ECRIS 2010

Online Proceedings

19th International Workshop on ECR Ion Sources

Grenoble, France
23-26 August 2010

Hosted by
Laboratoire de Physique Subatomique et de Cosmologie

ISSN 2222-5692

Foreword

The 19th International Workshop on Electron Cyclotron Resonance Ion Sources (ECRIS10) was held in the World Trade Center in Grenoble, France, from August 24th until August 26th, 2010. The workshop was hosted by the Laboratoire de Physique Subatomique et de Cosmologie.

The scientific program focused on the latest developments (performance, modeling and applications) of ECR ion sources along with the associated physics and technologies, including plasma physics, beam optics, beam diagnostics, magnet technology.

The ECRIS10 edition was clearly a success and gathered together 104 participants, demonstrating once again that the ECRIS community is very active. The workshop program featured 9 oral and 2 poster sessions. A special care was taken to allow PhD students to present their work during the sessions. The spirit of ECRIS workshop was still present since it provided opportunities for informal discussions and future collaborations in a relaxed atmosphere.

The 2nd edition of the Geller Prize – a biennial award for promising young scientists in the field of ECR Ion sources - was chaired by Richard Pardo and sponsored by the PANTECHNIK company. The selection committee was impressed by the quality of the young nominees and the choice was not easy. Finally, the award was given to Olli Tarvainen (JYFL-Finland) for his outstanding contribution to ECRIS science.

I hope that the participants will keep a nice souvenir of the sunny excursions, either the hike in the Chartreuse mountains or the train tour of La Mure and the Vizille castle gardens visit.

I would like to thank the agencies that funded the workshop: *CNRS/IN2P3*, *la METRO*, *Université Joseph Fourier*, *Mairie de Grenoble*; and also the industrial sponsors and exhibitors who helped a lot to balance the budget.

Since ECRIS08 edition, the workshop proceedings are published electronically on the JACoW web site, dedicated to Accelerator related scientific publications. I would like to thank the JACoW team, especially Marie Robichon, Christine Petit-Jean-Genaz and Volker Schaa, for their constant help and training before and after the workshop to make these proceedings possible.

Finally, I would like to thank the local organizing committee and the edition board for their very helpful contribution to make ECRIS10 a successful edition. I am now looking forward to the next ECRIS12 edition which will be hosted by the ANSTO laboratory near Sydney in Australia.

Sincerely yours,

Thomas Thuillier,
ECRIS10 Chair
Proceeding Editor
June 2011

Contents

Workshop Chair

Thomas Thuillier	LPSC, France

International Advisory Committee

H. Beijers	KVI, Netherlands
S. Bogomolov	JINR, Russia
S.Gammino	LNS, Italy
D. Kanjilal	IUAC, India
H. Koivisto	JYFL, Finland
T. Lamy	LPSC, France
R. Leroy	GANIL, France
C. Lyneis	LBNL, USA
R. Pardo	ANL, USA
T. Nakagawa	RiKEN, Japan
P. Spaedtke	GSI, Germany
H.W. Zhao	IMP, China

Local Organizing Committee

J.Angot	LPSC, France
C.Favro	LPSC, France
T.Lamy	LPSC, France
M.L. Lombard (Secretary)	LPSC, France
M.Marie-Jeanne	LPSC, France
J.Riffault (Web)	LPSC, France
P. Sortais	LPSC, France
T. Thuillier (Chair)	LPSC, France

Editorial Board

T. Thuillier (Editor)	LPSC, France
M.Robichon (co-Editor)	ESRF, France
C.Renault	LPSC, France
E. Vernay	LPSC, France

ECRIS10 Workshop Photograph

SECRAL STATUS AND FIRST BEAM TEST AT 24GHZ

H. W. Zhao, W. Lu[1], L. T. Sun, X. H. Guo, X. Z. Zhang, Y. Cao, H. Y. Zhao,
Y.C.Feng, J. Y. Li, D. Z. Xie[2]
Institute of Modern Physics (IMP), Chinese Academy of Sciences, Lanzhou 730000
People's Republic of China

Abstract

SECRAL (Superconducting ECR ion source with Advanced design in Lanzhou) has been in routine operation at 18GHz for HIRFL (Heavy Ion Research Facility in Lanzhou) accelerator complex since May 2007. It has delivered a few highly charged heavy ion beams for the HIRFL accelerator and the total beam time so far has exceeded 3500 hours. To further enhance the SECRAL performance, a 24GHz/7kW gyrotron microwave amplifier has been installed and tested. Very exciting results were produced with quite a few new record highly-charged ion beam intensities. The latest results and reliable long-term operation for the accelerator have once again demonstrated that SECRAL is one of the best performance ECR ion source for the production of highly-charged heavy ion beams.

INTRODUCTION

SECRAL (Superconducting ECR ion source with Advanced design in Lanzhou) is a fully superconducting compact ECR ion source designed to operate at microwave frequency at 18-28GHz, which is dedicated for highly charged heavy ion beam production. SECRAL with an innovative superconducting magnet structure of solenoids-inside-sextupole [1-2], is different from all existing or under development high-magnetic-field superconducting ECR ion sources which utilize the conventional ECR magnetic structure of sextupole-inside-solenoids. The commissioning of the SECRAL at 18 GHz in 2006 and the experiments with double-frequency (18+14.5 GHz) heating in 2008 had yielded many world record ion beam intensities [2-3]. All these results and reliable operation have demonstrated that SECRAL performance at lower frequency is comparable or even better than those ECR ion sources operating at higher frequency of 28 GHz. To further enhance the performance of SECRAL and produce more intense highly charged heavy ion beams, a 24GHz/7kW gyrotron microwave generator was installed and SECRAL was tested at 24GHz. Some promising and exciting results at 24GHz with new record highly charged ion beam intensities were produced although the commissioning time was limited within a few weeks and RF power only 3-5kW. Bremstrahlung measurements at 24GHz have shown that X-ray is much stronger at higher RF frequency, higher RF power and higher minimum B field. An additional cryostat with five GM cryocoolers was installed at the SECRAL top to liquefy the boil-off helium gas to minimize the liquid helium consumption. The detailed results and the new development achieved at SECRAL in the past two years will be presented in this article.

SECRAL PRELIMINARY TEST RESULTS AT 24GHZ/3-5KW

To further enhance the SECRAL performance in production of highly charged heavy ion beams, finally a 24GHz gyrotron system with maximum output power 7 kW was chosen and installed. The SECRAL excellent results at 18+14.5 GHz double frequency heating for highly charged heavy ion beam production have convinced us that the best performance for SECRAL should be achieved at 24+18 GHz double frequency heating. The reason to choose 24GHz instead of 28GHz is that it is more difficult to compromise the magnetic field distribution for 28+18 GHz double frequency heating because the frequency difference is larger than that of 24+18 GHz. SECRAL does not need to couple very high RF power to reach the best performance because of its smaller plasma chamber, so 5-6 kW operational power is quite enough. The 24GHz transmission line and RF coupling system to SECRAL is similar to that developed at SERSE source [4-5]. The 24GHz transmission line from the gyrotron cabinet to the SECRAL source consists of arc detector, directional coupler, polarizer, mode convertor from T_{02} to T_{01}, mode filter, compensator, DC-breaker, 90-degree corrugated bend and bore-nitride microwave window, as shown in Fig.1. All components at the transmission line are water cooled and designed as compact as possible. The 24GHz microwave is coupled into the SECRAL source through the oversized waveguide WRC621D14. The 24GHz gyrotron system and all components at the transmission line were manufactured by Russia GYCOM.

The first beam tests at 24GHz were conducted in August 2009 with a stainless steel chamber in order to have quite stable beam. The beam commissioning has focused on Argon and Xenon beam production. The source extraction voltage was limited to 22kV due to the DC-breaker problem and the output power from the gyrotron system was limited to 5 kW due to problem of the high voltage power supply for the gyrotron cathode. The SECRAL magnet was set at 90%-95% of the maximum design field during 24 GHz beam tests in terms of the optimized beam and charge state, typically the axial injection field from 3.3 Tesla to 3.5 Tesla and the radial sextupole field at the chamber wall from 1.65 Tesla to 1.75 Tesla. The source conditioning at 24GHz was

[1] Also of the Graduate School of CAS.
[2] IMP visiting scientist.

conducted firstly with pure Oxygen. It turns out that the source conditioning and out-gassing at 24GHz take much longer time than that at 18GHz. Beam spectra obtained during the source conditioning at 24 GHz indicate that there are so many ion species coming out from the out-gassing and plasma sputtering to the chamber wall although the plasma chamber has been operated at 18GHz for more than one year. It took about one week for the SECRAL to raise the RF power more than 3.0 kW during the source conditioning, and the overloading due to out-gassing and higher power could happen sometimes. After one week continuously source conditioning, a stable plasma condition can be achieved easily at 3.0 kW and SECRAL can be tuned for stable beam production and optimization.

Figure1: SECRAL with 24GHz/7kW gyrotron system.

SECRAL commissioning for stable beam production was started from Ar^{12+} and Ar^{14+}. After two days optimized tuning to those key parameters, such as the magnetic field distribution, the main gas Argon, the mixing gas Oxygen, the coupled RF power, the biased probe voltage, the beam focusing from the solenoid lens and so on, some good results were produced at the 24GHz power level of 3-4 kW, for instance, 650 eμA of Ar^{12+}, 440 eμA of Ar^{14+}. SECRAL was switched to $Ar^{16+}$and Ar^{17+} beam tuning after $Ar^{12+}$and Ar^{14+}beam optimization. It seems much more difficult to achieve optimum plasma conditions for $Ar^{16+}$and Ar^{17+} productions at high RF power. Much more mixing gas Oxygen and main gas Argon is required, otherwise the plasma could be out of igniting. After some time tuning and optimization, only 149 eμA of Ar^{16+} and 14 eμA of Ar^{17+} were produced at about 4 kW RF power. The typical magnetic fields for Argon beam production are: B_{inj}=3.46 Tesla, B_{min}=0.68 Tesla, B_{ext}=1.6 Tesla and B_{rad}=1.74 Tesla. Probably longer time conditioning and Aluminium chamber are needed for higher charge state beam production.

SECRAL was commissioned with Xenon beam at 24GHz after Argon beam production. The emphasis was put on optimization of $^{129}Xe^{27+}$, $^{129}Xe^{30+}$ and $^{129}Xe^{35+}$ beams. Even after two weeks source conditioning, the out-gassing or some kind of plasma instability at high RF power still occurred from time to time which could result in beam instability and even overloading. However, stable plasma conditions for optimum tuning of $^{129}Xe^{27+}$ and $^{129}Xe^{30+}$ can be easily obtained because of two weeks source conditioning. After two days test and tuning, some new record Xenon beam intensities have been produced at 3.5 kW RF power of 24 GHz, such as 480 eμA of Xe^{26+}, 455 eμA of Xe^{27+}, 350 eμA of Xe^{28+} , 152 eμA of Xe^{30+} and 85 eμA of Xe^{31+}. Fig.2 shows a typical spectrum to optimize $^{129}Xe^{27+}$ at 3.5 kW RF power. The typical magnetic fields for Xenon beam production are: B_{inj}=3.3 Tesla, B_{min}=0.67 Tesla, B_{ext}=1.54 Tesla and B_{rad}=1.63 Tesla. The situation for production of highly charged Xenon beams such as Xe^{35+} and Xe^{42+} is similar to that of Ar^{16+} and Ar^{17+} beams at 24GHz. The optimum plasma conditions have not been found for those very high charge state Xenon beams. Fig.3 shows a spectrum to optimize $^{129}Xe^{34+}$ at 3.5kW. Xenon beam test at 24GHz had to be stopped because SECRAL was requested to deliver Kr beam for HIRFL accelerator.

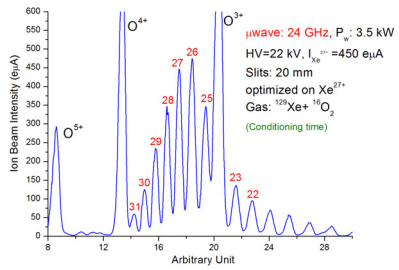

Figure 2: Spectrum to optimize $^{129}Xe^{27+}$ at 3.5 kW of 24GHz.

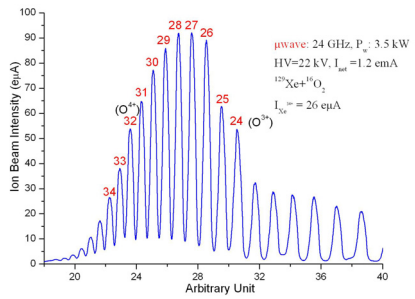

Figure 3: Spectrum to optimize $^{129}Xe^{34+}$ at 3.5 kW of 24GHz in September 2009.

Xenon beam test at 24GHz was conducted again in November 2009 after one month Kr beam operation at 18GHz. Surprisingly, the source tuning at high power 24GHz/3-4 kW was much better than previous test in terms of beam stability, beam intensity and charge state distributions for high charge state Xenon beams. Fig.4 shows a spectrum to optimize $^{129}Xe^{35+}$ at 5kW. By comparing with Fig.3 and Fig.4 and also taking into account the beam test condition, it seems that longer time source conditioning for higher charge state Xe beam at 24GHz is needed. Finally, a few new record Xenon beam intensities for higher charge state beams have been produced at 3.5-5 kW RF power of 24 GHz, such as 60 eμA of Xe^{34+}, 45 eμA of Xe^{35+}, 17 eμA of Xe^{38+} and 3 eμA of Xe^{42+}. Optimum test for very high charge state Xenon beams Q>42 needs to be done in near future. Unfortunately, a high voltage power supply for the

24GHz gyrotron system failed to work and SECRAL beam test at 24GHz had to be stopped.

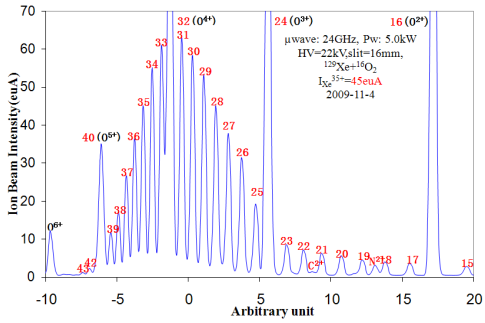

Figure 4. Spectrum to optimize $^{129}Xe^{35+}$ at 5 kW of 24GHz.

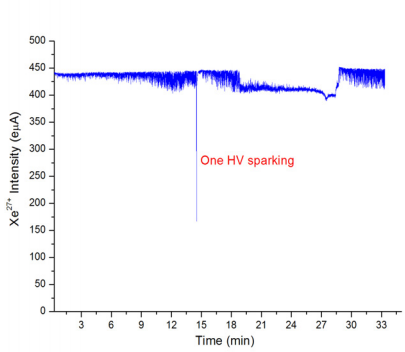

Figure5: $^{129}Xe^{27+}$ beam intensity instability at 3.5 kW rf power of 24GHz in September 2009

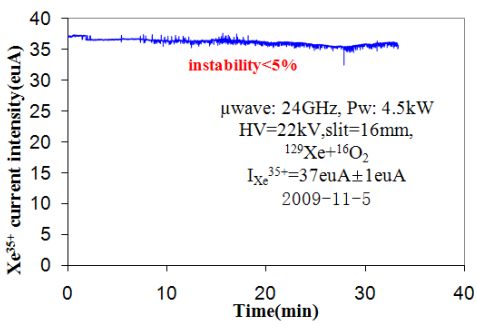

Figure 6: $^{129}Xe^{35+}$ beam intensity stability at 5 kW rf power of 24GHz in November 2009.

Generally speaking, beam stability at 24GHz is worse than that at 18GHz at the RF power level 3 kW. Fig.5 shows $^{129}Xe^{27+}$ beam intensity variation around 440 eμA during 30 minutes at the coupled RF power 3.5kW at 24GHz recorded in September 2009. Fig.6 shows $^{129}Xe^{35+}$ beam intensity stability around 37 eμA during 30 minutes at the coupled RF power 4.5kW at 24GHz recorded in November 2009.The beam intensity instability and big jump in the Fig.5 might be caused by the out-gassing and ECR discharge inside the 24GHz waveguide of the injection part. There is an ECR zone in the 24GHz waveguide in terms of the axial field distribution, where the pumping conductance is low and the vacuum is not good. It is easier to result in the out-gassing and the ECR discharge in that region. However, any evidence to support ECR discharge inside the 24GHz waveguide was not found after the source was opened. Beam instability at high power of 24GHz may not be understood completely and further experiments and studies are needed.

Table 1 lists the latest Xenon beam results achieved by SECRAL at 18GHz and 24GHz and comparison with recently published data from the high performance ECR ion source VENUS[6].

Table 1. Latest Xe beam results of SECRAL at 18GHz and 24GHz in comparison with other high performance ECR ion source (beam intensity: eμA).

		SECRAL	SECRAL	VENUS[6]
f (GHz)		*18(+14.5)*	*24*	*28(+18)*
P(kw)		<3.2	3-5	5-9
^{129}Xe	20^+	505		320
	27^+	306	455	270
	30^+	101	152	116
	31^+	68	85	67
	35^+	16	60	28
	38^+	6.6	17	7
	42^+	1.5	3	0.5
	43	1		

SECRAL OPERATION TO HIRFL ACCELERATOR

SECRAL ECR ion source has been put into operation to deliver highly charged heavy ion beams for the HIRFL accelerator complex since May 2007. SECRAL has been operated at 18GHz in an axial injection beam line of the HIRFL cyclotron and only dedicated to very high charge state heavy ion beams, while the other light ion beams with low charge state are provided by the room temperature ECR source LECR3. Four different ion beams, such as $^{129}Xe^{27+}$, $^{78}Kr^{19+}$, $^{209}Bi^{31+}$and $^{58}Ni^{19+}$, have been delivered to the HIRFL accelerator complex for various experiments. During operation the typical RF power of 18 GHz is 1.2-2.0 kW and extraction voltage is about 10-22 kV according to the cyclotron requirements. The operational beam intensity is typically around 100-150 eμA for $^{129}Xe^{27+}$, $^{78}Kr^{19+}$, and 50-70 eμA for $^{209}Bi^{31}$, $^{+58}Ni^{19+}$ (only 9.8 kV extraction voltage). The total operated beam time from SECRAL has been more than 3500 hours up to July 2010. SECRAL operation with higher charge state and higher beam intensity has made a great contribution to HIRFL performance enhancement in terms of beam energy and intensity.

REFERENCES

[1] H. W. Zhao, et al. Rev. Sci. Instrum. 79, 02A315 (2008).
[2] H. W. Zhao, et al. HEP&NP, 31, Supp. I, 8 (2007).
[3] H.W. Zhao et al, RSI, 81, 02A202 (2010).
[4] S.Gammino, et. al., Rev. Sci. Instrum., 72, 4090 (2001).
[5] D.Hitz, Advances in Imageing and Electron Physics, 144, 1 (2006).
[6] D. Leitner, et.al. Rev. Sci. Instrum. 79, 02C710 (2008).

INTENSE BEAM PRODUCTION WITH SUSI

L. T. Sun*, J. Brandon, D. Cole, M. Doleans, D. Morris, G. Machicoane, E. Pozdeyev, T. Ropponen, L. Tobos, National Superconducting Cyclotron Lab, MSU, East Lansing, MI 48824, USA

Abstract

SuSI ion source, a 3rd generation fully superconducting ECR ion source is now used for ion beam injection to the Coupled Cyclotron Facility since September 2009. Initial performances during the commissioning of SuSI (Superconducting Source for Ions) were mainly limited by the microwave power available from a single 18 GHz microwave amplifier, especially for the production of heavier ion beams. The Injection of SuSI was modified to add a second 18 GHz amplifier, to reach a maximum of 3.0 kW of RF power inside the plasma chamber. Production of heavy ion beams, such as Kr^{14+}, Bi^{30+} and U^{33+} is reported, to demonstrate the performance of SuSI. Additional studies were made with various ion source parameters to optimize the beam intensity within a normalized emittance of 0.9pi.mm.mrad as needed for the FRIB project and will be reported in this paper.

INTRODUCTION

As one of the latest developed fully superconducting electron cyclotron resonance ion sources (ECRIS) in the world, SuSI has been used for ion beam injection to the Couple Cyclotron Facility (CCF) since October 2009. Several ECRISs have been used for NSCL cyclotron operation, such as the 6.4 GHz SC-ECR [1] and the 14.5 GHz ARTEMIS [2]. The beam power available from CCF has steadily improved over the last few years due to an ongoing effort to improve both the performances of the ion source and the beam transport in the K500 injection line. But to further improve the performance of the coupled cyclotron facility (CCF), especially for heavy ion beams, a more powerful ion source that can produce more intense heavy ion beams with good beam quality is needed. In order to replace the aging 6.4 GHz ECR ion source, a new fully superconducting ECRIS SuSI was designed [3]. The source was completed and put into commissioning in early 2007 [4]. After some training of the superconducting coils, SuSI commissioning continued using an 18 GHz and a 14 GHz transmitter. Early results with gas and metallic beams showed that SuSI could produce high intensity of medium charge states of light to heavy ion beams [5]. In order to limit the beam transverse emittance propagating into the K500 injection line, a collimation scheme was developed and successfully tested. In the summer 2009, SuSI was successfully connected to the K500 cyclotron and put into operation since then. SuSI has now provided more than 1200 hours of operation to the CCF. Both gaseous and metallic ion beams have been produced, and good reliability and stability has been demonstrated. As a fully superconducting ECRIS with many flexibilities, SuSI has been used for basic ECRIS studies [6], beam developments and FRIB project R&D [7]. After a brief description of the new test setup of SuSI ion source, the latest results from SuSI will be presented.

*sunl@nscl.msu.edu

SUSI ION SOURCE UPGRADES

Several components of SuSI have been upgraded. In particular a New18GHz klystron amplifier has replaced the 14.5GHz klystron amplifier. This configuration provides a maximum 18GHz microwave power of ~3.0 kW. Also, at the outer surface of the plasma chamber, a 2mm thickness tantalum tube has been added to shield the strong bremsstrahlung radiation to protect the high voltage insulator from degradation. The high voltage insulator is a PEEK material tube that has much higher radiation tolerance than the acrylic tube used previously.

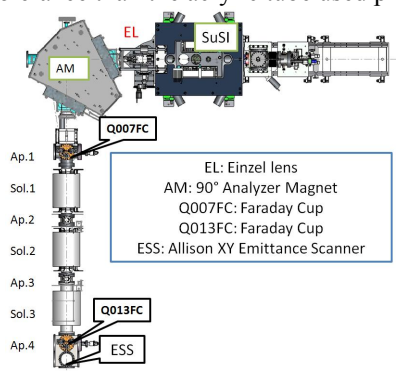

Figure 1: Layout plot of SuSI beam line.

Extracted beam is focused by an EINZEL lens with maximum operational voltage up to -30kV (negative voltage is proved with SuSI to give better ion beam transmission than that positive voltage can do, especially for intense beam transmission) and then analyzed by a 180mm gap 90° double focusing dipole magnet. Analyzed beam is detected by the faraday cup Q007FC with a 4-jaw slit in front of it. Past experience has showed that tuning the ion source for maximum intensity at this location may results in poor transmission through CCF. For example, large transverse emittance can lead to beam losses in the K500 cyclotron. Therefore, after the first analyzing faraday cup Q007FC, the SuSI beam line has been equipped with a setup to provide transverse collimation to the ion beam. The collimation is done by successive sets of apertures that cut the beam in transverse directions. A solenoid between every 2 apertures provides a possibility to do a rotation of the beam in phase space. Due to constraints in the space available, the collimation channel was designed to include four sets of slits and 3 solenoids. A drift space between each solenoid and each aperture is also included. The acceptance of the channel in the transverse direction is set by the size of the apertures. All the beam particles outside the acceptance of the collimation channel will be lost. 2 sets of steering

magnets are placed in front of Q007FC to align the beam through the collimation channel. The collimated beam current is read on a second faraday cup Q013FC situated just after the collimation channel. A set of Allison type XY emittance scanners are also installed to analyze beam quality. Fig. 1 shows the layout of the SuSI beam line.

Intense beam production

The Beam transmission with SuSI to the first analyzing cup Q007FC was found to change significantly with the total extracted drain current, 75 % to 80 % transmission are typically achieved with 1 to 2emA beams while less than 65 % was observed with drain currents exceeding 4 to 5 emA. The flexibility of SuSI axial magnetic field allows the modification of the ECR zone location to achieve more intense medium or low charge state ion beam production. Two experimental configurations have been tested with SuSI to produce intense medium charge state ion beams like 0.5emA Kr^{14+} and 350 eμA Xe^{20+}:

- Keep the radial, injection and minimum magnetic fields fixed, and move the ECR zone to the extraction while the extraction field is lowered when the ECR zone is closer to the extraction side. The ECR length is unchanged during the test. This is similar to the tests on room temperature ECRISs by adjusting the plasma electrode position [8]. (Test 1)
- Keep the radial, injection, extraction and minimum fields constant, and only move the ECR zone to the extraction side. The ECR zone length is kept unchanged. (Test 2)

For the two tests presented, the experimental procedure consisted to adjust the magnetic field configuration by changing the position of the end point of the ECR resonance zone. The magnetic configuration used for reference has the end point at 362mm from the front face of the first injection solenoid and is labelled "Z=0mm" position. The other magnetic field configurations are normalized to it, for example "Z=50mm" means the ECR zone has been moved to the extraction by 50mm. Table 1 shows the results of Test 1. The total drain current and Kr^{14+} beam intensity kept decreasing when moving the ECR zone end point position from 51mm to 72 mm. A possible explanation is that the extraction field kept decreasing for the different positions during the test which has a big impact on the plasma confinement and causes plasma loss. In the second test, where the maximum at extraction was kept the same, a different behaviour was observed. As shown in Fig. 2 and Fig. 3, the variation in the total drain current and Kr^{14+} beam intensity are characterized by successive maxima and minima along the change to the ECR zone position. A possible explanation is that the change of the ECR zone location impacts the coupling of the microwave with the ECR plasma. There is no obvious indication that the closer the ECR zone to the extraction aperture, the more medium charge state ion beam can be extracted. But the change of the ECR zone position modifies the beam extraction significantly, since at certain position more analyzed beam can pass through the collimation channel with the acceptance set at 0.9π.mm.mrad. That means the ECR zone position can not only regulate the ion source microwave cavity but also the intrinsic properties of the emitted ion beams. More investigation with intense beam production will be made in the future.

Table 1: Comparison of the data from Test 1

Z (mm)	Drain Current (emA)	Q007FC (eμA)	Q013FC (eμA)
51	5.20	320	203
55	4.61	279	176
60	4.26	287	205
72	3.72	255	186

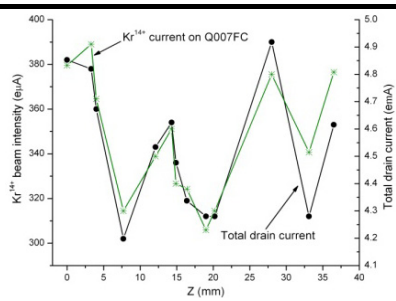

Figure 2: Kr^{14+} beam intensity and total drain current changes as the ECR zone movement (Test 2).

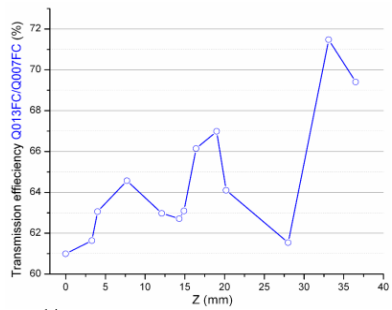

Figure 3: Kr^{14+} beam transmission efficiency through the collimation channel as the ECR zone movement (Test 2).

Production of high charge state ion beams

Although high charge state ion beams are not needed for CCF operations, high charge state ion beams of Xenon were produced to study the performance of SuSI. SuSI has many features that enable it to produce good results of high charge state ion beams. SuSI has a fully superconducting magnet to provide sufficient magnetic confinement for the operation at 18GHz, i.e. B_{rad}~1.3T, B_{inj}~2.6T, B_{ext}~1.3T. And the six independent solenoids make it more flexible to optimize the field configuration for high charge state ion production. The aluminium plasma chamber is also a very important part to improve the enhancement of high charge ions production, which has already been proved by many labs. Compared to other latest built fully superconducting ECRISs like VENUS [9], SECRAL [10] and RIKEN SCECRIS [11], SuSI has a more compact plasma chamber with an effective plasma volume typically around 3.6 litres, which makes it easier

to reach higher power density with reasonable RF power feeding. An additional 18GHz klystron amplifier was connected to SuSI which increases the available RF power up to ~3.0 kW and increases the power density up to 0.85kW/l. With more power density achievable on SuSI, it is convenient to learn the behaviour of the ion source performances via plasma heating power. The very high vacuum achievable at the source extraction side (low 10^{-8} Torr) helps the extraction and transmission of the high charge state ion beams like Xe^{42+}.

The typical test to produce high charge state ion beams was done with xenon. Fig. 4 gives the typical spectrum optimized for the production of high charge state xenon ion beams. With oxygen as the mixing gas, the charge state distribution can be easily tuned to be peaked on Xe^{31+}, so that higher charge state ion beams such as Xe^{39+}, Xe^{42+} and even Xe^{44+} can be easily distinguished on the spectrum. At lower power level, the high charge xenon beams such as Xe^{38+} can be barely seen in the spectrum, but when the power level is increased beyond 2.0kW, the beam intensity increases very fast. The maximum beam intensity is observed at the full microwave power of 3.0kW, with no indication of saturation. It is very positive that with more power injected into the plasma chamber, more intense xenon high charge state ion beams and even higher charge states are possible.

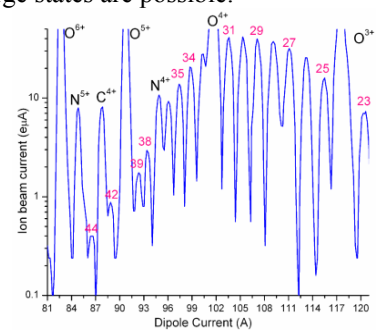

Figure 4: Typical xenon charge state distribution when optimizing for Xe^{38+}.

Production of refractory metal ion beams

The inductive oven developed at NSCL can generate a high temperature up to 2200°C, and has already been used to produce intense refractory metal beams for CCF operation or ECRIS R&D studies. For example, In 2009, more than 200eμA Ni^{12+} and 180eμA Ni^{17+} have been produced with SuSI. In recent years, intense uranium beam has become a worldwide interest. Because of its wide availability and stability even at high temperature, Uranium Oxide (UO_2) is a logical choice to try to produce Uranium ion beams. By design the rhenium tube works both as the recipient (susceptor) of eddy currents generated by the RF power supply and also as the crucible, it is possible to fill the rhenium directly with UO_2 powder. The first test indicated that UO_2 can be used to produce intense uranium ion beams. Although there is plenty of oxygen vapour produced at the same time, some oxygen gas is necessary to sustain the plasma. Fig.5 shows the spectrum when optimizing the production of U^{33+} beam. Within the limit of the inductive oven, 50eμA U^{33+} has been produced. The beam intensity was observed to be stable. Later examination of the experimental setup shows that there is only 100mg UO_2 that has been consumed and no obvious breakdown or burnt-out of the oven during the ~24hrs' real test, which demonstrates that inductive oven is good for the production of intense uranium beam with UO_2. Production of Uranium is limited at the moment by the amount of vapour available from the oven. More studies will be done in the near future to improve the performances of this technique.

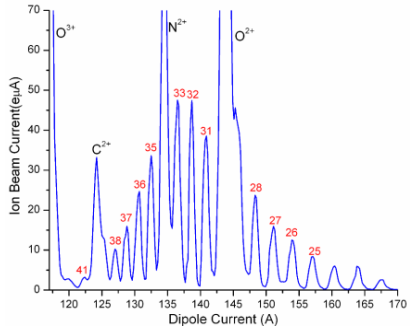

Figure 5: Spectrum obtained with UO_2 to provide uranium vapour.

Another typical method to produce refractory metal ion beams is ion beam sputtering and has also been tested with SuSI. A Ø10mm diameter uranium sample has been inserted on the axis of the ion source at the injection end. The large size of the sample provides a large cross section for the ion bombardment ions and the central-positioned sample enables the best acceptance of uranium by the plasma volume. Water cooling to the sample has also been considered. Since SuSI has a ~450mm mirror length and more than 130mm long ECR zone, the cross section to capture the sputtered material is much bigger than conventional ECR ion sources. Different support gases such as $^{16}O_2$, $^{18}O_2$, ^{20}Ne and ^{40}Ar have been tried during the test. Argon gas gives the best efficiency while $^{18}O_2$ gas provides higher charge states. U^{33+} and U^{34+}were the typical charge states optimized, and more than 86eμA $U^{33+}$and 95eμA U^{31+} have been detected on Q013FC. A disadvantage of the SuSI collimation channel is the poor mass resolution that can be achieved. For heavier ion beams such as Uranium, the lack of resolution requires to close the slits and aperture strongly in order to separate charge state effectively. However the transmission then decreases and in the case of the Uranium measurements was around 50 %. More details regarding the sputtering setup and measurements can be found in these proceedings [12].

R&D FOR FRIB

SuSI has been used to do beam studies for FRIB. In particular ion beam brightness has been investigated for high intensity ion beams. For the FRIB project, the ion beam transverse emittance should not exceed 0.9π.mm.mrad (full normalized) For heavy elements that will require transport of two charge states to reach the

desired beam current on the production target a smaller emittance is needed, (0.6π.mm.mrad) per charge state. By using the collimation channel set at 0.9π.mm.mrad or 0.6π.mm.mrad, it is possible by measuring the transmitted current through the channel to assess the proportion of beam within the acceptance of the FRIB linac. For FRIB project, 640eμA $^{18}O^{6+}$ and 378eμA $^{40}Ar^{8+}$ are needed and the corresponding full geometric emittance is 200π.mm.mrad and 275π.mm.mrad for 25kV/q energy respectively. Fig. 6 shows the emittance achieved by SuSI for oxygen and argon after the collimation channel. On the other hand for heavier beam such as Krypton 400eμA of $^{86}Kr^{14+}$ was measured on Q007FC, but only 250 eμA $^{86}Kr^{14+}$ can pass through the 0.9π.mm.mrad collimation channel to Q013FC, which means a 62.5% transmission efficiency.

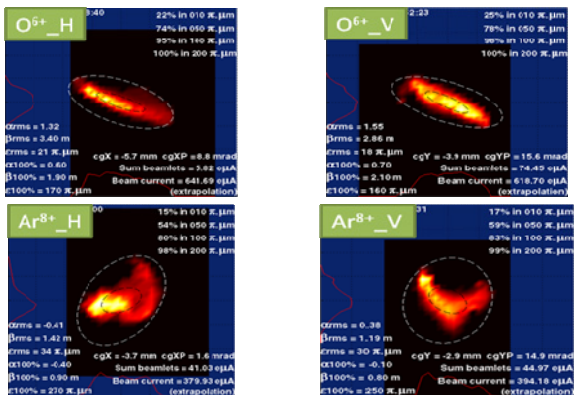

Figure 6: Horizontal and vertical beam emittance plots for 700eμA O^{6+} and 400eμA Ar^{8+} respectively.

CONCLUSION

SuSI ion source can now be operated at more than 3.0 kW at 18GHz and has demonstrated outstanding performances for a wide variety of beams from medium to high charge states. In particular, more than 380eμA Xe26+, 276eμA Xe27+ and 91eμA Xe30+ have been produced. Good intensity of ion beams of high charge states have also been produced with SuSI, such as 22 eμA Xe34+, 3.2eμA Xe38+and 0.35eμA Xe44+. Several other tests on SuSI have also provided solid results. For instance, UO2 was used for the first time with an inductive oven to produce intense uranium ion beams. About 50eμA U33+ has been successfully produced. Also beam sputtering with a uranium sample has provided a beam intensity of 86eμA U33+. As a summary, the latest results from SuSI are listed in Table 2.

A third 18GHz klystron amplifier will increase the value up to 1.3kW/l. SuSI is still on the way to challenging the limit of ECRIS performances at 18GHz. Following the frequency scaling laws, higher frequency ECR heating is also planned with SuSI. A 24GHz/10kW gyrotron amplifier is scheduled to be connected in FY2011.

Table 2: Latest beam results from SuSI

^{86}Kr	Q	I (eμA)	^{58}Ni	Q	I (eμA)
	14	500		12	200
^{129}Xe	20	350		17	180
	26	380	^{209}Bi	27	180
	27	276		28	190
	30	91		29	150
	34	22		31	76
	35	14.5		33	53
	38	3.2		36	9
	39	1.8		41	6
	42	0.95		46	2.5
	44	0.35	$^{238}U^{*}$	31	95
				32	95
				33	86

* obtained with sputtering method

REFERENCES

[1] T. Antaya, S. Gammino, Rev. Sci. Instr. 65 (1994) 1723.

[2] H. Koivisto et al., "ARTEMIS -the new ECR Ion Source for the Coupled Cyclotron Facility at NSCL/MSU", Proceedings of the Workshop on the Production of Intense Beams of Highly Charged Ions, Catania, Italy, September 2000, Italian Phys. Soc. Conf. Proc. p.135, 72 (2001).

[3] P.A. Zavodszky et al., Nucl. Instr. and Meth. in Phys. Res. B 241 (2005) 959.

[4] P.A. Zavodszky et al., "First commissioning results of the SuSI ECRIS", Cyclotron'07, Giardini Nexos, October 2007, p.283 (2007); http://www.JACoW.org.

[5] G. Machicoane, D. Cole and P. Zavodszky, "Commissioning results of the 18GHz fully superconducting ECR ion source SuSI", ECRIS'08, Chicago, September 2008, MOCO-B03, p.14 (2008); http://www.JACoW.org.

[6] T. Ropponen et al., "Bremsstrahlung and ion beam current measurements with SuSI ECR ion source", ECRIS'10, Grenoble, August 2010, WECOAK04, this proceedings; http://www.JACoW.org.

[7] G. Machicoane et al., "ECR ion sources for the Facility for Rare Isotope Beams (FRIB) project at Michigan State University", ECRIS'10, Grenoble, August 2010, MOCOBK01, this proceedings; http://www.JACoW.org.

[8] T.Nakagawa, Nucl. Instr. and Meth. in Phys. Res. B 226 (2004) 392.

[9] D. Leitner et al., Nucl. Instr. and Meth. in Phys. Res. B 235 (2005) 486.

[10] H. W. Zhao et al., Rev. Sci. Instrum. 81(2010) 02A202.

[11] T. Nakagawa et al., Rev. Sci. Instrum. 81(2010)02A320.

[12] D. Cole et al., "Early uranium ion production in SUSI and a low power survey of offset axial sputtering", ECRIS'10, Grenoble, August 2010, MOPOT16, this proceedings; http://www.JACoW.org.

STATUS OF RIKEN SC-ECRIS

T. Nakagawa#, Y. Higurashi, J. Ohnishi, RIKEN, Hirosawa 2-1, Wako, Saitama 351-0198, Japan
T. Aihara, M. Tamura, SAS, Ohsaki 1-17-6, Shinagawa, Tokyo 141-0032, Japan.

Abstract

To increase the beam intensity of highly charged heavy ions for RIKEN RIBF project, we constructed and tested the RIKEN new SC-ECRIS. After producing the first beam in the spring of 2009, we tried to optimize the ion source condition for maximizing the beam intensity with 18GHz microwave. We observed that the gentler field gradient and lager ECR zone size give higher beam intensity. Based on these studies, we produced 550μA of Ar^{11+} and 350μA of Ar^{12+} at the RF power of 1.8kW. In this summer, we will try use the 28GHz microwave to increase the beam intensity.

INTRODUCTION

Since middle of the 1990s, RIKEN has undertaken construction of new accelerator facility so-called Radio Isotope Beam Factory (RIBF) [1] and successfully produced 345MeV/u U beam (~0.4pnA on target) in 2008[2]. Using it, more than 40 new isotopes were produced with the in-flight fission reactions for only 4 days experiment.[3] It is clear that the intense U beam is strong tool to produce new isotopes in the region of medium mass nuclei and to study the mechanisms of the r-process in nuclear synthesis. For these reasons, the intense U beam is strongly demanded. To meet the requirement, we started to construct the new superconducting ECR ion source (SC-ECRIS) which has an optimum magnetic field strength for the operational microwave frequency of 28 GHz in the summer of 2007. In the end of 2008, we obtained the 102% of the designed value for the magnetic field strength. In the spring of 2009, SC-ECRIS produced first beam with 18GHz microwaves. Till now, we made various test experiments to increase the beam intensity of highly charged heavy ions with 18 GHz microwave [4].

In this article, we present the structure of the new ion source, new experimental results and the future plan to meet the requirements.

SC-ECRIS

The detailed structure of the ion source was described in refs [4, 5]. Schematic drawing of the Sc-coils is shown in Fig.1. For operation of 28GHz microwave, the B_{inj}, B_{ext} and B_r are 3.8, 2.2 and 2.2T, respectively. The main feature of the ion source is that it has six solenoid coils for producing magnetic mirror for the axial direction. Using this configuration, one can change the magnetic field gradient and ECR zone size independently. This magnetic system allows us to produce "conventional B_{min} "and so-called "flat B_{min}" [6] configurations. For keeping the superconductivity, the cryostat is equipped with three small GM refrigerators with 4 K, 20K and 70 K stages and operated without supplying liquid He after poured once. Amount of the liquid-He in the cryostat is ~500 L. The nine current leads made of high temperature superconducting material are used to minimize the heat load to 4 K stage. The heat load to 70 K stage is 123 W caused by copper current leads, supports of a cold mass and radiation through the multi-layer insulation. In the winter of 2009, we installed one GM-JT refrigerator, which have total cooling power of 5W at 4K, to increase the cooling power.

#nakagawa@riken.jp

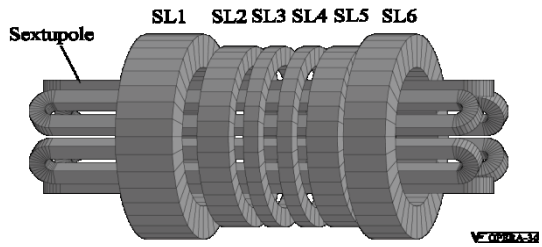

Figure 1: Schematic drawing of the Sc-coils.

EXPERIMENTAL RESULTS

The one of the strong interests for increasing the beam intensity of highly charged heavy ions are the effect of the resonance surface size and field gradient at ECR zone. As described in the previous section, the ion source has six solenoid coils for creating the mirror magnetic field. Using these coils, the ECR surface size can be changed without changing the average magnetic field gradient. Fig. 2 shows the beam intensity of Xe^{20+} as a function of the average magnetic field gradient for several ECR zone sizes at the RF power of 500W. For investigating these effects, B_{inj}, B_{ext} and B_r were fixed to 2.3, 1.2 and 1.3T, respectively. The extraction voltage was fixed to 17kV. It is clearly seen that the beam intensity increases with decreasing the field gradient. Furthermore, it seems that the beam intensity is higher for larger zone size at same field gradient. Fig. 3 a) and b) show the ratio of highly charged Xe beam intensity between two conditions. The ratio between two different field gradients increases with increasing the charge state (fig.2 a)) on the other hand, the ratio between different zone sizes are almost constant and independent on the charge state (Fig.3 b)). It is well-known that the energy transfer from microwave to electron increases with decreasing the gradient. It means that the electron temperature becomes higher at the gentler field gradient. The production rate of the higher charge state Xe ions increases with increasing the electron

temperature. For this reason, we observed the phenomena shown in Fig.3 a).

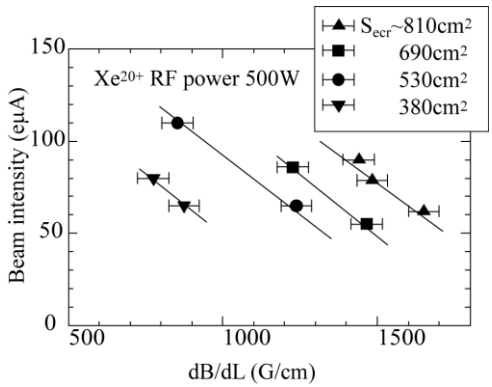

Figure 2: Beam intensity of Xe^{20+} as a function of average field gradient for several ECR zone size.

Fig. 4 shows the beam intensity of Ar^{11+} as a function of average magnetic field gradient for several ECR zone size. We can see the same tendency as Xe^{20+} case except for the beam intensity at gentler field gradient (dB/dL < 800G/cm). The beam intensity saturated or even decreased with increasing field gradient in this region.

The estimated beam intensities (dashed line) are shown in this figure. Simultaneously, we measured the heat load of the X-rays. (see Fig. 5) It is clearly seen that the heat load increases with decreasing field gradient. The heat load of the cryostat is strongly dependent on the X-ray energy, i.e., higher energy X-ray gives large heat load. It means that the very high energetic electron generate at dB/dL<800G/cm. We observed same tendency for Ar^{12+} and higher RF power (>1kW). It is still unclear why we do not obtain higher beam intensity in this region. To understand this phenomenon, we need further investigations.

Fig. 6 shows the beam intensity of Ar^{11+} as a function of RF power under two conditions (A and B). The conditions (field gradient and ECR zone size) A and B are shown in Fig.4. The beam intensity increases with increasing RF power up to 1.8kW and we obtained 500 eμA of Ar^{11+}.

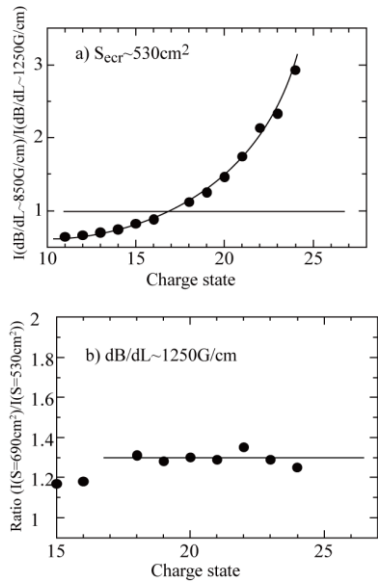

Figure 3: Ratio of beam intensity between two conditions

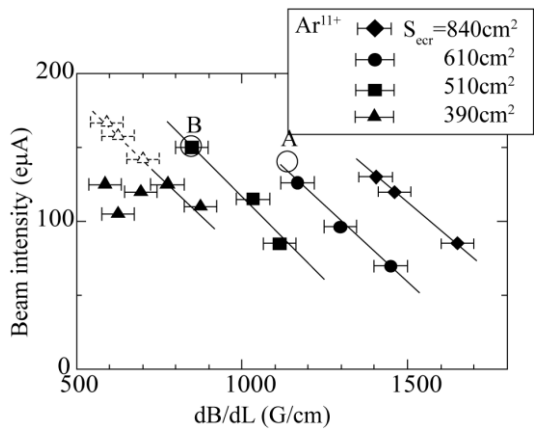

Figure 4: Beam intensity of Ar^{11+} as a function of average field gradient for several ECR zone size.

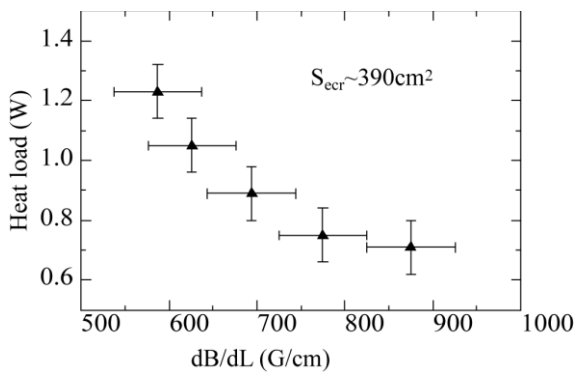

Figure 5: Heat load of the cryostat as a function of average field gradient

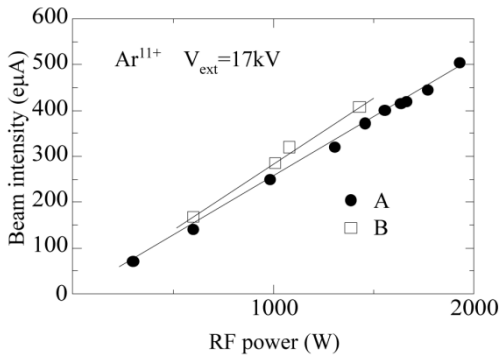

Figure 6: Beam intensity of Ar11+ as a function of RF power.

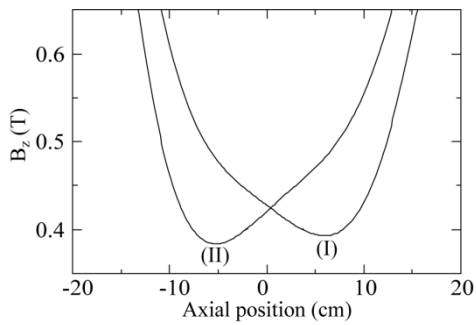

Figure7: magnetic field strength in the B_{min} region

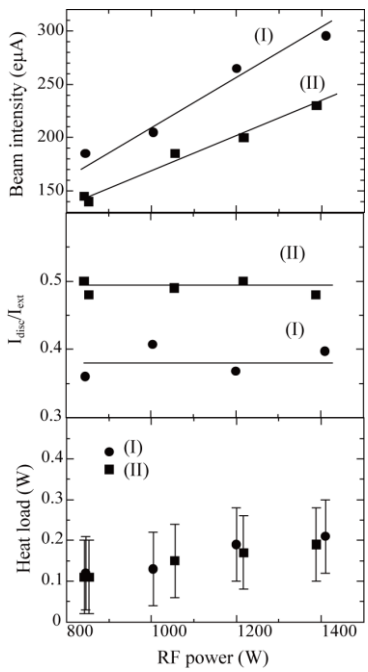

Figure 8: Beam intensity of Ar^{11+} (upper), ration between the extracted beam and biased disc current (middle) and heat load (lower) as a function of RF power

Fig. 7 shows the magnetic field distributions (I) and (II) in the B_{min} region. Fig. 8 shows the beam intensity of Ar^{11+}, ratio between biased disc current and extracted current, and heat load for two cases ((I) and (II)) as a function of RF power.

The beam intensities in case (I) are always higher than those in case (II). The average field gradient and ECR zone size for case (I) is same as those for case (II). The heat load of X-ray for case (I) was almost same as those for case (II) (lower figure). It means that the electron energy distribution may be same. Main difference is the position of the B_{min}. As shown in Fig.8, it seems that the ratio between the extracted beam intensity and current of biased disc in case (I) is always higher than those in case (II). It may indicate that the plasma flow to the extraction in case (I) is higher than that in case (II). To understand this mechanism, we need further investigation.

FUTURE PLAN

It is obvious that the higher frequency gives higher beam intensity of highly charged heavy ions, if we can make optimum magnetic field distribution for higher frequency. To increase the beam intensity of highly charged U ions, we will operate the new SC-ECRIS with 28GHz microwave instead of 18GHz after moving the ion source to the ion source room for new injector system of the RIBF in the summer of 2010. The 28GHz gyrotorn was already installed and tested at RIKEN in this spring of 2010. In the winter of 2010, the test with uranium will be made to meet the requirement of the RIKEN RIB factory project

CONCLUSIONS

We investigated the effect of the magnetic field gradient and ECR zone size on the beam intensity of highly charged heavy ions, independently. In this experiment, we clearly observed that the gentler field gradient and large zone size gives higher beam intensity. We also observed that the beam intensity was saturated or even decreased at smaller zone size and very gentle field gradient. To understand these phenomena, we need further investigation.

REFERENCES

[1] Y. Yano, Nucl. Instrum. Methods B261(2007)1009
[2] N. Fukunishi et al, PAC'09, Vancouver May 2009, MO3GRI01
[3] T. Ohnishi et al, JPSJ in press
[4] T. Nakagawa et al, Rev. Sc. Instrum. 81(2010) 02A320
[5] J. Ohnishi et al, High Energy Physics and Nuclear Physics 31(2007)37
[6] G. D. Alton, and D. N. Smithe, Rev. Sci. Instrum. 65(1994)775

STATUS OF THE VENUS ECR ION SOURCE

D. Leitner*, C.M. Lyneis, M. Leitner, A. Hodgkinson, T. Loew, P. Ferracin, G.L. Sabbi
Lawrence Berkeley National Laboratory, Berkeley, CA 94720, USA
G. Machicoane, E. Pozdeyev
National Superconducting Cyclotron Laboratory, Michigan State University, East Lansing, MI 48824, USA.

Abstract

The status and future developments of the 28-GHz VENUS (Versatile ECR for NUclear Science) Electron Cyclotron Resonance (ECR) ion source after the two years repair are presented. The fully superconducting ECR ion source VENUS serves as prototype injector for the Facility for Rare Isotope Beams (FRIB) project at Michigan State University (MSU) [1] as well as injector ion source for the 88-Inch Cyclotron at Lawrence Berkeley National Laboratory (LBNL). As such the source has produced many record beams of high charge state ions as well as high-intensity, medium charge state ions. As the FRIB project has now entered the preliminary design phase, LBNL is involved in the design of two new VENUS-like ECR injector ion sources for the FRIB facility. This paper will review the design changes for the FRIB injector, which will allow the installation of the FRIB injector source on a 100 kV platform. In support of the FRIB ion sources design systematic measurements of the heat load due to bremsstrahlung from the plasma for different magnetic fields have been performed and are presented. Finally, a possible future upgrade path for the FRIB injector using an advanced Nb_3Sn magnet structure is described.

A VENUS LIKE ECR ION SOURCE FOR THE FRIB INJECTOR

Fig. 1 shows the current installation of VENUS at the LBNL 88-Inch Cyclotron. The VENUS cryostat operates in a closed loop mode without additional helium transfers after the initial cool down as required for an installation on a high voltage platform as needed for the FRIB front end, but uses liquid nitrogen to cool the normal conducting leads. To adapt this design for the FRIB injector, the liquid nitrogen needs to be eliminated. In addition, the 4K cooling power will have to be increased. Finally, the extraction voltage needs to be enhanced.

HV insulation

The VENUS source high voltage insulation will need to be enhanced to allow reliable extraction at 40kV extraction voltage.

Pre-cooling of the normal conducting leads

The VENUS ECR ion source uses liquid nitrogen to dissipate the up to 70 watts of heat load from the normal conducting copper leads under full excitation. For FRIB the liquid nitrogen pre-cooling will be replaced by a single stage cryocooler.

4K cooling power

The VENUS cryostat is currently using four two stage Gifford-McMahon (GM) cryocoolers providing a total of 6W cooling power at 4K. But measurements of the x-ray heat load into the cryostat at the VENUS source, the SECRAL source, and the SC RIKEN indicate that more cooling power will be needed for the FRIB injector (see section3). For this purpose, three design options are currently being evaluated. In the first option a combination of two 2-stage and two 3-stage cryocoolers would provide a total cooling power of 13 W at 4K. Only minimal design changes are necessary for this option. Alternatively, we are evaluating the possibility of installing a compact external helium liquefier onto the HV platform, or the possibility of developing an insulated 100kV liquid helium fill line. While technically challenging, the last two options would have the advantage that ample cooling power would be available for potential future upgrades such as double frequency heating with 24 GHz or installing a higher frequency (>40GHz) Nb_3Sn based ECR ion source on the platform.

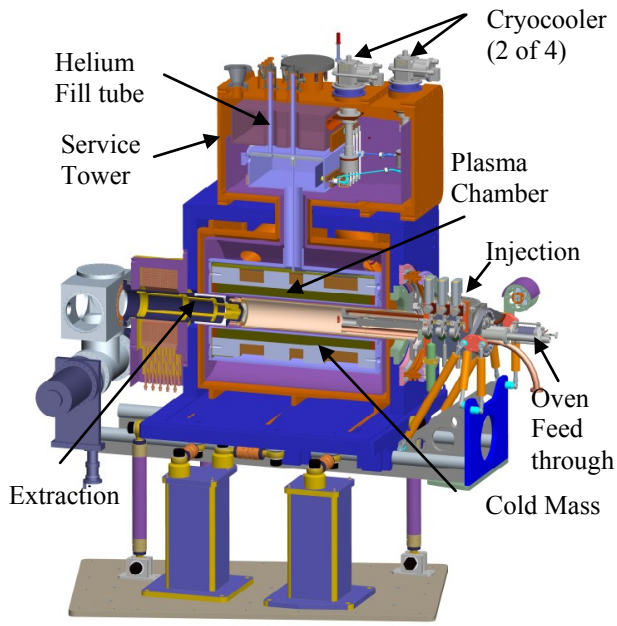

Figure 1: Mechanical layout of the VENUS ion source and cryogenic systems as installed on the vault roof of the 88-Inch Cyclotron

* Corresponding Author: Leitnerd@nscl.msu.edu

STATUS OF THE VENUS SOURCE

In January 2008, the VENUS ECR ion source experienced a major setback when one of the sextupole leads evaporated following a lead quench caused by an insufficient liquid helium level in the cryostat. At the 2008 ECR workshop in Chicago [2], we analyzed the failure mode and reported on the repair efforts, which were completed this year. Table 1 summarizes the chronology of the complex and long VENUS repair. In June of 2010 VENUS was finally re-installed at the 88-Inch Cyclotron and the magnet was tested to full excitation without quenches. The first 18 GHz plasma was achieved on July 9th 2010 and the first 28 GHz plasma was ignited on July 21st 2010, which marked the end of this long and difficult repair.

Table 1: Chronology of the VENUS source SC lead failure and its repair

Event	Date	Comments
Quench	1/24/2008	Sextupole magnet does not reenergize
Cryostat opened	1/28/2008	Sextupole coil #1 lead identified as cause
Service tower machined opened	2/29/2008	10 cm of lead # 1 had vaporized
Cable samples tested	3/2008	Lead damage extents into the cold mass
Cold mass extracted	4/15/2008	Wire samples taken
Wire tests completed	6/2008	Wire performance tested and leads are spliced and doubled up
Cold mass prepared for magnet testing	6-8/2010	
Magnet tested in external dewar at LBNL	9/12/2008	Reaches full field without quenches
Cryostat reconstruction complete	11/2009	Transfer to the 88-Inch
First cool down attempt	12/7/2009	He transfer tube weld fails during cool down
Open upper cryostat	2/2010	Replace internal helium fill line tubes
Cryostat repair complete	4/05/2010	Transfer to the 88-Inch
Installation on the roof	4/15/2010	Ion Source re-assembled
Cool down and magnet test	6/16/2010	Reaches full field without quenches
18 GHz	7/9/2010	First plasma and beam
28 GHz	7/21/2010	First 28 GHz operation, repair completed

During the repair, many improvements have been incorporated to prevent a similar accident. In particular, the lead cooling was enhanced by adding copper fins to the sextupole current leads for better heat transfer and the liquid helium level indicator was interlocked.

VENUS re-commissioning results

The VENUS ECR ion source commissioning was started with 18 GHz and two weeks later the 28 GHz waveguide was reconnected to the source as well. After about 2 weeks of conditioning with oxygen, ion beam tests using ^{124}Xe were conducted to assess the performance of the source after the repair. Table 2 shows some performance results before the repair and a few results from the re-commissioning experiments.

Table 2: A few VENUS ion source performance values before and after the repair. Ion beam intensity of the SECRAL ECR ion source are reported as reference[3].

	VENUS 28+18 GHz	SECRAL (24 GHz)
Results VENUS 2006-2008		
O^{6+}	2860 eμA	2300 eμA
O^{7+}	850 eμA	810 eμA
Ar^{12+}	860 eμA	510 eμA
Ar^{16+}	270 eμA	149 eμA
Ar^{17+}	36 eμA	14 eμA
Xe^{27+}	270 eμA	450 eμA
Xe^{30+}	116 eμA	152 eμA
Re -commissioning (3 weeks) VENUS 8/2010		
Xe^{26+}	480 eμA	480 eμA
Xe^{27+}	411 eμA	450 eμA
Xe^{30+}	211 eμA	152 eμA
Xe^{32+}	108 eμA	85 eμA (31+)
Xe^{35+}	38 eμA	45 eμA

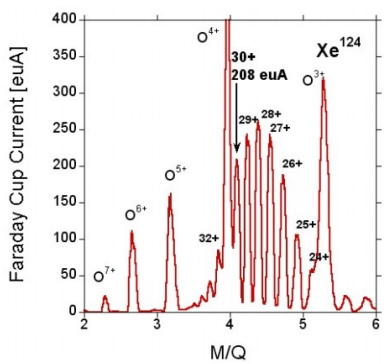

Figure 2: Xenon spectrum for medium to high charge states after the re-commissioning.

As an example Fig. 2 shows a high charge state spectrum optimized for Xe^{30+}, for which the ion beam in-

tensity was almost doubled compared to previous results from 2008 (see table 2). The re-commissioning results demonstrate that the VENUS source performance is far from being saturated and that it would benefit from further optimization. It also shows that for the highest charge states (e.g. Xe^{35+}) further conditioning is necessary.

X-RAY LOADING INTO THE CRYOSTAT

One of the surprising experimental observations during the development and early commissioning of the VENUS ECR ion source were the large amounts of x-ray radiation produced. These x-rays are a hazard for personal and also present a problem for the cryostat if they are absorbed into the coldmass [4]. In order to specify the cooling power for the FRIB injector source, systematic studies of the x-ray intensity and hot energy tail in dependence of various source parameters were conducted using all three LBNL ECR ion sources.

These studies showed that:

- X-rays can add several Watts of heat load to the cryostat and are a major challenge for present and future ECR ion sources (see Fig. 3)
- The maximum observed electron energy and heat load to the cryostat are both strongly dependent on the magnetic field gradient at the resonance zone (see Fig. 3 and [4])
- The maximum observed electron energy is strongly dependent on the microwave frequency[4]
- The energy spectrum shows a strong angular anisotropy[5]

During commissioning tests in 2010, the heat load into the cryostat for 28 GHZ operation was measured for a wide range of Bmin/Becr ratios. Fig. 3 shows the dependence of the heat load in W per kW of rf power injected into the plasma. Up to 1 W per kW was measured for a Bmin/Becr ratio of 0.8 percent.

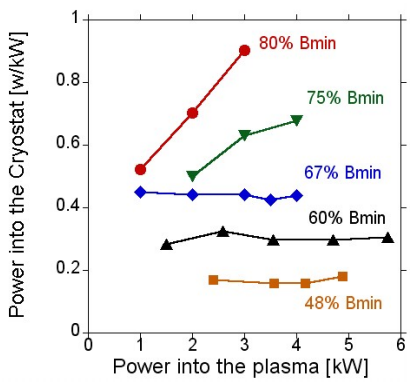

Figure 3: Added heat load into the cryostat due to bremsstrahlung absorbed by the coldmass per kW of microwave power injected into the cryostat for 28 GHz operation.

The VENUS cryostat has currently a total of 6 W of 4K cooling power available with no He consumption. The cryostat has a static 4K heat load of 2.5 W. Another 700 mW are added when the magnets are fully excited to 28 GHz fields. That leaves about 2.8 W of additional cooling power for the heat load due to absorbed x-rays. The results presented in figure 3 clearly demonstrate that for the FRIB injector source the 4K cooling capacity will need to be substantially enhanced compared to the VENUS source to enable tuning of the source over its full magnetic range.

FOURTH GENERATION ECR ION SOURCES

The continuing demand for higher intensities and the complexity of SC magnet structures make their development timely. Modern superconducting ECR ion sources are presently all utilizing Niobium-Titanium alloy (NbTi), since it is ductile and allows simple fabrication methods for wires and cables. However, NbTi performance is ultimately limited by its upper critical field of about 10 T at 4.2 K. The magnetic field strengths necessary for 56 GHz operation require a peak field in the magnet coils of 12-14 T, which cannot be achieved using conventional NbTi conductor. Nb_3Sn has an upper critical field limit of about 20 T at 4.2 K, but is much more difficult to use. A complex structure such as an ECR magnet has never been built in Nb_3Sn. As a first step, LBNL has proposed to build a prototype 56 GHz ECR ion source magnet structure (see Fig. 4) based on Nb_3Sn. It is designed for magnetic peak fields of 8T at injection 5 T at extraction and 4.2 T at the plasma chamber wall and peak fields of up to 15 T on the coils [6, 7].

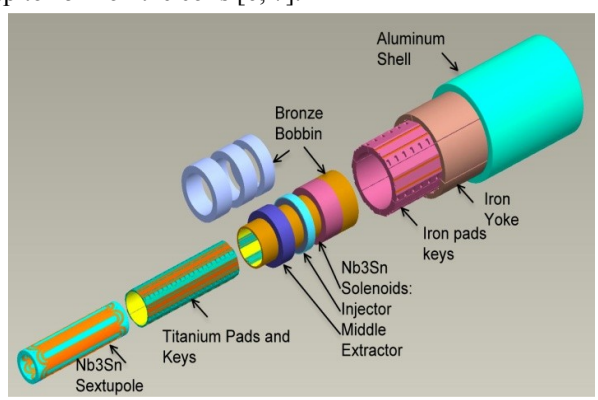

Figure 4: Assembly layout of the Nb_3Sn cold mass.

REFERENCES

[1] G. Machicoane, M. Doleans, et al., in 19th Intern. Workshop on ECR Ion Sources, Grenoble, (2010), JACoW http://www.jacow.org/
[2] D. Leitner, J.Y. Benitez, et al., in 18th Intern. Workshop on ECR ion sources, Chicago, (2008), JACoW http://www.jacow.org/
[3] H. W. Zhao, L. T. Sun, et al., Rev. Sci. Instrum. , 79 (2008): p. 02A315.
[4] D. Leitner, C.M. Lyneis, et al., RSI, 79 (2008): p. 033302.
[5] J. Noland, J. Y. Benitez, et al., RSI, 81 (1), (2010).
[6] P. Ferracin, S. Caspi, et al., in PAC'09, Vancouver, (2009),
[7] P. Ferracin, S. Caspi, et al., RSI, 02A309 (2010).

ECR ION SOURCES FOR THE FACILITY FOR RARE ISOTOPE BEAMS (FRIB) PROJECT AT MICHIGAN STATE UNIVERSITY*

G. Machicoane, M. Doleans, O. Kester, E. Pozdeyev, T. Ropponen, L. Sun, E. Tanke, X. Wu
National Superconducting Cyclotron Laboratory, Michigan State University, East Lansing, MI 48824, USA.
D. Leitner, 88 inch cyclotron Lawrence Berkeley National Laboratory, Berkeley CA 94720

Abstract

Once operational, the Facility for Rare Isotope Beams (FRIB) will open the possibility to gain key understanding in nuclear science and in particular regarding the properties of nuclei far from the valley of stability or the nuclear processes in the universe. In addition it will also allow experimenters to test fundamental symmetries. The production of rare isotopes with FRIB will be achieved, using a heavy ion driver linac that will accelerate a stable isotope beam to 200 Mev/u and deliver it on a fragmentation target. FRIB aims to reach a primary beam power of 400 kW for light to heavy elements up to uranium. To meet the intensity requirement, two high performance ECR ion sources operating at 28 GHz will be used to produce high intensity of medium to high charge states ion beams. Plans regarding initial beam production with the ECR ion sources and beam transport through the front end will be discussed.

INTRODUCTION

The Facility for Rare Isotope Beams (FRIB) (formerly referred to as RIA - Rare Isotope Accelerator) will provide intense beams of rare isotopes for a wide variety of studies in nuclear science. In particular it will help to deepen the current understanding of nuclear structure and help develop a comprehensive model of nuclei. In nuclear astrophysics, it will allow astrophysicists to model and understand the origin and evolution of elements in the cosmos and will permit sensitive tests of the fundamental symmetries of nature. Finally it will provide the scientific community with a source of rare isotopes to develop new applications for medicine, stockpile stewardship and improve applications that benefit from the use of radioisotopes. The FRIB facility is based on a heavy-ion linac with a minimum energy of 200 MeV/u for all ions at a beam power of 400 kW. To minimize the cost of the conventional facility, the layout of the accelerator follows a double folded geometry. The linac has been designed to accelerate ions with a charge to mass ratio higher than 1/7. The first segment with superconducting λ/4 cavities will accelerates the ion beam to 17 MeV/u and will be followed by a folded section that includes a charge stripper and a 180º magnetic bend. A second section with superconducting λ/2 cavities will accelerate ions to 108 Mev/u and again will be followed by a 180º magnetic bend but without charge stripping. A final accelerating section will allow the ion beam to reach 200 Mev/u for all ions up to uranium. The facility will have a production target for in-flight production of rare isotopes. A three-stage fragment separator will be used to prepare fast rare isotope beams with high-purity that can be used at velocity for fast-beam experiments. A multiconcept beam stopping facility will provide thermalized ion beams for stopped beam experiments or for reacceleration at energies up to 3 MeV/u for uranium.

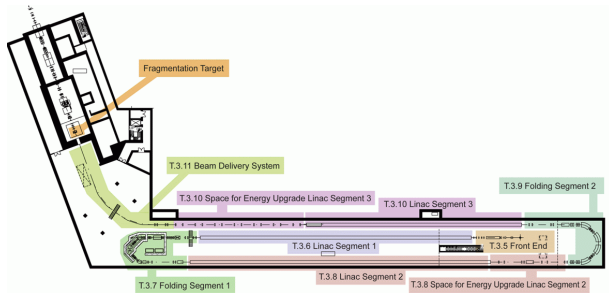

Figure1: Layout of the FRIB driver linac.

FRIB FRONT END

The main functions of the FRIB front end will be on one hand to produce the ion beam using an ECR ion source and on the other hand to prepare the beam for injection into the superconducting linac by providing an initial beam acceleration to 0.3 MeV/u through a Radio Frequency Quadrupole (RFQ) and to ensure proper beam matching in the longitudinal and transverse directions. The front end includes the following segments: First heavy ion beams for FRIB will be produced from high performance ECR ion sources operating at 28 GHz. Two ion sources are necessary to ensure maximum beam availability through redundancy. The initial ion beam energy after extraction from the ion source will be 12 keV/u. This corresponds to an accelerating voltage around 90 kV for U^{33+}. Such a potential difference can not be achieved directly in one acceleration gap at the ECR extraction and a high voltage platform will be used to reach the initial required energy. Then, following the high voltage platform, an achromatic charge to mass selection system will be used to minimize transverse emittance growth in particular for heavy ion beams. The low energy beam transport section (LEBT) will include a transverse collimation system to ensure that the full normalized transverse beam emittance does not exceed the acceptance of the Superconducting linac.

An ion beam chopper is also included in this section to reduce the average beam intensity without impacting the nominal beam bunch intensity for safe tuning and

* Work supported by US DOE Cooperative Agreement DE-SC0000661

operation of the machine. A multi-harmonic buncher operating at a fundamental frequency of 40.25 MHz will then change the DC beam produced by the ECR ion source to a pulsed beam for injection into the RFQ. Finally a Medium Energy Beam Transport (MEBT) section will match the beam coming out of the RFQ to the first segment of the superconducting linac and catch beam particles not accelerated by the RFQ.

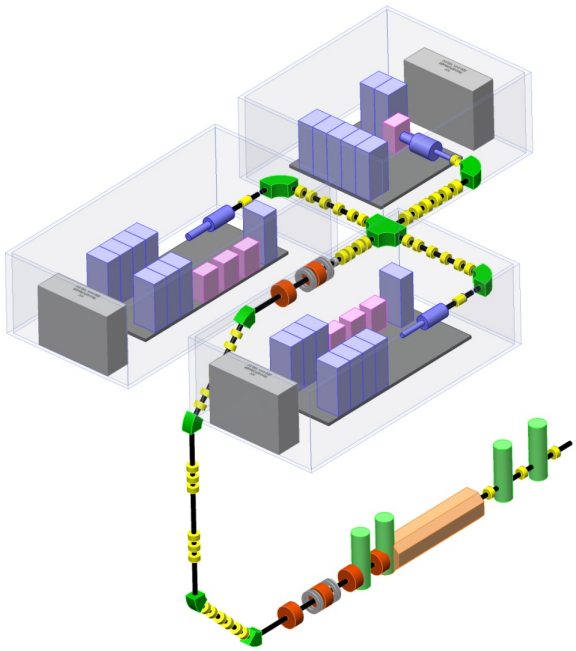

Figure 2: Front end for FRIB. Two ECR ion sources on high voltage platforms will provide the primary ion beam. Each ion source is followed by an achromatic charge selection system. Beam is then transported into the linac tunnel where the RFQ is located. A light ion source on a third platform is shown for future upgrade.

REQUIREMENTS FOR FRIB ECR ION SOURCE

The most stringent requirement on the ECR ion sources is the beam intensity needed to reach 400 kW on the fragmentation target for heavy ions and in particular uranium. From the final beam power and the beam energy per nucleon, the particle beam current on target can be easily calculated and gives 8.1 pμA for ^{238}U. Conservative estimates for beam losses through the LEBT and the charge stripping section provide a transmission of 64 % for uranium from the source to the target therefore raising the initial beam requirement from the ECR ion source to 12.7 pμA. The design of the superconducting linac imposes an initial charge state not lower than U^{33+} which leads to an electrical current of 424 eμA. This current exceeds by approximately a factor two, the highest performance demonstrated for U^{33+} with the ECR ion source VENUS [1]. Therefore, to reach the final beam power in the production target, the driver linac will accelerate concurrently two charges states for heavy ion beams. This approach has been selected for ions heavier than xenon. Table 1 summarizes intensity requirements and expected transmission for various elements. It is clear from the table that the FRIB project does not require the ECR ion source to produce very high charges states but rather medium charges state ion beams. Of course the possibility to produce higher charge states without diminishing too heavily the beam intensity could be a strong advantage if the accelerating gradient in the RF cavities are somewhat lower than projected.

Table 1: Projected intensity and charge state needed from the FRIB ECR ion source for various elements once the facility operates at full power (400 kW)

	A	Z	Q-ECR	Transmission (%)	I-ECR (eμA)	I-ECR (pμA)
Argon	40	18	8	0.8	378	47.3
Calcium	48	20	11	0.8	468	42.5
Nickel	58	28	12	0.8	365	30.4
Krypton	78	36	14	0.8	331	23.6
Tin	112	50	18	0.72	354	19.7
Xenon	124	54	20	0.72	334	18.5
Lead	208	82	27,28	0.64	392	14.3
Bismuth	209	83	28,29	0.64	404	14.2
Uranium	238	92	33,34	0.64	424	12.7

In addition, to the requirement on the beam intensity shown in table 1, the ion beam transverse phase space distribution has to be within the acceptance of the RFQ and superconducting linac. In particular, beam dynamic calculations show that the full normalized emittance for one charge state ion beam has to be within 0.9 pi.mm.mrad, while, for the acceleration of two charge states, each individual charge state should have a full normalized emittance smaller than 0.6 pi.mm.mrad.
Variations in beam intensity from the ECR ion source beyond a few percent can lead to frequent retuning of the machine and should be minimized. Fast beam variations exceeding 10 kHz can lead to beam loading of the RF cavities and could increase beam losses in the linac. Recent measurements at MSU for low intensity uranium with the ECR ion source SuSI using a scope with a capability of Fourier analysis showed that the ion beam did not have oscillations of the beam intensity exceeding a few kHz. The amplitude of the AC variations however could reach between 5 to 10% of the DC value.

CONCEPTUAL DESIGN

The selected approach for the conceptual design of the FRIB ECR ion source is to use the ECR ion source VENUS design developed at LBNL with added modifications that reflect the experience gained with the ion source construction and operation. This approach is based on the following considerations. First, the primary operating frequency for the FRIB ECR ion source should be 28 GHz in order to reach the highest electron density

in the ECR plasma as demonstrated by the VENUS ion source. Choosing an operating frequency beyond 28 GHz, would require further development and progress of ECR ion source technology. Such developments are less likely to mature within the timeframe of the FRIB project. An additional microwave generator operating at a frequency between 18 GHz to 24 GHz should also be added. Operation of the ECR ion source at 18 GHz could be beneficial for lighter ion beams. Second, the VENUS coil package has demonstrated the unique capability to run independently the hexapole from the solenoid coil despite strong interaction forces between the two coil system. In particular, innovative techniques were developed to improve the clamping of the coils using expendables bladders. Another technical choice was to use a large copper to superconducting ratio for the hexapole coil wire to improve its stability [2]. However, experience with the VENUS ion source has shown that the heat load induced by the radiation generated by the ECR plasma can add up to one watt for each kilowatt of microwave power at 28 GHz operation. Therefore, in order to inject a maximum of 10 to 12 kW of microwave power into the ECR ion source from a Gyrotron amplifier, an overall cooling capacity of 13 to 15 W at 4.2 K is needed even if we are to consider a low static load (1 W). This will require modifying the VENUS cryostat. Two cryocoolers with each a cooling capacity of 5W (single stage Gifford-McMahon Joule-Thomson crycooler) will be needed as well as additionals two stage Gifford-McMahon cryocoolers (1.5W) to reach the desired cooling capacity. An additional cryocooler will be also needed for the precooling of the HTc leads. Another possibility that has not been fully explored is to use circulating liquid helium to cool the ion source cryostat through a cold box installed on the high voltage platform. Although this solution offers many advantages, it also poses the problem as to where the compressor can be located and overall, requires a larger footprint.

CHALLENGES AND DEVELOPMENT

For medium mass ions to heavy ions the electrical currents shown in table 1 are close to the maximum performance reached by existing ECR ion sources. Therefore, to meet the requirement set by FRIB, most of the current extracted from the ECR ion source needs to be within the acceptance of the linac. Although several groups have measured beam emittance, this has often been at a relatively low intensity and full emittance at high extracted currents have seldom been reported. Two factors can contribute to emittance growth during beam formation. One is the angular momentum caused by the decreasing magnetic field in the extraction region. This contribution will in principle increase with higher operating magnetic field. The other is caused by space charge forces which can contribute significantly to emittance growth for drain currents exceeding several milliamperes. For higher charge states, the first effect could be mitigated by a smaller effective radius at extraction as evidenced by smaller measured emittance with higher charge states [3]. However more measurements are needed to fully characterize intense high charge states ion beams. For medium charge state ion beams it is unclear what fraction of the ion beam current can fit within the FRIB linac acceptance. Recent measurements at MSU with the ion source SuSI using an intense beam of Kr^{14+} (~400 euA) indicates that at least a third of the beam exceeds the required FRIB emittance 0.9 pi.mm.mrad [4].

It is anticipated that, during the operation of the FRIB facility, users will run experiments for several weeks with minimum interruption. The stability of the beam extracted from the ECR ion source will therefore be critical to successfully operate the facility at full power. In particular, for metallic beams, the techniques used to produce the initial vapour have to be optimized. Several techniques such as resistive oven [3], inductive oven [4] and sputtering [5] have already produced significant amounts of uranium beam but need to be further optimized. Initial estimation indicates that the material consumption needed to run the ion source could reach up to 10 mg/h assuming a 10 % efficiency. In addition, several new primary beams will have to be developed for FRIB such as ^{204}Hg or ^{82}Se. Some rare earth elements or refractory elements could also be added to the primary beam list.

OUTLOOK

As of August 2010, a Conceptual Design Report (CDR) for the FRIB project has been proposed and reviewed by the U.S Deparment of Energy. It is anticipated that during the fiscal year 2011, a preliminary design of the FRIB front end will be completed. In particular, technical solutions for the cryostat and coil package will be selected. Completion of the project is expected at the earliest in 2018. However, at least one high performance ECR ion source needs to be constructed and tested by early 2016.

REFERENCES

[1] D. Leitner, M. L. Galloway, T. J. Loew, C. M. Lyneis, I. Castro Rodriguez, and D. S. Todd Rev. Sci. Instrum. 79, 02C710 (2008)

[2] C. Lyneis,D. Leitner,M. Leitner, C. Taylor, and S. Abbott Rev. Sci. Instrum. 81, 02A201 (2010)

[3] D. Leitner, C.M. Lyneis, S.R. Abbott, R.D. Dwinell, D. Collins, M. Leitner, 16th Intern. Conf. on the ECR Ion Sources (ECRIS'04), Berkeley, California

[4] Lianting Sun, ECRIS 2010, these proceedings MOCOAK02.

[5] Dallas Cole ECRIS 2010, these proceedings MOPOT16.

PRESENT STATUS OF FLNR (JINR) ECR ION SOURCES

S. Bogomolov, A. Efremov, V. Loginov, A. Lebedev, N. Yazvitsky, V. Bekhterev, Yu. Kostukhov, G. Gulbekian, B. Gikal, V. Drobin, V. Seleznev, JINR, Dubna, Russia

Abstract

Six ECR ion sources have been operated in the Flerov Laboratory of Nuclear Reactions (JINR). Two 14 GHz ECR ion sources (ECR4M and DECRIS-2) supply various ion species for the U400 and U400M cyclotrons correspondingly for experiments on the synthesis of heavy and exotic nuclei using ion beams of stable and radioactive isotopes. The 18 GHz DECRIS-SC ion source with superconducting magnet system produces ions from Ar up to W for solid state physics experiments and polymer membrane fabrication at the IC-100 cyclotron. The third 14 GHz ion source DECRIS-4 with "flat" minimum of the axial magnetic field is used as a stand alone machine for test experiments and also for experiments on ion modification of materials. The other two compact ECR ion sources with all permanent magnet configuration have been developed for the production of single charged ions and are used at the DRIBs installation and at the MASHA mass-spectrometer. In this paper, present status of the ion sources, recent developments and plans for modernization are reported.

INTRODUCTION

Main theme of FLNR JINR is super heavy elements research. From 2000 up to 2010 more then 40 isotopes of elements 112, 113, 114, 115, 116, 117, 118 were synthesized in the laboratory.

At present four isochronous cyclotrons: U-400, U-400M, U-200 and IC-100 are under operation at the JINR FLNR. Three of them are equipped with ECR ion sources. In the DRIBs project for production of accelerated exotic nuclides as ^{6}He, ^{8}He etc. the U-400M is used as radioactive beam generator and U-400 is used as a post-accelerator. Layout of FLNR accelerators complex is presented at Figure 1 [1]. Red stars indicate the location of the ECR ion source.

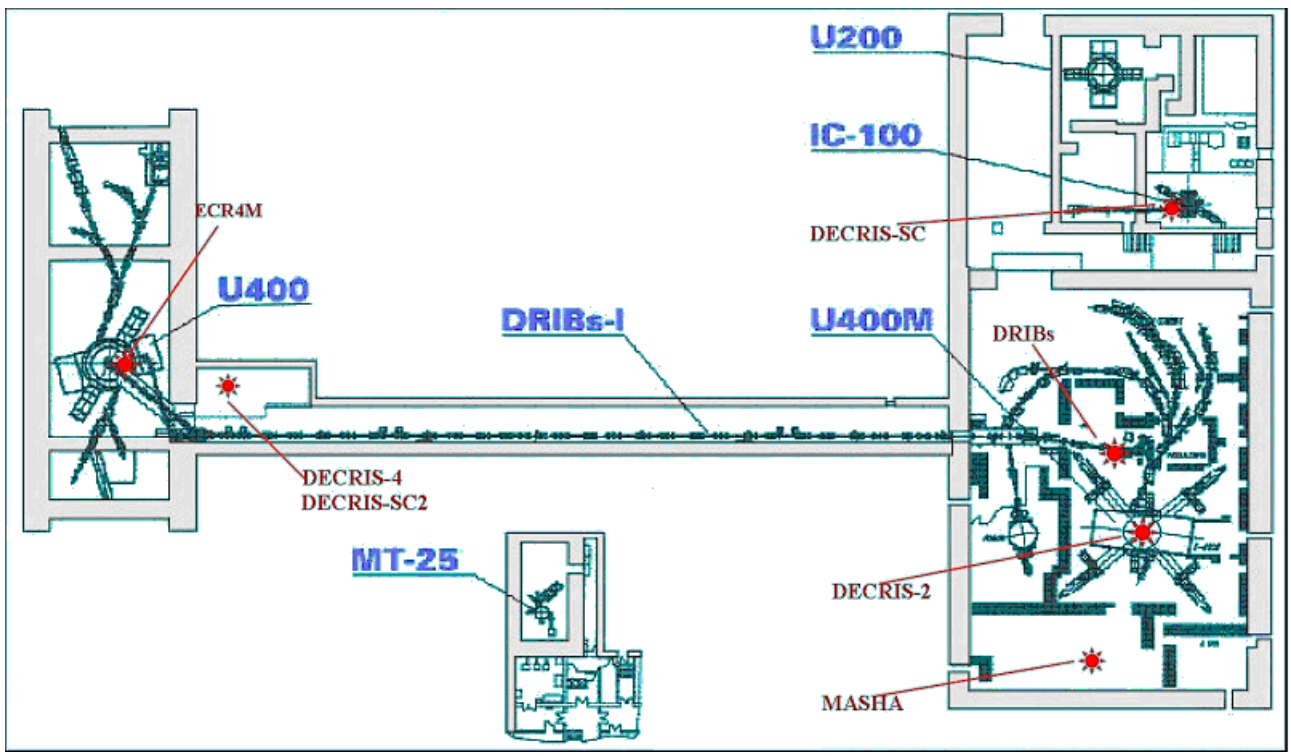

Figure 1: Layout of FLNR JINR accelerator complex. Red stars indicate the location of the ECR ion sources.

DECRIS-2 ION SOURCE

The ion source DECRIS-2 is in regular operation at the U400M cyclotron since 1995 [2]. Nowadays the main physical setups at the cyclotron U400M are the fragment-separators ACCULINNA and COMBAS. Besides, the accelerator is used for the secondary beam production at the DRIBs facility. Intensive beams of ^{7}Li, ^{11}B, ^{13}C, ^{15}N, ^{18}O ions with energies of 35 -55 MeV/nucleon on the U400M cyclotron provide good possibilities for generation secondary beams of ^{6}He, ^{15}B, ^{9}Li, ^{11}Li, ^{12}Be,

^{14}Be, ^{8}He. The intensity of light ion beams such as ^{7}Li or ^{11}B on the targets is (3÷5)10^{13} pps.

Typical intensities of ion beams, produced by DECRIS-2 source, are listed in Table 1.

Table 1: Typical intensities of ion beams (eμA), produced by DECRIS-2 source

Ion	Li	B	O	Ar	Kr	Xe
2+	300					
3+	70	200				
4+		80				
5+			660			
6+			450			
7+			40			
8+				600		
9+				340	100	
18+						45
20+						40

At present time the cyclotron ensures two acceleration modes:

- acceleration of high-energy ion beams up to 100 MeV/nucleon.
- acceleration of low-energy ion beams (the mode providing the beam energy of 4.5-9 MeV/nucleon was implemented in 2008). This low energy ion beams (such as ^{48}Ca) will be used for synthesis and study of new elements.

ECR4M ION SOURCE

The ECR4M source and the axial injection system were assembled and commissioned in 1996. First accelerated Ar beam was produced in November 1996 [3]. The main goal was to provide the intense beam of ^{48}Ca ions for the experiments on synthesis of super heavy elements at a minimal consumption of this enriched and expensive isotope. First experiment on the synthesis of superheavy elements with the beam of ^{48}Ca was performed in November 1997. Since that total operation time of the U400 amounts more than 70000 hours. About 66% of this time was used for acceleration of $^{48}Ca^{5+,6+}$ ions for research on synthesis and investigation of properties of new elements. The production of the ^{48}Ca ion beam was performed with the use of microoven with the maximal temperature of 900 °C and thin cylindrical Ta sheet placed inside the discharge chamber to prevent the condensation of metal at the chamber wall [4].

The modernization of the U400 axial injection, which included sharp shortening of the injection channel horizontal part, was performed. These changes allow us to increase the $^{48}Ca^{18+}$ ion intensity at the U400 output from 0.9 to 1.4 pμA

According to the plans of the reconstruction of the U400 cyclotron (U400R project) the project of the modernization of the ECR4M source was developed. This modernization include the increase of the plasma chamber diameter from 64 to 74 mm; production of the higher magnetic field in the injection region by insertion an iron plug in the injection side; waveguide UHF injection into plasma chamber. The modified magnetic structure of the ECR4M and the axial magnetic field distribution are shown at Figure 2.

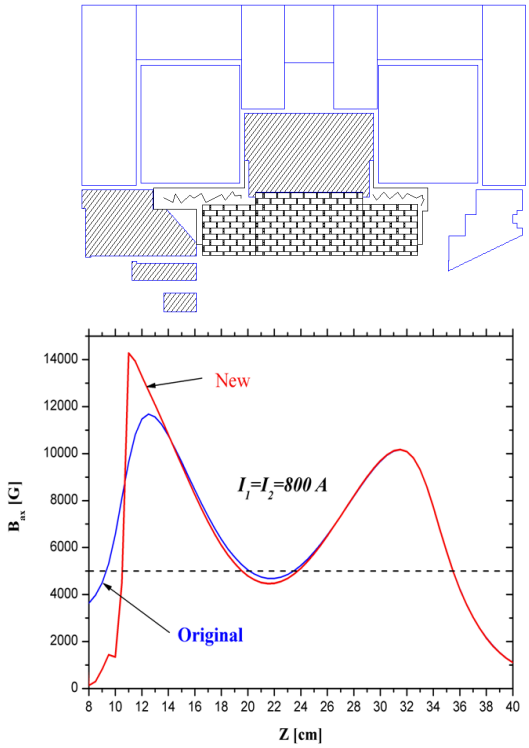

Figure 2: The modified magnetic structure of the ECR4M source (top) and axial magnetic field distribution (bottom)

DECRIS-4 ION SOURCE

The DECRIS-4 ion source [5] was designed for the use as an injector of heavy multiply charged ions for the U-400 cyclotron as well as a "charge breeder" for the second phase of the DRIBs project. The design of the magnetic structure of the source was based on the idea of the so-called "magnetic plateau". The axial magnetic field is formed by three independent solenoids enclosed in separated iron yokes. Since 2005 the source is in operation at the test bench and is used for the experiments in the solid state physics and for beam development.

Test experiments on production of Ti ion beam were performed. The best results were obtained using MIVOC method with $(CH_3)_5C_5Ti(CH_3)_3$ compound, first used by Jyvaskyla group [6]. More than 60 μA of $^{48}Ti^{5+}$ were produced in stable mode, but there is a problem in synthesizing such a compound from a small quantity of enriched ^{50}Ti. Also the titanium isopropoxide was tested with MIVOC method, but the results were very pure, not more than 1 μA of $^{48}Ti^{5+}$ were produced.

Also TiF_4 was tested using the microoven. The compound was loaded into the crucible with thin capillary, and microoven was moved further from the plasma chamber. About 10÷20 μA of $^{48}Ti^{5+}$ were obtained in stable mode of operation, the further increase of intensity leads to instability of source regime due to overheating of crucible by plasma.

DECRIS-SC ION SOURCE

DECRIS-SC is a hybrid type electron cyclotron resonance ion source using permanent magnet hexapole, providing the radial magnetic field at the plasma chamber wall of 1.3 T, and a set of four superconducting solenoids to make min-|B| structure suitable for operation up to 28 GHz [7]. The compact refrigerator of Gifford-McMahon type is used to cool the solenoid coils. At present the operating frequency of the source is 18 GHz.

Since May 2004 the source is in regular operation at the IC-100 cyclotron for production of polymer membranes and solid state physics. Accelerated beam currents are listed in Table 2.

Table 2: Typical intensities of ion beams (eμA), accelerated at the IC-100 cyclotron

Ion	A/Z	Current, μA
$^{22}Ne^{4+}$	5.5	0.7
$^{40}Ar^{7+}$	5.714	2.5
$^{56}Fe^{10+}$	5.6	0.5
$^{86}Kr^{15+}$	5.733	2
$^{127}I^{22+}$	5.773	0.25
$^{132}Xe^{23+}$	5.739	1.2
$^{184}W^{31+}$	5.9355	0.035

DECRIS-SC2 ION SOURCE

Using the experience obtained during construction and operation of the DECRIS-SC source the new source DECRIS-SC2 was developed [8]. The source is planned to be used at the U-400M cyclotron to replace the conventional ECR ion source DECRIS-2. For ECR plasma heating the existing microwave system (14 GHz) will be used.

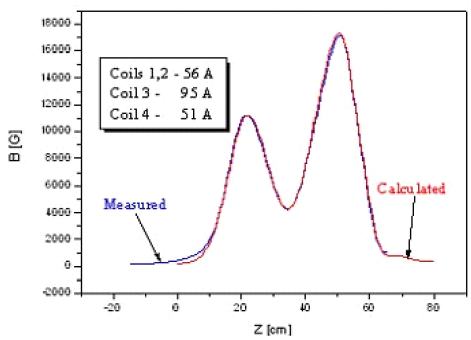

Figure 3: Axial magnetic field distribution of the DECRIS-SC2 source

The design of the superconducting magnet system of the new source differs essentially from the previous one. To decrease the weight and dimensions of the system it was decided to produce the vacuum vessel from chromium plated soft steel, so it will simultaneously serves also as a magnetic yoke. The superconducting magnet system passed the full test. The axial magnetic field distribution is shown at Figure 3. The source is completely assembled and installed at the test bench for beam tests.

ECR ION SOURCES FOR RADIOACTIVE ION BEAMS

The DRIBs (Dubna RIB) project has been running since 2002 [9]. The primary ion beams (^{7}Li or ^{11}B) from U400M are used for production nuclides as ^{6}He, ^{8}He at the target (Be or C). The produced radio-nuclides transported from hot catcher by diffusion into ECR ion source [10] where are ionized. The 2.45 GHz ion source is dedicated for production of singly charged radioactive ion beams. The magnetic configuration of the source is made with three radially magnetised permanent magnet rings. That allows to create pseudo-closed resonance surface. For the primary beam (^{7}Li) intensity of 3 pμA the intensity of accelerated ^{6}He beam reaches of 5 10^{7} pps.

The similar type of the ECR source is used at the MASHA (Mass Analyser of Super Heavy Atoms). The magnetic configuration of this source is made with two permanent magnet rings. The easy axis of the each magnet ring is directed along the axis of the magnetic system.

REFERENCES

[1] G. Gulbekian and CYCLOTRONS Group, "Status of the FLNR JINR Heavy Ion Cyclotrons," in *Proc*. of *14th Int. Conf. on Cyclotrons and Their Applications* (Cape Town, South Africa, 1995), pp. 95–98.

[2] A.Efremov, V.B.Kutner, A.N.Lebedev, V.N.Loginov, N.Yazvitskiy and H.Zhao. "Dubna electron cyclotron resonance ion source DECRIS)-14-2: Results of the first operation" Rev. Sci.Instr. 1996, 67(3) p.980 – 982.

[3] Yu.Ts.Oganessian et al. "Axial injection system for the U-400 cyclotron with the ECR-4M ion source". JINR FLNR Scientific Report 1995 – 1996 Heavy Ion Physics. E7-97-206, Dubna 1997, p.270 – 276.

[4] V.B.Kutner, S.L.Bogomolov, A.A.Efremov, A.N.Lebedev, V.Ya.Lebedev, V.N.Loginov, A.B.Yakushev, and N. Yu. Yazvitsky, Rev. Sci.Instrum. **71**, p.860-862, 2000.

[5] M.Leporis, S.Bogomolov, A.Efremov and G.Gulbekian "The new ECR ion source DECRIS-4 (project)" Rev. Sci. Instr. 75 (5), 2004, p. 1492 – 1493

[6] H. Koivisto, J. Arje, R. Seppala, M. Nurmia "Production of titanium ion beams in an ECR ion source" NIM B, 187 (2002), p.111-116

[7] A.Efremov et al. "Status of the ion source DECRIS-SC" Rev. Sci. Instrum. **77**, o3A301, 2006.

[8] V.V.Bekhterev et al. "The project of the superconducting ECR ion source DECRIS-SC2" High energy physics and nuclear physics (HEP & NP) A Series Journal of the Chinese Physical Society (C) vol.31, Supp.I, Jul., 2007, p. 23 - 26

[9] B. N. Gikal, S. L. Bogomolov, S. N. Dmitriev, et al., "Dubna Cyclotrons - Status and Plans," in Proc. of Cyclotron04 Int. Conf. (Tokyo, Japan, 2004).

[10] A.Efremov, V.Bekhterev, S.Bogomolov et al., "The 2.45 GHz ECR ion source for the first stage of the DRIBs project", NIM B 204 (2003) p. 368 – 371

STATUS OF ION SOURCES AT HIMAC

A. Kitagawa, T. Fujita, M. Muramatsu, Y. Sakamoto,
National Institute of Radiological Sciences (NIRS), 4-9-1 Anagawa, Inage, Chiba 263-8555, Japan
T. Sakuma, N. Sasaki, T. Sasano, W. Takasugi,
Accelerator Engineering Corporation (AEC), 2-10-14 Konakadai, Inage, Chiba 263-0043, Japan
S. Biri, Institute of Nuclear Research (ATOMKI), H-4026 Debrecen, Bem ter 18/C, Hungary
A.G. Drentje, Kernfysisch Versneller Instituut (KVI), 9747AA Groningen, The Netherlands

Abstract

The Heavy Ion Medical Accelerator in Chiba (HIMAC) at the National Institute of Radiological Sciences (NIRS) was designed as a clinical dedicated facility. The carbon ions are utilized for the heavy-ion radiotherapy, so its production is the most important aim for ion sources at HIMAC. However HIMAC has a second essential task to operate as a facility for basic experiments. In that scope it accelerates many ions. In order to serve all HIMAC users at best, three ion sources have been installed. This report summarizes the status of the ion sources to produce carbon ions and to extend the range of ion species.

INTRODUCTION

The National Institute of Radiological Sciences (NIRS) was funded in 1957 and has been researching on the effects of radiation on the human body, protection from radiation, diagnosis and treatment of radiation injuries, and medical uses of radiation. The HIMAC (Heavy Ion Medical Accelerator in Chiba) project is one of the most important research subjects in NIRS [1], and it has successfully realized the heavy-ion radiotherapy with 140-400 MeV/u carbon beams since 1994 [2]. HIMAC was designed as a clinical dedicated facility, but it has as a second essential task to operate as a facility for basic experiments in e.g. biomedical and material science, physics and chemistry. In order to accelerate various ion species, two ECR ion sources and one PIG ion source are installed. The carbon ions for the daily treatment are mainly provided with a 10GHz ECR ion source called 'NIRS-ECR'[3]. The NIRS-ECR is sometimes utilized for lighter gaseous ions too. A PIG ion source, ('NIRS-PIG'), supplies relatively lighter ions, especially metallic ions by the sputtering method [4]. An 18GHz ECR ion source called 'NIRS-HEC', produces relatively heavier gaseous ions[5,6]. Since the three ion sources are almost occupied with daily operations, it's difficult to spend a time for the development to extend the range of ion species. The installation of a new local injector linac is scheduled to be completed in the spring of 2011. Another ECR ion source, called 'Kei2' had been developed as a prototype of a hospital specified facility[7], is now under commissioning for the new injector. It is expected that the other three ion sources will be free from the carbon production for the daily clinical operation. Several developments for these four ion sources are now in progress. The present status of carbon-ion production and the trial for the extension of the range of ion species with ECR ion sources are presented in this paper.

CARBON-ION PRODUCTION

Difficulty of carbon- ion production

The production of highly charged carbon ions with good stability and reproducibility is harder effort than other ions. NIRS-PIG realizes a very low-duty pulsed operation and a feedback of the arc power. In addition, its carbon vapour is supplied by sputtering from graphite resulting decreasing amount of carbon atoms in the chamber. So that, the lifetime can extend about one week [4]. However the change of conditions of consumptive parts like a cathode finally requires the tuning by manual operation. It's not satisfied for the medical requirement. Unfortunately, this difficulty is also true for the ECRIS, the source well known for its long lifetime and good performance for highly-charged ion production. Based on the experiences at NIRS-ECR and NIRS-Kei2, the performance of the ECR ion source is degraded due to carbon deposition on the parts, especially the chamber wall. In order to increase the intensity of highly charged carbon ions like C^{4+}, it's effective to feed hydro-carbonic C_xH_y gases[8]. However, the deposition is unavoidable under the use of such gases, and causes serious unfavourable effects.

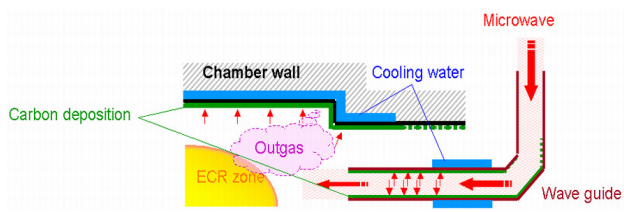

Figure 1: Microwave absorption on the dirty carbon deposited wall.

The microwave power absorbed on the walls of the waveguide and the plasma chamber increases with increasing the deposition on the walls. The less microwave power can reach into the ECR zone shown in Figure 1, thus the plasma density and the electron energy distribution must be low. When the microwave power is increased in order to compensate for this deficit, more loss of the microwave power causes heat-up of the walls and the heat-up induced the change of the vacuum pressure. As a result, reproducibility is much worse. In

order to solve the problem, we improved the water cooling system for plasma chamber and the waveguide, however the transmission efficiency is consequently worse. Therefore, the maximum power of the microwave amplifier must be sufficiently high.

The deposition on the wall of the plasma chamber also causes another unfavourable effect, i.e. a decreasing of the beam, especially for the higher charge-state ions due to the surface material of the plasma-chamber wall. Considering the particle loss fluxes in a 'normal ' ECRIS, the electron flux dominates the axial losses and the ion flux dominates the radial diffusion; both fluxes compensate in the conducting surface material forming the so-called 'Simon short circuit'. In the case some depositing material on the wall forming a dielectric surface, ions diffusing to the wall will charge up the surface of the wall and forms a repelling potential. Thus the loss fluxes are reduced, the short circuit is broken; this leads to better performance and the beam intensity increases [9]. This beneficial effect usually is called the 'wall-coating' effect shown in Figure 2B. However, when operating the source with carbon, the wall will be completely covered by carbon material, forming a well conducting surface layer shown in Figure 2C; it appears that the beam intensity gradually decreases. This is likely due to the 'adverse (or anti-) wall-coating' effect [3].

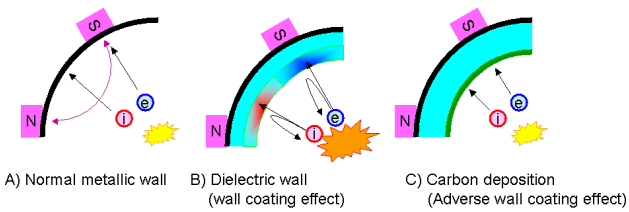

Figure 2: Adverse wall-coating effect in the carbon production.

Status of carbon-beam operation

The condition of the deposition on the wall depends on the operation parameters and it sometimes shows hysteresis. For example, oxygen gas removes the deposited carbon atoms from the wall shown in Figure 3. The varying of the condition immediately gives instability or bad reproducibility. The exchange of ionising gasses is especially undesirable.

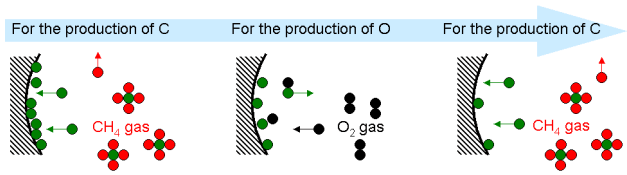

Figure 3: Cycle of carbon deposition on the wall.

In order to maintain enough reproducibility and stability under the dirty condition, the suppression of any change of the vacuum pressure due to the heat-up process is necessary. The cooling for the plasma chamber, the waveguide, and the extraction electrode are effective. Good thermal conductivity is a major consideration for the material of the chamber, because it does not affect the intensity due to carbon deposition. In this meaning, copper is also a good candidate. The extraction slit and the puller are also important heat-up parts. These are therefore made of molybdenum, and the puller is cooled by water. Pulsed operation is also effective to reach to a stable condition as soon as possible. Finally, we obtained typically 70 % decreasing of the beam after a few months of operation, but it's still available to produce a sufficiently intense and stable beam [3]. Although the beam intensity varies during the first few tens of minutes, it becomes fairly stable within 1 hour.

TRIAL FOR THE EXTENSION OF THE RANGE OF ION SPECIES

In order to extend the range of ion species with our ECR ion sources, the optimization of the extraction configuration, the gas mixing technique, and the MIVOC method gave successful results. We have reported the scope and history of our developments in Ref. [10]. The points to be considered for development are as follows.

- No ion source specialist is required for tuning.
- Since the ion sources are almost occupied for the daily operation, the short development time is only available.
- With the present ion sources' structure the required reproducibility and stability is fulfilled. New developments are in a way disturbing the situation.
- For developments one has to cope with 'dirty' plasmas and many contaminations in the available sources.

The high priority is assigned to the two-frequency heating technique and the MIVOC method at present. They are discussed in the next points.

Two frequency heating

Many reports pointed at the improvement of highly charged ion production by feeding multiple microwaves with different frequencies [11]. In an early stage of the development of two-frequency heating with the HYPER-ECR at the Institute for Nuclear Study, the University of Tokyo, we could confirm that the two different frequency microwaves using two klystron amplifiers (KLY) were absorbed at different ECR zones by observing the shapes of visible radiations [12].

In order to investigate the frequency dependence precisely, we added an additional travelling wave tube amplifier (TWTA) with a wide frequency range between 10 and 18 GHz to NIRS-HEC. We also concluded that it is also important to adjust one frequency to the other frequency[13]. Since our TWT had only a maximum power of 250 W at the former experiments, it was not enough to improve the performance.

The recent experiments were performed with NIRS-HEC which has an 18.0 GHz KLY with a maximum power of 1500W. An additional TWT system was added to NIRS-HEC. The frequency range and maximum power of TWTAs are 17.75 to 18.25GHz and 600W, respectively.

The detailed experimental setup had been described in Ref. [10].

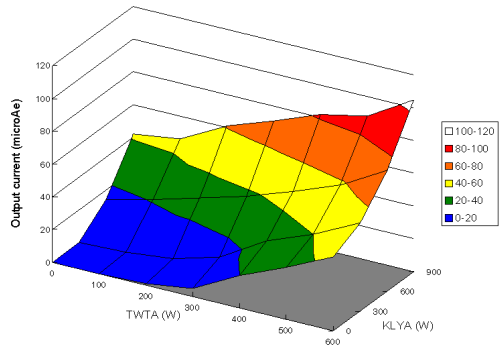

Figure 4: Calibration of microwave power from each amplifier.

The present experimental data were obtained with ^{132}Xe gas (isotopic enrichment 90%). Initially, the parameters of KLY, i.e., microwave power, amount of gas, magnetic field, extraction voltage, and so on, were optimised. Then, the frequency of TWT was optimised. Figure 4 shows a dependence of the output current of $^{132}Xe^{21+}$ on microwave power of KLY and TWT. The frequencies of microwave are 18.0 and 17.88 GHz, respectively. The relation of input microwave power and output beam current showed that 900 W by KLYA has the same effect as 600 W by TWTA. Both powers were measured by crystal detectors midway the chamber from the amplifiers. The two waveguides had the different loss of microwave. It seams that the transmission efficiency from KLY is likely about 2/3 of TWT. The microwave power of TWT was normalized by KLY power in Figure 5. The red line shows the output currents of $^{132}Xe^{21+}$ by TWT only. The blue line shows the output currents by KLY only. The broken blue line indicates the region of instable plasma. The green line shows the output currents by mixture of TWT and KLY. The green line was slightly lower than red and blue lines. Although we suppose interference with each other slightly occurred, the output current mainly depended on the total power of two frequencies.

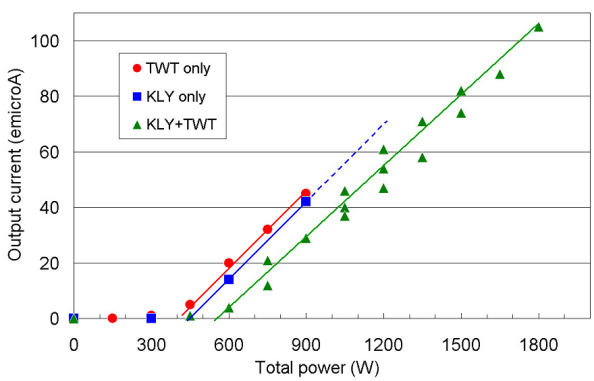

Figure 5: Dependence on total microwave power.

In the case of the total 1200W with 300W TWT and 900W KLY, when TWT was stopped and only KLY supplied, the beam intensity was decreased from 60eμA to 40eμA. When the microwave power from KLY was increasing, the output current was also increasing. However, the beam instability was appeared over 900 W as shown in Figure 6. The plasma collapsed every several milliseconds and recovered in about 1 ms. When TWT turned on in this situation, the beam stability was improved and the large output current was obtained.

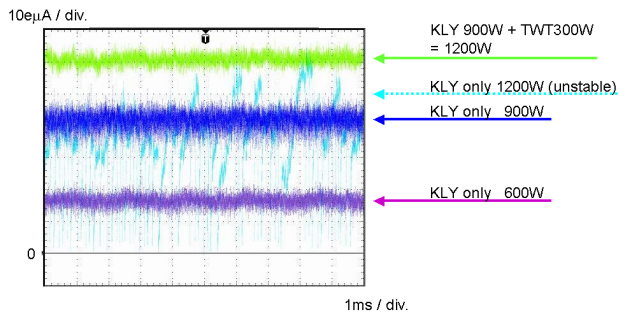

Figure 6: Limitation of microwave power for instability.

As a conclusion, the two frequency heating improved the beam intensity under the conditions of enough power and precise frequency tuning for the additional microwave. It seems it is mainly due to prevent the plasma instability. The effect appears to be most important on the higher charge states, therefore further study needed. The optimised microwave power is not saturated in our cases. Applying a more powerful TWT would be promising. For higher charge state ions, it is more effective.

REFERENCES

[1] Y. Hirao et al., Nucl. Phys. A 538, 541c (1992).
[2] D. Schulz-Ertner, H. Tsujii, Journal of Clinical Oncology, 2 , 953 (2007)..
[3] A. Kitagawa et al., Rev. Sci. Instrum. 79, 02C303 (2008).
[4] T. Miyata et al., Rev. Sci. Instrum. 71, 972 (2000).
[5] A. Kitagawa et al., Rev.Sci.Instrum. 69, 674 (1998).
[6] A. Kitagawa et al., Rev.Sci.Instrum. 73, 604 (2002).
[7] M. Muramatsu et al., Rev. Sci. Instrum. 76, 113304 (2005).
[8] A.G. Drentje, et al., IEEE Trans. Plasma Sci., Vol.36, No.4, 1502 (2008).
[9] A.G. Drentje et al., Rev. Sci. Instrum. 75, 1399 (2004).
[10] A. Kitagawa et al., Proc. of the 18th International Workshop on ECRIS, Chicago, 2008, p.92.
[11] Z. Q. Xie et al., Proc. of the 12th International Workshop on ECRIS, Wako, INS-J-182 (1995), p.24.
[12] A. Kitagawa et al., Rev.Sci.Instrum. 71, 1061 (2000).
[13] A. Kitagawa et al., Proc. of European Particle Accelerator Conf., Wien, 2000, p.1607.

RECENT ACTIVITIES AT THE ORNL MULTICHARGED ION RESEARCH FACILITY (MIRF)*

F.W. Meyer#, M.E. Bannister, J.W. Hale, C.C. Havener, H.F. Krause$, C.R. Vane, S. Deng, I.N. Draganić, P.R. Harris, Physics Division, Oak Ridge National Laboratory, Oak Ridge, TN 37831-6372 USA

Abstract

Recent activities at the ORNL Multicharged Ion Research Facility (MIRF) are summarized. A brief summary of the MIRF high voltage (HV) platform and floating beam line upgrade is provided. An expansion of our research program to the use of molecular ion beams in heavy-particle and electron collisions, as well as in ion-surface interactions is described, and a brief description is provided of the most recently added **I**on **C**ooling and **C**haracterization **E**nd-station (ICCE) trap. With the expansion to include molecular ion beams, the acronym MIRF for the facility, however, remains unchanged: "M" can now refer to either "Multicharged" or "Molecular."

THE MIRF UPGRADE PROJECT AND RECENT FACILITY ACTIVITIES

In order to enhance the capabilities of on-line experiments of the MIRF [1], a facility upgrade project was undertaken to add an all permanent magnet ECR source on a new 250 kV HV platform, and to modify the existing CAPRICE ECR source to inject a new floating beam line, from which beams could be decelerated into grounded end stations with final energies as low as a few eVxq, where q is the charge state of the analyzed beam [2][3][4]. An electrostatic trap end station was also added to the facility, for multi-second confinement of metastable-multicharged or hot-molecular ions to reduce their degree of internal excitation either for lifetime or subsequent cold collision studies [5].

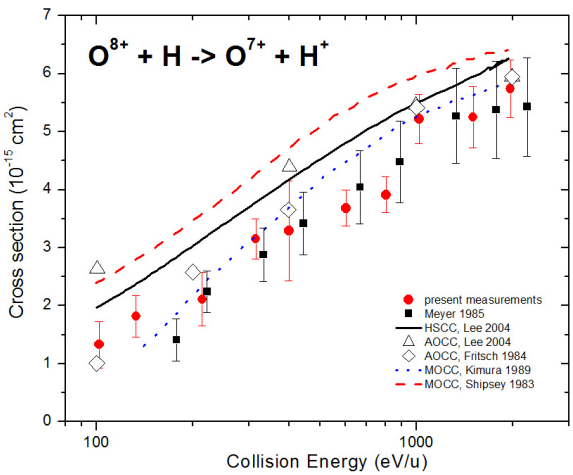

Figure 1: Results for O^{+8} – H electron capture [7].

Table 1: Performances of the MIRF ECR sources [6]

Ion		CAPRICE 10 GHz	Platform ECR source
Xe	+20	35 µA	52 µA
	+26	9	24
	+29	--	3
Ar	+8	500	510
	+11	70	90
O	+6	400	650
	+7	50	90

The new permanent magnet ECR source was designed and built at CEN-Grenoble, and has been previously described [6]. Table 1 summarizes typical multicharged ion performances for the CAPRICE and the new permanent magnet ECR sources injecting the low-energy and high-energy MIRF beam lines, respectively.

To illustrate the increased experimental capabilities made possible by the facility upgrade, Figure 1 shows recent results for electron capture by fully stripped oxygen ions from atomic hydrogen obtained with the upgraded ion-atom merged beams experiment. For these measurements, a well-collimated, small-cross section O^{8+} beam was merged with a fast ground-state atomic hydrogen beam produced by photodetachment, and the protons resulting from charge exchange collisions between the two fast beams monitored.

The present MIRF layout is shown in Figure 2. The facility is comprised of 5 on-line experiments fed by the new HV platform ECR source, and 3 on-line experiments injected from the new low-energy floating beam line.

*Work supported by the Office of Fusion Energy Sciences, and the Office of Basic Energy Sciences of the U.S. Department of Energy, under Contract No. DE-AC05- 00OR22725 with UT-Battelle, LLC. SD, ID, and PRH were appointed through the ORNL Postdoctoral Research Associates Program administered jointly by Oak Ridge Institute of Science and Education and Oak Ridge National Laboratory
#meyerfw@ornl.gov
$retired

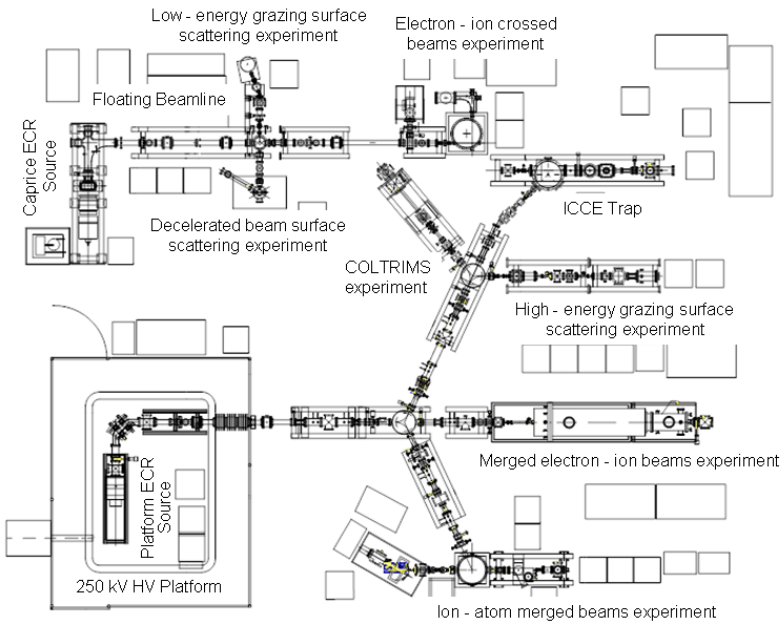

Figure 2: Present configuration of the ORNL Multicharged Ion Resarch Facility. A total of eight on-line experiments studying electron- and heavy-particle collisions, and ion-surface interactions utilize ion beams from either the new permanent magnet ECR ion source on the 250 kV HV platform or from the existing CAPRICE ECR ion source injecting the new floating beam line (see above).

Molecular ion beams

In addition to their well documented capability of highly charged ion production, both ECR sources in the MIRF have recently found increasing use for production of molecular ion beams as well, due to the increased programmatic focus of our research activities on the atomic collision and surface interactions occurring in the cool edge of magnetic fusion devices, and on electronic driven process in systems of increasing chemical complexity. Figure 3 illustrates synthesis of B and F mono- and di-hydride molecular ion beams in the CAPRICE ECR source plasma using a mixture of BF_3 and D_2 source gases that can be optimized by a combination of high source pressure and low rf power. These beams were required for exploration of electron impact dissociation of such molecular ions along iso-electronic sequences. Figure 4 illustrates synthesis of D_3^+ ions, again in the CAPRICE ECR source, from D_2 source gas at very high source pressures and low rf powers. Such beams, decelerated to a few eV, are used in our studies of low-energy chemical sputtering of C materials. Intense beams of molecular ions have been obtained using the all-permanent magnet HV platform ECR source as well [8]. However, extraction region discharges due to the poorer extraction region pumping of the permanent magnet source limit its high-source-pressure operation. The D_3^+ beams from the platform ECR source are typically lower

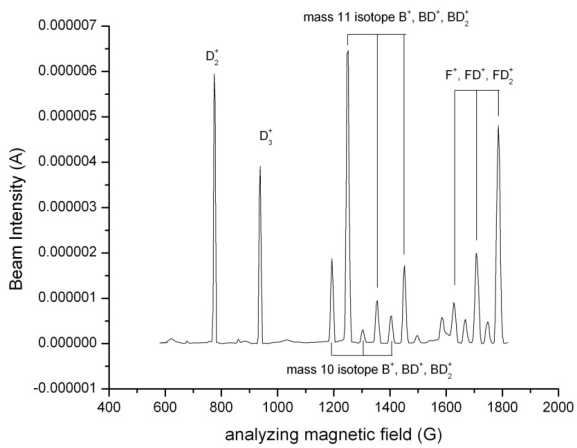

Figure 3: B and F mono- and di-hydride beam production by CAPRICE ECR gas mixing of BF3 and D2 at a total source pressure of 1x10-4 Torr and 4 W forward rf power.

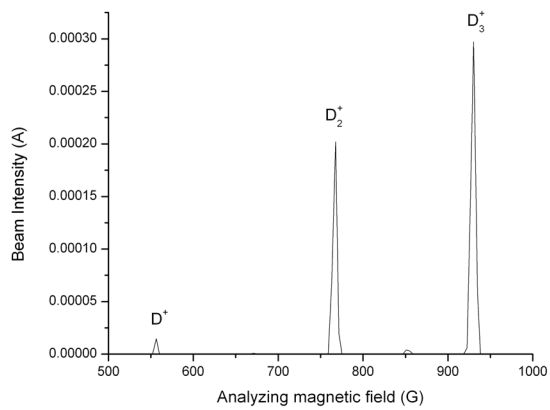

Figure 4: CAPRICE ECR D beams for a source pressure of 5x10-5 Torr and 10 W forward rf power.

in intensity than those produced with the CAPRICE, and, unlike Figure 4, can't be tuned to exceed the D_2^+ current.

ICCE Trap

The final element of the MIRF upgrade project was the development and installation of the **I**on **C**ooling and **C**haracterization **E**nd-station (ICCE) trap. This electrostatic trap is side-injected by a combination of 32° and 13° pulsed parallel plate deflectors, simplifying HV

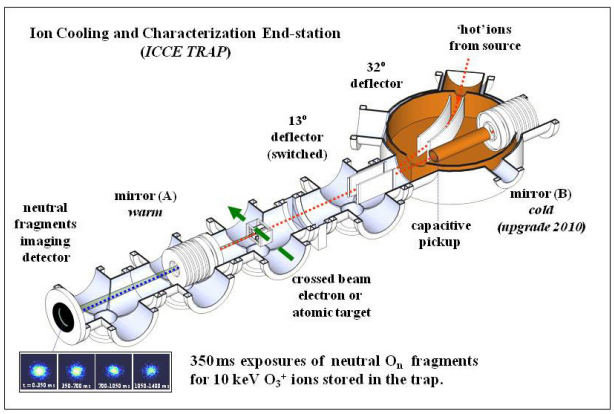

Figure 5: Schematic diagram of the ICCE trap [5].

switching and permitting DC operation of the two electrostatic end mirrors [5]. A neutral fragment imaging detector located outside one of the end mirrors is implemented to permit analysis of kinetic energy release during electron- or heavy-particle-induced dissociation of the trapped molecular ions. Figure 5 shows a schematic of the ICCE trap. Recently multi-second trapping of CO^+ ions has been achieved. In-situ electron and gas jet targets are being used to study electron and heavy-particle collisions of molecular ions as function of trapping times, i.e., as function of the degree of internal cooling of the trapped ions.

Plasma potential measurements

An issue of continuing interest is the determination of the ECR source plasma potential and the energy spread of extracted ions. These parameters impact the magnitude and uncertainties of impact energies of decelerated beams used in our low energy ion surface interaction studies [9] and thus must be known. In addition, knowledge of these parameters may improve fundamental insights into the ECR plasma dependences on pressure, microwave power, confinement magnetic fields, and elucidate the basis of the gas mixing effect. In-situ Langmuir probe measurements of MIRF CAPRICE plasma potentials have been reported in [10]. More recently, complementary measurements of plasma potentials based on retardation analysis of extracted ion beams [11] have been carried out, which are generally consistent with the in-situ probe measurements. A typical plasma potential and ion energy spread result from analysis of external beam deceleration is shown in Figure 6.

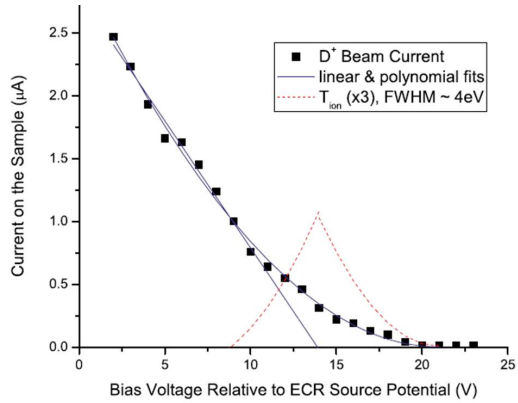

Figure 6: CAPRICE ECR plasma potential (~13.8 eV) and ion energy spread (~4 eV) deduced from retardation analysis of a D^+ ion beam extracted at a source pressure of $2x10^{-6}$ Torr and 6 W forward rf power [11].

REFERENCES

[1] F.W. Meyer in: J. D. Gillaspy (Ed.) "Trapping Highly Charged Ions: Fundamentals and Applications" (Nova Sciences Pub., New York, 2001) p. 117-165.

[2] F.W. Meyer et al., "The ORNL Multicharged Ion Research Facility Upgrade project," Nucl. Instrum. Methods Phys. Res. **B 242**, 71 (2006).

[3] F.W. Meyer, M.R. Fogle, and J.W. Hale, "The New ORNL MIRF Floating Beamline," Proceedings, 22nd Particle Accelerator Conference (PAC'07), Albuquerque, NM, June 25-29, 2007; IEEE Cat. No. 07CH37866, ISBN: 1-4244-0917-9, p. 3139.

[4] M.E. Bannister et al., "Control System for the ORNL MIRF High Voltage Platform", 2005 Particle Accelerator Conference, Knoxville, TN, May 16 – 20, 2005, published on CD, IEEE Cat. No. 05CH37623C, Piscataway, NJ, (2005).

[5] S. Deng et al., J. Phys. Conf. Ser. **194**, 142010 (2009), ICPEAC 2009, Kalamazoo, Mich., 22-28 July.

[6] D. Hitz, et al., "An All-Permanent Magnet ECR Ion Source for the ORNL MIRF Upgrade Project", AIP Conference Proceedings **749**, 123 (2005).

[7] C.C. Havener, I.N. Draganić, and D. Seely, in preparation for submission to Phys. Rev. A.

[8] I.N. Draganić et al., "Production of Molecular Ion Beams using an ECR Ion Source," submitted to Journal of Appl. Phys., Aug. 2010.

[9] e.g., H. Zhang and F.W. Meyer, J. Nucl. Mat. **390-91**, 127 (2009).

[10] H.J. You, F.W. Meyer, and K.S. Chung, "The Cold and Hot Electron Populations, Temperatures, and Their Transports in the Edge Plasma of the ORNL CAPRICE ECR Ion Source," Plasma Sources Sci. Technol. 18, 015004 (2009).

[11] P.R. Harris and F.W. Meyer, "Plasma Potential and Energy Spread Determination using Ion Beams Extracted from an Electron Cyclotron Resonance (ECR) Source," Rev. Sci. Inst. **81**, 02A310 (2009).

PK-ISIS: A NEW SUPERCONDUCTING ECR ION SOURCE AT PANTECHNIK

A. C. Villari#, C. Bieth, W. Bougy, N. Brionne, X. Donzel, G. Gaubert, R. Leroy, A. Sineau, O. Tasset, C. Vallerand, Pantechnik, Bayeux, France,
T. Thuillier, LPSC UJF CNRS/IN2P3 INPG, Grenoble, France

Abstract

The new ECR ion source PK-ISIS was recently commissioned at Pantechnik. Three superconducting coils generate the axial magnetic field configuration while the radial magnetic field is done with multi-layer permanent magnets. Special care was devoted in the design of the hexapolar structure, allowing a maximum magnetic field of 1.32 T at the wall of the 82 mm diameter plasma chamber. The three superconducting coils using Low Temperature Superconducting wires are cooled by a single double stage cryo-cooler (4.2 K). Cryogen-free technology is used, providing reliability, easy maintenance at low cost. The maximum installed RF power (18.0 GHz) is of 2 kW. Metallic beams can be produced with an oven (Tmax = 1400 °C) installed with an angle of 5° with respect to the source axis or a sputtering system, mounted in the axis of the source. The beam extraction system is constituted of three electrodes in accel-decel configuration.

Pantechnik has developed and improved its family of ECRIS in collaboration with research laboratories like GANIL and LPSC in France and IUAC in India. From this collaboration, the first ECRIS using He-free High Temperature Superconducting wire technology (HTS) was born in 2002: PK-DELIS.

The goals of that development were to reduce the power consumption of the coils from 200 kW to 15 kW, for avoiding liquid He in the superconducting coils and to demonstrate the feasibility of such hybrid HTS - permanent magnet (for the radial magnetic field) source. PK-DELIS works since then successfully at New Delhi.

The new source of Pantechnik is conceived for reaching optimum performances at 18 GHz RF frequencies. Moving to this direction, PK-ISIS, our new source, has much higher axial and radial magnetic fields (2.1 T axial B_{inj} and 1.32 T radial field in the wall), a larger plasma volume, variable B_{min} via an independent coil and a large and opened extraction region. Moreover, PK-ISIS integrates modern design concepts, like RF direct injection (2.5 kW availability), DC-bias moving disk, out-of-axis oven and axial sputtering facility for metal beams.

PK-ISIS delivers 5 to 10 times more beam intensity than the original PK-DELIS and/or shifting the charge state distribution to higher values.

PK-ISIS is built with Low Temperature Superconducting wire technology (LTS), but keeps the He-free concept, extremely important for a reliable and easy operation. The radial field circuit is permanent magnet made. Finally, PK-ISIS is also conceived for using in a High-Voltage platform with minor power consumption.

The intensities already obtained by PK-ISIS are listed in the Table 1 below. Please, note that these values were obtained during commissioning in the Pantechnik premises. *The intensities – mainly for metallic beams – should be taken as lower limits. Not all intensities were obtained after reaching the maximum magnetic field in the Superconducting coils.*

The problems we faced with the superconducting coils during the first commissioning were recently solved. PK-ISIS is running within the designed specifications.

Table 1: Beam intensities measured with PK-ISIS

Ion	Intensity (μA – electrical)
^{4}He (2+)	2,400
^{13}C (4+)	>500
^{13}C (6+)	50
^{14}N (5+)	>1,000
^{16}O (6+)	1,500
^{16}O (7+)	230
^{40}Ar (12+)	200
^{40}Ar (14+)	100
^{84}Kr (17+)	100
^{129}Xe (26+)	100
^{181}Ta (26+)	20
^{181}Ta (30+)	13
^{181}Ta (32+)	6
^{209}Bi (29+)	35
^{209}Bi (31+)	25
^{209}Bi (33+)	15

#antonio.villari@pantechnik.com

3D SIMULATION STUDIES AND OPTIMIZATION OF MAGNETIC HOLES OF HTS-ECRIS FOR IMPROVING THE EXTRACTION EFFICIENCY AND INTENSITIES OF HIGHLY CHARGED IONS

G. Rodrigues*, P.S. Lakshmy, Y. Mathur, R.N. Dutt, U.K. Rao, D. Kanjilal, A. Roy,
Inter University Accelerator Centre, Aruna Asaf Ali Marg, New Delhi 110067, India
R. Baskaran, Indira Gandhi Centre for Atomic Research, Kalpakkam 603102, Tamilnadu, India

Abstract

3D simulation studies using RADIA code have been performed to optimise the magnetic holes in the high temperature superconducting electron cyclotron resonance (HTS-ECRIS) ion source for improving the extraction efficiency and intensities of highly charged ions. The magnetic field improvements using simple techniques like optimisation of iron regions is found to be economical. The extraction efficiency can be increased three-fold in the case of a hexapole magnet depending on the level of the uniformity of the fields in the high and low regions. This technique further minimises localized heating of the plasma chamber walls which can improve the vacuum conditions in an ECR ion source. For superconducting sources where the x-ray heat load poses severe problems during operation, such a reduction of heating load is of great significance. The typical triangular pattern of the plasma impact observed on the plasma electrode of HTS ECRIS at various tuning conditions are reproduced by the simulations. Details of the simulations and experimental results will be presented.

INTRODUCTION

Today, ECR ion sources are being utilized as high current injectors for various accelerator projects around the world due to its simplicity, robustness, wide mass range of ions with excellent beam intensities and long lifetime as compared to other ion sources [1]. The backbone of this kind of source is based on a minimum B magnetic configuration where the electrons are confined to increase the probability of stripping ions to higher charge states. The design of this kind of magnetic configuration is based on well known ECR scaling laws. This study was undertaken to improve the extraction efficiency and especially the intensities of the highly charged ions. Earlier, experiments have shown that the optimum plasma electrode position inside the plasma chamber is not the same for the extraction of low, medium and highly charged ions. It was observed for the RIKEN [2] and JYFL ECR ion sources [3] that the intensities of highly charged ions increased as the plasma electrode was moved further away from the ECR zone. On the other hand, the intensities of medium charged ions, increased as the plasma electrode was moved closer to the ECR zone. Normally the extraction field, B_{ext}, should be slightly lower than the last closed magnetic surface, B_{last}, for the efficient production of highly charged ions [4]. A closer look led us to investigate further the magnetic configuration of the source at the extraction side. The magnetic field region at extraction (towards the exit of the hexapole) where the highly charged ions are extracted shows that there exist three weaker field regions (due to the use of a hexapole) where the plasma can still escape rather than being extracted. This is due to the radial component of the solenoid field which only partially cancels the radial field produced by the hexapole especially at the ends of the hexapole. It is expected that by further optimizing these weaker field regions, much higher intensities of highly charged ions can be extracted. Since no detailed work is available in the literature, except for a brief mention [5], it was important to perform 3D calculations of the combined magnetic field using the computer code RADIA [6]. Localized heating of the plasma chamber walls could be reduced which in turn would improve the vacuum conditions in the ECR ion source. For superconducting sources, the x-ray heat load which poses severe problems during operation and localised heating in the superconducting coils (quenches) can be further minimized.

MAGNETIC STRUCTURE OF AN ECRIS

In ECR ion source, combined magnetic field consisting of an axial and radial components generated by solenoid and a multipole magnet respectively is used. This kind of open magnetic field configuration is found necessary for good plasma confinement, stability and also for ease of extraction of the ions [1]. For efficient operation, the combined magnetic field structure should follow the well known ECR scaling laws ; the last closed surface should be at least twice that of the resonance field, B_{ecr}, within the plasma chamber, where B_{ecr} is the field required for the electron cyclotron resonance condition. In addition, the periphery of the plasma should be far away from the walls of the chamber to reduce the probability of melting of the plasma chamber. For a typical magnetic field configuration in conventional ECR ion sources, a triangular shape at both extremes is evident on the plasma electrode at extraction side and on the bias electrode if the electrode is in the form of a disc at injection side. The radial losses have a pattern on the plasma chamber wall which is symmetric corresponding to the orientation of the multipole, where the plasma impacts are oriented on the pole directions of the multipole. For the case of a multipole where order of the multipole, n =3 (sextupole) ,

*gerosro@gmail.com

the plasma has a three fold symmetry, similarly, if n =4 (octupole) , the symmetry is 4 fold. For most of the ECR ion sources, the multipole has been optimised for n = 3 for optimum performance. Generally, the magnetic structure is chosen so that the field confines the plasma in all possible directions as much as possible and losses to the walls of the plasma chamber are minimised.

3D SIMULATIONS OF THE MAGNETIC STRUCTURE OF HTS-ECR PKDELIS

During operations with the 18 GHz HTS-ECR PKDELIS ion source [7], it has been observed that the plasma impact on the electrode shows a triangular structure typical of ECR sources, but the extent of the losses inside the triangular pattern varies with different sources depending on the magnetic field configurations and tuning conditions. This is a normal observation found in ECR sources where a plasma electrode is used for defining the beam size during the extraction of the beam. In addition, the six loss areas can also be found on the inner chamber wall of these sources.

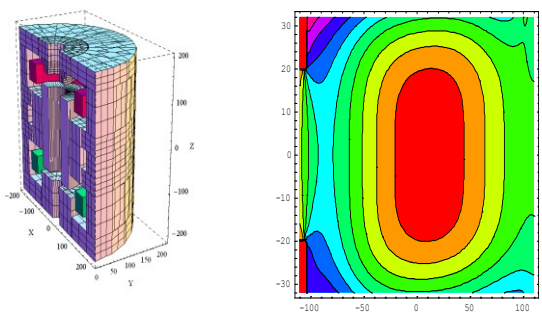

Figure 1: Magnetic structure built using RADIA

It means that most of the plasma was being lost to the electrode (diameter of plasma electrode 32 mm) than what was actually going through the extraction hole (hole diameter 12 mm). The plasma electrode positioned at the peak value of the extraction magnetic field (z = +82.5 mm), was not the correct position for extraction of high intensities of highly charged ions. This position was suitable for extraction of high intensities of low and medium charged ions. As pointed out by D.Hitz,[4] the best position to extract high intensities of highly charged ions is to place the plasma electrode at the position of B_{last}. By performing a 3D magnetic field simulation, the triangular structure was reproduced and matched well with the observed pattern. A model that was built to simulate the structure is shown in figure 1. The magnetic configuration clearly showed that the leaking plasma was going through the weaker regions of the magnetic field instead of being extracted through the plasma electrode where the field is relatively higher at positions close to the edge of the hexapole. This was supported by the model that close to the extraction area or the edge of the hexapole magnet, three weakest points of the total magnetic field existed. This is also true in the injection side and could also be improved by optimising these regions. For example, some sources have shown more plasma impacts on the injection side as compared to the extraction side of the source.

RESULTS AND DISCUSSION

We investigated by moving the electrode away from the ECR zone [7] which resulted in extracting higher intensities of highly charged ions of argon (figure 2, without the use of mixing gas, 150 µA of Ar^{11+}).

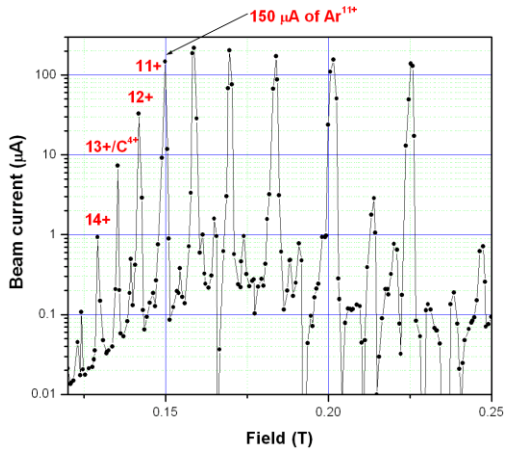

Figure 2: Charge state distribution optimised on Ar^{11+}

In addition, the shift in the charge state distribution (CSD) for argon (CSD peak at Ar^{10+}) was clearly seen at lower levels of RF power (400 W of absorbed power from 18 GHz klystron) than the case at higher levels of RF power (500W from 14.5 GHz TWT amplifier), where the charge state distribution peaked at Ar^{8+} using oxygen mixing gas, ~ 25 µA of Ar^{11+}), at position z = + 82.5 mm [8,9]. The best position was at z = +98 mm slightly inside the hexapole [7]. In this case, the field of the three magnetic holes should be higher than the field at the plasma electrode so that the plasma could be more efficiently extracted. This can be further improved by field shaping using iron material. The other possible solution could be to increase the length of the hexapole which may turn out to be more expensive; Three options effectively were looked into to see the improvement in optimising the field of the magnetic holes ; all simulations have been performed corresponding to the beam tuning conditions when the source was optimised for Ar^{11+} (injection coil current 120 A, extraction coil current 80 A); they are as follows ;

i) effect of incorporating iron ring close to the edge of the hexapole

The effect of incorporating iron rings close to the edge of the hexapole were simulated. The inner and outer diameters were chosen appropiately as 35 mm and 74.5 mm and the closest distance from the edge of the hexapole was 1 mm. Four rings of thickness 5, 10,15 and 20 mm were simulated at z = +98 mm.

ii) effect of incorporating iron ring further away from the edge of the hexapole

The effect of incorporating iron rings further away from the edge of the hexapole was simulated using inner diameters of 41mm, 54.8 mm and 69.5 mm and keeping the outer diameter fixed at 86.8 mm. The closest distance from the edge of the hexapole was 5 mm. Rings of varying thickness were simulated. at z = +98 mm. Figure 3 shows the correction after integrating all the iron rings.

iii) effect of increasing the length of the hexapole at the extraction side

The effect of increasing the length of the hexapole towards the extraction side in small incremental steps was simulated at z = +98 mm. It was found that the length of the hexapole should be made considerably longer (L=225 mm) to optimize the weakest magnetic field regions (shown in figure 4.) and the cost implications show that it is more economical to tune the magnetic field using iron as in cases (i) and (ii)

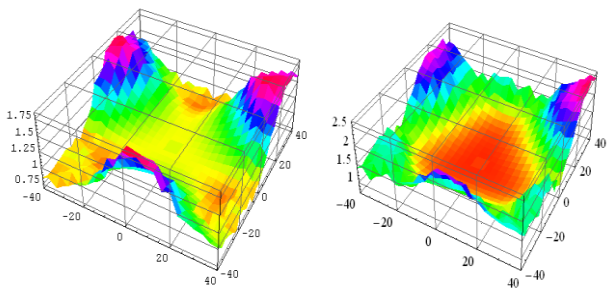

Figure 3: (left) View of three magnetic holes at z =+98 mm, before optimization (Right) optimized at z=+98 mm using iron rings integrated with the hexapole

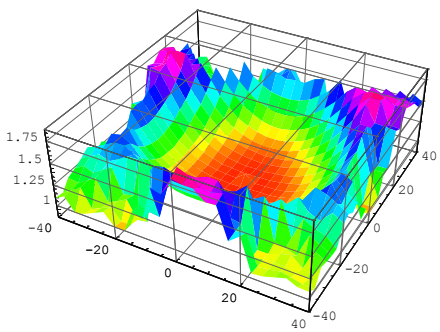

Figure 4: After optimization at z=+98 mm, using an extended hexapole of length 225 mm.

SUMMARY AND CONCLUSION

All the methods described to optimize the field in the weaker regions show definite improvements. It is expected that the efficiency of extracting the ions from the plasma should scale three-fold according to the uniformity in the fields. In principle, much higher intensities of highly charged ions can be extracted depending on the levels of the magnetic field. It is left to the designer to decide which is more advantageous and thereby optimize the best performance to cost ratio. In summary, the 3D simulations show that further improvements in the tuning of the magnetic field can be done for improvement of the extraction conditions in a typical ECR ion source. Besides, localized heating of the plasma chamber walls could be reduced which can further improve the vacuum conditions in an ECR ion source. The lifetime of synthetic high voltage insulators used between the plasma chamber and the cryostat can be increased further. For superconducting sources, the x-ray heat load which poses severe problems during operation and the localised heating in the superconducting coils can be further minimized.

ACKNOWLEDGEMENTS

One of the authors (G.R) would like to thank Department of Science & Technology (DST) for the help and support.

REFERENCES

[1] Geller R 1996 Electron Cyclotron Resonance Ion Sources and ECR Plasmas (Bristol: Institute of Physics Publishing)

[2] H.Higurashi et al., JYFL ECR workshop proceedings; T. Nakagawa, Y. Higurashi, M. Kidera, T. Aihara, M. Kase, Y. Yano, Nucl. Instrum. Methods. Phys. Res B226 (2004) 392; Higurashi et al, Nucl. Instrum. Methods. Phys. Res A510 (2003)206

[3] P. Suominen, O. Tarvainen, H. Koivisto, Rev. Sci. Instrum. Vol 75, No.5 (2004)1517

[4] D. Hitz, A. Girard , G. Melin, S. Gammino, G. Ciavola and L. Celona, Proc.15th Int.Workshop on ECR Ion Sources (University of Jvaskyla, Finland) JYFL Report 4/2002 pg.100

[5] X.Q. Xie and C.M. Lyneis, Proc.13th Int.Workshop on ECR Ion Sources, 1997, pg.16

[6] http://www.esrf.eu/Accelerators/Groups/InsertionDevices/Software/Radia

[7] G. Rodrigues, P.S. Lakshmy, R. Baskaran, D. Kanjilal, A. Roy, Rev. Sci. Instrum. Vol 81,02A323 (2010)

[8] C. Bieth, S. Kantas, P. Sortais, D. Kanjilal, G. Rodrigues, S.Milward, S. Harrison, and R. McMahon, Nucl. Instr. Meth. B 235 (2005) 498

[9] D. Kanjilal, G. Rodrigues, P. Kumar, A. Mandal, A. Roy, C. Bieth, S. Kantas, P. Sortais, Rev. Sci. Instrum.,77 (2006) 03A317

DESIGN STUDY OF A HIGHER-MAGNETIC-FIELD SC ECRIS AT IMP

D. Z. Xie*, W. Lu#, X. Z. Zhang and H. W. Zhao
Institute of Modern Physics (IMP), Chinese Academy of Sciences (CAS), Lanzhou 730000
People's Republic of China

Abstract

Development of ECR ion source has demonstrated that, as the empirical scaling laws summarized, higher magnetic field with higher operation frequency will greatly improve the source performance. Based on the great success of SECRAL at IMP, a higher-magnetic-field SC ECRIS is planned to meet the new accelerator demands. However, there are many practical issues in the design and construction of a higher-field SC ECRIS which need addressed. In this paper we will present and discuss the design features of the higher-field SC ECR with a maximum axial field of 7.0 T and a radial field of 3.5 T at the plasma chamber wall of ID 110 mm, and operating frequency up to 50 GHz.

INTRODUCTION

Performance of high-charge-state Electron Cyclotron Resonance Ion Source (ECRIS) has been greatly improving since its advent and especially in the past decade, thanks to the continuous increase of magnetic-field-strength and operating frequency. Although a full understanding of the detailed physics process involved in ECR plasma is still in the horizon, higher-magnetic-field combined with higher-operating-frequency remains nowadays the relatively easy and straightforward way to further the development of ECRIS. Based on the empirical scaling laws [1], there were a few fully superconducting (SC) ECRISs all built with NbTi magnets in the past decade. At safe current loadings (up to about 90% of its critical current), the highest field strength reaches 4 T on axis and 2 T at the plasma chamber wall of ID 100 to 140 mm for operating frequency up to 28 GHz. These SC ECRISs have significantly improved the ECRIS performance by a great factor in both the ion beam intensity and charge state. To further enhance the ECRIS performance to meet new demands, higher-field ECRISs have been proposed and are under design. The maximum field strengths are to reach 8 T on axis and 4 T at the plasma chamber wall by using the higher-critical-current Nb_3Sn wires to construct the SC magnets [2].

At the Institute of Modern Physics (IMP), the great success of SECRAL has demonstrated that further ECRIS performance is not only possible but also needed. The institute is planning a future facility of higher-energy and higher-beam-intensity for nuclear physics research. This new facility requires very intense ion beams, for example, at least 15 pμA of Bi^{31+} and about the same intensity of U^{33+} are to be extracted from the proposed accelerator. Such intense beam intensities require at least a new higher-field SC ECRIS that leads to this design study.

* Visiting Scientist
# Also of the Graduate School of CAS, Beijing 100049, P. R. China

A BRIEF REVIEW OF THE SC MAGNET STRUCTURES FOR ECRISs

Presently there are two different types of magnet structures used in the SC ECRISs. Figure 1 shows the "classical" structure, the sextupole coils sit inside the solenoid coils, that is used so far in all ECRISs but one. Because of the very strong Lorenz interaction forces, especially the repulsing force, the sextupole coils have to be ended at a good distance away from the solenoid coils so that the interaction forces can be reduced. The lengthy end extension results in a bulky magnet structure and cryostat. Sometimes a set of liquid-metal-filled bladders that increases the complexity of magnet fabrication is used to harness the very strong forces [3]. So far the best embodiment of the classical magnet structure remains to be the LBNL VENUS, the first ECRIS that has been designed and reached 4 T on axis and 2 T at the plasma chamber wall of ID 140 mm [4]. Its magnet assembly is wound with NbTi wires of high Cu/Sc Ratios of 3.0 and 4.0 for better thermal stability. Since 2002 it has been commissioning at 18, 28 GHz and double-frequency heating at 18+28 GHz with wave power up to ~10 kW and has produced very great performance. A few example beams produced with VENUS are listed in Table 1 below.

The "non-classical" magnet structure is shown in Figure 2. A striking feature of this structure is that the sextupole coils not only sit outside the solenoid coils but also ended right next to the solenoid coils. A set of simple cold irons, no bladders, is used to clamp down the magnet coils and reduce the stray field right inside the cryostat. This non-classical magnet structure results in a smaller magnet assembly and simplifies somewhat the fabrication process. The IMP's SECRAL is the first SC ECRIS built with this non-classical magnet structure. All the SECRAL magnet coils are wound with the NbTi wires of low Cu/Sc Ratio of 1.35. The field maxima are 3.6 T on axis and ~2.0 T at the plasma chamber wall of diameter of 126 mm. SECRAL had begun its commissioning at 18 GHz with maximum microwave power of about 3.5 kW in 2005. Though operated at lower magnetic fields, lower frequency and wave power, SECRAL has produced very compatible results in comparison to VENUS at higher fields, higher frequency and wave power. So far SECRAL has reliably provided more than three-thousand hours of ion beams to the IMP accelerators and sometimes the operation lasted months without system failures. SECRAL has recently begun its commissioning operation at 24 GHz and already shown better performance than at

18 GHz. Shown in Table 1 is a summary of a few example beams of SECRAL operating at 18 GHz and the preliminary results at 24 GHz [5], as well as VENUS performance for comparison. The great performances of SECRAL and VENUS have demonstrated that SC ECRIS is independent of the magnet structure, so long as a high-strength Minimum-B field is provided.

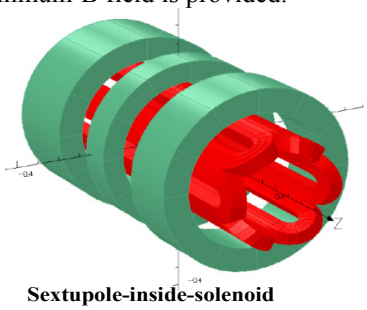

Sextupole-inside-solenoid

Figure 1: The classical magnet structure for ECRIS.

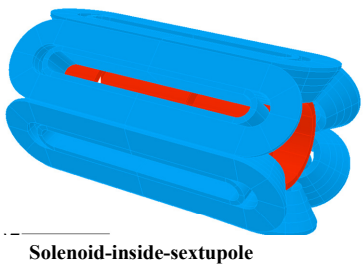

Solenoid-inside-sextupole

Figure 2: The non-classical magnet structure.

Table 1: Example Beams from SECRAL and VENUS

	Q	SECRAL 18 GHz <3.2 kW μA	SECRAL 24GHz 3-4 kW μA	VENUS 28 GHz 5-9kW μA
^{16}O	6+	2300		2860
	7+	810		850
^{40}Ar	12+	510	650	860
	16+	73	149	270
	17+	8.5	14	36
^{129}Xe	27+	306	455	270
	35+	16	45	28
	42+	1.5	3	0.5
^{209}Bi	30+	191		240
	41+	22		15
	50+	1.5		0.5

DESIGN OF A NEW HIGHER-FIELD SUPERCONDUCTING ECRIS

The studied SC ECRIS reported here is essentially a scaled-up version of SECRAL using Nb_3Sn wires to construct the magnets. The great success of SECRAL has demonstrated the advantages of the non-classical magnet structure in many ways, such as the performance, smaller magnet size and cost effectiveness. Therefore it is very natural to follow a good source as the first step to design a higher-field ECRIS, though it may not necessarily guarantee the best results. Figures 3 and 4 show the axial field and radial field profiles in which the peak axial field reaches 7 T at the injection region and the maximum radial field reaching 3.5 T at the plasma chamber wall of ID 110 mm, hoping a slightly smaller chamber could increase the wave power density and perform as well as a larger chamber. Figure 5 shows a histogram along a pole line at the maximum designed currents. As a norm, a maximum loading of about 90% of the critical current is assumed in this design. Table 2 lists a few key parameters of the new magnet assembly and of SECRAL for comparison.

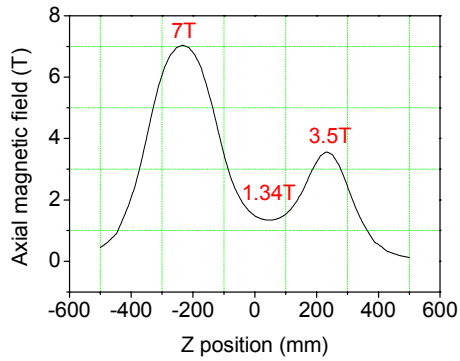

Figure 3: The axial field profile of the SC ECRIS under study. The maximum axial fields reach 7 T at the injection and 3.5 T at the extraction, respectively.

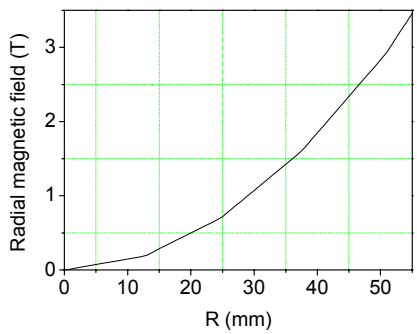

Figure 4: The radial field profile of the SC ECRIS under study which reaches 3.5 T at the plasma chamber of ID 110 mm.

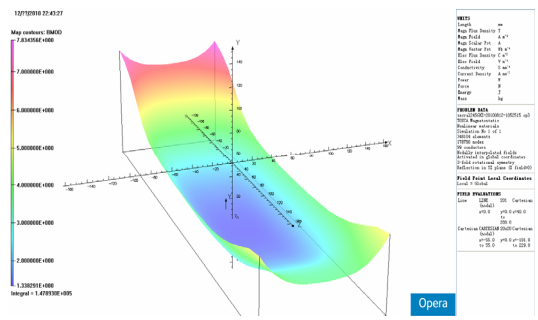

Figure 5: The histogram of the total field inside the plasma chamber that yields a maximum closed contour of 3.6 T inside the chamber at the designed electrode orifice.

Table 2: A Few Key Parameters and Comparison

	New ECRIS <50 GHz	SECRAL 24 GHz
Superconducting Wire	Nb_3Sn*	NbTi (F54)
Critical Jc	400 A /14 T	197 A /9 T
Sextupole Coil (Ampere-Turns)	1,167,000	627,000
Injection Coil (Ampere-Turns)	1,540,000	689,000
Middle Coil (Ampere-Turns)	36,000	162,000
Extraction Coil (Ampere-Turns)	551,000	272,000
Magnet Length (mm)	822	724
Max. Torque (N/M) (a Racetrack Coil)	69.7 E6	8.9 E6
Magnetic Peak Axial Field (T)	7	3.6
Magnetic Radial Wall Field (T)	3.5	1.8
Plasma Chamber ID/Volume (mm/L)	110/4	126/5

*: BRUKER NST 11000 A23 Ø1.0 mm Nb_3Sn wire was used in the design and F54 Ø1.0 mm NbTi wire was used in SECRAL.

DISCUSSIONS

With maxima of 7 T on axis and of 3.5 T at the plasma chamber wall, this magnetic configuration is strong enough, based on the High-B mode [6], to support an operating frequency up to about 50 GHz and it could further significantly enhance the ECRIS' performance. However before it can become a reality, there are a few important issues that must be well addressed. The first is the interaction force among the solenoid coils and the sextupole coils and its resulting torque that has been much more than quadrupled in comparison to the SECRAL. This much higher torque no doubt will pose a dilemma for the magnet clamping. A strong and possibly very deliberate clamping scheme may be required. Secondly, how do the strong interaction force and the huge torque experienced by the individual sextupole racetrack coil affect the Nb3Sn critical current have to be addressed. Though there have been successful high-field coils built with Nb_3Sn wires for non-ECRIS magnets [7], the ECRIS' magnet structure, a mixture of solenoids and a multipole, is more complicated than those simple solenoids or multipole only. Thirdly, unlike the NbTi wire, the Nb_3Sn wire has a pretty poor ductility and it requires a tedious after-coil-winding heat treatment that typically lasts at least one to two weeks at about 700 °C in order to reach its superior critical current. This third issue could lead to a very complex Nb_3Sn magnet fabrication process.

On the other hand, the NbTi magnet has fully demonstrated its workability with exercitation current very close to its critical limit in the built SC ECRISs with either the classical or the non-classical magnet structure. This is why the higher-critical-current Nb_3Sn wires are used in the design of the higher-field ECRIS magnets. However, using NbTi wire has a number of advantages over the uncertain Nb_3Sn wire. Will there be any other NbTi magnet structures that could produce about the same fields discussed above? We have recently begun a magnet structure exploration and the preliminary result is very encouraging and promising. At about the same 90% loading, a novel NbTi magnet structure may be able to produce a minimum-B filed of maximum fields of 6-6.5 T on axis and 3.5-4 T at the plasma chamber wall of IDs 160-180 mm. Somewhat higher radial fields could also be possible at the price of more deliberate structure designs. Furthermore, if this new magnet structure can be fabricated with the Nb_3Sn wires, the maximum fields could reach at least 10 T on axis and 5.5-6 T at the plasma chamber wall of the same diameters, respectively. With maximum fields of 10 T on axis and 6 T at plasma chamber wall, a 70 GHz or higher frequency ECRIS could then be realized which would be a milestone of more than halfway of a 120 GHz ECRIS that Dr. Geller had envisioned decades ago [8]. Unfortunately, this novel magnet structure needs a thorough investigation and hopefully a sound magnetic field calculation and profile design can be reported soon.

Higher magnetic field and operating frequency is the relatively easy way to enhance the ECRIS performance but it comes costly and will run up to the limit of the present superconducting magnet technology in the foreseeable future. To further ECRIS, we should also spend more efforts to investigate other techniques, such as lower frequency heating with a much higher-B mode configuration and microwave heating efficiency [9], etc.

ACKNOWLEDGEMENT

The authors are very grateful to Dr. L. T. Sun for his fruitful inputs and great helps in this study.

REFERENCES

[1] R. Geller, "Electron Cyclotron Resonance Ion Source and ECR Plasma", Institute for Physics Publishing, Bristol, p. 395 (1996).
[2] S. Prestemon *et al*, "Design of a NB_3SN Magnet for a 4th Generation ECR Ion Source", IEEE Trans. on Applied Superconductivity, 19(3), p. 1336 (2009).
[3] C. E. Tayler *et al*, "Magnet System for an ECR Ion Source", IEEE Trans. on Applied Superconductivity, 10(1), p. 224 (2000).
[4] C. M. Lyneis, Z. Q. Xie and C. E. Taylor, RSI, 69(2), p. 682 (1998).
[5] H.W. Zhao *et al*, RSI, 81, 02A202 (2010).
[6] T. Antaya & S. Gammino, RSI, 65(5), p. 1723 (1994).
[7] G. Ambrosio *et al*, "Development and Coil Fabrication for the LARP 3.7-m Long Nb_3Sn Quadrupole", IEEE Trans. on Applied Superconductivity, 19(3), p. 1231 (2009).
[8] R. Geller, IEEE Trans NS-26, 1979.
[9] B. Jacquot, private communications.

MEASUREMENT OF THE SIXTY GHZ ECR ION SOURCE USING MEGAWATT MAGNETS - SEISM MAGNETIC FIELD MAP*

M. Marie-Jeanne#, J. Jacob, T. Lamy, L. Latrasse, LPSC UJF CNRS/IN2P3 INPG, Grenoble, France
F. Debray, J. Matera, R. Pfister, C. Trophime, LNCMI CNRS UJF INSA UPS, Grenoble, France.

Abstract

LPSC has developed a 60 GHz Electron Cyclotron Resonance (ECR) Ion Source prototype called SEISM. The magnetic structure uses resistive polyhelix coils designed in collaboration with the French National High Magnetic Fields Facility (LNCMI) to produce a CUSP magnetic configuration. A dedicated test bench and appropriate electrical and water cooling environments were built to study the validity of the mechanics, the thermal behaviour and magnetic field characteristics obtained at various current intensities. During the last months, measurements were performed for several magnetic configurations, with up to 7000 A applied on the injection and extraction coils sets. The magnetic field achieved at 13000 A is expected to allow 28 GHz ECR condition, so by extrapolation 60 GHz should be possible at about 28000 A. However, cavitation issues that appeared around 7000 A are to be solved before carrying on with the tests. This contribution will recall some of the crucial steps in the prototype fabrication, and show preliminary results from the measurements at 7000 A. Possible explanations for the differences observed between the results and the simulation will be given.

SCIENTIFIC CONTEXT

LPSC Grenoble has initiated an ambitious research and development program for high frequency ECRIS, i.e. with a resonance frequency above 28 GHz. Such a program benefits greatly from LNCMI research on split magnets described in reference [1]. The use of LNCMI radially cooled polyhelix technology allows investigating several magnetic configurations with low fabrication costs and short delays in comparison to classical and superconducting ECR ion sources.

As a first step, the SEISM prototype was designed to produce a CUSP magnetic structure with a closed 60 GHz resonance zone at 2.14 T for a 30000 A current in the helices. Reference [2] recalls the main steps for the design of the prototype, including the results from magnetic, mechanical, hydraulic and thermal calculations.

Due to many uncertainties concerning hydraulic and thermal behaviour of such an innovative helix design, a dedicated test stand was built at LNCMI to study the coils characteristics obtained for various current intensities. The goal of such tests is to validate the magnetic field map at half-current using 2 of the 4 available power supplies of LNCMI, thus creating a closed 28 GHz resonance zone at 1 T for 15000 A in the coils.

*We acknowledge the financial support of the European Community under the European Commission Framework Programme 7 Design Study: EUROnu, Project Number 212372. The EC is not liable for any use that may be made of the information contained herein.
#melanie.marie-jeanne@lpsc.in2p3.fr

PROTOTYPE FABRICATION AND TESTS

Helices

Each helix was first machined with its final diameter, then rigidified by the insulators glued between its windings and finally adjusted to its final height. Helices fabrication process is shown on Fig. 1. According to thermal calculations, insulators had to be as narrow as possible (i.e. 2 mm wide) in order to limit local temperature rise in their centre. Thickness was calibrated to maintain a constant space between two windings (i.e. 0.32 mm thick) in order to avoid constraints on the helix. The difference of potential between two windings was expected not to exceed 10 V at 30000 A. Therefore, composite fibres already "pre-impregnated" (hence the name “pre-preg”) with the resin that would bond them to the windings surface have been chosen. Such pre-pregs can hold a maximum voltage of 35 kV/mm, and are easily cut to their final shape with an automatic cloth cutting machine. As calculated, 24 pre-pregs per winding were glued on internal helices H1 and H2, and 32 pre-pregs on external helices H3 and H4, in order to avoid windings distortion and contact under the magnetic field forces.

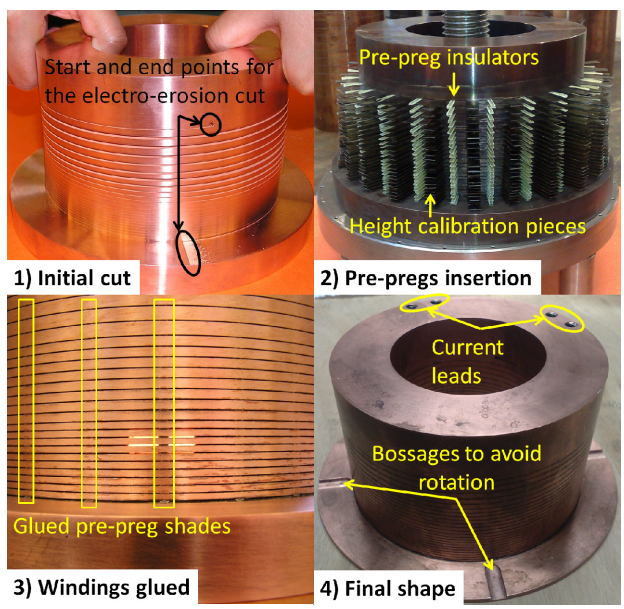

Figure 1: Inner injection helix H1 fabrication process from initial electro-erosion machining (1), through pre-preg insulators gluing (2, 3), to final adjustments in height and shape (4).

After forty hours of run at a 7000 A applied current, thermal and mechanical resistances of the outer coil insulators were checked by inserting an endoscopic camera. Mechanical resistance was validated, as pre-pregs were not displaced and still aligned vertically. Pictures were compared to samples of heated pre-pregs to estimate the temperature reached locally, which seemed to already exceed the temperature expected in the pre-preg centre. The maximum operating temperature being of 165 °C for the pre-pregs, other solutions will have to be investigated for magnetic field tests at full current intensity, where higher temperatures are expected.

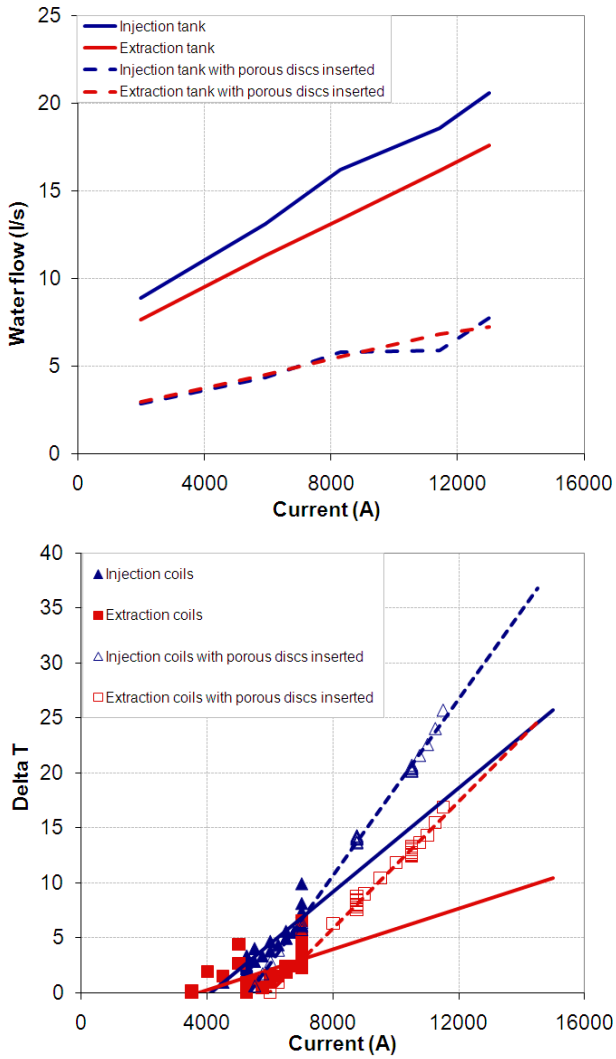

Figure 2: Water flow evolution with and without porous disks inserted (top) and consequences on the coils temperature (bottom)

Tanks

Water circulation in the tanks was first tested up to 18 bars and 18 l/s in each tank, with fake aluminium parts drilled with holes to simulate the water flux. Due to the inaccurate geometry of the water holes, loud cavitation noises could be heard and small damages could be observed on the aluminium. When applying 7000 A on the real copper helices, i.e. 10 bars and 12 l/s in each tank, with the water speed up to 14 m/s in the radial helices slit, cavitation noises could be heard too. In order to increase the pressure in the water outlet of SEISM without modifying the cooling of M5 magnet running in parallel, stainless steel porous discs soldered in flanges were installed on the water outlets of both tanks. The water flow through the prototype went down to half, but helices were still sufficiently cooled down, as can be seen on the graphs from Fig. 2.

Cavitation effects were successfully suppressed, and measurements could go on up to 10500 A current applied. However, because of the pressure difference between the two sides of the porous discs, one of them broke at 10500 A (19.5 bars – 7 l/s). An alternative to the porous discs will be needed to pursue the tests at higher current.

Setup for magnetic measurements

The magnetic field was measured on three horizontal axes along z, and on one radial axis (see Fig. 3), with two gaussmeters equipped with single-axis axial and radial Hall probes calibrated inside the M5 magnet. Two 300 mm-course jacks with a stepper motor allowed moving the Hall probe inside the prototype chamber. A LabView interface was developed to move the jacks to a given position and automatically acquire data.

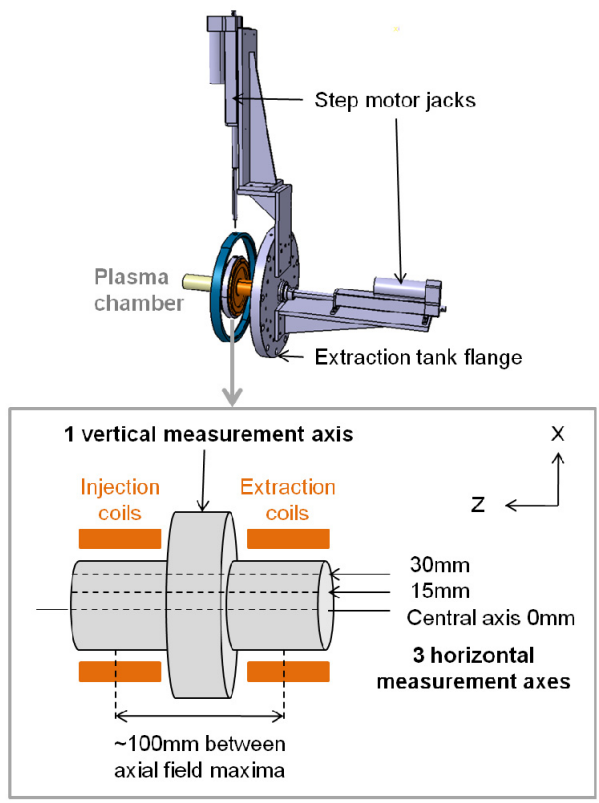

Figure 3: Scheme of the magnetic field measurement setup (top) and of the axes of measurement (bottom).

MEASUREMENTS RESULTS

As a first approximation, the magnetic structure can be considered as axi-symmetric. This is verified experimentally, as one measures a constant field at any angle for given x and z (see Fig. 4).

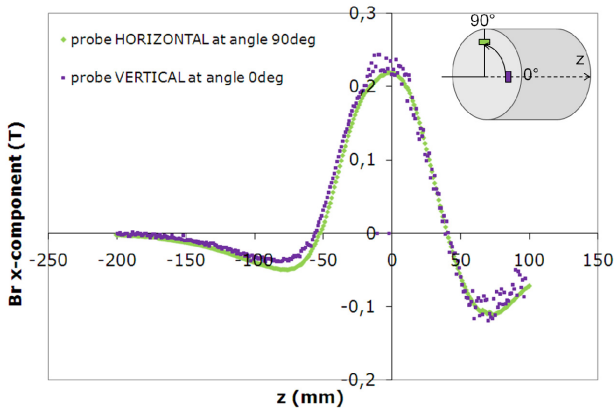

Figure 4: Radial field x-component measured on 15 mm-axis at different angles for 3500 A current applied.

By summing the axial and radial components of the field, one obtains the total magnetic field on three axes of the chamber (see Fig. 5).

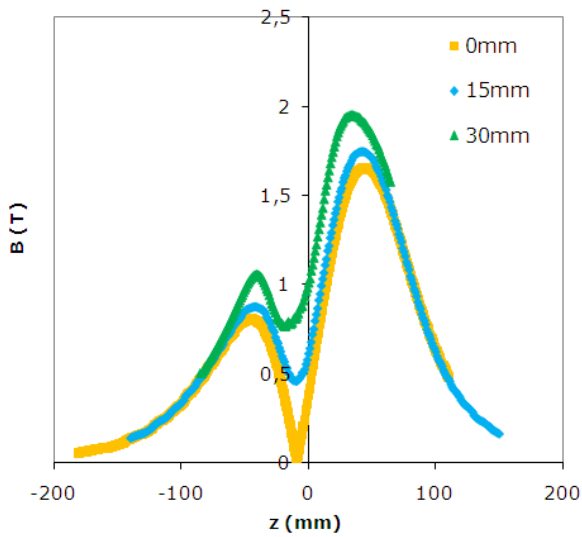

Figure 5: Total magnetic field measured at 7000 A on axes parallel to the coils axis at various distances from the centre.

One can deduce an approximate magnetic field map at 7000 A, shown on Fig. 6. Magnetic field zones at 0.5 T and at 0.64 T are closed within the chamber walls, respectively allowing ECR at 14 GHz and 18 GHz. The first iso-B touching the walls is at 0.76 T. Given the field linear scaling with intensity, one expects to measure a closed 1 T resonance zone at 14000 A.

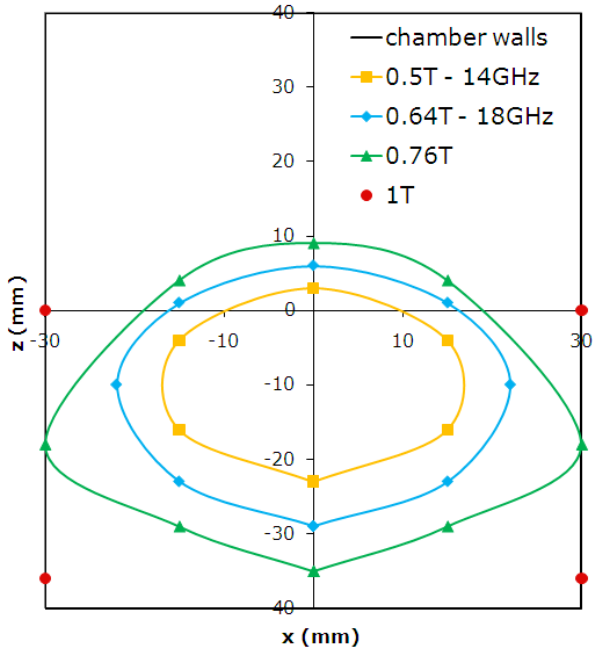

Figure 6: Approximate magnetic field map at 7000 A.

When comparing the measurements with the simulations, one finds a similar structure for the iso-B lines, with lower gradients close to the chamber walls and towards the extraction.

However, the resonance zone centre is displaced of about 5 mm towards the extraction. By measuring the magnetic field produced independently by the injection and extraction sets of helices, one finds that injection and extraction maxima are closer; the summed amplitude is thus lower, especially on the extraction side (see Fig. 7).

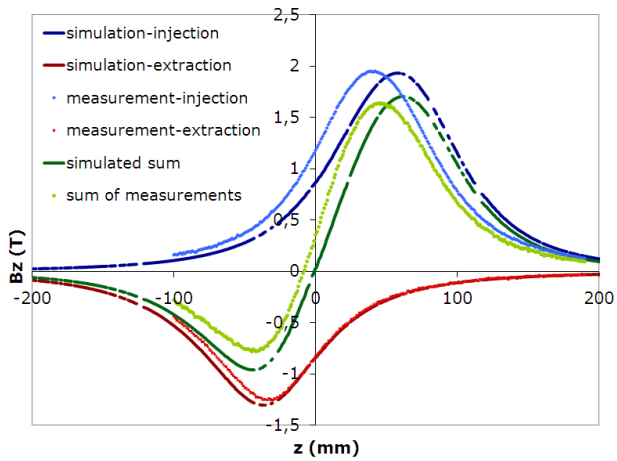

Figure 7: Comparison between measured and simulated (2D model) axial fields at 7000 A on the central axis.

Possible reasons for such discrepancies are being investigated. A mechanical error in the tank or in the helices positioning pieces would induce less than 1 mm displacement, as dimensions were measured within tolerances. The helix shape itself may be wrong, due to a difference between the real helix split (0.37 mm) and the

expected one (0.32 mm), causing less than 2 mm total displacement. Each helix magnetic centre should be carefully checked after dismounting. Finally, the comparison with the 2D calculation model may be inaccurate. Simulations are being run again within the 3D model. Temperature gradients in the windings (due to the presence of insulators) and in the cooling water (due to heat exchanges) induce non-linear effects that will be introduced in the calculation.

PERSPECTIVES

In order to carry on with the half-magnetic field tests, the stainless steel porous discs are currently being replaced. A proposal for two extra weeks of magnetic field was accepted and the run is to be scheduled during autumn 2010.

Given the first results presented here, one expects the magnetic structure to be valid for a 28 GHz resonance. Therefore, the design for the components of the source (plasma chamber, gas and microwave injection...) will be possible in 2011. A permanent room at LNCMI is under funding request for the first 28 GHz tests.

REFERENCES

[1] F. Debray, J. Dumas, S. Labbé−Lavigne, R. Pfister, C. Trophime, N. Vidal, F. Wilhelm, M. Enderle Design study of High Field Resistive Magnets for Diffraction Experiments, IEEE Trans. on Appl. Superconduc. Vol.20 Issue:3 664−667 Jun 2010.

[2] L. Latrasse, M. Marie-Jeanne, T. Lamy, T. Thuillier, J. Giraud, C. Fourel, C. Trophime, F. Debray, P. Sala, and J. Dumas, “SEISM: A 60 GHz cusp electron cyclotron resonance ion source”, Rev. Sci. Instrum. 81(2010) 02A324.

MULTIGAN®: A NEW MULTICHARGED ION SOURCE BASED ON AXISYMETRIC MAGNETIC STRUCTURE

L. Maunoury#, J.Y Pacquet. M. Dubois, P. Delahaye, P. Jardin, P. Lehérissier and M. Michel
GANIL, Caen, France
C. Pierret, CIMAP, Caen, France
X. Donzel, G. Gaubert, R. Leroy* and A.C.C. Villari, PANTECHNIK, Bayeux, France
S. Biri, ATOMKI, Debrecen, Hungary

Abstract

The regular ECR ion sources, allowing the production of multicharged ions, have openings only at their two ends. Based on the MONO1000 ECRIS [1] concept and experience, a new multicharged ECR ion source has been designed with a large opened space in the middle of the source enabling a direct contact with the ECR plasma. This source will combine the advantages of the axisymetric magnetic structures made only of permanent magnets with a high operating frequency.

The magnetic structure calculations as the mechanical design and stress will be described in details. An estimation of the electronic energy distribution has been calculated using the TrapCad code [2] and thus the performances of the source have been deduced. A rough calculation of the beam extraction and formation has also been calculated taking into account of the several fields (magnetic and electric) surrounding the extraction system.

The ion source presented in this paper is a prototype which shall validate the magnetic concept and which shall confirm the expected performances. The next step will be the design of an optimized ECRIS according to its future applications.

INTRODUCTION

In the framework of the SPIRAL1 facility upgrade, the design of a new ECR ion source ionizing radioactive metallic species in multicharged states is an alternate way in the actual NANOGANIII TIS system. It should contain open sides in order to have a close connection between the hot target and the plasma. Obviously the ECRIS should ionize the radioactive atoms with a high efficiency that requests to operate the ECRIS with a high value for the RF frequency. Based on an existing Mono1000 magnetic system, the prototype is under construction to demonstrate the ability of such an ECRIS to produce multicharged ions with an intermediate expected average charge state $\langle Q \rangle \geq 2$. This development is realized in collaboration with the Pantechnik company which has applications for this type of ECRIS.

MAGNETIC AND MECHANICAL DESIGN

The magnetic structure (principle has been used in two other ECRIS's [3,4]) takes back the two Mono1000 rings made of permanent magnets (NdFeB Vacodym 655HR) coupling with iron (ARMCO) which concentrates and transports the magnetic flux lines in the centre of the source. The magnetizations of the rings are similar and are aligned on the axis of the source. In our case, the trick is to shape the iron as to bring the maximum magnetic flux for creating a closed B iso-magnetic surface having a high value (here the last closed B iso-module reaches 4800 Gauss) far from the saturation of the iron (saturation value is 1.8T).

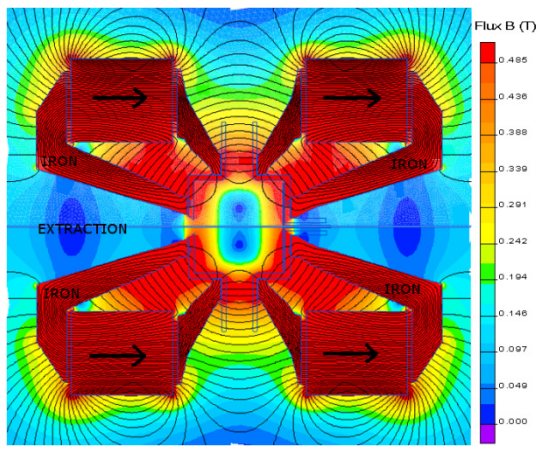

Figure 1: calculated magnetic structure with QuickField software

Figure 1 displays the output calculation made with the QuickField software: value of the total magnetic field at each point of the source. The magnetic field values decrease from the ECRIS wall down to almost 0 in the middle of the source. The magnetic field is lowered voluntarily in the extraction region in order to make a type of "ion funnel". Using a RF frequency of 7 GHz, corresponding to a resonant magnetic field of 2500 Gauss, the mirror ratio is 1.92.

After the iron design and the permanent magnet ring used, a mechanical design of the source has been realized. Figure 2 shows a sketch of the source. The ion source is relatively compact: length is 252 mm with a total diameter of 280 mm. The dimensions of the plasma chamber (grey) have been chosen such an RF wave with a frequency higher than 5.5 GHz can propagate inside the cavity. A movable disk is set on the back of the source, it has double objectives: RF tuning and plasma bias (negative voltage). Hence the RF is injected directly inside the cavity with a direct connection between the RF guide and the plasma chamber.

maunoury@ganil.fr
* also at GANIL

Mechanical calculations have been performed about the stress applied on different parts of the source. Reinforcements (blue) on the iron pieces had to be added due to the magnetic strengths applied on the plasma chamber. The maximum displacement is 0.04 mm. Thermal calculations have been also carried out.

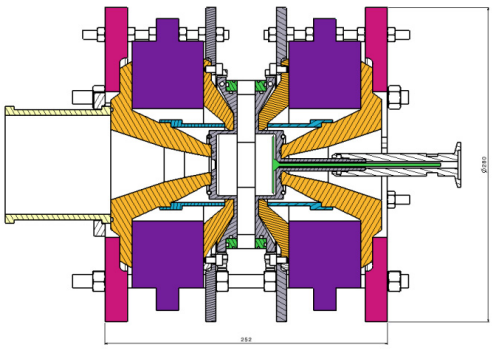

Figure 2: Mechanical design of the source

The maximum temperature elevation is around 70°C using 500W RF power and a water cooling down system. This will be still improved to get 50°C maximum.

TRAPCAD CALCULATIONS

The TrapCad code, developed by the Atomki ECR team, is a PC simulation tool which can be used to predict the general behavior of a source and, in a certain way, the performances of an ECRIS [5, 2]. TrapCad is only used to study the electron population and the ability of the source to heat up these electrons. It is why the calculation time is always below 50µs. In these conditions the particle collisions can be neglected (in the case of Multigan $1/\nu_{ee}$ ~ 200µs [6]). The typical fixed parameters for the TrapCad calculations were: 20000 initial electrons, energy range from 0.1 to 1 eV, electrons are randomly distributed on the ECR resonance surface. The variable parameters were the time, RF frequency and RF power. In the following, the electronic density in an ECR ion source, which varies with the square of the RF frequency, is taken into account. The electronic density reference is the Multigan ECRIS operating at 7 GHz.

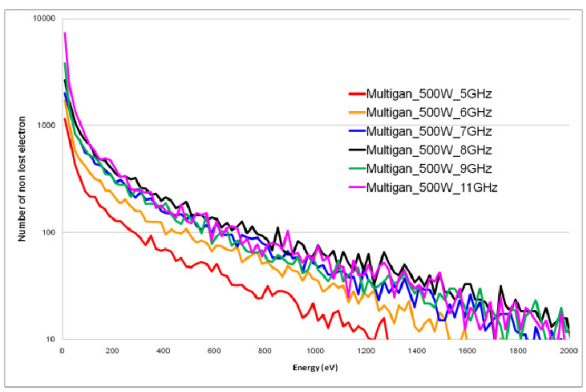

Figure 3: Evolution of the non lost electron distributions with the RF frequency of the injected wave

Figure 3 shows the evolution of the non lost (plasma) electron population with the RF frequency of the injected wave. The power and time were set to 500W and 1µs respectively. For RF frequencies below 7 GHz the non lost electrons are less energetic. From 7 GHz up to 11 GHz the distributions are really close but the 8 GHz is a little above. Another calculation at 7 GHz and 500 W of RF power gives an average energy of the non lost electrons of 380 eV. This energy is obtained in 5 µs.

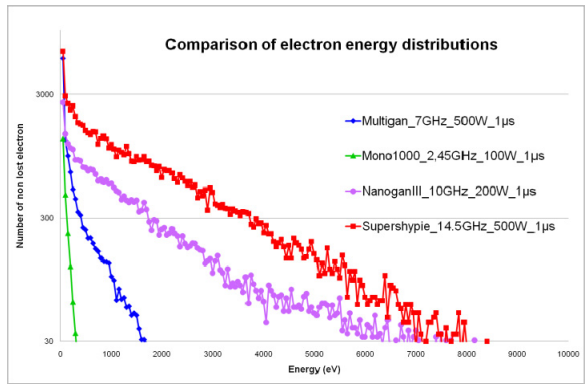

Figure 4: Non lost electron population for four ECRIS's

Let's consider now the case of phosphorus ions. Considering that the maximum single ionization cross section energy corresponds to energy of ~$10E_{ionization}$ for one charge state [7], it should be possible to ionize phosphorus atoms up to 5+ ($E_{ionization}$ = 67.9 eV). Regarding the reference [8], multicharged phosphorus ions have been already produced up to 2+ charge state with Mono1000 ECRIS at 100W of RF power. Figure 4 shows that, in the energy range of 1 – 700 eV (charge state range 1+ – 5+) the ratio of the non lost electrons population for Multigan 7GHz and Mono1000 2.45 GHz varies from 2.5 up to 100. These arguments reinforce the potential of multicharged ion production of this ECRIS. The Multigan non lost electron population is located between that of NanoganIII and Mono1000 as expected. These sources having an average charge state of 2.8 and 1 respectively [2], it is reasonable to expect for Multigan a value around 2.

EXTRACTION CALCULATIONS

A rough calculation of the extraction has been also carried out. Due to the high magnetic field gradient in the extraction region ~39 T/m, the ions extracted should be highly perturbated (it is roughly twice the SUPERSHyPIE ECRIS value). The extraction calculations are based on the methods described in [9]. In that paper, the space charge was neglected. The goal was to compute at first order the characteristics of the extracted beam. Figure 5 shows the extraction geometry which gives the best results. Another difficulty comes from the fact that the shape of the iron imposes a limitation of the possible shape of the first electrode. The plasma electrode is directly designed in the plasma chamber. Its aperture diameter is fixed at 7 mm. An intermediate electrode

(U_{inter}), biased positively, should have been added (figure 5) in order to get a small beam with an emittance value as small as possible.

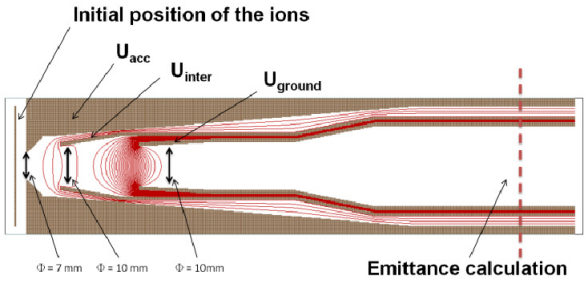

Figure 5: Sketch of the Multigan extraction geometry

As it is shown in figure 5, there are two regions: one between the plasma electrode and the intermediate electrode which is located inside the higher magnetic field gradient and the second region separating the intermediate electrode and the grounded electrode. The initial ions are made of phosphorus ions (mass = 31 u.m.a.) distributed either randomly or concentrated [9] on a disk of 10 mm diameter. They are located a few millimeter backward the electrode plasma biased at the plasma potential of 10V. Their initial energy is 0.5 eV and both the azimuthal and elevation angles vary from -90° to +90°. The charge states were fixed from 1 to 6 with a homogeneous number of ions: 2000 per charge.

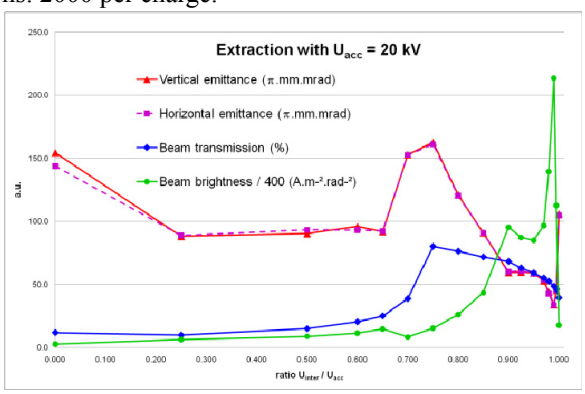

Figure 6: Evolution of the emittances, ion transmission and brightness of a phosphorous beam

The figure 6 displays the evolution of the emittances, ion transmission and brightness with the ratio R = U_{inter} / U_{acc}. The emittances present a plateau from R = 0.25 to 0.6 then a maximum for R = 0.75 and a diminution. The ion transmission which corresponds to the ratio of the ion number at the emittance calculation over the initial ion number follows roughly the same behaviour. The brightness which is more or less the ratio of this transmission over the emittances product increases slowly up to R = 0.8 and arises suddenly for reaching a maximum at R ~ 0.9 before dropping down. This can mean for R > 0.8 that the first extraction region acts smoothly on the ion angles for preparing them before to be focused by the second region which makes the main acceleration (90%).

CONCLUSION

A development of a new ECR prototype using the magnetic structure of the Mono1000 ECRIS has been undertaken by collaboration between GANIL laboratory and Pantechnik company. The objective is to get an ECRIS with large opened space in the middle of the source able to ionize atoms in multiply charged states with <Q> ≥ 2. It has been shown this new ECRIS is mechanically stable and the effective cooling of the plasma chamber allows injecting high RF power. The magnetic structure and the plasma chamber dimensions have been designed for RF waves with frequencies from 5.5 to 13 GHz. A movable electrode will serve for RF tuning and to bias negatively the plasma. The TrapCad code gave results for the expected performance of the source: the optimal RF frequency should be around 8 GHz. The distribution of the non lost electron population calculated is between those of the Mono1000 and NanoganIII ECRIS that reinforces our confidence in the potential of this source to produce multicharged ions. The preliminary extraction geometry calculations show that, despite the high magnetic gradient in the extraction region, it is possible to get a beam with reasonable emittance values. Pantechnik company built up a test bench where this prototype will be experimentally tested at the beginning of 2011. Depending on the results a new ECRISs will be specifically developed towards the objectives of each partner.

REFERENCES

[1] P. Jardin et al., "Mono1000: A simple and efficient 2.45 GHz electron cyclotron ion source using a new magnetic concept", RSI, 73, 789 (2002)
[2] L. Maunoury et al., "Studies of the ECR plasma using the TrapCad code", PSST, 18, 015019 (2009)
[3] C. Huet-Equilbec et al., "MONOBOB: A radiation-hard and efficient 2.45 GHz ECRIS dedicated to radioactive ion production", NIMB, 240, 752 (2005)
[4] F. Labrecque et al., "MISTIC: Radiation hard ECRIS", NIMB, 266, 4407 (2008)
[5] S. Biri, A. Derzsi, E. Kekete and I. Ivan., "Upgraded TrapCad code", High Energy Physics and nuclear Physics, 31 165 (2007)
[6] J.L. Delcroix and A. Bers, "Physique des plasmas", Savoirs Actuels / CNRS Editions (1994)
[7] S. Matt et al., "Experimental and theoretical determination of electron ionization cross sections for atoms, molecules and molecules ions relevant to fusion edge plasmas", Czechoslovak Journal of Physics, vol 48 (1998), Suppl 52
[8] L. Maunoury et al., "Production of charged (singly and multiply) phosphorous beams with electron cyclotron resonance ion source", RSI, 77, 03A324 (2006)
[9] L. Maunoury et al., "Extraction from ECR ion sources: a new way to increase beam brightness", proceedings of the International Workshop on ECRIS, Chicago, IL, USA, 224 (2008)

OPERATION OF KEIGM FOR THE CARBON ION THERAPY FACILITY AT GUNMA UNIVERSITY

M. Muramatsu#, A. Kitagawa, S. Hojo,
National Institute of Radiological Sciences, 4-9-1 Anagawa, Inage-ku, Chiba 263-8555, Japan
H. Miyazaki, T. Ueno, K. Sawada,
Sumitomo Heavy Industries, Ltd., 5-2 Soubiraki, Niihama, Ehime 792-8588, Japan
M. Tsuchiyama, S. Ueda, Y. Kijima,
Mitsubishi electric corporation, 1-1-2, Wadasaki-cho, Hyogo-ku, Kobe 652-8555, Japan
K. Torikai, and S. Yamada
Gunma University, 3-39-22 Showa-machi, Maebashi, Gunma 371-8511, Japan

Abstract

Carbon-ion radiotherapy is being carried out at Gunma University Heavy Ion Medical Centre (GHMC) since March 2010. A compact electron cyclotron resonance ion source (ECRIS) for GHMC, so-called KeiGM, supplies carbon 4+ ions for treatment. The general structure of KeiGM was copied from a prototype compact source, so-called Kei2. Based on experimental studies for production of carbon 4+ ions with a 10 GHz ECR source at the Heavy Ion Medical Accelerator in Chiba (HIMAC), so-called NIRS-ECR, the field distribution of the mirror magnet for Kei2 and KeiGM was designed. A microwave source with the traveling-wave-tube (TWT) was adopted for KeiGM, with a frequency range and maximum power of 9.75 - 10.25 GHz and 750 W, respectively. The KeiGM was installed in the GHMC facility in December 2008.

INTRODUCTION

The Heavy Ion Medical Accelerator in Chiba (HIMAC) at the National Institute of Radiological Sciences (NIRS) was the first heavy ion medical dedicated accelerator in the world [1]. Its aim has been to verify effectiveness and safety of heavy-ion radiotherapy. Carbon-ion radiotherapy (C-RT) started in 1994 and has mainly focused on the group of diseases in the whole body that are difficult to cure using conventional radiotherapy. The total number of patients enrolled by August 2009 was over 4,800 and various types of tumors have been treated. These results have clearly demonstrated the advantages of C-RT [2].

The Japanese government approved C-RT as a new treatment method in 2003, and promoted to development of new downsizing technologies under "the 3rd Comprehensive 10 year Strategy for Cancer Control (2004 – 2013)". NIRS carried out R&D studies for various components and designed a hospital-specified C-RT facility [3]. The construction of the Gunma University Heavy Ion Medical Centre (GHMC [4]) was funded by the Japanese government and Gunma prefecture beginning in 2006, and construction started in 2007 at the Centre site in Maebashi, Gunma. The technologies concerned were transferred from NIRS to Gunma University. GHMC will be a demonstration of the new C-RT facility. Gunma University already started a clinical trial since March 2010. A compact electron cyclotron resonance ion source (ECRIS) for GHMC, the KeiGM, is also based on the development of the ECRIS at NIRS [5]. This article presents the operation of KeiGM and the status of their daily treatment.

#m_mura@nirs.go.jp

CARBON ION THERAPY FACILITY AT GUNMA UNIVERSITY

In the design process, the following policies are considered to be important: (1) only high-energy carbon ions will be used in the facility to reduce the size and cost of the apparatus, and (2) beam characteristics should cover the same clinical beam characteristics as the HIMAC. Major specifications of the facility were determined on the basis of the statistics of clinical data from HIMAC. The reliable and well-established wobbler method with the respiratory-gated irradiation system was adopted for the beam delivery system [6]. It was decided to accelerate only carbon ions, with a maximum energy established at 400 MeV/n. This energy ensures a 25 cm residual range in water and, for example, carbon ions can penetrate the human body and reach the prostate through a patient's pelvis. Another important requirement of the new facility is to have two orthogonal beam lines directed toward the same isocenter. This beam line configuration is required in order to realize sequential beam irradiation from different directions with single positioning of a patient. As a conclusion, GHMC consists of the following parts; an ECRIS, a Radio-Frequency-Quadrupole linac (RFQ), an Interdigital-H mode Drift Tube Linac (IH-DTL), a synchrotron and four treatment rooms. Of these the first room will have a horizontal beam line, the second will have a horizontal as well as a vertical beam line, and the third will have a vertical beam line. The fourth room will be used for developmental studies for advanced irradiation techniques. A fast beam course and energy switching are also required for the same purpose. The major specifications of the facility are summarized in Table 1. The main building of the facility is about 65 m × 45 m, and it was completed at the end of October 2008.

Table 1: Major specifications of the therapy facility.

Items	Contents
Ion Species	Carbon ions only
Range	25 cm max. in water (400 MeV/n)
Field Size	15 cm × 15 cm max.
Dose Rate	5 GyE/min. (1.2×10^9 pps)
Treatment Rooms	3 (H, V, H&V)
	No rotational gantries
Fourth Room	Prepared for future developments
Irradiation Techniques	Respiration Gated; Single & Spiral Wobbling Methods; Layer-Stacking Method

KEIGM

KeiGM has been manufactured by Sumitomo Heavy Industries. Fig. 1 shows schematic view of the KeiGM with high voltage platform. The general structure including the magnetic field was copied from Kei2 [7]. Based on experimental studies with a conventional 10 GHz ECR source [8] at HIMAC, the field distribution of the mirror magnet for compact source was designed so that a charge distribution of carbon ions was optimized at 4+. A microwave source with the traveling-wave-tube (TWT) was adopted, with a frequency range and maximum power of 9.75 - 10.25 GHz and 750 W, respectively. Microwave power is fed into the plasma chamber through a rectangular wave guide from the axial direction. A biased disk is also used for optimizing. The plasma chamber is made of copper for a good cooling efficiency, in order to avoid a decrease in the magnetic field due to high temperature. The plasma chamber has an inner diameter of 50 mm. The vacuum pressures of the gas injection side and beam extraction side are 1.1E-6 Pa and 9.0E-7 Pa, respectively. Extraction voltage is 30 kV. The CH_4 gas was chosen for production of carbon ions. There are two reason for choose the CH_4 gas, (1) enough beam intensity of C^{4+} is obtained for medical use under the CH_4 operation; (2) there is experience of long operation of the source used the CH_4 gas at HIMAC. From our previous experience, other carbon compound gas (e.g. C_4H_{10} and C_2H_2) was better than the CH_4 for increasing the beam intensity of C^{4+} [9].

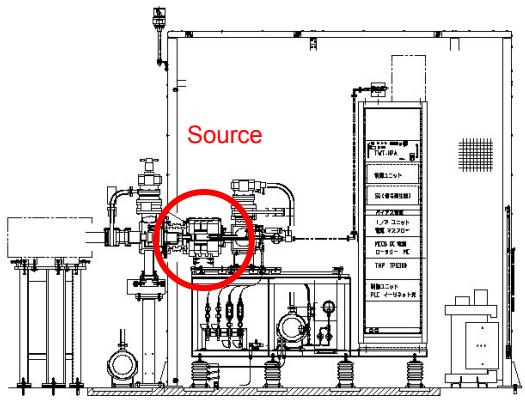

Figure 1: Schematic view of the KeiGM with high voltage platform.

Operation of KeiGM

KeiGM supplied the carbon ions from 7:30 in the morning to 0:00 midnight on weekdays. Fig. 2 shows trend graph of vacuum pressure at injection and extraction side, gas flow, microwave power, extraction voltage, current of the extraction power supply and C^{4+} beam intensity. The ion source starts in order of cooling water, the gas, the extraction power supply, and the microwave. All parameters of the ion source were fixed. The cooling water system for a whole of facility is started at 7:30. In this time, vacuum pressure in the extraction side change form 9.0e-7 Pa to 1.1e-6 Pa. The microwave power is applied to the ion source after 200 sec from start time. Beam intensity keeps changing for about 200 seconds after turning on the microwave power. All of beam parameter, intensity, profile, and so on, is reproduced at 1000 seconds every day.

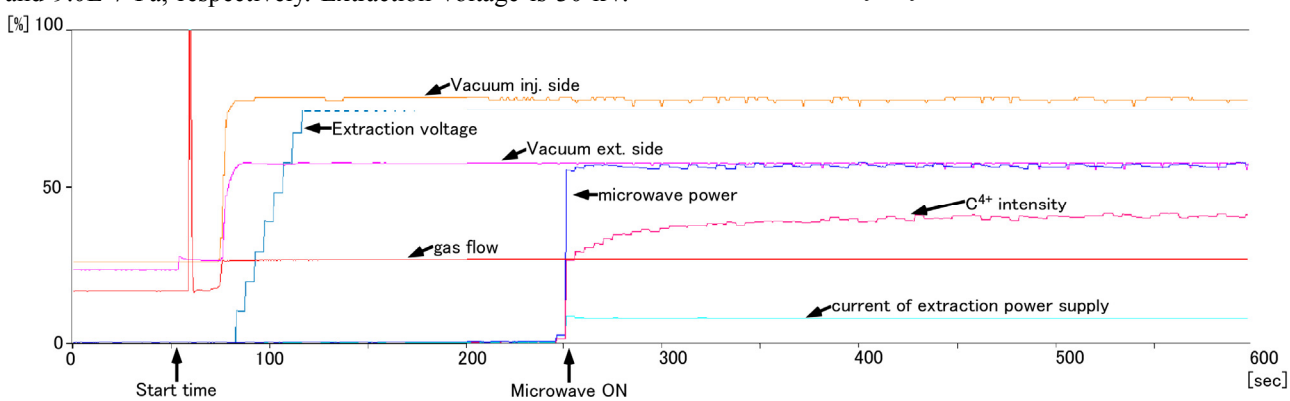

Figure 2: Trend graph of vacuum pressure at injection and extraction side, gas flow, microwave power, extraction voltage, current of the extraction power supply and C^{4+} beam intensity.

Fig. 3 shows a long term beam reproducibility from February to June 2010. The beam intensity decreased for 20% every three months. We thought that the operation parameters had not been optimized. Therefore, operation parameters were tuned on May 28. However, the beam intensity has increased slowly from May 28. It seems that the operation parameters are not yet optimized. The beam intensity of C^{4+} was 230 eμA at 30 kV extraction in June 9, 2010. The fluctuation of beam intensity was less than 10%. The operation parameters are as follows; the microwave frequency and power were 9.953 GHz and 300 W, respectively. CH_4 gas was fed, and the gas flow rate was 0.054 sccm. The extraction voltage was 30 kV. The repetition frequency and pulse width were 0.36 Hz and 50 msec, respectively. The voltage of the biased disk was -40 V.

Since at present KeiGM is the only ion source installed, all beams are supplied by KeiGM. In about 1600 hours operation between March and August, there was only one failure. It was due to breaking TWT amplifier after 14000 hours operation. The failure had been repaired by replacing of the amplifier.

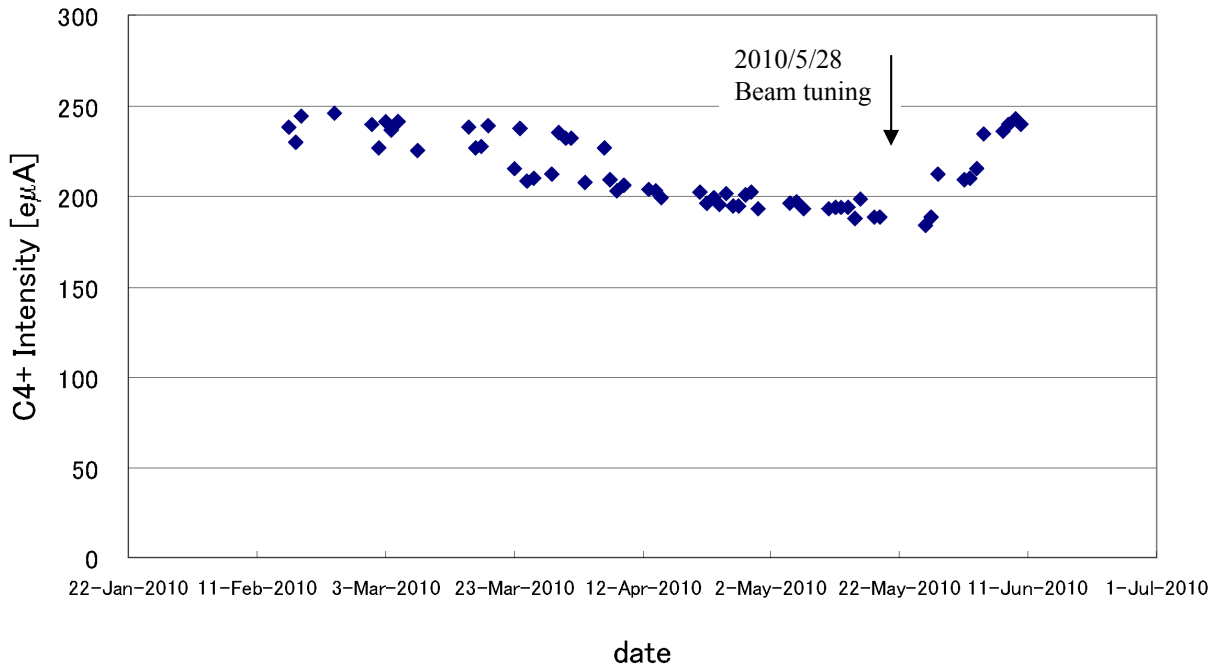

Figure 3: A long term beam reproducibility from February to June 2010.

CLINICAL TRIALS AT GHMC

Carbon ion radiotherapy started on March 16, 2010 at GHMC. Treatment is done in daytime from Monday to Friday. Gunma University has successfully treated the first 12 patients for the clinical trial until June 2010, thus the Japanese Ministry of Health and Labor Welfare approved GHMC as “advanced medicine”. Since June 2010, head and neck tumor, lung cancer and prostate cancer on advance medicine were started. The total number of patients enrolled by August 12, 2010 was 41.

REFERENCES

[1] K. Noda, et al., Proceedings of EPAC2004, Lucerne, Switzerland, 2634 (2004).
[2] H. Tsujii, et al., New Journal of Physics 10 (2008) 075009.
[3] K. Noda, et al., J. Radiat. Res. 48: Suppl. A A43 (2007).
[4] Satoru Yamada, Ken Yusa, Mutsumi Tashiro and Kota Torikai, Proceedings of NIRS-Etoile Joint Symposium 2009 on Carbon Ion Radiotherapy, Lyon, France, NIRS-M-218, 170 (2009).
[5] M. Muramatsu et al., Rev. Sci. Instrum. 81, 02A327 1-3 (2010).
[6] T. Kanai, et al., Int. J. Radiation Oncology Biol. Phys. 44, 201 (1999)
[7] M. Muramatsu et al., Rev. Sci. Instrum. 76, 113304 1-6 (2005).
[8] A. Kitagawa et al., Rev. Sci. Instrum. 65, 1087 (1994).
[9] A. G. Drentje, A. Kitagawa, M. Muramatsu, IEEE Trans. Plasma Sci. 36, 1502 (2008).

TWO-CHAMBER CONFIGURATION OF THE BIO-NANO ECRIS

T. Uchida#, H. Minezaki, Y. Yoshida, Toyo University, Kawagoe, Japan
S. Biri, R. Racz, ATOMKI, Debrecen, Hungary
A. Kitagawa, M. Muramatsu, NIRS, Chiba, Japan
Y. Kato, Osaka University, Suita, Japan
T. Asaji, K. Tanaka, Tateyama Machine Co. Ltd., Toyama, Japan

Abstract

We are studying the application of the electron cyclotron resonance ion source (ECRIS) for the new materials production on nano-scale. Our main target is the endohedral fullerenes. There are several promising approaches to produce the endohedral fullerenes using an ECRIS. One of them is the ion-ion collision reaction of fullerenes and aliens ions to be encapsulated in the mixture plasma of them. Another way is the shooting of ion beam into a pre-prepared fullerene layer. In this study, the new device configuration of the Bio-Nano ECRIS is reported which allows the application of both methods. The basic concept and the preliminary results using Ar gas and fullerene plasmas are described.

INTRODUCTION

The Bio-Nano ECRIS was designed for new materials production on nano-scale [1,2]. Our main target is the endohedral fullerene, where endohedral means some alien atoms are encapsulated inside the fullerene cage. The endohedral fullerenes have much potential in medical care, biotechnology and nanotechnology. In particular, endohedral Fe-fullerene can be applied as a contrast material for magnetic resonance imaging or microwave heat therapy. There are several promising approaches to produce the endohedral fullerenes using an ECRIS. One of them is the ion-ion or molecule-ion collision reaction of fullerenes and aliens ions to be encapsulated in the mixture plasma of them. Here we call it the plasma method. Another way is the shooting of ion beam into a pre-prepared fullerene layer. Here we call it the ion implantation method.

One of our team has been successfully synthesized the endohedral N-fullerene using the plasma method [3]. Also the endohedral N-fullerene were synthesized using ion implantation method by S. Abe et al. [4]. In addition, several kinds of atomic species, such as Li, Na, K, Rb, and Xe were encapsulated into the fullerenes by ion implantation method [5,6,7]. However, the number of the atomic species, which are successfully encapsulated into fullerene cage, is limited. Also the yield of endohedral fullerenes is not enough to develop them for above-mentioned practical applications.

In this study, the new device configuration of the Bio-Nano ECRIS is reported which allows the application of both the plasma and the ion implantation methods. The ions of the synthesized materials can be checked by in-situ extraction and analysis. This device configuration will make it possible to produce the endohedral-Fe fullerene and improve the yield of the endohedral fullerenes.

uchida_t@toyo.jp

DEVICE CONFIGURATION

Since 2006, we have developed and studied the Bio-Nano ECRIS with min-B configuration (see Fig. 1) [1,2,8]. Since 2008, the new device configuration, which we report in this paper, has been manufactured and tested.

Fig. 2 shows the schematic of the new device configuration. In contrast to the normal min-B ECRIS configuration, the plasma chamber is divided into two chambers by installing mesh electrodes and by installing an optional, second chamber (Fig. 3) which is also called processing chamber. Therefore we call this new device configuration the two-chamber configuration. The processing chamber is installed between the normal plasma chamber and the extraction box, and has 8 vacuum ports to host several connections like wave-guide, boat heater, substrate (plasma electrode) bias, substrate cooling, vacuum gauge, etc. In the gas injection side, a 2.45 GHz microwave can be introduced into the 1st chamber via coaxial waveguide. Also a 10 GHz microwave can be introduced in this chamber. There are several gas sources such as a resistance heating oven for fullerenes evaporation and an induction heating oven for iron evaporation, and a gas inlet for N_2, Ar, He, O_2, etc. Thus, we can make several plasmas in the 1st chamber. In the extraction-side 2nd chamber, a 10 GHz microwave can be introduced using a rectangular waveguide (WR75). We note that this frequency combination (2.45 GHz in the 1st chamber and 10 GHz in the 2nd chamber) was decided by some technical reasons and we do not consider them as the final solution. Later other frequencies are planned to be tested in both chambers.

An evaporation boat for fullerene is also installed in the processing chamber. The mesh electrode between the chambers and the plasma electrode can individually be biased to any DC voltage. The plasma electrode (frequently called also as collector or substrate holder) has a hole in its center to allow in-situ beam extraction.

Here let us explain the experimental procedure to produce the endohedral fullerenes using the two-chamber configuration. The gas ions to be encapsulated and the fullerene molecules or ions are generated in the 1st and the 2nd chambers, respectively. The injection of microwave into the second chamber and its power are

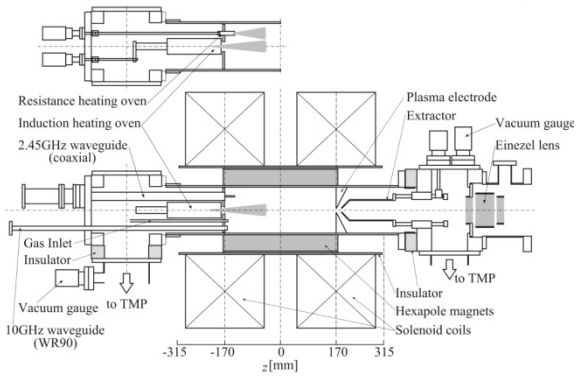

Figure 1: Schematic of the normal Bio-Nano ECRIS with min-B configuration.

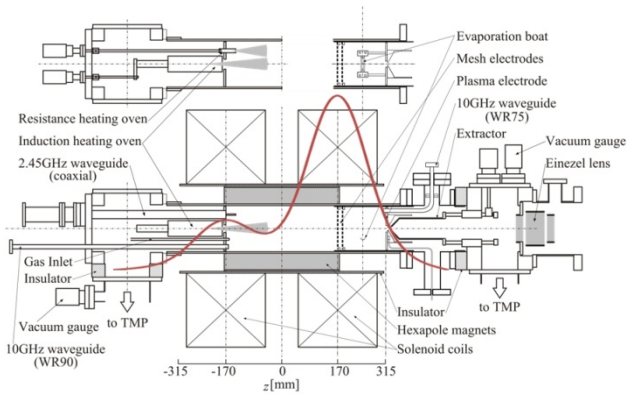

Figure 2: Schematic of the two-chamber Bio-Nano ECRIS with the optimized axial magnetic field distribution.

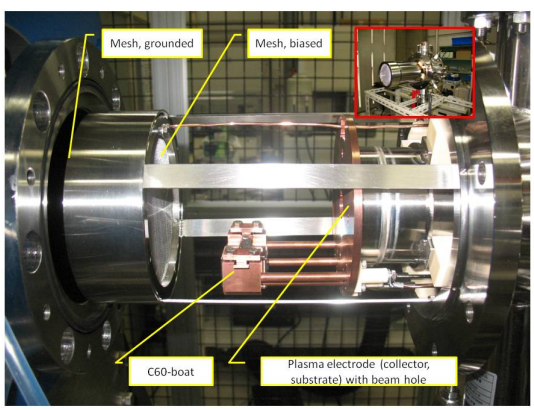

Figure 3: The second (processing) chamber before installation

optional. Thus C_{60} particles with any q charge can be produced in this chamber where q can be 1 (positive fullerenes) or 0 (neutrals) or -1 (negative ions). Furthermore, partly damaged positive fullerene ions can also be produced as C_{58}, C_{56}, C_{54}, etc. ions. The ions produced in the 1st chamber are extracted to the 2nd chamber through the mesh. This mesh actually is a double mesh. The one facing to the 1st chamber is grounded to the chamber and operates as many small plasma electrodes. The other mesh facing to the 2nd chamber is biased to some negative voltage and operates as many small puller electrodes. In the 2nd chamber vapor-phase ion-ion collision reaction can occur both in the plasma and on the surface of the collector plasma electrode. In the latter case ion implantation or ion beam deposition on the plasma electrode can be done. Thus, we expect that the endohedral fullerenes can be synthesized by ion-ion collision reaction or by ion implantation in the 2nd chamber. The ions in the 2nd chamber are in-situ extracted and analyzed. Also the ions of the synthesized materials can be collected by ion beam deposition and can be examined off-line using different materials analysis tools and methods.

RESULT

We checked the production of plasma in each chamber. The presence of the plasma was confirmed by extracting and analyzing the ions from each chamber. We measured the total extracted ion beam current in the straight beamline using a faraday cup FC1 (I_{FC1}), and the ion beam current for each ion in the analyzed beamline using a faraday cup FC2 (I_{FC2}). The extraction voltage throughout the whole experiment was 5.0 kV.

First, we checked the plasma production in the 1st chamber using Ar gas. Ar gas was supplied from the gas inlet at 0.3 sccm. Then the gate valve of the injection-side turbo molecular pump was closed in order to increase the chamber pressure to get the highest possible intensity of singly charged Ar plasma and beam. The pressure at the injection-side (P_{inj}) is 6.2×10^{-2} Pa, and that at the extraction-side (P_{ext}) is 9.1×10^{-4} Pa. The ion source was tuned for Ar^{+} beam. The ions were extracted through the second chamber as described. The mirror coil currents for both injection-side (I_{inj}) and extraction-side coils (I_{ext}) were 100 A and 340 A, respectively (see Fig 4). As will be shown later, we used a very unusual and asymmetrical magnetic field distribution in order to get resonance zones in both chambers. The 2.45 GHz microwave power of 40 W was fed (the forward power is 70W, and the reflected one is 30 W.). Without the bias voltages to the mesh and the plasma electrodes (V_{mesh} and V_{plasma}, respectively), we observed negative current on both electrodes (electron flow dominant). These currents on the two electrodes (I_{mesh} and I_{plasma}) increased toward zero with increasing the negative bias voltages. The I_{mesh} and I_{plasma} became zero at certain negative bias voltages. Then, we observed positive values of I_{mesh} and I_{plasma} at higher negative bias voltages (ion flow dominant). However we must always consider the contribution of both electrons and ions. Finally, the optimized V_{mesh} and V_{plasma} were -1 and -40 V, respectively which resulted in a near zero (-0.6 mA) I_{mesh} and 0.27 mA of I_{plasma}, respectively. The I_{FC1} is 12 μA. We could observe the I_{FC2} of 3.5 μA for Ar^{+}, I_{FC2} of 0.15 μA for Ar^{++}, and the ion currents due to the impurities such as H_2O^{+}, OH^{+}, O^{+}. If the ECRIS is optimized for the highest plasma electrode current then the axial magnetic field distribution changed (I_{inj} of 160 A, I_{ext} of 130 A) and the

resulted I_{plasma} was 0.7 mA. While this value is higher than the one optimized for FC1, is still not enough for macroscopic material collection. It means we need denser plasma in stage 1.

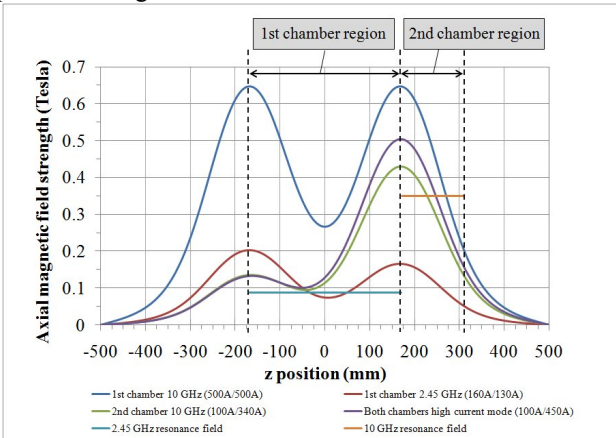

Figure 4: Magnetic field variations of the mirror coils.

Second, we checked the Ar plasma production in the 2nd chamber. First most conditions (mirror coil currents, gas flow rate, pressure, and two bias voltages) are set to the same values as the 1st chamber plasma. A 2.45GHz microwave was not fed in the first chamber. A 50 W 10 GHz microwave power was fed in the 2nd chamber. However, the plasma could not be ignited in the 2nd chamber. This is because the magnetic configuration is not B-minimum type in the 2nd chamber and there is no radial confinement (no hexapole here). If there is plasma in the 1st chamber, the plasma was ignited in the 2nd chamber easily, provided if the magnetic field distribution is suitable for the ECR condition in the 2nd chamber. The optimized I_{inj} and I_{ext} for plasma production in the 2nd chamber were 100 A and 340 A, respectively. This is a very unusual and asymmetrical magnetic field distribution. The high extraction peak however is necessary to get a resonance surface in the 2nd (processing) chamber. The resonance value of 10 GHz is 0.35 Tesla. The low injection peak was necessary to get a resonance zone (or at least a resonance point) in the 1st chamber where the resonance value of the 2.45 GHz frequency is only 0.09 Tesla. The magnetic field distribution in Fig. 4 thus is a result of several compromises. After setting this special magnetic field distribution we generated Ar plasma in the 1st chamber using 2.45GHz, under the above-mentioned conditions. Then, the 50W 10GHz microwave power was fed in the 2nd chamber. We observed the I_{FC1} of 10.8 µA. After that, the 2.45GHz microwave power could be turned off and we could still observe the extracted ion beam current. The I_{FC1} was 0.45 µA. This value is much smaller than that for the 1st chamber plasma. In order to increase the extracted beam current, we checked the effect of the 10GHz microwave power and the extraction-side mirror coil current. We could observe the increase of the I_{FC1} from 0.45 µA to 0.86 µA by increasing the microwave power from 50 W to 100 W. Also we observed the increase of I_{FC1} from 0.86 µA to 40 µA by increasing the I_{ext} from 340 A to 447 A. The I_{plasma} meanwhile was also increased from 0.36 mA upto 19 mA! We could confirm that the magnetic system is very effective to obtain high extracted beam current from the 2nd chamber but, of course, strongly prevents ions from the 1st chamber.

Finally, we tested the production of fullerene plasma in the 2nd chamber. We generated the plasma in the 2nd chamber using Ar mixing gas. Then we increased the evaporation boat current gradually. We used pure C_{60} powder (99.5% purity, nanom purple SU, Frontier Carbon Corporation) as fullerene source. We could observe the I_{FC2} of 100 pA for C_{60}^{+} and the I_{FC1} of 0.4 µA with the boat current of 37 A. The source conditions are as follows: Ar gas flow rate of 0.338 sccm, the P_{inj} of 8.7×10^{-2} Pa, the P_{ext} of 1.4×10^{-3} Pa, the I_{inj} of 139 A, the I_{ext} of 340 A, 10 GHz microwave power of 22 W, the V_{mesh} of -1 V, the V_{plasma} of -20 V. In order to increase the I_{FC2} for C_{60}^{+}, we examined the effect of the 10GHz microwave power and the I_{ext}. The I_{FC2} for C_{60}^{+} did not change with increasing the microwave power up to 40 W. We could observed the increase of the I_{FC2} for C_{60}^{+} from 100 pA to 45 nA by increasing the I_{ext} from 340 A to 400 A.

SUMMARY

The conclusions of the Ar-plasma and C_{60}-evaporation experiments in the two-chamber Bio-Nano ECRIS are summarized. The first and most important result is that the two-chamber configuration ECRIS works in each tested modes. The 1st chamber only operation mode works as traditional B-minimum ECRIS. In the 2nd chamber operation mode only a not-closed ECR-surface exists and both gaseous and C_{60} plasmas and ion beams can be produced. In the two chambers together mode however the configuration is strongly limited by the requirements for the 2nd chamber. A strongly asymmetrical magnetic field distribution is necessary where the extraction peak is much higher than the injection peak. The next technical steps in the two-chamber configuration experiments logically are the testing of other frequencies in the chambers. It can be the application of the same 10 GHz in both chambers or simply the exchange of the present two frequencies.

REFERENCES

[1] T. Uchida *et al.*, Proceedings of the 18th International Workshop on ECRIS, p 27 (2008).
[2] T. Uchida *et al.*, Rev. Sci. Instrum. 81 (2010) 02A306.
[3] S. Biri *et al.*, Rev. Sci. Instrum 77 (2006) 3A314.
[4] S. Abe *et al.*, Jpn. J. Appl. Phys. 45 (2006) 8340.
[5] E. E. B. Campbell *et al.*, J. Phys. Chem. Sol. 58 (1997) 1763.
[6] S. Watanabe *et al.*, J. Radioanal. Nucl. Chem. 255 (2003) 495.
[7] S. Watanabe *et al.*, Nucl. Instr. and Meth. in Phys. Res. B 206 (2003) 399.
[8] S. Biri *et al.*, High Energy Physics and Nuclear Physics - Chinese Edition Supplement 31 (2007) 156.

STUDY OF POTENTIAL APPLICATION OF COMPACT ECRIS TO ANALYTICAL SYSTEM *

M. Kidera#, K. Takahashi, RIKEN, Wako, Saitama 351-0198, Japan
Y. Seto, S. Kishi, NRIPS, Kashiwa, Chiba 227-0882, Japan
S. Enomoto, Okayama University, Kita-ku, Okayama 700-8530, Japan
T. Nagamatsu, T. Tanaka, Tokyo University of Science, Shinjyuku-ku, Tokyo 162-8601, Japan

Abstract

The objective of this study is to develop a desktop-sized system of element mass analysis (element analysis system) with a compact electron cyclotron resonance (ECR) ion source in the ionization section. This system is different from other element analysis systems in terms of the effective use of ionization by ECR plasma. A compact ECR ion source is required to fit in the desktop-sized element analysis system. This paper reports the development of the compact ECR ion source.

INTRODUCTION

An ECR ion source has been developed to meet the demands of users for accelerated heavy-ion beams with high intensity, highly charged ions, high stability, a small consumption rate of rare sample, and new ionic species production. The development of large ECR ion sources is underway at large-scale heavy-ion accelerator facilities. The application of ECR ion sources or ECR plasma to various areas, for example, the use of multicharged ions in the field of atomic physics, the ionization of fullerene [1] and charge state breeding [2], has yielded positive results. The basic mass analysis and ion detection technologies for general mass analysis systems have already been established. The ionization section in mass analysis devices, however, continues to undergo intense development because of the development of new ionization techniques.

In 2007, we developed an ECR ion source for an element analysis system (ECRIS-MS) used for isotope ratio measurement [3]. This ECR ion source is, however, very large as compared to the ionization section of ICP-MS systems typically used for element analysis. In the case of an element analysis system, its size, the ease of handling, etc., are important factors determining its applicability. Thermal ionization mass spectrometers (TI-MSs) and surface ionization mass spectrometers (SIMSs) having both merits and demerits, the improvement is still given to ionize of a difficult sample now. We developed a small-sized ECR ion source for realizing a desktop-sized element mass analysis system.

*This work was supported by a Grant-in-Aid for Scientific Research (KAKENHI: 20310100) from the Japan Society for the Promotion of Science (JSPS) and "R&D Program for Implementation of Anti-Crime and Anti-Terrorism Technologies for a Safe and Secure Society", Special Coordination Fund for Promoting Science and Technology of the Ministry of Education, Culture, Sports, Science and Technology, the Japanese Government
#kidera@kindex.riken.jp

FUNDAMENTAL CONSIDERATIONS IN FABRICATION OF COMPACT ECRIS

ECR plasma is nonequilibrium plasma; its ion temperature is low, although the electron temperature is high. It is advantageous to use ECR plasma sources in element analysis because the mass resolution is high when the ion temperature is low. No molecular ions are generated by the collision of radical ions, because ionization takes place in high vacuum, as compared to ionization by inductively coupled plasma. Further, numerous techniques have been developed to stably ionize gas and solid samples. In these techniques, it is necessary to maintain high vacuum in the plasma chamber. Therefore, the direct introduction of liquid samples is difficult. The directionality of development of the ECR ion source developed for the desktop-sized system differs significantly from the sources used in accelerators. A highly charged intense ion beam is not required, because the high-sensitivity channeltron detectors cannot receive intense ion beams. The charge number of the ions generated in the ECR plasma is optimized to 1+ and 2+. The stability of plasma is closely related to the accuracy of the measurement results. A confinement magnetic field has to be generated using permanent magnets if compact size and low-power consumption are the criteria for the source. A large magnetic field, however, cannot be generated with small permanent magnets. Therefore, the too high microwave frequency cannot be used significantly. In contrast, when an extremely low frequency is used, the miniaturization of the ECR ion source becomes difficult. Because the inside diameter of the magnet (i.e., plasma chamber diameter) cannot be small by the problem of the cutoff frequency. Fig. 1 shows plots of the diameter of circular waveguides (i.e., diameter of the plasma chamber) calculated from the lower cutoff frequency in the TE11 mode and the resonance magnetic field strength for microwave frequencies from 1 GHz to 32 GHz. It is necessary to miniaturize the mass analysis and detection sections.

For a compact and high-performance system, a small-sized quadrupole mass spectrometer or an ion-trap-type mass spectrometer is a promising candidate for the mass analysis and detection sections. In the case of time-of-flight spectrometers, miniaturization is difficult. Because the size of system is increased with the use of pulsed power supplies for time-of-flight method.

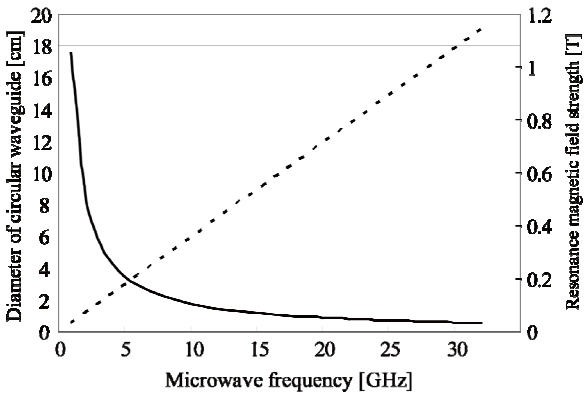

Figure 1: Microwave frequency vs. lower diameter of circular waveguide in TE11 mode and resonance magnetic field strength. The solid line indicates the diameter and the dashed line indicates the magnetic field strength.

FABRICATION OF PERMANENT MAGNET

The permanent magnet for the compact ECR ion source was manufactured by Hitachi Metals, Ltd. Fig. 2 shows a photograph of this magnet. The main specifications of the permanent magnet are listed in Table 1. For a microwave frequency of 5.76 GHz, the lower limit diameter of the chamber calculated from the cutoff frequency is 30.5 mm.

Table 1: Main Specifications of Magnet

Mirror magnet	
Maximum field strength	
Injection side	0.38 T
Extraction side	0.33 T
Minimum field strength	0.16 T
Hexapole magnet	
Maximum field strength	0.58 T
Size	
Outer diameter	100 mm
Inner diameter	45 mm
Length	150 mm
Weight	7 kg

Even if the cooling mechanism is installed outside the chamber because the inner diameter of the magnet is 45 mm, the inner diameter is an enough size. Distributions of magnetic field strength in the axial and radial directions are shown in Fig. 3 and 4, respectively. A commercially available quadrupole mass spectrometer is selected for the mass analysis and ion detection sections. When this spectrometer is installed in the ECR ion source equipped with a magnet, it is necessary to consider the leakage magnetic field from the magnet. The distribution of magnetic field strength from the edge of the magnet to a distance of 150 mm in the axial direction is shown in Fig. 3.

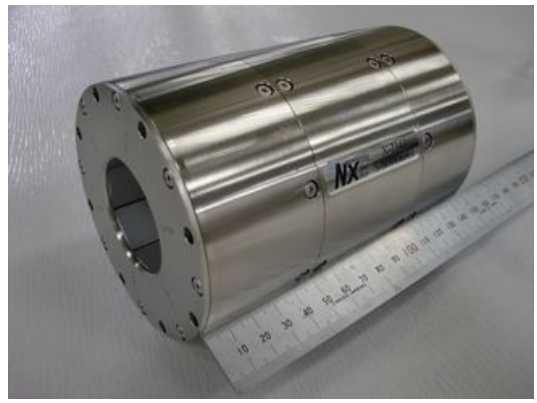

Figure 2: Photograph of permanent magnet for compact ECR ion source.

The spectrometer is not significantly affected by the leakage magnetic field if it is about 200 mm from the edge of the magnet. A solid-state-type microwave amplifier operating at a frequency of 5.76 GHz with an output power of about 100 W was used.

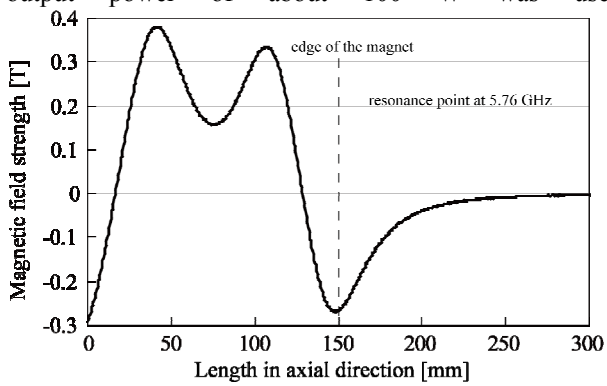

Figure 3: Distribution of mirror magnetic field strength. The region from 0 mm to 150 mm is inside the magnet.

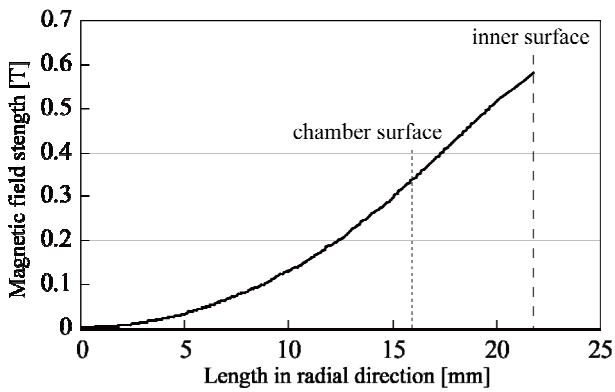

Figure 4: Distribution of magnetic field strength of hexapole magnet. The region from the center of the magnet to its inner surface is shown.

The amplifier does not contain a signal generator, and its dimensions, including a cooling mechanism with a heat sink and a fan, are 300 × 200 × 200 mm. The transportation line for the ion beam from the extraction electrode to the quadrupole mass spectrometer consists of

an einzel lens and an XY deflector electrode. Fig. 5 shows photographs of the einzel lens and XY deflector electrode. The ions accelerated by an extraction voltage of about 150 V are transported to the 1-mm-diameter injection hole of the quadrupole mass spectrometer. The entire system, including the abovementioned components, a vacuum pumping system, a control system, and the cooling system, is enclosed in a 100-L box.

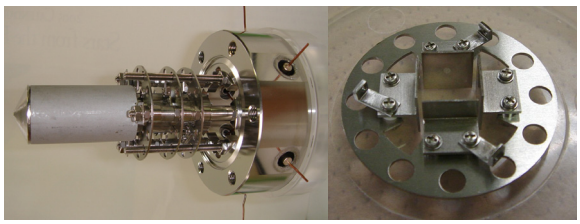

Figure 5: Photographs of extraction electrode and einzel lens (left) and XY deflector electrode (right).

SUMMARY AND FUTURE STUDIES

A desktop-sized element mass analysis system with a compact ECR ion source in the ionization section has been developed. The conditions for the compact ECR ion source to be installed in the desktop-sized element mass analysis system were determined, and the permanent magnet for the compact ECR ion source was fabricated considering these conditions.

We plan to use this system for the high-sensitivity detection of contaminants (especially, metallic floating particles) in the atmosphere. Most mass analysis techniques involve sample preparation processes, the use of expendable supplies, and setting up of a sample holder etc. for the introduction of the sample. In contrast, the use of the ECR ion source simplifies the analysis by facilitating the direct sampling of air, generation of ECR plasma in air, and ionization of the elements in air. Therefore, this system is effective for the automatic long-term monitoring of environmental conditions. The use of the ECR ion source is expected to expand the application range of desktop-sized element mass analysis system.

REFERENCES

[1] T. Uchida, H. Minezaki, K. Tanaka, M. Muramatsu, T. Asaji, Y. Kato, A. Kitagawa, S. Biri, and Y. Yoshida, Rev. Sci. Instrum. 81 (2010) 02A306.

[2] T. Lamy, J.L. Bouly, J.C. Curdy, R. Geller, A. Lacoste, P. Sole, P. Sortais, T. Thuillier, J.L. Vieux-Rochaz, K. Jayamanna, M. Olivo, P. Schmor, and D. Yuan, Rev. Sci. Instrum. 73 (2002) 717, DOI: 10.1063/1.1429778.

[3] M. Kidera, K. Takahashi, S. Enomoto, Y. Mitsubori, A. Goto, and Y. Yano, Eur. J. Mass Spectrom. 13 (2007) 239, DOI: 10.1255/ejms.883.

NEUTRALISATION OF ACCELERATED IONS AND DETECTION OF RESULTING NEUTRALS

T. Peleikis[#], L. Panitzsch, M. Stalder, IEAP, Kiel, Germany

Abstract

At the University of Kiel, the Department of Experimental and Applied Physics is running an ECR ion source in order to, amongst others, calibrate space instruments designed to measure solar wind properties and suprathermal particles. The ion source is able to produce medium to highly charged ions which are then accelerated by an electrostatic field up to 400keV per charge. In order to extend the particle spectrum from ions to neutral atoms we are planning to install a device for the beam particle neutralisation. It will be used to calibrate instruments which measure neutral particles. This device will be located downstream from the sector magnet and the acceleration-stage. The sector magnet separates the ions by their m/q ratio. This way the type and the energy of the ions can be determined before the neutralisation. Neutralisation can be achieved either by passing the ions through a thin carbon foil (thickness ~88nm) or through a gastarget (thickness ~6mm, pressure ~0.1mbar) where charge-exchange occur. The remaining ions behind the neutraliser will be suppressed by an electrostatic separator. Both methods will alter the beam properties and lead to a divergence in energy and an angular spread of the beam. Simulations regarding these effects will be discussed. The overall progress on this project will be presented.

Paper not received

[#] peleikis@physik.uni-kiel.de

HIGH CURRENT PRODUCTION WITH 2.45 GHZ ECR ION SOURCE

A. Coly#, T.Lamy, T. Thuillier, UJF CNRS-IN2P3 INPG, Grenoble, France
G. Gaubert, A. Villari, Pantechnik, Bayeux, France

Abstract

A new test bench has been installed at LPSC dedicated to 2.45 GHz ECR Ion Sources characterization. Several magnetic structures have been tested around the same plasma cavity. For example, a current density of 70 mA/cm2 has been measured with the MONO1000 source lent by GANIL. An original ECRIS, named SPEED (for 'Source d'ions à aimants PErmanents et Extraction Dipôlaire'), presenting a dipolar magnetic field at the extraction is also presented.

Paper not received

colyarona@yahoo.fr

IONIZATION EFFICIENCY OF A COMIC ION SOURCE EQUIPPED WITH A QUARTZ PLASMA CHAMBER

P. Suominen, T. Stora, CERN, Geneva, Switzerland
P. Sortais, J. Médard, LPSC, Grenoble, France

Abstract

Increased ionization efficiencies of light noble gases and molecules are required for new physics experiments in present and future radioactive ion beam facilities. In order to improve these beams, a new COMIC-type ion source with fully quartz made plasma chamber was tested. The beam current stability is typically better than 1 % and beams are easily reproducible. The highest efficiency for xenon is about 15 %. However, the main goal is produce molecular beam including radioactive carbon (in CO or CO_2), in which case the efficiency was measured to be only about 0.2 %. This paper describes the experimental prototype and its performance and provides ideas for future development.

INTRODUCTION

The ISOLDE facility at CERN produces a wide range of radioactive ion beams due to a long history on target and ion source development. Because the radioactive isotope production is very limited, the most important ion source parameters are high ionization efficiency, selectivity and reliable operation under intense radiation. Currently used ion sources (mainly laser (RILIS [1]) and arc discharge –type ion sources (VADIS [2])) do not efficiently ionize light noble gases, such as helium, and molecules, such as CO, CO_2, N_2 and NO. These beams were previously planned to be produced with 1+ ECR ion sources operating at 2.45 GHz (for example MINIMONO [3]). However, due to new and more efficient RF coupling of COMIC-type ion sources [4], we expect to advance in 2.45 GHz ECRIS utilization for radioactive beam production.

Q-COMIC

The new COMIC source (Fig. 1) designed by LPSC/Grenoble incorporates special features such as a plasma chamber fully made of quartz (Q-COMIC), which should provide chemically favourable conditions for molecular ion beam production, especially for CO_2. The beam is mainly formed between plasma (hole diameter 3.1 mm) and intermediate electrodes, which have 1.5 – 3 kV potential difference over 10 mm gap. The intermediate electrode is important in minimizing the effect of using different operation voltages to the beam formation and shape. Comprehensive emittance measurements will be performed in near future. Results are expected to be similar to those of standard COMIC [4].

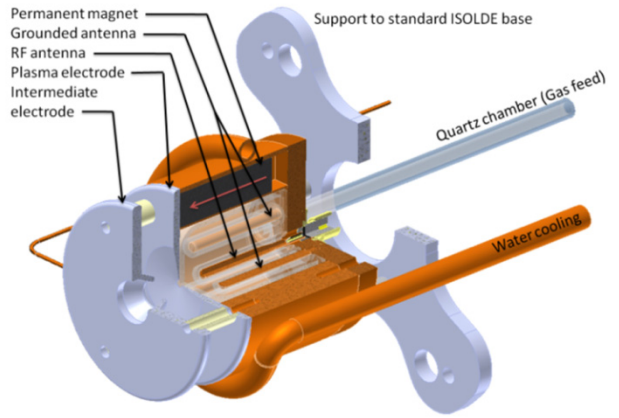

Figure 1: Schematic of Q-COMIC.

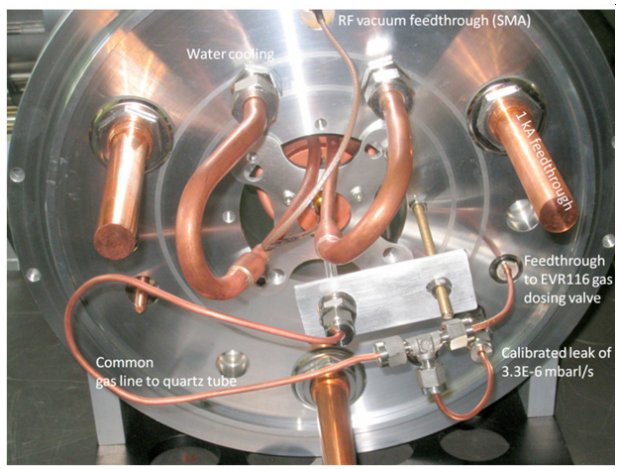

Figure 2: Q-COMIC setup and gas injection system

The source is placed inside a standard ISOLDE target base (Fig. 2), in vacuum. Consequently, a water cooling system is necessary to protect the NdFeB -permanent magnets from overheating. In this prototype unit there is no target container (between 1 kA current feedthroughs, Fig. 2) and the gas of interest (simulating a radioactive gas from target) is injected through a calibrated leak of 3.3E-6 mbarl/s (value corresponding air). The buffer gas is injected into the system by using a Pfeiffer EVR116 gas dosing valve operated by a RVC300 controller unit. Gas injection system calibration was verified with a calibrated helium leak detector.

The microwave power generator is Kuhne Electronic GmbH “KU SG 2.45-30A” operating at 2.45 GHz and capable of injecting up to 30 W microwave power. The plasma ignites typically at the pressure level of about 5E-5 mbar (at the extraction) when employing the full microwave power. However, at higher pressure of to 1E-2

mbar the ignition can be achieved already at 10 W. After the plasma is ignited the power can be decreased down to 2.7 W still maintaining the plasma. All the experiments were performed at ISOLDE off-line mass spectrometer using 30 kV acceleration voltage. An example of measured spectrum is shown in Fig. 3.

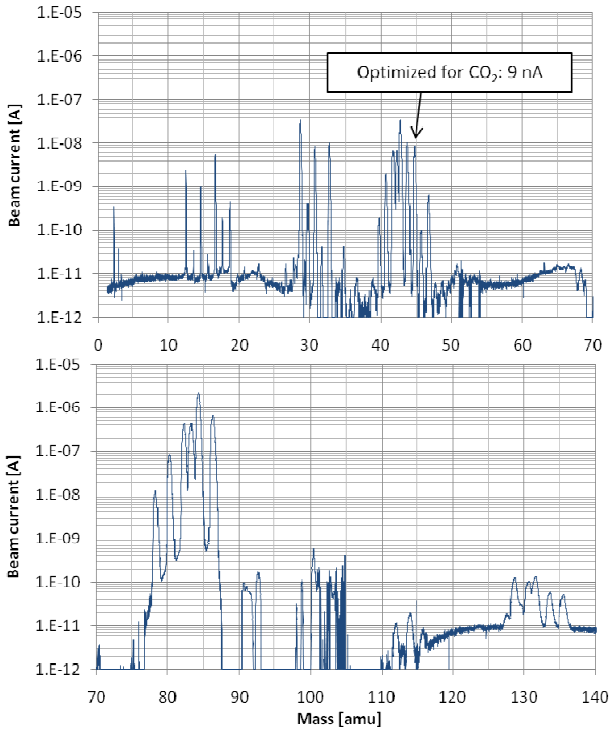

Figure 3: Spectrum when injecting 11.3 pμA of CO_2 in to the source with krypton as a buffer gas.

GAS EFFICIENCY

Experiments were performed by a) injecting only one gas and b) injecting CO_2 through a calibrated leak (simulating radioactive CO_2 from target) and a buffer gas for igniting and maintaining plasma.

A. *Injection of one gas*

In order to measure the influence of pressure (leak) on the gas efficiency, krypton was injected through the buffer gas dosing valve. The highest gas efficiency achieved was 6 % when injecting 62 pμA (4E-5 mbarl/s over 1.2 bar) of natural krypton (where ^{84}Kr abundance is 57 %). Comparable measurement was done also for argon and nitrogen. Results are shown in Fig. 4. In the case of nitrogen, it should be noted that this is a molecular beam of N_2 (atomic nitrogen beam current is typically 10 % of molecular N_2 beam with 28 W of forward microwave power).

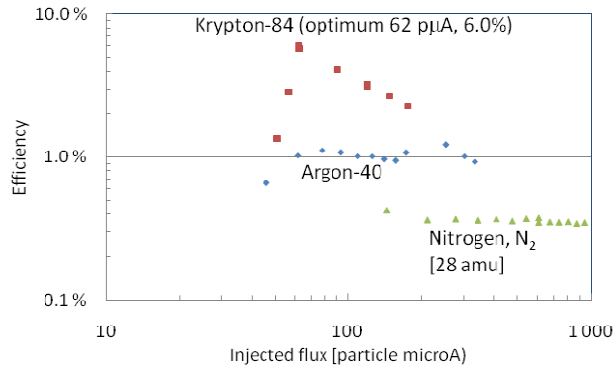

Figure 4: Gas efficiency as a function of injected flux

B. *Injection of CO_2 with a buffer gas*

Buffer gases tested with CO_2 were: nitrogen (N_2), argon, krypton and xenon. To verify the origin of monitored peak, the pressure of CO_2 injection line was altered from 0.5 bar to 1.5 bar (corresponding CO_2 injection from 5.1 pμA to 15.4 pμA). In the case of nitrogen the "CO_2 beam" was almost independent of CO_2 injection pressure. Possible explanation could be the formation of N_2O molecule having a same mass with CO_2. In the case of argon, krypton and xenon CO_2 beam intensity was a function of the pressure and the measured gas efficiency remained constant. The summary of the results is shown in table 1.

Table 1: CO_2 gas efficiency for different buffer gases

Buffer gas	**CO_2 gas efficiency**
Argon	0.09 %
Krypton	0.12 %
Xenon	0.22 %

DISCUSSION AND SUMMARY

Fig. 5 shows a summary of the gas efficiencies as a function of mass. All the measurements, except CO_2, fit very well on the dashed trend curve. The values for helium, neon and xenon were not measured with a single gas injection, but by injecting a gas-mixture of 20%-xenon, 20%-krypton, 20%-neon and 40%-helium. Krypton efficiency in this case was 5.9% (separately measured 6 %) indicating that the other compounds were not drastically affecting to the measured efficiency.

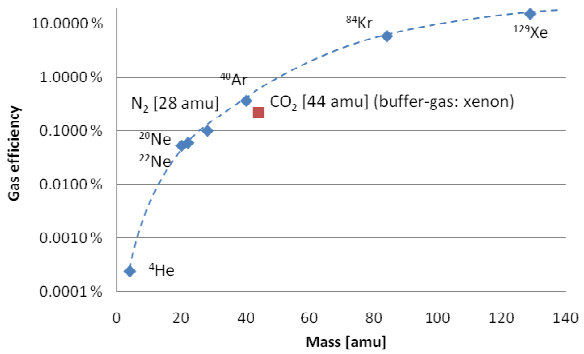

Figure 5: Summary of the measured gas efficiencies

It seems that the higher masses are ionized and extracted more efficiently than lower masses. This behaviour looks very similar to the kinetic theory of gases where $v_{rms} \propto \sqrt{(1/M)}$.

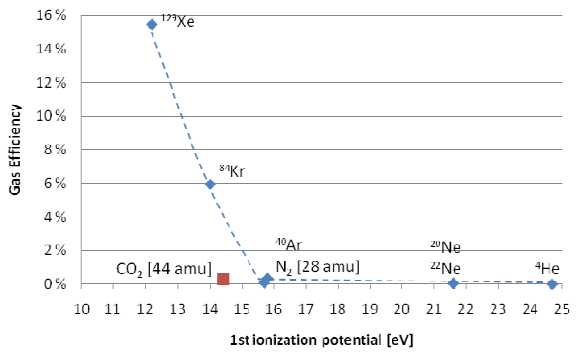

Figure 6: Gas efficiency as a function of the first ionization potential

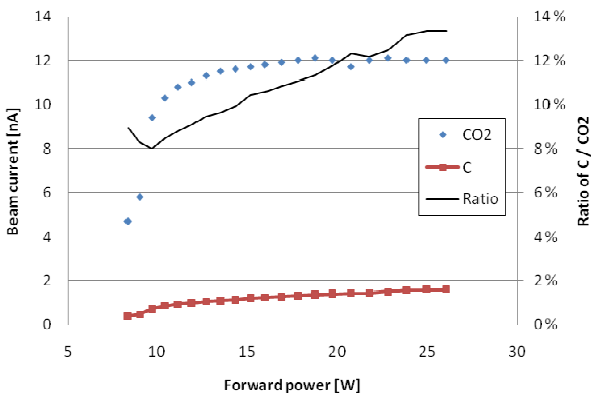

Figure 7: CO_2 breaking to C

Fig. 6 shows efficiencies plotted as a function of the first ionization potential of the ion. Also in this case CO_2 does not follow the tendency of the other tested gases. Possible explanation is that the CO_2 molecule is breaking in the plasma (C=O bond energy is only 8.3 eV). This was studied by measuring the CO_2 and C ion production as a function of microwave power. Fig. 7 shows that above 15 W of microwave power, the production of CO_2 saturates while the production of C increases with the power.

Table 2: Molecule dissociation and recombination

Ion	Mass [amu]	Beam current [nA]
C	12	2.4
O	16	5.6
O_2	32	10
CO_2	44 (also N_2O)	8.7
N	14	1
N_2	28 (also CO)	34
NO	30	8.7
NO_2	46	0.65
Kr	84	2 200
H_2O	18	0.47

Table 2 summarizes the relevant peaks of the spectrum shown in Fig. 3. Calculation of the total amount of oxygen in peaks O, O_2, NO and NO_2 suggests that some of the carbon is missing. However, after opening the source no visible carbon contamination was found on the quartz chamber.

The next step is to use oxygen (O_2) as a buffer gas, which is expected to improve C + O_2 recombination and therefore the CO_2 beam production. Additional plan is to test a plasma electrode with 0.3 mm extraction hole. This should increase the pressure inside the plasma chamber and reduce the amount of neutrals lost to vacuum pumps.

ACKNOWLEDGEMENTS

This research project has been supported in part by ISOLDE-collaboration, CERN/EN-department and a Marie Curie COFUND grant (PCOFUND-GA-2008-229600) to the CERN Fellowship Programme under the European Commission's 7th Framework Programme.

REFERENCES

[1] V.N. Fedosseev, et al, Nucl. Instrum. Methods Phys. Res. B 266/19-20 (2008) 4378.
[2] PhD thesis, univ. polyt. Bucarest, L. Penescu (2009)
[3] F. Wenander, W. Farabolini, G. Gaubert, P. Jardin, J. Lettry, Nucl. Phys. A, 746 (2004) 659
[4] P. Sortais, T. Lamy, J. Médard, J. Angot, L. Latrasse, and T. Thuillier, Rev. Sci. Instrum. 81 (2010) 02B31

HE2+ SOURCE BASED ON PENNING DISCHARGE WITH ADDITIONAL 75 GHZ ECR HEATING

I. Izotov#, A. Vodopyanov, S. Golubev, D. Mansfeld,
IAP/RAS, Nizhny Novgorod, Russia
G. Yushkov, Institute of High Current Electronics, Tomsk, Russia

Abstract

It is well known that one can reach high average charge of ions in the ECR plasma by increasing plasma density and decreasing neutral gas pressure. ECR discharge could be realized at very low gas pressure, but discharge breakdown takes longer time when gas pressure is low. So, it is impossible to realize ECR discharge with limited microwave heating pulse duration at gas pressure lower certain threshold value. This problem could be solved with help of trigger plasma, which should be ignited at low gas pressure in the trap with high magnetic field. This fore plasma could help to decrease ECR plasma breakdown time significantly and make it possible to realize ECR plasma at very low pressure in pulse operation regime. We suggest penning type discharge as a trigger discharge for fast breakdown of pulsed ECR plasma. Penning type discharge glows at as low pressure as needed. Discharge was realized in the simple mirror magnetic trap at pressure about 1E-5 mbar. Helium was used as an operating gas. Significant plasma density (about 1e11 cm-3) was obtained at the moment just before microwave heating pulse started. Gyrotron radiation with frequency of 75 GHz, microwave power up to 200 kW and pulse duration up to 1 ms, was used for plasma heating. In the present work the fully striped helium ions were demonstrated, average charge of ions in the plasma was equal 2. Temporal evolution of charge state distribution was investigated. Charge state distribution over helium pressure was also studied.

Paper not received

izotov@appl.sci-nnov.ru

THE LIGHT ION GUIDE CB-ECRIS PROJECT AT THE TEXAS A&M UNIVERSITY CYCLOTRON INSTITUTE

G. Tabacaru, D. P. May, Cyclotron Institute, Texas A&M University, College Station, 77843 TX, U.S.A.
J. Ärje, JYFL, Jyväskylä, Finland

Abstract

Texas A&M University is currently configuring a scheme for the production of radioactive-ion beams that incorporates a light-ion guide (LIG) coupled with an ECRIS constructed for charge-boosting (CB-ECRIS). This scheme is part of an upgrade to the Cyclotron Institute and is intended to produce radioactive beams suitable for injection into the K500 superconducting cyclotron. The principle of operation is the following: the primary beam interacts with a production target placed in the gas cell. A continuous flow of helium gas maintains a constant pressure of 500 mbar maximum in the cell. Recoils are thermalized in the helium buffer gas and ejected from the cell within the gas flow through a small exit hole. The positively charged recoil ions (1^+) are guided into a 2.43 m long rf-only hexapole and will be transported in this manner on-axis into the CB-ECRIS (Charge Breeding – ECRIS). The CB-ECRIS will operate at 14.5 GHz and has been specially constructed by Scientific Solutions of San Diego, California for charge-boosting [1]. An overall image of the entire project will be presented with details on different construction phases. Specific measurements and results will be presented as well as future developments.

PROJECT OVERVIEW

In 2005 the Cyclotron Institute at Texas A&M University initiated a facility upgrade project [2]. This project will extend the research capabilities as a stable beam facility with moderate rare beam capabilities. This will be achieved by re-activating the 88" Cyclotron to deliver high intensity light-particle and heavy-ion beams, to be used for production of rare isotopes for acceleration in the existing K500 Cyclotron. The plan is to produce radioactive species for re-acceleration by the existing K500 Cyclotron. The main items of the scientific program that drive this project are summarized as: nuclear astrophysics (the extension of the Asymptotic Normalization Coefficients method and study of the (^{3}He,d) reactions), nuclear structure (study of the Giant Monopole Resonances and the cluster structure of the nuclei using the radioactive beams), fundamental interactions and nuclear thermodynamics (multifragmentation). We are expecting also to gain valuable experience in the development of radioactive ion sources and different methods of diagnosis for weak beams.

The project is divided in three tasks: a) recommission the existing 88" Cyclotron and install new beam lines; b) construct light-ion and heavy-ion guides and produce and transport 1^+ radioactive ions; c) charge boost radioactive ions, transport and accelerate in the K500 Cyclotron. Table 1 presents the new beams intended to be developed using the Light Ion Guide (LIG).

Table 1: Projected beam intensities from the LIG after K500 re-acceleration.

(p,n) reaction Product $T_{1/2}$	Max Energy [MeV/A]	Intensity [particles/sec]
^{27}Si (4.16s)	57	5.4×10^3
^{50}Mn (0.28s)	45	2.1×10^4
^{54}Co (0.19s)	45	5.4×10^3
^{64}Ga (2.63m)	45	3.5×10^4
^{92}Tc (4.25m)	35	3.5×10^4
^{106}In (6.20m)	28	5.4×10^4
^{108}In (58.0m)	28	2.7×10^4
^{110}In (4.9h)	26	5.4×10^4

PRODUCTION OF RADIOACTIVE IONS

The Light-Ion Guide (LIG) will produce radioactive species mainly from (p,n) reactions. The beam (a proton beam around 30 MeV) interacts with a production target (e.g. ^{27}Al) placed in a gas cell. In the gas cell helium gas is flowing continuously at constant pressure of 500 mbar maximum. The recoil ions (e.g. ^{27}Si from ^{27}Al(p,n)^{27}Si)) are trapped in the buffer gas and ejected at a 90° direction (with respect to the beam direction) through a small exit hole [3]. All ions created in the gas cell are collected and transported by a rf-only hexapole: a resonant structure similar to the RFQ in a residual gas analyzer. The large flow of helium gas is evacuated by a differential pumping system. The ions are then injected into a Charge Breeding ECRIS (CB-ECRIS) source which will ionize them to higher charge states. The radioactive species are injected into the K500 Cyclotron and re-accelerated. The primary beam (proton beam) will exit the gas cell and will be stopped in the beam dump. Figure 1 shows an engineering drawing of the LIG coupled with the CB-ECRIS. The main new feature of the device is the rf-only hexapole with a length of 2.43 m. Extensive calculations performed with SIMION [4] software confirm early theoretical approaches [5] where it was shown that all the particles entering the central region of the hexapole should have almost 100 % transport efficiency. The rf-only hexapole is a non-selective device, meaning that all

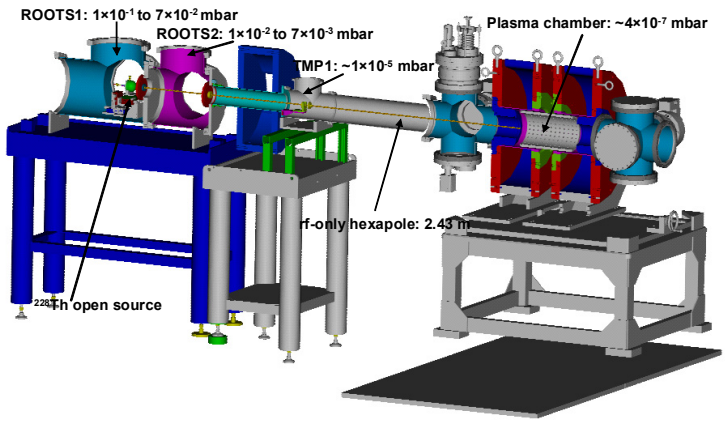

Figure 1: Engineering drawing of the Light Ion Guide coupled with the CB-ECRIS.

ions, singly and possibly doubly charged, as well molecular ions, are transported with the same efficiency, independent of their mass-to-charge ratio.

DEVELOPMENT OF THE LIGHT ION GUIDE

At the Cyclotron Institute we developed, built and tested a prototype of the Light Ion Guide that will only suffer minor modifications for future operation. The vacuum system consists of two large chambers and a 2 m long beam tube for connection to the CB-ECRIS. The chambers are pumped with ROOTS blowers (2000 m^3/h and 1000 m^3/h pumping speed) and the beam tube is pumped with a turbo molecular pump (520 l/s pumping speed). Two similar turbo pumps are coupled also at the injection and extraction side of CB-ECRIS. Figure 1 indicates the helium pressures in the different sections of the device.

Inside the first vacuum chamber, stands a semispherical gas cell (volume of about 50 cm^3) with an exit orifice: 1 and 2 mm in diameters were used. Between the cell exit and the inlet of the CB-ECRIS plasma chamber is a 2.43 m long rf hexapole divided into three sections: two of 1 m and one of 0.43 m. The hexapole is made from 2 mm brass rods placed on a circle pattern with diameter of 6 mm (equivalent with an interior diameter of the hexapole of 4 mm).

The device was initially developed with ionized gas created by two high-voltage spark electrodes inside the gas cell. We were able to produce a few mA of current, mainly ionized helium and ionized impurities. The transported current (a few nA) was measured at the end of the rf hexapole on a Faraday cup. Figure 2 presents, as an example, a graph of the transported current at the end of the first 1 m long section rf hexapole as a function of the pressure inside the gas cell. The discharge voltage and current were 227 V and about 3.5 mA, respectively. The production of the ions via the spark method has drawbacks: the high voltage needed to ignite the spark accelerates the ions, and at the end of the rf hexapole the ions gain about 180 eV in energy. This energy is too high for the injection into the CB-ECRIS.

In order to eliminate the described feature, and reproduce more closely the future on-line operation, we decided to use an open radioactive source (^{228}Th) as the recoil-ion source. An effort to use a heated alkali source was unsatisfactory due to the fact that the continuous flow of helium in the gas cell prevents attaining the temperature where the alkali source will start releasing the products. Inside the gas cell the daughters from ^{228}Th are released continuously and they are thermalized by the helium gas. In order to have maximum stopping efficiency of the radioactive products, a pressure of 30 mbar of helium was used. The daughters are injected into the rf-only hexapole within helium flow by applying a small (approx. 10 - 50 V) acceleration (guiding) voltage between the cell exit and the hexapole inlet. The same voltage will control the injection energy of the recoil ions into the CB-ECRIS plasma chamber. In this preliminary experiment the recoil ions were transported to a collector plate (aluminized mylar), placed at the inlet of the CB-ECRIS plasma chamber. The collector plate is backed by a silicon detector. The alpha particles coming from the products pass through the collector plate and are detected with the Silicon detector. The decay series of ^{228}Th include ^{216}Po with a half life of 145 ms. This is an excellent candidate to test our device: the half-life is short enough to provide a reasonable counting rate and is long enough to be charged boosted in the CB-ECRIS. The first tests, without CB-ECRIS plasma, were successful: we were able to measure about 50 alphas/sec coming from the ^{216}Po. We measured also the energy of the ^{216}Po ions, and found that the energy spread is only around 1 eV (see Figure 3). This extra energy will have to be taken into account for stopping the products in the plasma of the CB-ECRIS. The CB-ECRIS is now operational. A Sample of Oxygen spectrum is shown in Figure 4

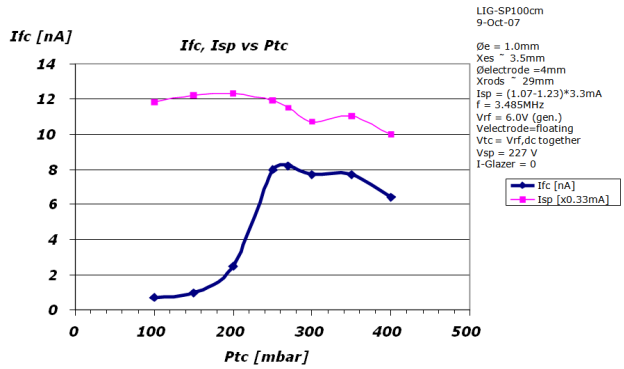

Figure 2: Faraday Cup current (Ifc) vs. the pressure in the gas cell (Ptc).

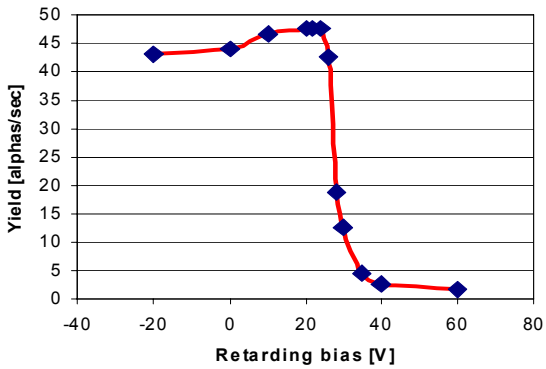

Figure 3: The retarding bias is a measure of the energy of the ions. The radioactive products exhibit an energy of 20-25 eV approximately. The acceleration voltage was 24 V.

FUTURE PLANS

Much further development of this system is necessary before it can produce a usable beam of highly charged radioactive ions with high efficiency for further re-acceleration in the K500 cyclotron. Two major directions should be followed to achieve the proposed efficiencies. The first is to find optimum parameters in the operation of the gas cell in conjunction with the rf-only hexapole. We need to determine the factors that will lead to high efficiency extraction of the radioactive products from the gas cell and high efficiency transport of the products to the CB-ECRIS. The second direction is to determine the ideal conditions for injection and extraction of the highly charged products from the CB-ECRIS with maximum efficiency. In pursuing these two directions the efficiencies of different sections of this system need to be measured along with finally the efficiency of the entire system.

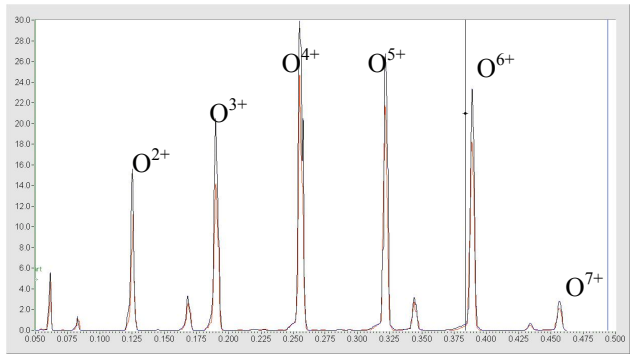

Figure 4: Oxygen spectrum (analyzed current vs. charge to mass ratio) for the CB-ECRIS.

Acknowledgments

The authors would like to thank the staff of the Cyclotron Institute Texas A&M University for the commitment to their work. This work is supported by the U.S. Department of Energy under Grant number DE-FG02-93ER40773.

REFERENCES

[1] W. D. Cornelius, Design of a Charge-Breeder Ion Source for Texas A&M University , ECRIS 2008, 18th International Workshop on ECR Ion Sources, Chicago, Illinois USA, http://cern.ch/AccelConf/ecris08/papers/weco-b01.pdf.

[2] "A proposed facility upgrade for the Texas A&M University Cyclotron Institute", http://cyclotron.tamu.edu/facility_upgrade.pdf

[3] J. Ärje et al., Nucl. Instr. and Meth. A247, 431 (1986).

[4] SIMION: Industry standard charged particle optics simulation software. http://www.simion.com/

[5] C. Hagg and I. Szabo, Intl. Jour. of Mass Spectrometry and Ion Process, 73 (1986) 295-312.

DRAGON: A NEW 18 GHz RT ECRIS WITH A LARGE PLASMA CHAMBER*

W. Lu[1], D. Z. Xie[2], X. Z. Zhang and H. W. Zhao
Institute of Modern Physics (IMP), Chinese Academy of Sciences, Lanzhou 730000
L. Ruan, F. C. Song, B. Xiong, S. Yu and J. Yuan
Institute of Electrical Engineering (IEE), Chinese Academy of Sciences, Beijing 100190
People's Republic of China

Abstract

Building a strong radial magnetic field with a permanent sextupole magnet for an ECRIS is extremely challenging so that the conventional wisdom recommends a small but not optimal plasma chamber that is typically of ID less or equal to 80 mm. A new 18 GHz RT ECRIS, DRAGON, with a large bore permanent sextupole has been designed and is under construction at IMP. Its plasma chamber is of ID 126 mm, the same as that of the superconducting ion source SECRAL, with maximum radial field strength reaching 1.5 T at the plasma chamber wall. The overall magnetic strengths of DRAGON, with maximum axial fields of 2.7 T at the injection and 1.3 T at the extraction, are very similar to those of SECRAL operating at 18 GHz and hopefully its performance. The source solenoid magnets are cooled by medium evaporation at about 50 °C. In addition, the source is thickly insulated for beam extraction at 50 kV and higher voltage up to 100 kV can be explored. This article will present the design details and discussions of this new ion source.

INTRODUCTION

In recent years ECRIS has made tremendous progress with the continuing increase of magnetic field and higher operating frequency in which the fully superconducting (SC) ECRIS takes the leading roll, while the great contribution from the Hybrid ECRIS remains to be realized. A room temperature (RT) ECRIS has the advantages of easy operation and lower cost in comparison to a SC ECRIS but with lower performance. Because of the filed strength and ac power consumption restraints, there are essentially no new improvements on the RT ECRIS since the great success of the GTS [1]. However, there are still possible rooms to further enhance the RT ECRIS' performance for cost effective applications that do not require super performance.

An RT ECRIS consists of a set of water cooled resistive solenoids and a permanent sextupole magnet. The resistive solenoids are typically made of hollow-conductor cooled by de-ionized pressurized-water. As the field strengths keep increasing for better source performance, building a strong radial magnetic field with a permanent sextupole magnet is extremely challenging. So far all the permanent sextupoles are built with a small plasma chamber of ID less or equal to 80 mm to reach a strong radial field of ~1.2 to 2 T without/with iron tips [2]. These small plasma chambers are not optimal as evidenced by the larger chambers of the SC ECRISs at about the same field profiles. An embodiment is the IMP's SC ECRIS, SECRAL, which has demonstrated great performance [3] while operating at 18 GHz with axial field maxima of 2.5 T on the injection and 1.3 T at the extraction regions and a radial field of 1.4 T at the plasma chamber wall of ID 126 mm. If an RT ECRIS can duplicate these magnetic fields with the same large plasma chamber and can produce about the same performance, it would definitely be a good improvement on RT ECRIS that comes with much lower cost and easier source operation.

In this article, we will present and discuss the design features of DRAGON, the new 18 GHz RT ECRIS being constructed at IMP, Lanzhou, China.

THE NEW 18 GHZ RT ECRIS WITH A LARGE PLASMA CHAMBER

Figure 1 shows the overall features of DRAGON. Figure 2 shows the axial field profile that reaches 2.7 T at the injection with an iron plug field booster and 1.3 T at the extraction. Figure 3 shows the calculated radial field at the plasma chamber of ID of 126 mm reaches 1.4 T and 1.5 T if six small iron tips are embedded in the plasma chamber cooling channels. Shown in Figure 4 is a cross-section view of the sextupole magnet with a simple easy-axis rotation. DRAGON's plasma chamber volume is about 6 litters, about 15% larger than the SECRAL for a slightly larger ECR volume. The maximum source magnet power consumption is about 400 kW. This new RT ECRIS has a few new features in comparison to the existing RT ECRISs:

Large Bore Sextupole

Most of the high-field RT ECRISs use a Halbach-sextupole [4] of small bore that is typically made of M equal-size sections with the easy-axis rotating $8\pi/M$ from section to the next. Such an easy-axis rotation poses a risk of regional de-magnetization when the field approaching certain strength [5]. In addition the fabrication of such a Halbach-sextupole requires very complex and delicate magnet-block cutting and assembling.

[1] Also of the Graduate School of Chinese Academy of Sciences, Beijing 100049, P. R. China
[2] Visiting Scientist
* This collaboration project was supported by the Research Foundation of Chinese Academy of Sciences.

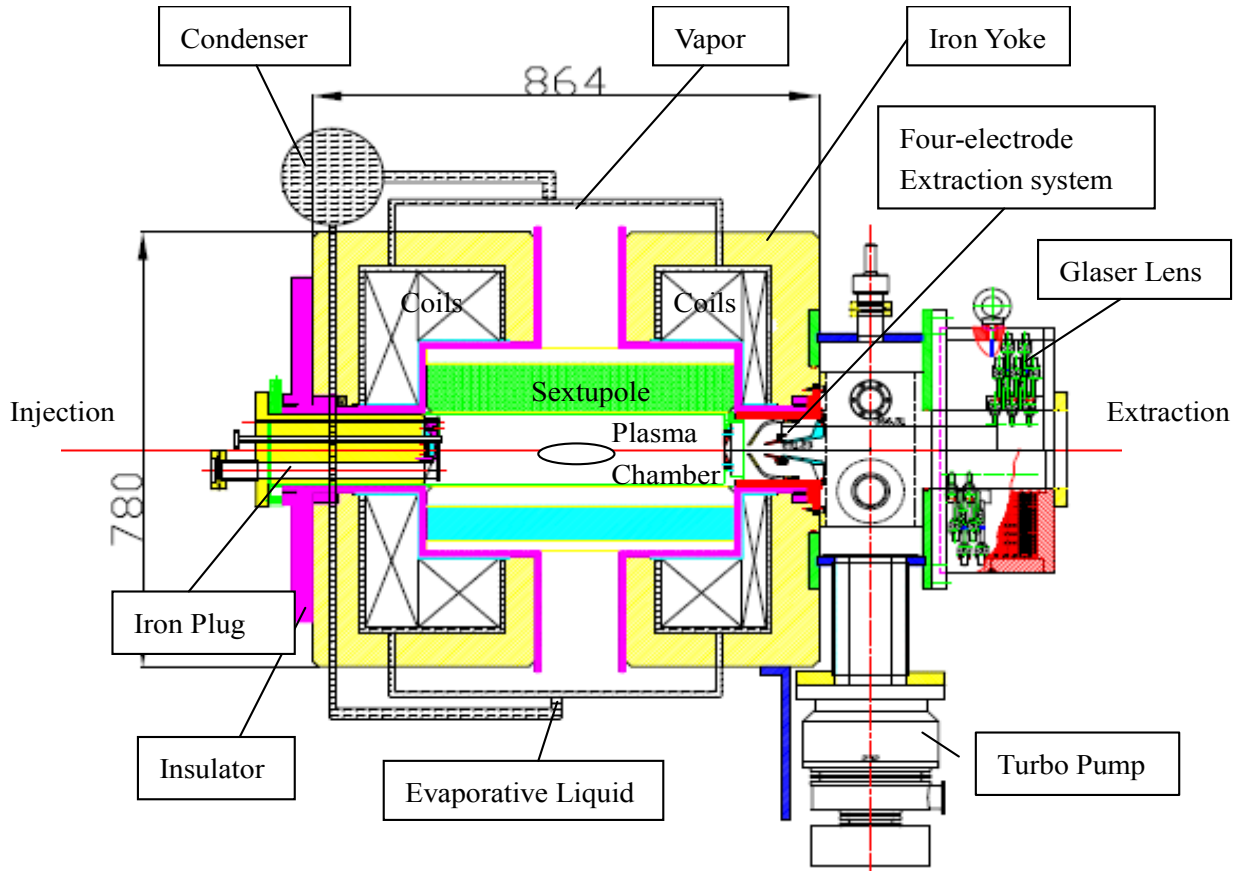

Figure 1: An elevation schematic view of DRAGON. No mechanical pumping at the injection side for simplicity but it may be added in the future. The evaporative cooling condenser and its related pipes are not in scale.

Though the Halbach-sextupole yields the highest field strength, a simplified large-bore non-Halbach-sextupole with about 2% lower field strength and easier fabrication, is being built for DRAGON. This large bore sextupole consists of six sectors and each sector is made of many simply-shaped magnet blocks with simple easy-axis rotation to essentially eliminate the regional de-magnetizations from the adjacent permanent magnet blocks. The DRAGON sextupole bore is of ID 134.5 mm that is large enough to support a stainless steel water-cooled plasma chamber of ID 126 mm, the same size as in SECRAL. This sextupole are made of N50M permanent magnets with an OD of 320 mm and a length of 526 mm.

Evaporative Medium Cooled Solenoids

A new cooling method, evaporative medium cooling at atmosphere pressure and at about 50 °C, may safely and cost effectively increase the coil excitation current density is explored in DRAGON. Typically the RT magnets are cooled with de-ionized pressured-water and it is very costly if the excitation current density reaching above 10 A/mm^2 and magnet power approaching a few hundreds kW. A proprietary evaporative cooling medium [6], developed by the Institute of Electric Engineering, CAS, has a few advantages over the conventional de-ionized pressured-water cooling. The DRAGON magnet coils are wound with solid copper conductors, instead of the normal hollow copper conductors, with adequate cooling channels. Just like the case of LHe cooling the superconducting magnets, the RT magnets are submerged in the cooling medium at atmosphere pressure without any pressure-resistant pipes/tubes and pressure-caused leaks. The high latent-heat-medium evaporates at about 50 °C and efficiently carries away the heat from the magnets. The maximum excitation current density for DRAGON is about 13 A/mm^2 and the magnet power reaches ~ 400 kW for the production of the maximum axial fields.

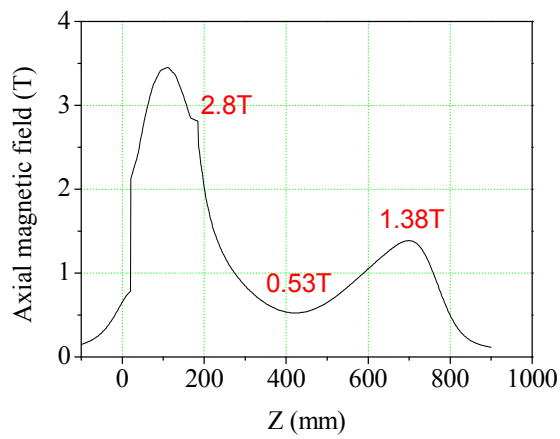

Figure 2: The axial field profile of DRAGON. With an iron plug field booster the maximum axial field reaches 2.7 T at the surface of the bias probe in the injection.

Higher Voltage Beam Extraction

So far the routine maximum ion-beam-extraction from the high-charge-state ECRISs is about 30 kV for the accelerators. However, there are applications where higher beam voltage is required and a practical solution is installing the ECRIS on a high-voltage (HV) platform. However a HV platform comes with many unfavourable consequences, such as higher cost and very inconvenient operations. Higher voltage ion beam extraction from ECRIS could eliminate or reduce the voltage requirement of an HV platform thus to lower the system cost with easier operations. As a study, DRAGON is thickly insulated with 10 mm thick materials so that higher voltage beam extraction can be explored. The goal is to achieve routine 50 kV beam extraction and hopefully to explore beam extraction up to 100 kV with a four-electrode (accel-accel-decel) beam extraction mechanism for better beam transport.

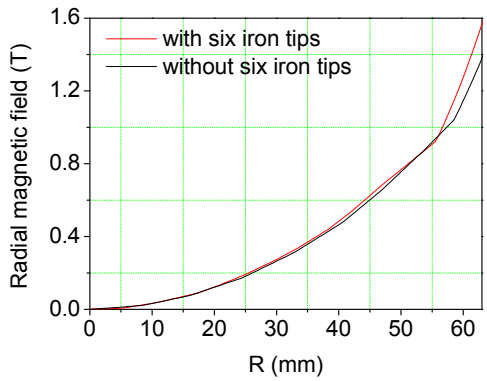

Figure 3: The DRAGON radial field reaches 1.4 and 1.5 T (red line), with six small iron tips embedded in the chamber cooling channels, at the plasma chamber inner surface of ID 126 mm.

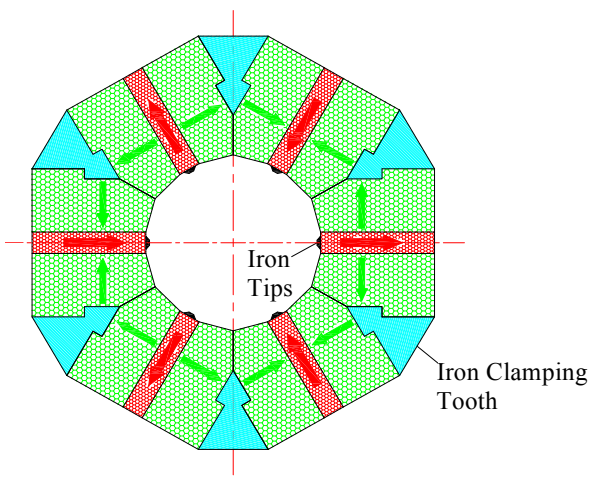

Figure 4: A cross-section view of the DRAGON's sextupole and its easy-axis orientation. There are six 10x2.5 mm^2 small iron tips embedded in the cooling channels to boost the field strength by about 0.1 T and the blue hatched regions are the iron clamping teeth.

DISCUSSIONS

As presented above, the overall parameters of DRAGON are very close to those of SECRAL operating at 18 GHz and the GTS as listed in Table 1. So it is reasonably to expect that DRAGON should be able to perform well at least compatible with the GTS. DRAGON can also operate at 14 GHz alone or double-frequency (14+18 GHz) heating with maximum wave power of about 3.5 kW of any one of the three operation modes. DRAGON is the first high-charge-state RT ECRIS that has been built with a plasma chamber of ID more than 100 mm. Its plasma chamber volume is 6 Litters that is quadrupled in comparison to GTS. This large difference could clearly evidence the effects of a large chamber to the ECRIS performance once DRAGON is being commissioned in about two years.

There is no mechanical pumping, at least in the early development, in the injection side of DRAGON for simplicity. Without the injection mechanical pumping, DRAGON may not be able to produce the highly-charged ion beams as SECRAL does, but hopefully compatible intense multiply-charged heavy ion beams, such as Xe^{27+}, Bi^{32+} and U^{33+}. In addition, the higher voltage beam extraction will help the heavy beam transport and decent beam intensities should be expected.

Table 1: Main Parameters of DRAGON, GTS and SECRAL operating at18 GHz

	DRAGON	GTS	SECRAL
Operating Frequency (GHz)	14. – 18	14 - 18	18
Resonance Length (mm)	14 GHz: 120 18 GHz: 135	14 GHz: 95 18 GHz: 145	105
Plasma Chamber (mm)	L: 480 ϕ: 126	L: 300 ϕ: 80	L: 420 ϕ: 126
Max. Axial Injection field (T)	2.7	2.5	2.5
Max. Chamber Radial field (T)	1.5	1.2	1.4

REFERENCES

[1] D. Hitz et al, NIM, B 205 (2003) 168.
[2] T. Thuillier et al, RSI, 77, 03A323 (2006).
[3] H.W. Zhao et al, RSI, 81, 02A202 (2010).
[4] K. Halbach, NIM, 187 (1981) 109.
[5] Z.Q. Xie and T. Antaya, "The PERMAG Code", Report MSUCL-622, Michigan State University, East Lansing, 1987.
[6] L. Ruan et al, "The comparison of cooling effect between evaporative cooling method and inner water cooling method for the large hydro generator", Proc. of ICEMS, p. 67 (2007).

TESTS OF THE VERSATILE ION SOURCE (VIS) FOR HIGH POWER PROTON BEAM PRODUCTION*

S. Gammino#, L. Celona, R. Miracoli, D. Mascali, G. Castro, G. Ciavola, INFN-LNS, Catania, Italy
F. Maimone, GSI, 64291 Darmstadt, Germany and Univ. of Catania, D.M.F.C.I, Catania, Italy
R. Gobin, O. Delferrière, G. Adroit, F. Senèe, CEA-Saclay, DSM/IRFU, Gif sur Yvette, France

Abstract

The sources adapted to beam production for high power proton accelerators must obey to the request of high brightness, stability and reliability. The Versatile Ion Source (VIS) is based on permanent magnets to produce an off-resonance microwave discharge (the maximum field value on the chamber axis is around 0.1 T). It operates up to 75 kV without a bulky high voltage platform, producing several tens of mA of proton beams and monocharged ions. The microwave injection system and the extraction electrodes geometry have been designed in order to optimize the beam brightness. Moreover, the VIS source ensures long time operations without maintenance and high reliability. A description of the main components and of the source performances is given in the following. A brief summary of the possible next developments is also presented, particularly for pulsed mode operations, that are relevant for some future projects (e.g. the European Spallation Source of Lund).

INTRODUCTION

The layout of the VIS source is reported in figure 1. The source body consists of a water-cooled copper plasma chamber (100 mm long and 90 mm diameter) surrounded by permanent magnets [1]. The plasma chamber is coupled with a 2.45 GHz magnetron through a microwave line that has been deeply studied with tools for high frequency structures simulations in order to optimize the impedance match, to maximize the electric field in the plasma chamber and to reduce the microwave losses in the 80 kV DC-break. [2,3].The magnetic system is composed by three NdFeB rings permanent magnets; the stainless steel separation rings and inner and outer iron components has been adapted to the production of an almost flat magnetic field profile along the whole plasma chamber. Moreover, the magnetic field quickly falls in the extraction region along the axis and off axis as for other sources [4], thus minimizing the stray field effect on the extracted beam as well as the Penning discharges in the first gap. The ionic component of the plasma produced in the chamber is then extracted by means of a four electrodes extraction system. It consists of a plasma electrode made of molybdenum at 65 kV voltage, two water cooled grounded electrodes and a 3.5 kV negatively biased screening electrode inserted between them to stop the secondary electrons due to residual gas ionization, backstreaming to the extraction area. The VIS extraction has been optimized to work around 40 mA and a theoretical value of 0.07 π mm mrad normalized emittance has been calculated, i.e. fulfilling the requirement of high brightness. The low energy beam transport line (LEBT) allows the beam analysis and it consists of a focusing solenoid, a four-sector diaphragm to measure the beam misalignments, a Direct-Current Current Transformer (DCCT), a 30° bending magnet and an insulated beam stop to measure the beam current. author should submit the PostScript and all of the source files (text and figures), to enable the paper to be reconstructed if there are processing difficulties.

The emittance has been measured by means of an emittance measurement unit (EMU) provided by the CEA/Saclay SILHI group described in detail in ref[5]. The EMU was not originally considered in the design of the LEBT of VIS, but with minor beam line changes it has been easily installed.

Figure 1: The VIS Source with the Emittance Measurement unit.

EMITTANCE MEASUREMENTS

The emittance measurements have been carried out for different positions of the permanent magnets to check the role of the fine magnetic field tuning on the beam. For each position (see fig.2) we investigated the emittance variation by changing the puller voltage, the microwave power and the gas pressure.

For the different operational parameters, the beam current ranges from 30 to 50 mA for an extraction voltage of 60 kV and an extraction aperture of 8 mm.

*Work supported by the 5th National committee of INFN and INFN Strategic Project NTA-HELIOS
#Gammino@lns.infn.it

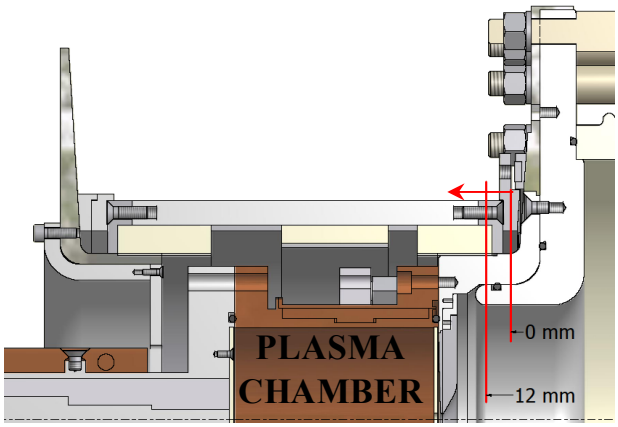

Figure 2: A cross section of the VIS body source: the permanent magnets assembly has been moved towards the injection side.

The figure 3 shows the comparison of the beam current for different magnetic settings and microwave power ranging from 600 to 1200 W.

Similar results have been observed for lower pressures but the peaks observed in the configurations 2÷4 mm are less pronounced.

An example of emittance measurements when the permanent magnets have been shifted toward the injection side of 8 mm is shown in figure 4.

Figure 5 shows the proton fraction against the microwave power measured when the permanent magnet are in the 4 mm configuration. It can be observed a value increasing continuously with the microwave power from 76 to 89 %. Moreover, by changing the permanent magnet position in step of two millimeters (i.e by slightly varying the magnetic induction on the extraction and injection sides) the proton fraction measured was always higher than 80 % for a RF power ranging from 0.4 to 1 kW.

In figure 6 the measurements carried out for different values of gas pressure are plotted with the permanent magnets in the 4 mm configuration. It can be observed that the beam divergence has the lowest values when the pressure (measured with a gauge mounted on the ground flange of the extraction column) is about $2.5 \cdot 10^{-5}$ mbar. Different values of extraction voltage have been used ranging from 55 to 65 kV: even at 55 kV the beam emittance was approximately 0.1 π mm mrad at 400 W.

During the tests we decided to not use the gas injection in the beam line to increase the space charge compensation, as observed for TRIPS [6], because the emittance values were already satisfactory at these current levels.

Figure 7 shows one of the worst emittance plot (ε_N=0.174 π mm mrad at 900 W) which presents the typical shape due to the solenoidal field aberrations. These asymmetries in the emittance have been observed mostly for large power.

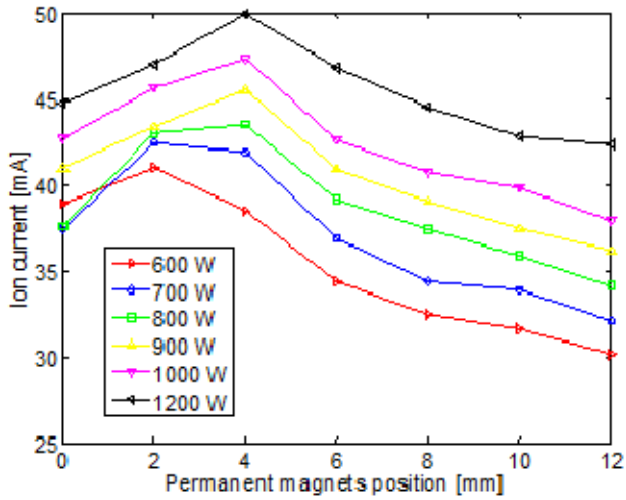

Figure 3:Total beam current vs. permanent magnets position for $P_{source}=2.3 \cdot 10^{-5}$ mbar and V_{ext}=60 kV.

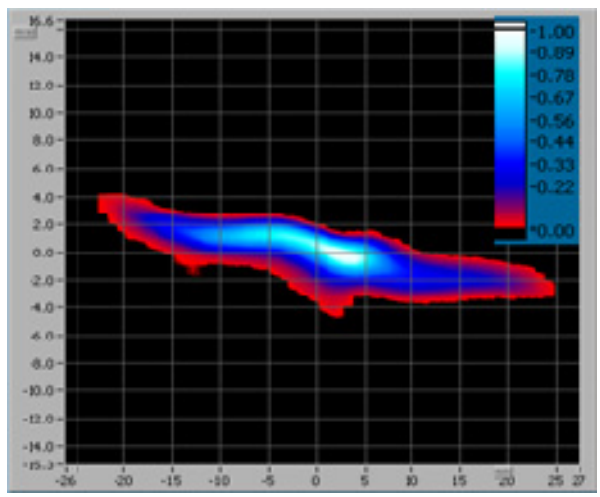

Figure 4: Beam emittance measurements ($P_{source}=2.3 \cdot 10^{-5}$ mbar, I=42 mA, ε_N=0.143 π mm mrad, P_{rf}= 1000 W and V_{ext}=60 kV).

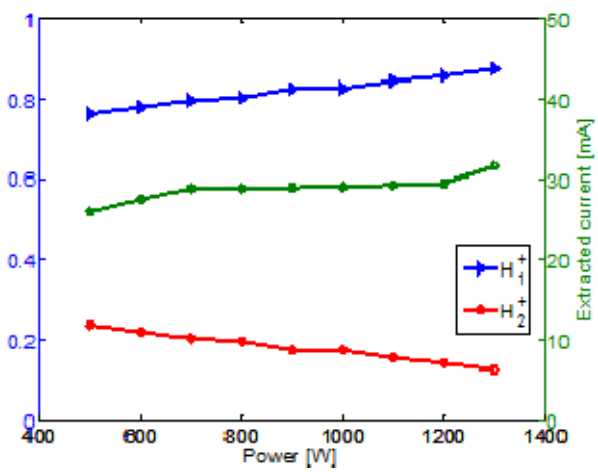

Figure 5: Proton fraction and extracted beam current vs microwave power for P_{source}=1.5•10-5 mbar.

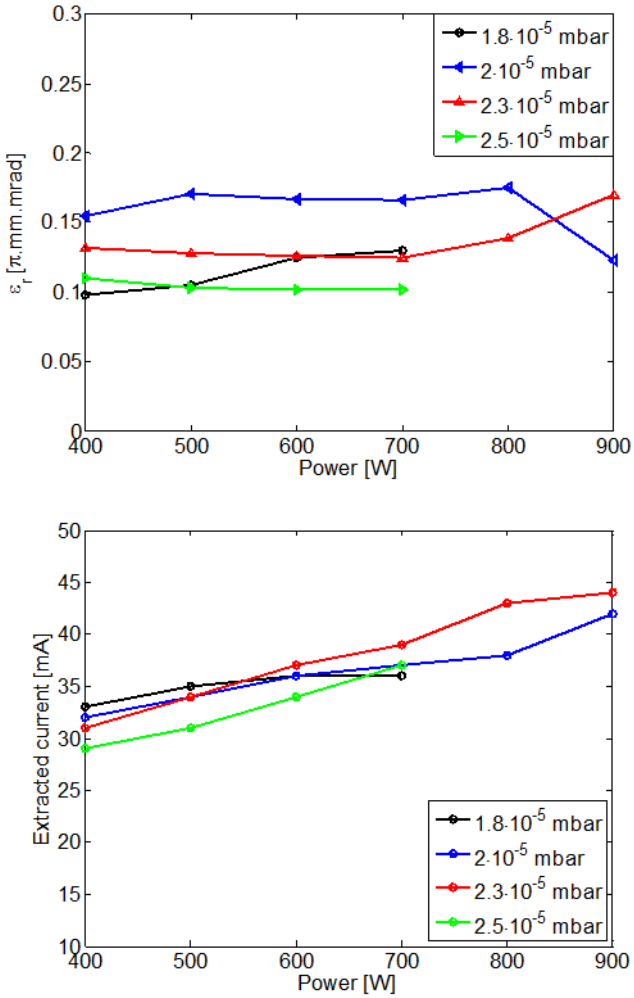

Figure 6: Variation of beam emittance at 60 kV for different pressure values (top). Extracted current at 60 kV for different pressure values (bottom).

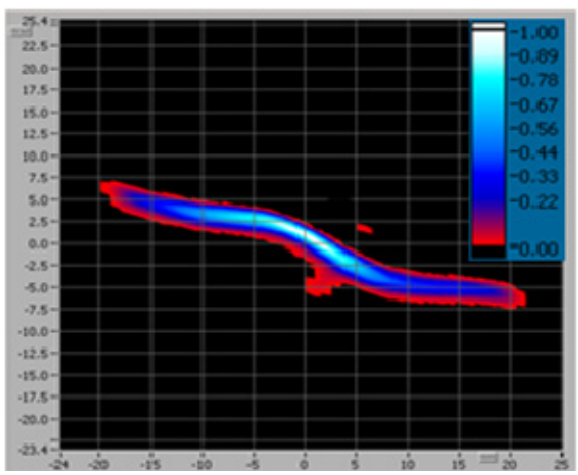

Figure 7: Proton beam emittance measured (P_{source}=2.3•10^{-5} mbar, I=42 mA, ε_N=0.174 π mm mrad, P_{rf}= 900 W).

PERSPECTIVES

The VIS source will be used in the next two years as a testbench for new techniques to improve the beam brightness, ranging from the use of different methods to couple the microwave power to the plasma, to the use of electron donors and of different methods to neutralize the space charge. A different scheme of plasma excitation will be also tried, according to the R&D developed at INFN-LNS in the frame of the NTA-HELIOS experiment. A particular emphasis will be given to the operations in pulsed mode, with the 4% duty cycle needed for the project of the Linac for the European Spallation Source (ESS) at Lund, Sweden, and to the limitation of the emittance growth which may occur in the LEBT.

Table 1: Main requirements of the beam for ESS.

Input	**Nominal**	**Upgrade**
Average beam power	5.0 MW	7.5 MW
Macro-pulse length	2.0 ms	2.0 ms
Pulse repetition rate	20 Hz	20 Hz
Proton kinetic energy	2.5 GeV	2.5 GeV
Peak coupler power	1.0 MW	1.0 MW
Beam loss rate	<1.0 W/m	<1.0 W/m
Output	**Nominal**	**Upgrade**
Duty factor	0.04	0.04
Average pulse current	50 mA	75 mA
Ion source current	60 mA	90 mA
Total linac length	418 m	418 m

ACKNOWLEDGEMENTS

The contribution of L. Allegra, N. Gambino and F. Chines is gratefully acknowledged.

REFERENCES

[1] F. Maimone et al, "JACoW, A Service to the Accelerator Community", EPAC'08, Genoa, June 2008, MOPC151, p. 430 (2008); http://www.JACoW.org.
[2] F. Maimone et al, Proc. of 23rd Symposium on Plasma Physics and Technology, Prague, Acta Tecnica CSAV 53 (2008) 333.
[3] L. Celona et al, Rev. Sci. Instrum. 71 (2000) 771.
[4] R. Gobin et al, Rev. Sci. Instrum. 77 (2006) 03B502.
[5] R. Gobin et al, Rev. Sci. Instrum. 75 (2004) 1414.
[6] L. Celona et al, Rev. Sci. Instrum. 75 (2004) 1423.

MONOBOB II : LATEST RESULTS OF MONOCHARGED IONS SOURCE FOR SPIRAL2 PROJECT

M. Dubois, P. Jardin, O. Bajeat, C. Barue, C. Canet, M. Dupuis, J.L. Flambard, R. Frigot, C. Leboucher, N.Lecesne, P. Lecomte, P. Leherissier, F. Lemagnen, L. Maunoury, B. Osmond, J.Y. Pacquet, A. Pichard
GANIL, bd Henri Becquerel, BP 55027, F-14076 Caen cedex 05, France

Abstract

Among the sources which can be installed in the radioactive ion production module of SPIRAL II, a singly-charged ECRIS has been chosen to produce ions from gaseous elements. Its characterization is under way on a test bench at GANIL. Extraction, transport and response time results are presented.

INTRODUCTION

In the frame of the SPIRAL II project [1] (Système de Production d'Ions Radioactifs Accélérés en Ligne phase II), four techniques of ion source (IS) have been chosen to cover a large range of radioactive ions, *i.e.* FEBIAD and LASER [2] IS's for condensable elements, surface IS [3] for alkalis, and ECRIS [4] for gaseous elements. These sources can be installed in a vacuum chamber named "production module" which contains mainly the radioactive element production target and the IS. To limit the transient time of the atom from the target to the IS, the source is installed very close to the target. In this hostile environment, a standard ECRIS including permanent magnets and non mineral insulators cannot withstand the radiation dose more than few days, what must be compared to the three months of continuous operation expected. Then the techniques and materials available to design the sources are limited and only singly-charged IS can be built. To reach the charge states required by the post accelerator CIME [5] the delivered beams are then injected in a charge-booster [6].

The most interesting isotopes are the shortest lived ones; unfortunately, their production yields in the target decreases with their half-lives, and their losses tends to increase during the atom-to-ion transformation process as their half-lives decrease. The efficiency of each step of the process, diffusion of the isotopes out of the target, effusion up to the IS, ionization and transport must then be as high as possible to make the most of the isotopes produced in the target. By difference with stable elements, the process must also be as fast as possible to limit the losses by radioactive decay.

In this paper, we report the measurements of the beam transport from the exit of the ECRIS up to the Faraday cup situated after a magnetic mass spectrometer, the emittance measurement and the measurement of the atom-to-ion transformation time in the ECRIS.

DESCRIPTION OF THE SETUP

For gases, the production module includes a carbon converter, a uranium carbide target with its oven, a transfer tube and an ECRIS (Fig. 1). A primary beam of deuterons impinges the carbon of a wheel in front of the UC target, producing a flux of neutrons which induces the fission of the uranium. As the target is maintained at 2000°C, the fission fragments diffuse out of target material, effuse up to the ECRIS via the transfer tube and are ionized in a time and with an efficiency depending on the tuning of the source and of the element.

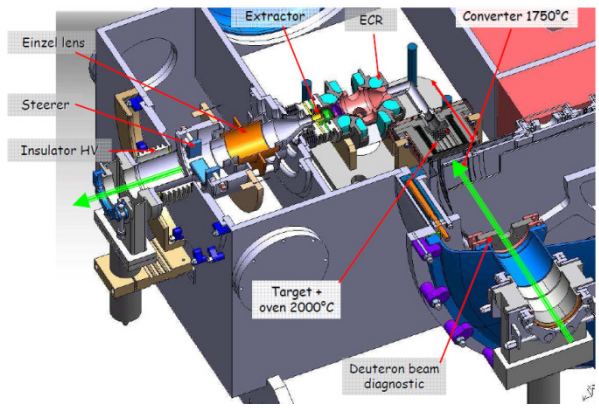

Figure 1 : Production module

The ions leave the IS trough the hole of the plasma electrode (7 mm in diameter) placed in front of the extraction electrode (14 mm in diameter, and with a tuneable position). The potential difference was maintained at 15 kV. After acceleration, the beam passes through an Einzel lens (with tuneable position), a magnetic mass analyser, an emittance meter (removable), before reaching a Faraday cup.

For safety reasons, in the frame of SPIRAL II operation, the TISS will be installed in a vacuum chamber where the pressure must be lower than 10^{-5} mbar after outgassing. During the present tests, the vacuum chamber reproduces these vacuum conditions, but the UC pills were replaced by carbon pills.

Two fast valves were installed on the TISS: one at the opposite of the plasma electrode hole to measure the response time of the source, and one on the target container, at the opposite of the aperture towards the IS to measure the contribution of the target to the response time of the TISS.

Fast valves were fed with a mixture of He, Ne, Ar, Kr, and Xe. Support gas was N_2, 0_2 being forbidden in case of carbon target at high temperature (max 1500°C).

TRANSPORT OPTIMISATION

The optimal distance between the extraction and plasma electrodes has been found equal to 31 mm. The transport of the beam from the exit of the ECRIS up to the Faraday cup has been estimated by comparing the total

current of the peaks present on the spectrum and the total current delivered by the ECRIS. The position of the lens and of its voltage were tuned to maximize the current of the N_2^+ beam in the Faraday cup, as this ion beam is the most abundant and then mainly govern the value of the transport (Fig. 2).

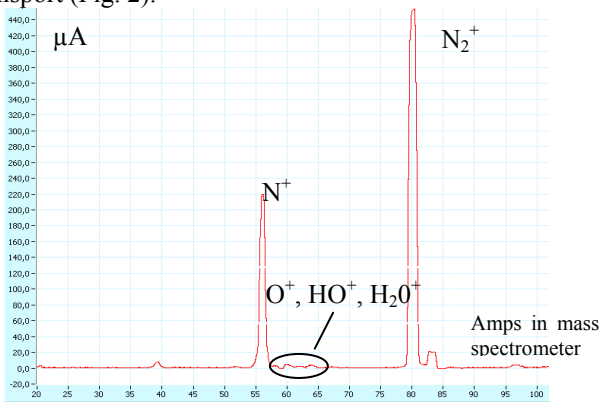

Figure 2: typical spectrum of the source after mass spectrometer after outgassing.

The total current delivered by the source was maintained between 640 µA and 810 µA, what is close to the maximum of this source. Once a transport close to 100% has been obtained, the emittance has been measured for Ar^+ (Fig. 3) and N_2^+ beams. More than 85% of the beam is included in an ellipse of 80 π.mm.mrad, which corresponds to the acceptance of the low energy beam line.

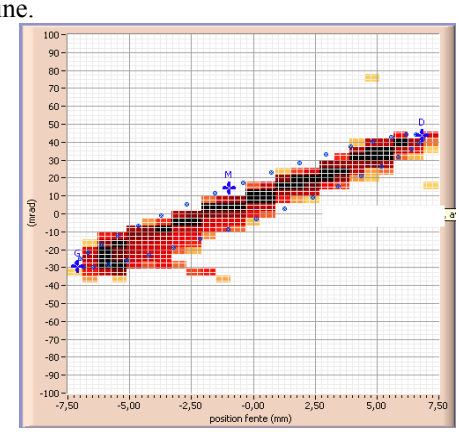

Figure 3: Emittance of the $^{40}Ar^+$ beam for a total current extracted from the source of 735 µA. The ellipse corresponds to the geometrical acceptance of the low energy beam line (80 π.mm.mrad).

This result should be improved by increasing the magnetic field of the ECRIS in the extraction region. During the tests, this magnetic field was not optimum owing to a limitation of the power supplies, and will be improved during the next tests. The emittance of the ECRIS being considered as the most important among the IS chosen, all the beams extracted from these ISs should be easily transported in a 80 π.mm.mrad beam line.

RESPONSE TIME

The source was fed with N_2 and ~50 W of RF power (less than 5 W of reflected power) to reach a total current between 640 µA and 810 µA at the exit of the source. Gas pulses of ~1.4 ms long were injected in the source, containing natural He, Ne, Ar, Kr and ^{129}Xe (Fig.4). The magnitude of the electrical pulses controlling the aperture of the valve was tuned to limit the perturbation to value lower than 5 µA induced on the plasma and thus on the total current. The ion beam of interest was selected with the spectrometer and the shape of the ion pulses was recorded on the Faraday cup. The intensities of the ion pulses being of the order of 10 nA, several pulses were added to increase the statistic. To reject the 50 Hz noise, the repetition period of the pulses was different from a multiple of 20 ms.

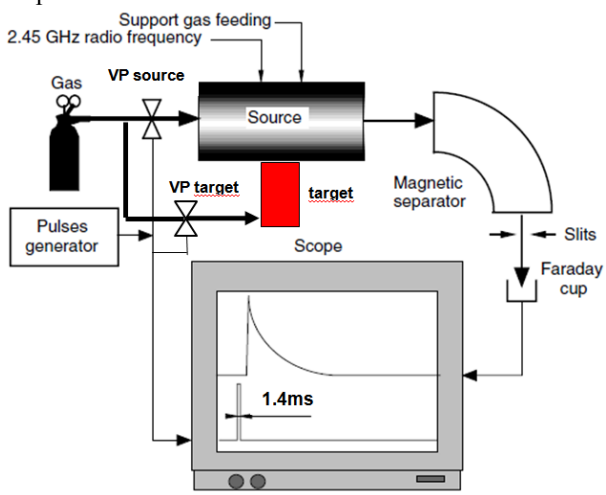

Figure 4 : Set up scheme

During the following measurements, the temperature of the target was equal to 1000 K. Owing to two half discs placed in the transfer tube, the target and the ECR plasma were not in direct regard. This TISS being dedicated to the production of isotopes of noble gases, this chicane stops the direct effusion of condensable element from the target to the source.

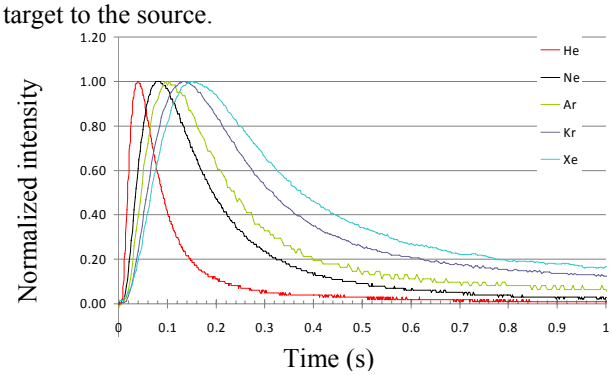

Figure 5: Time responses (s) of the TISS for He, Ne, Ar, Kr and Xe injected through the target. The target was the largest one, including 19 cylinders of 80 carbon pills each.

We recorded the response time of the atom-to-ion transformation for different gases in the same working

conditions of the source, as gases were simultaneously injected (Fig. 5). The response time increases with the mass of the gas.

This effect is mainly attributed to the effusion of the atom in the whole cavity of the TISS, and should then depend on the square root of the mass of the element considered

If the time scale of each response is compressed according to the ratio $\sqrt{M_{He}/M_X}$ (where M_X corresponds to the mass of the gas X and M_{He} is the mass of He), the different responses should be identical if only effusion governed the time responses. In fact, within this compressed scale representation, the time response decreases with the mass of the element (Fig. 6).

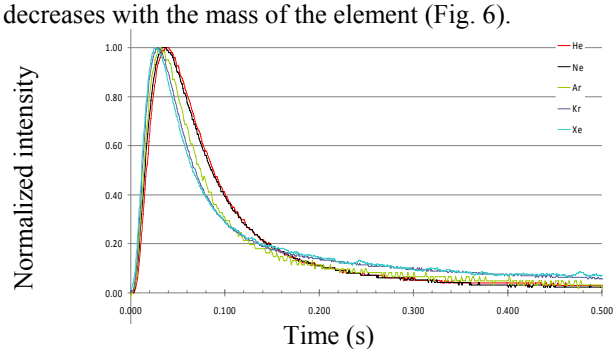

Figure 6: time responses of the TISS after time scale transformation. Injection has by the target (VP target).

To understand it, measurements were performed with injection of gas directly in the source (VP source). After time scale transformation (Fig.7), the result show is due to the first ionization potential which decreases with the mass and leads to ionization rates higher for heavier elements. In case of radioactive isotopes, this observation is of first interest since the global atom-to-ion transformation process of heavier elements will be shortened by ionization efficiency, increasing the ion production rate.

The contribution of this effect to the reduction of the global response time is relatively small (some tens or hundreds of ms) compared to the effusion time of the isotopes out of the target labyrinth (Fig. 5). But in case of short lived isotopes, the size of the target could be reduced to limit the inner-target effusion time.

TECHNICAL FEEDBACK

The TISS has been designed to withstand the dose around the UC target. Materials are only non-magnetic metals and mineral insulators. The TISS being installed under vacuum, the mechanical precision between the parts is sufficient to insure the tightness.

After several weeks of operation with a carbon target in its vicinity, the ECRIS still works but the total operation time has not been precisely measured. A layer of carbon appears on the wall of the plasma chamber but its thickness must be very low since the color of the wall metal is still visible. The carbon deposition is an important concern especially for RF window: if covered by carbon, the RF power will be reflected, and the window will be destroyed by temperature increase.

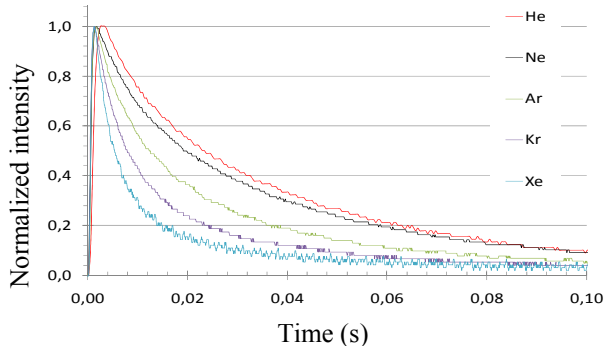

Figure 7: Time responses of the source for He, Ne, Ar, Kr and Xe in the same plasma conditions, after time scale transformation. Injection of gas in the source (VP source).

The carbon in the ECRIS comes from the target and its oven, which includes several parts in graphite. When the target is at high temperature, the carbon reacts with oxygen coming from the outgassing and is transported up to the source as CO or CO2 molecules, which are present in the source spectrum (Fig. 2, right part).

When the outgassing is less important, the presence of oxygen decreases and the carbon disappears from the spectrum. The system has then to be well outgassed before operation to avoid carbon concerns.

REFERENCES

[1] M. Lewitowicz, 'The SPIRAL 2 Project', Nuclear Physics A, Volume 805, Issues 1-4, 2008

[2] N.Lecesne et al., 'GISELE: A resonant ionization laser ion source for the production of radioactive ions at GANIL', Rev. Sci. Instrum. 81, 02A910 (2010)

[3] A. Pichard at al., 'Development of a surface ionization source for the SPIRAL 2 project', Rev. Sci. Instrum. 81, 02A908 (2010)

[4] C. Huet-Equilbec et al., 'MONOBOB: A radiation-hard and efficient 2.45-GHz ECRIS dedicated to radioactive ion production', Nucl. Instr. and Meth. in Phys. Res. B 240 (2005) 752–761

[5] Cime Working Diagram, 'http://pro.ganil-spiral2.eu/users-guide/accelerators/spiral-beams'

[6] T. Lamy et al., 'Charge breeding method results with the phoenix booster ECR ion source', Proceedings of EPAC 2002, Paris, France

THE DESIGN OF 28 GHZ ECR ION SOURCE FOR THE COMPACT LINEAR ACCELERATOR IN KOREA

B. S. Lee#, M. Won, Korea Basic Science Institute, Busan, Republic of Korea

Abstract

The construction of a compact linear accelerator is in progress by Korea Basic Science Institute. The main capability of this facility is the production of multiply ionized metal clusters and the generation more intense beams of highly charged ions for material, medical and nuclear physical research. To produce the intense beam of highly charged ions, we will construct an Electron Cyclotron Resonance Ion Source (ECRIS) using 28 GHz micrewaves. For this ECRIS, The design of a superconducting magnet, microwave inlet, beam extraction and plasma chamber was completed. Also we are constructing a superconducing magnet system. In this presentation, we will report the current status of development of our 28GHz ECRIS.

Paper not received

bslee@kbsi.re.kr

THE DESIGN STUDY OF SUPERCONDUCTING MAGNET SYSTEM FOR AN ADVANCED ECR ION SOURCE*

M. Won#, B. S. Lee, Korea Basic Science Institute, Busan, Republic of Korea

Abstract

The Korea Basic Science Institute is developing a superconducting magnet system for 28 GHz Electron Cyclotron Resonance Ion Source (ECRIS). We are investigating in order to realize compact size, economic operation and generation of high current beam. Although companies and researchers have valuable experience, skill and ability in designing of superconducting magnet for ECRIS, they did not exactly proposed a excellent superconducting magnet system for ECRIS because many superconducting magnets were not required. Of course they do if we required many magnets for the various applications of ECRIS. In this presentation, we have filed reports of former researcher and we have discussed the realization of ECRIS over 35 GHz.

*Work was supported by KBSI grant D30300
mswon@kbsi.re.kr

A LOW POWER SURVEY OF RADIAL-OFFSET AXIAL SPUTTERING AND HIGH INTENSITY URANIUM PRODUCTION FROM AXIAL SPUTTERING IN SUSI*

D. Cole, G. Machicoane, T. Ropponen, L. Sun, and L. Tobos, National Superconducting Cyclotron Laboratory, Michigan State University, East Lansing, MI 48824, USA.

Abstract

Results of a low power survey of axial sputtering, to test sputtering efficiency at incremental radial offsets from on axis position, is reported. Also, prototype axial sputtering hardware has been tested in the SuSI ion source and the uranium ion production results is discussed.

INTRODUCTION

The National Superconducting Cyclotron Laboratory (NSCL) depends on each of its ECR ion sources for production of all required primary beams found on the Coupled Cyclotron Facility user beam list. A schedule of beam development for the SuSI ECRIS [1], supporting the NSCL experimental program since Fall 2009, is ongoing. Parallel efforts toward development of Uranium beams from SuSI are being pursued at this time. The process of producing uranium beams from axial sputtering has been investigated and is being developed.

The SuSI plasma chamber injection baffle is 100mm in diameter and therefore has limited area for installation of RF waveguides, gas port, biased disk, and RF inductive oven or resistive oven assemblies. The need to install a sputter target, for possible uranium beam development, on an already congested surface led to the question of where a sputter target must be located. Intuitively, the sputter surface would seem to be best on the plasma chamber axis, but the possibility of sputtering at positions radially offset from the axis and the relative sputter efficiency at such positions was unknown.

In December of 2009 a simple survey of relative sputter efficiency of radially off-axis sputter target positions and at increasing axial insertion toward the plasma was done. Based on the results, a prototype on axis sputter assembly was built, tested and is presented in this paper.

LOW POWER SURVEY OF SPUTTER TARGET POSITION

In December of 2009 a survey of radial offset sputtering was performed, The survey was done at very low RF power (500W) due to the sample not being cooled and the risk of X-ray damage to the plasma chamber insulation, which had not at that time been upgraded to tantalum shielding and PEEK insulation [2]. Considering the uranium target geometry, sputtering on the side of a cylindrical surface, was expected to be very inefficient. The sputter target was swept through an arc into the radial loss line and finally to the on axis position (see Fig. 1).

*Work supported by National Science Foundation under grant PHY-0606007

Measurements of uranium production intensities were made at radial positions of 0mm, 9mm, 18mm, 27.5mm and completely away from plasma interaction. The injection baffle was generally located on the injection field maximum. At each radial offset position the sample sputter surface was initially 10mm from the injection baffle surface and then moved longitudinally toward the plasma by increments of 5mm. The sputter target was biased over a limited range of 0 to -2kV.

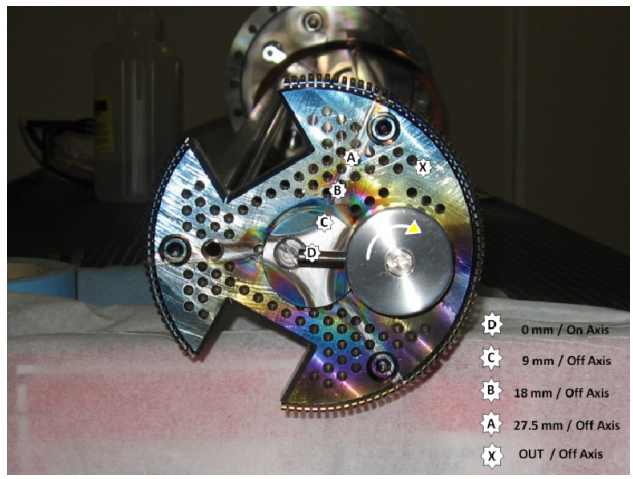

Figure 1: Low Power Radial-Offset Sputter Survey Hardware.

In addition to the survey, a small uranium sample with a diameter of 5 mm was mounted on axis and inline with the plasma chamber axis. It was positioned longitudinally 25mm above the injection baffle surface (toward the plasma). The baffle was located at the injection field maximum. A low power survey of sputter efficiency was done moving the sample into the plasma chamber in 5mm increments. Additionally, an assortment of support gases was tried.

Results of Survey

Results of the survey are shown in figure 2. It was clear that the Uranium sputter production yield is highest on the axis of the plasma loss cone, (0 mm radial offset). Sputter production does occur along the radial loss line with a sputter efficiency that is remarkably uniform from 9mm to 27.5 mm radius. In general the sputter yield increased with axial insertion of the sample from 0 – 15 mm and with target bias voltage from -1 kV to -2kV.

Sputter yield increased with heavier mass support gases, with oxygen and neon being reasonable choices for middle to high uranium charge states. Argon sputters very efficiently, but being a poor mixing gas drives the charge

state distribution toward lower charge states with robust sputtering.

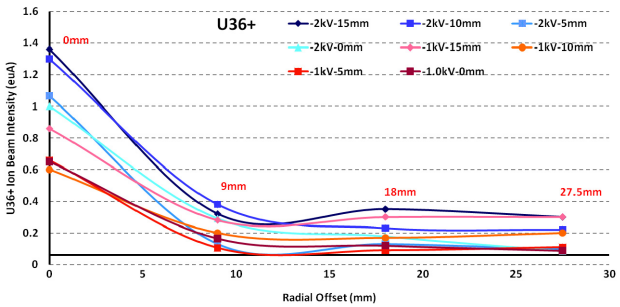

Figure 2: Uranium Sputter Yield Using ^{16}O Support Gas with Radial and Axial offset at -1kV and -2kV bias.

Based on this survey, a prototype sputter assembly was built utilizing a larger diameter and water cooled uranium target. The target was mounted on axis with a longitudinal adjustment of 50mm and bias voltage range of 0 to -5kV. An assortment of support gases and mixtures of support gases would be evaluated.

SuSI URANIUM BEAM PRODUCTION FROM ON AXIS SPUTTERING

In June 2010 the first attempt was made to sputter uranium axially and at higher power in the SuSI ECRIS to meet the Coupled Cyclotron Facility primary beam list requirements at NSCL. The prototype sputter hardware consisted of a water cooled 10 mm diameter and 15 mm long depleted uranium target mounted inline with the plasma chamber axis (see Fig. 3). The injection baffle is adjustable through a range of +/- 50mm around the injection field maximum; generally the baffle was left very near the injection field maximum. The sputter target surface was located 2 mm above the injection baffle surface toward the plasma. The sputter target could be inserted up to 50mm further toward the plasma relative to the baffle position.

Because the on axis location of the sputter target displaced the biased disk, the bias disk was replaced with a biased ring with internal diameter of 19 mm allowing the sputter target to travel through the ring (see photo). The uranium sputter target could be biased from 0 to -5kV and the biased ring could be biased from 0 to -2kV. It should be noted that the biased ring worked well, however the bias voltage required for the ring to perform as well as the original disk was about a factor of ten higher or -700 to -1000 V. Additionally, the biased ring ceased having an effect on beam intensity when the sputter target bias reached about -4kV.

The sputter production was evaluated changing target axial position, bias voltage, and support gases while tuning the source field and RF power to optimize performance and stability. Performance was measured primarily by the intensity of U^{33+} at the end of the SuSI collimation channel. During the uranium development, the transport efficiency of beam produced by SuSI through the collimation channel using 10mm - 12mm slits was about 50% due to efforts to obtain best resolution of charge states. Beams were developed using various support gases alone and in combination.

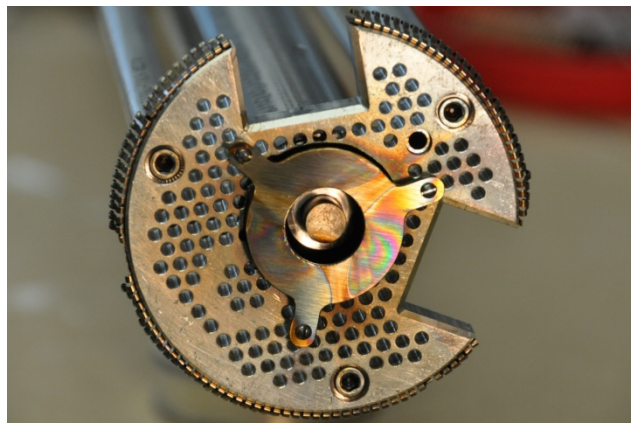

Figure 3: High Power Axial Sputter Hardware.

Results of Initial High Power Test

Low intensity uranium ion production, on the order of 20euA of U^{33+}, began immediately without the target being biased. This can be explained by considering that there is enough target interaction with the normal flow of ions leaving the plasma on axis through the loss cone to initiate sputtering. Beam intensity increased greatly with increased target bias voltage. While generally, sputter yield increases with insertion of the target toward the plasma, the sputtering was so robust at higher power and voltage that the best axial position was the starting position of 2 mm above the injection baffle and toward the plasma. Biased ring and biased target voltages were adjusted together producing increasing intensity until the target bias reached -4kV and the ring bias, no longer helping, was reduced to less than -100V.

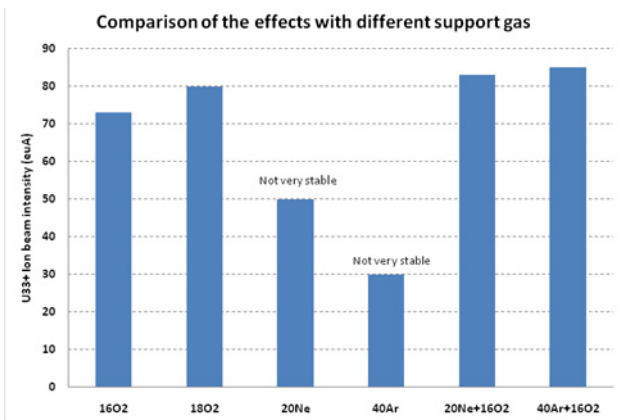

Figure 4: Uranium Sputter Yield Using Various Support Gases and Combinations.

Beam production increased with RF power and was ultimately limited by maximum power available at the time of 2.5 kW with a maximum drain current of about 5mA. Gas mixing advantage was gained using oxygen but best sputter efficiency required gases with higher mass, as illustrated in Fig. 4, for the production of U33+. It appears

that the best performance for higher charge state uranium production used a combination of ^{16}O and ^{20}Ne (see Fig. 5), while best performance for lower charge states ,< 34+, was achieved with a combination of ^{16}O and ^{40}Ar.

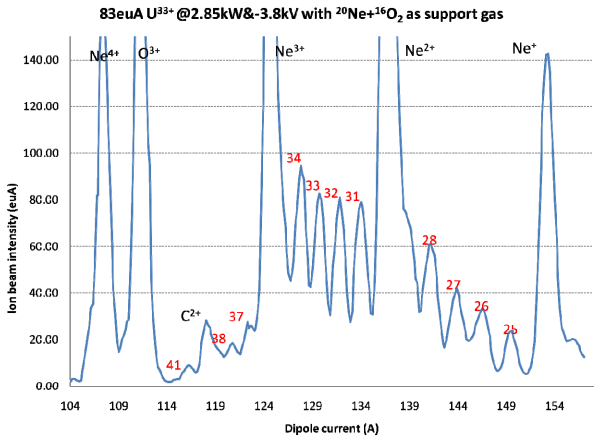

Figure 5: Higher Uranium Charge State Distribution Sputtering With Neon and Oxygen.

The sputter pattern on the surface of the sputter target shows that the effective interaction area is greater than the 10 mm diameter of the target. Also, the sample was misaligned 1 mm radially resulting in significant loss of sputtered material available to the plasma. Uranium production averaged 30 euA over 105 hours and consumed 211 mg or 2mg / hr.

Further development, scheduled Fall 2010, will include a redesign of the sputter equipment to allow the target to be withdrawn at least 25mm behind the injection baffle, increase the target size to 25mm diameter, and increase RF power capability beyond 3kW.

REFERENCES

[1] P. A. Zavodszky et al, Proc. 17th Int. Workshop on ECR Ion Sources and Their Applications (2006, Lanszhou, China)

[2] L. T. Sun et al, Proc. 21st Int. Workshop on ECR Ion Sources and Their Applications (2010, Grenoble, France)

TESTS OF A NEW AXIAL SPUTTERING TECHNIQUE IN AN ECRIS*

R. Scott#, R. Pardo, R. Vondrasek, Argonne National Laboratory, Argonne, IL 60439, U.S.A.

Abstract

Axial and radial sputtering techniques have been used over the years to create beams from an ECRIS at multiple accelerator facilities. Operational experience has shown greater beam production when using the radial sputtering method versus axial sputtering. At Argonne National Laboratory, previous work with radial sputtering has demonstrated that the position of the sputter sample relative to the plasma chamber wall influences sample drain current, beam production and charge state distribution. The possibility of the chamber wall acting as a ground plane which influences the sputtering of material has been considered, and an attempt has been made to mimic this possible ground plane effect with a coaxial sample introduced from the injection end. Results of these tests will be shown as well as comparisons of outputs using the two methods.

INTRODUCTION

There are two Electron Cyclotron Resonance Ion Sources (ECRIS) in operation at the ATLAS facility at Argonne National Laboratory. The ECR charge breeder (ECRCB) has been dedicated primarily for charge breeding development and production as the Californium Rare Ion Beam Upgrade CARIBU comes online. ECR2 has become the primary stable beam producer at ATLAS using a variety of techniques including gas injection, oven, and sputtering. Sputtering was developed at Argonne [1] and has been used often on both sources. ECR2 is an evolved version of an AECR-U [2] type ECRIS. While radial sputtering has been heavily used, axial sputtering has not been characterized on this specific source. A new co-axial sputtering technique has been tested and compared with radial and axial methods in hopes of better understanding this form of metal ion production. The characterizations obtained could also be useful for final development of the Actinide Accelerator Mass Spectroscopy project [3].

SPUTTERING TECHNIQUES

Three sputtering methods were used during the course of this evaluation. Efforts were made to provide consistency of measurements. The same negative bias power supply was used for all tests for repeatable voltage and current measurements. Single frequency (~14GHz) RF inputs at prescribed power levels as well as similar source bake out conditions were maintained. Oxygen was used for support with no additional gas mixing. The injection side bias disk was grounded to eliminate another variable. Standard radial, standard "bare" axial, and axial with grounded sleeve techniques are described next.

*Work supported by the U.S. Department of Energy Office of Nuclear Physics, under contract No. DE-AC02-06-CH11357

#rscott@phy.anl.gov

Standard Radial

This method is the preferred for sputtering at ATLAS. ECR2 has a generous radial port to allow up to a 5mm diameter sample to be inserted. The sample is inserted through an air-lock/insulator assembly toward the plasma into a pumping port that exists in a gap between the hexapole bars (see Fig. 1 below).

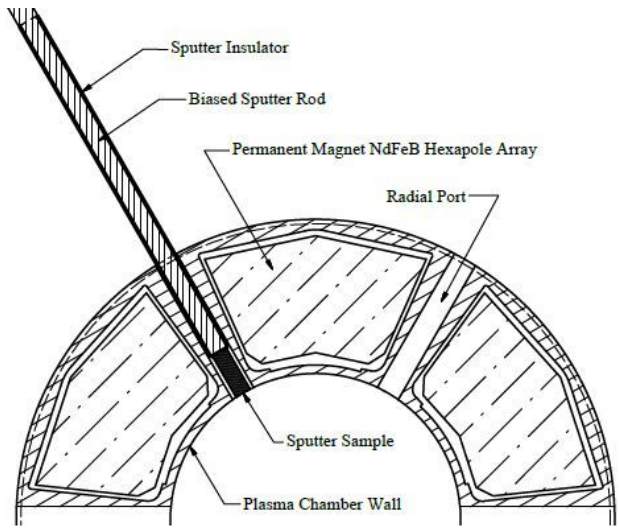

Figure 1: Section view of standard radial sputtering.

Typical gaps between the port wall and the sample are between 0.25 mm and 1.25 mm. Through previous experimentation with ECR2 the ideal location for sputtering has been found where the face of the sample is even with the plasma chamber wall. This location was chosen for our tests. Beam current and consumption rate measurements as well as radial sputtering parameters were used as a comparison to the 2 axial methods.

Standard Axial

Although radial sputtering is preferred, it cannot always be used. The use of radial ports spreads the magnet bars apart increasing the plasma chamber bore and weakening the hexapole magnetic confinement. Many groups omit this gap (and port) for this reason. Also, fundamental design constraints for all-permanent magnet ECRIS and 3rd and 4th generation superconducting ECRIS do not allow for radial ports. In these cases sputtering is only allowable axially.

Typically a sample is attached to a biased rod and inserted into the plasma chamber injection end (see Fig. 2). A location with an existing hole in the shaping plug was chosen. It is offset 2.2 cm from the centerline of the plasma chamber and in between the magnetic loss lines, evidenced by the plasma star on the biased disk, which

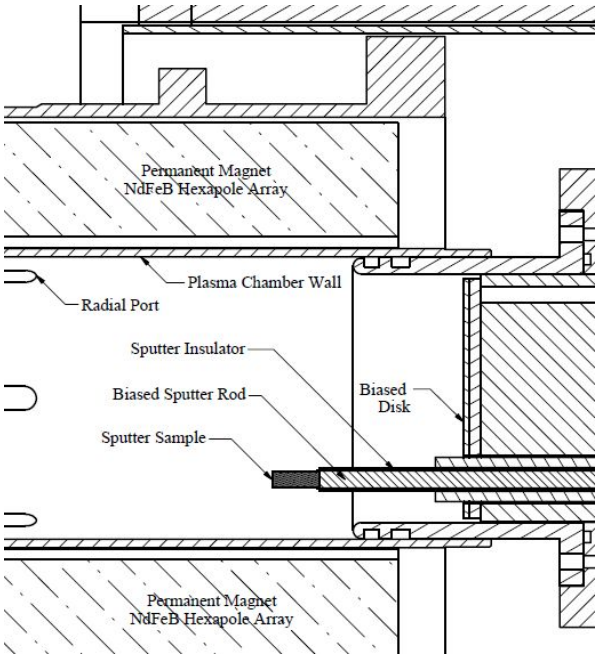

Figure 2: Standard axial sputtering.

helps minimize the effect of plasma heating on the sample.

The rod was attached to an available 5 cm travel linear motion feed-thru (LMFT) as the ideal location for sputtering was unknown. In this case the full sputter sample is exposed in the plasma chamber as well as the floating AlO_2 insulator. Others have used no insulator, leaving the biased rod of material other than that of interest exposed in the plasma chamber.

Axial with Grounded Sleeve

This modified axial method uses the same technique described above with biased rod, sputter insulator and attached sample. The assembly was placed co-axially inside a sleeve (grounded to the plasma chamber) which travelled with the sample. The face of the sample is even with the face of the ground sleeve (see Fig. 3). The assembly was inserted with the LMFT. In these tests the same axial insertion point was used as well as distances travelled into the plasma chamber by the assembly. The gap between the sputter sample and the ground sleeve was equal to that of the radial sample to port wall gap for each material used. Two sleeves were fabricated of 6061 Al, which is the same material as the plasma chamber wall. One is oval shaped at the tip to more closely replicate conditions at the radial port where only two points are closest to the sample. This sleeve was used with a large diameter Ag sample. The 2nd sleeve has a round opening at the tip and was used with the smaller diameter Ti sample. For all instances using this method, $^{27}Al^{7+}$ production (possibly attributable to the sleeve) never exceeded 50% more than the corresponding bare axial case.

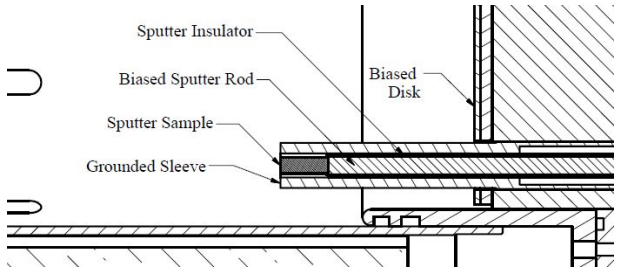

Figure 3: Axial sputtering with ground sleeve.

BEAM TESTS

Ideal Axial Position

It has been shown that beam current with axial sputtering varies with position relative to the plasma and with solenoid current [4]. Position vs. beam current was first plotted for $^{107}Ag^{21+}$. Initial position chosen was flush with the bias disk for both standard axial and axial with ground sleeve. The step size used was 1.2 mm when farther from the plasma and 0.3 mm when closer to the plasma. At each position the source was tuned using gas, solenoids and RF power. Both standard and sleeve cases measured maximum beam current at the farthest travel of 5.2 cm from the bias disk. This suggests the optimal location is likely closer to the plasma than the LMFT was able to travel. For Ti, adjustments were made within the limitation of the already fabricated ground sleeve to start travel at 1 cm past the bias disk and end 6.2 cm past the disk. Using the same sequence, optimal position for $^{48}Ti^{13+}$ was found to be at full travel suggesting that the true ideal location is closer to the plasma than could be measured. Sputter bias was removed at optimal locations resulting in immediate beam current drops of up to 50% with gradual declines thereafter as wall recycling tapered. This was done to insure that the major component of the beam output was due to sputtering and not plasma heating. All further data was taken at the closest location allowed by the existing apparatus.

Sputtering with Silver

Silver was chosen for its refractory properties, ease of sputtering and low number of stable isotopes creating a simple charge state distribution. In all cases the ECRIS was tuned for the intermediate charge state of 21+. Axial w/sleeve and standard axial were tested successively. Maximum outputs after a few days of conditioning were 18.1 μA for axial w/sleeve and 18.8 μA for standard axial. Maxima were achieved at the same RF power and in this case solenoid settings. Sputter voltage was then decreased to achieve 18.1 μA for standard axial for comparison. The sputter bias power was ~3X higher and the sputter drain current was ~4X higher for the bare sample vs. the sample with the grounded sleeve (see Table 1). The charge state distribution (C.S.D) was shifted slightly higher for the ground sleeve case. Maximum measured output for radial was 27 μA. The sputter voltage was not pushed further for fear of melting the

Table 1: Summary of Silver Production

Technique	use rate (mg/hr)	107/21+ (μA)	sputter V (kV)	sputter I (mA)	sp pwr P (W)	14 GHz (W)	ext I (mA)	sol. 1 I (A)	sol. 2 I (A)	V1(Torr)
Radial	1.7	18.3	0.58	0.43	0.25	280	1.91	528	519	1.80E-07
Axial w/sleeve	---	18.1	3.7	0.1	0.37	245	1.45	495	490	2.10E-07
Axial bare	4.2	18.1	2.7	0.46	1.24	249	1.5	494	490	1.90E-07

Table 2: Summary of Titanium Production

Technique	use rate (mg/hr)	48/13+ (μA)	sputter V (kV)	sputter I (mA)	sp pwr P (W)	14 GHz (W)	ext I (mA)	sol. 1 I (A)	sol. 2 I (A)	V1(Torr)
Radial	0.03	2.2	0.51	0.46	0.23	350	2	501	514	2.70E-07
Axial w/sleeve	.22	2.2	6.5	0.55	3.58	352	2.5	455	476	2.30E-07
Axial bare	0.81	2.2	3.1	1.1	3.41	350	1.8	522	483	2.20E-07

sample. Radial sputtering gave a much lower C.S.D. and required more RF power to achieve 18.3 μA compared to the two axial methods above.

Sputtering with Titanium

Titanium was chosen as a contrast to silver. It is more difficult to produce at high beam currents. It's C.S.D. slightly overlaps that of silver which was tested beforehand, so the most abundant isotope at lowest charge state without conflict $^{48}Ti^{13+}$ was chosen for these tests. Axial w/sleeve, standard axial and radial methods were tested successively. Maximum outputs after a few days of conditioning were 2.2 μA for axial w/sleeve, 5 μA for standard axial and 16 μA for radial. At an averaged 1 μA output for all methods, consumption rate was highest for standard axial, followed by ~4 times less for axial w/sleeve. Radial sputtering consumed another ~ 7 times less than axial with sleeve. Sputter current and power vs. consumption rate did not trend perfectly but there is believed to be some relation between the three (Table 2). Preliminary emittance measurements show a more divergent beam for standard axial vs radial. This could be from the exposed biased sample and insulator disrupting the plasma. Normalized (x,y) in mm mrad were (.094,.149) for axial vs. (.057,.090) for radial. Scheduling conflicts prohibited emittance measurement of axial with ground sleeve. It is hoped that all of these measurements can be done in more depth in the future.

REMARKS

The ground plane effect proposed cannot significantly be proven from these efforts. There is a definite difference between some of the operating parameters of the standard sputter and the sputter with grounded sleeve techniques. Consumption rates and drain currents are significantly different for the two methods. It may be that the radial technique helps to shield the majority of the sample and the ungrounded "floating" insulator from the plasma allowing sputtering from a finite surface. Use of a grounded co-axial sleeve may help to replicate this aspect of radial sputtering.

Maximum silver output was similar between standard axial and axial w/sleeve. For titanium, maximum output was double for standard axial compared to axial w/sleeve. Either the sample material or the type of sleeve (oval tip for silver and round tip for titanium) could have influenced these results.

Higher sputter voltages are observed for all axial vs. all radial results. This may be due to the further location from the plasma of the axial samples. It was observed that as the LMFT was retracted, beam current could be restored by increasing sputter voltage.

If allowable, future plans are to bring samples closer to the ECR resonance zone and to water cool the ground sleeve.

REFERENCES

[1] Harkewicz R, Billquist P, Greene J, Nolen J, Pardo R, Rev Sci Instrum., 1995, **66**: 2883

[2] Vondrasek R, Scott R, Pardo R, "Magnetic Field Upgrade of Argonne National Laboratory 14 GHz ECR Ion Source", Proceedings of the 10th International Conference on Ion Sources, Rev. Sci. Instrum., 2004, **75**: 1532

[3] Pardo R, Vondrasek R, Scott R, Kondev F, Palchan T, Kondrashev S, Paul M, Collon P, Youinou G, Salvatores M, Palmotti G, Mcgrath C, Imel G, "Plans for Laser Ablation of Actinides into an ECRIS for Accelerator Mass Spectroscopy", These Proceedings.

[4] Gaelens M, Loiselet M, Ryckewaert G, Proceedings of the 9th International Conference on Ion Sources, Rev. Sci. Instrum., 2002 **73 (2):** 714

FIRST A/Q=3 BEAMS OF PHOENIX V2 ON THE HEAVY IONS LOW ENERGY BEAM TRANSPORT LINE OF SPIRAL2

C. Peaucelle#, CNRS-IN2P3, IPN Lyon, France
J. Angot, P. Grandemange, T. Lamy, T. Thuillier, CNRS-IN2P3, LPSC Grenoble, France
J-L Biarrotte, CNRS-IN2P3, IPN Orsay, France
D. Uriot, CEA Saclay, SACM France.

Abstract

The heavy ions low energy beam transport line (LEBT) of Spiral2 built at LPSC Grenoble is fully operational since the beginning of 2010. This LEBT has been calculated and designed to hold permanently 15 mA of multi charged ions extracted from the source at 60 kV extraction high voltage. The LEBT is shortly described. The PHOENIX V2 ECRIS is presently installed on the LEBT and first beam tests results are reported. A daily reliable beam of 1 mAe of O6+ beam at 45 kV has been obtained with a high LEBT transmission efficiency of 90. Preliminary Argon tuning shows a reproducible beam of 130 µA of Ar12+ beam. Improved currents are expected in the future. Associated emittance measurements, beam profiles are also presented. The future program, including A-PHOENIX restart, and planned improvements on the LEBT are discussed.

INTRODUCTION

The present configuration of Spiral 2 accelerator [1] features two electron Cyclotron resonance ion source (ECRIS) that produce either heavy or light ion beams. These beams are selected by a low energy beam transport line (LEBT) before being injected in an 88 MHz radio frequency quadrupole and a superconducting linear accelerator. LPSC is in charge of the assembly and commissioning of the heavy ion LEBT. This line is currently equipped with the PHOENIX V2 ECRIS, shortly described later.

THE HEAVY ION LOW ENERGY BEAM LINE

This new line, displayed on Fig. 1 was calculated and dimensioned by GANIL, CEA/IRFU and IPNO [2] to hold permanently 15 mA of total ionic beam current extracted from a heavy ion source at 60 kV voltage.

First, a solenoid is placed immediately after the ECR ion source. Then stand a quadripole triplet and a double-focusing 90° bending magnet designed with simple flat shimmed pole. An associated hexapole located before the dipole is used to reduce the non-linearities induced by such a dipole. Two faraday cups (FC) are available: one in front of the ECRIS extraction to measure the total ionic current and the second after the dipole to measure the selected beam. The overall transmission efficiency of the beam line can be deduced from these two measurements. The LEBT is also equipped with 3 profilers to centre the beams, a set of 3 motorized slits to clean the beam and perform the mass resolution through the dipole. Next, two Allison type emittancemeters are located after a second quadrupole triplet.

#peaucelle@ipnl.in2p3.fr

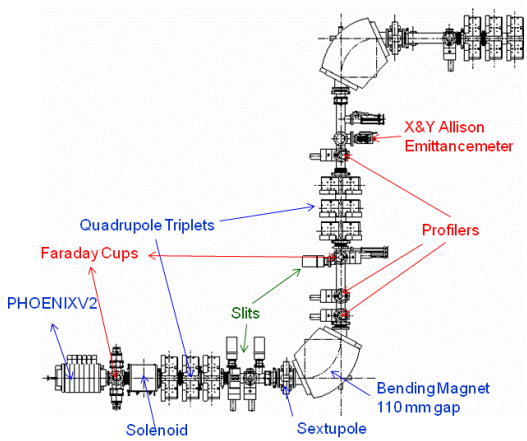

Figure 1: general sketch of the LEBT.

The LEBT uses ultra high vacuum standards for vacuum in order to minimize charge exchange in the accelerator. The pumping system is designed to reach 1.10^{-8} mbar in the whole beam line during high current production operation. Concerning the control command system, EPICS (Experimental Physics and Industrial Control System) [3] was chosen by Spiral 2 project.

THE PHOENIX V2 AND A-PHOENIX HEAVY ION SOURCES

In a first step the 18 GHz ECR ion source PHOENIX V2 [4] (see Fig. 2) is installed on the LEBT to commission it. This source has already been tested with Ar, Xe, O and He beam. Several upgrades have been made to improve the performance of this ECRIS: a water-cooled bias disk was added and new design of iron yoke allows increasing the magnetic field at the injection side from 1.7 T to 2.1 T now. The new injection flange designed accepts an oven reaching 1600°C performed by GANIL to produce ion metallic beam.

A-PHOENIX is a compact hybrid ECR ion source [5, 6] with two High Temperature Superconducting (HTS) coils and an innovative large permanent magnet hexapole. The magnetic structure allows reaching 2T radial magnetic field and 3T axial magnetic confinement. A-PHOENIX is designed to operate with frequencies from 18 to 28 GHz.

Because of the weld break of one the HTS cryostat, experiments on A-PHOENIX stopped in December 2009.

After repairing, the HTS coil was tested successfully during July 2010 and A-PHOENIX is now ready to restart up its commissioning.

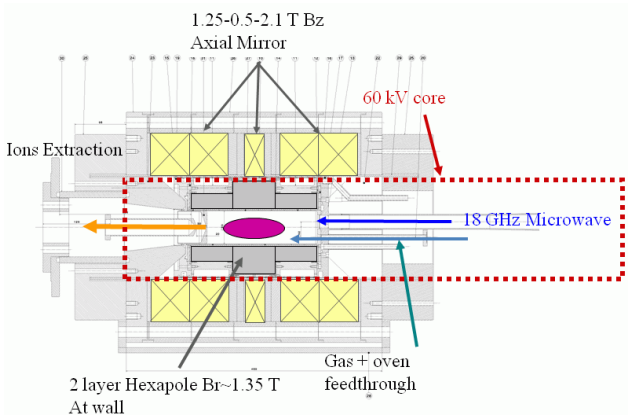

Figure 2: Phoenix V2 ion source.

The ultimate experiments done in 2009 tended to show that the low performances of the ECRIS at 18 GHz are due to a weak RF coupling. In order to improve this point, important modifications of the injection flange design have been done. The position of RF power injection was moved closer to the axis of the source; the bias disk mechanics was improved and a large welded below has been installed in order to move very easily the whole injection by 80 mm inward. Its construction is now finished and this system will be tested in late 2010.

STATUS OF THE LEBT AT GRENOBLE

The LEBT is completely assembled and operational at Grenoble since the beginning of 2010. A photo of the system is available on Fig. 3. As expected The LEBT vacuum system is able to hold ~1-2.10^{-8} mbar even at high ionic currents. Different beams such as Oxygen, Argon, Calcium and Xenon have been extracted and analyzed at a high voltage extraction up to 47 kV.

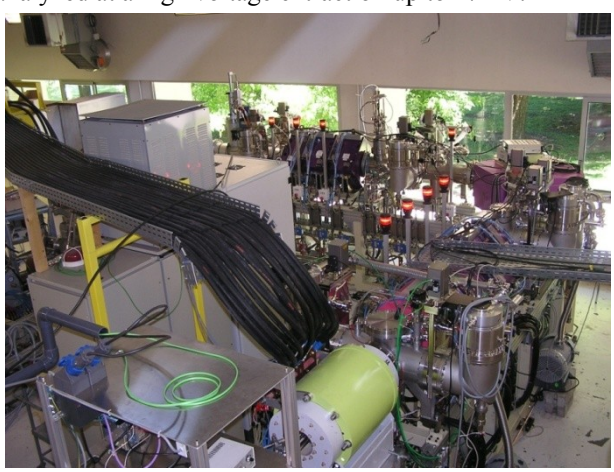

Figure 3: Phoenix V2 ion source and LEBT line at Grenoble.

Concerning transport beam dynamics, simulations was validated experimentally by measurements on FCs, profilers and emittancemeters with Argon, Xenon and Oxygen beams. Transverse emittance between 0.15 and 0.4 pi.mm.mrad normalized RMS depending of the beam is usually measured in both planes (see Fig.4).

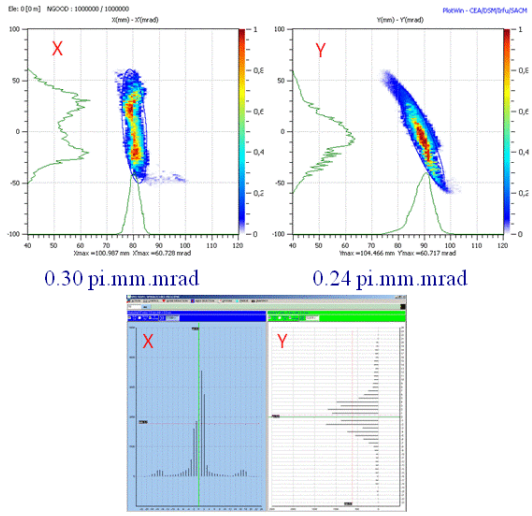

Figure 4: emittance measurements (up) and profiles (bottom) for 800 µAe O^{6+} at 45 kV.

The whole optic devices are tuned through an automatic algorithm developed from the TraceWin code [7] so that the LEBT can be optimized in two modes [8]: the first one corresponds to the smallest size on the profiler immediately after the dipole (optimized beam selection) while the second corresponds to the highest current on the second FC. Once the optics is optimized, the LEBT transmission reaches 90% in most cases. Besides, Phoenix V2 produces a very stable and reliable beam. The resolving power of the dipole has been studied and validated using a Xenon beam at 40 kV: $^{132}Xe^{25+}$ and $^{16}O^{3+}$ beams are not fully separated when slits between the dipole and the second FC are completely opened. Helped with the beam dynamic algorithm, it was possible to tune the optics and get rid of the oxygen keeping only Xenon beam with the analysis slits being opened at ± 5 mm (see Fig.5).

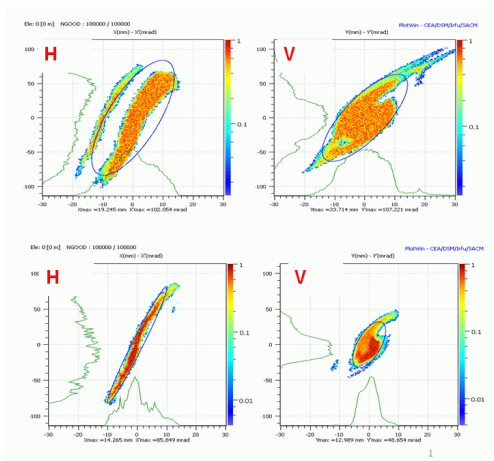

Figure 5: resolving power of the dipole validated with emittance measurements when slits are fully opened (up) and opened at ± 5 mm (bottom) for $^{132}Xe^{25+}$ at 40 kV.

The nominal performance in Oxygen beam was obtained in July 2010 at 45 kV and 1 kW of RF power: a $^{16}O^{6+}$ beam of more than 1 mA was produced with a very good transmission (95%). The associated ionic spectrum is displayed on Fig. 6. Measured transverse emittance was 0.3 pi.mm.mrad norm. rms in horizontal plane and 0.24 pi.mm.mrad norm. rms in vertical plane.

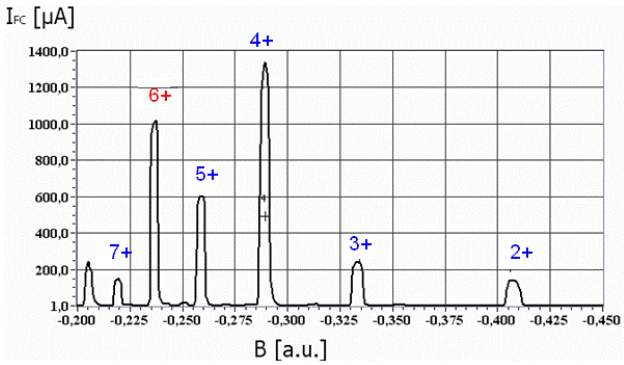

Figure 6: Oxygen spectrum at 45 kV with He gas mixing.

Tests with Argon beam have also been performed in summer 2010. 130 µA beam of $^{40}Ar^{12+}$ was produced at 40 kV. The associated ionic spectrum is presented on Fig.7. This result was obtained with few oxygen buffer gas. The $^{40}Ar^{12+}$ emittances, displayed on Fig.8, were measured to be 0.3 and 0.25 pi.mm.mrad normalized RMS in the horizontal and vertical planes respectively. One should note that the tests were done on a short time and a limited microwave power set to 1 kW. Improvement of these performances is expected in the future.

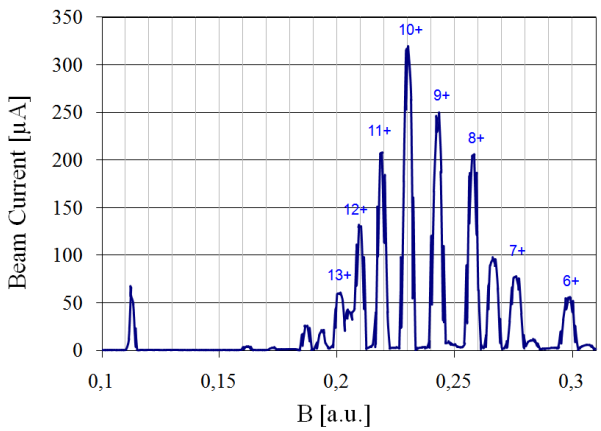

Figure 7: Argon spectrum at 40 kV optimized for Ar^{12+} production.

PROSPECTS

The LEBT beam tests will continue with PHOENIX V2 ECRIS especially with metallic ion beams using the large capacity oven (LCO) from GANIL. The present ECRIS extraction system must be modified to reach the high voltage specifications: an intermediate extraction electrode set to 30 kV will be added to safely hold the 60 kV high voltage required.

Once this last milestone is fulfilled, The A-PHOENIX research and development will restart at 18 GHz and continue at 28 GHz until mid 2011. The goal being to choose by mid 2011 the starter ECRIS to be moved in 2012 at GANIL. If A-PHOENIX shows better performance than PHOENIX V2, it will be installed on the LEBT for ultimate tests before moving to GANIL.

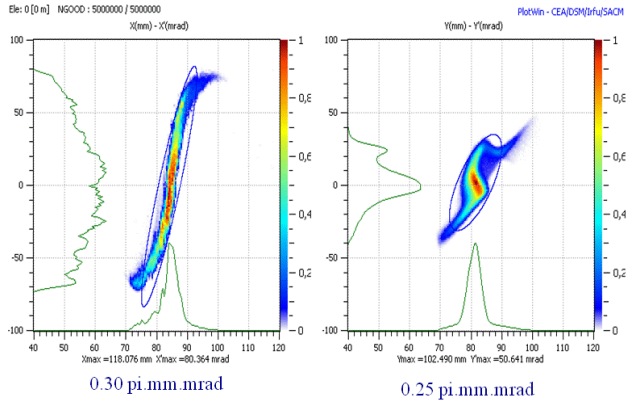

Figure 8: Argon 12+ emittance at 45 kV.

REFERENCES

[1] R. Ferdinand, Patrick Bertrand, "Status and challenges of the Spiral 2 utility", LINAC'10, Tsukuba, Japan.
[2] T. Junquera, "Status of the construction of the Driver Accelerator at Ganil", LINAC'08, Vancouver, Canada.
[3] http://www.aps.anl.gov/epics/.
[4] T. Thuillier, J.L. Bouly, J.C. Curdy, E. Froidefond, T. Lamy, C. Peaucelle, P. Sole, P. Sortais, J.L. Vieux-Rochaz, D. Voulot, "High Intensity Ion Beams Prospects for Accelerators with PHOENIX 28 GHz", EPAC'02, Paris, France.
[5] T. Thuillier, T. Lamy, L. Latrasse, J. Angot, "First plasma of the A-Phoenix electron cyclotron resonance ion source", ICIS'07, Jeju, Korea.
[6] T. Thuillier, T. Lamy, C. Peaucelle, P. Sortais, "Status report of the heavy ions source research and development for Spiral2", ICIS'10, Gatlinburg, USA.
[7] See http://irfu.cea.fr.Sacm/logiciels/index.php.
[8] J-L. Biarrotte, D. Uriot, O. Tusk, T. Thuillier, C. Peaucelle, P. Bertrand, C. Barué, "First beams produced by the Spiral-2 injectors", LINAC'10, Tsukuba, Japan.

TRACE SPACE RECONSTRUCTION FROM PEPPERPOT DATA

H.R. Kremers*, J.P.M. Beijers, V. Mironov, J.Mulder, S. Saminathan, S. Brandenburg,
Kernfysisch Versneller Instituut, Groningen, The Netherlands

Abstract

In this paper we present a simple model that we developed to reconstruct the 4D trace space distribution from the convoluted spatial images of a pepperpot emittance meter. Straightforward analysis of the images is hampered because of multiple and/or overlapping beamlets emerging from a single hole in the pepper plate. The model allows us to unambiguously assign each transmitted beamlet to its corresponding hole in the pepper plate from which it emerged. We will illustrate our analysis model with the reconstruction of the 4D trace space distribution behind the analyzing magnet of a He^{1+} beam extracted from an electron cyclotron resonance ion source.

INTRODUCTION

It is well known that electron cyclotron resonance ion sources (ECRIS) produce ion beams with relatively large emittances, i.e. several tens of π mm-mrad or even larger. Such low-quality ion beams are difficult to transport to and inject into an accelerator with high efficiency. Much work is therefore being devoted to better understand and improve low-energy ion beam transport. At KVI we made some progress by a combined effort of detailed beam transport simulations and measurements of beam profiles and emittances. This is reported in an accompanying paper to these proceedings [1]. To measure the 4D beam emittance of low-energy multiply-charged ion beams we built a pepperpot emittance meter and installed it in the image plane of the analyzing magnet [2]. However, overlapping and multiple beamlets emerging from a single hole in the pepper plate complicate a straightforward reconstruction of the 4D trace-space of the ion beam. This paper presents a simple method that we developed to overcome this problem. After a brief description of the emittance meter the above-mentioned problem will be illustrated with an emittance measurement of a 21 keV He^{1+} beam. Then the analysis method will be outlined that we developed to unambiguously reconstruct the 4D trace-space distribution of the ion beam.

PEPPERPOT EMITTANCE METER

The KVI4D emittance meter combines the pepperpot and scanning techniques to measure the 4D trace-space distribution of ion beams which have a large divergence and narrow width in the horizontal plane and a small divergence and large width in the vertical plane [2]. This is done by stepping a pepper plate with a linear array of holes aligned in the vertical direction horizontally through the beam and measuring the images of the transmitted beamlets at each step with a position-sensitive detector positioned 59 mm downstream of the pepper plate. The pepper plate is a 25 μm tantalum foil, mounted on a water-cooled copper block, with a vertical row of 20 holes each with a diameter of 20 μm and a pitch of 2 mm. The step width in the horizontal direction depends on the desired resolution, and is typically around 0.5 mm. We installed the pepperpot emittance meter near the focal plane of the 110° analyzing magnet.

An emittance measurement consists of measuring a series of spatial images of the transmitted beamlets, one at each horizontal step. As an example we measured the emittance of a 21 keV He^{1+} beam. The horizontal step size was set at 0.56 mm and we measured 39 spatial images of the transmitted beamlets from which the 4D trace-space distribution has to be reconstructed. A single spatial image taken at the horizontal position of x=-4 mm is shown in Fig. 1a. Also the location of the holes in the pepper plate is indicated. Fig. 1a clearly shows that there are i) more beamlets than there are holes and ii) some of the beamlets are overlapping. This complicates the analysis.

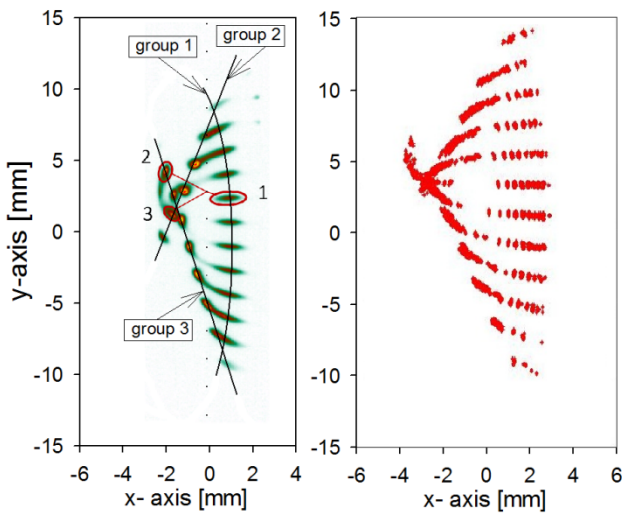

Figure 1: Measured a) and simulated b) spatial image obtained with the KVI4D emittance meter of transmitted beamlets with the pepper plate positioned at x=-4 mm for a 21 keV He^{1+} beam.

THE ANALYSIS

As already mentioned above the measured spatial images sometimes show both overlapping beamlets and, particularly around the median plane, multiple beamlets emerging from a single hole. From the systematic trend in the series of 39 images we could connect each beamlet with the hole in the pepper plate from which it emerged. An example is shown in Fig. 1a where three beamlets are connected that emerge from one hole. In addition, it

* kremers@kvi.nl

appeared convenient to classify all the beamlets into three groups with identical behavior. These are also indicated in Fig. 1a. In order to check our assignments we performed a detailed simulation of the beam transport from the ECRIS plasma electrode through the analyzing magnet to the scintillation screen of the emittance meter. The simulation method is described in more detail in Ref. [1]. The simulation result is shown in Fig. 1b and confirmed our initial assignments. Although 10^6 particles were used in the simulation, the calculated image has a much more granular appearance than the measured one. This is caused by the fact that the pepper plate intercepts most of the particles. The simulation also showed that the beamlets belonging to group 1 follow the more paraxial trajectories through the analyzing magnet, while the group 2 and 3 beamlets make a relatively large vertical angle (either positive or negative) with the median plane.

In order to reconstruct the 4D trace-space distribution we have to disentangle the overlapping beamlets. This was done by using an ellipse fitting routine to determine the center coordinates (x_c^i, y_c^i) of every beam spot in the plane of the scintillation detector, with the label i denoting the group to which each spot belongs. Next we fitted the center coordinates with a two-dimensional second-order polynomial according to:

$$x_c^i = \sum_{m,n=0}^{2} a_{mn}^i x_s^m y_s^n \; ; \; y_c^i = \sum_{m,n=0}^{2} b_{mn}^i x_s^m y_s^n \qquad (1)$$

with (x_s, y_s) the coordinates in the scintillation plane. The fit results in 18 coefficients for one group, i.e. 9 coefficients for x_c^i and 9 for y_c^i. Knowing the center coordinates of all the beam spots and the center coordinates of the holes in the pepper plate to which they belong, it is straightforward to reconstruct the 4D trace-space density $\rho(x,y,x',y') = \Sigma_i \rho^i(x,y,x',y')$ of the ion beam. Here, (x,y) are the center coordinates of the holes in the pepper plate and $x' = (x_s - x)/L$, $y' = (y_s - y)/L$ and L = 59 mm the distance between the scintillation screen and the pepper plate.

TRACE-SPACE DISTRIBUTIONS

From the 4D trace-space distribution $\rho(x,y,x',y')$ we can calculate various 2D projections by integrating over the two other coordinates. For example, the 2D spatial distribution $\rho(x,y)$ is obtained from $\rho(x,y,x',y')$ by calculating

$$\rho(x,y) = \iint \rho(x,y,x',y')dx'dy'. \qquad (2)$$

This is illustrated in Fig. 2 for the He^{1+} beam showing the groups i=1, i=2,3, all three groups and the simulated spatial profile. The spatial profiles show a strong second-order aberration which we attribute to the analyzing magnet [1].

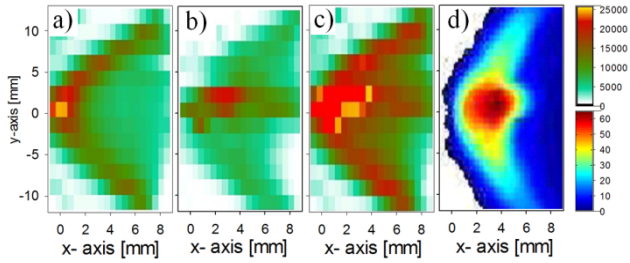

Figure 2: Spatial distribution of a 21 keV He^{1+} beam behind the analyzing magnet. a) group 1 ions; b) group 2,3 ions; c) all ions; d) simulated 2D profile.

For the horizontal trace-space distribution $\rho(x,x')$ (x-x' emittance) we get

$$\rho(x,x') = \iint \rho(x,y,x',y')dydy'. \qquad (3)$$

This is shown in Fig. 3 for the different ion groups together with a simulated emittance distribution. Both the measured and simulated x-x' trace-space distributions show a diverging beam, although the simulated distribution is less diverging than the measured one. Interestingly, the ions in group 2 and 3 have a relatively large negative offset in angle, i.e. their deflection angles are less than 110°. We will investigate this further in the next section.

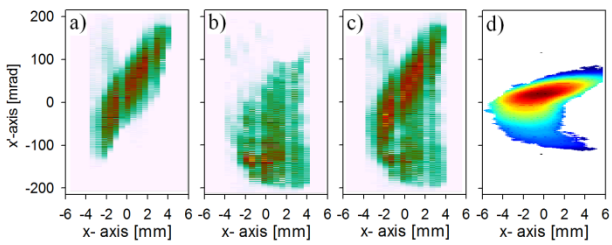

Figure 3: Horizontal x-x' emittance distribution of a 21 keV He^{1+} beam behind the analyzing magnet. a) group 1 ions; b) group 2,3 ions; c) all ions; d) simulated x-x' emittance distribution.

The vertical trace-space distribution $\rho(y,y')$ (y-y' emittance) is given by

$$\rho(y,y') = \iint \rho(x,y,x',y')dxdx'. \qquad (4)$$

Fig. 4 shows some of the vertical emittance distributions summed over all three ion groups. In Fig. 4a a partial vertical emittance is plotted, i.e. measured at the horizontal position x = 5.6 mm. This figure clearly shows that from the holes close to the median plane y = 0 three different beamlets emerge, i.e. one with a very small vertical angle and two with larger positive and negative vertical angles. The S-shape suggests a third-order aberration, which is probably caused by the pole face rotation of the analyzing magnet. Figs. 4b and c show the measured and simulated vertical emittances summed over all three ion groups, respectively. The characteristic

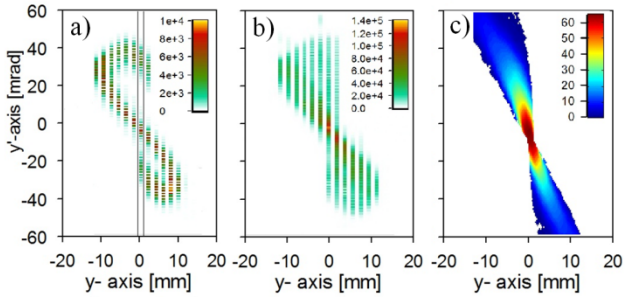

Figure 4: Vertical y-y' emittance distributions of a 21 keV He^{1+} beam behind the analyzing magnet summed over all three ion groups. a) y-y' emittance at the horizontal position x = 5.6 mm; b) total y-y' emittance; c) simulated y-y' emittance distribution.

bowtie shape of the y-y' emittance results from integration over the x coordinate.

BACKTRANSFORMATION

In order to investigate the horizontal imaging properties of the analyzing magnet further we constructed its transfer map T up to second order from the ion trajectory calculations described in Ref.[1]. The transfer map T projects a trace-space vector x(0) at the end of the ground electrode of the ECRIS extraction system to its corresponding vector x(1) in the image plane of the analyzing magnet. Using the inverse map T^{-1} we then projected each 4D point x(1) back to its corresponding point x(0), i.e. $x(0)=T^{-1}x(1)$, and from this we have calculated the 4D trace-space distribution $\rho^0(x,y,x',y')$ of the ions at the end of the ground electrode.

As an example we show in figure 5 the spatial distributions of the ions projected back from the image plane of the analyzing magnet to the end of the ground electrode before the magnet. Plotted are the spatial distributions of the group 1 ions, the ions of groups 2 and 3 and of all ions. The figure confirms that group 1 ions follow more or less paraxial trajectories. Ions belonging to groups 2 and 3 on the other hand are offset in both x and y coordinates with respect to the group 1 ions. Their starting positions are horizontally shifted to the inward side of the analyzing magnet and are vertically shifted above and below the median plane. The ions belonging to groups 2 and 3 follow trajectories that probe the fringe field of the analyzing magnet more than the group 1 ions do and are therefore deflected less.

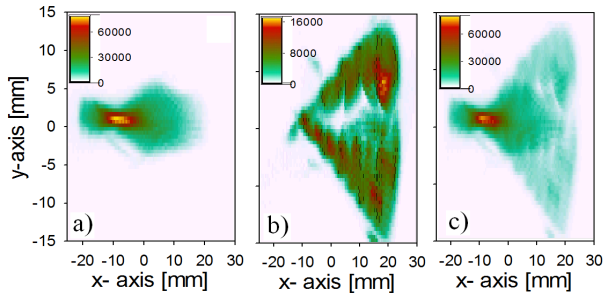

Figure 5: Back transformed spatial distributions of 21 keV He^{1+} ions at the end of the ground electrode before the analyzing magnet calculated from the measured trace-space distribution in the image plane of the magnet. a) group 1 ions; b) group 2,3 ions; c) all ions.

CONCLUSIONS

We have developed a method which allows us to reconstruct the 4D trace-space distribution of a low-energy ion beam from measured spatial images of a pepperpot emittance meter in the presence of multiple and overlapping beam spots. The method is illustrated with a detailed analysis of the 4D trace-space distribution of a 21 keV He^{1+} beam measured in the image plane of the analyzing magnet. We find that in our case the measured trace-space distributions are to a large extent determined by the ion-optical properties of the analyzing magnet. The measured trace-space distributions agree reasonably well with detailed beam transport simulations.

REFERENCES

[1] S. Saminathan et al., these proceedings.
[2] H.R. Kremers, J.P.M. Beijers, S. Brandenburg, DIPAC07 Proc. Triëste, p. 169-171, 2007.

PLASMA-TO-TARGET WARP SIMULATIONS OF URANIUM BEAMS EXTRACTED FROM VENUS COMPARED TO EMITTANCE MEASUREMENTS AND BEAM IMAGES *

D. Winklehner#, D. Todd, LBNL, Berkeley, CA 94704, USA
D. Grote, LLNL, Livermore, CA 94551, USA
D. Leitner, J. Benitez, M. Strohmeier, LBNL, Berkeley, CA 94704, USA

Abstract

This work presents the latest results of an ongoing effort to simulate the extraction from ECR ion sources and the Low Energy Beam Transport (LEBT). Its aim is to help understand the influence of parameters like initial ion distributions at the extraction aperture, ion temperatures and beam neutralization on the quality of the beam and to provide a design-tool for extraction- and transport-systems. Simulations of multispecies beams (Uranium of charge state 15+ to 42+ and Oxygen) extracted from the VENUS ECR ion source are presented and compared to experimentally obtained emittance values.

INTRODUCTION

The superconducting Versatile ECR ion source for NUclear Science (VENUS) [1, 2], was developed as the prototype injector for the Facility for Rare Isotope Beams (FRIB) and as injector ion source for the 88" – Cyclotron at Lawrence Berkeley National Laboratory [3, 4]. Like most ECR ion sources VENUS operates in a minimum B field configuration which means that a magnetic sextupolar field for radial confinement is superimposed with a magnetic mirror field for axial confinement. Consequently:

- Ions are extracted out of a region with high axial magnetic field (in VENUS typically 2 T) which then continuously decreases as the ions move along in axial direction, adding a rotational component to the beam.
- Due to the sextupolar field, the total magnetic field inside the source is not rotationally symmetric and thus the spatial distribution of ions at extraction resembles a triangle rather than a circle [5].

Furthermore, the extracted beam often consists of more than 30 different ion species with different mass-to-charge ratios which makes modeling even more complicated. The work described here represents the current status of a long-term effort to create a highly adaptable, advanced simulation script utilizing the well-established particle-in-cell (PIC) code WARP [6].

SIMULATIONS

Many of the issues regarding the extraction simulation and the beam transport through the beam line have been addressed in earlier work by D. Todd et al. (e.g. [5, 7]) and will only be reviewed briefly here.

* This Research was conducted at LBNL and was supported by the U.S. Department of Energy under Contract DE-AC02-05CH11231.
# dwinklehner@lbl.gov

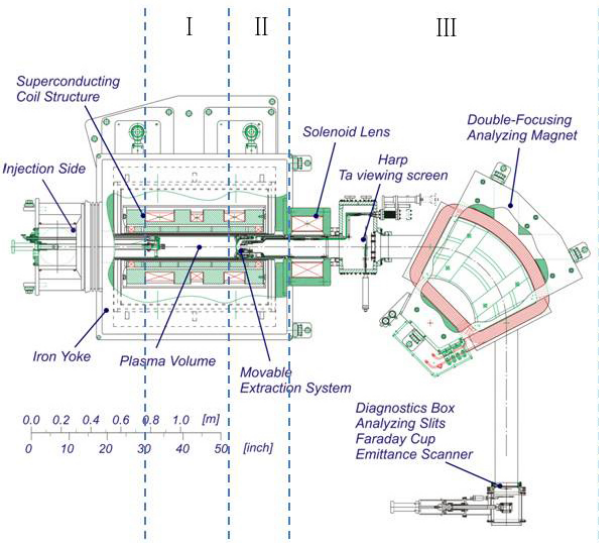

Figure 1: VENUS source and LEBT layout.

Initial Conditions

(See Figure 1, region I: Inside the plasma) For this work, a semi-empirical approach to obtain initial conditions on the plasma side of the extraction simulation was taken: VENUS's biased disk on the far side of the source is kept at a voltage of -50 V to -100V, thus providing the ions with enough kinetic energy to sputter the surface. A triangle with sharp edges was found to be etched into the disk, showing the spatial distribution of the ion beam on the injection side of the source. Because the ions are cold (a few eV) resulting in small Larmor radii it is reasonable to assume that they mainly follow the magnetic field lines. In addition, there is no reason why the direction towards the biased disk should be preferred, thus it can be argued that a similar ion beam distribution can be found on the extraction side of the source. To obtain the initial conditions the following recipe was used for each species: 10000 ions are randomly distributed on a triangle corresponding to the sputtered triangle and are given a random velocity corresponding to a Boltzmann distribution with a peak temperature of 2 eV. Then, each particle's respective gyro-motion guiding-centre is calculated and the field-line originating at that point is tracked through the source. At the respective end-point, an appropriately scaled Larmor radius is applied and the particle is put on a random point on a circle with this scaled radius around the guiding-centre. Because travelling through the

source's magnetic field leads to a shift from the ion's transversal velocity to the longitudinal velocity component, velocities are recalculated from the scaled Larmor-radius in the end. A detailed description of the method can be found in [8] and the references therein.

Extraction

(See Figure 1, region II: The extraction system) WARP includes both a two-dimensional, axially symmetric plasma sheath extraction model similar to IGUN [9] and a three-dimensional sheath extraction model comparable to KOBRA [10]. In order to allow for sufficient resolution at the plasma sheath while keeping the simulation time reasonable, the following two-step approach has been taken:

1. An axially symmetric beam with the same species parameters, currents and energies as the triangular beam is extracted using the two-dimensional model. The beam is tracked through the simulation several times, until a relaxation of the combined potential of applied fields and self-fields has been reached.
2. The obtained potential is stored and used as an applied field in the second step, where the beam is initialized with the obtained triangular particle distributions and the simulation is run in three-dimensional mode.

Previous tests against a full 3D simulation have confirmed the validity of this approach [5].

Beamline Transport

(See Figure 1, region III: The beam line) Since the longitudinal velocity in the remaining beam line is much higher than the transverse, a two-dimensional Poisson solver can be used to simulate the beam line transport (slice mode). The longitudinal self-fields are neglected but the motion through the three dimensional analyzing magnet fields is simulated [5]. The beam-influencing components in the beam transport simulation are (see Figure 1):

- The solenoid field of the source
- The solenoid lens (Glaser-lens)
- The dipole analyzing magnet

Table 1: Simulation parameters

Parameter	Value	
Total extracted current	1.6 emA	4.6 emA
Ion mean Temperature	2 eV	2 eV
Uranium Ekin (longitudinal)	~3 eV	~3 eV
Electron Temp. (in sheath)	5 eV	5 eV
Source Voltage	20 kV	22 kV
Puller Voltage	-2 kV	-3 kV
Bmax at extraction	2.1 T	2.1 T
Extraction Aperture ↔ Puller	31.5 mm	21.6 mm

RESULTS

One of the most important beams for FRIB are high intensity medium charge state uranium beams [11]. Uranium beam data from VENUS is thus available and benchmarking this data against simulations is of particular interest. Two simulations are compared to each other and to experimental results: 1.6 emA and 4.7 emA total extracted current. The respective species distributions and currents in eμA were calculated from experimentally obtained VENUS spectrums. The key initial parameters of the simulations are listed in Table 1.

Simulation Results

Figure 2 shows a typical horizontal beam envelope plot for a multispecies Uranium beam simulation.

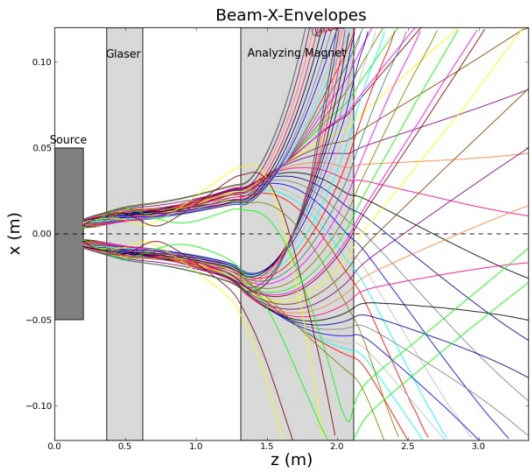

Figure 2: Horizontal beam envelopes (1-rms) of a 4.6 mA Uranium beam, optimized for q = 35+. Note the 'warping' of coordinates to simulate the bend. Different focusing and bending of different species is clearly seen.

Figure 3-Figure 5 show simulation results comparing different neutralization levels and extracted currents. The magnetic emittance displayed for comparison was calculated according to [12] by

$$\varepsilon_{mag}^{xx'-rms-norm} = 0.032 \cdot r^2 \cdot B_0 \cdot \frac{1}{M/Q}.$$

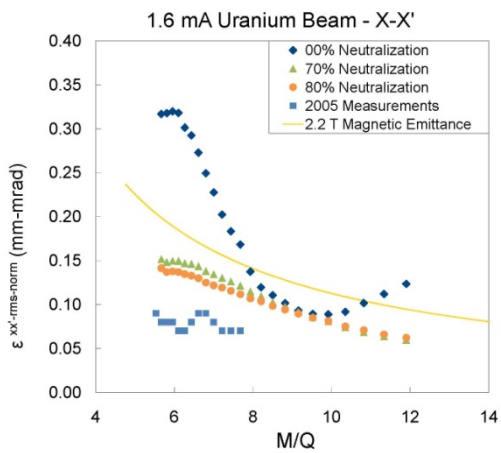

Figure 3: 1.6 mA Uranium run. Comparison of horizontal emittances for different neutralization levels in simulation with a measurement series from 2005.

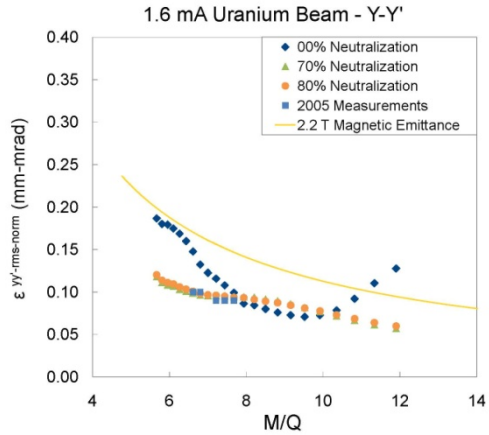

Figure 4: 1.6 mA Uranium run. Comparison of vertical emittances for different neutralization levels with a measurement series from 2005.

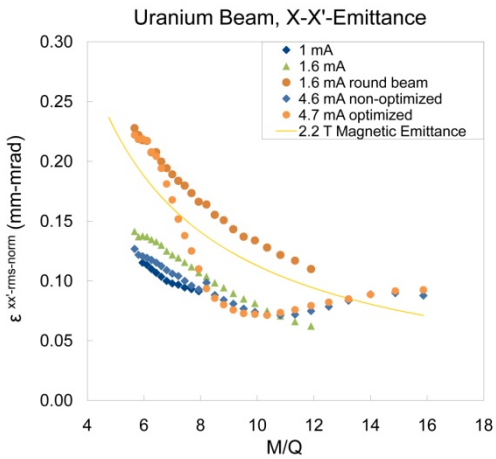

Figure 5: Comparison of horizontal emittances for simulations using different total extracted currents and beam shapes (triangular where not noted otherwise). All simulations were run with 80% neutralization.

Discussion

As seen in Figure 4, the vertical emittances produced by the simulations fit well with the measured values. The offset in horizontal emittance could be a result of one of the following:

- Not all species were included into the 1.6 mA simulation due to computer memory issues,
- For simplification, the size and shape of the initial triangles was set the same for all species.
- Initial conditions like ion and electron temperatures were 'guessed'.

All of the above will be subject to further systematic analysis. In Figure 5, an emittance minimum can be observed in the region of m/q = 9 for the 4.7 mA beam. This might prove useful when it comes to the acceptance of the accelerator subsequent to an ECRIS and will also be investigated further.

CONCLUSION

The status of the efforts to create an adaptable simulation code for beam extraction from an ECR ion source using WARP has been presented. It is now possible to simulate multispecies beams with more realistic initial particle distributions and a high number of species in 3D mode with a high grid resolution. Emittance values are reproduced within reasonable margins by the simulations. Future work will aim to better understand the physics leading to the initial conditions and beam neutralization.

ACKNOWLEDGEMENTS

This work was supported by the Director, Office for Energy Research, Office of High Energy and Nuclear Physics, Nuclear Physics Division of the U.S. Department of Energy under Contract DE-AC02-05CH11231.

REFERENCES

[1] M. Lyneis et al., New Results with the superconducting ECR Ion Source VENUS, RSI 75 (2004).
[2] D. Leitner et al., Next generation ECR ion sources: First results of the superconducting 28 GHz ECRIS - VENUS, Nuclear Instruments and Methods in Physics Research Section B 235, 486 (2005).
[3] R.C. Pardo et al., Heavy-Ion Beams Required for the RIA Accelerator, RSI 75, 1427 (2004).
[4] D. Leitner et al., Status report of the 28 GHz superconducting electron cyclotron resonance ion source VENUS (invited), Review of Scientific Instruments 77, 03A302 (2006).
[5] D. S. Todd et al., Comparison of particle-in-cell simulation with experiment for the transport system of the superconducting electron cyclotron resonance ion source VENUS RSI 77 (2006).
[6] David P. Grote et al., The WARP Code: Modeling High Intensity Ion Beams in 16th intern. Workshop on ECR Ion Sources, edited by M. Leitner (AIP, Berkeley, CA, 2004).
[7] D. S. Todd et al., Simulation and beamline experiments for the superconducting electron cyclotron resonance ion source VENUS, (AIP, 2008), p. 02A316.
[8] D. Winklehner et al., Comparison of extraction and beam transport simulations with emittance measurements from the ECR ion source VENUS, in 14th Beam Instrumentation Workshop, edited by LANL (JACoW, Santa Fe, New Mexico USA, 2010).
[9] R. Becker, and W. B. Herrmannsfeldt, Igun - A program for the simulation of positive ion extraction including magnetic fields, (AIP, 1992), pp. 2756.
[10] INP, KOBRA3-INP (INP, Junkernstr. 99, 65205 Wiesbaden, Germany.
[11] D. Leitner et al., High intensity production of high and medium charge state uranium and other heavy ion beams with VENUS, (AIP, 2008), p. 02C710.
[12] A. Septier, Focusing of charged particles (Academic Press,, New York, 1967), Vol. 2

PRODUCTION OF HIGHLY CHARGED U ION BEAM FROM RIKEN SC-ECRIS

Y. Higurashi[#,1], T. Nakagawa[1], J. Ohnishi[1] ,H. Haba[1], E. ikezawa[1], M. Fujimaki[1], Y. Watanabe[1], M. Komiyama[1], M. Kase[1], A. Goto[1], O. Kamigaito[1], T. Aihara[2], M. Tamura[2], A. Uchiyama[2],
[1] RIKEN Nishina Center 2-1 hirosawa Wako, Saitama JAPAN, 351-0198
[2] SHI Accelerator Service, Ltd. 1-17-6 ohsaki, Shinagawa-ku Tokyo JAPAN, 141-0032.

Abstract

In 2008, we produced 345 MeV/u beam (~0.4pnA on target) for RIKEN RIBF. To increase the U beam intensity, we produced U^{35+} from RIKEN SC-ECRIS with sputtering method. To maximize the beam intensity, we made various test experiments. We obtained 2~0.7 pμA of highly charged U ion (27~35+) at the RF power of ~1.2kW.

INTRODUCTION

In 2008, we produced 345 MeV/u U beam (0.4 pnA on target) and observed more than 40 new isotopes with in-flight fission reaction for only 4 days experiments [1]. This experiment shows that the intense U beam is strong tool to produce very neutron rich nuclei and to study the r-process in nuclear synthesis. Using 18 GHz RIKEN ECRIS, we only produced 2~4 eμA of U^{35+} beam, which was much lower than the required beam intensity for RIKEN RIBF. For this reason, to meet the requirement, we constructed new SC-ECRIS which has the optimum magnetic field strength for 28GHz.[2] In the autumn of 2009, we obtained first beam of U^{35+} from RIKEN-SC-ECRIS with 18 GHz microwave. Since then, we tried to increase the beam intensity of highly charged U ion beam.

In this article, we report the results of the test experiment for production of highly charged U ion beam.

SC-ECRIS

The detailed structure of the SC-ECRIS and the test experiment was described in refs. 2, 3. For operation of 28 GHz microwaves, the B_{inj}, B_{ext} and B_r are 3.8, 2.2 and 2.2 T, respectively. The main feature of this ion source is that it has six solenoid coils to produce mirror magnetic field at the axial direction. Using this configuration, one can change the magnetic field gradient at ECR zone and ECR zone size independently. To keep the superconductivity, the cryostat is equipped with three small GM refrigerators. The amount of liquid He is about 500 L. The cooling power at 4 K is about 1 W. It was reported that the higher microwave frequency gives stronger heat load. [4] To keep the superconductivity against the heat load, we need stronger cooling power for cryostat. For this reason, we installed GM-JT refrigerator (cooling power of 5 W at 4 K) to increase the cooling power in the end of 2009.

[#]higurasi@riken.jp

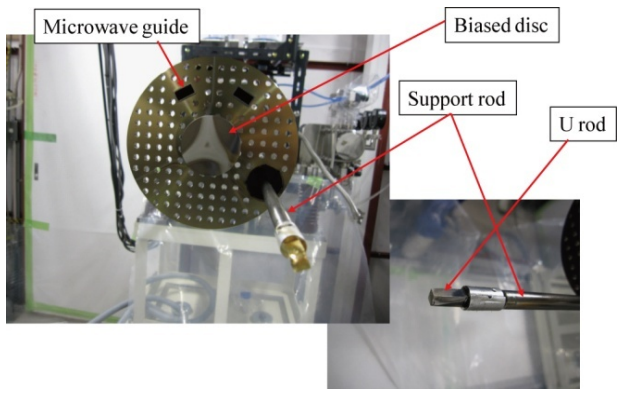

Figure 1: Photograph of the RF injection side and U rod.

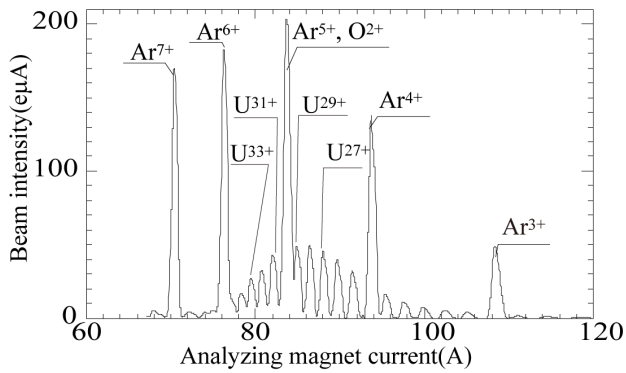

Figure 2: Charge state distribution of the U ion, when using the O2+Ar gas as an ionized gas.

U BEAM PRODUCTION

Fig. 1 shows the photograph of the RF injection side. To produce U ion beam, we used the sputtering method. As shown in Fig. 1, the metal uranium was installed at off-center axis. The metal U was supported by supporting rod. The position of rod was remotely controlled within the error of ~0.2mm. The support rod was water cooled for minimizing the chemical reaction between metal uranium and material of uranium holder at high temperature. The rod position and high voltage for sputtering were optimized for maximizing the beam intensity of highly charged U ions.

For investigating the support gas effect, we used the O_2 , Ar and Ar+O_2 gas as an ionized gas. Fig. 2 shows the charge distribution of the highly charged U ion with using O_2+Ar gas. The RF power was 980 W. The extraction voltage was 17 kV.

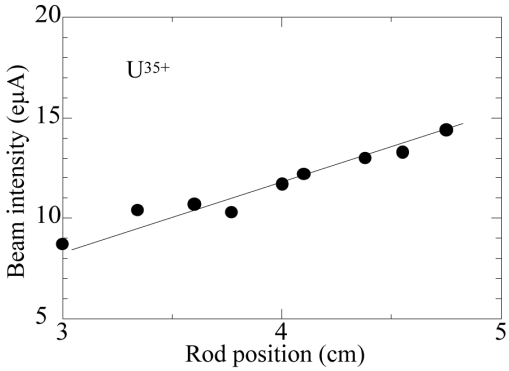

Figure 3: Beam intensity of U^{35+} as a function of rod position.

Beam intensity of U^{35+} as a function of rod position and high voltage are shown in fig.3 and 4, respectively. The RF power was ~900 W. The extraction voltage was 15 kV. B_{inj}, B_{min}, B_{ext} and B_r were 2.3 T, 0.46 T, 1.1 T , 1.3 T respectively. The beam intensity was increased linearly with increasing high voltage for sputtering. The beam intensity is very sensitive to the rod position as shown in Fig.3. The beam intensity increased linearly when moving the rod toward the ECR zone.

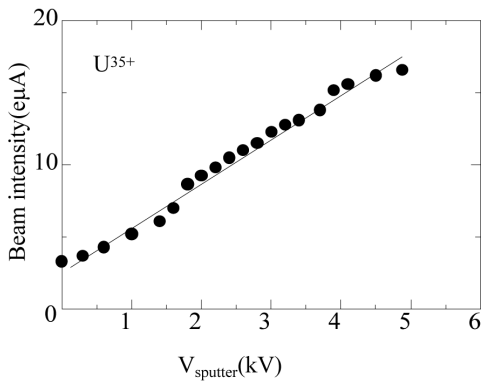

Figure 4: Beam intensity of U^{35+} ion as a function of sputtering voltage.

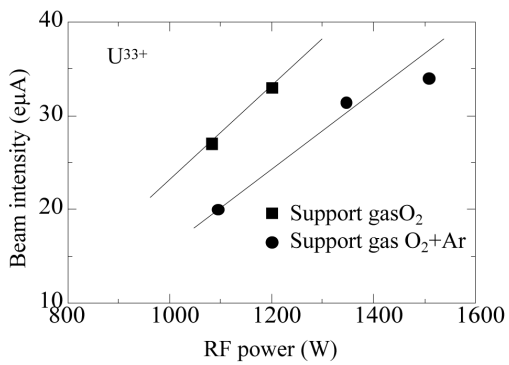

Figure 5: Beam intensity of U^{33+} as a function of RF power, when using O_2(closed squares) and O_2+Ar (closed circles)gases as an ionized gas

Fig. 5 shows the beam intensity of U^{33+} as a function of RF power in case of O_2+Ar gas. The beam intensity for O_2 gas was always higher than those for O_2+Ar at the same RF power. However, for lower charge state of heavy ions(<31+), the beam intensity for O_2+Ar gas was higher. Fig. 6 shows the beam intensity of U^{33+} and U^{35+} as a function of RF power in case of O_2 gas. In Fig. 7, the beam intensity for lower charge state of U ions (31+,33+) are shown. We obtained ~50 eμA of U^{31+} at the RF power of 1.2 kW.

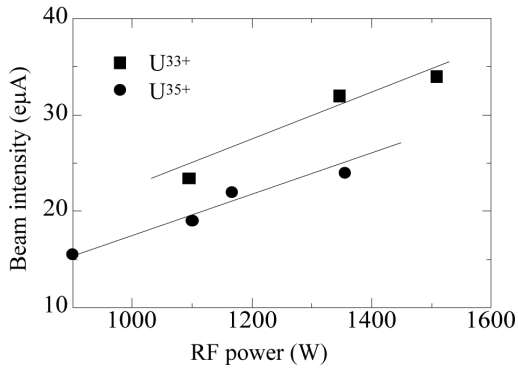

Figure 6: Beam intensity of $U^{33+}$and U^{35+} as a function of RF power, when using O_2 gas.

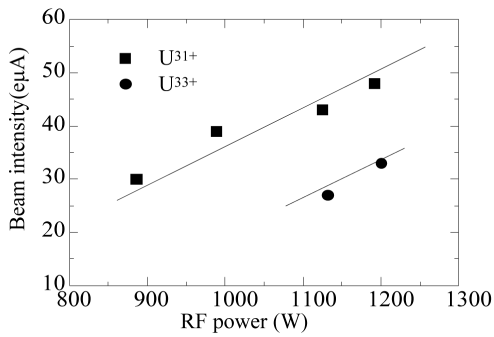

Figure 7: Beam intensity of U^{31+} and U^{33+} as a function of RF power, when using O_2+Ar gas.

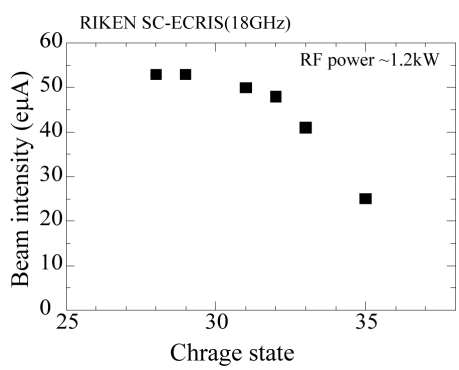

Figure 8: Beam intensity of highly charged u ion at the RF power of ~1.2 kW.

Fig. 8 shows the beam intensity of highly charged U ions at the RF power of ~1.2 kW. It is noted that the beam intensities were not saturated in this test experiment as shown in Figs.3~7. Because the power density of RF power in this experiment was very low (~100 W/L). We may obtain higher beam intensity at the higher sputtering voltage and RF power.

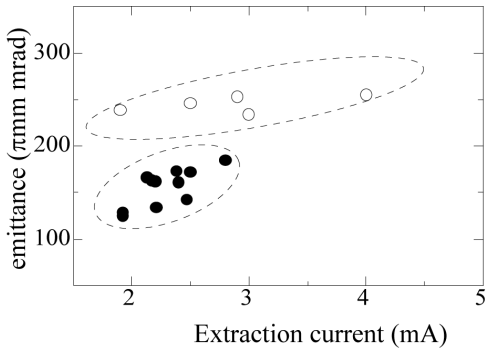

Figure 9: Y emittance (4 rms), when using O_2 gas(closed circles) and O_2+Ar gas (open circles).

Fig. 9 shows the 4 rms emittance as a function of extracted current, when using O_2 gas (open circles) and O_2+Ar gas (closed circles). The values of the 4 rms emittance are calculated with:

$$\varepsilon_{rms} = 4\sqrt{< x^2 >< x'^2 > - < xx' >^2}$$

The emittance was increased with increasing the extracted current. Furthermore, it seems that the emittance for O2+Ar gas was smaller than that for O2 gas at the same extraction current. To understand it, we may need more systematic study.

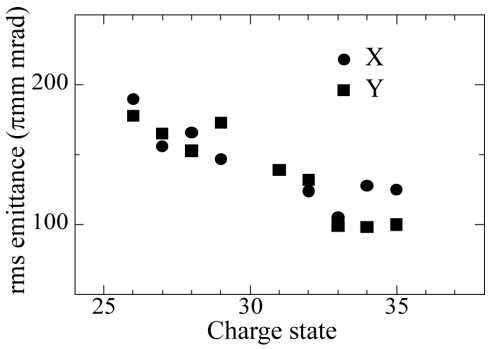

Fig.10: Rms emittance for highly charged U ion.

Fig. 10 shows the X and Y emittance (4 rms) for highly charged U(26~35+) ions. The emittance decreased with increasing the charge state at same extraction voltage. In this experiment, we obtained the 4 rms emittance of ~ 120 πmm mrad for U^{35+}. This is smaller than the acceptance of the accelerator of the RIKEN RIBF (~160 πmm mrad). It means that we can accelerate almost of the U^{35+} beam (~20 eμA) produced form RRIKEN SC-ECRIS at present. This intensity is ~10 times as high as the intensity from RIKEN 18 GHz ECRIS. From these results, we may obtain ~4 pnA of U ion beam at the energy of 345 MeV/u on target for production of RI beam.

CONCLUSIONS AND FUTURE PLAN

We obtained 0.7~2 pμA of highly charged U ion beams (35~27+) from RIKEN SC-ECRIS with sputtering method. For higher RF power and sputtering voltage, we may obtain higher beam intensity, because the beam intensity was not saturated in the test experiment. We observed that the emittance for O_2+Ar gas was smaller than those for O_2 gas. To confirm it, we need further investigation.

From this autumn, we will use the 28 GHz gyrotron to increase the beam intensity of U^{35+}. To produce U vapour, we will make a test experiment with high temperature oven.

REFERENCES

[1] T. Ohnishi, "Identification of 45 new neutron-rich isotopes produced by in-flight fission of a 238U beam at 345MeV/nucleon" JPSJ in press.
[2] J. Ohnishi et al, 6th Annual Meeting of Particle Accelerator Society of Japan p637(2009).
[3] Y. Higurashi et al, 6th Annual Meeting of Particle Accelerator Society of Japan p377(2009).
[4] D. Leitner et al, Rev. Sci. Instrum. 79 02A325(2008).

PREGLOW PHENOMENON ORIGIN AND ITS SCALING FOR ECRIS

I. Izotov#, A. Sidorov, V. Skalyga, V. Zorin, IAP RAS, Nizhny Novgorod, Russia

Abstract

Preglow effect investigation is one of topical directions of ECR ion sources development at present. Preglow is of interest for efficient short-pulsed multicharged ion source creation. Particularly, such source of intense beams of shortliving radioactive isotopes multi-charged ions is one of key elements in "Beta-Beam" European project [1]. Use of Preglow-generating regime of an ECRIS operation is a promising way of pulsed high-intense multi-charged ion beams production with much shorter edges in comparison with usual operation regime. The first theoretical investigations of Preglow phenomenon were performed in references [2, 3]. Numerical simulations made with the updated theoretical model allow authors to propose more physical and intuitive explanation of Preglow phenomenon origins. Obtained dependences of Preglow characteristics on experimental conditions offer a scaling for a wide range of ECRISes.

INTRODUCTION

The preglow effect was first observed in experiments in LPSC (Grenoble, France) and later modeled theoretically in the works [2,3]. Theoretical model of ECR discharge development in a magnetic trap of an ECR MCI source, modified as compared to [2], allowed us to simulate the process of preglow peak more accurately and to assess dependence of its parameters on experimental conditions. The performed theoretical research and results of the numerical modeling give a new, more physical and clear insight into the nature of the preglow effect. We investigated preglow peak duration and intensity as a function of parameters controlled in experiments. Besides, we found a dimensionless parameter characterizing the regime of plasma confinement in the source trap that universally defines the preglow properties and may be used as scaling for a wide class of available and future experimental facilities. These results are also presented in the paper.

PHYSICAL INTERPRETATION OF PREGLOW

Theoretical research demonstrated that the condition necessary for the existence of multicharged ion current burst at the beginning of the pulse, i.e., preglow, is intense heating of electrons by microwave radiation at the initial stage of gas breakdown that must be sufficient for formation and maintaining for some time of superadiabatic energy electron distribution function (EEDF, see [3]). The EEDF form ensures efficient neutral gas ionization due to the presence of electrons in the energy region corresponding to maximum ionization cross-sections, on the one hand, and allows "storing" higher energy (compared to the maxwellian EEDF with the same mean energy) of "hot" electrons whose lifetime in the trap is large in comparison with the characteristic time of discharge evolution, on the other hand. Hereinafter, under plasma energy content we understand the quantity $w=<E>*Ne$, where $<E>$ is average electron energy over EEDF, and Ne is electron concentration.

With a definite combination of parameters of seed plasma, the concentration of neutral particles at the beginning of the discharge and characteristics of heating microwave radiation, there may occurs a situation when the energy stored at the initial stage of plasma breakdown is much higher than its energy content at the steady-state stage of discharge combustion. Fast withdrawal of this excess energy in the form of an intense flux of charged particles from the trap gives rise to a preglow peak. In other words, at the stage of avalanche-like growth of plasma concentration, when its magnitude reaches a high enough level, the energy stored in hot electrons as well as the energy of microwave radiation is expended on intense gas ionization. This energy reserve makes it possible in a short time to create plasma with concentration and temperature higher than those attainable by means of microwave radiation. A particle flux from the magnetic trap, too, may be much higher than the steady-state one. Note that, if the power of microwave radiation is so small that sufficient energy cannot be stored, there will be no preglow effect. Nor will it occur in the case of too large power, when all the electrons, even with total-lot gas ionization, are heated up to maximum energies.

The said above may be readily illustrated by means of numerical modeling of the evolution of ECR discharge within the framework of the considered theoretical model. Results of computation of the dynamics of plasma energy content, its concentration and density of particles flux from the trap at the initial stage of discharge are presented in fig. 1 for the following parameters: 28 GHz, 200 W/cm^2.

It is clearly seen from the time plots in fig. 1 that, by the time the particle flux from the trap starts to grow, the plasma energy content is almost an order of magnitude higher than the steady-state level and termination of the stored energy release exactly coincides with termination of the burst of particle flux, after which the discharge parameters take on steady-state values. The preglow current peak intensity (the ratio of the amplitude of peak current to a steady-state value) in this case is the larger, the higher the maximum plasma energy content was in comparison with the steady-state one.

#izotov@appl.sci-nnov.ru

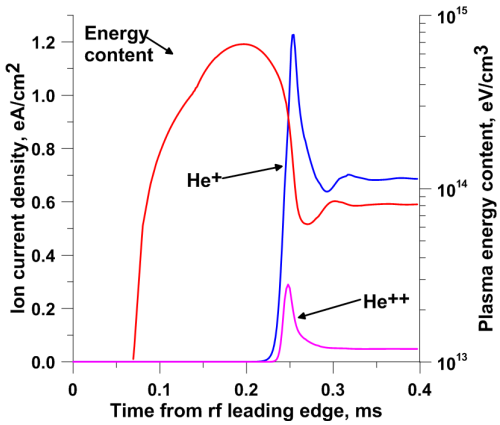

Figure 1: Plasma energy content & ion current density

Temporal parameters of preglow peak depend on how active neutral gas ionization is (i.e., on ionization rate, hence, on particle concentration) and on how fast the particles may withdraw "excess" stored energy from the trap, i.e., on their lifetime. As plasma lifetime, its concentration and temperature are interrelated quite intricately, it is very difficult to give a comprehensive analysis of the preglow effect without numerical simulation. In the next section we present results of simulations.

NUMERICAL SIMULATION

It is convenient to investigate preglow characteristics using the parameters based on Gaussian approximation of preglow peak [2]. *Imax* is maximum value of peak current (current density), *Time(Imax)* = *Tmax* is the time period from the beginning of heating pulse to attaining maximum current, *FWHM* is full width at half maximum.

Numerical simulation was performed using the code created by the authors on the basis of the model described in [3]. The variable parameters in the computations were the following: heating radiation frequency f, microwave radiation flux density p, and initial concentration of atoms N_{a0}. All the other parameters were constant: magnetic trap length L=20 cm, mirror ratio R=5, initial plasma concentration $N_{e0}=10^5$ cm^{-3}, initial electron temperature T_{e0} =1 eV. Frequency f was varied within the 28-60 GHz range corresponding to the frequencies of available and developed ECRIS. Power density p was varied in a wide range accessible to state-of-the-art ECRIS. The operating gas was helium.

We introduce parameter *RP* (stands for regime parameter) as ratio between gasdynamic and classical electron lifetime: $RP = \tau_{gd} / \tau_{cl}$ (see [3]). This parameter characterizes the regime of plasma confinement that is realized at a given moment of time. For $RP \gg 1$ the regime is collisional or quasi-gasdynamic, whereas for $RP \ll 1$ it is collisionless or classical regime of confinement. Initial conditions of ECR gas breakdown unambiguously determine the confinement regime at the steady-state stage of the discharge and, consequently, the magnitude of *RP*.

Preglow intensity *Int* (the ratio of peak current amplitude to current at the quasi-stationary stage of the discharge) as a function of RP at a steady-state stage of the discharge is plotted in fig. 2 for different power densities at the frequency of 28 GHz. The highest intensity of the 2nd ion preglow (solid lines in the graph) is attained at the power of 100-500 W/cm^2 with the initial density of atoms of 4-6*10^{12} cm^{-3}.

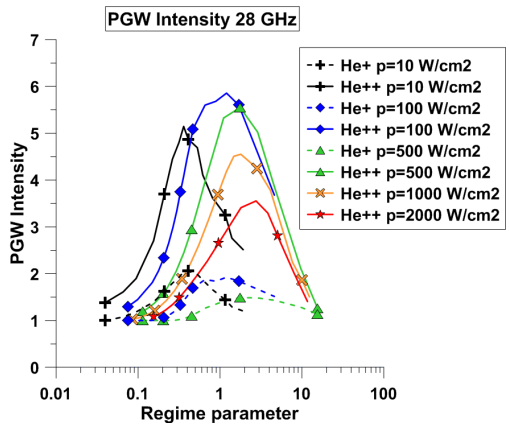

Figure 2: Preglow *Int*.

The curves for preglow intensities lie primarily in the region $0.1<RP<10$ outside which the preglow effect is not observed (as follows from definition, Int=1 corresponds to the absence of preglow peak in current oscillogram). This means that a preglow peak is generated only in a plasma in the intermediate state in terms of confinement regime, i.e., when RP~1. At $RP \gg 1$, which corresponds to a fully filled loss cone and a strongly collisional plasma, preglow is not formed because of a small lifetime of particles – energy is not stored due to its intense withdrawal. In the opposite case, at $RP \ll 1$, energy is not stored either because of a small number of collisions and, as a consequence, insufficient ionization multiplication of electrons.

An oscillogram of current densities of the 1st and 2nd helium ions in the regime corresponding to maximum preglow intensity of the 2nd ion (p=100 W/cm^2, N_{a0}=5*10^{12} cm^{-3} -> RR=1.5) as well as the time dependence of plasma energy content are shown in fig. 1.

FWHM of the preglow peaks is plotted as a function of *RP* in fig. 3. Clearly, unlike fig. 2, where power greatly influences maximum intensity and to a lesser degree position of *RP* maxima, the curves in fig. 3 almost coincide. This is attributed to the fact that preglow *FWHM* is defined by plasma lifetime that is rigorously related to *RP*. It is apparent from figs. 2 and 3 that an intense preglow peak with a duration of several tens of microseconds may be generated.

Simulations showed that the increase in frequency has an insignificant impact on the preglow peak intensity. In the 20-100 GHz range, the preglow intensity of the 2nd ion increases by 12% only, and the preglow intensity of the1st ion remains almost unchanged. The insignificant growth of preglow intensity with increasing frequency

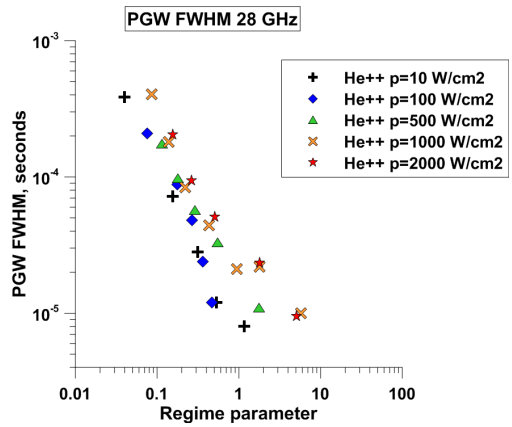

Figure 3: Preglow *FWHM*.

(other parameters being fixed) is explained by the fact that maximum possible electron energy in the superadiabatic regime is related to frequency by $E_{max} \sim f^{1/2}$ [3], hence, the energy average over EEDF that defines energy storage at the initial stage of the discharge also depends on frequency as $<E> \sim f^{1/2}$. Taking into consideration that preglow parameters weakly depend on the absolute magnitude of initial energy storage, we obtain a very weak dependence of these parameters on heating radiation frequency.

Note that, when the power of heating radiation is increased, for attaining intense preglow one has to increase the initial concentration of atoms too so as to maintain *RP* within the existence range of preglow, which in turn leads to increased plasma density that may exceed the cut-off density value for the used frequency. Preglow intensities as a function of steady-state plasma density are shown in fig. 4 for different values of power. The diagram was constructed for 60 GHz, but with allowance for the weak dependence of preglow parameters on frequency, it may be used for assessing preglow parameters at other frequencies also, if plasma density is lower than a critical one. The diagram also shows cut-off concentrations for some typical frequencies.

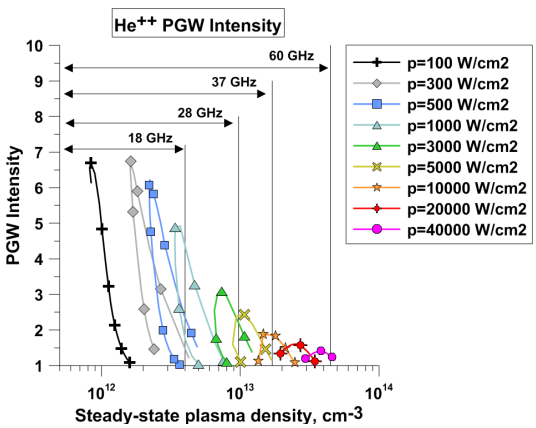

Figure 4: Preglow *Int*.

Besides preglow intensity and peak duration, an absolute value of current (current density in our case) is a parameter important for applications. As a supplement to fig. 4, fig. 5 gives a diagram of maximum current densities in the preglow peak.

It is clear from figs.4 & 5 that it is impossible to produce intense Preglow with current density higher than 1 eA/cm^2 using low power radiation sources at a frequency of 18 GHz and less.

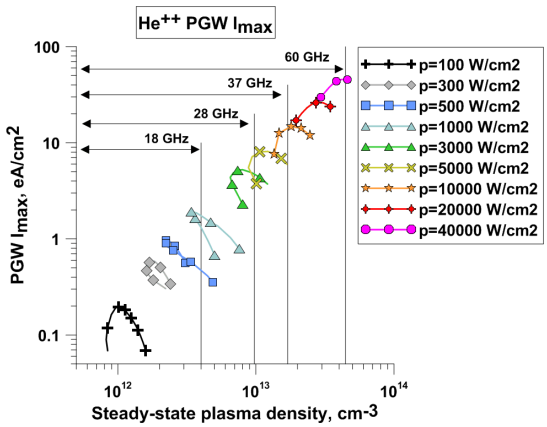

Figure 5: Preglow *Imax*.

CONCLUSION

The results presented provide an insight into the origin of the preglow effect and dependence of its principal parameters (intensity, half-width, and others) on the characteristics of microwave radiation and initial conditions of gas breakdown in a source trap. This effect may be observed in all ECR sources almost independent of characteristics of the used microwave radiation; a proper choice of gas pressure may ensure a regime of ion current burst at the beginning of the pulse. Results of the numerical simulation confirm that the preglow effect is promising for creating a short-pulse ECR source of multicharged particles. The proposed scaling demonstrates that an ECR source with plasma heating by radiation at a frequency of 37 GHz and higher seems to be the most effective in terms of currents, preglow intensity and mean ion charge.

ACKNOWLEDGMENTS

Work was performed in frame of realization of federal targeted program “Scientific and pedagogical labour force for an innovative Russia” for 2009 – 2013 yy.

We acknowledge the financial support of the European Community under the European Commission Framework Programme 7 Design Study: EUROnu, Project Number 212372. The EC is not liable for any use that may be made of the information contained herein.

REFERENCES

[1] (ONLINE) http://beta-beam.web.cern.ch/beta-beam/task/diverse/mandate.htm

[2] T. Thuillier et all. Rev. Scient. Instrum., 79, 02A314, 2008.

[3] I. Izotov et all. IEEE Trans. Plasma Sci.36, 1494, 2008.

"PREGLOW" INVESTIGATION IN ECR DISCHARGE AT 37 GHZ, 100 KW

V.G. Zorin, V.A. Skalyga, I.V. Izotov, S.V. Razin, A.V. Sidorov, Institute of Applied Physics of Russian Academy of Sciences, 46 Ul'yanova st., Nizhny Novgorod, Russia, 603950*
T.Lamy, T. Thuillier, The Laboratoire de Physique Subatomique et de Cosmologie UJF-IN2P3-CNRS, 53 Av. Des Martyrs, 38026 Grenoble Cedex, France.

Abstract

Multicharged ion beams generation in "Preglow" regime is now considered as the main way of short pulsed ion source creation for "Beta Beam" project [1]. The "Preglow" effect has been investigated at a several laboratories (LPSC, JYFL, IAP RAS). The effect was discovered at LPSC on PHOENIX ion source using 18 GHz radiation for plasma heating. Investigations at 14 GHz frequency were made at JYFL. Theoretical analysis demonstrated the advantage of MW frequency increase. Theoretical calculations predict possibility of "Preglow" peaks generation with duration about tens microseconds and rather high average ion charge. At present time at LPSC a joint construction of a new generation ECR ion source with 60 GHz gyrotron plasma heating is running.

As a continuation of previous research at 14, 18 and 28 GHz at present work results of experimental and theoretical "Preglow" effect investigations at SMIS 37 setup with 37,5 GHz MW plasma heating are reported. Received data are important as fundamental result in physics of ECRISs and at the same time it is the next step on the way of 60 GHz SEISM facility creation.

"Preglow" effect was observed and investigated in experiments with ECR discharge stimulated with gyrotron radiation @ 37.5 GHz, 100 kW. Received dependencies of the "Preglow" parameters are in good correspondence with results of numerical simulations. It was shown in experiments that generation of "Preglow" peak with duration about 30 μs is possible.

INTRODUCTION

Investigation of the preglow effect is one of the topical trends in the field of ECR sources of multicharged particles. This effect is, basically, generation of a sharp burst of multicharged ion (MCI) current at the beginning of a microwave pulse, which ensures gas breakdown and plasma confinement in an ion-source magnetic trap. The interest in the preglow effect is associated with prospects of creating an efficient short-pulse MCI source. Such sources are currently in great demand for research in nuclear physics and physics of elementary particles to be carried out on accelerators of new generation.

The preglow effect was first observed in experiments in LPSC and later modeled theoretically in the works [2, 3]. Present work is devoted to experimental demonstration of preglow effect in ECR ion source with gyrotron plasma heating @ 37 GHz, 100 kW.

* sva1@appl.sci-nnov.ru.

FORMULATION OF THE PROBLEM

In frame of short pulse creation problem first of all it is necessary to perform the analysis of gas breakdown dynamics dependences on different parameters.

A microwave breakdown of a rarefied gas in a magnetic trap under the ECR conditions may be separated conventionally into two stages [4], for which the rate of plasma density growth are determined by basically different processes. At the first stage the main process is ionization of the neutral gas by collisions with hot electrons; plasma density grows exponentially, the degree of gas ionization is less than unity, low-charge ions dominate in the distribution of ions over their charge states, and the power absorbed in the plasma is much less than the power of the microwave pumping. At the second stage the rate of density growth slows down significantly, the process of ion peeling goes further, their charge becomes higher, and the power absorbed by the plasma is equal to the power of the microwave pumping, approximately.

Electron energy distribution function (EEDF) which determines plasma life time and efficiency of gas ionization is rather different on those two stages. As it was shown in [2] that transition from breakdown to quasi-stationary stage could be attended with a unexpected transient peak of multicharged ions current. This effect was called preglow [2] and it looks very promising as a way of short pulses creation. Its amplitude and duration are depends on initial breakdown conditions which also determine discharge steady state parameters. It was shown that Preglow peak with duration about of a few tens of microseconds and high average ion charge could be created only with using of microwave with high frequency (more than 30 GHz) and power.

In present work experimental results obtained on SMIS 37 [5] stand demonstrating creation of short pulses under conditions of powerful plasma heating with gyrotron radiation @ 37 GHz are observed.

EXPERIMENTAL SETUP

The experimental research presented in this work was carried out on the SMIS 37 shown schematically in fig. 1.

A gyrotron generating linearly polarized radiation at the frequency of 37.5 GHz, with the power up to 100 kW, and pulse duration up to 1.5 ms was used as a source of pulsed microwave radiation.

In the greatest majority of the experiments the field in the magnetic plugs of the system was 2 Tesla.

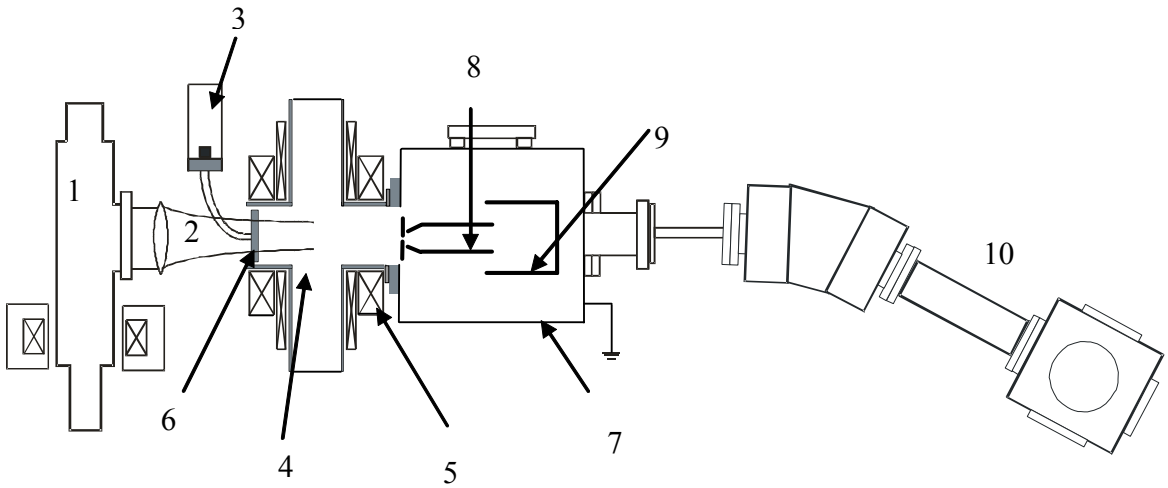

Figure 1: SMIS 37 experimental stand. 1 – gyrotron, 2 – MW beam, 3 – pulsed vacuum valve, 4 – discharge chamber, 5 – magnetic trap coils, 6 – quartz window, 7 – diagnostic chamber, 8 - extractor, 9 – Faraday cup, 10 – ion analyzer.

The operating gas was inlet into the trap along the axis of the magnetic system through a 20-cm long quartz tube with internal diameter of 5 mm; the tube was soldered at the centre of the input quartz window.

Ion extraction and ion beam formation were achieved by means of a traditional two-electrode extracting system. A plasma electrode was placed at an arbitrary distance from the trap plug. Maximum 55 kV voltage was supplied to the extractor. Total ion current was measured by a Faraday cup mounted on the magnetic trap axis. The cup had an input window 35 mm in diameter and intercepted the entire ion beam passed through the extractor puller.

Spectral analysis of the extracted beam of positive ions was performed by means of a magnetostatic analyzer.

EXPERIMENTAL RESULTS

As it was mentioned investigations of non-stationary generation of multicharged ions in Preglow regime in ECR sources are carried out in many laboratories. Typical oscillogram of Ar^{6+} ion current obtained on Phoenix experimental facility at LPSC [2] with plasma heating by 18 GHz radiation is presented in fig.2.

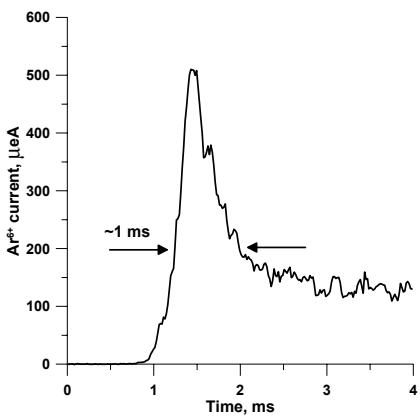

Figure 2: Typical Ar^{6+} current oscillogram on Phoenix 18 GHz facility.

It is evident that formation time of the peak in such conditions is too long for "Beta Beam project".

In experiments on SMIS 37 the Preglow effect was also successfully observed. The Preglow peak duration in this case was about 20 μs, and that is much sorter than shown in fig.3.

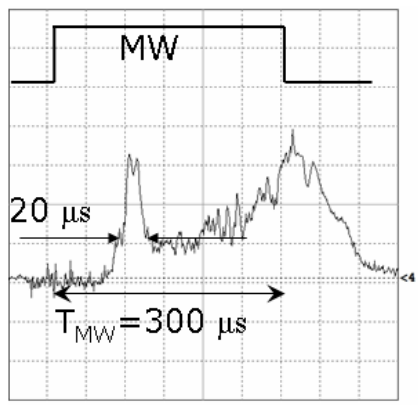

Figure 3: Total ion current.

Experimentally obtained dependences of peak parameters suit well to theoretical calculations. In present work the dependence of qualitative form of ion current pulse on initial neutral gas pressure is presented. In fig 4. a sequence of Faraday cup oscillograms obtained with increase of the pressure in discharge chamber is shown.

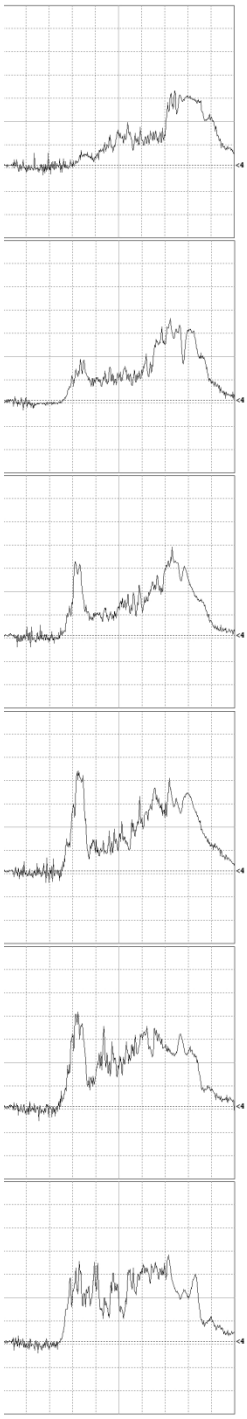

Figure 4: Oscillograms of total ion current in conditions of slight increase of gas pressure in discharge chamber.

Preglow peak could be observed in some narrow range of the pressure what was theoretically predicted in [3].

In such conditions the average ion charger in this peak could be high enough. In fig.5 corresponding ion spectrum in nitrogen is presented.

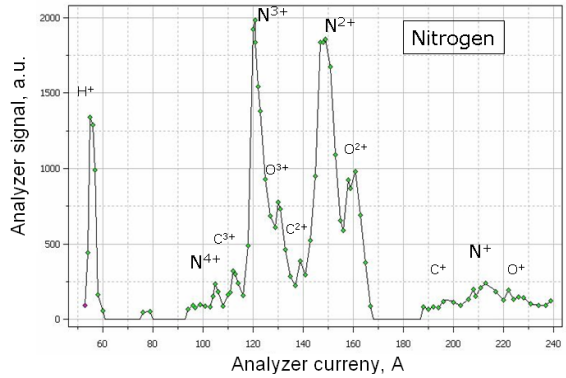

Figure 5: Ion charge state distribution. Nitrogen was used as operating gas.

CONCLUSIONS

Obtained results obviously demonstrate perspective of heating microwaves frequency increase for production of short pulsed multicharged ion beam.

ACKNOWLEDGMENTS

Work was performed in frame of realization of federal targeted program “Scientific and pedagogical labour force for an innovative Russia” for 2009 – 2013 yy.

We acknowledge the financial support of the European Community under the European Commission Framework Programme 7 Design Study: EUROnu, Project Number 212372. The EC is not liable for any use that may be made of the information contained herein.

REFERENCES

[1] http://beta-beam.web.cern.ch/beta-beam/.

[2] T. Thuillier, T. Lamy, L. Latrasse, R. Geller, I. Izotov, A. Sidorov, V. Skalyga, V. Zorin, M. Marie-Jeanne. Study of pulsed electron cyclotron resonance ion source plasma near breakdown : The Preglow. Review of Scientific Instruments, 79, 02A314 (2008).

[3] I.Izotov, A.Sidorov, V.Skalyga, V.Zorin, T.Lamy, L.Latrasse, T.Thuillier. Experimental and Theoretical Investigation of the Preglow in ECRIS. IEEE Transactions on plasma sciense, Vol. 36, No 4, p. 1494 (2008).

[4] V. Skalyga, V. Zorin, V. Izotov, A. Sidorov, T. Lamy, P. Sortais, T. Thuillier. Gas Breakdown in ECR ion Source // Review of Scientific Instruments. v.77, n3, p. 03A325-1 – 03A325-3 (2006).

[5] S.V. Golubev, S.V. Razin, A.V. Vodopyanov, V.G. Zorin. Trans. Fusion Technol. 35, 288 (1999).

TIME EVOLUTION OF PLASMA POTENTIAL IN PULSED OPERATION OF ECRIS*

O. Tarvainen#, H. Koivisto, T. Ropponen and V. Toivanen, University of Jyvaskyla, Finland
Y. Higurashi and T. Nakagawa, Institute of Physical and Chemical Research (RIKEN), Japan

Abstract

The time evolution of plasma potential has been measured with a retarding field analyzer in pulsed operation mode with electron cyclotron resonance ion sources at JYFL and RIKEN. Three different ion sources with microwave frequencies ranging from 6.4 to 18 GHz were employed for the experiments. The plasma potential was observed to increase 10-75 % during the preglow and 10-30 % during the afterglow compared to steady state.

INTRODUCTION

Electron Cyclotron Resonance Ion Sources (ECRIS) exhibit fast transient peaks of extracted ion beam currents at the leading and trailing edges of the applied microwave pulse [1,2]. The fundamental difference between these transients, called preglow and afterglow, is the charge state distribution (CSD) of extracted ion beams - low charge ions (LCI) exhibit preglow while the afterglow boosts the beam currents of highly charged ions (HCI). Studies [1,3,4] of the preglow are driven by the aim of creating a short-pulsed multi-charged ion source with high ionization efficiency. The afterglow mode is utilized e.g. for injection into circular accelerators [5] as it offers intensive beams of HCI.

In order to gain understanding on the plasma processes associated with these transients we measured the time evolution of plasma potential during the microwave pulse. Furthermore, the results allow us to estimate beam transport properties during the transients as the variations of the plasma potential are reflected to the beam energy spread.

EXPERIMENTAL PROCEDURE

The plasma potential of an ECRIS can be deduced by measuring the exact energy of extracted ion beams. The study presented in this article was performed with retarding field analyzers described in detail in references 6 (JYFL) and 7 (RIKEN). Three different ion sources, the JYFL 6.4 GHz ECRIS, the JYFL 14 GHz ECRIS, and a room temperature 18 GHz ECRIS at RIKEN, were employed for the experiments. The retarding field analyzer was located in the beam line downstream from the analyzing magnet to allow charge state dependent studies of the plasma potential. The output of the klystron was controlled by pulsing the input signal from a solid state oscillator with an rf-switch controlled by a pulse generator. The pulsing signal was also used as a trigger for the data acquisition. The klystron gain i.e. attenuator setting was kept constant. The voltage regulated power supply for the retarding electrode was floating on the high voltage of the ion source. This eliminates the error due to small fluctuations of the source bias, typically associated with the plasma breakdown. Signals from the retarding field analyzer and Faraday cup were measured across a resistor and stored with an oscilloscope. Schematic of the measurement setup is shown in Figure 1.

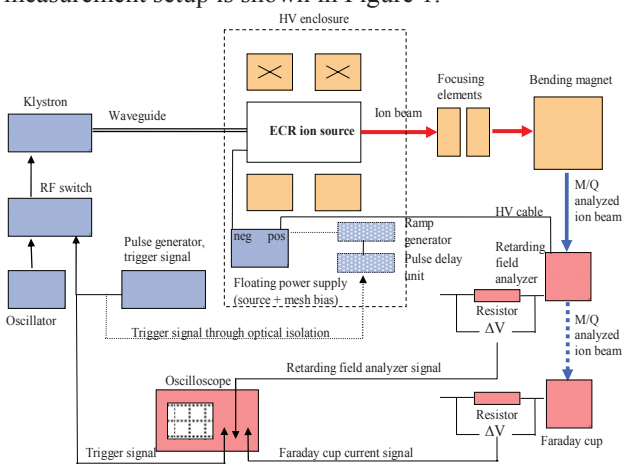

Figure 1: Schematic of the measurement setup.

Two slightly different methods were used for controlling the bias voltage of the retarding field analyzer. The more elegant method utilizes floating, optically isolated, pulse delay unit and voltage ramp generator. The trigger signal was fed into a pulse delay unit gating a fast (1 ms) linear voltage ramp from a signal generator. Adjustment of the pulse delay (measured from the leading edge of rf pulse) was used for selecting the time window for ramping the retarding voltage and acquiring the IV-curve for deducing the plasma potential as described in reference 6. This method was used always when possible i.e. when the variations of the plasma potential were found to be slower than the voltage ramp time of 1 ms, limited by the four-quadrant bias power supply.

Unfortunately, it was observed that this condition does not hold during the preglow and afterglow. For studying fast variations of the plasma potential (preglow and afterglow) the retarding voltage was fixed to a constant value for the duration of the microwave pulse. Increasing the retarding voltage in discrete steps between consecutive pulses makes it possible to deduce the plasma potential at arbitrary time within the microwave pulse after reconstructing IV-curves from the data.

The goal of the experiments was to compare the plasma potential during preglow and afterglow transient with the steady-state value with frequencies from 6.4 to 18 GHz.

* Work supported by the Academy of Finland under the Finnish Centre of Excellence Programme 2006-2011 (Nuclear and Accelerator Based Physics Programme at JYFL).
#olli.tarvainen@jyu.fi

The density of seed electrons at the moment of microwave turn-on affects the characteristics of the preglow [3] and, thus, the effect of seed electrons on the time evolution of plasma potential was studied at JYFL. Seed electrons were produced by sustaining a low density plasma with low power cw microwaves from a TWTA. The power dependence of the plasma potential time evolution was studied at RIKEN. Helium and Argon plasmas were used for the experiments and the source settings, i.e. power, neutral gas pressure and magnetic field, were chosen to correspond to typical operational values of the ion sources.

EXPERIMENTAL RESULTS

He^{2+} ion beam was used for studying the plasma potential during the preglow with the JYFL ECR ion sources (6.4 and 14 GHz). The delay between plasma breakdown and first observation of extracted He^{2+} is less than 0.2 ms [3]. Microwave pulse pattern with on-time of 1.76 s and off-time of 5.9 s was used in order to assure that the plasma potential reaches a steady-state value and to drain the magnetic bottle from well-confined electrons between the pulses. The plasma potential and He^{2+} ion beam current following the microwave turn-on (at t = 0 ms) are presented in Figure 2. The plasma potential peaks immediately after the plasma breakdown being 30 – 50 % higher than the saturation value. The peak of the plasma potential coincides reasonably well with the preglow in the case of 14 GHz ion source. In the case of 6.4 GHz a similar peak of plasma potential was observed although the preglow is virtually non-existent.

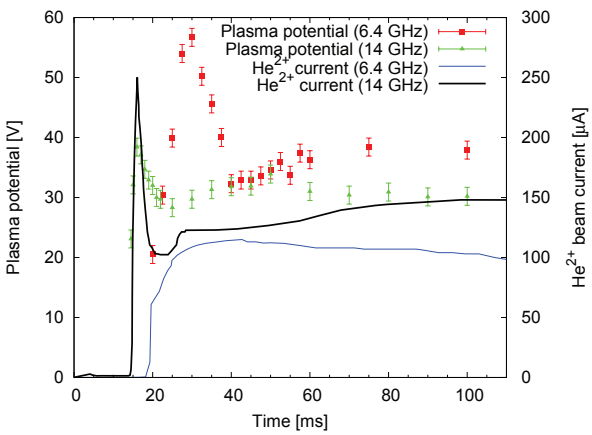

Figure 2: Preglow plasma potential and He^{2+} ion beam current of the JYFL ion sources.

It was observed with the JYFL 14 GHz ECRIS that while providing seed electrons clearly enhances the preglow ion beam current of He^{2+} and allows a faster plasma breakdown, the time evolution of plasma potential is unaffected as shown in Figure 3.

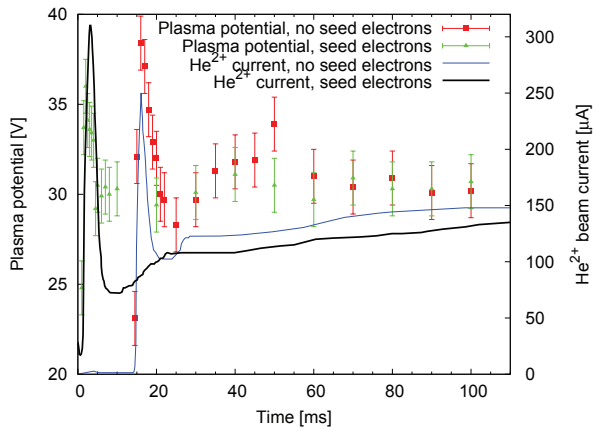

Figure 3: Preglow plasma potential and He^{2+} ion beam current with and without seed electrons (JYFL 14 GHz ECRIS).

Argon plasmas also exhibit similar transient behavior in the very beginning of the microwave pulse (confirmed at JYFL and RIKEN). Figure 4 shows a result from the 18 GHz ECRIS at RIKEN. Microwave pulse pattern with on- and off-times of 100 ms (i.e. duty factor of 50%), resulting into presence of notable amount of seed electrons, was used. The plasma potential was measured with Ar^{9+} ion beam.

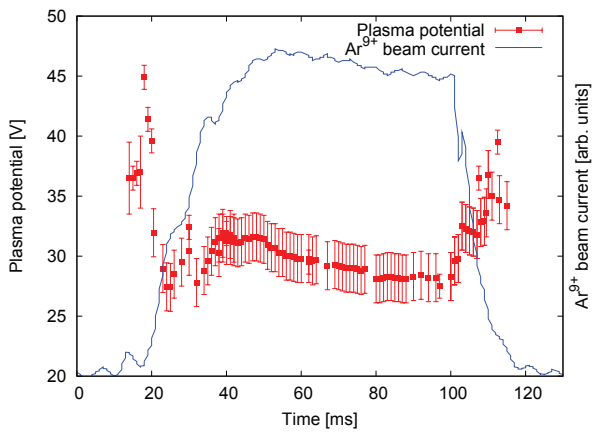

Figure 4: Plasma potential and Ar^{9+} ion beam current of the RIKEN 18 GHz ECRIS.

The peak of the plasma potential in the beginning of the microwave pulse is reached far before the beam current of Ar^{9+} reaches steady-state. The behavior highlights the fact that during the preglow the plasma is populated by low charge state ions increasing the plasma potential. The RIKEN 18 GHz ECRIS was also used for studying the time evolution of plasma potential at different microwave powers. The results are displayed in Figure 5.

The peak value of the plasma potential remains practically constant while the steady-state value increases at higher power (plasma density). The relaxation time decreases with increasing power. Saturation was not reached with 100 ms pulses for 100 W of power (indicated by the arrow associated with the data point).

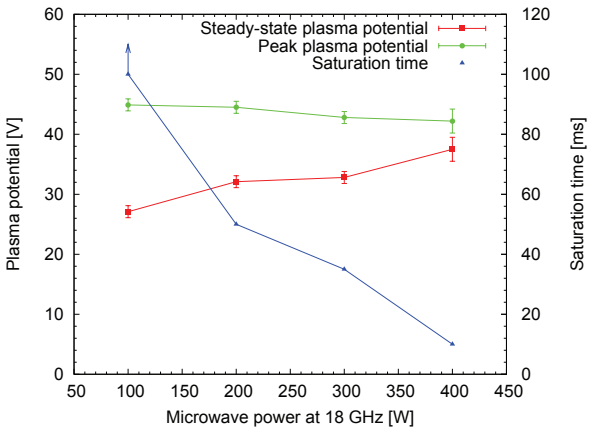

Figure 5: The effect of microwave power on the behaviour of the plasma potential (18 GHz).

Figure 4 shows also that the plasma potential increases momentarily during the plasma decay (afterglow). Similar behavior during the afterglow was observed with the JYFL ion sources. The magnitude of the afterglow fluctuation of the plasma potential was less pronounced at lower frequencies. i.e. lower magnetic field affecting the plasma confinement. The relative increase of the plasma potential during the preglow and afterglow transients for the three ion sources are listed in Table 1. The range of the values corresponds to varying ion source settings (however, a full parametric study is still desirable).

Table 1. Comparison of the relative increase of plasma potential (argon) during the preglow and afterglow.

Ion Source	Preglow / Steady-state plasma potential	Afterglow / Steady-state plasma potential
JYFL 6.4 GHz	1.06 – 1.12	1.09 – 1.14
JYFL 14 GHz	1.13 – 1.47	1.17 – 1.28
RIKEN 18 GHz	1.13 – 1.66	1.04 – 1.34

DISCUSSION

The conclusion of our studies can be summarized as follows: the plasma potential is higher during the plasma build-up and decay compared to steady-state conditions. However, the processes explaining the potential fluctuations are different for preglow and afterglow.

It is believed that the preglow peak of low charge state ion currents is caused by abrupt change in plasma energy content (electron energy distribution function, EEDF) [4]. At low ionization degree, the microwave power is sufficient to heat the electron population to high energies corresponding to so-called superadiabatic EEDF. The average electron energy collapses with exponentially increasing plasma density, which results to burst of electron losses from the plasma. Due to lower mobility, the loss rate of ions cannot match the loss rate of electrons. The difference in particle fluxes is compensated by the formation of plasma potential. High electron loss rate associated with the transition from superadiabatic EEDF to bi-Maxwellian one forces the plasma potential to peak in the process. The effect is presumably amplified by the fact that the preglow CSD is concentrated on LCI. High plasma potential is required to retard electrons and, on the other hand, supply LCI with enough velocity to balance the fluxes of negative and positive charge. As the mean charge of ions increases, the potential drops and reaches steady-state value. The damping of the plasma potential fluctuations seems to be faster with increasing microwave power and frequency i.e. increasing plasma density in steady-state. This is most likely due to increased rate of ionization pushing the CSD towards equilibrium in reduced time.

Plasma potential peaking during the preglow implies that any application, relying on running an ECRIS in pulsed mode and utilizing the preglow transient, must take into account the increased energy spread of the ion beam causing the bending and focusing properties of the ion beam differ from those of a cw beam. It is plausible to claim that the space charge compensation degree of the ion beams in pulsed mode is lower than cw beams, which could deteriorate the beam quality even further. This has been noted in experiments at JYFL [3] in which the bending magnet (energy spread) and solenoids (space charge compensation / beam particle distribution) had to be tuned differently when switching from cw beams to pulsed beams (preglow).

According to the prevailing understanding afterglow peak of HCI is initiated by a burst of cold electrons escaping the plasma [2]. As the microwave power is turned off, growing number of cold electrons populate the loss cone of the magnetic bottle in velocity space because they are not being heated perpendicular to the magnetic field anymore. It has been argued [8] that this process changes the magnitude and spatial distribution of the plasma potential reducing the confinement of ions. Our experiments suggest that the ion confinement is indeed reduced during the afterglow due to increased plasma potential, which results to a fast transient peak of HCI expelled from the plasma, followed by diffusive decay.

REFERENCES

[1] I.V. Izotov, A.V. Sidorov, V.A. Skalyga, V.G. Zorin, T. Lamy, L. Latrasse, T. Thuillier, IEEE Transactions on Plasma Science, 36, 4, Part 2, (2008), p. 1494.
[2] G. Melin et al., Rev. Sci. Instrum. 61, 236, (1990).
[3] O. Tarvainen, T. Ropponen, T. Thuillier, J. Noland, V. Toivanen, T. Kalvas, and H. Koivisto, Rev. Sci. Instrum. 81, 02A303 (2010).
[4] I. Izotov et al. in these Proceedings.
[5] C. E. Hill and K. Langbein, Rev. Sci. Instrum. 69, 643, (1998).
[6] O. Tarvainen, P. Suominen, and H. Koivisto, Rev. Sci. Instrum. 75, 3138 (2004).
[7] H. Higashijima, W. Takai, T. Nakagawa, Y. Higurashi, M. Kidera, and A. Goto Rev. Sci. Instrum. 79, 02B505 (2008).
[8] R. Geller, Proc. Intl. Conf. on Physics of Highly Charged Ions, Giessen, p. 117 (1990).

MICROPULSES GENERATION IN ECR BREAKDOWN STIMULATED BY GYROTRON RADIATION AT 37,5 GHZ

V.Skalyga*, V. Zorin, I. Izotov, S. Golubev, S. Razin, A. Sidorov, A. Vodopyanov
Russian Academy of Sciences, 46 Ulyanova st., Nizhny Novgorod, Russia, 603950

Abstract

Present work is devoted to experimental and theoretical investigation of possibility of short pulsed (< 100 μs) multicharged ion beams creation.

The possibility of quasi-stationary generation of short pulsed beams under conditions of quasi-gasdynamic plasma confinement was shown in recent experiments. Later another way of such beams creation based on "Preglow" effect was proposed. In present work it was demonstrated that in the case when duration of MW pulse is less then formation time of "Preglow" peak, realization of a regime when ion current is negligible during MW pulse and intense multicharged ions flux appears only when MW ends could be possible. Such pulses after the end of MW were called "micropulses". In present work generation of micropulses was observed in experiments with ECR discharge stimulated by gyrotron radiation @ 37,5GHz, 100 kW. In this case pulses with duration less than 30 μs were obtained. Probably the same effect was observed in GANIL where 14 GHz radiation was used and pulses with duration about 2 ms were registered [1].

In present work it was shown that intensity of such micropulse could be higher than intensity of "Preglow" peak at the same conditions but with longer MW pulse. The generation of micropulses of nitrogen and argon multicharged ions with current of a few mA and length about 30 μs after MW pulse with duration of 30-100 μs was demonstrated. The low level of impurities, high current density and rather high average charge make possible to consider such micropulse regime as perspective way for creation of a short pulsed ion source.

INTRODUCTION

Realization of the European programme for neutrino oscillations research, "Beta Beam Project" [2], requires that short-pulse (10 to 100 μs) beams of multicharged ions of radioactive gases (^{6}He or ^{18}Ne) with high gas efficiency be created. A possible way to achieve formation of such beams is associated with the use of a pulsed ECR source of multi-charged ions (MCI). Application of modern classical ECR ion sources for this is not feasible, since the time of gas breakdown and the plasma density's reaching the stationary level is long (over 1 ms) as compared with the required pulse duration. In [3] possibility of gas breakdown process shortening by using of microwave radiation with higher frequency for plasma heating was demonstrated theoretically. Plasma life time decreases with increase of its density (plasma density could be increased by using of higher frequency microwaves) in the case of classical plasma confinement [4] and reaches its minimum value determined by quasi-gasdynamic plasma outflow from the trap though magnetic plugs [5]. That is why present work is devoted to experimental demonstration of short pulsed multicharged ion beams creation possibility in ECR ion source with gyrotron plasma heating with frequency 37 GHz and power 100 kW. Such parameters of microwave heating are much higher than in traditional ECR ion sources [6]. In the article two regimes of short pulsed beams generation are discussed: quasi-stationary and non-stationary.

FORMULATION OF THE PROBLEM

To solve a problem of short pulse creation, first of all it is necessary to perform the analysis of gas breakdown dynamics dependences on different parameters.

In the very beginning of microwave breakdown of a gas in a magnetic trap under the ECR conditions the main process is ionization of the neutral gas by collisions with hot electrons; plasma density grows exponentially, the degree of gas ionization is less than unity, low-charge ions dominate in the distribution of ions over their charge states, and the power absorbed in the plasma is much less than the power of the microwave pumping. Electron energy distribution function (EEDF), which determines plasma life time and efficiency of gas ionization, has a form corresponding to superadiabatic regime of electron heating in a mirror trap under ECR condition. Average energy of electrons in this case is as high as hundreds kilo electron-volts [7]. Energy content of plasma grows with plasma density. Plasma confinement time is rather high. If one stop microwave pulse on this stage, ionization would continue as long as electron temperature is high. In this case appearing of ion beam after end of microwaves pulse is possible like it happen in afterglow mode.

*Corresponding author :
sva1@appl.sci-nnov.ru

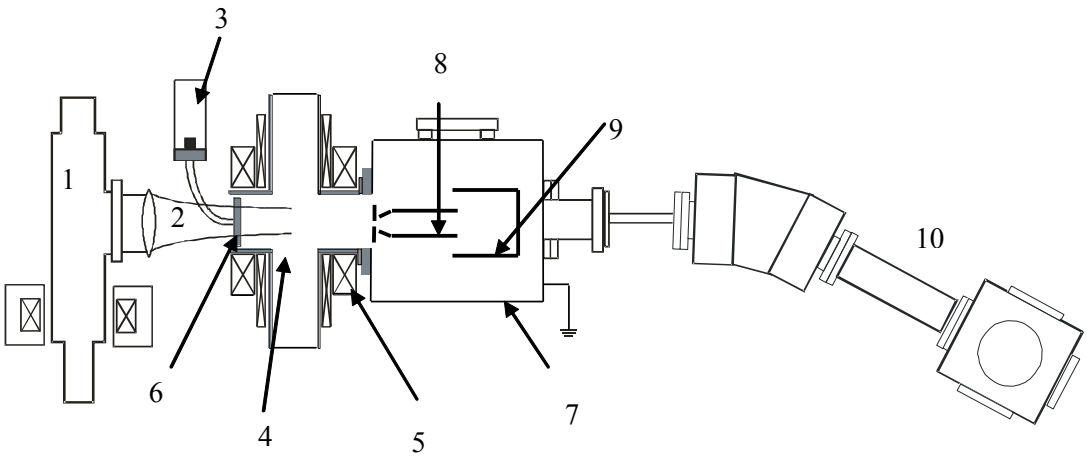

Figure 1 SMIS 37 experimental stand. 1 – gyrotron, 2 – MW beam, 3 – pulsed vacuum valve, 4 – discharge chamber, 5 – magnetic trap coils, 6 – quartz window, 7 – diagnostic chamber, 8 - extractor, 9 – Faraday cup, 10 – ion analyzer.

Experimental results obtained on SMIS 37 [8] stand demonstrating creation of short pulses under conditions of powerful plasma heating with gyrotron radiation @ 37 GHz are described in the present work.

EXPERIMENTAL SETUP

The experimental research presented in this work was carried out on the SMIS 37 shown schematically in Figure 1.

A gyrotron generating linearly polarized radiation at the frequency of 37.5 GHz, with the power up to 100 kW, and pulse duration up to 1.5 ms was used as a source of pulsed microwave radiation.

Mirror or cusp magnetic traps was created by 2 pulsed solenoids. In the greatest majority of the experiments the field in the magnetic plugs of the system was 2 Tesla.

The operating gas was inlet into the trap along the axis of the magnetic system through a 20-cm long quartz tube with internal diameter of 5 mm; the tube was soldered at the center of the input quartz window.

Ion extraction and ion beam formation were achieved by means of a traditional two-electrode extracting system. A plasma electrode was placed at an arbitrary distance from the trap plug. Maximum 55 kV voltage was supplied to the extractor. Total ion current was measured by a Faraday cup mounted on the magnetic trap axis. The cup had an input window 35 mm in diameter and intercepted the entire ion beam passed through the extractor puller.

Spectral analysis of the extracted beam of positive ions was performed by means of a magnetostatic analyzer.

EXPERIMENTAL RESULTS

Quasi-stationary short pulse generation

The aim of experiments was investigation of time dynamics of the discharge and efficiency of multicharged ions generation. To realize the minimum time of gas breakdown together with high ionization rate the next experimental conditions were tuned: microwave power, neutral gas flux into the source, neutral gas pressure, magnetic field of the trap. For plasma confinement a cusp magnetic trap was used. As a result of tuning discharge evolution time about 15 μs was obtained. In Figure 2 an example of total ion current oscillogram when 50 μs microwave pulse was used for plasma heating is presented.

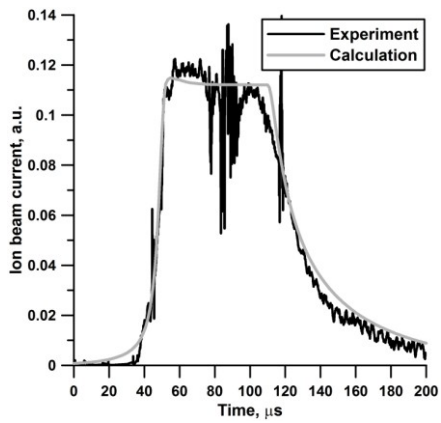

Figure 2. Total ion current. 1 – current measured with Faraday cup , 2 – numerical simulation for corresponding parameters.

As follows from Figure 2 the time of current rising is about 15 μs, and it is enough for creation of the pulses with duration of 30 μs and more, that meets the challenge of the "Beta Beam project". In those experiments the plasma flux density through the plugs of the trap was equal to 2 A/ cm^2.

Non-stationary short pulse generation

Study of a possibility of shortening of ion beam pulse was started with study of Preglow effect. The effect was found and described in [7]. Later it was studied with higher (37 GHz) frequency of MW pumping. Three left

oscilogramms in Figure 3 show this effect. Further shortening of microwave pulse leads to only one maximum on the oscilogramm (right oscilogramms in Figure 3) which appeared a certain time later of end of the microwave pulse.

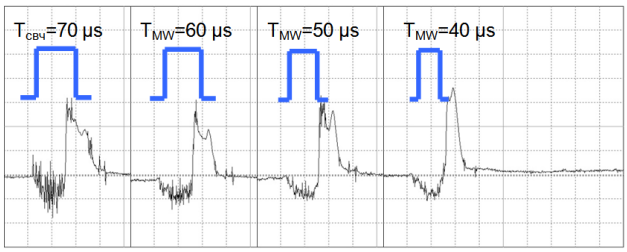

Figure 3. Ion current of Ar^{4+} versus microwave pulse duration. Negative signal on the oscilogramms is electric noise.

Such short pulse after the end of microwaves was called "micropulse". Temporal evolution of ion beam current may be described in frame of the model developed in [7]. In the beginning of the breakdown while plasma density is low electrons could accumulate a lot of energy which could course an efficient ionization after the end of MW pulse. Fast density growth and average electron energy decrease after MW pulse leads to intense peak of ion current. So nature of micropulses is close to afterglow, but with starting of afterglow peak not from steady state regime of discharge flow but from breakdown stage.

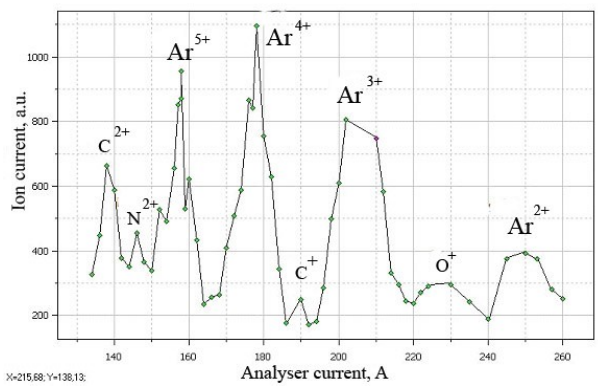

Figure 4. Ion charge state distribution for Argon.

In such conditions the average ion charger in this peak could be high enough. In Figure 4 corresponding ion spectrum in argon is presented.

CONCLUSIONS

Obtained results obviously demonstrate perspective of heating microwaves frequency increase for production of short pulsed multicharged ion beam.

ACKNOWLEDGMENTS

Work was performed in frame of realization of federal targeted program "Scientific and pedagogical labor force for an innovative Russia" for 2009 – 2013 yy.

We acknowledge the financial support of the European Community under the European Commission Framework Programme 7 Design Study: EUROnu, Project Number 212372. The EC is not liable for any use that may be made of the information contained herein.

REFERENCES

[1] L. Maunoury at all. Sev. of Scient. Instr. 79, 02A313 (2008)

[2] http://beta-beam.web.cern.ch/beta-beam/.

[3] V. Skalyga, V. Zorin, V. Izotov, A. Sidorov, T. Lamy, P. Sortais, T. Thuillier. Gas Breakdown in ECR ion Source // Review of Scientific Instruments. v.77, n3, p. 03A325-1 – 03A325-3 (2006).

[4] Pastoukhov V.P.. Review of Plasma Physics, v.13, p.203 (1987).

[5] Mirnov V.V., Ryutov D.D. Pisma v Zhurnal Theknicheskoi Fiziki., v.5,p. 678 (1979).

[6] R. Geller, Electron Cyclotron Resonance Ion Sources and ECR Plasmas. UK, London, Institute of Physics Publishing (1996).

[7] T. Thuillier, T. Lamy, L. Latrasse, R. Geller, I. Izotov, A. Sidorov, V. Skalyga, V. Zorin, M. Marie-Jeanne. Study of pulsed electron cyclotron resonance ion source plasma near breakdown: The Preglow. Review of Scientific Instruments, 79, 02A314 (2008).

[8] S.V. Golubev, S.V. Razin, A.V. Vodopyanov, V.G. Zorin // Trans. Fusion Technol. 35, 288 (1999).

BEAM, MULTI-BEAM AND BROAD BEAM PRODUCTION WITH COMIC DEVICES*

P. Sortais#, T. Lamy, J. Médard, J. Angot, UJF CNRS-IN2P3 INPG, LPSC, Grenoble, France
C. Peaucelle, IPNL, Grenoble, France

Abstract

The COMIC discharge cavity is a very versatile technology. We will present new results and devices that match new applications like: molecular beams, ultra compact beam line for detectors calibrations, quartz source for on-line application, high voltage platform source, sputtering /assistance broad beams and finally, a quite new use, high energy multi-beam production for surface material modifications.

In more details, we will show that the tiny discharge of COMIC can mainly produce molecular ions (H_3^+). We will present the preliminary operation of the fully quartz ISOLDE COMIC version, in collaboration with IPN-Lyon, we will present a first approach for a slit extraction version of a three cavity device, and after discussing about various extraction systems on the multi discharge device (41 cavities) we will show the low energy broad beam (2 KV) and high energy multi-beams (10 beams up to 30 KV) productions.

We will specially present the different extraction systems adapted to each application and the beams characteristics which are strongly dependent on the voltage distribution of an accel-accel two electrodes extraction system.

THE COMIC PRINCIPLE

The basic principle of the COMIC (COmpact MIcroonde & Coaxial) discharge have been previously presented [1]. This principle is a very basic and low power way of plasma generation and we will present here the different discharge customization ways for beam, broad beam of multi-beam generation. The plasma is ignited between a quarter wave antenna and grounded couplers where the over voltage can reach the Paschen's conditions (Fig.1). This discharge is magnetized by a small gradient of a magnetic field that reach ECR conditions at the level of this over voltage. The weak generated plasma (roughly 5eV and 5 10^{10} cm^{-3}, measured after 5 mm of diffusion outside the cavity) is very suitable for molecular and monocharged ion production .The very small confinement time allows the creation of non negligible current densities in the range of 0.1 to 10 mA/cm^2. The consequence of these compromises is the use of relatively high gas flux by respect to a high confinement ECR source.

*Work supported by GRAVIT (Grenoble Alpes Valorisation Innovation Technologies) under grant ND-77-2009.
#sortais@lpsc.in2p3.fr

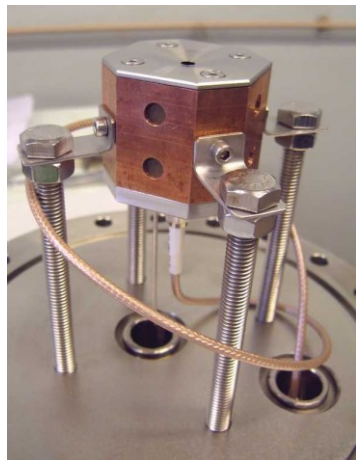

Figure 1: The elementary COMIC discharge.

We can see (Fig.2) an optimization for the production of H_3^+ molecular ions (15 µAe with 1 mm extraction hole). Due the poor pumping of hydrogen we have observe the breaking of the 20 KV H_3^+ in two peaces : H_2^+ at 13.6 and H^+ at 6.8 KV and also H^+ at 10 KV coming from 20 KV H_2^+. The production of high currents of hydrogen could be done only with a strong pumping dedicated to hydrogen.

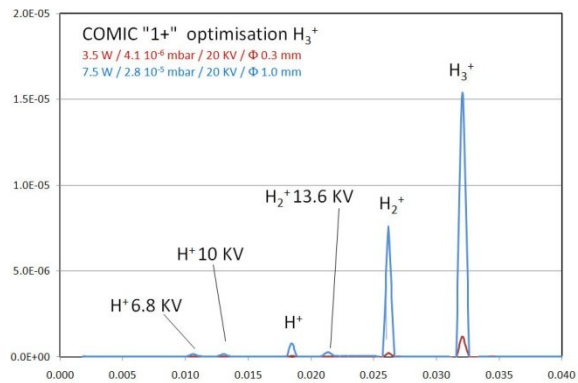

Figure 2: H_3^+ optimisation with partial energy beams generated by gas interaction of H_3^+ and H_2^+.

MONOBEAM / MONOCAVITY DEVICES

Due to the small size and low power operation, it is easy to match a COMIC source to compact devices.

A first one, now under assembly, is a moveable beam line for detectors calibrations. The purpose here is to deliver very low ion and electron currents (down to some

p/s) but with a high reliability. Inside a compact line (50 cm in length and 16 cm in diameter) it would be possible to focus or defocus the beam, with or without ion selectivity (Fig.3) for energy up to 50 KV. A Wien filter module can be placed in front of the source in order to get ionic selectivity up to the mass 20.

A second device is the so-called Q-COMIC, developed for ISOLDE/CERN that is a special version including a fully quartz gas and plasma chamber for ionisation of radioactive gas (Fig.4). The current and functioning point are very close to the COMIC one but here all the wall of the plasma chamber are quartz recovered from the gas injection to the current extraction [2].

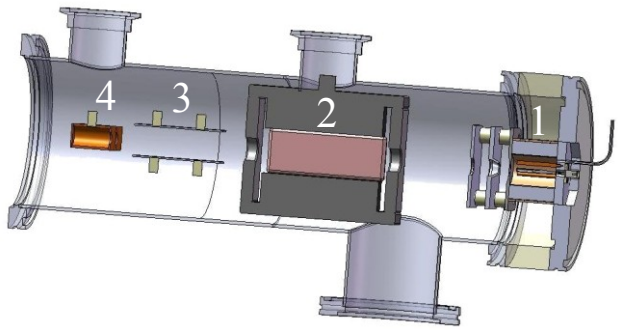

Figure 3: Moveable mini beam line for the MIMAC detector (1 - source, 2 Wien filter (or H deflector) -, 3 – V deflector, 4 – Faraday cup)

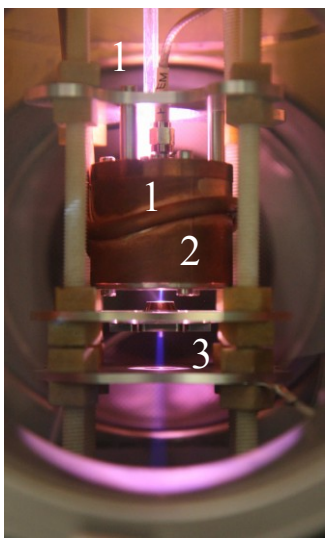

Figure 4: Q-Comic with quartz plasma chamber (1 - quartz, 2 - source, 3 - beam)

MONOBEAM / MULTICAVITY DEVICES

The principle of the COMIC discharge can be use also to generate slit or broad beams. A first device called T-COMIC (including three discharges) has been built in order to improve the reliability of Xenon beams initially produced with a Bernas ion source on a high voltage platform (Fig. 5). Here the microwave device has been introduced exactly inside the same volume and at the same place that the filament source. The plasma of three cavities feeds a small diffusion gap and after this gap a plasma electrode with a small rectangular slit extracts the beam extract the beam. Preliminary current measurements show a current density similar to a Ø 4 mm extractor (4 mA/cm2) but here produced as a slit beam (2 per 12 mm). The optical qualities of this beam are very similar to the Bernas one, so the possibility of matching the beam to the optical system of the high voltage platform is performed without problems (Fig. 6).

Figure 5: T-COMIC with up to three discharge and plug & play by respect to a filament source.

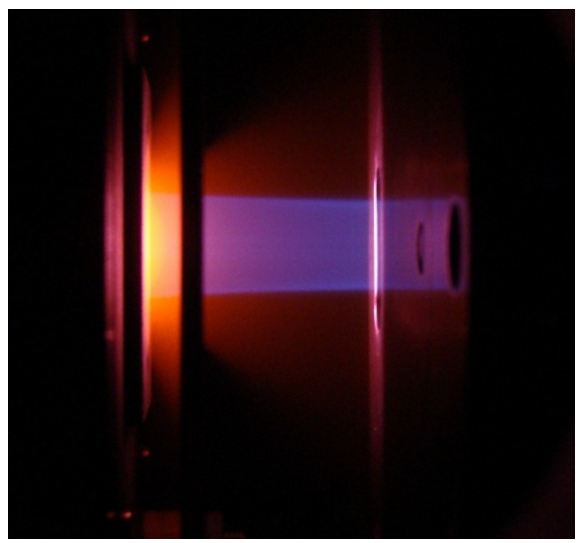

Figure 6: “Slit” beam produced with T-COMIC (1 mA, Ar, 30 KV, 20 W , 2.45 GHz, one cavity excited).

We can see (Fig. 7) the machine called COMIC-Array that is made of 41 cavities distributed over a square of 16 cm per 16 cm. Between each cavity a small magnet magnetizes four adjacent discharge volumes. Therefore, more than 50 % of the surface (41 times Ø 2 cm) can be used as a plasma diffuser so the plasma can be homogenized after some centimetres from the plane of the

discharges. This broad beam can be produced by the progressive activation of eight independent cavities and extraction after a diffusion gap of 9 mm like. This very preliminary test already shows that it is possible to build a large beam from the activation of small and well optimized discharges followed by the mixing of the different plasmas produced by each cavity. The beam (Fig. 8) is produced with a gas flux in the 41 cavities of about 1 mbar.l.s-1, but only 8 cavities are activated (only 8 transmitters available at this time) for an extracted current of 22 mAe at 2 KV.

Figure 7: COMIC-array low energy with grid extractor (gap size : 4 mm)

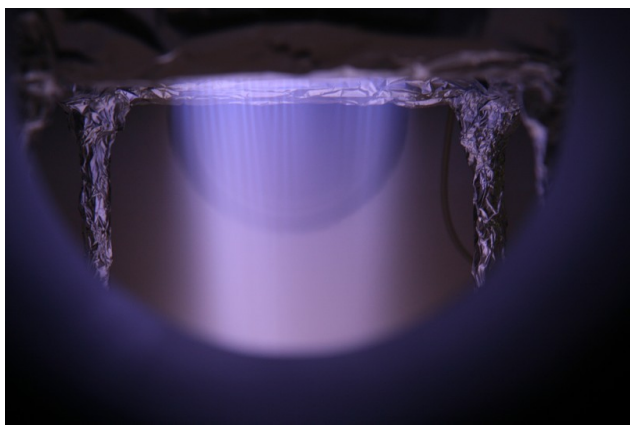

Figure 8: Low energy (2 KV) broad beam produced with COMIC-array (9 per 6 cm / 8 discharges).

MULTIBEAM / MULTICAVITY DEVICES

Such device can also be used at higher voltages (some tens of KV). In this case all the 41 cavities are closed by the plasma electrode so the discharge panel become just a juxtaposition of 41 independent COMIC ion sources (Fig. 9). The extraction system is a simple two gap extractor made of two plates with 13 holes of extraction. We can see (Fig. 10) 10 beams of Xenon produced in parallel. A strong defocus can be obtained just by tuning of the intermediate voltage and thus we can obtain a mixing of the different beams at a distance of some ten centimetres.

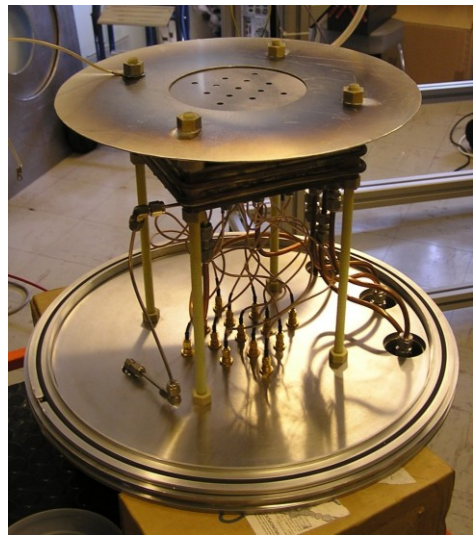

Figure 9: COMIC-array high energy with double gap extractor

Figure 10: 10 beams at 25 KV/ Φ 2mm of Ar (roughly 150 µA per beam) the "target" plate is placed at 10 cm from the extractor.

CONCLUSION

By the use of a small, simple and reliable microwave device it is possible to customize various devices for plasma or ion beam applications. Lot of new other customizations are possible.

REFERENCES

[1] P. Sortais, T. Lamy, J. Médard, J. Angot, L. Latrasse, and T. Thuillier, Rev. Sci. Instrum. 81 (2010) 02B31

[2] MOPOT06, P. Suominen, T. Stora, P. Sortais, J. Médard, these proceeding.

STATUS OF THE HIGH CURRENT PERMANENT MAGNET 2.45GHZ ECR ION SOURCE AT PEKING UNIVERSITY*

S. X. Peng#, Z. Z. Song, J. X. Yu, H. T. Ren, M. Zhang, Z. X. Yuan, P. N. Lu, J. Zhao, J. E. Chen, Z. Y. Guo, Y. R. Lu, SKLNPT, Peking University, Beijing 100871, China

Abstract

Several compact 2.45 GHz Electron Cyclotron Resonance Ion Sources (ECRISs) have been developed at Peking University for ion implantation [1], Separated Function Radio Frequency Quadrupole project (SFRFQ)[2] and for the Peking University Neutron Imaging FaciliTY project (PKUNIFTY) [3]. Studies on 2.45 GHz ECR ion sources are concentrated on methods of microwave coupling and microwave window design, magnetic field generation and configuration, as well as the extraction electrodes structure. Investigation also covers the influence of the size of plasma chamber on the discharge efficiency and species factor. Up to now, our sources have produced 25 mA of O^+ ion, 40 mA of He^+ ion, 10 mA of N^+ ion, 100 mA of H^+ ions and 83 mA of D^+ ions, respectively.

INTRODUCTION

In recent years the production of high current beams is a key point for many research projects [4]. The 2.45 GHz electron cyclotron resonance (ECR) ion sources, invented 30 years ago by Sakudo [5] and Ishikawa *et al.* [6] for industrial applications, are the suitable candidates of producing high current and high brightness proton, deuteron, oxygen and other mono-charged light ion beams. The special characteristics of 2.45 GHz ECR sources, such as high ion current density, compact structure, high reliability, ability to operate in both CW and pulsed mode, good reproducibility and low maintenance, make it popular as a High Current Ion Source in the world [7-10].

Research on the 2.45 GHz high current ECR ion source at Peking University (PKU) can trace back to 1980's [10]. Since then, several 2.45 GHz ECR sources were developed for different purposes [1-3]. Fig.1 is a schematic configuration diagram of the PKU ECR ion source developed for Peking University Neutron Imaging FaciliTy (PKUNIFTY) project (PMECR IV, see below). As shown in fig.1, special designed alumina dielectric microwave window is used for the microwave coupling between the rectangle microwave guide and plasma chamber. The axial magnetic field needed by the ECR in the plasma chamber with 2.45 GHz rf wave is provided by three permanent magnet rings, so the source is named PMECR ion source. Its out diameter and its length are 10 cm, and its weight is less than 5 kg. The discharge chamber is a cylinder with diameter about 40 mm and length of 50 mm. For beam extraction, a 45° angle cone-expansion type electrode is used to suppressing the beam divergence. Heretofore, we have got several tens of milliampere of various gas ions, such as H^+, D^+, He^+, N^+ and O^+ [1][11][12][13][14]. Now the PMECR I ion source is routinely delivering ion beams for Separated Function Radio Frequency Quadrupole (SFRFQ) project [2] and the PMECR IV, for PKUNIFTY project [3].

The technical achievements and progresses on methods of magnetic field generation and configuration, source body structure, microwave coupling, and beam extraction electrodes design of PKU 2.45GHz ECR ion source in the past decades will be described in this paper.

MICROWAVE COUPLING METHODS

The microwave system of an ECR ion source is used to generate 2.45 GHz microwave and transport the microwave to the ion source. At PKU, the system is a very simple one with a microwave generator, a magnetron cavity, a circulator or isolator, a tuner, some rectangular waveguide, a high voltage break wave guide (HV break) and a coupling part with source body. The tuner (manual three-stub or automatic stub) is adapted for matching the waveguide to plasma impedance, which enhances the plasma density and finally increases the current density of the extracted beam. The WR340 and WR284 rectangular waveguides were compared during the source running. Results show that using the WR340 rectangular waveguide can save more than 30% microwave power comparing with the WR284 to obtain the same beam current extracted at the same conditions [12].

The microwave coupling part refers to the matching unit to adapt the standard rectangular waveguide to the source body. Ridged waveguide, dielectric microwave window and antennas are the three ways to fulfil the coupling. Most Labs, such as Chalk River National Laboratory, Saclay/CEA [15][8], are using a ridged waveguide to match the microwave line with source body. At PKU, ridged waveguide, dielectric microwave window as well as T-shape antenna were tested at the early stage of ECRIS development [11][1][12]. The presence of antennas is not convenient to the routine operation because of periodical maintenance. Experimental results show that the function of dielectric microwave windows with special design is equivalent to a ridged waveguide for microwave coupling between the microwave line and the discharge plasma. As shown in fig.1, the dielectric microwave window for 2.45GHz ECR ion source at PKU which consists of an alumina block with dielectric constant 9 is special design for microwave coupling. It works as vacuum sealing as well. In the meantime, a piece of thin BN or SiN disk toward the plasma is used to protect the microwave window from the bombarding of electrons. The lifetime of SiN is longer than BN for

*Work supported by NSFC No. 10675015 and 10455001.
#Sxpeng@pku.edu.cn

window protection [13], which has been proved by the recent research on the D^+ ion source developed for PKUNIFTY project. With dielectric microwave window, the microwave system is more compact compared with using ridged waveguide.

By inserting a HV break in our microwave line, the tuner, the isolator, the microwave cavity and the microwave generator can be operated on ground voltage. It has been proved that this design is very robust and safety.

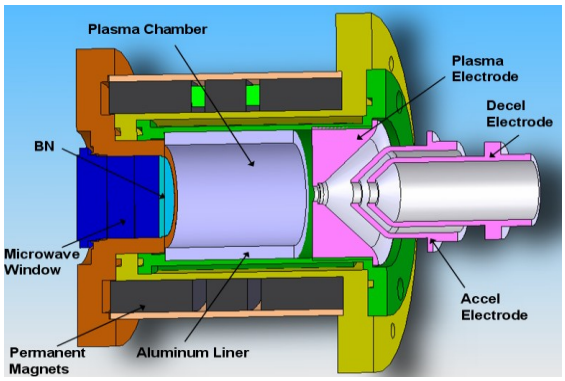

Figure 1: Schematic diagram of 2.45 GHz ECR ion source in PKU.

MAGNETIC FIELD GENERATION AND SOURCE BODY FABRICATION

In microwave discharge ion sources, the magnetic field along the plasma chamber axis is effective on the ionization process because it forces the electrons to circulate around the field lines and increases the ionization probability. Different theoretical approaches exist about plasma ignition in High Current Ion Source operating at 2.45 GHz that depends on the shape and value of the maximum magnetic field with respect to B_{ECR} = 875 Gauss [16].

The axial magnetic configuration can be provided by three ways, which are electromagnetic coils [7][8][16][17], electromagnetic coil plus permanent magnetic rings [1], or permanent magnetic rings only [1][18]. The magnetic field distribution and strength can be adjusted when the electromagnetic coils are used. But in the case of using permanent magnets only, the magnetic field is unchangeable after source assembling.

BEAM FORMATION AND HANDLING

The beam extraction system design is depended on requirements of the accelerator. Special attention should be paid to the electrode design in order to minimize the electric field on the electrode surface, beam divergence angle, beam emittance and the spark risks. The most important parameters in extraction system design are the angle of the conical section of the plasma electrode and the ratio *S* defined as the radius of extraction aperture of plasma electrode over the distance from plasma electrode to the downstream electrode.

So simulation using suitable software is needed in the permanent magnet design, and the special attention should be paid to avoid high stray field at the extraction side, which may result in Penning discharge within the extraction region. The advantages of using permanent magnets are obvious. For example, with permanent magnets the size of the components at high voltage becomes smaller, the power supplies operated on high voltage platform is no longer needed, and the structure of the ion source body is more compact. Also the ion beams produced by PMECR ion source have better stability and reliability in comparison with the solenoid coil system for long term operations [4]. By replacing solenoids and its power supplies with several permanent magnetic rings, the manufacture cost of an ion source drops a lot.

At PKU, the study on the methods of magnetic field generation and magnetic fields configuration for 2.45GHz ECR ion source started at 1990's [1]. We have tested solenoids, solenoid plus permanent magnet rings and only permanent rings. For plasma generation, they did not make any difference. Recently we focused on permanent magnetic rings for our source (PMECR I, II, III and IV) because it is more safety (less components placed at high voltage), compact (smaller source body) and economic.

Unlike the permanent magnetic rings used at CEA/Saclay, that each ring is made of 24 elementary NdFeB magnets assembled in an aluminium shell [18], we use two or three NdFeB permanent magnet rings to form the magnetic field for plasma producing as shown in Fig.1. Fig.2 shows several typical magnetic field configuration curves we have used [12]. The source operated well with all the three magnetic field distributions, and the best one for the source performance is the magnetic field distribution A, which produces two high density plasma regions at both end of the discharge chamber. Further study results indicate that the beam current is very sensitive to the B value at the extraction aperture position, but not sensitive to the magnetic field strength at the microwave window [13].

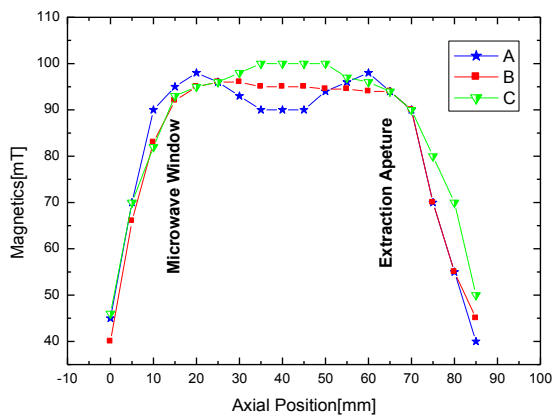

Figure 2: Axial magnetic field profiles of the permanent magnet.

At PKU, studies are focused on a classical three electrode system on test bench and for PKUNIFTY

project. Emphases are concentrated on how to decrease beam divergence, suppress emittance growth within LEBT and increase the beam transmission efficiency in LEBT [2, 3, 14]. Study shows that an appropriate angle of the conical section of the plasma electrode and a suitable suppression voltage are important parameters for beam formation and handing. For example, we replaced the original plat electrode with a cone apex angle of 90° for SFRFQ project, the peak oxygen current at RFQ entrance increased from 9 mA to 25 mA [14]. On our LEBT test bench, a set of flat electrodes was used before 2008. The aperture diameter of plasma electrode was 5 mm, and of suppressing electrode and grounded electrode was 8 mm. The acceleration gap and the deceleration gap were 6 mm and 2 mm, respectively, and the suppression voltage was set to 2 kV. In such a case more than 100 mA proton beam could be easily obtained at 50 kV extraction voltage and its normalized rms emittance is about 0.2 π.mm.mrad [12], but its beam half divergence angle was larger than 100 mrad. At the end of 2008, we replaced those plat electrodes with a set of 90° cone - expansion type one, as shown in Fig.1. The emission aperture has a diameter of 6 mm with thickness of 2 mm followed by an expansion cylinder with diameter of 8 mm and thickness of 2 mm. The aperture diameter of the puller electrode and the ground electrode is still 8 mm and their thickness is 3 mm. The acceleration gap and the deceleration gap are 12 mm and 3 mm, respectively. The half divergence angle of the beam reduced to 64 mrad at 2 kV suppression voltage. When the suppression voltage increased to 2.8 kV, the half divergence angle dropped to 35 mrad further, the normalized rms emittance is about 0.13 π.mm.mrad for 100 mA H^+ ion beam at 50 kV, and the beam transmission efficiency on LEBT test bench increased from 75% to 93% [14]. Also a 40 mA He^+ and more than 10 mA N^+ ion beams have been extracted on this test bench with a normalized rms emittance less than 0.2 π.mm.mrad and a half divergence angle less than 40 mrad. The extraction system for PKUNIFTY project is a copy of 90° cone - expansion type [3]. About 83 mA total current deuteron beam has been extracted at 50 kV with half divergence angle less than 70 mrad, and its normalized rms emittance is less than 0.18 mm mrad.

X-ray shielding is another issue outside the acceleration column, especially when operator is on the spot. By embedding the whole accelerator columns into the metal vacuum box above the pump for LEBT test bench and D^+ injector, radiation outside the accelerator columns was reduced to background lever when operated at 50 kV for H^+ ion beam generation [3].

DISCUSSIONS

After the investigation for several decades, a series of compact permanent magnetic 2.45 GHz ECR ion sources has been developed to deliver high current beam for different accelerator projects at PKU. About 25 mA of O^+ ion, 10 mA of N^+ ion, 100 mA of H^+ ions and 83 mA of D^+ ions can be produced with those compact PMECR sources. Recently, 40 mA of He^+ ion beam at 50 kV was also obtained on our LEBT test bench. For all the beams the normalized rms emittance is less than 0.2 π.mm.mrad, the half divergence angle is smaller than 70 mrad. The possible further improvements might be investigated depending on the requirements. Beside higher current and higher brightness, beam divergence is another important parameter for an ion source. Moreover, attentions should be paid to magnetic field shielding and space charge compensation within extraction region. Plasma diagnosis is going to be performed in a new PM ECR source (PMECR V) so that we can understand the behaviour of gas discharge inside the discharge chamber better.

REFERENCES

[1] Zhizhong Song, Dong Jiang, and Jinxiang Yu, Rev. Sci. Instrum. 67, 1003 (1996).
[2] S. X. Peng, M. Zhang, Z. Z. Song, et. al., Rev. Sci. Instrum. 79, 02B706 (2008).
[3] H. T. Ren, S. X. Peng,_ M. Zhang, et. al., Rev. Sci. Instrum. 81, 02B714 (2010).
[4] S. Gammino, L. Celona, G. Ciavola, et. al., Rev. Sci. Instrum 81, 02B313 (2010).
[5] N. Sakudo, Rev. Sci. Instrum. 49, 940 (1978).
[6] J. Ishikawa, Y. Takeiri, and T. Takagi, Rev. Sci. Instrum. 55, 449 (1984).
[7] L. Celona, G. Ciavola, S. Gammino, et. al., Rev. Sci. Instrum. 75, 1423 (2004).
[8] R. Gobin, P.-Y. Beauvais, O. Delferrière, et. al., Rev. Sci. Instrum. 79, 02B303 (2008).
[9] Gobin, R., Blideanu, V., Bogard, D., et. Al., Rev. Sci. Instrum. 81, 02B301_2010.
[10] Zhao Kui, Song Zhizhong, Wang lifang, et. al., Proceedings of The Third Symposium on Ion Sources and Beams, Lanzhou, China, Sep.,1987 (in Chinese).
[11] Zhizhong Song, Shixiang Peng, Jinxiang Yu, et. al., Rev. Sci. Instrum. 77, 03A305 (2006).
[12] S. X. Peng, R. Xu, J. Zhao, et. al., Rev. Sci. Instrum. 79, 02A310 (2008).
[13] M. Zhang, S. X. Peng, H. T. Ren, et. al., Rev. Sci. Instrum. 81, 02B715 (2010).
[14] R. Geller, Electron Cyclotron Resonance Ion Sources and ECR Plasmas_IOP, Bristol, 1996.
[15] S. K. Jain, Akhilesh Jain, P. R. Hannurkar, et. al., Rev. Sci. Instrum.78, 053301 (2007).
[16] T. Taylor and J. F. Mouris, Nucl. Instrum. Methods Phys. Res. A 336, 1_1993_.
[17] R. Gobin, G. Charruau, O. Delferrière, et. al., Rev. Sci. Instrum., 03B502 (2006).

DEVELOPMENT OF 14.5 GHZ ELECTRON CYCLOTRON RESONANCE ION SOURCE AT KAERI*

Byung-Hoon Oh, Sang-Ryul In, Kwang-Won Lee, Chang Seog Seo, Jung-Tae Jin, Dae-Sik Chang, Seong Ho Jeong, and Chul-Kew Hwang, KAERI, Daejeon, Korea.

Abstract

A 14.5 GHz ECRIS has been designed and fabricated at KAERI (Korea Atomic Energy Research Institute) to produce multi-charged ion beam (especially for C^{6+} ion beam) for medical application. The magnet system has cupper conductor solenoid coils and a permanent magnet hexapole. A welded tube with aluminium and stainless steel is used for an ECR plasma chamber to improve the production of secondary electron. A Krystron supplies microwave energy to the plasma. A movable beam extractor with 8 mm aperture covers different species and different charge numbers of the beam. Fabrication and initial experimental results on ECR plasma are discussed in this paper.

INTRODUCTION

A heavy ion accelerator for cancer treatment [1] by a cyclotron or a synchrotron is planned in Korea. As an important activity of this project a 14.5 GHz ECRIS has been designed and fabricated. The main design goal of the ion source is to produce C^{6+} ions with a current level of several tens of electro-microampere, and to meet this goal key parameters were designed as summarized in Table 1.

In this paper the design and fabrication results of the ion source, and the initial experimental results on the ECR plasma are described. An image camera and an optical sensor with a photo multiplier (PM) tube near the beam extraction aperture, and a NaI(Tl) detector at the outside of a beam extraction chamber with multi-channel analyzer (MCA) system to measure the X-ray spectrum were used to understand the characteristics of the ECR plasma.

SOURCE DESIGN AND FABRICATION

To get high current for the fully striped carbon ions with 14.5 GHz frequency strong-field ECR ion source, as shown in Fig. 1, was designed. The solenoid coils are composed of two axial coils to make mirror fields in both sides of the chamber and one trim coil at the center to control the layer of the resonance region (B_{min}). There are also three different yokes to make effective and strong axial field at the both ends of the ECR plasma region such as main yokes, hexapole fixing yokes and chamber yokes as shown in Fig. 2. The volume of the chamber yoke at the input side is maximized except the needed openings for microwave injection, vacuum pumping, and gas injection. Their positions and shapes are designed to minimize magnetic reluctance in the magnetic circuit. The hexapole [2] is composed of NdFeB permanent magnet. The sector number and outer diameter are optimized to make a strong hexapole field with a fixed inner diameter.

*This study was performed as a part of Nuclear R&D Program funded by the Ministry of Education, Science and Technology of Korea.

Table 1: Design Parameters of KAERI ECRIS

Parameters	Values
Microwave Max. Power	2.0 kW
B_{inj}	1.65 T
B_{ext}	1.1 T
B_r max	1.1 T
Max. Mirror Ratio	3.3
Chamber Inner Diameter	68 mm
Chamber Length	320 mm
Beam Extraction Diameter	8 mm
Beam Extraction Voltage (Max.)	30 kV
I_{C6+}	> 20 μA

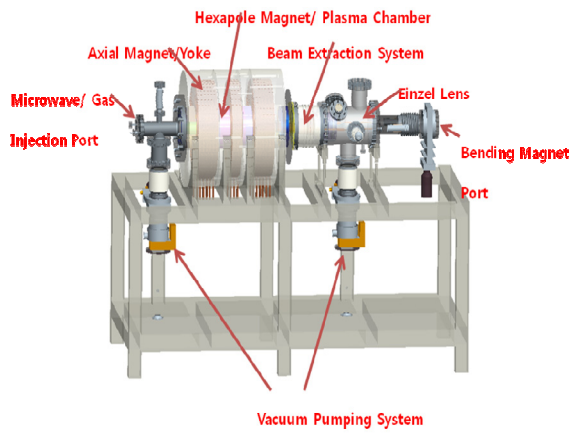

Figure 1. Main structure of KAERI ECR ion source.

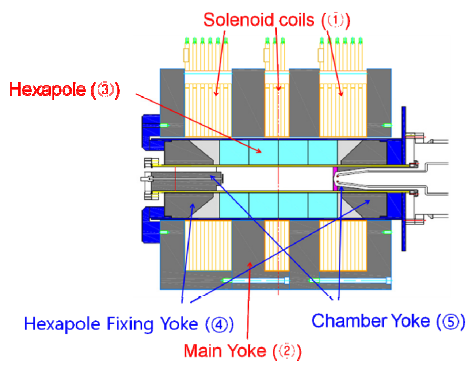

Figure 2. Inner structure of magnets and insulators.

An aluminium tube (5 mm wall thickness) welded with stainless steel (SUS 304) flanges is used for an ECR plasma chamber to improve the production of secondary electrons. A 2 kW Krystron supplies the microwave energy to the plasma. Microwave is injected in an axial direction at the off-axis position from the center to protect RF window from back streaming electrons. A movable beam extractor with 8 mm aperture covers different species and different charge numbers of the beam. And a movable Einzel lens with the beam extraction grid controls beam divergence. To make a simple insulation structure the vacuum chamber and the hexapole including the inner yokes are insulated from other components with G10 cylinder (5.5 mm thickness) and nylon covers at both sides of the chamber as shown with blue colour in Fig. 2. Two pumping system composed of 230 l/sec TMPs at RF input side and beam extraction side maintain the base pressure at the order of 10^{-8} mbar. A shielding box of 10 mm around the solenoid coils and 20 mm around the beam extraction side is installed to shield the high intensity and high energy Bremsstrahlung X-rays from the ECR plasma.

FIELD MEASUREMENT RESULTS

The field components of B_r, B_θ and B_z have been measured by a three dimensional probe to certificate the magnetic structure of the fabricated ECRIS system. The measured B_θ components after fixing the hexapole structure at the chamber wall position (r=34 mm) with the angle resolution of 15° is shown in Fig. 3. It shows that the measured value (about 1.3 T) is higher than the estimated one (1.2 T) by a field calculation code. The difference between the measured and the calculated one comes from the position shift of a θ–component sensor in a three dimensional probe. The measured and calculated results of the axial field with the chamber yokes along the center line are shown in Fig. 4. The mirror field at the entrance region could be increased higher than 1.7 with a proper cooling. At the exit region, mirror field of more than 1.1 T also could be possible.

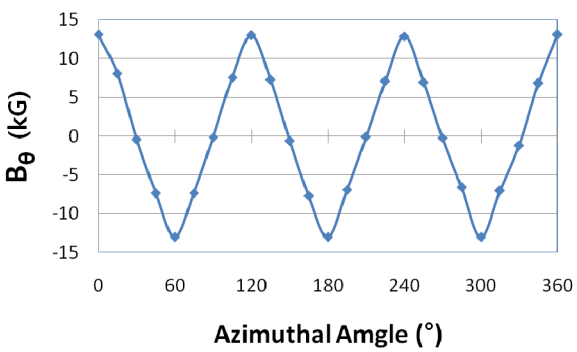

Figure 3. Measured B_θ at the chamber wall position (r = 34mm) with a hexapole structure.

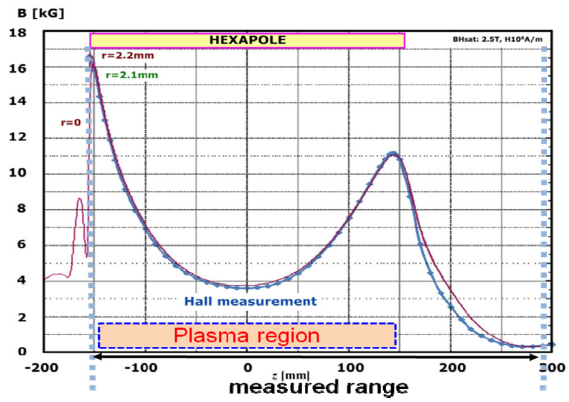

Figure 4. The magnetic field at the beam center (r=0 mm) with complete magnet structure of KAERI ECRIS. The coil currents are 700A, 300A, 700A for coil A, trim coil and coil B respectively.

ECR PLASMA EXPERIMENT

The charge state and the current of the beam from the ion source are closely related with the electron temperature and density of the ECR plasma. Three different tools such as image camera, optical sensor and X-ray detector are used to check the characteristics of the ECR plasma.

Camera Image

There are limited apertures through which ECR plasma could be seen. A small image camera is inserted instead of the beam extraction grid of the ion source, and ECR plasma is observed by the camera through the beam extraction hole. Fig. 5 shows the images of the ECR plasma through the hole (8 mm diameter) depending on the current value of the trim coil. The current changes B_{min} value and the layer structure of the ECR zone, and it changes the characteristics of the ECR plasma. They show that as B_{min} is approached to the ECR resonance frequency by increasing the current of the trim coil the light intensity is decreased, but on the other hand X-ray intensity is increased.

Optical sensor and PM Tube

An optical sensor is installed instead of the camera to measure the light intensity of the ECR plasma. The signal is amplified by a PM tube. Fig. 6 shows the measured result of the light intensities from the argon ECR plasma depending on gas pressure and microwave input power. The light intensity increases as pressure and microwave power are increased.

Bremsstrahlung X-ray

X-ray shielding was not considered seriously at the first design of the 14.5 GHz ECR ion source, but the X-ray dose from the ECR plasma was very high during some operation conditions even with 6 mm lead shielding around the beam extraction system (Fig. 1). Therefore X-ray spectrum and radiation dose were measured with

NaI(Tl) detector to estimate the needed shielding thickness around the ion source.

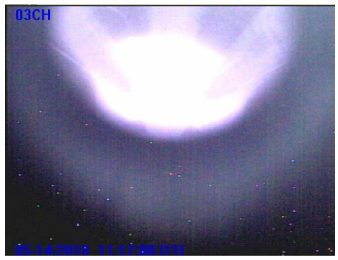

(a) When trim coil current is 0 A ($B_{z\,min}$ = 0.22 T).

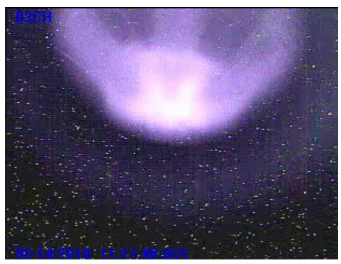

(b) When trim coil current is 200 A ($B_{z\,min}$ = 0.31 T).

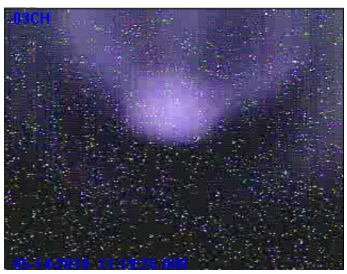

(c) When trim coil current is 500 A ($B_{z\,min}$ = 0.48 T).

Figure 5. Camera images of the ECR plasma that are seen through the beam extraction hole.

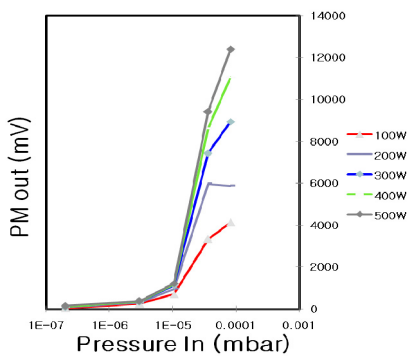

Figure 6. Light intensities from the ECR plasma depending on Argon gas pressure and input power.

A detector without collimator is positioned at the outside of the ion source near the beam monitoring chamber, which is fabricated with 3 mm thickness stainless steel (Fig. 1). The dimension of the NaI(Tl) detector is 50 mm(D) x 50 mm(L) and the pulse shaping time is 1 μsec. Energy calibration was made by a Cs-137 gamma ray source, which has 0.031 MeV and 0.661 MeV energy peaks. Gas was not supplied during this measurement but discharges could be started even at the base pressure of ~10^{-8} mbar. The pressure increases up to ~10^{-6} mbar with the plasma ignition.

The energy distribution of Bremsstrahlung X-ray from the ECR plasma [3, 4] is closely related with the electron energy distribution function. The spectrum change with trim coil current is shown in Fig. 7 when the microwave input power is 100 W. It clearly shows that electron heating efficiency changes with the field strength of B_{min}. The optimum condition for the electron heating is supposed to be made around the trim coil current of 450 A. At this current the value of B_{min} is 0.45 T (0.87*B_{ECR}). Fig. 8 and Fig. 9 show another X-ray spectrums when microwave input power is 250W and 500W respectively. X-rays, whose energies are higher than 2 MeV, were detected when trim coil current is 450 A at 250 W input power. And the peak energy of the X-ray decreases again with the microwave input power. It looks like there is an optimum value of input power for the KAERI ECR ion source between 250 W to 500 W. This value is relatively small compared with the results of other sources [5].

Because of the shield layers between the ECR plasma and the detector such as chamber wall, extraction grid and/or other components of the ECR ion source, the X-ray distribution at low energy region should be deformed much by the attenuation by the shields. But the distribution at higher energy region can have relatively useful information on the electron distribution function of the ECR plasma. The electron temperatures estimated by the high energy tails of the measurement data are summarized in Fig. 10. We are planning to make more detailed measurement form the pure ECR plasma with proper collimators [3] in a near future.

SUMMARY

The fabrication of KAERI ECR ion source had been finished, and the test was started. During the initial test of the ECR plasma energy spectrums at the outside of the ion source depending on different operation condition were measured. It was found that the measured spectrums at the outside of the ion source without collimator also give some information on the KAERI ECR ion source. As the installation of the shielding structure of the source has been finished recently, next experiments on ECR plasma and multi-charged ion beam will be started.

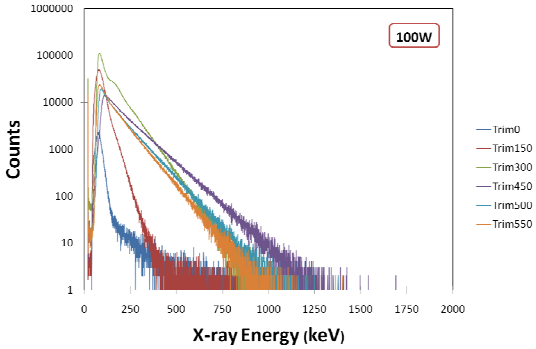

Figure 7. X-ray spectrums depending on trim coil currents when microwave input power is 100 W.

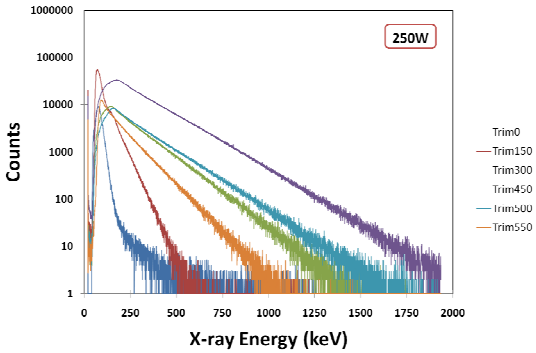

Figure 8. X-ray spectrums depending on trim coil currents when microwave input power is 250 W.

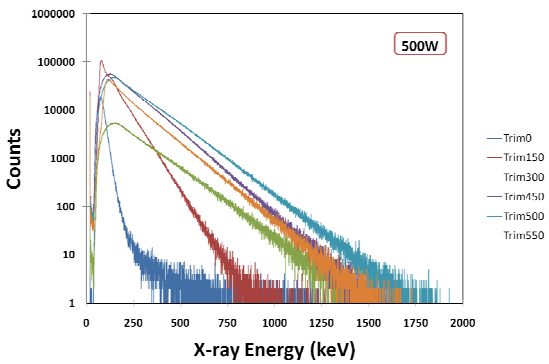

Figure 9. X-ray spectrums depending on trim coil currents when microwave input power is 500 W.

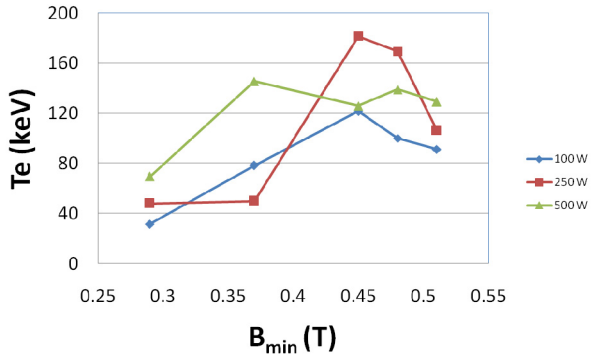

Figure 10. Calculated electron temperature of the ECR plasma based on the X-ray spectrum of high energy tail.

REFERENCES

[1] A. Kitakawa, M. Muramatsu, T. Fujita, W. Takasugi, S. Wakaesami, S. Biri, A.G. Drentje, Proceeding of 18th International Workshop on ECR Ion Sources, Chicago (2008) 88.

[2] Byung-Hoon Oh, Chang Seog Seo, Sang-Ryul In, and Tae-Seong Kim, Rev. Sci. Instrum. 81, 02A317 (2010).

[3] J.Y. Benitez, J.D. Noland, D. Leitner, C. Lyneis, D.S. Todd, and Verboncoeur, Proceeding of 18th International Workshop on ECR Ion Sources, Chicago (2008) 74.

[4] G. Rodrigues, P. S. Lakshmy, Y. Mathur, U. K. Rao, R. N. Dutt, P. Kumar, A. Mandal, D. Kanjilal, and A. Roy, Proceeding of 18th International Workshop on ECR Ion Sources, Chicago (2008) 101.

[5] Y. Higurachi, T. Nakagawa, M. Kidera, T. Aihara, M. Kase, and Y. Yano, Proceeding of 16th International Workshop on ECR Ion Sources, Berkeley (2004) 71.

MASS SPECTROMETRY WITH AN ECR ION SOURCE

M. Hotchkis#, D. Button, ANSTO, Menai, Australia

Abstract

Several groups [1-3] have demonstrated the usefulness of ECR ion sources in forms of mass spectrometry, for the detection of rare long-lived radioisotopes, trace elements and stable isotope ratios. Mass spectrometry imposes strict constraints on the ion source. First, the ion source must be free of backgrounds at the same m/q ratio as isotope of interest. Backgrounds take several forms, including beams generated from residual gas or other materials in the source, either of the element of interest, or other elements which cause isobaric or other m/q ambiguities. Second, the ion source must exhibit a minimum 'memory' effect from sample to sample. We are interested in isotopic ratios of carbon, nitrogen and oxygen. These elements are ubiquitous in vacuum systems and so this work has its own particular challenges, especially in relation to the design and operational characteristics of the ion source. Initial work has revealed retention effects which reduce the sample clear out rates, and cause persistent backgrounds [4]. We will present results of our most recent efforts to control these problems.

[1] P. Collon et al., Nucl. Instrum. Methods B 2004; 223/224: 428.
[2] M. Kidera et al., Eur. J. Mass Spectrom. 2007; 13: 239.
[3] M. Hotchkis et al., Rapid Comm. Mass Spec. 2008; 22: 1408-1414.
[4] D. Button and M.A.C. Hotchkis, Proc. 18th ECRIS Workshop, Sept 15-18, 2008, Chicago, USA, http://www.JACoW.org/.

Paper not received

#mah@ansto.gov.au

PLANS FOR LASER ABLATION OF ACTINIDES INTO AN ECRIS FOR ACCELERATOR MASS SPECTROSCOPY*

R.C. Pardo#, F.G. Kondev, S. Kondrashev, C. Nair, T. Palchan, E. Rehm, R. Scott, R. Vondrasek, Argonne National Laboratory, Argonne, IL , USA,
M. Paul, Racah Institute of Physics, Hebrew University, Jerusalem, Israel
P. Collon, Nuclear Structure Laboratory, University of Notre Dame, Notre Dame, IN, USA
G. Youinou, M. Salvatores, G. Palmotti, C. McGrath, Idaho National Laboratory, Idaho Falls, ID, USA
G. Imel, Idaho State University, Pocatello, ID, USA

Abstract

A project using Accelerator Mass Spectrometry (AMS) at the ATLAS facility to measure neutron capture rates on a wide range of actinides in a reactor environment is underway. This project will require the measurement of many samples with high precision and accuracy. The AMS technique at ATLAS is based on production of highly-charged positive ions in an electron cyclotron resonance ion source (ECRIS) followed by linear acceleration. We have chosen to use laser ablation as the best means of feeding the actinide material into the ion source because we believe this technique will have more efficiency and lower chamber contamination thus reducing 'cross talk' between samples. In addition construction of a new multi-sample holder/changer to allow quick change between multiple samples is part of the project. The status of the project, design, and goals for initial off-line ablation tests will be discussed as well as the overall project schedule.

INTRODUCTION

Advanced nuclear fuel cycles are currently under evaluation in order to assess their potential to cope with new requirements of radioactive waste minimization, optimization of resource utilization, and reduced risk of proliferation. This assessment should account for several key features of the fuel cycle, including irradiated fuel processing, innovative fuel development and fabrication, waste characterization, and disposal. In some cases, the impact of nuclear data and their associated uncertainties can be crucial in order to further explore an option, or to reject it. The need for accurate data has been pointed out in recent studies devoted to Generation-IV systems, see e.g. [1]. The very high mass actinides can play a significant role in the feasibility assessment of innovative fuel cycles. As an example, the potential build-up of ^{252}Cf when recycling all transuranics in a light water reactor, leads to increased neutron emissions that could impact the fuel fabrication process. As a consequence, the poorly known nuclear data of higher mass transuranics need to be significantly improved.

At present, there is data to provide some information on the performance of these isotopes in reactor environments, but up to now, there has been little emphasis on the quality of these data and few reliable uncertainty estimates have been provided. This situation is due to the difficulty to make both integral and differential cross section measurements for these isotopes.

The objective of this project is to obtain valuable integral information about neutron cross sections for actinides that are of importance for advanced nuclear fuel cycles in a relatively short time compared to the more standard, and time consuming, route which consists of irradiating samples in a reactor and then performing chemical analysis to characterize the different isotopes produced during irradiation.

The proposed work intends to develop an original approach that takes advantage of two experimental facilities: the neutron irradiation capabilities of the Advanced Test Reactor (ATR) at the Idaho National Laboratory and the Accelerator Mass Spectrometry (AMS) capabilities of the Argonne Tandem Linac Accelerator System (ATLAS)[2] at Argonne National Laboratory.

The novelty of this approach relies on the use of AMS which is expected to provide very sensitive measurements of the production of different actinides that are built up during the irradiation, up to the highest mass isotopes. AMS at ATLAS can detect down to about 10^6 atoms in samples consumed in the ion source, which is out of the range of more classical chemical analysis traditionally used to analyze irradiated fuel samples.

In order to succeed in this project, the work can be decomposed into three major steps:

1. Preparation and irradiation of some pure actinide samples in ATR. The samples that are available at INL and which are of interest for advanced reactor fuel cycles are the following: ^{232}Th, ^{235}U, ^{236}U, ^{238}U, ^{237}Np, ^{238}Pu, ^{239}Pu, ^{240}Pu, ^{241}Pu, ^{242}Pu, ^{241}Am, ^{243}Am and ^{248}Cm.

2. Measurements of the amount of the different isotopes produced in the irradiated samples at ATLAS.

* This work is supported by the U.S. Department of Energy, Office of Science, Office of Nuclear Physics, under DOE Idaho Operations Office Contract DE-AC07-05ID14517 as well as by the ANL Contract DE-AC02-06CH11357 and by the ATR National Scientific User Facility.
# pardo@phy.anl.gov

3. Using the results of the measurements, derive information on (n, γ), and (n,2n) cross sections on the target and daughter isotopes. An effort will be made also to derive, if possible, fission yields.

In this report we will focus on the requirements of the AMS program and the novel aspects that will be implemented at the ECR ion source at ATLAS to carry out this research program. The requirements of precision and accuracy to obtain useful results are discussed more fully in [2]

AMS AT ATLAS

The principle of AMS at ATLAS [4] differs from conventional tandem-accelerator AMS by the injection of highly-charged positive ions followed by their linear acceleration. In this scheme, the high-velocity electrons of the ECRIS plasma strip the ions to high charge states, a process in some sense inverse to the stripping of fast ions in a solid or gas target used in a tandem accelerator. Similarly, the ECRIS ion stripping dissociates any existing molecular ions, an essential feature of AMS.

The requirements placed on the AMS measurements to be performed at ATLAS are quite challenging. These challenges include high-precision isotope ratio measurements, minimization of cross-talk between samples, efficient use of milligram samples, and the processing of an unprecedented number of samples for a facility as complex as ATLAS. Unique element (Z) identification is desirable, but is not expected to be possible except for specific cases.

The measurement configuration for ATLAS will use the ECR-II ion source, significantly modified as discussed below, as the source of ions. After acceleration and deceleration (increasing the accelerator m/q resolution but keeping the ion energy within acceptance range of analytical elements) in the ATLAS linac to approximately 1 MeV/u, the actinide ions of interest will be counted in the focal plane of the Fragment Mass Analyzer (FMA). The major challenges are discussed in the succeeding paragraphs.

Precision Requirements

Only ^{14}C AMS has consistently achieved precision levels in the <1% regime. This has been achieved in dedicated facilities, principally by the fast cycling of the accelerator setup between the rare isotope (^{14}C) and a normalizing abundant isotope (^{13}C). Except for specific cases, counting statistics are not the problem. Knowing the transmission between the measurement point for the stable reference and the detector of the AMS isotope is often the limiting parameter for uncertainty in the final result. This problem will be tackled by developing an improved automation of the accelerator scaling required to measure the various isotopes or ion species and an automated sample changer to allow rapid changes between various samples. In many cases of interest, the measurement time for each sample will be only a few minutes for adequate measurement statistics. But the lack of known absolute standards, the possibility of cross-talk between samples, and instabilities in the accelerator are the significant problems that must be addressed to achieve the precision goals.

A recent AMS experiment on ^{146}Sm [5] has required that we develop an approach to measuring the absolute transmission of the accelerator and detector system and has highlighted the need to run ATLAS is an extremely stable mode. It has also demonstrated that it is feasible to switch rapidly (by computer control of the machine components' setup) between a rare and abundant isotope (in a way similar to that used for ^{14}C), thus improving control over the accelerator transmission. Because of this ongoing work and the additional techniques discussed here, we believe we can achieve the required stability and characterization of the transmission in order to enter this regime of precision.

Small Sample Size and Cross-Talk

A major feature of AMS is the ability to analyze small samples. At ATLAS the AMS activities always are focused on samples of a few milligrams. For this project, it is important that we deal with many small samples. The smaller the samples, the less are the radiological problems associated with handling α-emitting actinides for ATLAS operation. The need to measure many small samples as quickly as possible pushes us to develop efficient sample changing techniques for the ECR source and material delivery techniques which minimize source contamination.

We believe the best approach for this situation is to develop laser ablation for the feeding of sample material into the source. With laser ablation, a very small and controllable amount of sample material can be introduced into the source without introduction of extraneous material from the sample holder. Also the distribution of emission of ablated material in laser irradiation tends to obey a cos θ law which is expected to improve the efficiency of capture of ions into the plasma and thereby reduce wall contamination. Finally, the form of the sample material (metal, oxide, etc) is less critical than with the sputtering or oven technique.

The ECR-II source will also be equipped with a quartz liner. The quartz liner will keep the main body of the source relatively clean of actinides, thus simplifying cleanup. Furthermore, there is some operational evidence that cross talk among samples is reduced. This effect has been observed with other AMS projects at ATLAS. A negative to using a quartz liner is that source performance as measured by charge-state distribution and maximum beam intensity is somewhat reduced. But the beam energy is limited by the bending power of the FMA system and use of high charge state ions is not required. A mass-to-charge ratio of ~8-9 should be quite adequate for these measurements.

Ion identification and counting

One of the major challenges of actinide AMS at ATLAS is the need for separation or discrimination of a desired species from backgrounds of ions having similar mass-to-charge ratios present as chemical impurities or interference of ion-source materials. This discrimination is best achieved at ATLAS by using the FMA which has a very large dispersive power and can analyze very heavy ions. A proof of concept and first measurements of rare species in the actinide region were successfully performed [4] (since this experiment considerable improvement has been made in the focal-plane detector of the FMA). The typical setup consists in accelerating and decelerating a desired ion so that its energy matches the electric-rigidity acceptance of the FMA. Stripping at the FMA target position (the only one along the machine) allows the heavy ions to reach the high charge state needed for magnetic-rigidity acceptance of the FMA.

In the case of actinide nuclei, Z identification at the energies compatible with the FMA acceptance is likely to be impossible. However, the high redundancy of energy, energy-loss and time-of-flight signals available from that detector is expected to contribute to the mass-to-charge determination and to a high level of background discrimination.

LASER AND SOURCE CONFIGURATION

Laser Parameters and Configuration

Laser ablation into an ECR source was first developed at ATLAS [6] and used as a plasma diagnostic tool[7] and has since been used by a number of other labs to explore the coupling of laser produced ions into an ECR source. The technique has not been used routinely for ion production and will require development for this application. The controlled release of materials into the plasma by well-focused laser light will eliminate the significant material buildup often seen in the region of the oven throat or beside the sputter cones, two techniques widely used for sample feeding to the ECRIS. This inefficient, indiscriminate injection of material into the source not only reduces the overall sensitivity of the method but is a major source of cross-contamination between samples. Our experience with lasers in the past indicates that the laser ablation approach will be much cleaner, but must be shown to work for this application.

In this application we plan to use an axial geometry. The laser beam will be brought into the source through the extraction aperture as shown in Fig. 1. The properties of the laser to be used in this application are:

- λ =1064 nm
- ≤1011 W/cm2
- 8 ps pulse width
- Rep Rate up to 400 Hz
- Laser beam size ~7 mm maximum
- less than 1 mm diameter spot on sample
- Pulse energy: variable, up to 10 mJ/p.

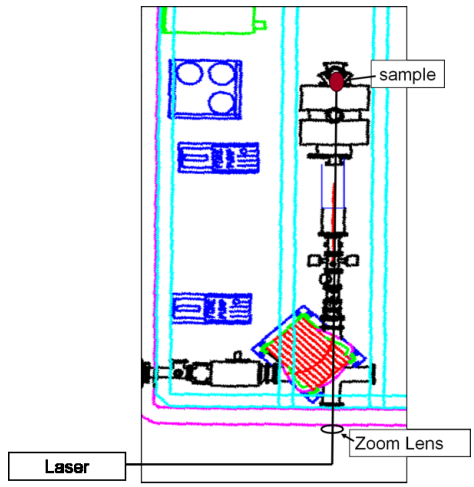

Figure 1: Axial geometry of laser ablation into the ATLAS ECR-II.

This project has an unprecedented number of samples that need to be characterized. Typically AMS experiments at ATLAS have needed to process less than 10 samples for any one experiment. This project envisions sample numbers of around 50 or more. An entirely new approach to sample processing is required. In addition, the desire to rapidly switch between measuring an irradiated sample and the original sample requires a different approach.

We have designed a multi-sample changer that will be installed in the injection side of the ECR ion source. This changer, shown in Fig. 2, can accept 20 samples and will be able to alternate between the various samples without breaking vacuum. The change time will be only a few seconds.

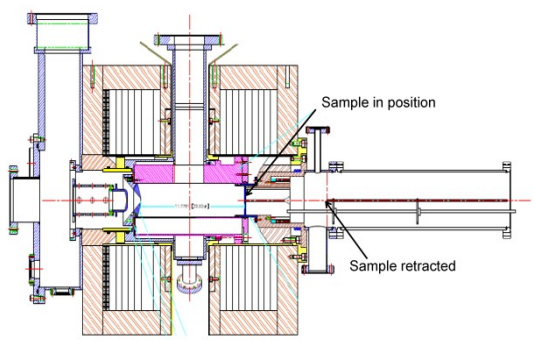

Figure 2: ECR-II cross-section with multi-sample changer shown

The laser is expected to be delivered in the Fall of 2010. Off-line ablation measurements will be made in late 2010 and installed at the ECR source by the Spring of 2011. Initial measurements on reference samples will be made in late 2010 to study backgrounds and

establish Z sensitivity of the detectors. The multisample changer will be ready for installation by the summer of 2011 and initial samples will be ready for measurement in late 2011.

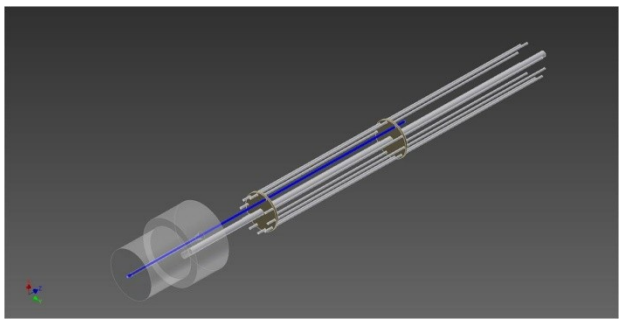

Figure 3: 3-D perspective of multi-sample changer assembly. The samples are pre-mounted on individual rods which can be rotated into position and inserted in the ECR ion source.

REFERENCES

[1] M.Salvatores, "Nuclear Data for Advanced Fuel Cycles", Proc. Int. Conf. IEMPT-10, Mito, Japan, 6-10 October 2008

[2] G. Youinou, M. Salvatores, M. Paul, R. Pardo, G. Palmiotti, C. McGrath, F. Kondev, G. Imel, "An Integral Reactor Physics Experiment to Infer Actinide Capture Cross-Sections From Thorium To Californium With Accelerator Mass Spectrometry", Eleventh International Conference on Nuclear Data for Science and Technology, Jeju Island, Korea, 2010.

[3] L.M. Bollinger et al, Nucl. Instr. and Meth. B, 79 753(1993)

[4] M Paul, D Berkovits, I Ahmad, F Borasi, J Caggiano, C N Davids, J P Greene, B Harss, A Heinz, D J Henderson, W Henning, C L Jiang, R C Pardo, K E Rehm, R Rejoub, D Seweryniak, A Sonzogni, J Uusitalo, R Vondrasek, "AMS of heavy elements with an ECR ion source and the ATLAS linear accelerator", Nucl. Instr. and Meth B 172, (2000), 688.

[5] N Kinoshita, T Hashimoto, T Nakanishi, A Yokoyama, H Amakawa, T Mitsugashira, T Ohtsuki, N Takahashi, I Ahmad, J P Greene, D J Henderson, C L Jiang, M Notani, R C Pardo, N Patel, K E Rehm, R Scott, R Vondrasek, L Jisonna, P Collon, D Robertson, C Schmitt, X D Tang, Y Kashiv, H Nassar and M Paul, J. Phys. G: Nucl. Part. Phys. 35, 014033 (2008)

[6] R. Harkewicz, J. Stacey, J. Greene, R.C. Pardo, Rev. Sci. Inst. 65(4), 1104(1994).

[7] R C Pardo, et al., Rev. Sci. Inst. 75 (5), 1427(2004)

ENHANCEMENT OF ECR PERFORMANCES BY MEANS OF CARBON NANOTUBES BASED ELECTRON GUNS*

F. Odorici, M. Cuffiani and L. Malferrari, ,INFN-Bologna, 40127 Bologna, Italy
R. Rizzoli and G. P. Veronese, CNR-IMM and INFN-Bologna, Bologna, Italy
L. Celona, S. Gammino#, D. Mascali, R. Miracoli, F. P. Romano, N. Gambino,
G. Castro and G. Ciavola, INFN-LNS, 95123 Catania, Italy and CSFNSM, 95125 Catania
T. Serafino, Univ. Messina, 98100 Messina, Italy

Abstract

The CANTES experiment at INFN-LNS tested the use of carbon nanotubes (CNTs) to emit electrons by field emission effect, in order to provide additional electrons to the plasma core of an ECR ion source. This technique was used with the Caesar source, demonstrating that the total extracted ion current is increased and that a relevant reduction of the number of "high energy" electrons (above 100 keV) may be observed. The injection of additional electrons inside the plasma increases the amount of cold and warm electrons, and then the number of ionizing collisions. Details of the construction of CNTs based electron gun and of the improvement of performances of the Caesar ECR ion source will be presented.

EXPERIMENTAL SET-UP

The ECR ion source CAESAR, operating at INFN-LNS laboratories as injector of the K-800 Superconducting Cyclotron since 2000, has been used as testbench for the CANTES technique,.

In the past, several passive techniques for the injection of secondary electrons were tested [1], with the purpose to increase the electron density and to prolong the ion lifetime in the plasma, enhancing the ionization probability. For example alumina was tested as source of secondary electrons [2].

Active materials, like ferroelectric cathodes, such as PBZT doped with 2 % of Bi_2O_3, have been employed because of their capability of producing high emission yields of energetic electrons [3]. However, their robustness is not sufficient for stable applications into ECRIS. In fact, they showed not only a lack of reliability, but also a limited resistance in plasma environment, and they failed after short time.

During this experiment, we tested a new active technique which makes use of CNTs-based electron guns. In our set-up, two electron guns are placed on a copper plate connected to the RF waveguide, that is usually employed as bias disk in the CAESAR source. A potential in the range 0-2.5 kV, is then applied between the chamber and the waveguide, and the same potential is used to produce the emission field (i.e. the extraction field) between CNTs and the anodic grid.

At an earlier stage, CNTs samples of the same type as used for CAESAR have been tested in microwave discharge plasma (MDIS), in order to preliminary verify if electron and ion collisions can damage them. The adopted MDIS apparatus operates at 2.45 GHz and generates, in presence of an off-resonance magnetic field, a weakly ionized and strongly collisional plasma because of the low electron temperature (T_e<10 eV) and high pressure (0.4 mbar). Tests were made both for air plasma and nitrogen plasma. Results were collected in fall of 2008 and they have shown that CNTs exposed to intense plasma milling (up to 4 mA/cm^2 current density and 300 C/cm^2 of integral dose) have been damaged in presence of oxygen (air plasma) but were perfectly resistant to nitrogen plasma. After the response of this preliminary test-bench, CNTs cathodes have been used for tests in ECR ion sources.

The CNTs electron gun used for the test is made of three elements: a CNTs cathode obtained on a 300 µm thick silicon substrate, a 150 µm thick mica spacer and an anodic copper grid with quad cells of 350 µm side. CNTs eject electrons because of the field emission effect, i.e. quantum tunneling, which is obtained by applying an electric field higher than 3-4 V/µm.

The gun elements are kept together by a MACOR holder, on which the electrical connection is obtained by an evaporated gold track. The MACOR holder is then fixed on a copper plate, i.e. the bias disk of the source, connected to the waveguide of the plasma chamber. The anodic grids are linked to the ground potential of the plasma chamber wall by means of copper creeping contacts. Two of such electron guns were mounted on the same bias disk during the experimental tests. A picture of a CNTs sample and the assembled guns is shown in Figure 1. The CNT e-gun scheme inside the plasma chamber is shown in figure 2 and the CAESAR source during the experiment is shown in figure 3. Prior to the plasma test, each CNTs sample was tested in terms of field emission, by means of a custom-designed apparatus [4]. The field emission properties of similar samples (i.e. CNTs arrays in free-standing porous alumina foils) were already tested [5] and found to be able to produce current densities up to 10-40 mA/cm^2. Emission measurements for the samples tested in CAESAR (i.e. CNTs arrays in porous alumina on silicon), gave even better results, with

*Work supported by 5th Nat. Comm. of INFN (CANTES experiment).
#gammino@lns.infn.it

current densities up to 50-100 mA/cm^2. The emission surface in our samples was set to about 0.1 cm^2, by using a mica spacer with a 3 mm diameter central hole (Fig. 1). The measurements of X-rays emitted by the CAESAR's central plasma region have been carried out by using an HPGe detector (High Purity Germanium), collimated through lead shielding blocks, in order to suppress secondary X-rays coming from electrons impinging on the lateral walls of the plasma chamber. The detector was surrounded by additional lead in order to minimize the leakage of the X-ray radiation around the main collimator. The collimation hole was 1 mm^2 .

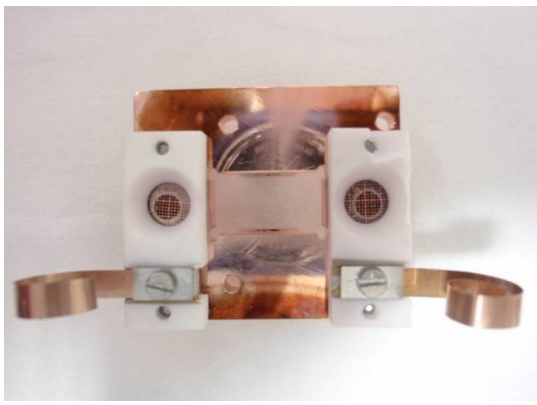

Figure 1: The CAESAR waveguide, holding two CNTs electron guns. The copper creeping contacts are used to put the extraction grid at the same potential of the chamber, while the CNTs are put to negative potential with respect to the chamber.

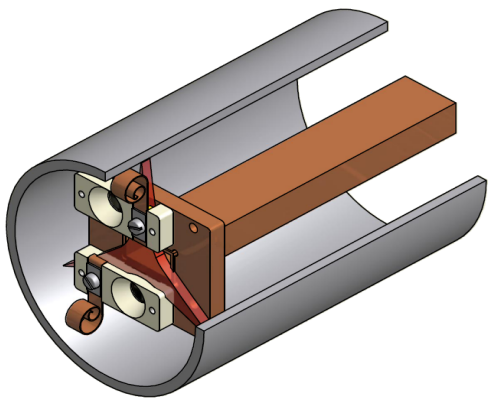

Figure 2: The scheme of the CNTs electron gun.

RESULTS AND DISCUSSIONS

The charge state distribution has been measured at different RF power and voltages applied to the CNTs electron gun for the Kr, working at fixed pressure. The Kr^{11+} extracted current has been taken as reference, for comparison of results. The extracted currents can be compared with those obtained when the CNTs electron gun was switched off. The beam current exceeded the one obtained with the biased disk already at 1 kV, as it can be observed in fig. 4. In spite of the small emission area, an increase of 30-70% was obtained in any case. (about 40% for Kr^{11+}).

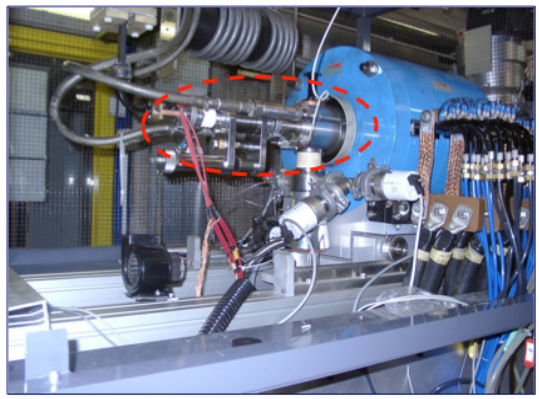

Figure 3: The CAESAR source injection section.

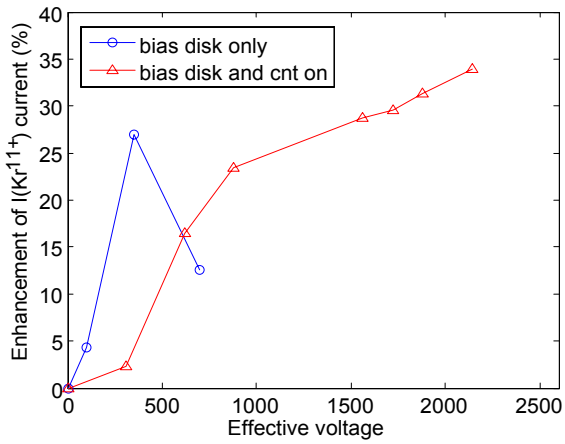

Figure 4: Comparison of produced Kr^{11+} current when using conventional biased disk or emitting CNTs.

Figure 5 shows the extracted current for Kr^{11+} when the CNTs emission is switched on and off, in a time window of 30 seconds and with a RF power of 35 W. The "jump", which takes place immediately after the electron emission from CNTs, was obtained with 2500 V applied to the CNTs extraction grid. It is also interesting to note the afterglow-like peak when the electron gun is switched off, which is similar to the one observed in pulsed operations. The limited time allotted for this experiment did not permit to check if the CNT's afterglow peak and the RF afterglow may be combined to obtain further enhancement of the current peak values.

CNTs provide additional and even more important benefits to ECR plasmas, as they contribute to the total suppression of the hot electrons component, that is evident above 1000 V. The same effect is not evident when using a conventional biased disk. Although the not perfect collimation of the detector cannot permit to

extrapolate quantitative estimations on electron spectral temperature, it is however evident in fig. 6 that the number of the hottest electrons decreases.

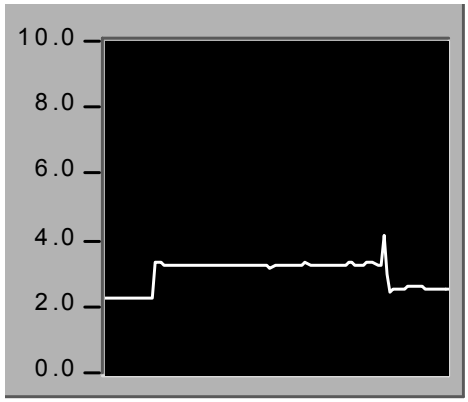

Figure 5: Trend of the Kr^{11+} current (in μA) during the switching on-off of CNTs emission, in a time window of 30 seconds. The CNTs applied voltage was 2500 V, at 35 W RF power.

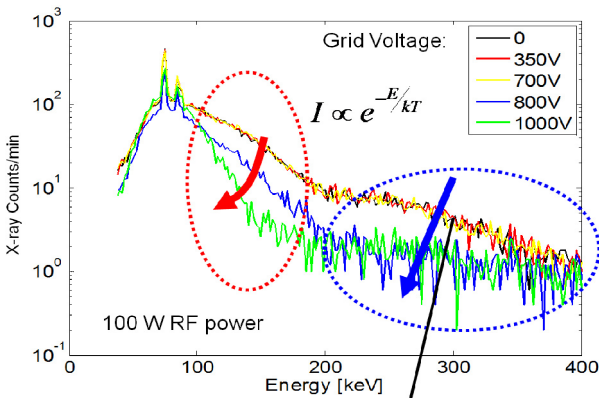

Figure 6: Axially emitted X-ray spectra for different voltage values and RF power of 30 W.

By providing additional cold electrons to the plasma, the average energy decreases as a larger number of electrons will share the same amount of energy injected into the plasma chamber by means of the microwave (the RF power is kept constant).

Measurements at low power shown in figure 6 are similar to the ones collected at 100 W and 150 W, demonstrating that the contribution of CNTs is effective in all cases (either for the current increase and for the damping of hot electron generation), and that the optimal CNTs' voltage increases with the power. Confirmations of these results came also by measurements at different values of the pressure in the chamber, even if some fluctuations in the maximum enhancement factor were evident. In all cases the counting rate of the X-rays above 100 keV was strongly damped. Long run measurements were also done. In fig. 7 the current plot during a 24 hours tests is shown, with all parameters fixed (gas input, power, magnetic field).

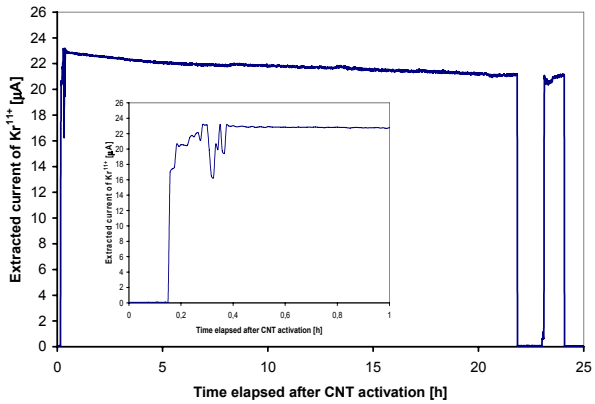

Figure 7: Current plot during a 24 hours test.

The small decrease is correlated to plasma chamber outgassing, which changed the pressure conditions inside.

CONCLUSIONS

We have observed a relevant reduction of the number of higher energy electrons after the injection of the electrons emitted by the CNTs-based electron gun. The current gain was between 30 and 70%. Once that a full comprehension of the phenomenon will be gained, this last result may be applied to modern ECRIS which performances are strongly limited by the occurrence of such hot electrons, especially when large power and frequencies above 18 GHz are used.

The use of CNTs-based emitters has solved robustness problem which emerged when ferroelectric cathodes were used. For the presented tests, their period of operation was limited to some tens of hours. Future experiments on ECRIS will focus on reliability tests, for one week or more.

ACKNOWLEDGEMENTS

The support of the 5th National Committee of INFN (CANTES experiment) is gratefully acknowledged.

The authors wish to thank Salvo Marletta, Maurizio Castro, Luciano Allegra, Salvo Vinciguerra, at INFN-LNS, and Michele Furini at INFN Bologna, for their help in supporting the experiment during its preparation and data taking.

REFERENCES

[1] S. Gammino, A.G. Drentje, J. Sijbring, Rev.Sci. Instr., 63,(1992) 2872

[2] S. Gammino et al., Rev. Sci. Instr. 77 (2006) 03B511

[3] I. Boscolo et al., Applications of ferroelectric cathodes to enhance the ion yield in the CAESAR source at LNS, Proceedings of EPAC 2000, Vienna, Austria, 1631.

[4] R. Angelucci et al., Phys. E 42 (2010) 1469

[5] R. Angelucci et al., Phys. Status Solidi C 6, N. 10, (2009) pp. 2164-2169.

A NEW BETSI TEST BENCH AT CEA/SACLAY

S. Nyckees, G. Adroit, O. Delferrière, R. Duperrier, Y. Gauthier, R. Gobin, F. Harrault,
C. M. Mateo, O. Napoly, B. Pottin, Y. Sauce, F. Senée, O. Tuske, T. Vacher,
CEA/Saclay, DSM/IRFU/SACM, F- 91191-Gif/Yvette, France.

Abstract

By the 90s, CEA has undertaken to develop the production of high intensity light ion beams from plasma generated by electron cyclotron resonance (ECR). Important results were obtained with the SILHI source in pulsed or continuous mode. Presently, CEA/Saclay is now involved in the construction of different injectors dedicated to large infrastructures like IFMIF or SPIRAL2. Other installations are also interested by high intensity ion sources like ESS or FAIR.

To improve and test new sources, a new test bench named BETSI (Banc d'Etudes et de Tests des Sources d'Ions) is now operating for several years. Low energy beam line diagnostics consist of a Faraday cup, cameras and a species analyzer. The SILHI emittance scanner can also be installed on the beam line. On this test bench, different permanent magnet source configurations are tested.

INTRODUCTION

In the middle of the 90s, CEA/Saclay developed the SILHI source, operating at 2.45 GHz and based on the Chalk River (Canada) principle. More than 100 mA proton or deuteron beams are routinely produced in pulsed or continuous mode. To answer new machine requests, specific source designs have already been performed. For example, a permanent magnet source has been developed to fit in with the 5 mA deuteron expected beam for Spiral 2. Then, to answer the IFMIF (International Fusion Material Irradiation Facility) high intensity deuteron beam request (125 mA), a copy of the SILHI source with a 4 electrode extraction system has been proposed.

Since the IPHI project will enter in a new phase of development, the availability of the SILHI platform will be reduced for source developments. Therefore, the construction of the new test bench named BETSI (described in the following section) has been decided [1]. Up to now, a new accelerator column designed for the Spiral2 ion source has been installed and tested on this test bench. Several simulations have been realized to find an optimization of magnetic configuration.

THE BETSI TEST BENCH

The Low Energy Beam Transport

The BETSI test bench is dedicated to study the influence of the source parameters on the beam characteristics. It operates up to 50 kV and ignites continuous or pulsed hydrogen plasma with a 2.45 GHz magnetron. The LEBT is composed of a pair of solenoids that has to reduce beam divergence and focus it into a classical mass analyzer magnet (Fig. 1).

Between the pair of solenoids and the analyzer magnet, a pumping and diagnostic box is installed. The analyzing part is composed of a vertical and horizontal viewport for CCD camera diagnostics and a vertical movable Faraday cup. Pumping of LEBT is realized by a turbo molecular pump of 1000 l/s, it allows easily obtaining vacuum of 10^{-4} Pascal. A beam stop with magnetic electron reppeler is installed after the mass analyzer for ion beam intensity measurement.

Currently, the two old solenoids have been installed close to each other to obtain a magnetic field as high as possible to focalize the extracted beam. But the field strength is not high enough to focalize H_2^+ or H_3^+. New solenoid, including vertical and horizontal steerers has been designed and built to replace them. It length is 310 mm (including the magnetic shielding) with a maximum magnetic field of .85 T. It will be installed during the next months.

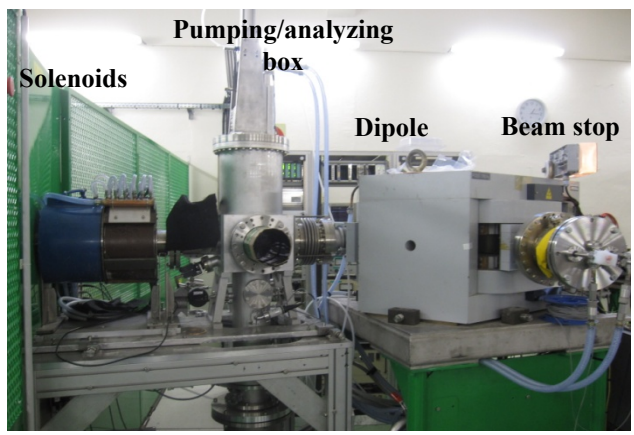

Figure 1: The LEBT of BETSI test bench

The analyzer magnet is a 104° dipole with a radius of 400 mm and double focusing corners. The magnetic field homogeneity within 110 mm from the axis is better than 10^{-3}, for a maximum transverse field of 230 mT. The dipole chamber height is 80 mm. The analyzer dipole is monitored by a Labview program and allows to realize spectra in order to dissociate the three H^+, H_2^+ and H_3^+ species in the beam. A species analysis with transport optimization of both H^+ and H_2^+ is presented in Fig. 2. This optimization is obtained by varying pair of solenoids focalization field. These measurements have been done by successively optimizing H^+ and H_2^+ transport in order to really determine the effective species fractions.

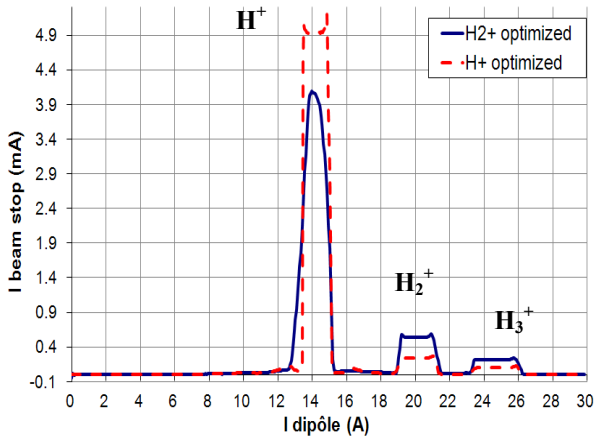

Figure 2: Spectra obtained by analyzer dipole

Easy source system assembly

Ion sources are positioned on a movable table on the test bench that allows quick and easy connection to the beam line. Plasma chamber and RF window are water cooled and the gas injection system is located on high voltage platform close to the source insulated table (Fig. 3). The radio frequency wave injection is produced by a magnetron located at ground potential and fed to the plasma chamber via rectangular waveguides and a DC break. For small extraction hole on the plasma electrode (due to low expected current) an additional pumping is installed on the high voltage table (between the bend and the ridged transition). Such additional pumping allows minimizing the impurity production.

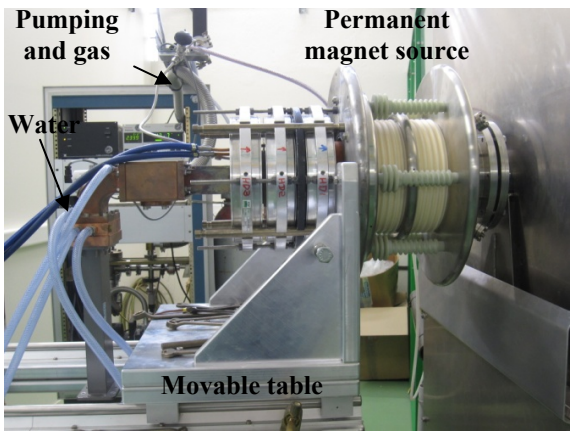

Figure 3: Source on movable table

PERMANENT MAGNET SOURCES

SILHI test bench experiments

First tests with permanent magnets sources were realized on SILHI test bench. The magnetic field is provided by several ring-shaped permanent magnets (with axial orientation) instead of 2 solenoidal coils.

A source with 3 magnets and appropriate shieldings has been installed. Electromagnetic simulations have been carried out to reproduce at best the SILHI source magnetic field profile on the axis. Even if the ECR resonance has been easily adjusted, first experiments showed Penning discharges occurred in the extraction system with the SILHI extraction system [2]. It came from the particular permanent magnet configuration built without shielding. To reduce the magnetic field in that accelerator column, an iron shielding was introduced as close as possible to the extraction hole (Fig. 4).

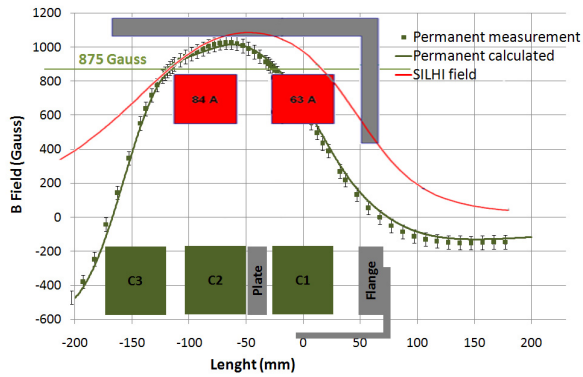

Figure 4: Simulation of iron tube effect on magnetic field with permanent magnet

On the BETSI test bench, the accelerating column (Fig. 5) diameter is reduced from 400 to 200 mm [3] that implies changing the electrode shape and size, which has as consequences to modify electric field distribution in the far axis region. Thus with this new accelerating column, no Penning discharge is occurred for mainly magnetic configurations.

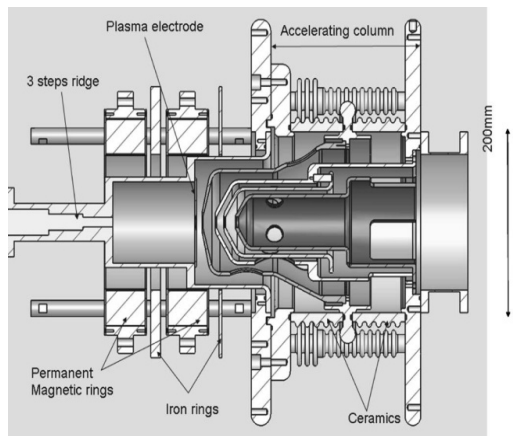

Figure 5: SPIRAL2 permanent magnets source

Magnetic optimization on BETSI

The developments realized on BETSI test bench are focused on magnetic optimization of permanent magnet sources. In order to simplify the shielding, several magnetic simulations were realized with 2 or 3 permanent magnets rings (Fig. 6). Field map shows the role of iron plates or flange for increasing magnetic field on axis at the ring position or reduce fringe field in the accelerating column. White zones correspond to field higher than 0.2 T.

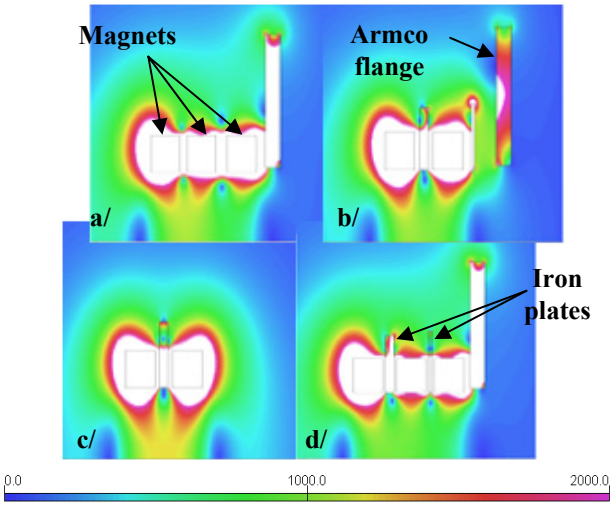

Figure 6: B field map for different permanent magnetic configurations (a/ 3 magnets, 1 flange; b/ 2 magnets, 1 flange, 2 plates; c/ 2 magnets, 1 plate; d/ 3 magnets, 1 flange, 2 plates)

The best results were obtained with 2 permanent magnets and 2 plates (one of 15 mm thick located between the 2 magnets, and the second one of 5 mm on the extraction electrodes side) shown in Fig. 7. The two resonant zones of 87.5 mT were respectively located near radio frequency input and near plasma extraction electrode. A 5.7 mA total beam was extracted with 86 % of H^+ (Tab. 1).

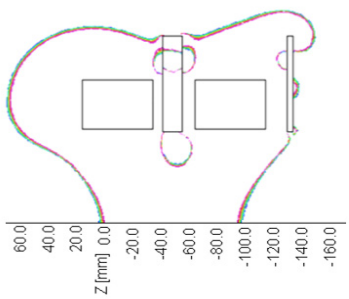

Figure 7: Optimized magnetic configuration and 87.5 mT ECR location

Table 1: Source and beam characteristics

SOURCE CHARACTERISTICS			BEAM CHARACTERISTICS		
Electrode Φ3mm					
Gas flow	0.95	sccm	**Total current**	5.75	mA
Pressure	$5.1.10^{-6}$	Torrs	**H^+ max current**	4.97	mA
e^- Filter	-1.5	kV	**H_2^+ max current**	0.54	mA
HTEI	20	kV	**H_3^+ max current**	0.24	mA
HT	40	kV	**H^+/total**	86.41	%
PHF	550	W	**H_2^+/total**	9.45	%
Pulsed time	50	ms	**H_3^+/total**	4.14	%

The SILHI emittance scanner has been installed on the diagnostic box after the solenoids. A normalized emittance of 0.012 π.mm.mrad has been measured with a 2 mA proton beam extracted at 20 keV through a 3 mm diameter hole (Fig. 8). To produce such beam, the RF injected power reached 800 W.

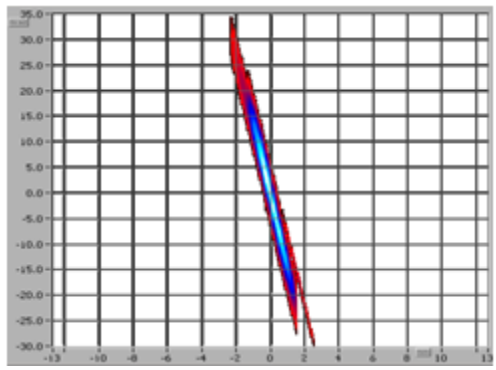

Figure 8: 2 mA H^+ beam emittance after the solenoids

CONCLUSIONS AND PERSPECTIVES

The new test bench named BETSI is now operating at CEA/Saclay, it allows developing and testing new ions sources and beam diagnostics. Several permanent magnets sources have already been tested. A configuration with 2 magnets and appropriate shieldings allowed extracting 5 mA of H^+ at 40 keV with a 3 mm electrode diameter.

Moreover a new ion source and two other diagnostics are under installation in order to better understand the role of plasma chamber size and shape on the plasma-wave interaction. A plasma light emission diagnostic using spectroscopy is also under development for ECR plasma electronic temperature measurements. A second diagnostic will allow measuring the absorbed power by the plasma using wide-band reflectometry technique.

ACKNOWLEDGEMENTS

The authors would like to thank all the persons involved in BETSI project for their advices and help.

REFERENCES

[1] O. Tuske, "BETSI, a new test bench for ion source optimization at CEA SACLAY", Proc. of ICIS, Jeju, Korea, 2007.

[2] R. Gobin, "Development of a Permanent Magnet Light Ion Source at CEA/Saclay", Rev. Sci. Instrum. 77, 03B502 (2006).

[3] R. Gobin, "Development of a permanent magnet ECR source to produce 5 mA deuteron beam at CEA/SACLAY", Proc. Of LINAC04, Lübeck, Germany, 2004.

MICROGAN ECR ION SOURCE IN A VAN DE GRAAFF ACCELERATOR TERMINAL

G. Gaubert, O. Tasset-Mayé, A.C.C. Villari, C. Bieth, W. Bougy, N. Brionne, X. Donzel, A. Sineau, C. Vallerand, PANTECHNIK, Bayeux, France.
C. Chaves, T. Gamboni, W. Geerts, G. Giorginis, R. Jaime Tornin, G. Lövestam, W. Mondelaers, EC-JRC-IRMM, Institute for Reference Materials and Measurements, Geel, Belgium

Abstract

The Van de Graaff accelerator at IRMM works since many years providing proton, deuteron and helium beams for nuclear data measurements. The original ion source was of RF type with quartz bottle. This kind of source, as well known, needs regular maintenance for which the accelerator tank must be completely opened. The heavy usage at high currents of the IRMM accelerator necessitated an opening about once every month. Recently, the full permanent magnet Microgan ECR ion source from PANTECHNIK was installed into a new terminal platform together with a solid state amplifier of 50 W, a dedicated dosing system for 4 gases (with respective gas bottles H2, D2, He and Ar), and a set of dedicated power supplies and electronic devices for the remote tuning of the source. The new system shows a very stable behaviour of the produced beam allowing running the Van de Graaf without maintenance for several months.

INTRODUCTION

The high intensity quasi mono-energetic neutron source at IRMM is driven by a vertical 7 MV Van de Graaff accelerator (VDG) producing either continuous or pulsed ion beams [1]. The accelerator is operated 24 hours a day and seven days a week. The maintenance cycle with the original RF source was about once a month. In order to improve availability of the machine as well as the operation of the ion source, it was decided to replace the RF source with an ECR ion source and also update the high voltage platform.

The Microgan ECR ion source [2] working at 10 GHz is now providing single-charged or multi-charged ions like proton, deuteron, helium and argon.

We will recall the principle of this ion source adapted to the existing beam line before describing the Van de Graaff accelerator high voltage platform constraints and technical solution adopted. The command and control hardware/software will be discussed. Finally, beam results in term of tuning, intensity and stability will be presented.

Microgan Ion source

The Microgan is an ECR ion source, for which the magnetic circuit is entirely made with permanent magnets both for the radial and longitudinal fields, so the total electrical power is extremely low. The minimum B structure (Fig. 1) is made to work with a 10 GHz RF wave. This source can work with RF power up to 200 W (if water cooled) depending on the element and charge state needed.

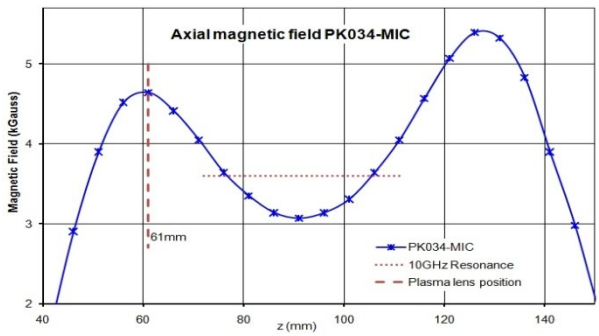

Figure 1: Microgan axial magnetic field

In this application, the requirement of 60 µA intensity for all beams (see table 1), led us to work with 50 W of maximum RF power if the plasma chamber is not cooled.

Table 1: Microgan intensities & VDG requirements

Usual guaranteed intensities (in µAe)							**VDG**
Ions/Q	1	2	3	4	5	8	1
H	7000						60
D							60
He	5000						60
O	4000	400	170				
P	2000	1200	700	200	20		
Ar	2000	1290	600	220		20	

Nevertheless, the ion source produces too high intensity with respect to the Van de Graaff limitations and the emittance of such an ECR ion source. Simulations with QuickfieldTM software and beam transport calculations combined with measurements done on a dedicated test bench at the Pantechnik's factory, that reproduced the first part of the accelerator, rendered the final set-up as shown in Fig. 2.

The plasma electrode aperture has been reduced to 3 mm in diameter. A simple gap extracting puller is followed by an Einzel lens to adapt the beam at the entrance of the present 30° analysing magnet. The plasma electrode aperture has been reduced to 3 mm in diameter. A simple gap extracting puller is followed by an Einzel lens to adapt the beam at the entrance of the present 30° analysing magnet.

This magnet is useful to clean the beam from contamination, especially to remove the molecular beams. We optimized the mechanical size of each element in order to maximize the analysed beam characteristics (size and intensity) in the buncher that is used for the pulsing system.

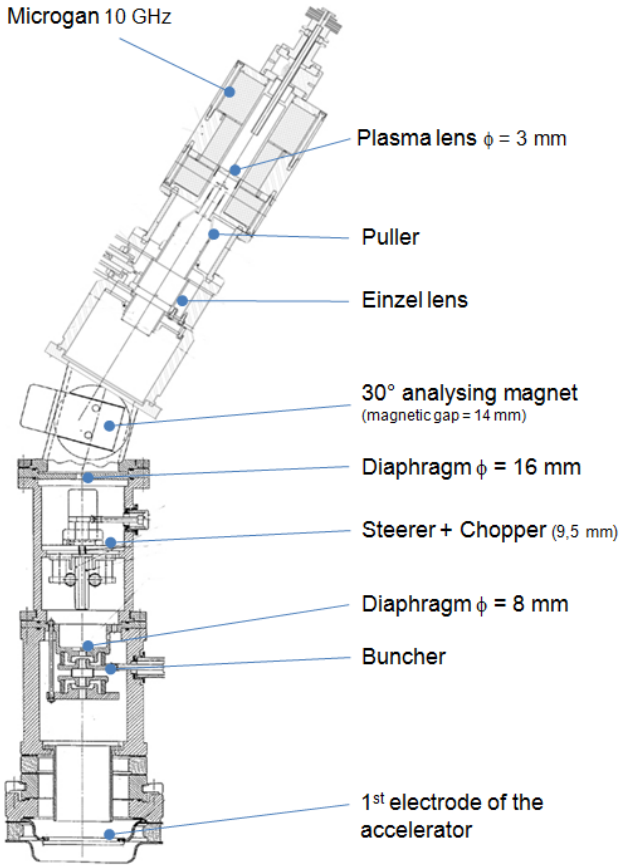

Figure 2: Overview of the VDG beam line before the high energy acceleration

VDG PLATFORM AND CONSTRAINTS

The Van de Graaff accelerator terminal is filled with up to 15 bars of a mixture of dry N2 (80 %) and CO2 (20 %) with a minor adding of SF6. This condition led us to test all critical parts that have to work under this pressure condition. A 15 bars test tank was built and used to test all mechanical components as well as electronic devices while powered (see Fig.3.a). Thus, the solid state 10GHz RF amplifier was tested together with the coaxial to wave guide designed feed-through. This component has to work at high pressure and in the same time has to be sealed with a leak rate under vacuum side better than 10-9 mb.l.s-1. The RF signal is generated with a DRO followed by a remote DC control attenuator allowing the RF power control.

Mechanical constraints were taken into account also for the gas system which is fully high pressure proof. The dosing valves (Pfeiffer UDV type, see Fig.3.b) are under atmospheric pressure in a dedicated closed container allowing a reliable behaviour. Four gas circuits are connected to the two dosing valve in the way that gas mixing of argon and helium allows producing multi-charged ions of argon (see Fig.3.c). Gas changing from proton to deuteron or helium and argon is remote controlled. About 3 hours are needed to change ion. The life time of a full gas bottle is several months of usage.

Special efforts were made to minimize the size of all equipment on the high voltage platform as the space is limited. On the other hand, the lack of any cooling liquid on the high voltage platform required the use of some pressure proof fans to cool down ECR components.

The most important electrical constraint is the low total power available on the high voltage platform (about 1500 W at 400 Hz AC current). A part of it (50 W maximum) is used by the RF amplifier and the rest is used for the electronic devices and power supplies.

Since the Van de Graaff is operated at high voltage up to 7 MV, all electrical components need a hard protection against electrical sparks and discharges. This protection is achieved by placing the components in dedicated shielded boxes where all cables (power and signals) are plugged on special CEM protected feed-through.

The last constraint is given by the charge the belt of the Van de Graaff is able to provide which corresponds to about 200 µA of ion beam current. That's why the full current of the source has been reduced with a small plasma lens aperture (3 mm) and a low RF power (few watts). The analysing magnet allows the selection of the ion beam of interest together with a stable behaviour of the column with almost 60 µA for each kind of ions.

3.a) Pressure test tank

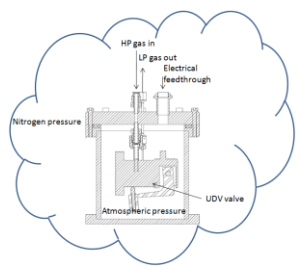

3.b) Dosing valve system

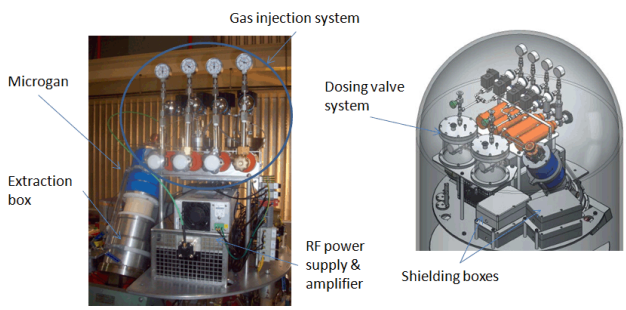

3.c) high voltage platform view

Figure 3

SIMULATIONS, TRANSPORT, TEST BENCH

Simulations of the electric field of the extraction system have been carried out with the QuickField™ software (see Fig. 4). The puller with a 10mm aperture is facing the plasma electrode with a 25mm gap. It's immediately followed by an Einzel lens. This system can operate with a 15 to 30 kV extraction potential, while the Einzel lens potential is about 2/3 of the extraction. Beam calculation have been carried out with TRANSPORT[1] software (Fig. 5) and predicted a high efficiency of the beam focussing at the entrance of the bending magnet (100 %) and ensuring more than 40 % of the full collimated beam in the the buncher system.

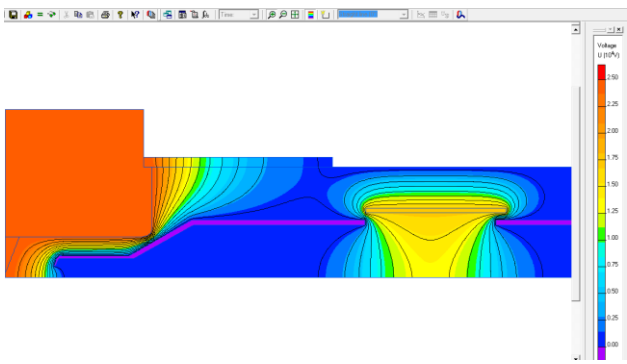

Figure 4: Extraction and focussing electric field simulation

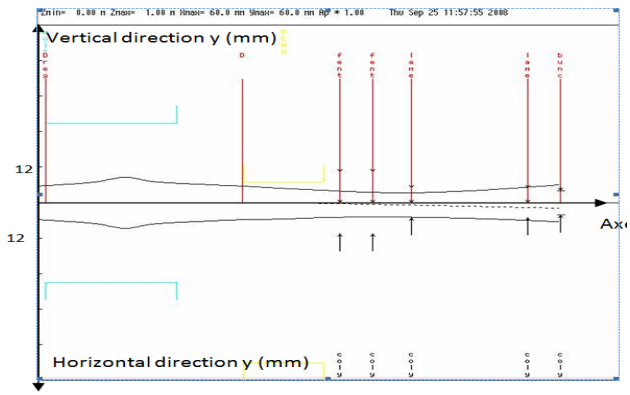

Figure 5: Vertical and horizontal D+ beam envelope

Those results were verified on the dedicated test bench built at Pantechnik's factory. The maximum beam size measured was 12 mm in diameter at the entrance of the magnet. The diaphragm at the entrance of the buncher with an 8mm aperture clearly reduces by about 60 % the beam intensity.

This bench was also used to find out the best parameters in terms of transport together with the more stable beam parameters for the tuning of the ion source (gas, RF, extraction mechanical adjustments).

[1]TRANSPORT PSI software

COMMAND & CONTROL

The hardware consists of 3 CNA control modules (from Group3 company) to control all signals (D/A) for the gas system as well as the RF amplifier and generator ones (Fig. 6). They are all connected together in series with optic fibers. The main tank of the Van de Graaf is equipped with a single optic feed-through and the last fiber is going to the command and control room. A dedicated computer running a Labview™ software controls the ion source and the extraction system.

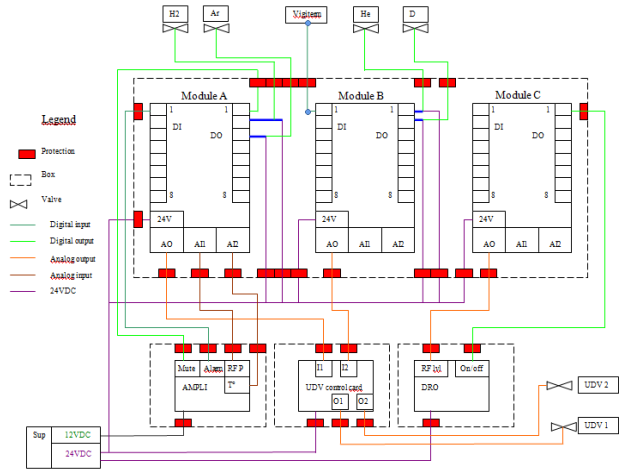

Figure 6: C&C hardware principle

RESULTS

On site acceptance tests have been successfully carried out in May 2010. The easy tuning of the system was demonstrated as well as the high reliability. The required intensities were measured at 3 MeV acceleration voltage on the accelerator column. Table 2 below shows the different parameters and intensities obtained at the bottom of the column, i.e. vertical position of the Faraday Cup. One should note that each beam has been identified with the mass spectrometer after the 3 MeV acceleration.

Table 2: Beam currents and parameter

Ion	P col	Uext	I ext	P RF	Gaz	U einzel	I CF25
Type	10^{-6} torr	turns	mA	W	Type	kV	µA
H^+	1.13	33	1.2	14.8	H_2	27.75	65
D^+	1.21	26	1.5	14.9	D_2	20.72	75
D_2^+	1.21	26	1.5	14.9	D_2	20.72	>100
He^+	0.92	26	<1	10.3	He	20.31	62

The H^+ beam at 60 µA was maintained without any operator neither regulation loop during 48 hours (see Fig. 7) to demonstrate the stability of the system. “Night and day effect” (temperature variation) was observed and induced +/-5 % change on the beam intensity for which the requirement was +/-20 %.

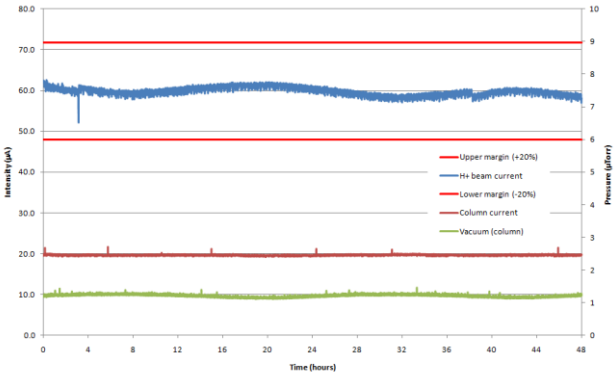

Figure 7: Beam stability recording

CONCLUSION

A new high voltage terminal in the Van de Graaf accelerator at the IRMM laboratory including a MicroganECR ion source was installed and commissioned in May 2010. It was demonstrated that the new system fulfilled the difficult constraints of such accelerator with high pressure conditions and an electrostatic sparking environment. H+, D+ and He+ beams were measured with the required intensities. The H+ beam stability was demonstrated through 48 hours operation without any intervention.

The system is supposed to have a high reliability and will allow to reduce the number of periodical maintenance of the machine.

Further tests are now needed to verify the ability of the system to work in the pulsed mode using the present chopper-buncher system.

[1] http://irmm.jrc.ec.europa.eu/html/about_IRMM/laboratories/The_Van_de_Graaff_laboratory.htm
[2] C. Bieth et al., RSI, 71, 899 (2000)

AN ECR TABLE PLASMA GENERATOR

R. Rácz[1, 2, #], S. Biri[1], J. Pálinkás[1, 2]
[1]Institute of Nuclear Research (ATOMKI), Hungary, H-4026 Debrecen, Bem tér 18/c
[2]University of Debrecen, Hungary, H- 4010 Debrecen, Egyetem tér 1.

Abstract

A compact ECR plasma device was built in our lab using the "spare parts" of the ATOMKI ECR ion source. We call it "ECR Table Plasma Generator". It consists of a relatively big plasma chamber (ID=10 cm, L=40 cm) in a thin NdFeB hexapole magnet with independent vacuum and gas dosing systems. For microwave coupling two low power TWTAs can be applied individually or simultaneously, operating in the 6-18 GHz range. There is no axial magnetic trap and there is no extraction. The technical details of the plasma generator and preliminary plasma photo study results are shown.

THE ATOMKI-ECRIS

In the ATOMKI a room-temperature, variable frequency ECR ion source operates as a stand-alone device to produce plasmas and ion beams from a variety of materials. So far H, He, N, O, Ar, Kr, Xe (from gases) and F, Ni, Fe, Zn, C, C_{60}, Zn, Pb (from solids) plasmas and beams were produced. The technical details and the recent applications of the ECRIS are shown elsewhere [1, 2]. The homepage of the ECR Laboratory [3] stores lots of information and photos.

The ATOMKI-ECRIS is a modular ion source which means that some of its main sub-systems are variable or changeable. It has two plasma chambers. The first one (internal diameter ID=5.8 cm, length L=20 cm) serves for highly charged ions (HCI) and a bigger one (ID=10 cm, L=20…40 cm, variable) was designed to host large-size, low charged plasmas (LCP). Both plasma chambers can be fit into their own NdFeB hexapole magnet which have logically appropriate IDs for the plasma chambers [4]. In Fig. 1 the plasma chambers and hexapoles are shown. Two room-temperature solenoid coils with optional iron plugs build the axial mirror trap of the ECRIS. The main microwave source is a klystron amplifier operating at 14.3 GHz frequency, with transmitted power between 5 and 1000 W. Occasionally we use a second microwave source which is one of our three travelling wave tube (TWT) amplifiers. The TWTAs can deliver microwave power up to 20 W in a wide frequency range (6-18 GHz).

The original goal was the usage of these two configurations (HCI and LCP) alternatively. But the frequent ECRIS disassembling and re-building sometimes caused inconvenience and the starting-up times (pumping down, plasma aging, etc.) was too long, occasionally 2-5 days. Furthermore, after more than 10 years of operation time our ECR laboratory owns many spare parts and devices (as pumping systems, vacuum measurement units, gas dosing tools, ovens, electrical and motion feedthroughs etc).

Therefore we decided to build a second ECR facility from the spare parts of the "big" ECRIS. It became a compact device which can be placed even on a table so we call it "ECR Table Plasma Generator". Its main elements are:

- plasma chamber (ID=10.2 cm, L=20-40 cm, variable), SS, double walled, water-cooled,
- NdFeB hexapole radial trap (L=24 cm, Br=0.65 T at chamber wall), Halbach-type,
- WR62 and WR90 connections
- microwave oscillator (HP 8350B + plug-ins)
- TWT amplifiers (max 20 W) with frequency 6-18 GHz (variable). One or two microwaves can be coupled.
- three vacuum ports for electrical or motion feedthroughs, for ovens, probes, etc.
- observing window or sample holder (alternative)
- gas dosing system, turbopump vacuum system.

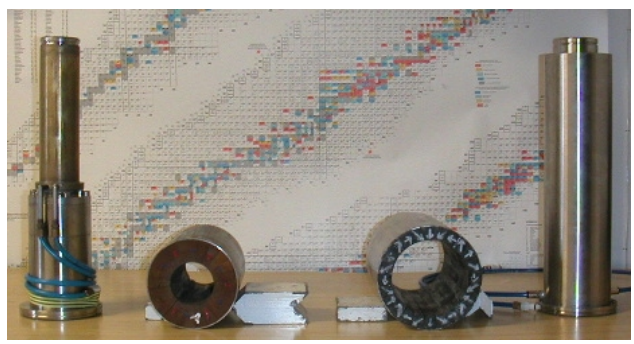

Figure 1. The HCI plasma chamber with its strong hexapole (left) and the LCP chamber with the large, weak hexapole (right).

The device is not equipped however, with axial magnetic trap (there are no coils or axial magnets) and there is no extraction system at all. In Fig. 2 the Table Generator is shown with explanation texts.

The first tests of the table device passed off without any major problems. A relatively high pressure (10^{-4} mbar) is necessary to ignite the plasma without a closed ECR-zone. In Fig. 3 residual gas plasma is shown. The strong asymmetry is caused by the side position of the gas tube.

#rracz@atomki.hu

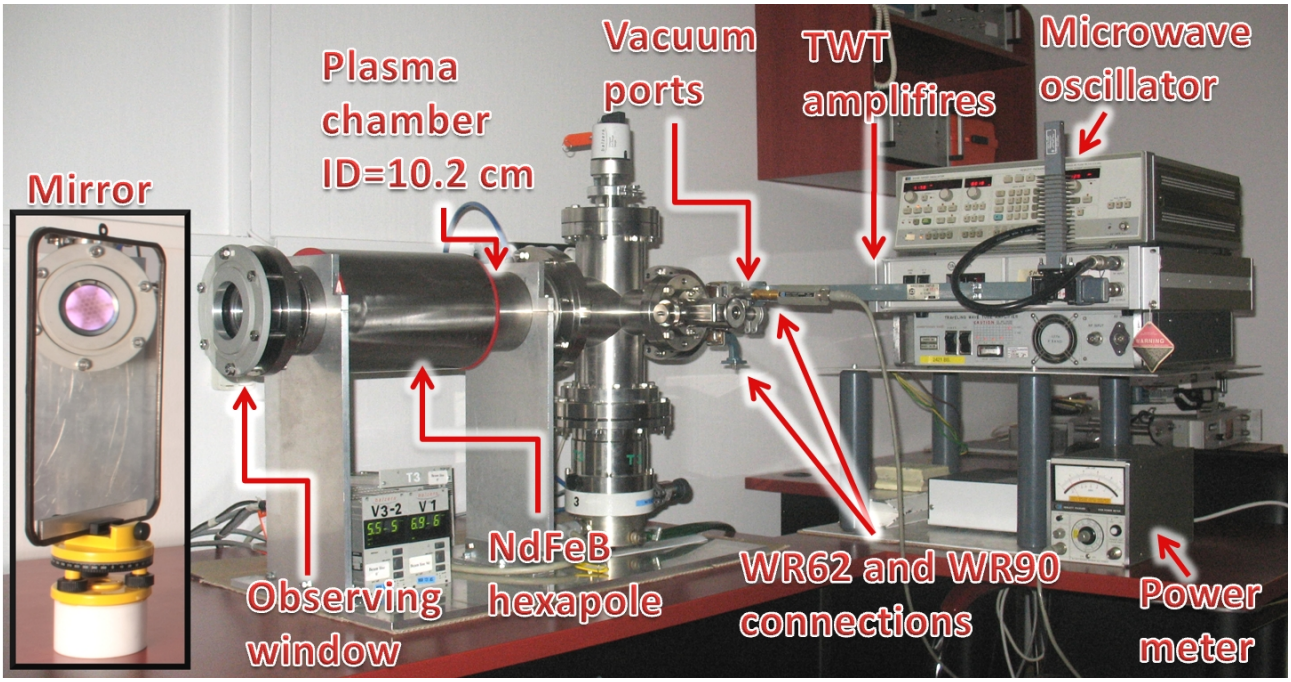

Figure 2. The ECR Table Plasma Generator of ATOMKI.

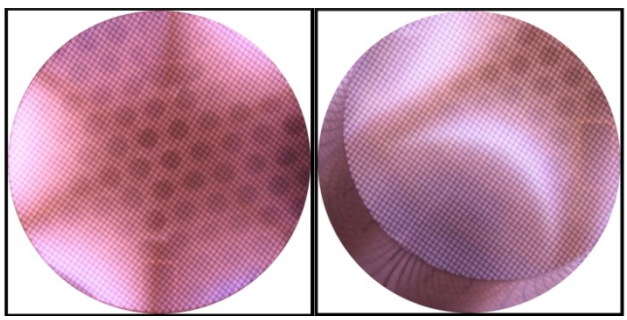

Figure 3. Typical plasmas produced by the ECR Table Plasma Generator. On-axis (left) and off- axis (right) views. Diameter of the resonant zone (7.14 cm) is larger than the diameter of the observing window (6.5 cm).

The intended fields of usage of the plasma generator are:

- A simple, cheap and safe educational working place for students.
- To prepare, to practice or to test measurements with electrostatic movable Langmuir probes.
- To prepare, to practice or to test plasma diagnostic measurements in the visible light and X-ray ranges using cameras and spectrometers.
- To cover and/or to modify solid surfaces with plasma particles, including with fullerene ions.
- To test and practice special microwave modes (pulsed power, frequency sweeper, double frequency etc.).

In the rest part of this paper the results of the first experiments carried out by the help of the ECR Table Plasma Generator, are shown.

VISIBLE LIGHT PLASMA STUDY

First we used the plasma generator to prepare and test a plasma diagnostic measurement in the visible light range.

The traditional visible light photos show the axial projection or integration of the ECR plasma spider in 2D but actually they contain enough information to build 3D pictures of the plasma. We are working out a method to get as much axial spatial information as possible. Fig. 4 shows the experimental setup.

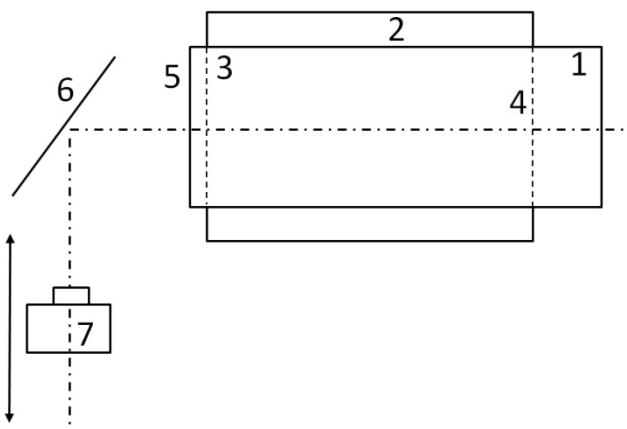

Figure 4. Experimental setup to take visible light photos at the Plasma Generator. Plasma chamber (1), hexapole magnet (2), meshes (3, 4), quartz window (5), mirror (6), camera (7).

Our 2D/3D method is based on elementary optical calculation. The lenses give exactly sharp images from the points of the objects plane. Points which are suited front of or back of the objects plane produce sharp images in front of or back of the film plane. These points form CoC (Circle of Confusion) on the film (Fig. 5.). There

exists a limit of the CoC (1/20mm), which allow sensing sharp images. t_{back} and t_{front} mean the distances of the levels (back of and front of the object distance) from where the lens make 1/20mm CoC on the film plane.

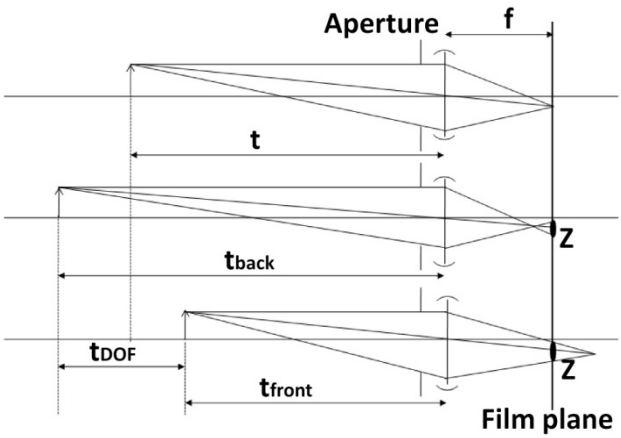

Figure 5. Imaging of the lens.

These distances define another distance: the Depth of Field (DOF).

$$(1)\quad t_{back} = \frac{t}{1+\frac{(t-f)zR}{f^2}}$$

$$(2)\quad t_{front} = \frac{t}{1-\frac{(t-f)zR}{f^2}}$$

$$(3)\quad t_{DOF} = t_{back} - t_{front}$$

Where *t* is the object distance, *f* is the focal length, *d* is the diameter of the aperture, *R=f/d* is the iris value *z* is the diameter of the tolerated COC [5].

According to these equations we can reach very low DOF value applying long focal distance (250 mm), low iris value (5.6) and very close object distance (1.1 m). With these settings the calculated DOF is 9.2 mm. Assuming a partly transparent plasma with homogeneous intensity distribution in visible light range we can get a 9.2 mm thick slice of the plasma in the given object distance using intensity filtering in the low intensity range (Fig. 6.).

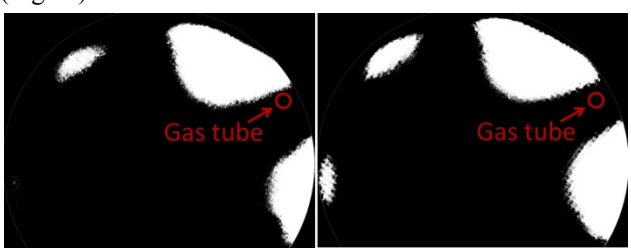

Figure 6.Ttypical slices of the plasma. The object distance was at 50mm (left) and 10mm (right) distance from mesh 4 (fig.4). The red circle shows the contour of the gas tube.

The intensity of the points which come from region out of DOF is significantly lower than those come from region inside of the DOF limit. In order to map axially through the plasma we took photo series by moving the camera on the axis in 10mm steps with unchanged camera settings.

These slices reconstruct the axial spatial distribution (3D image) of the plasma (Fig. 7).

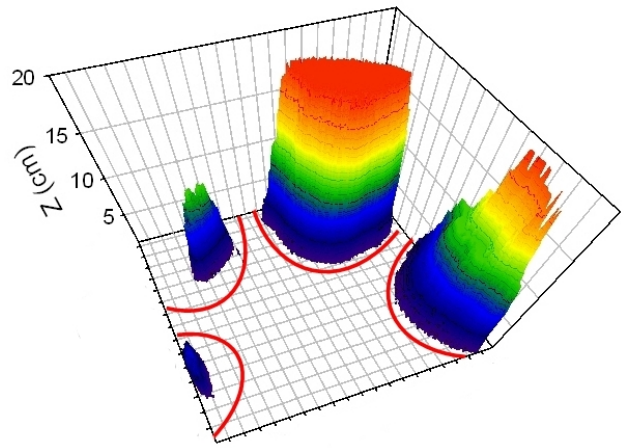

Figure 7. 3D picture of the plasma produced by the ECR Table Plasma Generator. Red lines show the theoretical contour of the hexapole-produced plasma.

We found that the position of the gas tube determine the structure of the plasma. Where the gas was injected the plasma appears close to the injection. However the other parts of the plasma appear at different axial distance from the injection plane (mesh 4 in Fig.4.)

We work out this method further and, in the near future, we want to answer the question: taking 2D axial photos only, is it possible to reconstruct the 3D map of a real ECR ion source plasma?

REFERENCES

[1] S. Biri, J. Vámosi, A. Valek, Z. Kormány, E. Takács, J. Pálinkás, Nucl. Instrum. Methods **B**124 (1997) 427.

[2] S. Biri, I. Iván, Z. Juhász, B. Sulik, Cs. Hegedűs, A. Ifj. Jenei, S. Kökényesi, J. Pálinkás, Proceedings of the 18th Int. Workshop on ECRIS Chicago, Ill. USA, 15-18 Sept., 2008. 41-47

[3] The homepage of the ATOMKI ECRIS Laboratory. www.atomki.hu/ECR

[4] S. Biri, A. Derzsi, É. Fekete, I. Iván, High Energy Physics and Nuclear Physics 31 (2007) 165.

[5] O. Jennrich, Ein Blick auf die Scharfentiefe, (1999) Avaible from (in German): http://www.traxel.de/foto/drf/schaerfentiefe.pdf

USING MASS-FLOW CONTROLLERS FOR OBTAINING EXTREMELY STABLE ECR ION SOURCE BEAMS

X. Donzel#, W. Bougy, N. Brionne, G. Gaubert, A. Sineau, O. Tasset-Mayé, C. Vallerand,
A.C.C. Villari, PANTECHNIK, Bayeux, France
R. Leroy, GANIL, Caen, France

Abstract

Beam stability and reproducibility is of paramount importance in applications requiring precise control of implanted radiation dose, like in the case of hadrontherapy. The beam intensity over several weeks or months should be kept constant. Moreover, the timing for changing the nature of the beam and, as a consequence, the tuning of the source should be minimized. Standard valves usually used in conjunction of ECR ion sources have the disadvantage of controlling the conductance, which can vary significantly with external conditions, like ambient temperature and inlet pressure of the gas. The use of flow controllers is the natural way for avoiding these external constraints. In this contribution we present the results obtained using a new model of Mass-flow controller in the Supernanogan [1] source, for production of C^{4+} and H^{3+} beams. Extremely stable beams (+/- 2.5%) without retuning of the source over several weeks can be obtained. The reproducibility of the source tuning parameters can also be demonstrated.

GAZ SYSTEM

The previous Pantechnik's gas system using UDV 140 thermo-valve has been replaced by Mass flow-controller but keeping in state the rest of the system (see Fig. 1).

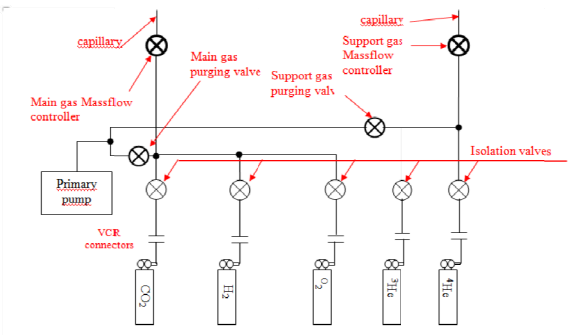

Figure 1: Schematic Gas System

The sensor's principle [2] inside the Mass flow-controller is made of a stainless steel capillary tube with resistance thermometer elements (see Fig. 2). A part of the gas flows through this bypass sensor, and is warmed up by heating elements. Consequently the measured temperatures T1 and T2 drift apart. The temperature difference is directly proportional to mass flow through the sensor. In the main channel Bronkhorst Company applies a patented laminar flow element consisting of a stack of stainless steel discs with precision-etched flow channels. Thanks to the flow-split the sensor output is proportional to the total mass flow rate. The minimum flow with this system is 0.014 mln/min until 0.06ml_n/min at max aperture.

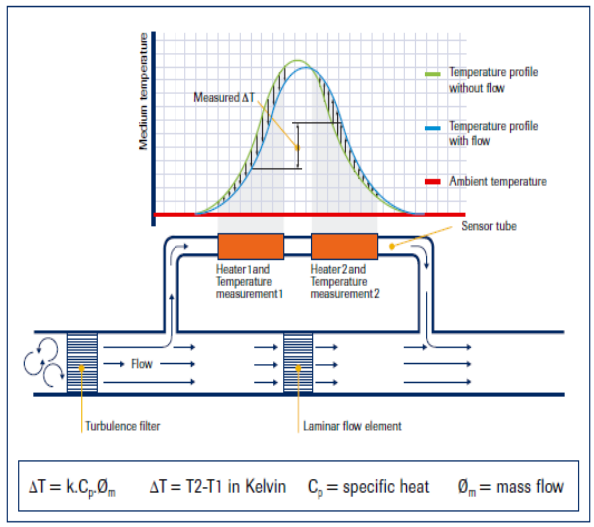

Figure 2: Mass-Flow sensor's principle

SYSTEM REACTIVITY AND STABILITY WITH TEMPERATURE

The behaviour of the Mass flow controller has been studied for different temperature variations.

Reactivity with sudden temperature changes

We recorded the current beam during 6400s and forced the temperature of the test room from 22°C to 14°C in 25 minutes (Fig. 3 & Table 1). The Mass-flow is only sensitive to very high variation of temperature.

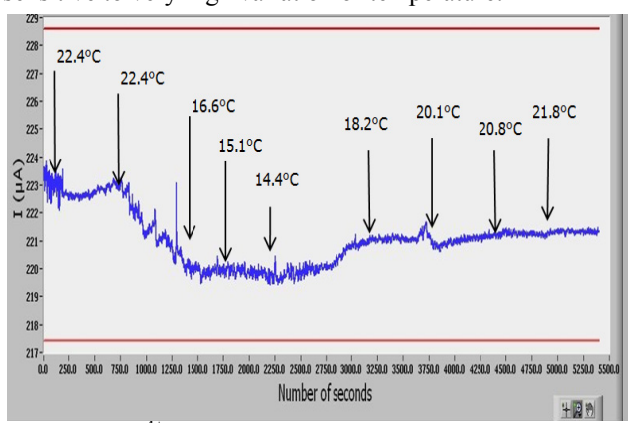

Figure 3: C^{4+} current with huge temperature's room variations.

xdonzel@pantechnik.com

Nevertheless, it stays under stability requirements limit (223µA +/- 2.5%).

Table 1: Test-room's temperatures

Time (s)	Temperature °C	I(µA)
0	22.4°C (start stability file)	223
600	22.4°C (start air cooler, set to 16°C)	223.5
1200	16.6°C	220
1800	15.1°C	220
2400	14.4°C (stop air cooler)	220
3000	16.6°C	221
3600	18.2°C	221
4200	20.1°C	221
4800	20.8°C	222
5400	21.2°C	222

Beam evolution during long term period

The Fig. 4 graphic shows the evolution of the beam during 1 hour using UDV valves and Mass Flow Controller.

The big wave observed is due to the start and stop of the air-conditioning system in Pantechnik's test-room.
The Mass-flow is insensitive to low variation of temperature (+-2°C) which is a requirement for Hadrontherapy [3].

The mean noise is lower with Mass Flow, the reason is the following: The gas mixing rate between support and main gas is maintained constant with the two Mass Flow while it can change with UDV140.

The Fig. 5 shows the evolution of the beam during 10 hours using UDV valves. The test with Mass-flow is in progress at Marburg's Hadrontherapy Center.

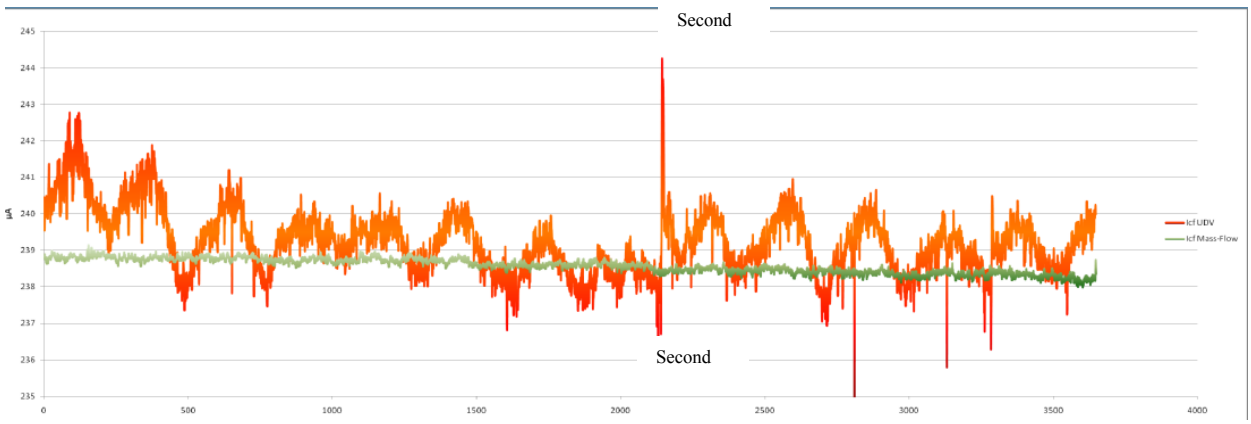

Figure 4: C^{4+} stability during 1 hour.

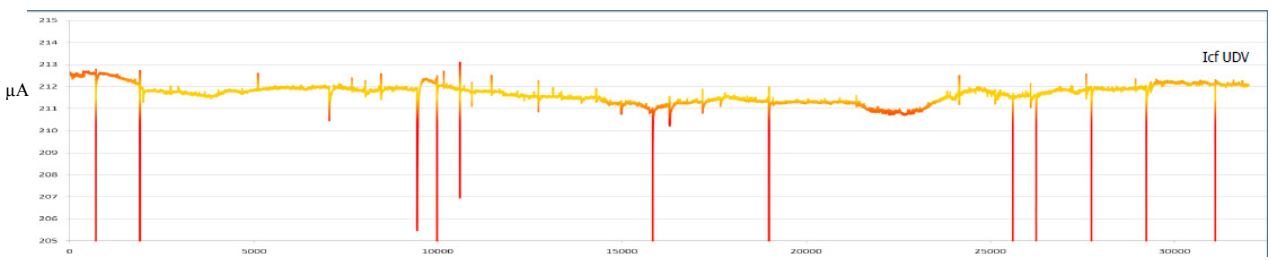

Figure 5: C^{4+} stability during 10 hours.

SYSTEM REPRODUCIBILITY WHEN CHANGING THE FLOW

In order to demonstrate the reproducibility of the system, the flow of the He gas has been changed and came back to the original value (see Fig. 6). There is no hysteresis effect like in UDV dosing valve and the reactivity is <5s.

The flow can be adjusted to the set point with a ramp (arrows 2, 4, 5, 6) or without (arrows 1, 3).

The flow has been changed with a step= 0.5% (of the max aperture) on arrow 1 and 2.

The ion source is insensitive to changes smaller than 0.5% for this tuning.

On arrows 3, 4 and 5, 6, the flow has been changed with a step=+/-1.25% , the ion beam current is restored.

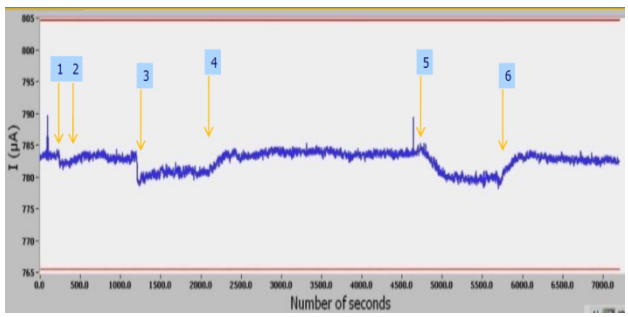

Figure 6: System reproducibility with He^{+}.

INJECTION PRESSURE ACCACCURACY

Fig. 7 & 8 display the result of test made on Supernanogan with injection turbo-pump. A calibration curve has been done on 2 different gases in order to investigate the behaviour of the valve and its resolution. We recorded (by step of 0.1% of the maximum flow) the injection pressure (without beam).

The opening is linear and the step resolution is around 1.4E-7 mbars.

The response time is less than 3s for small step.

The range goes to 2.10^{-7} to 5.10^{-5} mbar with He Gas and 2.10^{-7} to 2.10^{-4} mbar with H_2.

We conclude that we can have a very good accuracy on the flow. Nevertheless, further tests with others gases and high charge state will be studied in a close future.

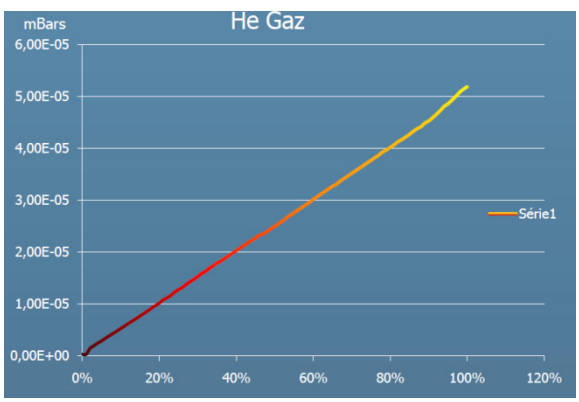

Figure 7: System reproducibility with He.

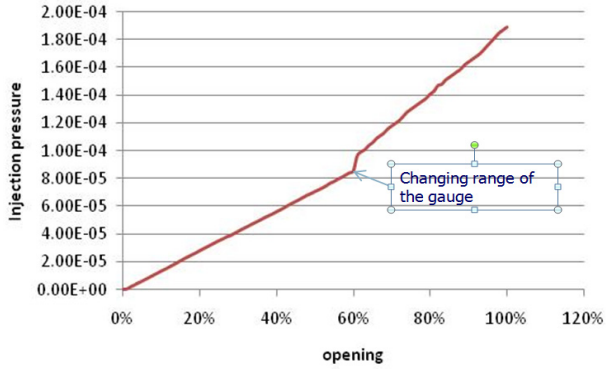

Figure 8: System reproducibility with H_2

The step at 60% for H2 (Fig. 8) is due to the range of the Injection Pressure monitor (10E-5 to 10E-4) so it changes calibration (Pirani gauge).

NEXT STEP: SMART BENCH FOR ECR SOURCE (AUTOMATIC SOURCE)

We already know that UDV valve provided a good stability [4] but the main defaults in this system are:

- The high sensibility to the temperature's variations.
- Hysteresis shape of valve thermo-mechanical response.

The main issue for having a stable beam from an ECR Ion source is the precise control of the gas flow.

Today, we can consider building a smart system for producing Ion beam dedicated to hadron therapy with:

- A high reproducibility of beam parameters.
- An insensibility to low temperature variation.
- And a stable beam with a good Emittance during several weeks without any intervention of operators.

The future system will allow selecting the type of ion (example C^{4+}) and the intensity (200µAe). The system will self-adjust Gas, Focus, Puller, RF-tuner, Frequency and RF power parameters for reaching the desired values after several minutes.

REFERENCES

[1] C. Bieth, Nucleonika 48 (2003) S93
[2] http://www.bronkhorst.fr
[3] J. Lettry,L. Penescu, J. Wallner, and E. Sargsyan, Rev. Sci. Instr. 81 (2010) 02A328
[4] T. Winkelmann, R. Cee, T. Haberer, B. Nass, and A. Peters, Rev. Sci. Instr. 81 (2010) 02A311

PRELIMINARY DESIGN OF BLISI, AN OFF RESONANCE MICROWAVE PROTON SOURCE

Slobodan Djekic, Ibon Bustinduy, David de Cos, David Fernandez-Cañoto, Jorge Feuchtwanger, Hooman Hassanzadegan, Igor Rueda, Juan Luis Munoz, ESS Bilbao, Bilbao, Spain
Daniel Cortazar, ESS Bilbao, Bilbao and Universidad de Castilla-La Mancha, Ciudad Real, Spain
F. Javier Bermejo Bilbao, Bilbao, Spain
Victor Etxebarria, Josu Jugo, Joaquin Portilla, University of the Basque Country, Bilbao, Spain
Miguel Angel Carrera, Julio Huguet Galipienzo, AVS, Eibar, Spain
Julio Lucas Elytt Energy, Madrid, Spain

Abstract

A new high current off resonance microwave H^+ source is currently in the last stages of design at ESS-Bilbao, in collaboration with two external companies Elytt and AVS. The design is intended to be a high-stability, high-current ion source capable of delivering a 70 mA proton beam with a 70 keV energy.

INTRODUCTION

The Bilbao Center for Accelerator Science and Technology is a large scale accelerator facility under construction in Spain. Its main headquarters have been inaugurated at the University of the Basque Country (UPV/EHU) campus at Leioa, Biscay. The first machine of the future facility will be a high intensity Proton Linear Accelerator. The first part of such a proton LINAC will be BLISI – Basque Light Ion Source Injector, that is to be completed within two years.

The main parts of the future BLISI Ion Source are magnetic structure, microwave system, gas inlet system and extraction system. The first two parts are designed in collaboration with Elytt. They are consists of a water-cooled plasma chamber that sits between two independently powered magnetic coils that generate the ECR magnetic field, a CPI 2.7 GHz klystron which provides the microwave energy and a fully controlled microwave system to minimize reflected power and improve the source overall performance.

The gas inlet system is designed for simultaneous introducing of two gases and it will have an automatic control loop for the gas flow stabilization.

The extraction system has been designed in collaboration with AVS. It will consist of a movable tetrode system designed for a maximum acceleration potential of 70 kV, the shape of the electrodes is at an earlier design stage at ESS-Bilbao.

The list of the desired parameters of the BLISI proton beam is given in Table 1.

We will present the current layout of the source, simulations and schematics of the source.

MAGNETIC STRUCTURE

The magnetic structure of the BLISI Ion Source consists of two solenoid coils divided into two pancakes and shielded by an iron yoke. The coils will be powered via four power supplies for higher flexibility in shaping of the magnetic field configuration. The coils are remotely movable via use of two stepping motors with a linear accuracy of 20 μm.

General Consideration

For optimal microwave power absorption in plasma chamber that will enhance production of high current of single charged ions one has to provide the special magnetic field configuration. Experimentally has been proven that such configuration has to have electron cyclotron resonance (ECR) conditions at both ends of the chamber and across the chamber to have a flat field around 10% higher then ECR field [1]. For our working frequency of 2.7 GHz corresponding resonance field will be B_{ECR} = 96.4 mT, so we have to provide flat magnetic field of around 106 mT through the whole length of the plasma chamber. We have considered two different solutions for the BLISI magnetic structure configurations.

Magnetic Field Proposals

In the first proposed magnetic structure, a plasma electrode and its support are made of magnetic material so they have a strong influence on the overall magnetic field shape. It is shown on the left part of the Fig.1.

Table 1: Expected proton beam characteristics

Proton Beam Parameters	Values
Beam energy	70 keV
Total current	80 mA
Proton fraction	>85 %
Emittance	<0.2 π mm mrad
Availability	98 %
Reliability	170 hours
Duty Factor	3 % to 10 % (pulsed beam)
Pulse	1.5 to 2 ms
Repetition Rate	Up to 50 Hz
Klystron	2 kW @ 2.7 GHz

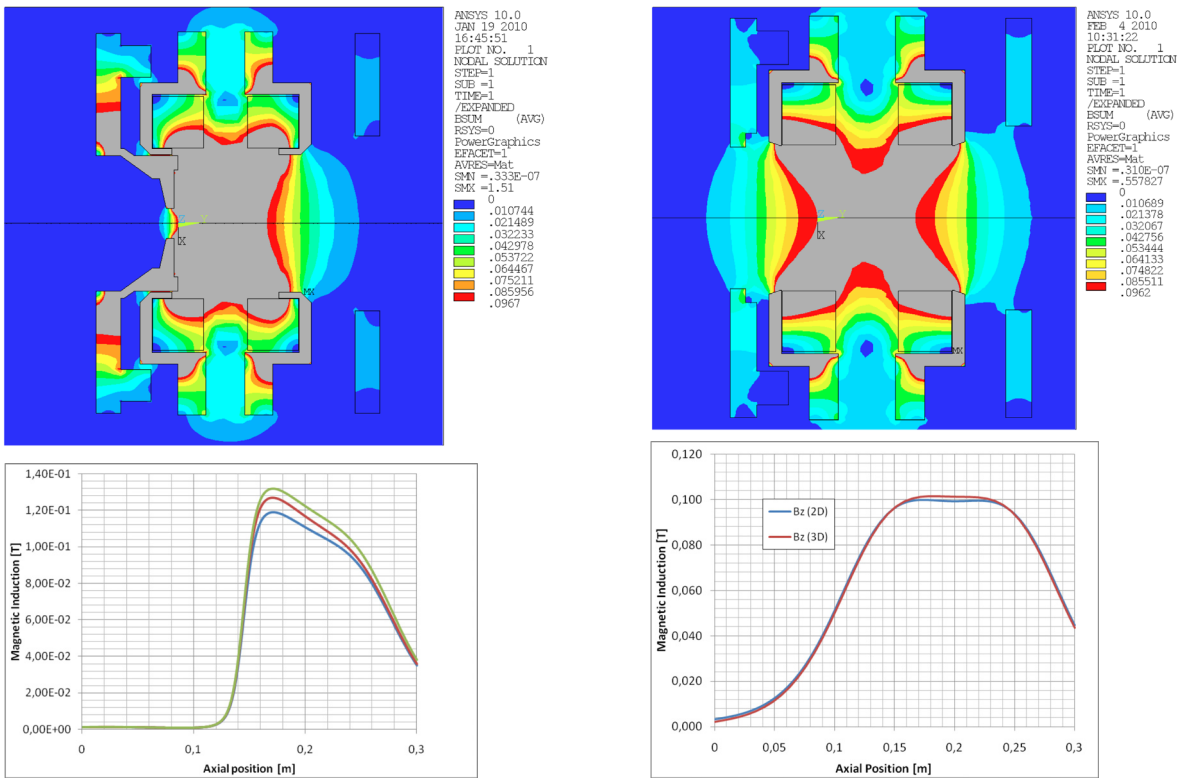

Figure 1: Magnetic Field Simulations for two cases of interest. On the left side the plasma electrode and its support are made of magnetic material, and on the right side of the figure they are made of non-magnetic one.

This solution has advantages that a magnetic field easily reaching values from 10% to 30% higher then $B_{ECR,}$ and also it provides a very good magnetic shielding of the extraction region. This can drastically improve the ion extraction. But the big disadvantage is that magnetic field shape isn't flat. This will probably detoriate microwave absorption and consequently creation of an overdense plasma necessary for the high proton current production.

So we have proposed another solution, shown on the right side of the Fig.1. The plasma electrode and its support part have been made of non-magnetic material and simulation has been done. Magnetic field will be almost constant along the plasma chamber having a value of 100 mT, that is just above the resonance. This will allow for a better plasma formation and higher plasma density, but will increase the magnetic field in extraction region up to 500 mT that will involve a risk of sparks and higher divergence of the extracted ion beams.

Deeper understanding of this problem is necessary and we will perform a detail test of the both proposed solutions in our future plasma laboratory that is already under construction.

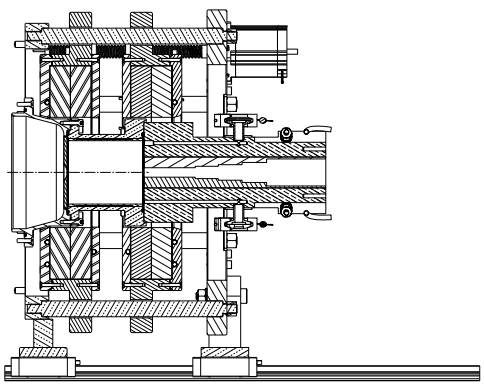

Figure 2: Layout of BLISI.

MICROWAVE SYSTEM

The microwave system of the BLISI consists of commercially available CPI klystron generator of 2 kW, working at 2.7 GHz, bidirectional couplers, circulator, waveguides and four stub automatic tuning unit (ATU) from Sairem company. Waveguide transition for coupling with the plasma chamber, electronics for ATU and electronics for pulsing the klystron amplifier will be designed and engineered by us. The plasma chamber (see Fig.2) will be made of copper in cylindrical shape with diameter 80 mm and length of 97 mm to provide optimal microwave coupling. It will be water-cooled and having at the both ends boron-nitride disks as electrons donors, this is necessary for efficient production of the high current proton beams.

The main reason for using klystron instead of magnetron is because it is easier for maintenance and better for pulse mode operation.

The 2.7 GHz working frequency has been chosen since it will generate higher plasma density.

GAS INLET SYSTEM

A special care has been taken in designing a gas inlet system that includes a PID regulator for creating an automatic control loop. It consists of a gas dosing valve, automatic gas pressure control unit, isolation valve and pressure gauge (see Fig.3). Our aim is to ensure a stable and reliable work for hundreds of hours even in case of long and/or short term changes in outside temperature or some others instabilities that can happen in the vacuum system and plasma fluctuations during a pulse mode operation.

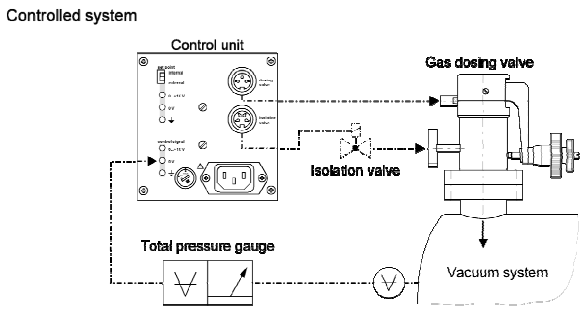

Figure 3: Layout of the gas inlet system.

For experimental determination of the PID parameters of the control unit of the gas regulation system we are building an ion source test stand. A pressure gauge will be directly connected to the plasma chamber that will give us exact knowledge on the pressure inside the chamber. This will open possibility to derive relation (semi-empirical equation) between the magnetic field profile, microwave power (and frequency) and neutral gas pressure and the plasma parameters: ion density, electron temperature and plasma potential.

The gas inlet system will consists of two separates lines for simultaneous introducing of hydrogen (or deuterium) and additional gases like oxygen or even water vapour.

EXTRACTION SYSTEM

The extraction system consists of 4 electrodes (see Fig. 4). The first one is plasma electrode attached to the plasma chamber and ion source body. So it is elevated to the voltage of the HV platform, i.e. 70 kV. Another 3 electrodes are packed in the extraction column and separated via two alumina insulators from the HV platform.

These three electrodes will be remotely movable as an entire group. That means we will keep the fixed distance between them, and change only acceleration gap – distance between them and plasma electrode. In such a way we have opportunity to experimentally optimize acceleration gap according to possible different extraction voltages, ion current density and different ion species (protons and deuterons). It will also allow for comparison of our ion extraction simulations with the experimental results for identical plasma parameters, since we can change the acceleration gap without breaking a vacuum.

The first and the third electrode of this group are grounded and water cooled. They serve for shaping of the ion beam. The second one, so called repeller, shall be on negative voltage of 3kV serving for the electron suppression.

We have paid a special attention to provide a good vacuum condition inside the extraction column, drilling additional wholes on the support parts of the electrodes. For reducing electron production in the HV column, and consequently minimizing X-ray radiation in vicinity of the source a special kofoidal protectors has been installed.

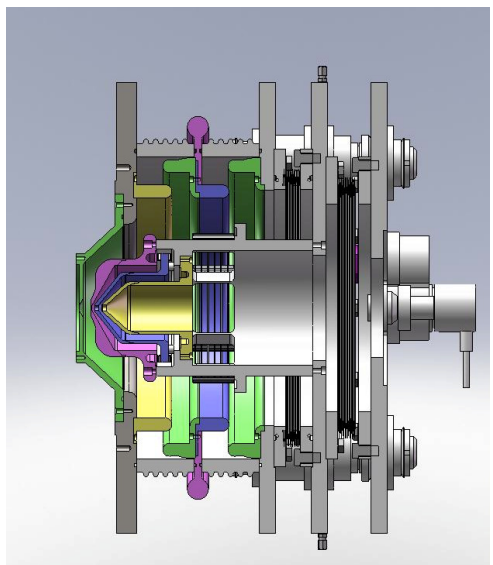

Figure 4: Layout of extraction system.

CONCLUSION

We have presented a preliminary design and status of construction of BLISI, an off resonance microwave source. Improvements have been done in all crucial parts of the BLISI comparing to designs of the similar proton sources [2],[3]. Extensive set of test measurements in the plasma laboratory, that we are building at the same site, will allow us for very a detailed performance check. The main target is reaching the overall reliability of the BLISI of minimum 170 hours.

REFERENCES

[1] T. Taylor and J.F. Mouris, Nucl. Instr. Meth. **A 336**, 1 (1993)
[2] J.D. Sherman et al. Rev. Sci. Instr. **73,** 917 (2002)
[3] R. Gobin et al. Rev. Sci. Instr. **73**, 922 (2002)

PERFORMANCE OF THE LBNL AECR-U WITH A TWTA

J. Benitez#, D. Leitner, M. Kireeff-Covo, C.Lyneis,
Lawrence Berkeley National Laboratory, Berkeley, USA

Abstract

The Advanced Electron Cyclotron Resonance - Upgrade ion source (AECR-U) at the Lawrence Berkeley National Laboratory has successfully utilized double frequency microwave heating (14.3 GHz and 10.4 GHz) for several years [1]. Recently a traveling wave tube amplifier (TWTA), providing frequencies in the range of 10.75GHz-12.75GHz, was added as a secondary heating frequency, replacing the previous 10.4 GHz Klystron. The TWTA opens the possibility to explore a wide range of secondary frequencies and a study has been conducted to understand and optimize its coupling into the AECR-U. In particular, the reflected power dependence on heating frequency has been mapped out with and without the presence of plasma. A comparison is made to determine how the presence of plasma, confinement fields, and other source parameters affect the reflected power and if and how the amount of reflected power can be correlated to the source ion beam performance.

[1] Z. Q. Xie and C. M. Lyneis, RSI 66 (1995).

Paper not received

jybenitez@lbl.gov

MEASUREMENTS OF BREMSSTRAHLUNG RADIATION AND X-RAY HEAT LOAD TO CRYOSTAT ON SECRAL *

H. Y. Zhao [#,‡], W. H. Zhang [#], Y. Cao [#,†], H. W. Zhao [#], W. Lu [#,†], X. Z. Zhang [#], Y. H. Zhu [#], X. X. Li [#], and D. Z Xie [#]
[#]Institute of Modern Physics, Chinese Academy of Sciences, Lanzhou 730000, China
[†]Graduate School of Chinese Academy of Sciences, Beijing 100049, China

Abstract

Measurement of Bremsstrahlung radiation from ECR (Electron Cyclotron Resonance) plasma can yield certain information about the ECR heating process and the plasma confinement, and more important a plausible estimate of the X-ray heat load to the cryostat of a superconducting ECR source which needs seriously addressed. To better understand the additional heat load to the cryostat due to Bremsstrahlung radiation, the axial Bremsstrahlung measurements have been conducted on SECRAL (Superconducting Electron Cyclotron Resonance ion source with Advanced design in Lanzhou) with different source parameters. In addition, the heat load induced by intense X-ray or even ϒ-ray was estimated in terms of liquid helium consumption. The relationship between these two parameters is presented here. Thick-target Bremsstrahlung, induced by the collision of the hot electrons with the wall or electrode of the source, is much more intensive compared with the radiation produced in the plasma and, consequently, much more difficult to shield off. In this paper the presence of the thick-target Bremsstrahlung is correlated with the magnetic confinement configuration, specifically, the ratio of B_{last} to B_{ext}. And possible solutions to reduce the X-ray heat load induced by Bremsstrahlung radiation are proposed and discussed.

INTRODUCTION

Driven by the increasing demand of heavy ion accelerators devoted to nuclear physics and high energy physics for more intense and higher charge state heavy ion beam, the technology of highly charged ECR (Electron Cyclotron Resonance) ion sources have been developed dramatically in the past decades. The production of more intense and higher charged state heavy ions can be realized by the increase of the plasma density and confinement time and, according to the scaling laws [1], finally realized by the enhancement of the frequency and power of the microwave and the magnetic confinement field. In the past twenty years, beam intensities of highly charged heavy ions produced by ECR ion sources have increase by a factor of 10-100 for different ions. However, nowadays the trend of ECR ion sources towards to higher microwave frequency and power and higher magnetic field is limited not only by the technological limits of microwave and superconducting magnets but also by the presence of intense high-energy X-ray flux produced by electron-ion collisions in the plasma or electron-wall collisions, which is severe especially for superconducting ECR ion sources because the X-ray can lead to substantial heat load to the cryostat. The presence of high energy electrons, with energy up to 1 MeV, in third generation ECR ion sources has been proved experimentally [2], [3]. The collisions of these high energy electrons with plasma ions lead to Bremsstrahlung radiation. In addition, some lost electrons strike on the chamber wall or the electrode and, consequently, thick-target Bremsstrahlung is produced. The produced X-ray deposits energy in the structure of ion sources, and turns out to be substantial heat load to the cryostat in the case of superconducting ECR ion sources.

To better understand the heat load of SECRAL, the axial Bremsstrahlung spectra have been measured at 24 GHz with different source parameters, and the heat load to the cryostat was estimated in terms of LHe (Liquid Helium) consumption simultaneously.

In some cases, the plasma electrons lose confinement and strike on the structure of the source, which leads to thick-target Bremsstrahlung that is much more intense and with much higher energy compared with the radiation produced in plasma. Obviously, this kind of radiation should be avoided in the point view of the reliable operation of the source. The axial Bremsstrahlung measurements have been carried out in different magnetic confinement configuration to provide insights about the thick-target Bremsstrahlung in ECR ion sources.

EXPERIMENTAL SETUP

The bremsstrahlung spectra were measured with an HPGe (High Purity Germanium) detector. To measure the axial radiation, the HPGe detector was located behind the straight-through port of the 110° analyzing magnet. The signals produced by the detector were amplified and shaped by a main amplifier, then sent to a MCA (Multi-Channel Analyzer) and finally displayed and stored on a PC (personal computer).

*Work supported by the nature Science Foundation under Contract No. 10225523 and 60706006
‡zhaohy@impcas.ac.cn

The main challenge in the measurements of Bremsstrahlung is to build an effective collimation system. The original system used in the previous measurements [4] turned out to be not effective to keep the counting rate reasonably low in the case of high frequency and high power. So a new collimation system has been designed and constructed. The collimation comprises two copper blocks and one lead block. The first copper collimator is positioned just behind the straight-through port of the analyzing magnet, about 2.5 m away from the plasma electrode of the source. It is 100 mm long and has a 1 mm circle aperture. The function of this collimator is to reduce the number of the photons that enter the rest of the collimation system. The second copper collimator, 100 mm long and with a 3 mm circle aperture, is placed 850 mm away from the first one. The last collimator, a lead block with an aperture of 10 mm, is located directly before the detector. The last two collimators are used to prevent the X-ray photons scattered by the surrounding material from entering the detector. With this system, the dead time of the acquiring system decrease from tens of percent to less than one percent.

AXIAL BREMSSTRAHLUNG RADIATION AND HEAT LOAD TO CRYOSTAT AT 24GHz

As presented in [3], the X-ray flux increases with the 24 GHz RF power and the axial minimum magnetic field Bmin. Here we focus on the correlation of the axial Bremsstrahlung radiation and the heat load to the cryostat at 24 GHz. The heat load to the cryostat is estimated in terms of LHe consumption. The LHe consumption of the source at different 24 RF power or different Bmin is presented as a function of the axial Bremsstrahlung radiation energy, which is estimated by integration of the spectra in the whole energy range. The LHe consumption increases with the X-ray radiant energy as expected. However the dependence is not linear.

The non-linear relation between the axial radiant energy and the LHe consumption can be explained as follows. Firstly, the radiant energy in our study is in the axial direction while the LHe consumption is mainly correlated with the radial X-ray radiation. According to ECRIS physics, the high energy electrons in ECR plasma are energized primarily in the radial direction. Thus the X-ray radiation of ECR plasma is highly anisotropic. With the increase of the RF power and B_{min}, the electron energy increases and the power radiated by electrons during collisions tends to be more forward, and then the anisotropism becomes more pronounced. In other words, the radial radiation may increase quicker with the RF power and B_{min} than the axial one. Secondly, this may be attributed to the shielding effect of the chamber. The chamber used in this study is enclosed with a 1.5 mm thick tantalum tube to reduce X-ray absorbed by the cryostat. The attenuation effect of tantalum has been measured with axial radiation. The experimental result shows that the tantalum almost has no effect for the radiation above 500 keV. But as shown in previous research, the electron energy increases with the increasing power and Bmin. So the shielding effect of the tantalum weakens as the high energy component increases.

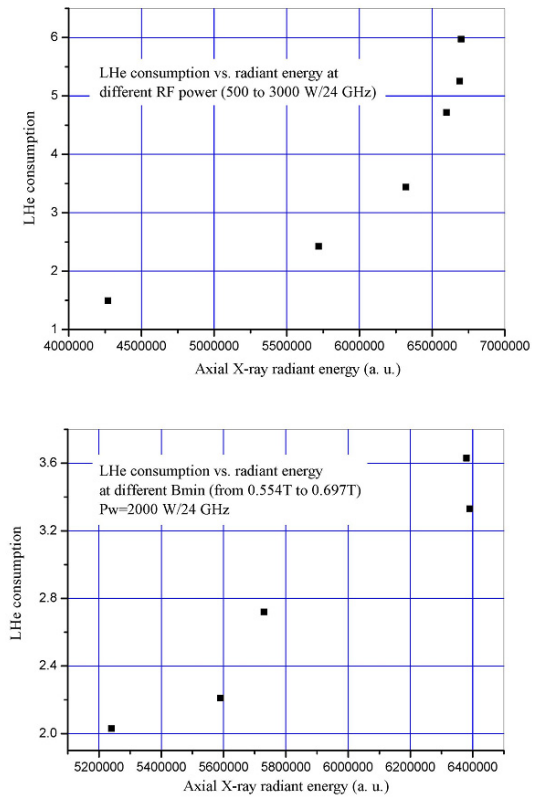

Figure 1: The LHe consumption as a function of the axial radiant energy.

Anyway, the non-linear increase of the LHe consumption with axial radiant energy demonstrates that the problem of X-ray heating turn to be much more severe for higher frequency and power ECR ion sources with higher magnetic confinement field.

THICK-TARGET BREMSSTRAHLUNG AND MAGNETIC CONFIGURATION OF ECRIS

As found in a previous experimental research [5], there is a sudden increase both in X-ray flux and energy of the axial Bremsstrahlung spectra with the increase of B_{rad} or the decrease of B_{ext}. In [5] the sudden change of the spectra is attributed to thick-target Bremsstrahlung. To confirm this, systematical experiments have been carried out on SECRAL at 18 and 14.5 GHz RF power. The experimental results are presented in Fig. 2.

The spectra were measured at different B_{rad} or B_{ext}. In one group of data, only one field was varied and the other one kept constant. As shown in Fig. 2, no matter which field is varied, the jump of the spectra is only correlated

with the ratio of the B_{last} to B_{ext}; the value of B_{last} is estimated by

$$B_{last} = \sqrt{B_{ext}^2 + B_{min}^2} \quad (1)$$

These results turn to be the further confirmation of the statement in [5]. When $B_{last}>B_{ext}$, the thick-target Bremsstrahlung will be produced in the axial direction; on the contrary, the thick-target Bremsstrahlung will be produced mainly in the radial direction when $B_{last}<B_{ext}$.

Therefore from the point view of X-ray heating, both situations of $B_{last}>>B_{ext}$ or $B_{last}<<B_{ext}$ should be avoided in the operation of ECRISs.

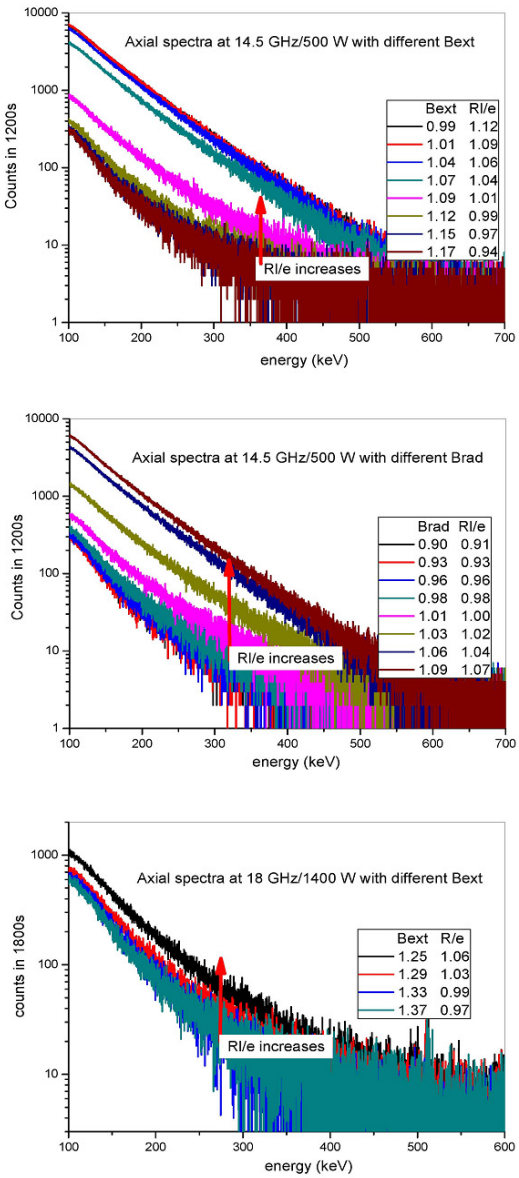

Figure 2: Axial Bremsstrahlung spectra with different magnetic configuration (Rl/e is ratio of B_{last} to B_{ext})

CONCLUSIONS

As one of key issues in the development of ECRIS, the heat load to cryostat induced by Bremsstrahlung radiation is addressed in this paper. The possible solutions to this problem can be summarized as follows,

Firstly, the heavy-metal shielding is the simplest method to reduce the influence of Bremsstrhlung radiation on the cryostat. However the shielding is just effective against radiation with energy below 500 keV. So this method turns out to be incapable in high frequency and high power ECRIS.

Secondly, by choose appropriate ratio of B_{last} to B_{ext} the thick-target Bremsstrahlung radiation can be avoided effectively. And this can decrease both the intensity and the energy of produced Bremsstrahlung radiation to a large extent.

In addition, it was found in our experiments the Bremsstrahlung radiation in an aluminum chamber was lower than that in a stainless steel one at the same source condition. This may be due to the effect of an aluminum chamber to maintain the ambipolarity in the plasma [6], [7], but further experiments and analysis are necessary to confirm this.

REFERENCES

[1] R. Geller, Electron Cyclotron Resonance Ion Sources and ECR plasma (IOP, Bristol, 1996)
[2] C. Lyneis, D. Leitner, D. Todd, and S. Virostek, Rev. Sci. Instrum. 77, 03A342 (2006)
[3] H. W. Zhao, L. T. Sun, W. Lu, and X. Z. Zhang, Rev. Sci. Instrum. 81, 02A202 (2010)
[4] H. Y. Zhao, H. W. Zhao, X. W. Ma, and H. Wang, Rev. Sci. Instrum. 79, 02B504 (2008)
[5] H. Y. Zhao, H. W. Zhao, L. T. Sun, and H. Wang, Plasma Sources Sci. Technol. 18, 025021 (2009)
[6] K. E. Stiebing, L. Schachter, and S. Dobrescu, Rev. Sci. Instrum. 81, 02A326 (2010)
[7] L. Schachter, K. E. Stiebing, and S. Dobrescu, Rev. Sci. Instrum. 81, 02A330 (2010)

EFFECTS OF MICROWAVE FREQUENCY FINE TUNING ON THE PERFORMANCE OF JYFL 14 GHz ECRIS*

V. Toivanen†, V. Aho, P. Jones, J. Kauppinen, H. Koivisto, P. Peura, T. Ropponen‡,
O. Tarvainen, J. Ärje, JYFL, Jyväskylä, Finland
L. Celona, G. Ciavola, S. Gammino, INFN-LNS, Catania, Italy
D. Mascali, INFN-LNS and CSFNSM, Catania, Italy
A. Galatà, INFN-LNL, Legnaro, Italy

Abstract

Measurements have been carried out at the Department of Physics, University of Jyväskylä (JYFL) to study the effects of microwave frequency fine tuning on the performance of JYFL 14 GHz electron cyclotron resonance ion source. The frequency was varied within an 85 MHz band around the normal operation frequency of 14.085 GHz. The radial bremsstrahlung emission was measured for plasma diagnostics purposes and mass separated ion beam currents extracted from the ion source were recorded at the same time. Also, beam quality studies were conducted by measuring the ion beam emittance and shape with and without enhanced space charge compensation achieved by increased neutral gas pressure in the beam line. The obtained results are presented and possible origins of observed phenomena in measured quantities are discussed.

INTRODUCTION

The microwave frequency fine tuning has become an interesting subject concerning the enhancement of ECR ion source capabilities. In this method the ECRIS microwave frequency is altered in a narrow frequency band around the normal operation point to achieve improved source performance. Studies done by L. Celona et al. have given promising results showing strong frequency dependent variations in ion beam currents and beam shape [1]. Encouraged by these results, similar experiments were conducted with JYFL 14 GHz ECRIS including studies of mass separated ion beam currents and emittance. The results were promising but the origin of many phenomena were still left unanswered [2]. It was clear that additional measurements were needed. This paper presents the results of the latest frequency tuning measurements conducted at JYFL.

ELECTROMAGNETIC MODE STRUCTURE

When microwaves are fed into an ECRIS plasma chamber in vacuum, certain kinds of electromagnetic field structures can be excited inside. With frequencies around 14 GHz and typical plasma chamber dimensions these electromagnetic modes are closely packed and have separation of the order of some MHz [3]. Thus only a slight change in the feeding microwave frequency can induce a notable difference in the electric field structure on the ECR surface.

It is not clear how the situation changes when the chamber is filled with anisotropic inhomogeneous plasma. If the mode structure behavior remains, it should affect the electron heating efficiency, charge state distribution, ion dynamics and confinement time in the plasma, having an obvious influence on the characteristics of the ion beam [4].

EXPERIMENTAL PROCEDURE AND RESULTS

All measurements were conducted with JYFL 14 GHz ECR ion source [5]. The local 14.085 GHz oscillator was replaced with Rohde & Schwartz signal generator set to sweep a frequency range of 14.050 - 14.135 GHz in 100 seconds. The klystron was set to maintain constant power output during the sweeps. A signal given by the signal generator at the beginning of each sweep was used for triggering and time stamping of all time resolved data acquisition. Bremsstrahlung was measured radially from the plasma chamber with a germanium detector. The ECRIS and beam parameters were collectively measured with a computerized data acquisition system. The quality studies of m/q separated beams were conducted by measuring the beam emittance with an Allison type emittance scanner and the beam shape with a KBr scintillation screen at discrete frequencies. In these measurements the enhancement of space charge compensation (ESCC) was achieved by feeding argon into the beam line section between the ECRIS and the analyzing magnet resulting to beam line pressure of $4 \cdot 10^{-6}$ mbar. More details of similar gas feeding method can be found from reference [6]. All measurements were performed using argon beams with charge states between 5+ and 16+, except the transmission studies, where oxygen and krypton beams were also used. The ion source tuning was performed with 14.085 GHz frequency.

Beam current, bremsstrahlung and reflected power studies

The ion beam currents exhibited a clear oscillating behavior with varying microwave frequency. The fluctuations

* Work supported by the Academy of Finland and Nyyssönen foundation. LNS team acknowledges the support of the INFN Strategic Project NTA-HELIOS.
† E-mail: ville.toivanen@jyu.fi
‡ Currently at NSCL/MSU, East Lansing, Michigan, USA.

increased with increasing charge state of the ion beam. With low charge states the current remained practically constant, but with the highest up to 50% variations were seen during the frequency sweep compared to the normal operation frequency. Similar oscillations were seen also in the bremsstrahlung emission and the behavior was matched with the oscillations seen in the reflected microwave power (see Fig. 1). This suggests that the current variations are caused mainly by fluctuations in the transmitted power.

As the behavior of reflected power has had an important role in the earlier discussions concerning the existence of mode structure inside the plasma chamber [2], and is clearly reflected in the behavior of beam current and bremsstrahlung emission, a special effort was given to further study its origin. When the sweep time and the frequency range were varied, the location of the maxima and the minima of the oscillations remained unchanged, ruling out the possibility of outside interference with fixed frequency. Varying the ion source parameters, such as neutral gas pressure, magnetic field and microwave power, had no distinctive effect to the location of the minima and maxima either. When the length of the plain wave guide between klystron and ion source (before high voltage and vacuum breaks) was varied, the number of maxima in a fixed frequency range changed. The number of maxima increased with increasing wave guide length and vice versa. It was also observed that with high powers the location of maxima drifted slightly towards lower frequencies with time. This was caused by increasing wave guide length due to heat expansion. To further study the connection between the oscillations of reflected power and plasma conditions inside the ion source, the plasma chamber was disconnected from the wave guide and replaced with a low-VSWR (voltage standing wave ratio) load element. The measurements were repeated with the load element at different locations along the wave guide with and without the high voltage break. It was observed that the high voltage break increases the measured reflected power significantly (by a factor of about 4) but does not change the oscillating behavior. The oscillations remained, as can be seen in Fig. 2 and the number of maxima depended clearly on the wave guide length. This indicates that the oscillatory fine structure of the reflected power is not connected to the mode structure inside the plasma chamber.

The oscillating behavior seems to be connected to a phase dependent phenomenon. When the phase of the electromagnetic wave is calculated at the end of the wave guide, it is observed that the consecutive reflected power maxima correspond to phase shift of $\pi/2$ ($\lambda/4$). This relation holds very well for all the measured cases.

In the measurements with the plasma chamber there is a clear increase in the reflected power with the highest frequencies, a phenomenon which is not seen with the load element. This effect most probably originates from the plasma. However, comparing the signals with the load element and the plasma chamber shows that possible narrow frequency range (a few MHz) effects coming from the

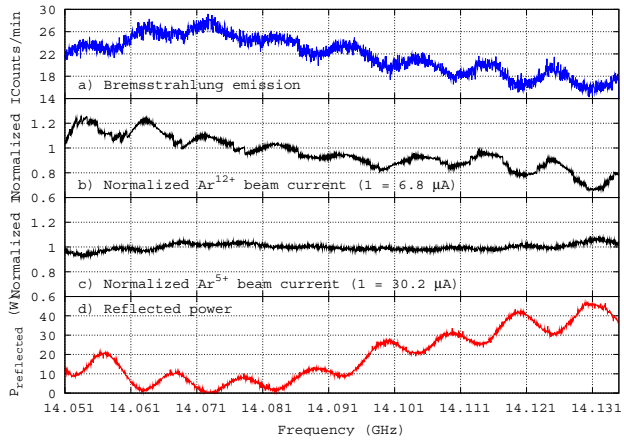

Figure 1: The bremsstrahlung count rate, normalized Ar^{12+} and Ar^{5+} beam currents and the reflected power with varied frequency. Constant forward power of 460 W. Note with the bremsstrahlung count rate that only relative efficiency calibration was used for the detector.

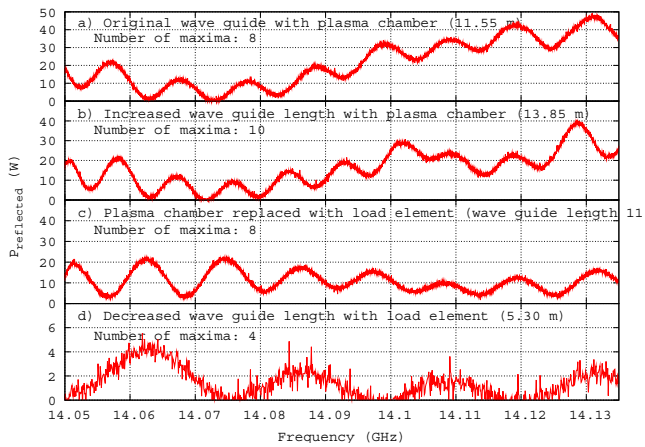

Figure 2: Reflected power with load element or plasma chamber and varied wave guide length. All cases with the same ECRIS settings and 500 W of forward power.

chamber must be very weak compared to the effects caused by the wave guide system. This makes it very difficult to say anything about the mode structure inside the plasma chamber using the reflected power signal in the case of JYFL 14 GHz ECRIS.

Beam quality and transmission studies

Changes of up to tens of percent were seen in the beam emittance with varying frequency compared to the normal operation point (see Fig. 3). These variations correlated well with changes in the structure of the beam profile and beam current instabilities. The behavior was very sensitive to the ion source settings and variation of any parameters could change it radically.

With ESCC the beam emittance was lowered signifi-

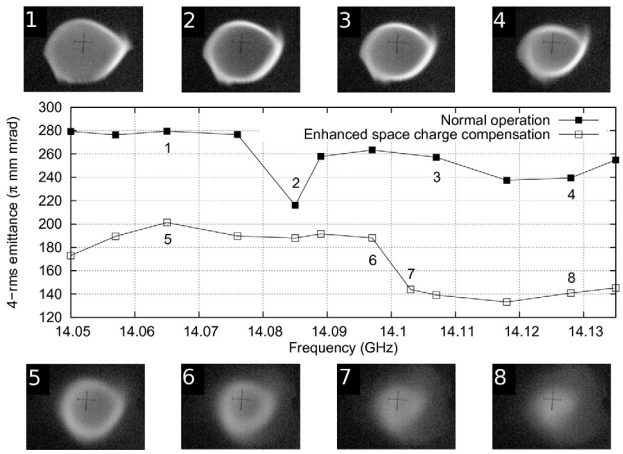

Figure 3: 4-rms emittance of Ar^{9+} with and without ESCC and beam profiles at selected frequencies.

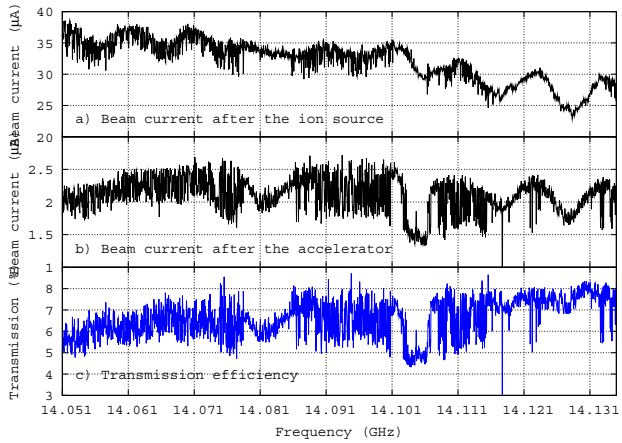

Figure 4: Ar^{12+} beam currents and transmission with varying frequency. Constant forward power of 667 W.

cantly. At low frequencies the general behavior of the emittance remained mostly unchanged. However, at around 14.1 GHz the emittance exhibited a steplike change accompanied by a change in the beam structure. The low and medium charge states, which normally have a hollow beam shape, became uniform and the emittance was lowered significantly. At the same time the profiles of high charge states expanded, became less dense and the beam emittance increased.

Transmission through the K-130 cyclotron was studied using $^{16}O^{6+}$, $^{40}Ar^{12+}$ and $^{82}Kr^{22+}$ beams. The beam currents were optimized through the injection line and the cyclotron. After this, the frequency was varied and the beam currents after the ion source and after the cyclotron were recorded. The transmission was also measured for a set of discrete frequencies, each optimized separately through the system. The frequencies were chosen based on changes in the beam emittance and profile. The results are presented in Table 1. The transmission of O^{6+} is considerably lower than what is normally achieved due to tuning problems with

Table 1: Transmission efficiency T and maximum ion beam current I_{max} after the cyclotron for frequency sweeps and separately tuned discrete frequencies.

	Frequency sweep		Discrete frequencies	
Beam	T (%)	I_{max} (μA)	T (%)	I_{max} (μA)
$^{16}O^{6+}$	1.0 - 1.4	2.9	1.2 - 1.4	2.7
$^{40}Ar^{12+}$	4.5 - 8.0	2.6	3.8 - 7.4	2.2
$^{82}Kr^{22+}$	2.5 - 9.0	1.3	6.1 - 7.5	1.1

the accelerator. The transmission for Ar^{12+} sweep is presented in Fig. 4.

DISCUSSION

The studies presented in this article show that microwave frequency fine tuning does produce clear variations to many of the measurable quantities connected to the performance of the JYFL 14 GHz ECRIS. However, the varying input power makes it difficult to separate which effects are caused by the frequency variations and not the power fluctuations. This is the case especially with the beam currents. The beam emittance and profile exhibited clear variations which were further strenghtened with the ESCC. These effects on the beam quality were clearly reflected as significant variations in the transmission efficiency.

Compared to the behavior reported in [1], the reflected power and consequently the reflection coefficient behavior is vastly different with JYFL 14 GHz ECRIS. The results presented in [1] were obtained from measurements with a Caprice type ECR ion source. Compared to JYFL 14 GHz ECRIS, which is of the A-ECR type, the microwave coupling scheme is radically different. The Caprice source has a multistage coupling from wave guide to coaxial microwave feeding into the plasma chamber, as JYFL 14 GHz ECRIS uses rectangular wave guide all the way into the plasma chamber. As presented in this paper, the wave guide system at JYFL produces strong variations into the reflected power, which obscures any other possible narrow frequency range effects that could be seen in the signal. However, there seems to be some behavior present at broader frequency band. Whether this has something to do with the possible mode structure inside the plasma chamber, it is difficult to say without further studies.

REFERENCES

[1] L. Celona et al., Rev. Sci. Instrum. 79, 023305 (2008).

[2] V. Toivanen et al., Rev. Sci. Instrum. 81, 02A319 (2010).

[3] F. Consoli et al., Rev. Sci. Instrum. 79, 02A308 (2008).

[4] L. Celona et al., Rev. Sci. Instrum. 81, 02A333 (2010).

[5] H. Koivisto et al., Nucl. Instrum. Meth. B 174 (2001) 379-384.

[6] V. Toivanen et al., Nucl. Instrum. Meth. B 268 (2010) 1508-1516.

MEASUREMENT OF THE DIAMAGNETIC CURRENT ON THE LBNL 6.4 GHz ECR ION SOURCE

J. Noland#, J. Benitez, M. Kireeff Covo, D. Leitner, C. Lyneis, LBNL, Berkeley, CA 94720, USA.
J. Verboncoeur, Department of Nuclear Engineering, UC Berkeley, Berkeley, CA 94720, USA.
O. Tarvainen, Department of Physics, University of Jyvaskyla, Jyvaskyla 40500, Finland.

Abstract

A method of measuring the diamagnetic current on the LBNL 6.4 GHz ECR ion source is described. The diamagnetic signal is proportional to the rate of plasma formation and decay. Furthermore, the integrated signal can be used to estimate the total plasma pressure, or energy density, and can thus be used to study the warm and hot electron populations in an ECR plasma.

INTRODUCTION

ECR ion source (ECRIS) plasmas are capable of creating large amounts of high energy x-rays[1]. These x-rays present hazards to personnel and can add a substantial heat load to the cryostat of superconducting ECRIS's. As the heating frequency is increased, the problem will only worsen. In order to understand the production of x-rays in ECRIS plasmas, it is important to understand the electron heating mechanism, as it is the high energy electrons that are responsible for the creation of penetrating x-rays.

One common, non-invasive, high temperature plasma diagnostics that can be used to study high energy electrons is measurement of the plasma diamagnetic current. This diagnostic has been successfully applied to ECRIS plasmas previously[2]. Plasma diamagnetism is related to the energy density of all charged particles in the plasma. In a typical ECRIS plasma, though, the diamagnetic currrent is dominated by warm and hot electrons[3].

This paper describes the methods used to record diamagnetic signals on the LBNL 6.4 GHz ECRIS[4]. First,the theory of plasma diamagnetism is briefly discussed. In the second section of the article we discuss the diamagnetic loop experimental setup. Finally, examples of typical diamagnetic current measurements made over the course of our study are shown.

PLASMA DIAMAGNETISM

Charged particles orbit around magnetic field lines in such a way that the magnetic field created by their motion opposes the externally applied magnetic field. If a plasma is uniform, i.e., no density or temperature gradients, then the currents created by neighboring charged particles will cancel, and no net current will exist. If, on the other hand, gradients are present in a plasma a net current can arise. This macroscopic current creates a magnetic field that acts to decrease any external magnetic field, and is thus called a “diamagnetic” current. A common method of measuring the diamagnetic current is to use a loop of wire that is wrapped around the plasma chamber.

#jdnoland@lbl.gov

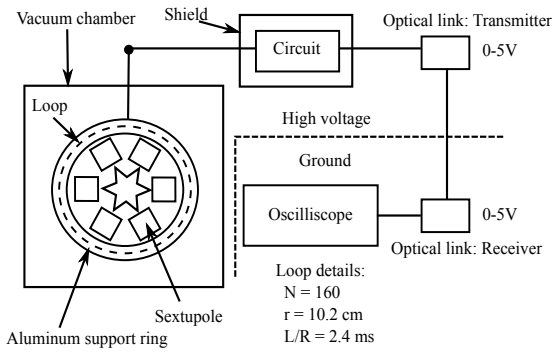

Figure 1: Experiment setup of diamagnetic loop used for plasma energy density measurements.

As the plasma in an ECR ion source forms or decays, the changing diamagnetic current creates a time varying magnetic field that opposes the steady, external magnetic field. By Faraday's law, an electric field is created. The electric field is responsible for creating a voltage across the leads of the diamagnetic loop, which is what is ultimately measured.

The electromotive force (emf) in the diamagnetic loop can be written:

$$\epsilon = -N\frac{d\phi}{dt}, \tag{1}$$

where N is the number of turns in the diamagnetic loop, and Φ is the total magnetic flux passing through the loop. Starting with Eq. 1, the following equation relating the integrated diamagnetic signal to the plasma pressure can be derived [5]:

$$\int^{t} \epsilon_p\, dt = \frac{\pi \mu_0 r_0^2}{B_0} nkT, \tag{2}$$

where r_0 is the plasma radius, and nkT is the plasma pressure due to all particles in the plasma. To arrive at this equation it is assumed that the velocity distribution is isotropic so that the pressure tensor reduces to a scalar, that the plasma can be represented by the ideal MHD equilibrium equation, and that the density profile is given by:

$$n = n_0 \exp\left(-(r/r_0)^2\right). \tag{3}$$

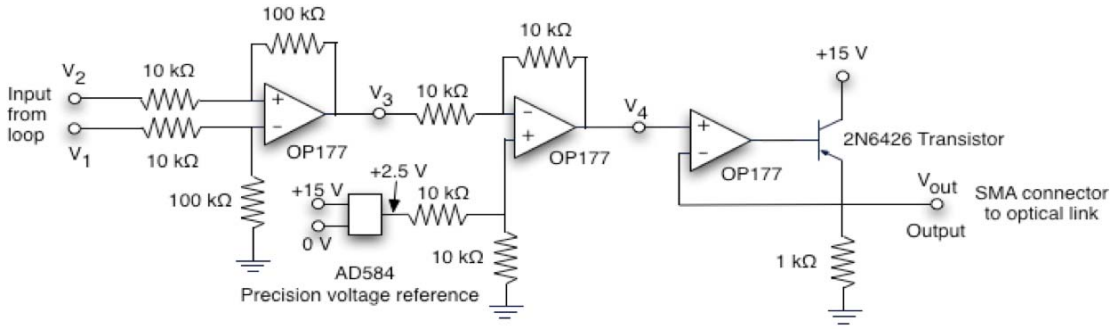

Figure 2: Diagram of circuit used to process diamagnetic loop signal.

EXPERIMENTAL SETUP

The experimental setup used to measure the diamagnetic signal is shown in Fig. 1. The diamagnetic loop is located within the vacuum chamber of the ECR. It is wound upon an aluminum support ring, which is, in turn, placed onto the sextupole structure. The leads of the diamagnetic loop are brought out of the vacuum chamber with a feed through. The loop and aluminum support ring are in electrical contact with source, and so float up to high voltage as the extraction voltage of the source is increased.

The raw signal from the loop is processed by a circuit, described in greater detail in the following section. Both the external portion of the feed through and the circuit are contained in an aluminum enclosure to prevent pick up of external noise.

To bring the diamagnetic loop signal outside of the high voltage cage that surrounds the ECR, a fiber optic cable is used. The processed signal from the circuit is first sent to an optical transmitter through an SMA cable, and then to the optical receiver through the fiber optic cable. Finally, the signal is sent to an oscilloscope where it is saved to a Compact Flash card. To reduce noise in the signal the averaging feature of the oscilloscope is used. For each data point, 128 microwave power on/off cycles are averaged. The data is processed on a PC using a simple Mathematica notebook. We can estimate the plasma energy density using Eq. 2.

Figure 3 shows the approximate location of the aluminum support structure upon which the diamagnetic loop is wound. The loop itself is made of magnet wire and is circular with an approximately square cross section (1.27 cm by 1.27 cm). It has a mean radius of approximately 10.2 cm and has 160 turns. The resistance of the loop is approximately 4 ohms, and its inductance is approximately 9.7 mH. The time constant of the loop (L/R) is thus approximately 2.4 ms. We expect, then, the diamagnetic loop will be able to follow changes in plasma energy density that occur on time scales greater than approximately 10 ms.

Loop circuit

Figure 2 shows a diagram of the circuit used to process the diamagnetic loop signal. The circuit consists of three major sections: a differential amplifier, a level shifter, and, finally, a driver section, required to power the analog optical link transmitter. The circuit does not have an analog integrator, as we have chosen to perform the integration on a PC.

The final output voltage of the circuit is given by:

$$V_{out} = -10(V_2 - V_1) + 2.5$$

The offset of 2.5 V is required because the optical link transmitter and receiver used both require a voltage between 0-5 V. The loop signal, though, is both positive and negative, depending on whether the plasma is forming or decaying. The final voltage signal is sent to the optical link transmitter through an SMA cable.

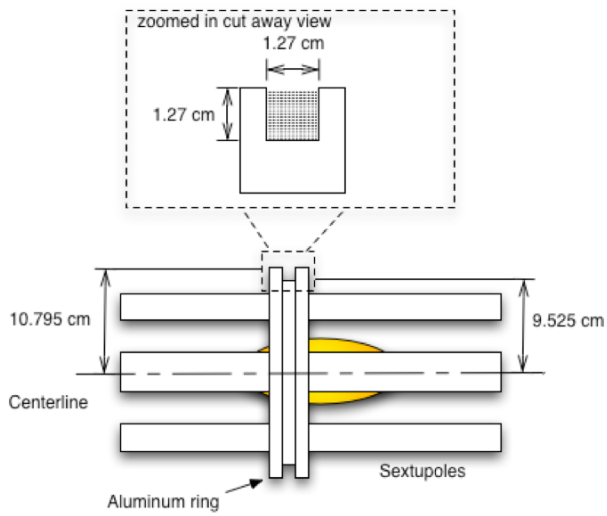

Figure 3: Approximate position of aluminum support ring. Drawing not to scale.

RF pulsing circuit

In order to measure a diamagnetic signal, which relies on changes in plasma density, an ECRIS must be operated in pulsed mode. Figure 4 shows a schematic of the pulsing method used in this study.

A signal generator is used to create the desired microwave pulse pattern. The signal is then sent to the Gunn Diode Modulator (GDM). The GDM is needed to provide the correct voltage and current values to drive the Pin Absorptive Modulator (PAM). When the output signal from the GDM is greater than zero, the PAM does not attenuate the oscillator signal. If the output signal from

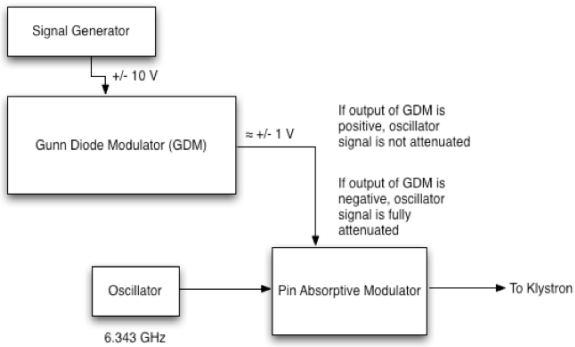

Figure 4: Diagram of klystron pulsing circuit.

the GDM is negative the PAM fully attenuates the oscillator signal, and the klystron power output is zero. Delays introduced with this method are on the order of microseconds. Plasma formation and decay time scales, though, are on the order milliseconds, and so the delays are ignored.

EXAMPLES OF EXPERIMENTAL DATA

Figure 5 shows an example of an unintegrated diamagnetic signal. The large, positive spike occurs when the microwave power is turned on. The smaller, negative spike occurs when the microwave power is turned off. Because the induced voltage is proportional to the rate of plasma formation, Fig. 5 indicates that the plasma forms at a faster rate than it decays.

The relative plasma energy density as a function of microwave power is shown in Fig. 6. The plasma energy density is calculated by integrating the initial, positive

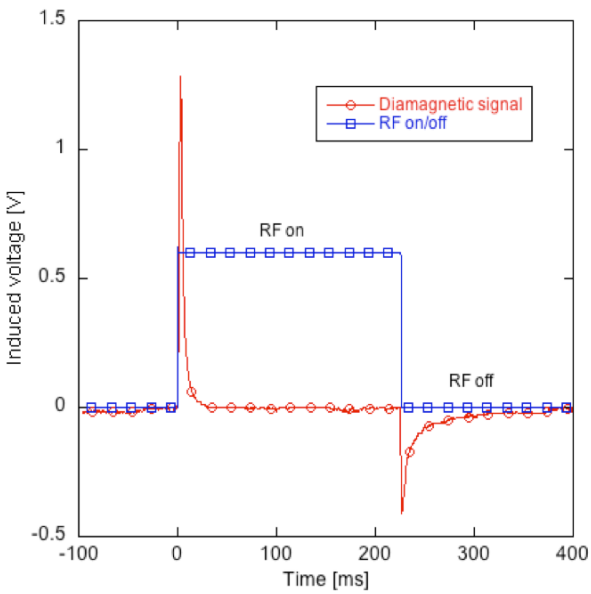

Figure 5: Diamagnetic loop signal. Argon plasma.

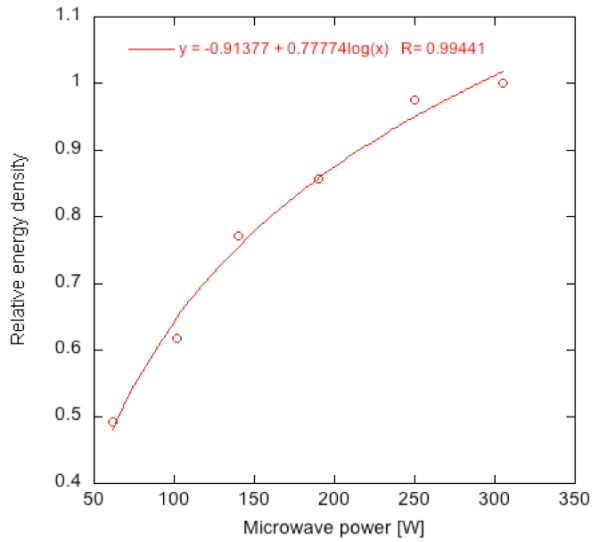

Figure 6: Relative plasma energy density versus microwave power. Argon plasma

spike and using Eq. 2. The relative plasma energy density is seen to increase logarithmically with microwave power.

SUMMARY

In this paper we have described a method of measuring diamagnetic signals on the LBNL 6.4 GHz ECR. This diagnostic is useful for understanding the behaviour of the warm and hot electrons confined in the plasma as source operating parameters are varied.

It is seen that the plasma energy density, as estimated using the integrated diamagnetic signal, increases logarithmically with the microwave power, and that the plasma forms at a faster rate than it decays at.

We will make a similar set of measurements on the LBNL 14 GHz AECR-U in a future experiment. More detailed explanations of the results and experimental setup discussed in this paper will be available in future articles [6,7].

REFERENCES

[1] D. Leitner, J. Benitez, C. Lyneis, D. Todd, T. Ropponen, J. Ropponen, H. Koivisto, and S. Gammino, Rev. of Sci. Inst. 79 033302 (2008)

[2] C. Barue, M. Lamoureux, P. Briand, A. Girard, and G. Melin, Journal of Applied Physics 76 2662 (1994)

[3] G. Melin, F. Bourg, P. Briand, J. Debernardi, M. Delaunay, R. Geller, B. Jacquot, P. Ludwig, T.K. Nguyen, L. Pin, M. Pontonnier, J.C. Rocco, and F. Zadworny, Rev. of Sci. Inst. 61 236 (1990)

[4] C. Lyneis, "Operating experience with lbl ecr source," International Conference on ECR Ion Source and their Applications, p. 42-56 (1987)

[5] F. Chen, Introduction to Plasma Physics and Controlled Fusion, 2nd ed. Plenum Press (1984)

[6] To be submitted to Plasma Sources Science and Technology.

[7] To be submitted to Journal of Instrumentation.

MICROWAVE FREQUENCY DEPENDENCE OF THE PROPERTIES OF THE ION BEAM EXTRACTED FROM A CAPRICE TYPE ECRIS

F. Maimone[1,2], K. Tinschert[1], P. Spädtke[1], J.Mäder[1], J. Roßbach[1], R. Lang[1],
[1]GSI Helmholtzzentrum für Schwerionenforschung GmbH, Planckstr. 1, 64291 Darmstadt,Germany
[2]Universita' degli Studi di Catania, D.M.F.C.I, Viale A. Doria 6, 95125 Catania, Italy
L. Celona[3], [3]INFN-LNS, Via S. Sofia 62, 95123 Catania, Italy

Abstract

In order to improve the quality of ion beams extracted from ECR ion sources it is mandatory to better understand the relations between the plasma conditions and the beam properties. The present investigations concentrate on the analysis of different beam properties under the influence of various applications of frequency tuning and of multiple frequency heating. The changes in the microwave frequency feeding the plasma affect the electromagnetic field distribution and the dimension and position of the ECR surface inside the plasma chamber. This in turn has an influence on the generation of the extracted ion beam in terms of intensity, shape and emittance. In order to analyze the corresponding effects, measurements have been performed with the CAPRICE-Type ECRIS installed at the ECR Injector Setup (EIS) of GSI. The experimental setup uses a microwave sweep generator which feed a TWTA (Traveling Wave Tube Amplifier) covering a wide frequency range from 12.5 to 16.5 GHz. This arrangement provides a precise determination of the frequencies and of the reflection coefficient along with the beam properties. A sequence of viewing targets positioned inside the beam line monitors the beam shape evolution.

INTRODUCTION

The increasing request of higher energies for higher charge states pushes towards the development of more performing ECR ion sources or to the research of methods to enhance the performances of the existing ones. The tuning of the microwave frequency feeding the plasma can be a promising technique even if a better understanding of this effect is mandatory. In 1998 the ORNL CAPRICE-Type ECRIS was used to demonstrate how the frequency domain technique was useful to enhance the ECRIS performances [1]. In 2008 several measurements were carried out with the CAPRICE ion source at GSI in order to investigate the frequency tuning effect on the extracted Helium beam intensity and shape [2]. In 2009 an experiment was carried out at JYFL in order to measure the effect of the frequency tuning on the intensity, quality and emittance of a mass separated Argon beam [3]. In both of these last tests the frequency was swept over a narrow range of ±40 MHz around the Klystron center frequency of 14.5 GHz and in the 14.04-14.13 GHz range, respectively. In the present experiment the frequency tuning effect has been analyzed in the 12.5-16.5 GHz frequency range. The availability of a TWTA driven by a signal generator gave the possibility to change the source operating frequency with steps of a few hundred kHz. This experiment allows to analyze the beam properties when the ECRIS operative frequency sweeps over a wide range of 4 GHz, and hence for increasing ECR surfaces. The influence on lower and higher charge states has been analyzed for different source conditions concerning the magnetic field configuration, the gas pressure and the power setting.

EXPERIMENTAL SET-UP DESCRIPTION

The CAPRICE-Type [4] ECR ion source used for this experiment is equipped with a 1.2 T maximum radial magnetic field. The plasma chamber dimension was 179 mm of length and 64 mm of diameter. The RF power was provided by a TWTA working in the 8÷18 GHz frequency range and able to provide an output power higher than 650 W in the frequency range of 12÷18 GHz. The input of the amplifier was driven by a signal generator able to sweep from 1 to 20 GHz. According to the maximum manageable power reflected to the amplifier, it has been restricted to work at a power of 100 W and in the frequency range of 12.5÷16.5 GHz. The use of a waveguide microwave isolator covering this frequency range and handling up to 650 W could allow to work with higher powers. The frequency steps were set to 200 kHz with a dwell time of 20 ms for each step. Then the duration of one measurement was around 400 seconds. Two directional couplers of high directivity were inserted in the waveguide line in order to measure the forward power and the reflected power with two microwave power probes. The experiment has been carried out with Argon and Helium as a support gas at gas pressures of 3.9÷5 $*10^{-6}$ mbar. The ion currents of the charge states Ar^{7+}, Ar^{8+} and Ar^{9+} have been measured with a faraday cup; the drain current of the high voltage power supply of the extraction has been recorded as well. The extraction voltage was set to 15 kV; a -2 kV voltage was applied to the screening electrode. Viewing targets could be remotely inserted at three positions along the beam line in order to monitor the beam shape evolution right after the extraction, the focused beam and analyzed beam [5]. KBr was used as target coating material for this experiment.

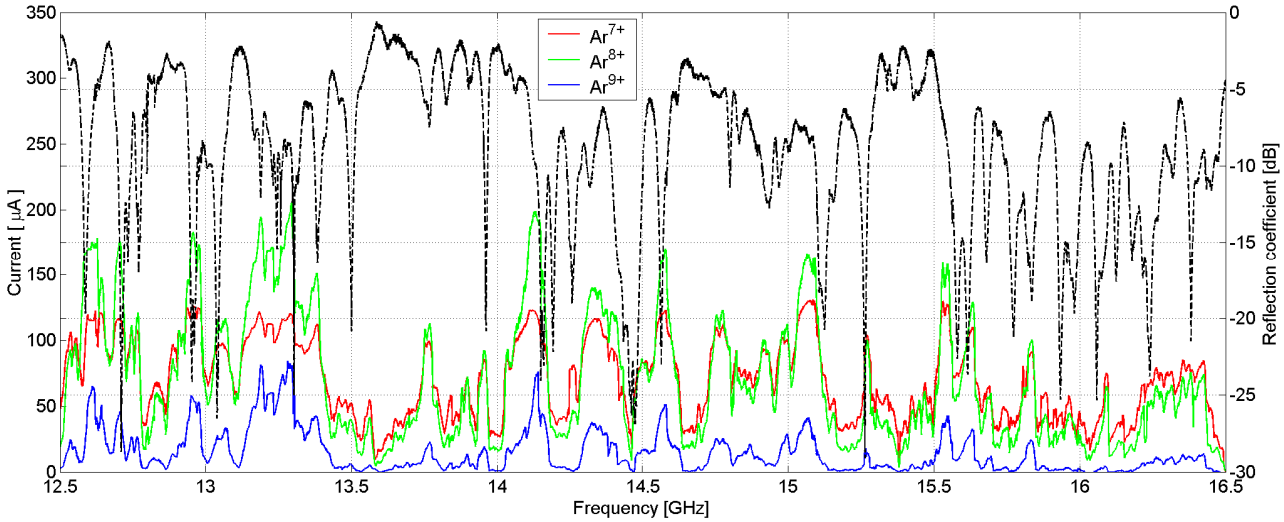

Figure 1: Reflection coefficient and current evolution vs. microwave frequency (the coloured solid lines refer to the left scale while the dashed black line is the reflection coefficient referring to the right scale).

RESULTS AND DISCUSSION

Different measurements have been carried out by sweeping the frequency and setting different ion source parameters, i.e. injection and extraction magnetic field values, gas pressure and microwave power.

The source parameters were set to operate with a charge state distribution with a maximum on the Ar^{8+} (by feeding the plasma with 100 W microwave power at 14.5 GHz). An Ar^{8+} current of 85 μA and a drain current of 2.36 mA were obtained. From these source conditions the frequency sweep was started by ramping the signal generator from 12.5 GHz up to 16.5 GHz, while the reflection coefficient, the Ar^{7+}, Ar^{8+}, Ar^{9+} currents and the drain current were recorded simultaneously.

The evolution of the reflection coefficient with the frequency is shown in figure 1. As expected by the previous experiments the matching impedance between the cavity filled by the plasma and the electromagnetic wave is strongly dependent on the frequency [1-3]. It is remarkable that the plasma properties are also changing considerably with varying frequency. The strong correlation between the peaks of the reflection coefficient and the current amplitude are clearly visible around the frequencies where the reflection coefficient is higher than -9.54 dB (matching condition). The relationship between the resonance frequencies and the heating efficiency has been theoretically analyzed and particle in cell codes has been used to correlate the electromagnetic field patterns and the electron cyclotron resonance surface. [6] However it is not possible with our analysis to determine the electromagnetic field patterns (modes) related to these peaks. The comparison of the current evolution in the frequency range indicated above is presented in figure 1. It is clear how the current amplitude is affected by the choice of the operative frequency. Looking at the Ar^{8+} current it ranges from a few μA up to 200 μA. The experimental results were clearly reproducible in several runs thus confirming the reliability of the measurements. The evolution of the Ar^{7+} and Ar^{8+} currents is similar, but the amplitude is different. In fact at the frequencies where both currents present a peak, the Ar^{8+} is quite higher than the Ar^{7+}(for instance at 14.119 GHz the difference between the two currents is 80 μA). The opposite behaviour is visible for the minima of the current amplitudes where the Ar^{7+} is higher than the Ar^{8+}. In the range 15.64-16.5 GHz the currents of the higher charge states, i.e. Ar^{9+}, tend to lower values even if the reflected power is less than 10%. This seems to be due to the confining magnetic field restricting the source operation to lower frequencies. It has been also observed that the drain current evolution is following the trend of the three charge states presented in figure 1.

In order to have a complete comprehension of the sweep effects on the ionization process, the charge state distribution has been analyzed for different frequencies. It has been decided to restrict the analysis to the frequency range of 14-15 GHz. Several frequencies have been considered where peaks and minimum amplitudes occur. In figure 2 the charge state distribution is presented for four different frequencies. The 14.5 GHz value is the normal operation frequency of the CAPRICE ion source; 14.46 GHz and 14.119 GHz are the frequencies where respectively the minimum and the maximum Ar^{8+} current were measured in the 14-15 GHz frequency range. The charge state distribution related to the 14.0 GHz operation is also reported in order to show how important the electromagnetic field pattern and the choice of the frequency are. In fact the charge state distributions at 14.0 GHz and at 14.46 GHz are quite similar even if the amount of power feeding the plasma was more than doubled. In the first case the reflection coefficient (indicated in the legend of the figure 2) was -2.3 dB, more than one half of the power was reflected, and in the second case it was -25.8 dB , the impedance matching condition was fulfilled and almost no power was reflected. It is also interesting that for the frequencies where the higher charge states are favoured,

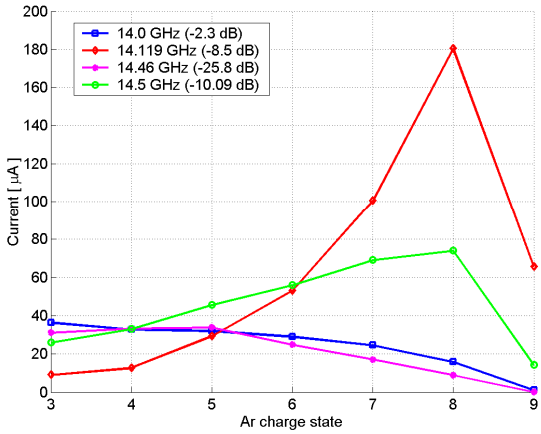

Figure 2: Ar charge states distribution for four significant operating frequencies.

The current of lower charge state is decreasing and vice versa. The analyzed charge state distributions confirm that the frequency tuning is more affecting the higher charge states (at 14.119 GHZ the current enhancement respect to the 14.5 operation frequency is 244% for the Ar^{8+} and 456% for the Ar^{9+}).

The enhancement of the current is not the only effect of the frequency sweeping, in fact also the quality, the shape and the emittance of the ion beam are varying. The use of beam viewing targets has proven to be a favourable technique to monitor the beam shape and a promising beam diagnostic tool. The images recorded after the extracted beam focusing solenoid (VT2 position) and in the diagnostic box after the mass/charge selection dipole (VT3 position) are shown in figure 3. Here the same frequencies are chosen as in figure 2. The Ar^{8+} beam is shown on the right column and the focused beam images also refer to the Ar^{8+} magnetic field setting. At 14.0 GHz and 14.46 GHz, which are the frequencies where the Ar^{8+} presents a minimum point, the focused beam shape seems to remain unchanged in the orientation of the arms (at 14.0 it is a little bit brighter, also according to the higher intensity measured at the faraday cup). At 14.119 GHz the focused beam is a little bit bigger and brighter than the one at 14.5 GHz and in both cases the orientation of the arms is turned by more then 40° clockwise with respect to the 14-14.6 GHz beam shapes. An emittance variation is clearly expected and in the next measurement session a pepper pot device will be used to analyze the emittance.

CONCLUSIONS

The experiment reported here has confirmed again how the frequency and the corresponding electromagnetic field feeding the plasma affects the ECRIS performances. The complete results of the measurements for the several source parameters settings together with the results of the multiple frequency heating experiment will be published soon.

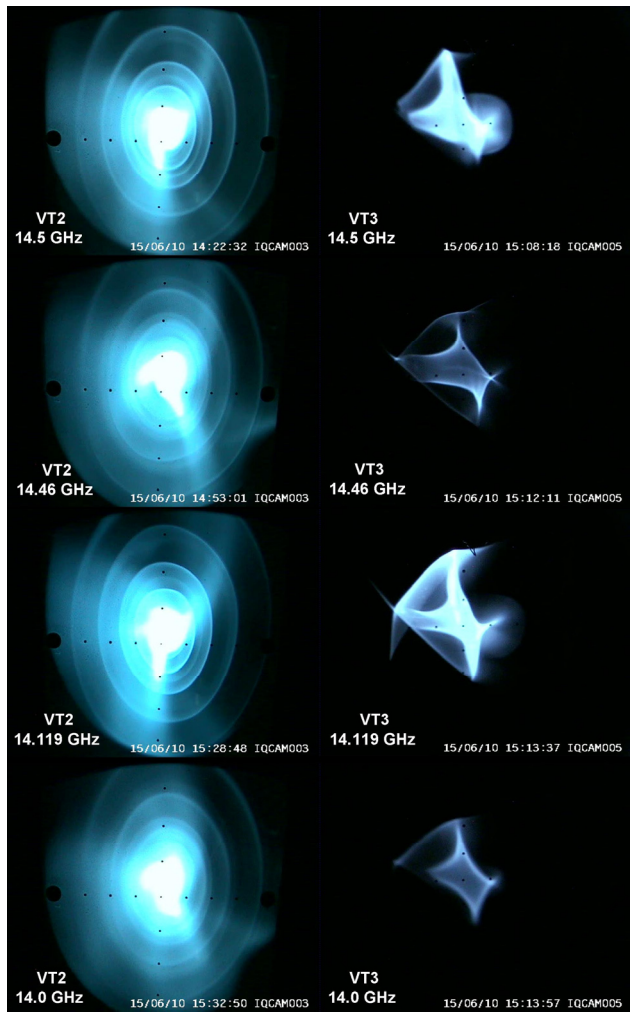

Figure 3: Ar^{8+} beam viewed at the targets located after the focusing solenoid (left column) and after the dipole (right column).

ACKNOWLEDGEMENTS

W. Kaufmann and P. Moritz are warmly acknowledged for the precious support provided for the arrangement of the experimental set-up

REFERENCES

[1] G.D. Alton et al., Rev. Sci. Instrum. 69, n° 6,1998.
[2] L. Celona et al., Rev. Sci. Instrum. 79, 023305,2008.
[3] V. Toivanen et al.,Rev. Sci. Instrum. 81,02A319,2010.
[4] D. Hitz et al., Proc. 11th Int. Workshop on ECRIS, Groningen 1993, KVI-Report 996,1993.
[5] J. Mäder et al., Rev. Sci. Instrum. 81,02B720,2010.
[6] D. Mascali et al., Rev. Sci. Instrum. 81,02A334,2010.

INFLUENCE OF INITIAL PLASMA DENSITY AND MEAN ELECTRON ENERGY ON THE PREGLOW EFFECT

I. Izotov#, A. Sidorov, V. Skalyga, V. Zorin, IAP/RAS, Nizhny Novgorod, Russia
H. Koivisto, O. Tarvainen, V. A. Toivanen, University of Jyvaskyla, Finland

Abstract

The investigation of the Preglow effect is driven with the aim of creating a short-pulsed multicharged ion source. Recent experimental investigations have revealed strong influence of seed electrons, i.e. initial plasma density, on the amplitude and duration of the Preglow peak [1]. Present work, consisting of experiments and simulations, is dedicated to further investigation of the Preglow dependence on initial plasma density and electrons energy. Experimental investigation was performed at University of Jyvaskyla (JYFL) with the A-ECR type ECRIS operated with 14 GHz frequency. Helium was used for the study. An initial ionization degree of the gas was varied by changing the pulse duration and duty factor. Time-resolved ion currents of He+ and He2+ were recorded. Calculations were made by using 0-dimensional model described in references [2], [3] and based on the balance equations for the particles confined in the magnetic trap. Results of simulation are compared with experimental Preglow peaks and discussed. Good agreement between experimental data and simulation encourages us to conduct a further study, aimed at optimizing the Preglow by tuning source parameters and initial plasma conditions.

[1] O. Tarvainen et all. R.S.I., 81, 02A303, 2010
[2] T. Thuillier et all. R.S.I., 79, 02A314, 2008
[3] I. Izotov et all. IEEE Trans. Plasma Sci. 36, 1494, 2008.

Paper not received

izotov@appl.sci-nnov.ru

OPTIMIZED EXTRACTION CONDITIONS FROM HIGH POWER-ECRIS BY DEDICATED DIELECTRIC STRUCTURES

L. Schachter[1], K. E. Stiebing[2], S. Dobrescu[1]

[1] National Institute for Physics and Nuclear Engineering (IFIN-HH), P.O. Box MG-6, Bucharest, Romania; [2] Institut für Kernphysik der Johann Wolfgang Goethe- Universität(IKF), Max- von-Laue- Straße 1, D-60438 Frankfurt/Main, Germany

Abstract

The MD-method of enhancing the ion output from ECR ion sources is well established and basically works via two mechanisms, the regenerative injection of cold electrons from an emissive dielectric layer on the plasma chamber walls and via the cutting of compensating wall currents, which results in an improved ion extraction from the plasma. As this extraction from the plasma becomes a more and more challenging issue for modern ECRIS installations with high microwave power input, a series of experiments was carried out at the 14 GHz ECRIS of the Institut für Kernphysik in Frankfurt/Main, Germany (IKF). In contrast to our earlier work, in these experiments emphasis was put on the second of the above mechanisms namely to influence the sheath potential at the extraction by structures with special dielectric properties. Two different types of dielectric structures, Tantalum-oxide and Aluminium oxide (the latter also being used for the MD-method) with contrastingly different electrical properties were mounted on the extraction electrode of the IKF-ECRIS, facing the plasma. For both structures an increase of the extracted ion beam currents for middle and high charge states by 60-80 % was observed. The method is able to be applied also to other ECR ion sources for increasing the extracted ion beam performances.

INTRODUCTION

The MD-method, using special insolating structures with high secondary electron emission coefficients, to enhance the ion output from ECR ion sources is well established and has been extremely successful. In second generation ECRIS sources (e.g. typically sources with 14GHz microwave systems at maximum powers of 2kW), enhancement factors for the highest charge states (e.g. Ar 16+) of up to 100 have been measured and were clearly attributed to the enrichment of the plasma by cold electrons form the secondary emission effect [1,2]. In a dedicated experiment an increase of the plasma density and electron temperature was observed for the Frankfurt 14GHz source equipped with a MD-liner as compared to the standard stainless steel source.

In a series of experiments it also could be shown that the secondary emission is only part of the mechanism that leads to the particularly good results for the highest charge states. A second effect clearly is the isolating properties of such a layer, which blocks all fast recombination currents and hence restores the ambipolarity at those parts of the surface of the plasma chamber where the structure is installed. This enhanced ambipolarity leads to considerably longer ion dwell times and hence serves to augment especially the high charge states by a better ion breeding.

It also has been demonstrated that, also with a MD-structure best results are obtained when the extraction from the source is optimized by carefully shaping the extraction conditions by a biased disk and that this can still be improved by using a MD-structure at the extraction electrode. This additional improvement was ascribed rather to the isolating properties of the MD-structure at the extraction electrode than to its secondary electron emission [3].

This allows for "tailoring" a MD structure to the needs of a respective installation. While a deficit in electron density may best be compensated by the secondary electron effect, for new generation sources with much better plasma densities and temperatures the improvement of the ion extraction by a MD extraction electrode my more appropriate.

In order to support this argumentation we have carried out a new series of experiments, where we have investigated the role of the dielectric character of the MD-structure by inserting two types of structure into the Frankfurt 14 GHz ECRIS, the very successful Al-MD structure with high secondary electron emission coefficient but only moderate dielectric constant and a Ta-MD structure which has a poor secondary electron emission but a distinctly higher dielectric constant as compared to the Al-MD.

EXPERIMENTAL SET-UP

The experiments reported in this article have been carried out at the 14GHz ECRIS installation at the Institute für Kernphysik, Frankfurt, Germany (IKF-ECRIS). Dielectric structures of Tantalum oxide and Aluminium oxide (denoted here as Ta/Al-MD electrode) were successively installed on the plasma electrode facing the plasma. The structures were made of 1 mm of pure Tantalum or Aluminium plates. The MD liner in this experiment was similar to those used in our previous experiments. It covers the radial walls of the plasma chamber on a length of 150 mm centred at the hexapole magnet.

All measurements were performed at the same operating parameters of the source: 15 kV extraction voltage, 1000 W operating RF power and with pure argon as working gas. The beam was optimized for the 12+ and 14+ charge states respectively. Typical values of the vacuum during operation were (3-5) x 10^{-7} mbar in the plasma chamber, measured at the injection flange and (7-8) x 10^{-8} mbar in the extraction area. A biased stainless steel electrode (biased disk) was located at the injection side of the plasma chamber. It's axial position and the voltage was adjusted in order to maximize the intensity of the extracted ion currents measured in a Faraday cup behind the 90 ° analysing magnet.

RESULTS AND COMMENTS

In order to better unveil the role of dielectric properties, it is meaningful to reduce the influence from the secondary emission effect as far as possible. This is best done by using a "standard" Al-MD liner installed at the radial plasma chamber walls for all experiments discussed here, because it strongly enhances the plasma density and any further contribution to secondary electron enhancement from the MD-electrode can be neglected. At the same time this resembles the best condition of the plasma that can be achieved in the IKF ECRIS because the presence of an Al-MD liner leads to an increase of the plasma electron density by a factor of 2.5 and the electron temperature by a factor of 1.7 [4]. The influence of this is demonstrated by comparing the charge-state-distributions (CSD) for the reference source and for the source equipped with a Al-MD-liner in Fig. 1. It is evident that the intensity of a typical intermediate charge state of argon (e.g. Ar^{12+}) is increased by a factor of 4, whereas Ar^{14+} (representing high charge states) is increased by a factor of 8.

Fig.1 also shows the influence of a Ta-MD-electrode, additionally installed on the plasma electrode. While the MD-liner considerably changes the shape of the CSD in the region of intermediate and high charge states, the additional Ta-MD-structure has only negligible influence on the shape of the CSD but clearly enhances the extracted ion currents in this whole range of charge states. This can be explained by the above described difference between both structures. While the Al-MD-liner enhances plasma density and temperature, leading to the observed considerable increase of high charge states in the CSD, the additional presence of the Ta-MD electrode improves the extraction of the ions from the plasma by suppressing the ion losses by wall currents at the extraction hole. It does not contribute, however, to a change of the plasma parameters. This is also shown by another experiment, where we installed a Ta-MD liner, which represents essentially an insulator, in the source (Fig. 2). The Ta-MD liner had exactly the same size and position as the Al-MD liner. Besides the fact that the Ta-MD liner had no

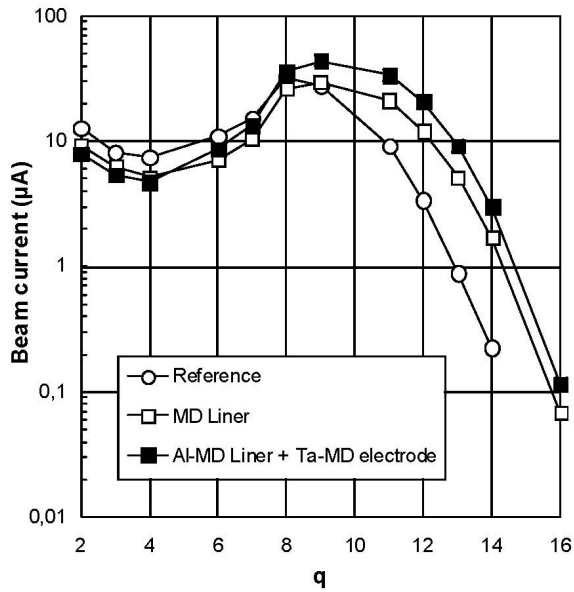

Figure 1: Charge state distributions (CSD) for Ar-ions for three different source configurations as indicated. The ion optics was optimized for the transport of Ar^{14+} ions the extraction voltage was 15kV, the RF power was 1kW.

markable emission of secondary electrons and hence did not influence the shape of the CSD very much, this scenario resulted obviously in a strongly reduced output from the source. Part of this reduction could then be restored by improving the extraction from the source again by adding the Ta-MD electrode.

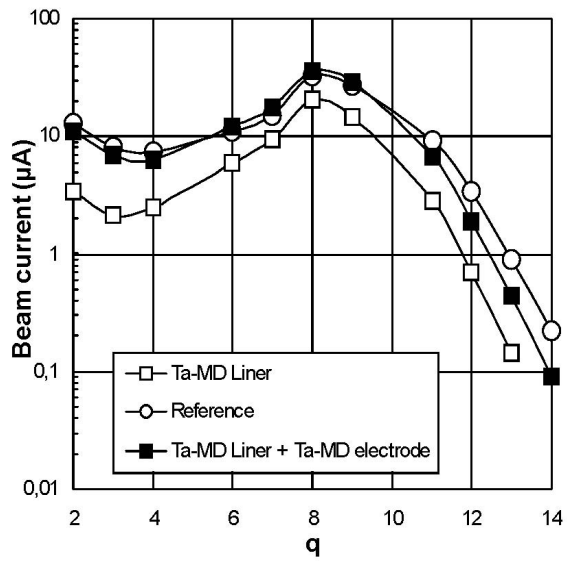

Figure 2: CSD for Ar-ions for different configurations as indicated. Ion optics, extraction voltage and RF power are identical to the ones given in Fig. 1.

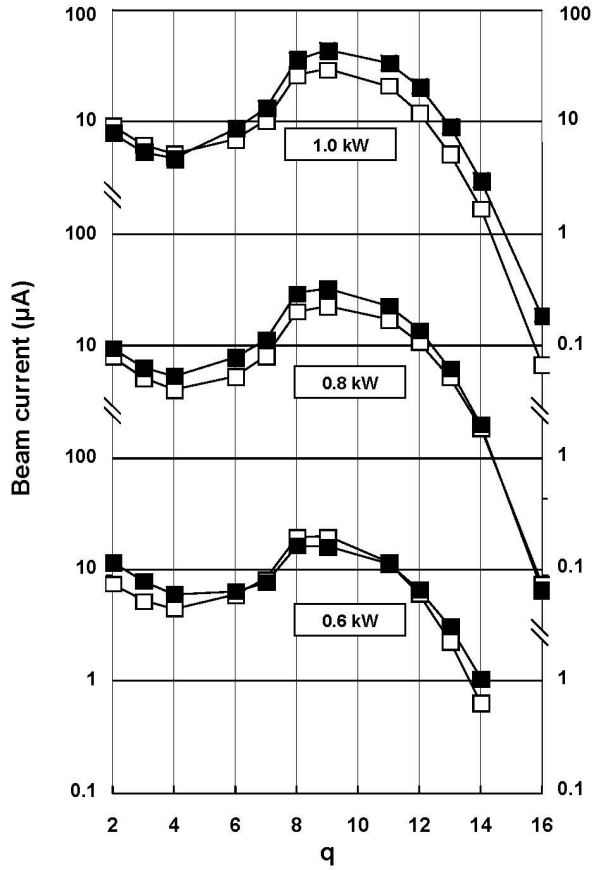

Figure 3: Comparison of CSD with (solid symbols) and without (open symbols) Ta-MD electrode for three different microwave powers as indicated in the figure. The ion optical transport was optimized for the transport of high charge states (Ar^{14+}) the extraction voltage was 15kV. The plasma parameters and extraction conditions were kept identical for the corresponding set of spectra.

All spectra, presented so far, have been measured at 1kW microwave power in order to demonstrate the usefulness of this method for high performance sources. It is well known that a careful shaping of the extraction conditions becomes more and more important the higher the source performance in terms of plasma density and temperature is. In Fig. 3 a series of measurements for different microwave powers is displayed. It is interesting to realize a "shift" of the effect towards higher charge states with increasing microwave power. While at 600 Watt some enhancement at the low-charge state-end of the CSD can be identified, at 1000 Watt clearly the range of intermediate and high charge states is enhanced, demonstrating that this method works the better, the higher the microwave power and hence the plasma parameters are.

The net contributions, given by the Ta dielectric structure are displayed in Fig. 4 as a function of the

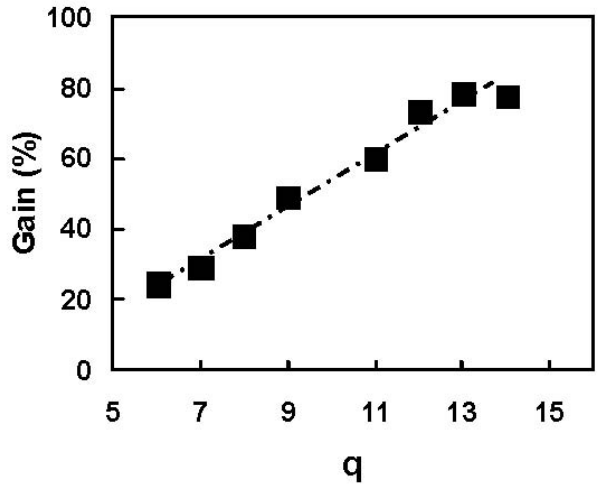

Figure 4: the net contributions from the Ta-structure: $G(q) = [I_{Ta\text{-}str}(q) - I_{std}(q)] / I_{std.}(q)$, $I_{std.}(q)$ is the ion current per charge state q for the source with stainless steel electrode and Al-MD-liner; $I_{Ta\text{-}str.}(q)$ is the configuration with a Ta-MD electrode in addition to the configuration of $I_{std.}(q)$.

charge state. A gain of 70-80%, relative to the standard source with Al-MD-liner and stainless steel electrode, can be observed for intermediate and high-charge-state Ar-ions.

The results demonstrate that dielectric structures on the extraction electrode introduce a new feature, which is not present in the standard ECRIS with stainless steel plasma electrode. An isolating structure at this position not only serves to cut the wall currents at the extraction, avoiding ion losses at this point, but also serves to improve the extraction conditions of ions by optimizing the sheath potentials at this point in such a way that a considerably higher amount of ions can be extracted through the extraction hole. The important factor is the positive charging of the plasma facing surface of the structure under electron bombardment. Here the degree of the charging, and hence the improvement factor, depends on the dielectric constant of the layer, which is distinctly higher for Ta-oxide than for Al-oxide, which we used for earlier studies.

REFERENCES

[1] L. Schachter, S. Dobrescu, Al. I. Badescu Singureanu; Rev. Sci. Instrum. 69, 706, (1998)
[2] L. Schachter, K. E. Stiebing, S. Dobrescu, et al. Rev. Sci. Instrum. 71, 918 (2000)
[3] L. Schachter, K.E. Stiebing, S. Dobrescu, T. Thuillier and T. Lamy; Rev.Sci. Instrum. 79, 02A329 (2008)
[4] L. Schachter, S. Dobrescu, K. E. Stiebing and J. D. Meyer; Rev. Sci. Instrum. 75, 1511, 2004

PERMANENT MAGNET ECRIS FOR THE KEK DIGITAL ACCELERATOR*

Leo Kwee Wah[1#], K.Okazaki[2], T.Arai[3], T.Adachi[1,3], K.Takayama[1,3,4], K. Koyama[3], and M.Wake[1,3]
[1]The Graduate University for Advanced Studies, KEK, Tsukuba, Ibaraki, Japan
[2]Nippon Advanced Technology Co. Ltd. (NAT), Tokaimura, Ibaraki, Japan
[3]High Energy Accelerator Research Organization (KEK), Tsukuba, Ibaraki, Japan
[4]Tokyo Institute of Technology, Nagatsuda, Kanagawa, Japan

Abstract

The KEK-Digital Accelerator (DA) is an induction synchrotron renovated from the KEK 500 MeV booster synchrotron [1]. Its concept was demonstrated in 2006 using the 12 GeV proton synchrotron [2,3], where a proton bunch was accelerated with pulse voltages generated by a transformer instead of RF cavity. In the KEK-DA, O, Ne, and Ar ions from the ECRIS embedded in the 200 kV high-voltage terminal (HVT) are directly injected into the ring though the low energy beam transport line. The permanent magnet ECRIS, in which a plasma is fired by x-band microwave pulses of 3 msec at 10 Hz, has been assembled at KEK. Its operational performance such as charge-state spectrum, emittance and current have been tested since the last year. Beam dynamics through the test bench is discussed as well as operational characteristics of the ECRIS.

INTRODUCTION

The KEK-DA is a recycling of the KEK 500 MeV PS-Booster, which was shut down in March, 2006, and is being renovated as the first DA.

The operational schematic of the ion source and LEBT to the KEK-DA is shown in Fig.1 [1,2]. An ion beam is directly injected into the KEK-DA from the ion source without a gigantic injector. In order to mitigate space-charge effects during injection, the ion beam is accelerated through a high voltage acceleration column of 185 kV.

A permanent magnet ECRIS is a unique solution when an ion source is mounted in a high voltage terminal, because it does not require a large amount of electric power and its size is small and its weight is less than 50 kg. Since 2008 a pulse-mode x-band ECRIS has been developed.

An Ar beam including Ar^{1+}~Ar^{8+} is extracted through the extraction electrode of 14-15 kV and focused in the downstream Einzel lens system and guided into the acceleration column with inner focusing electrodes and enters into the separation magnet to be selected a desired charge state (Z) ion beam. Through the quadrupole focusing channel, an A^{8+} beam pulse of 3-5 msec long is guided and chopped by an Einzel lens or electrostatic chopper placed at the downstream.

*Supported by Grant-In-Aid for Scientific Research (S) (KAKENHI No. 20224005)
#leokw@post.kek.jp

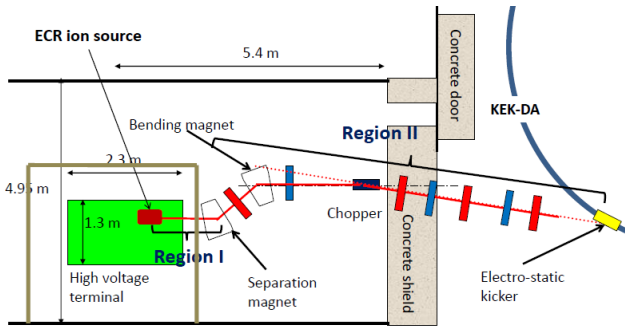

Figure 1: High voltage ion source and LEBT

ECRIS

The all-permanent magnet ECRIS has been built and tested over the last two years. Presently obtained results are discussed here. In addition remained issues are addressed.

Mechanical Design

The mechanical design of this ECRIS is shown in Fig. 2. It shows the complete assembly including two permanent ring magnets, hexapole magnet, return york, the microwave horn antenna and the extraction system with a screen to protect metal ions from spattering on the surface of the insulating ceramic pipe. The position of the antenna horn aperture can be optimized for matching. A plasma chamber with water cooling channels has been originally designed assuming a CW operation. As a result, the aperture size of 4cm in diameter is rather big compared with a similar x-band permanent ECRIS such as Nanogan [4].

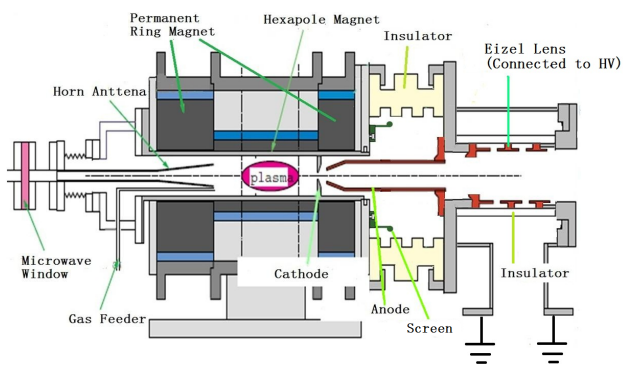

Figure 2: Schematic overview of the X-band ECR for The KEK-DA

Magnetic System

It is well-known that the high axial mirror ratio and a strong radial field inside the plasma chamber are important [5]. For our present ECRIS, the first peak flux density is (B_{peak1}) 7 kG, the second peak flux density (B_{peak2}) is 5.6 kG and the radial flux density (B_r) on the inner surface of the plasma chamber (r=20 mm) is 5 kG. The resonance flux density (B_{ECR}) is 3.3 kG for the frequency of 9.35 GHz. The empirical rule [5] tells us $B_r \sim 2\ B_{ECR}$ is desired. The actual field strength is a bit lower than this condition.

Microwave Heating

9.35 GHz microwaves are provided from a TWT with a maximum power of 700 W. In the present ECRIS, the microwave power in TE_{01} mode is uniformly irradiated in the plasma chamber from the rectangular horn antenna. Since the KEK-DA is operated at 10 Hz, the injection of ion beams at the same repetition rate is expected. An ion pulse is generated in a pulse mode, where the 5 msec long microwave pulse are fired at 10 Hz by controlling a seed pulse length of the TWT.

Extraction System

The geometrical shape of the anode hole biased at 14 - 15 kV and the grounded extraction electrode have been optimized by IGUN simulations. In the early stage, spattering of metal ions on the insulating ceramic pipe wall was serious to result in high voltage breakdown. The screen seen in Fig. 2 was quite effective to keep a clean surface from the direct spattering.

Test Bench

In order to investigate operational performances of our ECRIS including beam parameters and beam stability, a test bench have been constructed. It is divided into two portions: upper stream and downstream. The upper stream consists of a diagnostic device (Faraday Cup) just placed after the Einzel lens measured a total ion current. The beam is focused by a electrostatic quadrupole doublet (D)(F) and guided through the analyzer magnet to downstream. The downstream also consists of another doublet (F)(D) and to the diagnostic devices (Faraday cup and beam profile monitor) which are placed at the end point of the test bench as shown in Fig. 3.

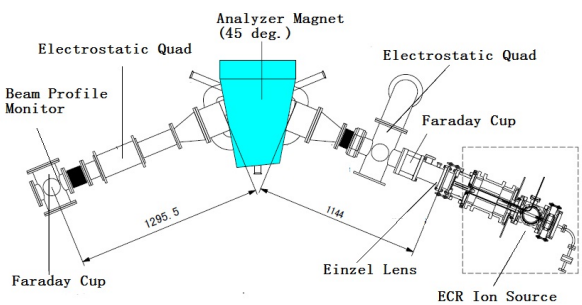

Figure 3: Schematic overview of test bench

Measurement Results

Charge-state spectrum of the extracted Oxygen, Neon and Argon beam were obtained by monitoring a beam current in the downstream Faraday cup. Figs. 4 and 6 show the pulse shapes for individual charge states at the gas flow rate of 0.05 SCCM for Argon and Neon.

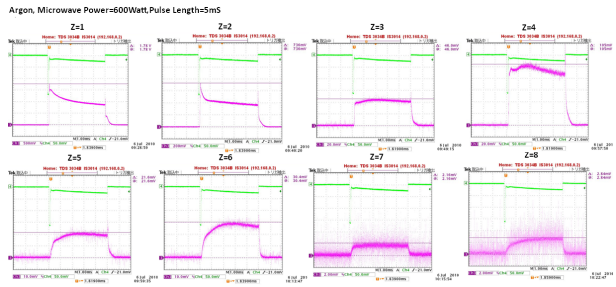

Figure 4: Waveform of ion current. Power/pulse length: 600W/5msec, upper green trace is the reflection signal of microwaves (Argon)

Absolute ion intensities have been obtained as a function of the microwave power. The results are shown in Fig. 5 and 7.

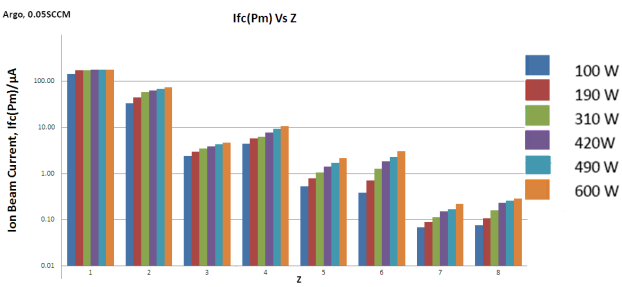

Figure 5: Ion current of an individual charge state for various microwave power (Argon)

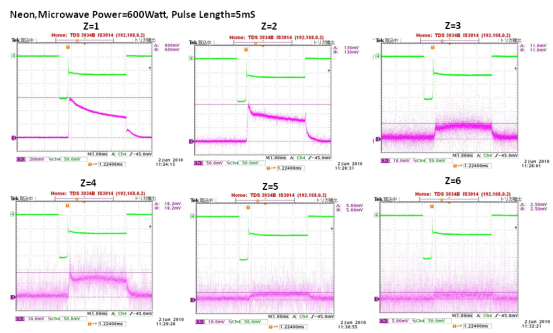

Figure 6: Waveform of ion current. Power/pulse length: 600W/5msec, upper green trace is the reflection signal of microwaves (Neon)

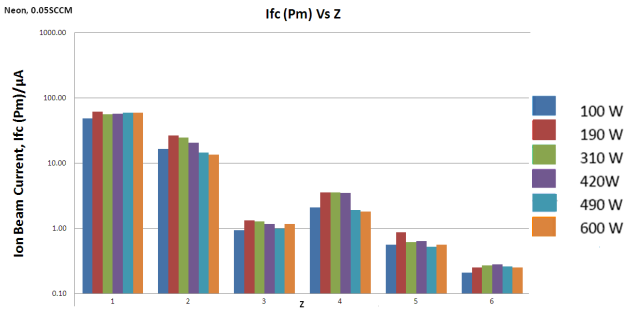

Figure 7: Ion current of an individual charge state for various microwave power (Neon)

Discussions

Achieved highest charge states for Oxygen, Neon and Argon were 6, 6 and 8, respectively. This fact can be explained by their ionization energy. According to reference [6], the ionization energy (ΔE) of $Ar^{7+\rightarrow 8+}$ is 143.5 eV, $Ar^{8+\rightarrow 9+}$ is 422.4 eV and $Ne^{5+\rightarrow 6+}$ is 157.9 eV, $Ne^{6+\rightarrow 7+}$ is 207.3 eV and $O^{5+\rightarrow 6+}$ is 138.1 eV, $O^{6+\rightarrow 7+}$ is 739.3eV . To obtain higher charge state ions, the electron energy must be sufficiently higher than the required ionization energy for a desired charge state. The achieved charge state of three species of ion suggested the density of high energy electron might be insufficient for ionization to the higher charge state. It is known that the electron confinement time in ECRIS increase as the mirror ratio of the magnetic field increases. This is crucial to obtain highly charged ions. Meanwhile, the so-called magnetic field scaling laws suggest that $B_{peak1}/B_{ECR} \sim 4$ and $B_r/B_{ECR} \sim 2$ are desired [7]. Their values in our present ECRIS are 2.1 and 1.5, respectively. The latter seems to be notably small.

Beam Dynamics

The IGUN simulator has been used to simulate the beam dynamics from the cathode to the anode and from the anode through the Einzel lens as shown in Fig. 8. The beam emittance and phase space plot are generated from the IGUN output.

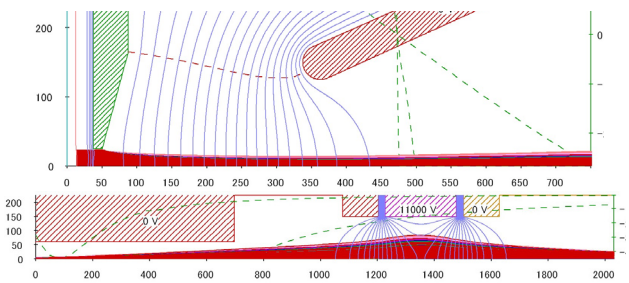

Figure 8: Beam envelope from the cathode to anode and from anode through Einzel Lens (IGUN simulation result)

IGUN simulations based on the Langmuir-Child law [8] give a space-charge limited ion current under an artificial assumption of a relative fractional ratio of charge states. In our calculations, the experimentally obtained fractional ratios were assumed. Consequently, the estimated space-charge limited current was in good agreement with the experimentally obtained total ion current.

The lattice function at the beginning of the test bench can be evaluated from the IGUN output. It is straightforward to calculate the beam envelope along the beam transport line using this initial value and lattice parameters which are uniquely determined by the voltage of electrostatic Q-lenses. It is interesting to compare the actual beam profile on the X-Y plane with the predicted result. For this purpose, a beam profile measurement was carried out using an emission plate of alumina placed at the end point of the beam line. Basic qualitative features of the observed profile were consistent with the predicted ones.

SUMMARY

Although our permanent ECRIS can deliver lower charge-state ions with a sufficient intensity, the intensity of higher charge-state ions is not enough. This could be attributed to the low B_r on the inner surface of the plasma chamber. In addition the region with $B=B_{ECR}$ is far from the central region. In order to improve both undesired features, installation of a thinner hexapole magnet into the inner aperture is underway.

ACKNOWLEDMENTS

The authors wish to thank Y. Arakida for providing an idea of profile monitoring, Shinozuka and Wakui of Tohoku University for their suggestions on remained issues and A. Takagi for his advice of voltage stabilizing.

REFERENCES

[1] K. Takayama, Y. Arakida, T. Iwashita, T. Dixit and K. Torikai, J. of Appl. Phys. 101, 063304 (2007).
[2] K. Takayama, Y. Arakida, T. Dixit, T. Iwashita, T. Kono, E. Nakamura, K. Otsuka, Y. Shimosaki, K. Torikai and M. Wake, Phys. Rev. Lett. 98, 054801 (2007).
[3] K. Takayama and R. Briggs (Eds.), Chapters 11 and 12 in Induction Accelerators (Springer-Verlarg, 2010) ISBN: 978-3-642-13916-1.
[4] J. Pivarc, J. of Elect. Eng. 55, 100 (2004).
[5] S. Gammino and G. Ciavola, Rev. Sci. Inst. 67, 155 (1996).
[6] Atomic Data and Nuclear Data Tables 65, 1-35 (1997).
[7] S. Gammino, G. Ciavola, L.Celona, M. Castro, F. Chines and S. Marletta, Rev. Sci. Inst. 70, 3577 (1999).
[8] I.G. Brown, The Physics and Technology of Ion Sources (2nd Edition), John Wiley & Sons, (2004), ISBN 3-527-40410-4.

LONG-TERM OPERATION EXPERIENCE WITH TWO ECR ION SOURCES AND PLANNED EXTENSIONS AT HIT

Tim Winkelmann, Rainer Cee, Thomas Haberer, Bernd Naas, Andreas Peters (HIT, Heidelberg)

Abstract

The HIT (Heidelberg Ion Beam Therapy Center) is the first treatment facility at a hospital in Europe where patients can be treated with protons and carbon ions. Since the commissioning starting in 2006 two 14.5 GHz electron cyclotron resonance ion sources are routinely used to produce a variety of ion beams from protons up to oxygen. The operating time is 330 days per year, our experience after three years of continuous operation will be presented. In the future a helium beam for patient treatment is requested, therefore a third ion source will be integrated. This third ECR source with a newly designed extraction system and a spectrometer line will be installed at a testbench to commission and validate this section. Different test settings are foreseen to study helium operation as well as enhanced parameter sets for proton and carbon beams in combination with a modified beam transport line for higher transmission efficiency. An outlook to the possible integration scheme of the new ion source into the production facility will be discussed.

INTRODUCTION

The facility of the Heidelberg Ion Beam Therapy Center (HIT) [1] is the first dedicated proton and carbon therapy facility in Europe. HIT is located at the university hospital in Heidelberg (Universitätsklinik Heidelberg, Germany).

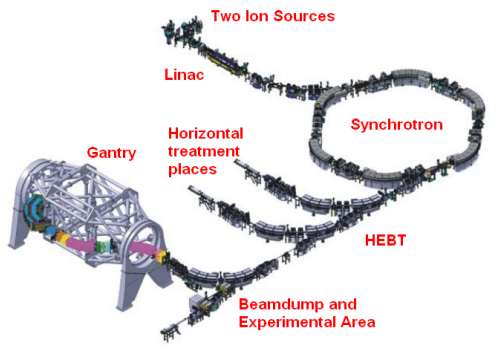

Figure 1: Overview of the HIT accelerator facility.

The beam production at HIT consists of two 14.5 GHz permanent magnet ECR ion sources from PANTECHNIK [2]. The 7 MeV/u injector linac [3] comprises the LEBT (Low Energie Beam Transport), a 400 keV/u radio frequency quadrupole accelerator (RFQ) [4,5], and a 7 MeV/u IH-type drift tube linac (IH-DTL) [3,4,5]. The linac beam is injected in a compact 6.5 Tm synchrotron [6] with a circumference of about 65m to accelerate the ions to final energies of 50 – 430 MeV/u, which is the key to the enormous variety of beam parameters provided by the HIT accelerator.

The maximum available beam intensity at the patient treatment place are 4·108 ions/spill for carbon and 1.6·1010 ions/spill for protons. With respect to the patient treatment, these intensities are sufficient, but for an effective quality assurance it will be important to reach the design parameters (C: 1·109 ions/spill, p: 4·1010 ions/spill). Taking into account the variable spill-length, the intensity shout be increased by a factor of 2.5 for carbon and protons.

The main contribution of particle losses is caused by the suboptimal transmission of the beam through the RFQ. Therefore the upgrade programme concentrates on a redesign of the RFQ [7]. In parallel we start to optimize the ion source performance for an improved brilliance to achieve a better adaption. Therefore we integrate a frequency variable microwave in a narrow range of 250 MHz around the 14.5 GHz center frequency. The frequency tuning is a method to optimize the electron cyclotron resonance ion source performances to maximize the extracted beam current and lower the beam emittance [8, 9, 10]. Furthermore for higher beam brilliance we designed a new extraction system.

LONG-TERM OPERATION EXPERIENCE

During the first three years of operation mainly carbon ions were used by 60 %, followed by hydrogen (38 %), helium (1 %) and oxygen (1 %). The continuous operation runtime of the two sources are 330 days per year 24h-operation!

Our challenge in the first three years of operation was the enhancement of the source components durability to stretch the time between maintenance intervals [10].

The operation-statistics (see Fig. 2) since summer 2007 of the two ion sources are: 97% of the time in operation, 2.9% of the time for planed maintenance shifts and 0.1% of the time are the “off time” caused by multiple RF-amplifier breakdowns. The time to exchange the defect amplifier by a spare part took mostly just one hour. By installing 3mm µ-metal shielding this instability is resolved in the meantime.

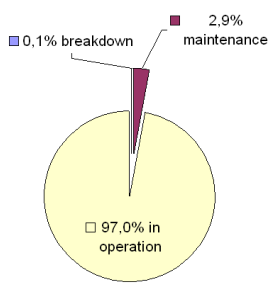

Figure 2: operation-statistic of the two ion sources at HIT, since summer 2007.

The required intensities given in table 1 were very stably achieved.

Table 1: Routinely used ion species and intensities behind the 90° analysing system.

Ion	I / eμA Used current	I / eμA Reachable current	U_{source} / kV
H_2^+	1200	1500	16
$^3He^{1+}$	500	500	24
$^{12}C^{4+}$	160	200	24
$^{16}O^{6+}$	150	150	21.3

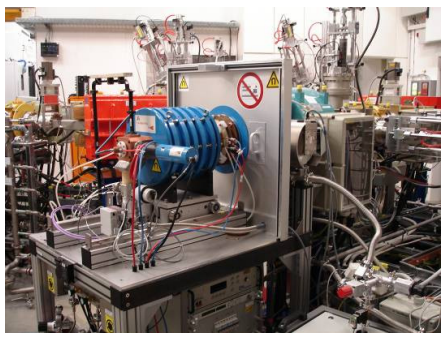

Figure 3: The 14.5 GHz high-performance permanent magnet ECRIS SUPERNANOGAN. This source was developed at GANIL, and is commercially available from PANTECHNIK S.A., France [2].

THIRD ION SOURCE

Presently the LEBT is designed for ion energies of 8 keV/u. At the moment there are two independent spectrometer lines (one for each ion source), a switching magnet which allows fast switching between the ion beams, a macro pulse formation and matching of the beam parameters to the entrance of the RFQ (Fig.4).

In 2009 it was decided to install a third ion source at HIT to offer Helium beam regularly for patient treatment in near future (Fig. 5).

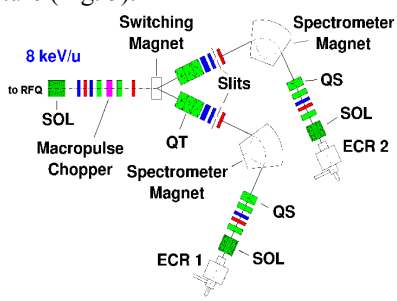

Figure 4: The existing low energy beam line (LEBT). SOL = solenoid magnet, QS = quadrupole singulet, QT = quadrupole triplet. Green: focusing and steering magnets, red: profile grids and tantalum screen, blue: beam current monitors

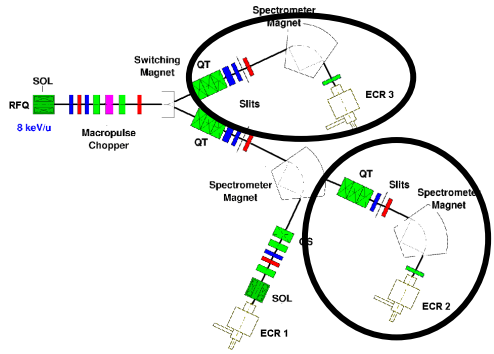

Figure 5: Possible schematic design of the LEBT including three ion sources.

All parts are delivered and will be pre-tested at a testbench.

The motivation for the shorter new design of the LEBT beam line is founded by lower space charge effects and by the geometry of the available LEBT space.

To test the "short" set up of the new spectrometer line (without Solenoid and Quadrupol (marked in Fig. 5)) a test bench is set-up now.

In May 2010 the factory acceptance tests (FAT) for the third ion source (SUPERNANOGAN) at Pantechnik has been started. For this test Pantechnik integrated in the acceptance test bench the new extraction system designed by HIT. We chose for the FAT a similar electrode design to the "old" Pantechnik extraction system with a 3mm smaller gap between plasma lens and puller electrode; another change to the original extraction system is the possibility to bias all three electrodes. After a week of conditioning the source fulfilled all tests. Pantechnik has begun in July the source installation at the HIT-Test-Bench.

TESTBENCH

A challenge for the installation planning was the integration of the new designed accel-decel-extraction-system (Fig. 6).

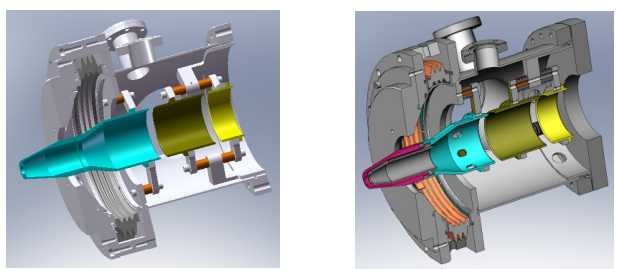

Figure 6: left: Extraction system for the ion source factory acceptance test at Pantechnik; right: The accel-decel extractionsystem, consisting of 4 electrodes set up for the HIT-Testbench

A goal for this set up (with a new extraction system and a "short" LEBT) is higher beam brilliance in comparison with the existing LEBT especially for the low LET-beams like helium and protons.

In the HICAT Technical Proposal [13] the use of 3He was recommended, but there are strong medical arguments to use 4He because of the less lateral straggling. In addition, the operation of a third ion species with the same A/Q = 2 value behind the stripper like for 12C6+ and 16O8+ will be much more efficient for keeping excellent accelerator settings for all ion species. For the risk mitigation measurement it is necessary to simulate a leak in the source and measure the potential "contaminating" output of 12C6+, 14N7+ and 16O8+ (same A/Q) at the "normal" operation setting for He.

A schematic design of the testbench is given in Fig. 7. The different testbench setup stages are also shown.

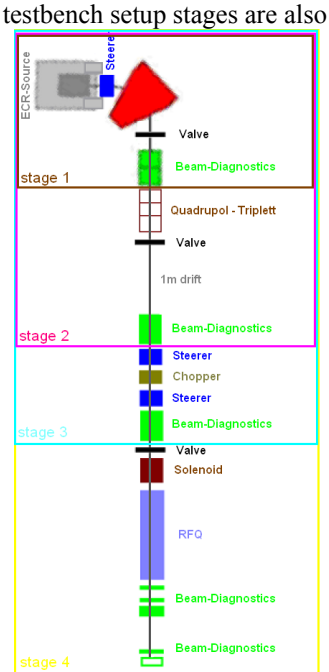

Figure 7: Test-Bench in 4 stages of expansion after every stages we integrate a slit grit emittance measurement device.

The aims for the different setups are:

Stage 1:

- Test of the optic for the new LEBT set up
- Acceptance test for the ion source with the new extraction system
- Parameter sets for helium (risk mitigation measurement), proton and carbon beams
- Improvement of the beam brilliance by changing the µ-Wave frequency [9]

Stage 2 and 3:

- Integration, and test, of a new designed pepper pot emittance scanner [11].

Stage 4:

- Investigation of the new RFQ with an enhanced electrode design and optimized alignment [12].

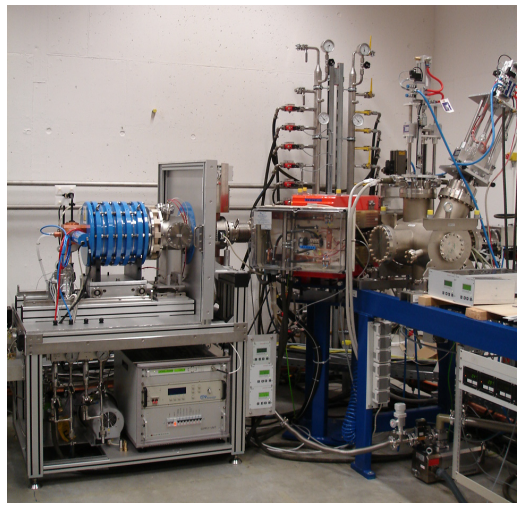

Figure 8: Test bench at HIT (stage 1)

REFERENCES

[1] Haberer et al., "The Heidelberg Ion Therapy Center", Radiotherapy and Oncology, Vol. 73 (Supplement2), P186-199,2004

[2] PANTECHNIK S.A., FRANCE.

[3] B. Schlitt et al., Proc. LINAC 2004, p. 51.

[4] A. Bechtold, PhD Thesis, J.-W.-Goethe University Frankfurt am Main, 2003. http://iaprfq.physik.uni-frankfurt.de/

[5] C. Kleffner et al., LINAC 2006, THP 089.

[6] A. Dolinskii, "The Synchrotron of the Dedicated Ion Beam Facility for Cancer Therapy, proposed fort he clinic in Heidelberg" EPAC 2000, Vienna

[7] R.Cee et al.,"Intensity Upgrade Programme for the HIT Injector Linac", EPAC08, Genoa, Italy, TUPP113

[8] WORK Microwave GmbH (http://www.work-microwave.de/work_home.htm)

[9] L. Celona, G. Ciavola, F. Consoli, S. Gammino, F. Maimone,D. Mascali, P. Spaedtke, K. Tinschert, R. Lang, J. Maeder,J. Roßbach, S. Barbarino, and R.S. Catalano, "Observationsof the frequency tuning effect in ECR ion sources", Rev. Sci.Instr. 79, 023305 (2008).

[10] T. Winkelmann et al.;"Progress in ion source injector development at the ionn beam therapy center HIT", Rev.Sci.Instrum.81, 02A311(2010)

[11] M. Ripert et al., "A Pepper Pot Emittance Device for 8 keV/u Light Ion Beams", BIW2010, Santa Fe, USA

[12] S. Yaramyshev et al., "Upgrade of the high current heavy ion front-end system of the GSI UNILAC" Prob.Atomic Sci.Technol. No 4, pp. 64-66, 2006.

[13] R. Bär, A. Dolinskii, H. Eickhoff, Th. Haberer, A. Peters, M.Rau, B. Schlitt, P. Spiller, *HICAT* - the Heavy Ion Cancer Therapy accelerator facility for the clinic in Heidelberg (Technical Description), GSI, December 2000.

CEA/SACLAY LIGHT ION SOURCES STATUS AND DEVELOPMENTS

R. Gobin*, G. Adroit, G. Bourdelle, N. Chauvin, O. Delferrière, Y. Gauthier, P. Girardot, F. Harrault, C. Marolles, C. M. Mateo, S. Nyckees, B. Pottin, Y. Sauce, F. Senée, O. Tuske, T. Vacher, C. Van Hille, CEA/Saclay, DSM/IRFU/SACM, F- 91191-Gif/Yvette, France

Abstract

After several years of high intensity light ion beam production with the SILHI source, CEA Saclay is now involved in the construction of different injectors dedicated to large infrastructures like IFMIF or Spiral 2. Other installations are also interested by high intensity ion sources. Such machines plan to produce and accelerate proton or deuteron beams in pulsed or continuous mode. The SILHI source, based on ECR plasma generation, already demonstrated its performance in both modes.

As a consequence, at present time the construction of 2 new injectors for Spiral 2 and IFMIF (source and low energy beam lines) is in progress at CEA/Saclay. This article will report on the status of both installations. It will also point out on ongoing developments. Such developments are mainly done with the new BETSI test bench operating for several months.

INTRODUCTION

In the beginning of the 90s, Chalk River (Canada) laboratory group demonstrated the production of intense single charge light ion beams with ECR sources operating at low frequency (i.e. 2.45 GHz). At CEA/Saclay, the SILHI source developments started in the middle of the 90,s. Since 1997 more than 100 mA proton or deuteron beams are routinely produced in pulsed or continuous mode with this source [1]. To optimize the beam transport in the low energy beam line, the extraction system was carefully designed and space charge compensation studies were undertaken. Moreover, to comply with new infrastructure requests, specific source designs have been performed.

As a consequence, permanent magnet sources have been developed to fit in with the 5 mA deuteron beam expected production in continuous mode for Spiral 2 [2]. Then, to answer the IFMIF (International Fusion Material Irradiation Facility) high intensity deuteron beam request (125 mA) [3], a copy of the SILHI source with a 4 electrode extraction system has been proposed. Table 1 summarizes the Spiral 2 and IFMIF requested characteristics at the injector and RFQ interface.

Such proposals were accepted and now both injectors for Spiral 2 and IFMIF are presently under construction at CEA/Saclay, as reported in the following sections. In parallel, the SILHI installation is used for optical diagnostic improvements or tests dedicated to the mentioned projects.

As reported in the last section, new developments have been undertaken towards beam profile reconstruction using tomography technique. It is also planned to install a new solenoid on the BETSI ion source test bench, in order to allow molecular ion focusing in front of the analyzing dipole.

All this work is performed within the PROFIIL (Plateforme de Recherche et d'Optimisation des Faisceaux Intenses d'Ions Légers) platform.

Table 1: Spiral 2 and IFMIF requests at the RFQ entrance.

Requests	Unit	Spiral 2	IFMIF
Particle type		(H^+), D^+	D^+ , (H_2^+)
Intensity	mA	0.15 to 5	140
Energy	keV	(20), 40	100
Emittance	π.mm.mrad	0.1	0.2
D^+ fraction		99	99
Mode		CW and pulsed	CW and pulsed

SPIRAL 2 INJECTOR CONSTRUCTION

Several years ago, permanent magnet source has been developed to produce several mA of H^+ or D^+ beams [4]. So, the Spiral2 ion source, presently installed at CEA/Saclay (Fig. 1) is also based on the ECR heating plasma, with a permanent magnet induced magnetic field. Magnet rings are composed of several individuals magnets glued together in an aluminum shell. Magnetic orientation follows the source axis. Shielding plates are positioned in order to concentrate the magnetic flux on source axis and to reduce fringe field which avoids Penning discharges inside the accelerating column. The resonant zone (of 87,5 mT) for plasma heating is located near the ridged transition-plasma chamber interface.

Extraction column is composed of 5 electrodes and is not water-cooled. The gaps are optimized for the lowest extraction RMS emitance: calculations were made for 10 mA of proton beam at 20 keV and also 10 mA of deuteron beam at 40 keV.

At end of 2009 the ion source has been tested with hydrogen gas injection in the plasma chamber, in pulsed and CW mode. The extracted ion beam was collected just at the end of the accelerating column in a Faraday cup equipped with an electron repeller electrode. A total beam of 12 mA has been extracted from the ion source without any characterization. Figure 2 presents repetitive 8 mA

*rjgobin@cea.fr

pulsed beam extracted (pulse width 200 ms at 1 Hz) with 700 W fed to the plasma chamber.

Fig. 1: Spiral 2 ion source on its HV table

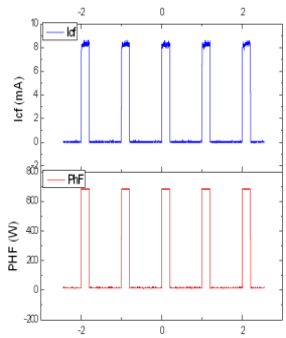

Fig. 2: H^+ beam produced with Spiral 2 source

The total LEBT (Low Energy Beam Transport) length from the source to the RFQ entrance, presently under construction (Fig. 3), will be assembled and characterized at Saclay.

Fig. 3: Spiral 2 LEBT under construction at Saclay

IFMIF INJECTOR CONSTRUCTION

In parallel, during the IFMIF-EVEDA (Engineering Validation and Engineering Design Activities) phase, CEA is in charge to build and characterize the injector (source + LEBT) at Saclay, before its transfer on the Rokkasho site in Japan.

The 100 keV beam energy request imposes to install the whole source and its ancillaries on a High Voltage platform. Since the magnetic shielding has been reduced to cover only the 2 coils, the IFMIF source design slightly differs from the SILHI one. Concerning the RF chain, the 2.45 GHz RF power is fed to the plasma chamber via an automatic tuning unit, rectangular waveguides, a 3 step ridged transition and a quartz window. A fast magnetron interruption system, developed by Sairem© is linked to the machine protection system. The water cooled plasma chamber is also equipped with 2 boron nitride disks at both extremities.

In order to minimize the beam divergence at the exit of the accelerator column, one of the most important changes compare to SILHI installation is the extraction system where the electrode number is reduced from 5 to 4 [5]. Such system allows keeping meniscus tuning with a puller to minimize beam looses on the electrodes. Then the puller is followed by the electron repeller and the grounded electrode.

Emittance growth has already been observed in the LEBT. As a consequence, to limit this effect, the length of the line has been reduced as short as possible. Numerous simulations were performed with the SOLMAXP code to better understand the space charge compensation evolution in the transport devices [6]. The use of short solenoids (310 mm long with shielding) allows limiting the total LEBT length at about 2.0 m.

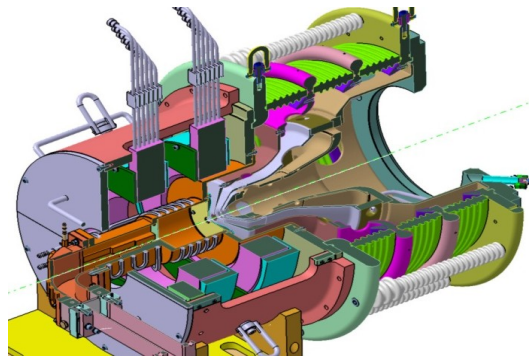

Fig. 4: IFMIF injector source and extraction system

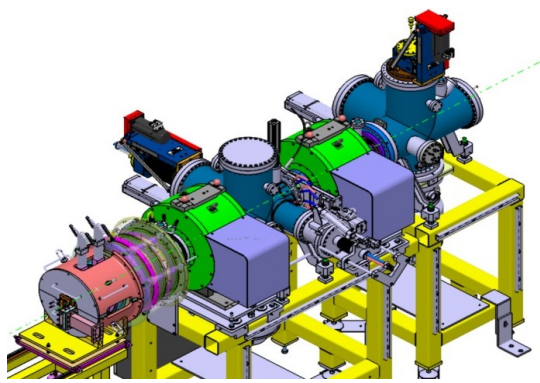

Fig. 5: General injector set up

SILHI AS DIAGNOSTIC TEST BENCH

As previously mentioned, both projects (Spiral 2 and IFMIF) need deuteron beams. Even at low energy, (D,d) reaction occurs when the D^+ beam interacts with implanted deuterium in the beam line material surfaces. Therefore beam losses (due to interceptive diagnostics or undesired particles) in the LEBT will lead to important neutron production.

To increase the reliability of the IFMIF injector which is more powerful than the Spiral 2 injector, great care has been done to minimize electronic devices inside the vault and to choose radiation hardened equipments. Following this strategy, the SILHI beam has been used to test CID (Charge Injection Device) cameras and a hardened fiberscope devoted to beam images transport towards a monochromator located outside the accelerator vault.

One CID8726DX6 camera from Thermo CIDTEC has been tested on the SILHI source with a 25 mm objective lens (Fig. 6). FWHM (full width at half maximum) beam profile comparison with CCD camera measurements showed quite good agreement; a difference of only few percent has been observed [7].

Comparative image acquisitions have also been done with and without a hardened fiberscope inserted between the beam line viewport and a CCD camera. The average FWHM difference with and without fiberscope remains in the range of 10 %.

As a consequence, several CID cameras and a 20 m long fiberscope with the characteristics summarized in Table 2 will be installed on the IFMIF injector.

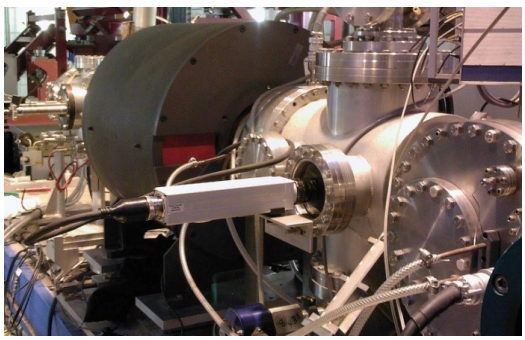

Fig. 6: CID camera tested on the SILHI source LEBT

Table 2: Fujikura fiberscope characteristics

Fiber Part No	FIGR-10
Number of picture elements	10000 +/- 1000
Image circle diameter (µm)	1100 +/- 100
Field of view	20 deg
Working distance	370 +/- 70 mm
Camera end	C-Mount camera lens

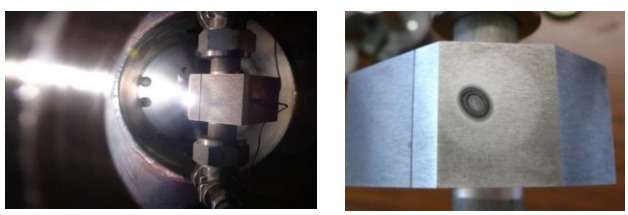

Fig. 7: Thermal screen models during and after test

High intensity beam power does not allow using the 3 gradient method (with optical profile) for emittance measurement. As a consequence, a classical Allison scanner, able to bear 15 kW cw beam, is presently under study. The thermal screen will be made of 2 water cooled copper block covered with tungsten wiles (assembled by brazing). The entrance slit will be defined by these 2 blocks. Two models, equipped with 2 thermocouples, have been tested with the SILHI beam (Fig. 7) to crosscheck the thermal simulations.

Beam density higher than 3 kW/cm^2 led to W tile deformation. In order to keep the slit width constant the beam power will have to be limited (roughly 1 kW/cm^2).

DEVELOPMENTS AND PERSPECTIVES

High intensity beam transport at low energy is a great challenge. In order to really well match the beam at the RFQ entrance, the beam characteristics such as position, profile, emittance, have to be perfectly known. Moreover, the beam power density can reach several 10 kW/cm^2. As a consequence, optical diagnostic development is ongoing for several years at CEA/Saclay. Presently, beam shape reconstruction using tomography technique is in progress within the DITANET Marie Curie European network [8].

To improve and test new sources, a new test bench named BETSI (Banc d'Etudes et de Tests des Sources d'Ions) is now fully operating for several months. It already allows source magnetic structure analysis as well as extraction system developments [9]. It also permits plasma emitted light analysis with a monochromator. In addition, BETSI is going to be renewed to be able to analyze each ion species produced by different tested ion sources. In particular, the molecular ions H_2^+ and H_3^+ are not sufficiently focalized before the analysis dipole. A new solenoid which is a copy of IFMIF solenoids able to focalize 175 mA beam in a strong focusing mode, has been built. It will be installed soon.

Since emittance investigation has been performed in pulsed mode with the SILHI source [10], FAIR project responsible decided to install such source with a 2 solenoid LEBT (built by CEA) to feed the future proton linac with up to 70 mA H^+ short pulsed beam at 4 Hz.

REFERENCES

[1] R. Gobin et al., Rev. Scient. Instrum. vol. 73, 924 (2002)
[2] Spiral 2 website: http://pro.ganil-spiral2.eu/spiral2
[3] A. Mosnier et al., “The injector prototype of the IFMIF-EVEDA project”, IPAC10 conference proc., Kyoto (Japan) May 2010
[4] R. Gobin et al., Rev. Scient. Instrum., vol. 77, 03B502 (2006),
[5] R. Gobin et al., Rev. Scient. Instrum., vol. 81, 02B301 (2010),
[6] N Chauvin et al., “Final design of the IFMIF-EVEDA low energy beam transport line”, PAC09 conference proc., Vancouver (Canada),
[7] F. Senée, “Diagnostics for high power ion beams with coherent optic fiber for IFMIF-EVEDA Injector”, DIPAC09 conference proc., Basel (Switzerland),
[8] DITANET website: http://www.liv.ac.uk/ditanet/
[9] S. Nyckees et al., “A new BETSI test bench at CEA/Saclay”, this conference.
[10] R. Hollinger et al., “High current proton beam investigations at the Silhi-LEBT at CEA/Saclay” LINAC06 conference proc., Knoxville, TN, (USA).

SHEATH FORMATION OF A PLASMA CONTAINING MULTIPLY CHARGED IONS, COLD AND HOT ELECTRONS, AND EMITTED ELECTRONS

H.J. You#, National Fusion Research Institute, Daejeon, Republic of Korea

Abstract

A model of sheath formation was extended to a plasma containing multiply charged ions (MCIs), cold and hot electrons, and secondary electrons emitted either by MCIs or hot electrons. In the model, modification of the "Bohm criterion" was given; thereby the sheath potential drop and the critical emission condition were also analyzed.

INTRODUCTION

It is quite well known since Geller's remarks [1] that ion confinement is an important factor in an electron cyclotron resonance ion source (ECRIS). Particularly, it has been pointed out that the ion confinement is closely related to the plasma potential, since many empirical techniques (wall coatings, secondary electron materials, electron injection and biased disks, and gas mixing) were found to lower plasma potential [2]. In this sense, the detailed sheath formation is very important in understanding how multiply charged ions (MCIs), bulk (cold and hot) electrons, and secondary electrons (either by MCIs and bulk electrons) are contributing to the plasma potential (sheath potential drop). The present study was motivated by the fact that the secondary electron yields are strongly dependent on the charge state of the ions and on the incident energy of electrons; secondary electron yield γ_j by ion bombardment is almost linearly proportional to the charge state j, so that the ratio γ_j / j reaches around unity for Ar^{8+} ion [3], and secondary electron yield γ_e by electron bombardment is typically larger than 0.5 for the incident energy larger than 100 eV [4]. Therefore, the contributions of the secondary electron emissions on the sheath formation would be severe if the charge state of ions and/or the energy of electrons are high.

MODEL

We consider an unmagnetized plasma composed of different MCIs, cold and hot electrons, and emitted electrons from the wall. The wall is located at x=0 and is contact with plasma, which is assumed to be zero. The electric field is also zero there. The wall potential V_w is negative with respect to the plasma potential V_s. We assume bi-Maxwellian electrons (cold and hot electrons), which has two different electron temperatures. The secondary electrons are assumed to be emitted from the wall with the same initial velocity v_{em}. The above all considerations are illustrated in Fig. 1.

The potential profile $V(x)$ in the sheath is obtained by solving Poisson's equation,

$$\frac{\mathrm{d}^2V(x)}{dx^2} = -\frac{1}{\varepsilon_0}\left[\sum_j e_j n_j(x) - e n_e(x)\right], \qquad (1)$$

where $n_e(x) = n_{ec}(x) + n_{eh}(x) + n_{em}(x)$, and n_j, n_{ec}, n_{eh}, and n_{em} are the densities of j-charged ions, cold electrons, hot electrons, and emitted electrons from the wall surface, respectively.

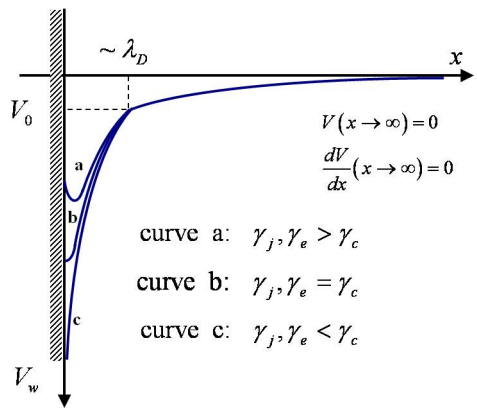

Figure 1: Sheath model & potential variations in front of the wall surface which emits electrons.

The behaviour of the j-charged ions can be described by continuity equation and momentum equation, therefore yielding following equation [5]

$$dn_j / dV = n_j e_j / m_j v_j^2, \qquad (2)$$

where m_j and v_j are the mass and velocity of j-charged ion.

The densities of cold and hot electrons are assumed to obey the Boltzmann relation,

$$n_{ec}(x) = n_{ec0}\exp(\psi), \quad n_{eh}(x) = n_{eh0}\exp(\psi). \qquad (3)$$

Here $n_{ec}(x)$ and $n_{eh}(x)$ are the cold and hot electron densities at x from the sheath edge, and n_{ec0} and n_{eh0} are the cold and hot electron densities at the sheath edge. The dimensionless potential ψ and the ratio (θ) of cold and hot electron temperatures (T_{eh}, T_{ec}) are defined in the following way:

$$\psi = -e\left(V_0 - V(x)\right)/kT_{ec}, \quad \theta = T_{eh}/T_{ec}. \qquad (4)$$

Therefore, ψ is a negative dimensionless potential measured with respect to the potential at the sheath edge.

#hjyou@nfri.re.kr

The density of the secondary electrons is given by continuity equation and energy conservation,

$$n_{em}(x) = n_{ems} \Big/ \sqrt{1-\psi/\psi_w - N^2\mu/2}\,, \tag{5}$$

with the introduction of the dimensionless potential drop and mass ratio of electron and ion:

$$\psi_w = -e\left(V_0 - V_p\right)\Big/ kT_{ec}\,, \quad \mu = m_e/m_j\,, \tag{6}$$

where the initial velocity v_{em} is assumed to the ion sound speed multiplied by a dimensionless factor N:

$$v_{em} = N\sqrt{kT_{ec}/m_j}\,. \tag{7}$$

Using Eqs. (1)-(7) and dimensionless variable $\xi = x/\lambda_D$, multiplying Eq. (1) with the field strength $dV/d\xi$, and then integrating yields

$$\varepsilon_0 E^2 + \left(\sum_j e_j \frac{dn_j}{dV} - e\frac{dn_e}{dV}\right)\Bigg|_{V=0} V = \text{const.} \tag{8}$$

Then Applying sheath edge condition (V→0 for ξ→0) gives const.=0 and yields general sheath condition

$$\left(\sum_j e_j \frac{dn_j}{dV} - e\frac{dn_e}{dV}\right)\Bigg|_{V=0} \le 0. \tag{9}$$

Engaging Eq. (2), the differentiations of Eqs. (3) and (5), and applying the general sheath condition (9) we have

$$\frac{kT_{ec}}{e^2}\sum_j \frac{e_j^2 n_{js}}{m_j v_j^2} \le n_{es}\,, \text{ where}$$
$$n_{es} = n_{ecs} + \frac{n_{ehs}}{\theta} + \frac{n_{ems}}{2\left(\psi_w - N^2\mu/2\right)}. \tag{10}$$

In spite of the discussions on the ion velocities at the sheath edge in multicomponent plasma, if we assume that all ions have the same velocity at the sheath edge [6], Eq. (10) can be written as

$$v_s^2 \ge \frac{kT_{ec}}{m_j}\sum_j \frac{e_j^2 n_{js}}{e^2 n_{es}}. \tag{11}$$

The ion velocity v_s at the sheath edge can be normalized by the ion sound speed $(kT_{ec}/m_j)^2$ and then be rewritten as

$$M^2 \ge \sum_j \frac{e_j^2 n_{js}}{e^2 n_{es}}. \tag{12}$$

According to the formalism in Ref. [7], we can use the relation between the flux of secondary electrons j_{em} from the wall and the fluxes of cold and the hot electrons j_{ec} and j_{eh}, and ions j_i to the wall. Here j_{em} is assumed to be proportional to j_{ec}, j_{eh}, and j_i in the form:

$$j_{em} = \gamma_e(j_{ec} + j_{eh}) + \gamma_j j_i. \tag{13}$$

The proportionality constant γ_e (γ_i) is defined as the number of emitted secondary electrons per incident electron (ion). j_{ec}, j_{eh}, j_{em}, and j_i can be given by

$$j_{ec} = en_{ecs}\exp(\psi_w)\sqrt{kT_{ec}/2\pi\mu m_j}\,, \tag{14}$$

$$j_{eh} = en_{ehs}\exp(\psi_w/\theta)\sqrt{kT_{ec}\theta/2\pi\mu m_j}\,, \tag{15}$$

$$j_{em} = j_{ems}N\sqrt{kT_{ec}/m_j}\sqrt{1-2\psi_w/N^2\mu}\,, \tag{16}$$

$$j_i = en_{es}M\sqrt{kT_{ec}/m_j}\,. \tag{17}$$

From Eqs. (13)- (17) we obtain

$$n_{ecs} = \frac{n_{es}\left(1-G_j\right)}{1+\beta+G_e},\ n_{ehs} = \frac{\beta n_{es}\left(1-G_j\right)}{1+\beta+G_e}, \tag{18}$$

$$\text{and}\quad n_{ems} = \frac{n_{es}\left(G_e + G_j(1+\beta)\right)}{1+\beta+G_e}, \tag{19}$$

where following variables have been employed:

$$\beta = \frac{n_{ehs}}{n_{ecs}},\ G_j = \frac{\gamma_j M}{\sqrt{N^2 - 2\psi_w/\mu}}, \tag{20}$$

$$\text{and}\ G_e = \frac{\gamma_e\left(\exp(\psi_w) + \beta\sqrt{\theta}\exp(\psi_w/\theta)\right)}{\sqrt{2\pi\mu\left(N^2 - 2\psi_w/\mu\right)}}. \tag{21}$$

Combining Eqs. (18) and (19), and inserting into Eq. (12) gives a newly modified form of Bohm criterion:

$$M = \sqrt{\sum_j \frac{j^2 n_{js}}{n_{es}} \frac{1+\beta+G_e}{\left(1-G_j\right)\left(1+\beta/\theta\right)\left(\frac{G_e+G_j(1+\beta)}{2\left(\psi_w - N^2\mu/2\right)}\right)}}. \tag{22}$$

Now the floating potential of the wall surface can be found by using the above Eq. (22), Eqs. (14)- (17), and following floating condition:

$$j_{tot} = j_i + j_{em} - j_{ec} - j_{eh} = 0. \tag{23}$$

Also, we can find the wall potential the critical condition occurs. As illustrated Fig. 1, if the emission of secondary electrons from the wall surface increases, the density of secondary electrons and consequently the negative charge in front of the probe eventually becomes so high that electric field at the wall surface becomes zero. This is called the critical emission where the emitted current starts to be space-charge limited. By applying the boundary condition

$$\left.\frac{d\psi}{d\xi}\right|_{\psi=\psi_w} = 0 \qquad (24)$$

we find the condition of the critical secondary emission,

$$0 = \frac{1}{1+\beta+G_e}\left[\begin{array}{l}\left(1-G_j\right)\left(\exp\left(\psi\right)-1\right)+\\ \beta\theta\left(1-G_j\right)\left(\exp\left(\psi/\theta\right)-1\right)+\\ +2\left(G_e+G_j\left(1+\beta\right)\right)\times\\ \times\left(\psi_p-\frac{N^2\mu}{2}\right)\left(1-\sqrt{1-\frac{\psi}{\psi-N^2\mu/2}}\right)\end{array}\right]. \qquad (25)$$

The formalism is described in more detail in a thesis [8].

RESULTS

The dependence of floating potential (ψ_f) of the wall is calculated by Eq. (23) and plotted as a function of the emission current ($J_{em}=j_{em}/j_0$, where $j_0=en_{es}(kT_{ec}/m_j)$) in Fig. 2(a). Here following sets of parameters are assumed: $\bar{j}=\sum_j I_j \big/ \sum_j \left(I_j/j\right)=1$, μ=4/1840, N=0, J_{em}=40, $G_e=2G_j$, and 7 combinations of (β, θ), where I_j is j-charged ion current obtained from the beam spectra. It is shown that the floating potential and its saturated potential (under high values of emission current) are strongly affected by the presence of hot electrons and the emission current (J_{em}). It is noted that sheath potential drop (floating potential) is significantly reduced by the emission current (J_{em}).

The critical emission potential (ψ_{w0}) implicated in Eq. (25) also can be calculated. Fig. 2(b) shows the dependence of ψ_{w0} and ψ_f on J_{em} for the following set of parameters: $\bar{j}$ =1, μ=4/1840, β=0.5, θ=6, J_{em}=40, $G_e=2G_j$, and three values of N=0, 50, 100. When J_{em} is increased, ψ_{w0} decreases and ψ_f increases, and then finally both values (ψ_{w0}, ψ_f) are merged to one value. Also, when the initial velocity (N) of the secondary electrons becomes higher, the critical emission potential (ψ_{w0}) is more slowly decreased with the emission current (J_{em}) and reaches a higher saturated value. It is also important to realize that that ψ_f and ψ_{w0} become independent of J_{em} when J_{em} is higher than critical emission current (J_{emc}) where critical emission occurs, and that even higher J_{em} is needed for the cases of higher initial velocities (N's) in order for ψ_f and ψ_{w0} to be independent of J_{em}.

Therefore, we conclude that the presence of hot electrons and emitted electrons strongly affects the sheath formation so that smaller hot electrons and larger emission current result in reduced sheath potential (or floating potential). However the sheath potential was found to become independent of the emission current J_{em} when $J_{em} > J_{emc}$ (or γ_e and $\gamma_i > \gamma_c$).

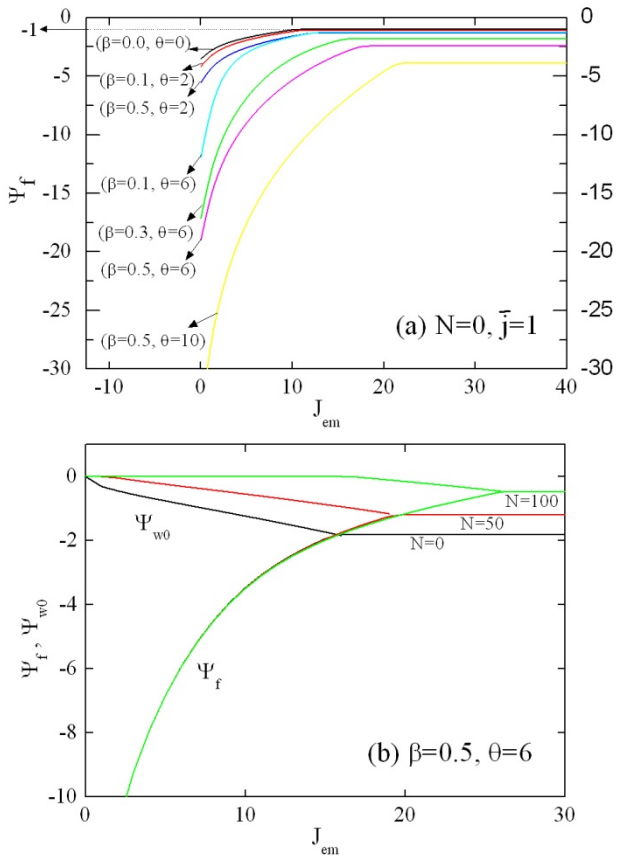

Figure 2: Floating potentials (ψ_f) and critical emission potentials (ψ_{w0}) dependent on the emission current (j_{em}) and the hot electron density and the temperature.

REFERENCES

[1] R. Geller, Electron Cyclotron Resonance Ion Sources and ECR Plasmas (Institute of Physics, 1996).
[2] A. G. Drentje, U. Wolters, A. Nadzeyka, D. Meyer, and K. Wiesemann, Rev. Sci. Instrum. 73, 516 (2002).
[3] B. Chapmann, Glow Discharge Process (John Wiley & Sons Pub., New York, 1980).
[4] L. Laska, J. Krasa, M. P. Stockli, and C. W. Fehrenbach, Rev. Sci. Instrum. 73, 776 (2002) and references therein.
[5] K. U. Riemann, IEEE Trans. Plasma Sci. 23, 709 (1995).
[6] N. Hershkowitz, Phys. Plasmas 12, 05502 (2002) and references therein.
[7] T. Gyergyek and M. Čerček, Contrib. Plasma Phys. 45, 89 (2005).
[8] H.J. You, Thesis Hanyang University, Seoul (2008).

CHARACTERIZATION OF THE MICROWAVE COUPLING TO THE PLASMA CHAMBER OF THE LBL ECR ION SOURCE

C. Lyneis , J. Benitez, D. Leitner, J. Noland, M. Strohmeier, LBNL, Berkeley, CA, USA
H. Kovisto, O. Tarvainien, Department of Physics, University of Jyväskylä, Finland

Abstract

The characteristics of the microwave coupling of the 6.4 GHz LBL ECR ion source were measured as a function of frequency, input power, and time dependence. The time dependence of the plasma diamagnetism and plasma loading of the ECR chamber were compared. The cavity modes in the LBL ECR plasma chamber are fairly widely spaced which makes it possible to locate frequencies, where a single RF mode is predominately excited. For one of these modes we were able to demonstrate that with no plasma in the cavity it is over-coupled. As the power is increased, the plasma density and the plasma loading both increase and the cavity becomes under-coupled. The experiments demonstrate that even for this low frequency, low plasma density source, the plasma loading strongly lowers the Q and the RF stored energy as the plasma builds up.

INTRODUCTION

The LBL ECR plasma chamber, which has a diameter to wavelength ratio of only 2, is not as over moded as many higher frequency ECR ion sources. This makes it possible to locate frequencies, where a single RF mode is predominately excited. In Table 1 the mode distribution between 6.2 and 6.5 GHz for the source is shown. This is approximate since it is based on a model with cylindrical geometry and the LBL ECR has a sextupole shaped chamber.[1] Using model calculations and accounting for dipole and multi-pole modes there are about 94 modes between 6 and 7 GHz or an average mode spacing of 10 MHz. In contrast a large high frequency source such a VENUS at 28 GHz has a mode spacing of roughly 26 kHz, which means no possibility to see quasi single mode excitation.

Table 1: Calculated Modes in the LBL ECR Plasma Chamber

Mode	Frequency in GHz
$TM_{01,16}$	6.236
$TE_{4,1,9}$	6.317
$TM_{0,2,8}$	6.325
$TE_{1,2,9}$	6.330
$TE_{3,1,13}$	6.339
$TE_{2,1,10}$	6.353
$TE_{0,1,14}$	6.362
$TM_{1,1,14}$	6.362
TE$1_{,1,17}$	6.374
$TM_{0,2,9}$	6.496
$TE_{4,1,10,}$	6.507

The LBL ECR can be analyzed as a transmission line terminated by a single port resonant cavity. The measurable variables are the frequency, incident power level, and the reflected signal. In this analysis, we treat the case of a single mode cavity or, equivalently, a multi-mode cavity where the modes are sufficiently separated with respect to their frequency response that they can be treated as a single mode cavity over a small delta in frequency.[2] This approximation works best at zero or low plasma densities in the source when the cavity Q is high. At higher plasma densities where the plasma loading increases the modes overlap and the approximation breaks down.

In a single port cavity the incident and reflected power can be measured. These data can be used to compute the adsorbed power and the coupling coefficient, β, which can be expressed as

$$\beta = \frac{\sqrt{P_i} \mp \sqrt{P_r}}{\sqrt{P_i} \pm \sqrt{P_r}} \qquad (1)$$

where P_i is the incident power and P_r is the reflected power. The choice of sign depends on whether the cavity is under coupled (upper sign) or over coupled (lower sign).

The coupling coefficient can be written alternatively as

$$\beta = \frac{Q_0}{Q_{ext}}, \qquad (2)$$

where Q_{ext} is the external Q-value of the cavity. For a single mode Q_{ext} is a constant dependent on the geometry of the coupling port and the electromagnetic distribution of the mode. In this paper, the calculation of the Q_0 includes all of the power adsorbed inside the cavity, whether it is due to the resistive walls or plasma adsorption.

The electromagnetic energy stored in the cavity (EM-fields), U, can be calculated from

$$U = \frac{Q_0 P_a}{\omega} = \frac{Q_{ext}}{\omega} \beta P_a, \qquad (3)$$

in which P_a is the absorbed power (reflected power P_r subtracted from the incident power P_i) and ω the microwave (angular) frequency. It follows that the energy stored in the EM-fields at any given time (plasma density), normalized with respect to the empty cavity value, can be written as

$$\frac{U_t}{U_{t=0}} = \frac{\beta_t\left(1-\left(\frac{P_r}{P_i}\right)_t\right)}{\beta_{t=0}\left(1-\left(\frac{P_r}{P_i}\right)_{t=0}\right)} \quad (4)$$

Equation 4 is written as a ratio because in these measurements it was not possible to directly measure or calculate Q0 although it can be estimated from the band width of the modes observed when dependence of the reflected power is plotted versus frequency.

EXPERIMENTAL MEASUREMENTS

For these measurements an adjustable microwave oscillator was used to drive a Varian klystron over the bandwidth of one of its channels, which are roughly 40 MHz wide. A small region of frequency between 6.34 and 6.37 GHz was measured in detail in the vicinity of the normal operating frequency for the source. In Fig. 1 the ratio of reflected to incident power is plotted without plasma and for 1, 2, 3, and 5 Watts of incident power. At these low powers, which are just enough to initiate a low density plasma, the effects of the plasma loading on the coupling coefficient can be observed. For example for the mode at 6.346 GHz, the reflected power at resonance first decreases between no plasma and 1 W, then increases. This indicates that with no plasma the cavity is initially over coupled and β is greater than 1. At 1 W it is close to unity coupling and it becomes more and more under coupled (β <<1) as the power is increased to 5 W. Two other changes occur as the plasma density increases with power. First the width of the resonance increases indicating increased plasma loading and the center frequency shifts up roughly 2 MHz, due to the change in the dielectric coefficient of the plasma.

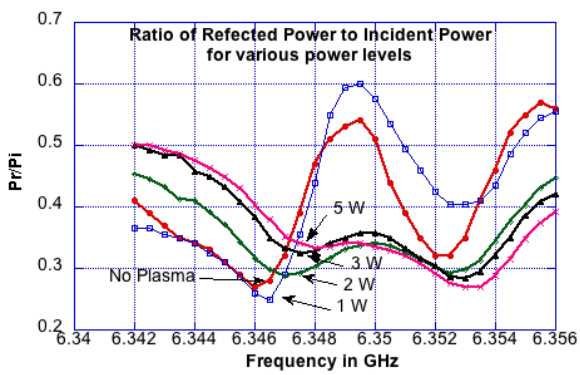

Figure 1: The reflected power ratio versus frequency at low RF incident power.

In Fig. 2 the reflected power ratio is shown for various powers between 40 and 250 W. Here the modes begin to overlap as the loading increases, but still the reflected power ratio continues to increase with incident RF power indicating that both Q_0 and β are decreasing.

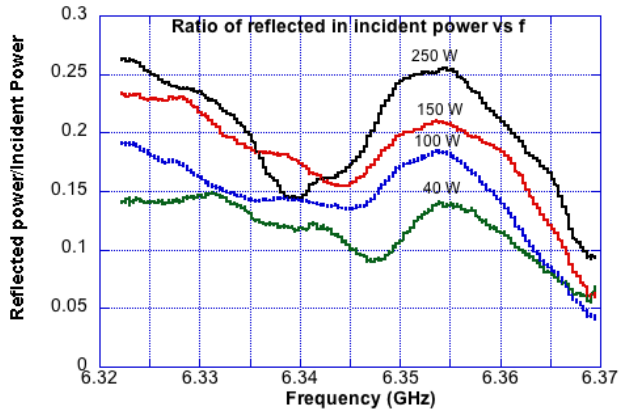

Figure 2: The reflected power ratio versus frequency for P_i from 40 W to 250 W.

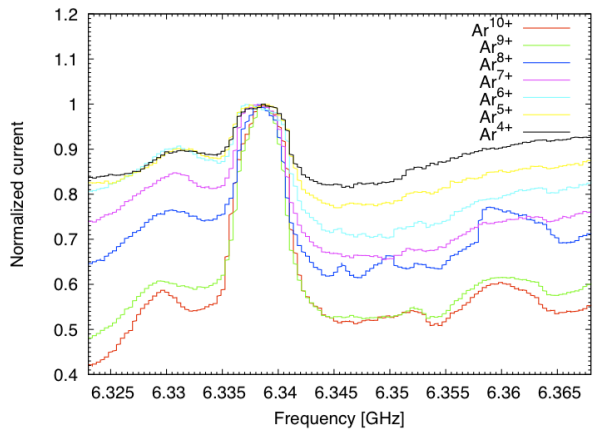

Figure 3: Ion currents for argon, normalized to their maximum value, as a function of frequency at 250 W incident power.

Figure 3 illustrates that for 250 W of incident power the production of high charge states is optimized at 6.337 GHz. For each charge state, the currents were normalized to1.0 at 6.337 GHz. For $Ar^{9+}$the beam current increases by a factor of two at the optimum frequency. This illustrates that outside a narrow frequency range of 5 MHz, the coupling efficiency between the RF modes and the plasma electrons decreases rapidly.

The response of the reflected to incident power ratio was measured as a function of time to study how the plasma build up affects the coupling microwave power to the plasma chamber cavity. The RF was switched on and the reflected power versus time was measured. The Q of this ECR chamber is relatively low and the microwave filling time is on the order of a μs, which is much faster than the times needed to build up plasma. The t = 0 time used below is a few μs after the RF is switched on when the RF field reaches its maximum value without plasma.

This is illustrated in Fig. 4 where the reflected power and the signal from the plasma diamagnetism loop are plotted versus time. The initial high reflected power drops to a minimum at 2ms as the coupling approaches unity and then increases as the plasma density grows. It reaches approximate equilibrium at roughly 3 ms. As the cavity goes from over coupled to under coupled the reflected power does not go quite to zero at unity coupling indicating an imperfect coupling network. However, it is clear from Fig. 4 that the loading increases quasi-monotonically with time and the Q decreases out to at least 3 ms. The diamagnetic loop signal on the other hand is proportional to the rate of change of the plasma diamagnetism (rate of change of plasma energy content), which peaks at about 3 ms. The integral of the loop signal is proportional to the plasma diamagnetism (plasma energy content) and following an apparent saturation in plasma density at 3 ms it continues to increase slowly implying that the hot tail of the electron energy distribution increases. This has little effect on the RF adsorption.

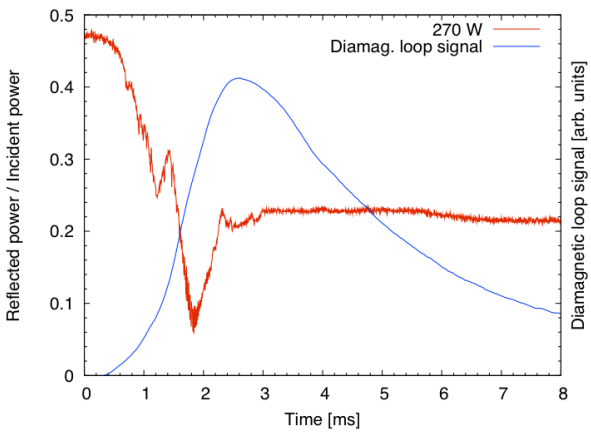

Figure 4: Reflected power ratio and the diamagnetic loop signal after RF turn on.

In Fig. 5 the electromagnetic energy of the microwave fields, normalized to the field at t=0, is plotted vs. time for slightly different conditions than Fig. 4. To compute the relative stored energy vs. time the measured values of Pr and Pi were used to compute the quantities in Eq. 4. The rapid drop at 5 ms is an artifact of the calculation of β near unity coupling where, as noted earlier, imperfections in the coupling network prevent the reflected power from going to zero at unity coupling. Fig. 5 shows the microwave stored energy reaches a maximum at turn on when there is no plasma loading and then decreases rapidly as the plasma density rises and loads down the cavity. Since the microwave electric field strength is proportional to the square root of the stored energy, it also decreases as the plasma builds up. A similar analysis showed that at 3 ms the Q_0 with plasma has decreased to only 10% of the initial Q_0 with no plasma.

A rough estimate of the Q_0 without plasma was made by using the full width half maximum values for the resonance width without plasma in Fig. 1. The Q_0 without plasma is 3000 to 5000 and as described above the Q_0 with plasma drops to one tenth that value.

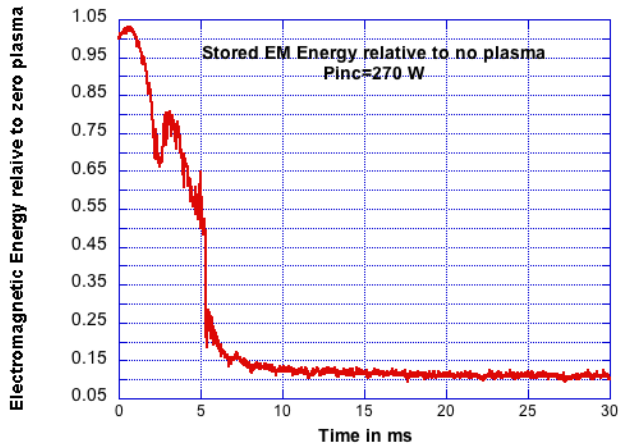

Figure 5: Relative stored power versus time calculated using Eq (4).

DISCUSSION

There are a number of models used to simulate the ECR heating of electrons in the plasma.[3] The two poorly understood inputs to these simulations are the microwave field distribution or mode and the strength of the RF electric fields. While the method described here is not applicable for highly over moded cavities, it is a reasonable approximation for the LBL ECR. With further effort and cold testing on the bench it would be possible to identify the modes excited, the zero plasma Q and then make very solid estimates of the RF electric fields. In any case, these measurements demonstrate that there are high RF fields only at the onset of an RF pulse and these fields are rapidly reduced by the plasma loading. For higher frequency sources, where the plasma density is much higher, the plasma loading will be even stronger and further damp the electric field strength.

Finally, these measurements indicate that the LBL ECR microwave coupling could be improved by using a waveguide directly inserted in the plasma chamber to increase the coupling strength, thereby making it similar to the coupling used on the AECR-U and VENUS sources.

REFERENCES

[1] The Physics and Technology of Ion Sources, John Wiley & Sons, New York, (1989) Ian Brown editor, p 219, 226

[2] J.C. Slater, Microwave Electronics, J.C. Slater, Van Nostrand, New York, (1963) p 51,76

[3] F. Consoli,_ L. Celona, G. Ciavola, S. Gammino, F. Maimone, S. Barbarino, R. S. Catalano, and D. Mascali, Rev. Sci. Instrum. 79, 02A308 (2008)

SOME CONSIDERATIONS ABOUT FREQUENCY TUNING EFFECT IN ECRIS PLASMAS*

D. Mascali, S. Gammino#, L. Celona, G. Ciavola, INFN-LNS and CSFNSM, Catania, Italy
L. Neri, R. Miracoli, N. Gambino, G. Castro, INFN-LNS and Università di Catania
F. Maimone, GSI, 64291 Darmstadt, Germany and Univ. of Catania, D.M.F.C.I, Catania, Italy

Abstract

In the recent past many experiments demonstrated that slight variations of the microwave frequency used for the ignition of ECRIS plasmas strongly influence their performances (frequency tuning effect) either in terms of extracted current, of mean charge state and of beam emittance. According with theoretical investigations, this phenomenon can be explained by assuming that the plasma chamber works as a resonant cavity: the excited standing waves, whose spatial structure considerably changes with the pumping frequency, globally influences either the energy absorption rate and the plasma spatial structure.

EXPERIMENTAL EVIDENCES

The experimental results collected during the last years in several laboratories (INFN-LNS, JYFL, GSI) have confirmed the validity of the Frequency Tuning Effect (FTE). Here we will report about two experiments with the ECR ion source of CNAO, Pavia, and with the CAESAR source of INFN-LNS (in this case we measured also the emitted X-rays at frequencies between 14.0 and 14.5 GHz). The experiments at CNAO evidenced the increase of the coupling efficiency with the RFQ: keeping constant all the other parameters, in Pavia the transmission was around 50-70%, while only a 30% of transmission was obtained at HIT with a "twin" accelerator and without FTE. Fig.1 shows the comparison between the extracted current and the reflection index. We can argue that resonant modes correspond to minima of reflection coefficient. Generally, the current signal is peaked on frequencies corresponding to modes (squared area b), because of the better coupling, but this is not a strict rule: in some cases (squared area a), although the matching of the microwave line with the source (cavity plus plasma) is optimal, and the extracted current remains low. Therefore we must distinguish between the microwave generator-to-plasma chamber coupling and the excited mode-to-plasma coupling. In the latter case, as formerly explained in [1, 2], the mode spatial structure plays the main role. According to simulations, the heating rapidity is strongly regulated by the electromagnetic field pattern over the resonance surface. This picture is not enough complete to describe all the consequences of the frequency tuning. Additional data information come from the data of Fig. 2.a and 2.b: from the X-ray measurements it follows that the high energy component of EEDF is not significantly affected by FTE (the magnetic field profile is the critical parameter, as demonstrated in [3]).

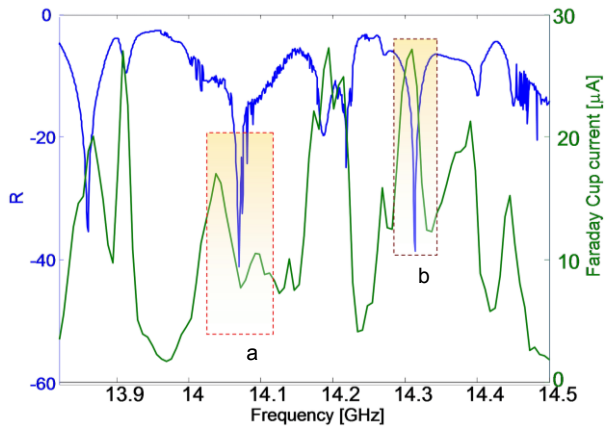

Figure 1: comparison between extracted current and reflection coefficient at different but close frequencies (test on the CNAO ECRIS).

Conversely the CSD (charge state distribution) reveals pronounced fluctuations for the highest charge states, as they are more sensitive to any change in heating rate. But the relationship between current and X-ray spectra is not straightforward. There are some frequencies (e.g. 14.38 GHz) which produce large amount of X-rays but relatively low currents and even a lower mean charge state. Considering the relation:

$$< q > \propto n_e \tau_i$$

being n_e the electron density and τ_i the ion lifetime, and assuming that the number of X-ray counts is somehow linked to the electron density, the results in Fig. 2 can be explained only by taking into account a possible influence of FTE on the ion dynamics (τ_i changes more than n_e).

This conclusion is confirmed by the other experimental data, which show how the frequency tuning affects the beam shape and emittance. At GSI [4] and JYFL in 2009 hollow beams have been obtained for some values of frequency, although no remarkable variations in the output current were observed. A plausible hypothesis is that cavity modes affects also the spatial plasma distribution, and consequently the ion dynamics, as discussed in [5]. Further confirmations come from the last experiment carried out at JFYL, focused on the beam transmission through the cyclotron, which varied even when the source output current did not change [6].

*Work supported by NTA – HELIOS Strategic Project and by 5th Nat. Comm. (INES experiment) of INFN.
#davidmascali@lns.infn.it

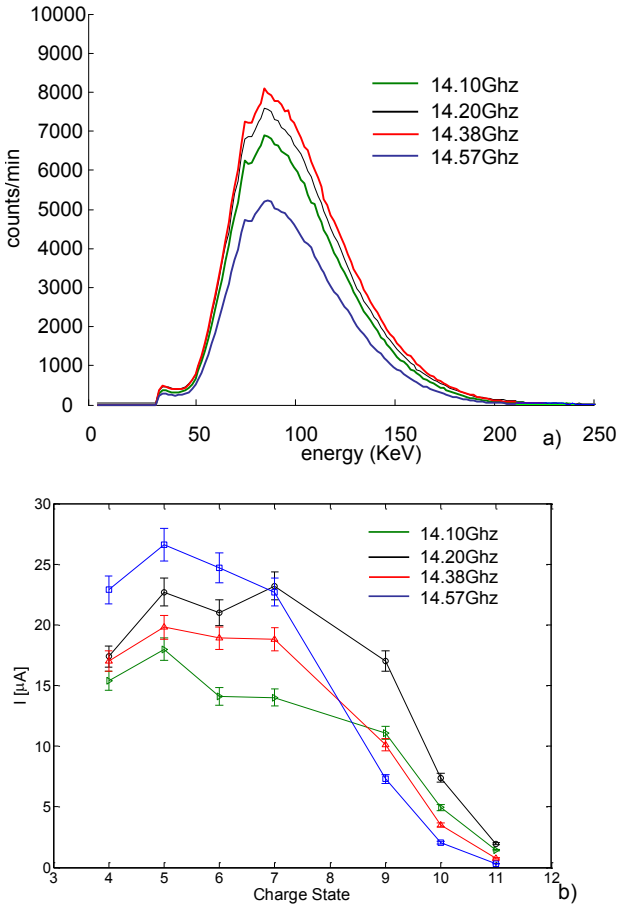

Figure 2: X-ray spectra (above) and CSDs (below) at different frequencies as measured with the CAESAR source.

THEORETICAL APPROACH

To reduce the calculation times for fully 3D collisional simulations of ECRIS plasma we can split the electron and ion dynamics, looking separately to their time evolution by using a Monte-Carlo (MC) collisional approach. 2D PIC simulations follow the electrostatic reciprocal interactions between electrons and ions on long timescales but assuming a collisionless plasma, and they can be used for a preliminary determination of plasma spatial distribution. In a fully 3D MC simulation the B-min field can be correctly reproduced, in Cartesian coordinates, by using the following formulas:

$$B_x = -B_1 xz + 2Sxy$$

$$B_y = -B_1 yz + 2S(x^2 - y^2)$$

$$Bz = \begin{cases} -B_0 + B_{inj} z^2 & \forall z < 0 \\ -B_0 + B_{ext} z^2 & \forall z > 0 \end{cases}$$

A SERSE-like device has been implemented in our code, with a plasma chamber length of 45 cm, and radius 6.5 cm. The magnetic field for 14 GHz (B_{ext}=1.2 T, B_{inj}=2.2 T, B_{min}=0.3 T, B_{hex}=1.2 T) is correctly reproduced with B_0=0.3 T, B_{inj}=25 T/m^2 , B_{ext}=36.5 T/m^2 and S=360. According to PIC calculations, because of the interaction with the electromagnetic field, working as an additional confinement tool, the ECRIS plasma separates into a high density plasma inside the resonance volume, and a lower density plasma in the outer resonance region. This situation can be adequately reproduced by the following formula for electron density [7]:

$$n_{ECRIS}(x,y,z) = 0.3 n_{cutoff} + \Sigma_i h n_{cutoff} \exp\left\{ -\frac{\left[B_{tot}(x,y,z) - (B_{ECR} - ki)\right]^2}{k^2} \right\}$$

which was used as input parameter for MC simulations. B_{tot} is the total magnetic field, h and k are two constants which ensure that the plasma density rapidly falls at the resonance plasma boundary in a few mm layer. This density is introduced into the following relation to calculate the collision probability, once known the characteristic time of Spitzer collisions for particles moving at velocity v:

$$P(t) = 1 - \exp\left(-\frac{t}{\tau_{coll}} \right) \qquad \tau_{coll} = \frac{M_{i,e}^2 2\pi\varepsilon_0^2 v_{i,e}^3}{n_e z^4 e^4 \ln\Lambda}$$

where z is the ion charge state (it is z=1 for electrons) and ln Λ the so called Coulomb logarithm. The MonteCarlo hybrid code solves the relativistic Landau equation [8] for electrons and a non relativistic equation for ions:

$$\frac{d\vec{v}}{dt} = \frac{q}{M}\left[\vec{v} \times \vec{B} + \vec{E}_s\right] \qquad (i)$$

$$\frac{d\vec{v}}{dt} = \frac{q}{m}\left(1 - \frac{v^2}{c^2}\right)^{3/2}\left[\vec{v} \times \vec{B}_S + \vec{v} \times \vec{B}_{em} + \vec{E}_{em} - \frac{1}{c^2}\left(\vec{E}_{em} \cdot \vec{v}\right)\vec{v}\right] \qquad (e)$$

where E_s is the electrostatic field over the resonance surface (from PIC simulations it is around V=20 V). This potential is perturbed by eventual fluctuations of the electron density [5].

The crucial assumption of our model is that the source chamber works as a resonant cavity even when filled by the plasma, which just shifts the resonance frequencies proportionally to the electron density, and introduces an absorption term in the eigen-field equation of the cavity. Experiments performed so far demonstrate that mode patterns still persist in high density absorbing plasmas [9].

MAIN RESULTS

Simulations are coherent with experiments: MC hybrid calculations make evident that the local absorbed power is much lower than the input one. The electromagnetic field was then calculated according to eigen-mode allowed in the aforementioned cylindrical chamber, with a field strength corresponding to a RF power of 1000W and Q=20000 [10]. The six first order differential equations which come out from either electron and ion vectorial equations of motion are solved by means of the 4th and 5th order Runge-Kutta routine implemented in MATLAB with time precision δt = 10^{-12} s (δt=10^{-9} s for ions), corresponding to about 10 points per gyroperiod. The trajectories of particles are followed for a fixed time interval Δt, after which the check of the collisions is done. If collisions are found, the velocity vector is rotated of 90° and the calculus restarts from this new coordinate.

Particles impinging on chamber walls are immediately removed from the calculation. Fluxes of electrons and ions, during their motion along the magnetic field, are stored with mm precision in a 3D array, which permits to visualize any density accumulation.

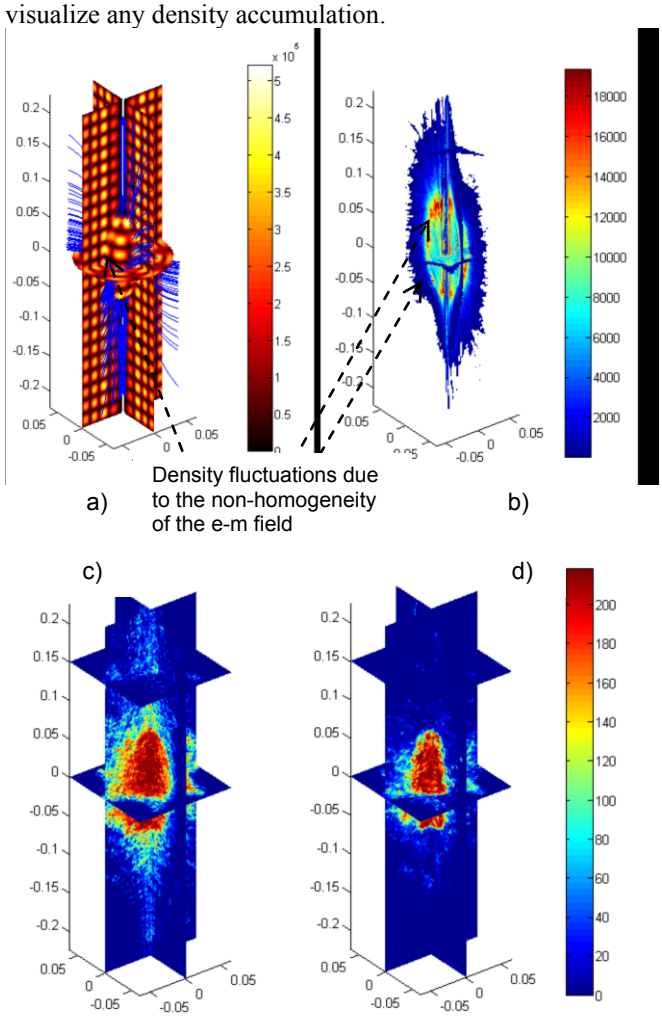

Figure 3: a) pattern of the electromagnetic field for 1000 W, TE4 4 23 mode, Q=2·104. b) longitudinal and transversal slices of electron density distribution (a.u.); c) d) comparison between simulated ion distributions (a.u.) for Ar plasma, with 1<q<4 (c), and 5<q<8 (d).

The most important results are shown in Fig. 3. MC hybrid approach reveals the existence of a strong non-homogeneity in plasma distribution: the largest part of electrons is well confined inside the resonance surface during the first 5 μs of life, confirming the results of 2D PIC simulations. Neither collisions are able to destroy the characteristic structure of plasma density, nor reciprocal electrostatic interactions among electrons and ions are able to do it, as observed in PIC simulations. MC show also that the density concentration in proximity of the resonance depends on the mode pattern (see Fig. 3.a) and b)), as well as the energy deposition into the plasma. Because of this additional effect of electromagnetic field on confinement and plasma structure, ions are partially reflected, partially accelerated when passing from inner resonance plasma to the outer one, fitting the shape of the electron density distribution. Ions are dynamically confined by collisions in the inner resonance-high density plasma; in the outer-resonance plasma, because of the lower density, the number of collisions drastically decreases and the ions feel the magnetostatic field. Localization of density perturbs the ion trajectories and the plasma surface corrugation scatters the ions along their path towards the extraction hole. According to the charge state, ions are then more or less scattered laterally or along the chamber axis, as confirmed by figures 3c) and 3d) (lower charge states are less confined). Simulations put also in evidence a depletion of plasma density in the near axis region: this may be at the basis of hollow beams. The only way to reduce the around axis accumulation of plasma, flattening the density, is the excitation of modes with maxima even in the region close to x=y=0.

In conclusion, simulations show that the different modes regulate the electron diffusion from cold to warm population, affecting the ionization efficiency; this is not sufficient to have high currents, because the ion scattering may make more rapid the losses of plasma particles, thus decreasing τ_i. Therefore the quality factor Q decreases although n_e remains about unchanged. In these cases also the emittance worsens. A proper handling of FTE may restore the conditions of good axial confinement, removing the hollow shape of extracted beam [6], and positively affecting the emittance. Hence FTE is a powerful technique to boost the performance of existing source without any large investments. Further efforts will be devoted to simulation methods, in order to self-consistently determine the dynamics of electron and ion density structures over very long timescales; more accurate predictions on ion beam properties will be possible.

REFERENCES

[1] S. Gammino et al., IEEE Transaction on Plasma Science, Vol. 36, 4, part II, August 2008.
[2] D. Mascali, Il Nuovo Cimento, DOI 10.1393/ncb/i2010-10899-9
[3] S. Gammino et al., Plasma Sources Sci. Technol. 18 (2009) 045016.
[4] L. Celona et al. Rev. Sci. Instrum. 79, 023305 (2008).
[5] D. Mascali et al., Rev. Sci. Instrum. 81, 02A334 (2010).
[6] V. Toivanen et al. these proceedings
[7] D. Mascali et al., accepted for publication in Rad. Eff. & Defects in Sol.
[8] L.D. Landau, E.M. Lifshitz (1975). The Classical Theory of Fields. Vol. 2 (4th ed.). Butterworth-Heinemann. ISBN 978-0-750-62768-9.
[9] L. Celona et al., accepted for publication on Eur. Phys Journal D.
[10] D. Mascali, PhD Thesis, Catania University, February 2009. Download at http://www.lns.infn.it/

STUDIES OF THE ECR PLASMA IN THE VISIBLE LIGHT RANGE

S. Biri[1#], R. Rácz[1, 2], J. Pálinkás[1, 2]
[1]Institute of Nuclear Research (ATOMKI), Hungary, H-4026 Debrecen, Bem tér 18/c
[2]University of Debrecen, Hungary, H- 4010 Debrecen, Egyetem tér 1.

Abstract

High resolution visible light (VL) plasma photographs were taken at the ATOMKI-ECRIS by an 8 megapixel digital camera. Plasmas were generated from gases of He, methane, N, O, Ne, Ar, Kr, Xe and from their mixtures. The analysis of the photo series gave many qualitative and numerous valuable physical information on the nature of ECR plasmas. It is a further challenging task to understand the colors of this special type of plasmas. The colors can be determined by the VL electron transitions of the plasma atoms and ions. Through the examples of He and Xe we analyze the physical processes which effect the characteristic colors of these plasmas.

INTRODUCTION

ECR plasmas can experimentally be investigated by two significantly different ways. Small-size electrostatic electrodes (Langmuir-probes) give local information on certain plasma parameters (density, potential) [1]. The other method is based on the fact that the plasma emits radiation in the infra-red (IR), visible light (VL), ultra-violet (UV) and X-ray (XR) regions of the electromagnetic spectrum. The main drawback of this method is that the recorded information always corresponds to integration or superposition over a specific line-of-sight in the plasma volume. In spite of this, the analysis of photos and spectra in any of these regions has shown that spatial imaging gives important and new insight into the plasma structure. XR-photons come from the walls of the plasma chamber or from the highly charged plasma ions. VL-photons however dominantly originate from atoms and low-charged ions excited by the cold electrons. Thus studying VL plasma photographs transforms information mainly on the spatial position and density distribution of the cold electrons.

As a continuation or supplement of our earlier successful X-ray studies [2] we made series of high-resolution VL plasma photos and movies in the ATOMKI ECRIS Laboratory. In [3] the effect of the basic setting parameters (gas pressure, magnetic field, microwave power) to the shape, color and structure of Ne, Ar and Kr plasmas were studied. In [4] the shape and intensity distribution of the VL-plasmas are compared with computer simulations and with XR-photos. The results and information presented in these two papers improve the understanding the ECRIS plasma. In the present paper a study is given on the colors of the ECR plasmas.

#biri@atomki.hu

EXPERIMENTAL SETUP

The technical details and the application fields of the ECR ion source of ATOMKI are shown elsewhere [5, 6]. The homepage of the ECR Laboratory [7] stores also lots of information and photos. The ATOMKI-ECRIS had to be partly re-constructed in order to take direct photos from the injection side. The extraction optical system was removed. The beamline was closed with a quartz vacuum window to observe the plasma in-situ. A mirror was placed at a distance of 100 cm from the plasma chamber in 45° angle in order to set the observers and the camera at a safe perpendicular 40 cm distance from the mirror and from the axes of the ion source. Two microwave amplifiers (14.3 GHz klystron and 8-12 GHz TWT) were connected to be used simultaneously or individually. The axial magnetic field was usually set 80% of its maximum value in order to form closed resonance zones in a wide range of frequencies so the typical peak values of the magnetic field were 0.88 Tesla. The pressure (measured in the injection box) was $(2\ldots5)*10^{-5}$ mbar when only one gas was injected. This pressure value is more than one order of magnitude higher than the optimal one for the production of highly charged ions, but corresponds to produce high current, singly charged beams by this ion source.

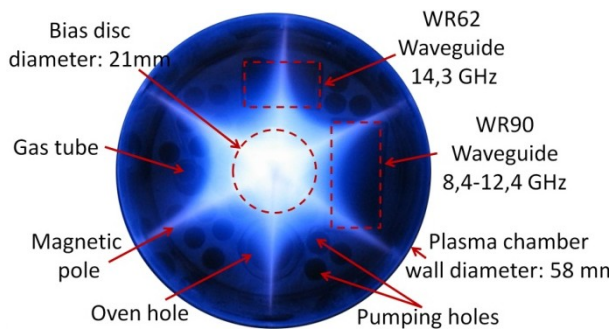

Figure 1. Typical axial image of the plasma. (Kr gas, microwave: 8.4 GHz, 10Wr, $2*10^{-5}$ mbar pressure) Plasma chamber, waveguides, bias disc, gas tube, oven hole, pumping hole can be seen.

When looking in the plasma chamber of an ECRIS the axial image of the plasma (Fig. 1.) in conformity with experimental setup can be seen. The photographs were taken by an 8 megapixel Canon digital camera. The ECR plasma is not an ideal photo model: its longitudinal length is about 20 cm, it is partly transparent and diffuse. To take systematically photo series we had to set manually the camera parameters. The typical exposure time was between 0.8 and 4 sec. Iris value was set to the maximum

R = 8 value. The minimum ISO value (80) was set to record the images with minimal noise.

After studying these photos and movies and observing the shape, structure and position of a high number of different kind plasmas, in one of our recent papers [3] we suggested that instead of "star" or "triangle" or "hexagon" the ECRIS-plasma would better be called "plasma-spider". Contrary to "normal" spiders this strange spider has only six legs: three at the injection side and another three at the extraction side, all originating from the middle plane region. The three arms or legs what we are seeing at both sides are fed by bunches of loss lines.

To obtain numeric information from such VL plasma pictures is possible only through the Analogue Digital Unit (ADU) values of pixels. ADUs store the color and intensity of the pixels.

THE COLOR OF THE PLASMAS

It is a challenging task to understand the color of different gas plasmas. We suppose that the plasma excitation is homogeneous throughout the VL region. The color of the plasma can be determined by visible light electron transitions (visible light energy spectrum) of plasma components (atoms and ions). According to the Schrödinger equation the excited atoms and ions emit photons with relative intensity and energy. Relative intensity of these spectral lines can be found in many handbooks. Through the example of Xenon and Helium we analyze the physical process which effects turquoise color of the Xenon plasma and pink color of the Helium plasma.

Fig. 2.a shows the VL-spectrum of the Xenon [8]. According to this spectrum we would expect violet or blue color Xenon plasma. However the human eye responds to electromagnetic radiation in the wavelength range from about 360 nm (violet) to 820 nm (red), with a peak sensitivity at near 555 nm (green). The detailed shape of this response curve depends on the individual person. Studies on representative samples of human subjects have led to adaption of a standard function relating the perceived brightness to the actual power of the spectral radiation.

This function (Fig. 2.b.) is the spectral luminous efficiency function, and it plays an important role in photometry. If we want to get real image from the color of the Helium and Xenon plasmas for the human eye, the intensity of the spectrum lines must be normalized with the spectral luminous efficiency function as it seen in Fig. 2.c.

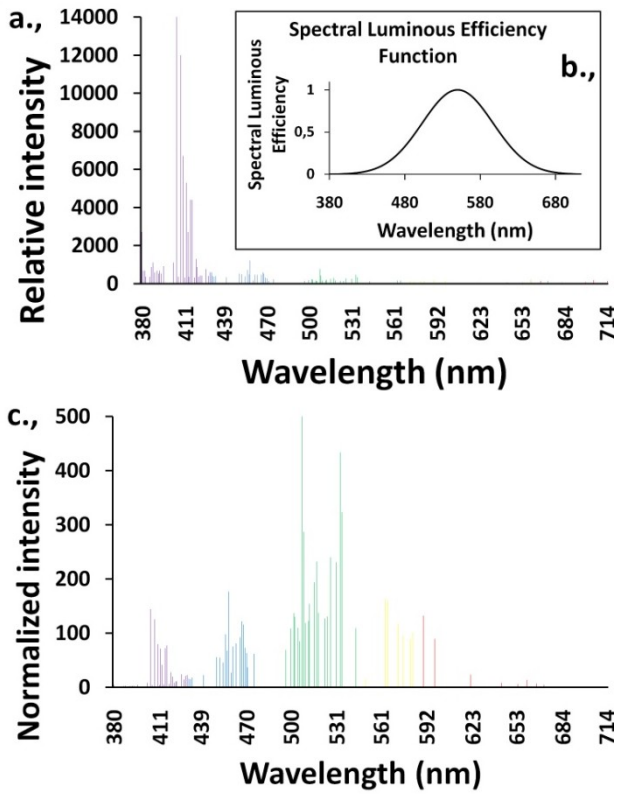

Figure 2. Xenon spectrum (a), the spectral luminous efficiency function (b) [8], Xenon spectrum normalized with spectral luminous efficiency function (c).

Any spectrum line assembly of a given gas can be decomposed to the primary colors (Red, Green, and Blue). Fig. 3.a. and 3.d. shows the decomposed spectrum [8] lines of Xenon and Helium. The normalized spectrum lines (like Fig. 2.c. in case of Xenon) were also decomposed to the primary colors and after that we got the complex light RGB values in case of Xenon and Helium (Fig. 3.b. and 3.e.). According to the Young-Maxwell-Helmholtz trichromatic theory (additive color mixing) calculated colors were created by a color mixing program using the RGB values. Fig. 3.c. and 3.f. show the Xenon and Helium plasma photos taken by us and the decomposed RGB values of these photos. There is a good visual agreement between the calculated normalised color and the real color of the plasmas and also between the RGB values of the decomposed normalized spectrum lines and of the photos. Thus this process is able to explain the color of ECR plasmas.

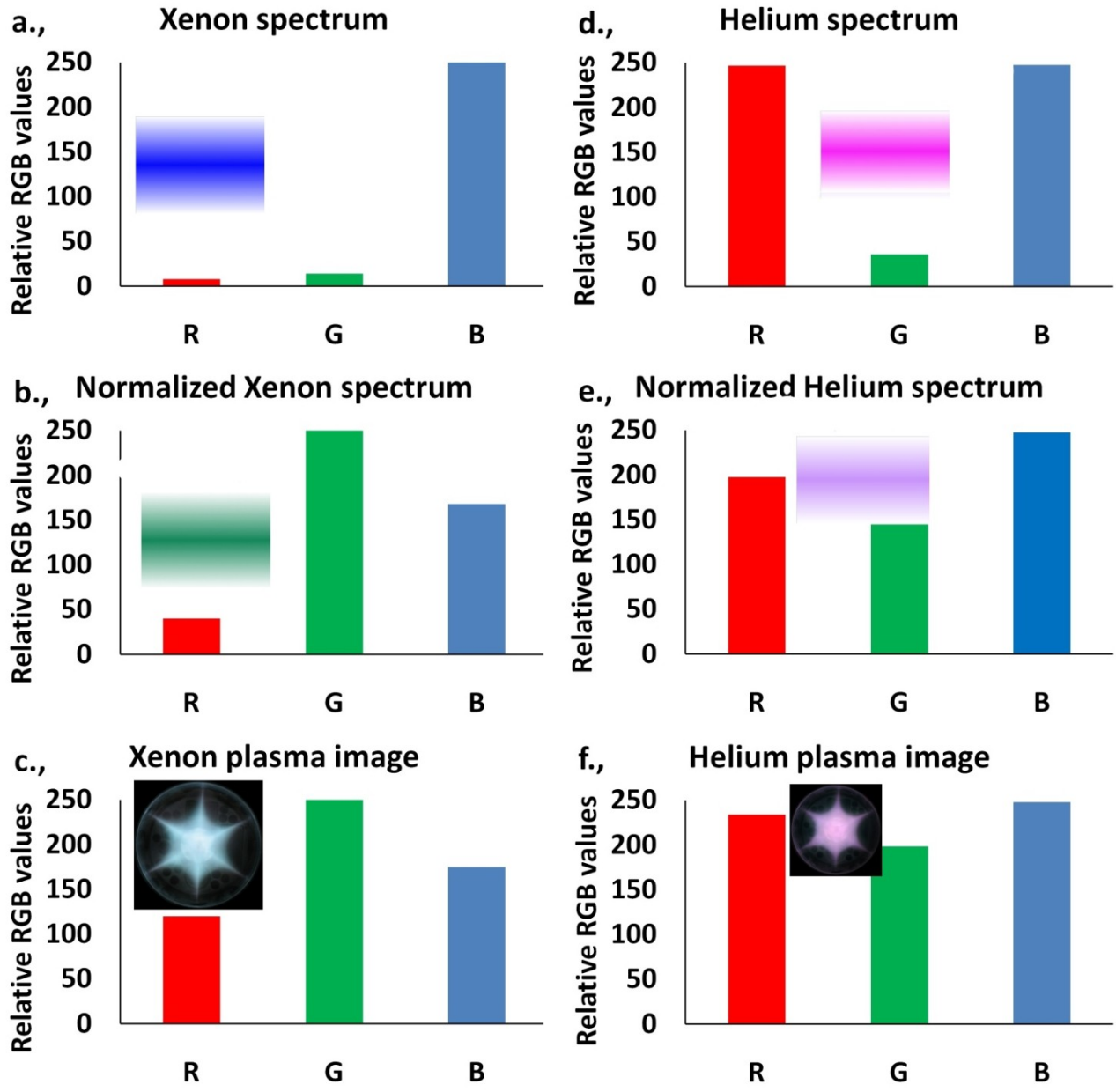

Figure 3.The original spectrum lines of Xenon (a) and Helium (d) and the normalized lines were decomposed to the primary colors (b, e) to get the RGB values. The insections show the superposition of the RGB values (a, d, b, e). 3.c. and 3.f. show the original Xenon and Helium plasma photos and the RGB values of these photos.

REFERENCES

[1] L. Kenéz, S. Biri, J. Karácsony, A. Valek, Nucl. Instrum. Methods B**187** (2002) 249-258.
[2] S. Biri, A. Valek, T. Suta, E. Takács, Cs. Szabó, L. T. Hudson, B. Radics, J. Imrek, B. Juhász, and J. Pálinkás, Rev. Sci. Instrum. **75** (2004) 1420.
[3] R. Rácz, S. Biri, J. Pálinkás, Rev. Sci Instrum. **81** (2010) 02B708.
[4] R. Rácz, S. Biri, J. Pálinkás, submitted to Plasma Sources Science and Technology, 2010.
[5] S. Biri, J. Vámosi, A. Valek, Z. Kormány, E. Takács, J. Pálinkás, Nucl. Instrum. Methods B**124** (1997) 427
[6] S. Biri, I. Iván, Z. Juhász, B. Sulik, Cs. Hegedűs, A. Ifj. Jenei, S. Kökényesi, J. Pálinkás, Proceedings of the 18th International Workshop on ECRIS Chicago, Ill. USA, 15-18 Sept., 2008. 41-47
[7] www.atomki.hu/ECR
[8] D. R. Lide (editor), CRC Handbook of Chemistry and Physics (CRC Press, London, 2008-2009)

BREMSTRAHLUNG AND ION BEAM CURRENT MEASUREMENTS WITH SuSI ECR ION SOURCE *

T. Ropponen†, D. Cole, G. Machicoane, A. Stolz, L. T. Sun, L. Tobos
National Superconducting Cyclotron Laboratory, Michigan State University

Abstract

The Superconducting Source for Ions (SuSI) [1] at the National Superconducting Cyclotron Laboratory at Michigan State University is a fully superconducting 3rd generation ECR ion source currently operated with two 18 GHz klystrons. The axial magnetic field is generated by six solenoid magnets which allow to control the magnetic field characteristics, such as resonance locations, mirror ratios and magnetic field gradients, almost independently. In this paper we will focus on the measurements done with different collimation geometries and we will show results comparing FlatB and normal Bmin operation. We will also discuss about the effect of different magnetic field gradients while keeping the length of the plasma and value of B_{min} as constants.

MEASUREMENT SETUP AND MAGNETIC FIELD PROFILES

The bremsstrahlung measurements presented in this paper are steady state high energy measurements. The bremsstrahlung events were recorded axially through the diagnostic port of the analyzing magnet using an Ortec p-type germanium detector. A small solid angle for the detection of bremsstrahlung was achieved using two collimators separated by 445 mm. Each collimator was made of lead for the outer parts and tungsten for the inserts. The layout of the collimator structure is presented in figure 1. The area at the extraction aperture of SuSI that was seen by the detector was about ⌀ 7 mm while SuSI plasma electrode has an opening of ⌀ 10 mm. In addition to these two collimators the existing lead shielding in the ECR area was put to use in order to decrease the amount of scattered radiation. First, a stand-alone lead shielding plate (25 mm of Pb, 6 mm of steel) positioned between the two collimators was used during the measurements. Second, the ECR area is confined using several large lead panels (13 mm of lead, 6 mm of steel) and one was positioned between the second collimator and the Ge detector. A 5 mm hole was drilled through both the shielding plate and the lead wall panel to allow the radiation to reach the detector. The distance from the plasma electrode to the detector was about 3.2 m. Figure 2 presents the general layout of the measurement setup.

The collimators were aligned through the injection flange using a laser and ^{133}Ba and ^{152}Eu sources were used for energy and relative efficiency calibration. Energy resolution of the setup was 2.14 keV at 80.997 keV, 2.97 keV at 443.965 keV and 6.15 keV at 1085.842 keV. Measurement time was fixed to 30 min per set and typical count rates at the detector varied between 2 kHz and 75 kHz. Background radiation has been subtracted from the data presented in this paper.

The measurements were conducted using analog NIM, CAMAC and VME electronics. The electronics is divided into two branches — the so-called slow branch for energy and the fast branch for timing information. Due to this arrangement, the system is capable of detecting pile-up events. Shaping time of the linear amplifier was set to 3 μs and the signal width was roughly 6 μs. When two or more

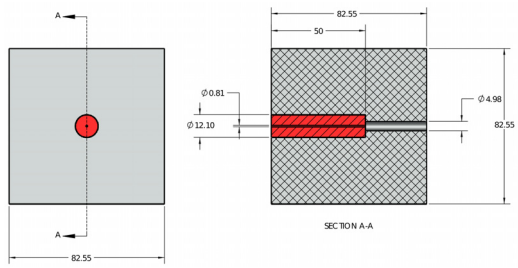

Figure 1: Cross-section view of the collimator structure. Both collimators that were used in the setup are identical. Lead is marked with gray color and tungsten insert with red. Dimensions are given in inches.

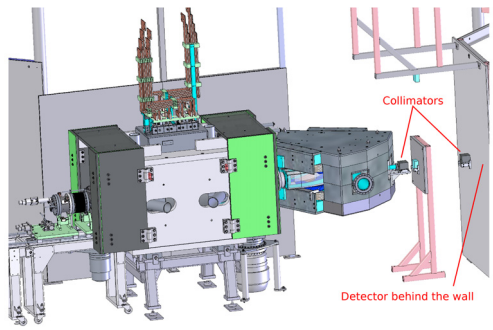

Figure 2: Layout of the measurement geometry. The first collimator is located next to the bending magnet flange (glass window) and the second one is attached to the ECRIS room wall. The stand-alone Pb shield is seen between the collimators. The detector was located behind the wall and was shielded with Pb blocks in order to decrease the background levels.

* This work was supported by the National Science Foundation under Grant No. PHY-0110253
† ropponen@nscl.msu.edu

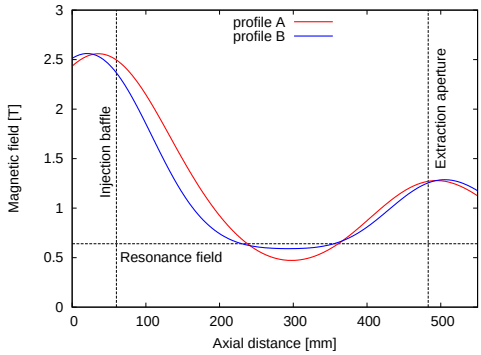

Figure 3: Magnetic field profiles for flatB and normal Bmin operation. See table 1 for details. Note that there is a difference of 0.1 T in the magnetic field at the injection baffle position.

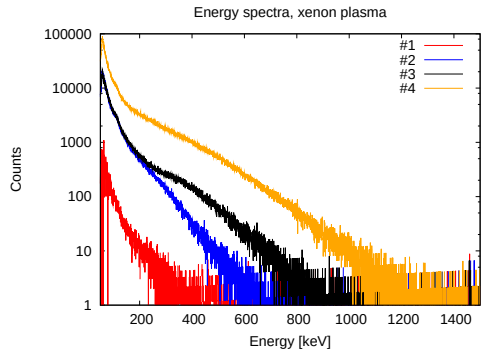

Figure 4: Energy spectra with different collimation geometries: #1 all collimators, #2 collimator at the dipole is removed, #3 Collimator at the dipole, Pb blocks inside the dipole and the stand-alone Pb shield are removed, #4 all the collimating elements except the Pb wall are removed. See also fig. 2.

Table 1: Axial magnetic field profile details. Resonance locations are given in same coordinates that are used in figure 3.

#profile	gradB (inj, ext)	plasma length	res. location (inj, ext)
A	-5.73 T/m, 5.01 T/m	124.5 mm	237.3 mm, 361.8 mm
B	-2.19 T/m, 2.25 T/m	127.1 mm	229.1 mm, 356.1 mm
C	-5.19 T/m, 4.75 T/m	125.4 mm	237.8 mm, 363.2 mm
D	-6.38 T/m, 5.39 T/m	124.3 mm	236.1 mm, 360.4 mm

events were observed within 20 μs they were considered to be pile-up events. The charge state distributions (CSDs) were recorded after the SuSI collimation channel [2].

For the FlatB measurements described in this paper we used the magnetic field profiles shown in figure 3. Field profile #A is used as a reference field and it is a starting point to normal operation with SuSI while producing medium charge states at 18 GHz. Position of the injection baffle, which was kept as constant during the measurements, the extraction aperture position and the resonance field for 18 GHz is marked in these figures. Value of 0 mm refers to the location of the entrance face of the first solenoid. The details of the profiles can be seen in table 1. The radial field was kept constant between measurement sets.

DIFFERENT COLLIMATION SCHEMES

The collimation scheme that was used in the measurements limits the area that the detector sees within the extraction aperture of SuSI. This means that we were mostly measuring radiation coming directly from the plasma processes and also some back-scattered radiation from the injection. We studied the effect of different collimation schemes and removed the collimators and additional shielding one-by-one increasing the area which the detector can observe. Energy spectra from this study, recorded using 1200 W of RF power and magnetic field profile #A, is presented in figure 4. The diameters of the circular areas at the extraction aperture position seen by the detector are roughly the following #1: 7 mm, #2: 62 mm, #3: 83 mm and #4: 4.7 m. It is noted that with collimation #4 the solid angle defined only by the hole in the Pb wall exceeds the size of the Ge crystal significantly at the location of the detector. Thus, the detector cannot observe all the radiation coming through the aperture. The endpoint energies presented in this paper are estimated by the eye due to the difficulties of obtaining endpoint energy from measurement data that is not entirely linear even at logarithmic scale.

With collimation #1, when the detector sees only the plasma, the endpoint energy of the spectrum lies a bit lower than 400 keV. With #2 we are observing roughly 650 keV and with #3 the endpoint energy is about 850 keV. When the last movable collimator is removed the endpoint energy rises to around 1200 keV. The difference between #1 and #2 is clearly the difference between just the plasma bremsstrahlung and the bremsstrahlung coming from the plasma and from the high energy electron losses towards the extraction. The difference between #2 and #3 is assumed to originate from the decreased shielding for scattered high energy radiation. With #4 the effect of collimation is almost non-existent and detector records both high count rates and energies over 1 MeV. It is clear, that the effect of the different collimation schemes is significant. Thus, if only the plasma bremsstrahlung is wanted to be studied a very tight collimation (within the extraction aperture) must be used. Comparing #2 and #3 reveals also the well-known issue concerning the impact of the scattered radiation on the shape of the spectrum.

In figure 5 the data from #4 is presented with and without efficiency correction and pile-up rejection. It is seen that the efficiency calibration has a clear impact on the shape of the low energy (0–120 keV) part and a smaller, but noteworthy, impact on the high energy (300 keV and higher) part of the spectrum. The efficiency calibration can thus

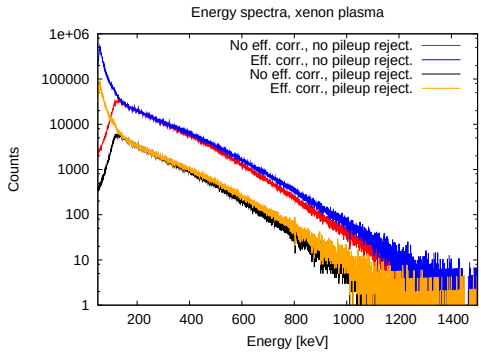

Figure 5: Energy spectra #4 (see fig. 4) with and without detector efficiency calibration and pile-up rejection.

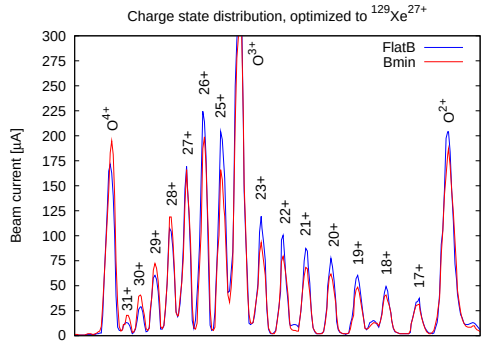

Figure 6: Xenon charge state distribution with normal B-min (profile #A) and Flat-B (profile #B) magnetic field profiles.

affect for example estimates for endpoint energies and values for spectral temperature (see table 2). The pile-up rejection does not seem to have such a clear impact on the slope i.e. spectral temperature but the endpoint energy can change significantly. In the case of this example (fig. 5), the endpoint energies change roughly from 1430 keV to about 1230 keV when the pile-up rejection is applied. Similar change (around 65 keV) is also observed with #1 (data not presented here). Count rates for background and measurement #1 were comparable, which means that pile-up rejection can be important also at low count rates.

FLATB VS. BMIN OPERATION

By tuning the SuSI magnetic field to very low gradients one has to accept the change of axial length of the plasma and B_{min} (see fig. 3). During this study the plasma length was varied from 124.5 mm to 127.1 mm with magnetic field profiles #A and #B, respectively. SuSI is capable of generating even lower gradient field profiles, but we choose not to use such a profile due to extremely high radiation levels. While the radiation monitor observing X-rays at the SuSI's extraction reported 6.1 mR/h with B-field profile #A (1500 W/18.0 GHz + 350 W/17.8 GHz) the level went up to 50 mR/h with profile #B with the same RF powers. When we tested a profile with even lower magnetic field gradient (0.79 T/m both injection and extraction) the radiation levels exceeded 31 mR/h already at 700 W. In addition to high radiation levels, it was observed that the plasma was very unstable and the source very sensitive to tuning, compared to normal Bmin operation, whenever a FlatB profile was used.

The charge state distributions of xenon plasma with oxygen as a support gas are presented in figure 6 and the corresponding bremsstrahlung spectra are shown in figure 7. It was found out that similar amounts of $^{129}Xe^{27+}$ beam current could be extracted when SuSI was tuned to Xe^{27+} with both profiles keeping the RF power constant. From the CSD it can be seen that during the FlatB operation slightly more low and medium charge states but less high charge

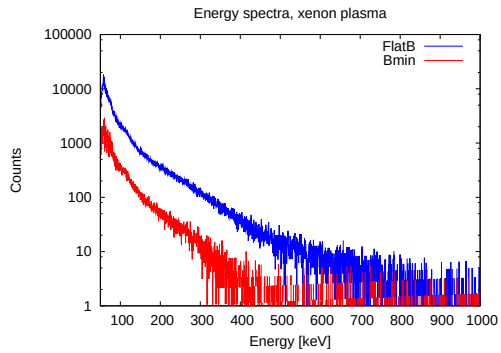

Figure 7: Energy spectra with normal Bmin (profile #A) and FlatB (profile #B) magnetic field profiles.

states are observed compared to Bmin operation. The difference can arise from the difference in the injection magnetic field (a slightly lower confinement with FlatB operation, see fig. 3) or from the magnetic field profile/gradient (differences in electron energy distribution). During the measurements the drain current of the source was relatively constant (4.4 mA and 4.5 mA with FlatB and Bmin, respectively) and the leak valve setting ratio between xenon and oxygen feed was 0.75 in both cases meaning that the gas mixing ratio was not playing a major part on the shape of the CSDs. Extraction pressures of 8.2e-8 and 9.5e-8 torr were recorded with FlatB and Bmin, respectively. By looking at the bremsstrahlung emission from figure 7 it is clear that the FlatB operation produces both higher count rates and significantly higher endpoint energies. It can be estimated that with FlatB operation the endpoint energies are in the area of 850 keV while with the normal Bmin operation the energies are below 450 keV. While the 2 mm Ta shield used around SuSI plasma chamber can decrease the radiation load of less than 400 keV photons effectively, it becomes more transparent to higher energies which are plenty in the FlatB operation. See table 2 for spectral temperatures.

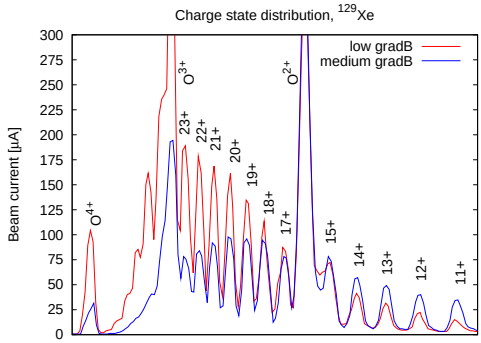

Figure 8: Xenon charge state distribution with different magnetic field gradients.

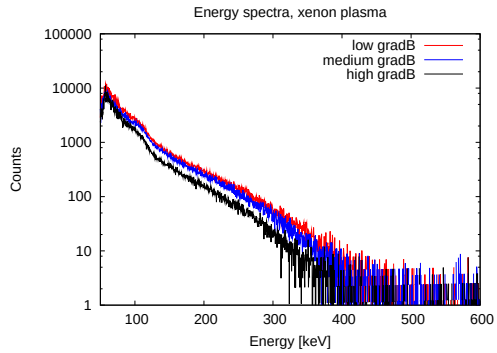

Figure 9: Energy spectra with different magnetic field gradients.

DIFFERENT GRADIENTS WITH FIXED PLASMA LENGTH AND B_{MIN}

The magnetic field gradient in the resonance zone can be tuned in SuSI within certain limits while other field characteristics are kept almost fixed. Plasma length varies only 1.1 mm between the different profiles and the maximum deviation in the B_{min} is 0.039 T. The ion source was tuned to $^{129}Xe^{20+}$ using the medium gradient (profile #A) and 1500 W of RF power. The source settings other than the magnetic field profile were not changed while using low (profile #C) and high (profile #D) gradient profiles.

The CDSs for medium and low gradient are shown in figure 8 where it can be seen that while the CSD is peaked at 20+ with the medium gradient profile the CSD is significantly different and peaking at 23+ when the gradient is lowered. Beam currents of charge states higher than 17+ are clearly increased and the beam intensity at 23+ is roughly 2.5 times higher. Drain currents were 5.0 mA in both cases and extraction pressures of 1.6e-7 and 1.4e-7 torr were recorded with medium and low gradient profiles, respectively. This suggests that while the source settings were kept relatively constant only very small changes in the magnetic field gradient can create significantly different plasma conditions.

Figure 9 shows that the count rates at the low energy part are roughly similar while there is a clear difference above 75 keV. The endpoint energies are 405 keV, 435 keV and 470 keV for high, medium and low gradient, respectively. For spectral temperatures, see table 2. As previously has been observed (see e.g. [3, 4]), the lower the gradient the higher the count rate, the endpoint energy and the spectral temperature. With these previous measurements the change in the magnetic field gradient also meant changing the B_{min} and length of the plasma. Because the length of the plasma and value of B_{min} were kept roughly constants in our measurements, it is experimentally confirmed for the first time that the value of the magnetic field gradient alone plays a major role especially in the ion beam and also in the radiation production.

DISCUSSION AND CONCLUSIONS

In the measurement described in this paper we have presented the importance of the efficiency correction and pile-up rejection event at very low count rates. We have also shown that while the FlatB operation can produce similar ion beam currents than normal Bmin operation, the radiation levels and photon energies are significantly higher if FlatB mode is used. This results into higher heat loads to cryostat systems. We also demonstrated that a slight change in the magnetic field gradient can significantly change the ion beam production when the length of the plasma and B_{min} are not changed. These observations favor constructing ECR ion sources with flexible axial magnetic field structures found at the moment only in SuSI and in SC-ECRIS in Riken [5].

Table 2: Spectral temperatures and endpoint energies [keV] for the different measurements. Fitting ranges for spectral temperatures are given in each section of the table.

different collimations, #4 (fig. 5) (fit range 600–800 keV)

no eff. corr. no pile-up reject.	eff. corr. no pile-up reject.	no eff. corr. pile-up reject.	eff. corr. pile-up reject.
118.9±0.6	129.9±0.7	117.7±1.3	128.5±1.5
1340±30	1430±30	1140±30	1230±30

FlatB vs. Bmin (fig. 7) (fit range 130–200 keV)		gradB (fig. 9) (fit range 130–200 keV)		
FlatB	Bmin	low gradB	medium gradB	high gradB
68.1±1.1	58.0±1.7	60.1±0.9	57.8±0.8	56.4±0.9
850±20	450±20	470±20	435±20	405±20

REFERENCES

[1] P. A. Zavodszky *et al.* Rev. Sci. Instrum. 77, 03A334 (2006).

[2] G. Machicoane *et al.* Conference presentation, ICIS2009 (2009).

[3] D. Leitner *et al.* Rev. Sci. Instrum. 79, 033302 (2008).

[4] T. Ropponen *et al.* Nucl. Instr. and Meth. A 600, p. 525–533 (2009).

[5] T. Nakagawa *et al.* Rev. Sci. Instrum. 81, 02A320 (2010).

MAXIMUM BREMSSTRAHLUNG ENERGY VERSUS DIFFERENT HEATING LIMITS*

H. Koivisto#, V. Aho, V. Toivanen, O. Tarvainen, P. Jones, J. Saren, P. Peura JYFL, Jyväskylä, Finland

Abstract

A comprehensive set of bremsstrahlung measurements has been performed at JYFL (University of Jyväskylä, Department of Physics) in order to understand the parameters affecting the heating of electrons. In order to extend the understanding of electron heating, a new set of measurements with the JYFL 6.4 GHz ECRIS has been conducted to study the parameters affecting the maximum bremsstrahlung energy. During the work the effects of microwave power and magnetic field were studied. The analysis of the experimental data focuses in comparing the results with theoretical stochastic electron heating limits.

INTRODUCTION

In addition to the high requirements for the magnetic fields in 3rd generation superconducting ECR ion source the total microwave power fed into the plasma chamber can be even 10 kW. Consequently, these operation conditions results in intensive bremsstrahlung emission, which gives an extra heat load to the cryostat. It has been attempted to decrease the load by increasing the x-ray shielding as has been done for example for VENUS at LBNL, Berkeley using 2 mm tantalum sheet. However, due to the very limited space the thickness of the shielding must be small and thus practically transparent to the high-energy part of photon spectrum.

Experiments studying the parameters affecting the bremsstrahlung emission have been performed in several laboratories. In addition, different simulation codes have been developed to model the electron heating process. The research work has clearly shown that the magnetic field structure has a strong effect on the energy of the bremsstrahlung emission. It is explained that this is due to the lower magnetic field gradient in the heating zone, which improves the heating efficiency. As an example, the measurements at Berkeley showed that the end-point energy of the photon emission almost doubled when the B_{min} of the VENUS was increased from 0.44 T to 0.64 T having total microwave powers of 8.8 kW and 6 kW, respectively [1]. It has also been shown that the microwave power increases both the end-point energy and especially the yield of the photon emission. The build up of hot electron population in ECRIS plasma has been studied also by S. Gammino et al. [2] using Canobbio theory where maximum energy W_{max} can be expressed as $W_{\max}(eV) = 1.5 \cdot 10^9 (E(V\,cm^{-1})/\omega_0)^{2/3}$. In this equation E is the electric field, ω_0 the microwave frequency and it is assumed that the ECR heating takes place in a so-called low gradient regime.

*Work supported by the Academy of Finland and Magnus Ehrnrooth foundation.

hannu.koivisto@phys.jyu.fi

These problems and observations gave a motivation to study the bremsstrahlung emission of an ECRIS also at JYFL. The objective of the work is to study parameters affecting the high-energy bremsstrahlung radiation. This work includes developing a hybrid simulation code [3], time resolved bremsstrahlung experiments (see e.g. [4]), and as a recent effort studying the parameters affecting the end-point energy of photon emission in continuous operation mode. In this article we present some results obtained when the ion source parameters affecting the end-point energy of bremsstrahlung radiation in steady state conditions have been varied. The results were compared to a stochastic heating limit theory in order to get more insight in the possibilities affecting the production of bremsstrahlung.

STOCHASTIC HEATING LIMITS

The ECR heating is considered to be stochastic if the phase between the electron and the wave is random in consecutive passes of resonance regions. When the electron gains energy the time between the successive passings of the resonance region decreases resulting to eventual loss of phase randomization, i.e. heating is not stochastic anymore. However, the energy can be increased even further until so-called adiabatic heating limit is reached. In this work the maximum bremsstrahlung energy produced by the JYFL 6.4 GHz ECRIS has been compared to the stochastic heating theory presented in ref. [5]. The theory states that the stochastic heating limit can be expressed as

$$W_s = 0.2\left[m_e L\left(1+\frac{l^2}{L^2}\right)\right]^{1/4} l\omega^{1/2}(eE)^{3/4} \qquad (1)$$

where E is the electric field of the microwaves at the resonance, $\omega = 2\pi f$ (f is the microwave frequency), m_e the mass of the electron, e is the unit charge, L is a parameter, which can be calculated from the axial magnetic field profile ($B = B_{\min}(1+z^2/L^2)$), where the resonances are at z = ± l. Here B_{min} is the minimum magnetic field and z the axial distance from this minimum. Adiabatic heating limit is defined to be $W_a = 5W_s$. With the aid of equation (1) the effect of electric field E (related to microwave power), gradient of the magnetic field B, microwave frequency f and axial distance l of resonance points (from B_{min}) on the adiabatic and stochastic limits can be studied. The *gradB* has been calculated from the magnetic field profile equation shown above. In this consideration the relativistic effect, power absorption and mode structure behaviour are neglected.

Figure 1 shows the adiabatic heating limit as a function of the electric field of microwaves at the resonance. The calculations correspond to typical operation parameters of

the JYFL 6.4 GHz ECRIS, i.e. *gradB = 1.5 T/m*, B_0 = 0.178 T and length *l* = 69 mm. Figure shows that using these values the typical experimental maximum bremsstrahlung energy of about 400 keV is reached with the electric field of about 1000 kV/m. The effects of length *l* and *gradB* on the adiabatic limit have been studied using this value for the electric field E. The effect of frequency *f* is omitted because of fixed frequency.

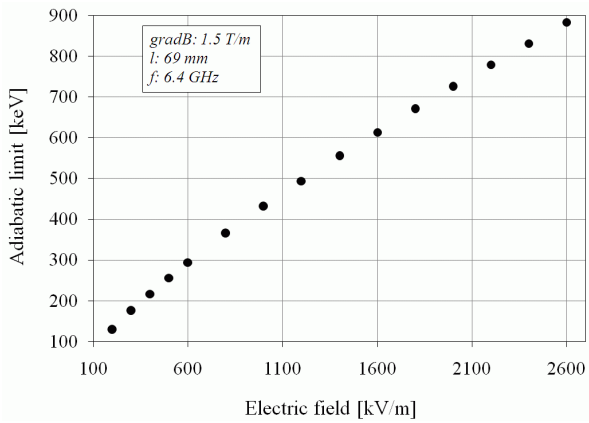

Figure 1: Adiabatic heating limit as a function of electric field *E* in the heating region.

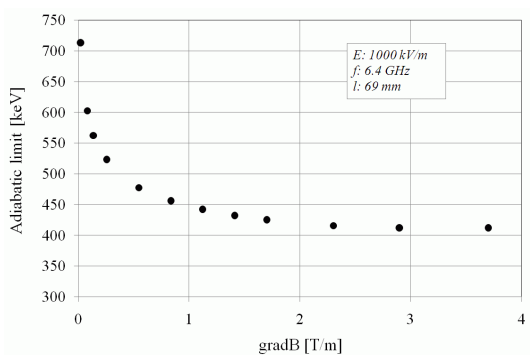

Figure 2: Adiabatic heating limit as a function of *gradB*.

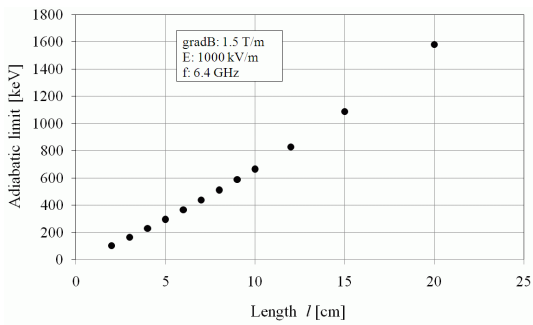

Figure 3: Adiabatic heating limit as a function of length *l* (*l* = distance between B_{min} and resonance zone).

Figure 2 shows the adiabatic heating limit as a function of *gradB* in the resonance region. The behaviour shows that the adiabatic limit starts to increase vigorously with relatively low values of *gradB*. However, these values are not reached in the resonance with the typical magnetic field settings of the JYFL 6.4 GHz ECRIS. The values of electric field *E*, frequency *f* and length *l* were kept constant resulting in unoptimized B_{min}/B_{res} -values (from 0.44 to 0.99). Figure 4 shows that the plasma size has a strong effect on the adiabatic heating limit. The 3rd generation ECR ion sources tend to have relatively large dimensions of the magnetic field, which can also explain the increase of measured bremsstrahlung energies. The larger distance between the resonances makes it possible to maintain stochastic heating at higher energies.

EXPERIMENTS

As Equation (1) shows four parameters are affecting the adiabatic heating limit in the heating region: electric field *E*, microwave frequency *f*, *gradB* and plasma size related length *l*. The validity of Eq. (1) was studied by extracting the end-point energies of the wall bremsstrahlung spectra produced by the JYFL 6.4 GHz ECRIS. The collimated photon emission was measured in the radial direction using Ge-detector. In reality this is not a true parametric study because it is virtually impossible to change only one parameter. For example, the changes in the magnetic field affect *gradB*, length *l* and consequently the electric field *E* simultaneously. In addition, the equation does not take into account the relativistic effect, which affects the effective length of *l* and *gradB* of the high-energy electrons. The heating can be limited also by the value of the maximum magnetic field and due to the increase of plasma density as a function of microwave power.

Figure 4 shows the experimental end-point energy of bremsstrahlung spectrum as a function of microwave power. As a comparison it also shows the heating limits estimated using Equation (1). The theory overestimates the adiabatic limit as can be seen in Figure 4. This might be due to the fact that the absorption of the electromagnetic wave in the resonance is not included. A new estimation was done starting with the Poynting vector and by including the Budden tunneling factor $P_t/P_0 = e^{-\pi\eta}$ for transmitted power, i.e.

$$E = Q\sqrt{\frac{2P_0 e^{-\pi\eta}}{\varepsilon_0 c \pi r^2}} \qquad (2)$$

where *r* is the radius of plasma chamber, *Q* is the quality factor and $\eta = n_e/(\epsilon_0 c|dB/dz|_{res}) = \alpha n_e$. The equation shows that the power absorption improves when *gradB* decreases. The measurements have shown for the ion source settings presented in Figure 4 that the bias disk current is proportional to $P^{0.27}$, where *P* is the microwave power. The power of *P* slightly varies with the operation parameters of the ion source. Now, assuming that the plasma density n_e is proportional to the bias disk current (i.e. $n_e = aP^{0.27}$, where *a* is the fitting parameter) and that stochastic limit W_s in Eq. (1) is proportional to $E^{3/4}$ the final form of the maximum energy is

$$W_{max} = AP^{3/8}e^{-BP^{0.27}} \qquad (3)$$

where A = 95 and B = 3πα*a*/8 = 0.16. As Figure 4 shows the fitting follows very closely the experimental data points if the power absorption of the electromagnetic

wave is included. In this treatment the constant Q value is assumed for simplicity.

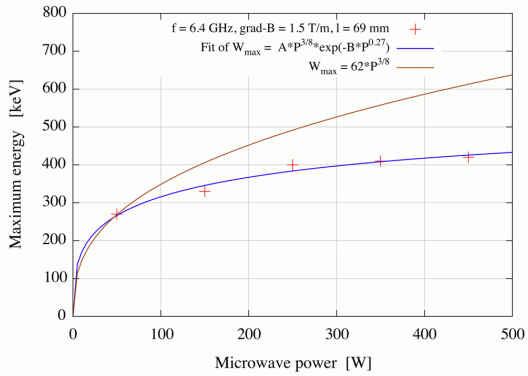

Figure 4: Maximum bremsstrahlung energy as a function of microwave power *P*.

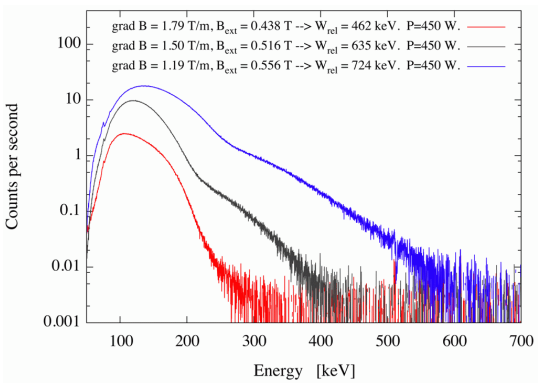

Figure 5: Effect of magnetic field settings on the bremsstrahlung energy and count rate.

Figure 5 shows the bremsstrahlung spectra for three different magnetic field configurations and Table 1 shows the corresponding data. As figure shows both the photon emission and the maximum energy increase when the B_{min} increases, i.e. the highest $W_{end\text{-}point}$ and the photon emission intensity are obtained with the lowest *gradB* value. However, in the case of conventional ECR ion source it is impossible to change only the *gradB*. Instead, the length *l* is also changed. In addition, it is possible that the electric field *E* is also changed due to changes in the plasma parameters. Consequently, the experiment cannot be used to define if the increased $W_{end\text{-}point}$ energy is caused because of decreased *gradB*. As Table 1 shows the equation (1) fails to predict the maximum energy seen in the bremsstrahlung spectrum (compare $W_{end\text{-}point}$ and W_a). This is discussed in the discussion chapter.

Table 1: Table shows the data corresponding to Figure 5. The energies $W_{end\text{-}point}$ are estimated from spectra shown in Figure 5, W_a is the adiabatic heating limit and $W_{rel,max}$ is the energy corresponding to resonance at B_{ext}.

$gradB_{res}$ [T/m]	B_{min} [T]	B_{ext} [T]	*l* [mm]	$W_{end\text{-}point}$ [keV]	W_a [keV]	$W_{rel,max}$ [keV]
1.19	0.199	0.556	52.4	620	322	724
1.50	0.178	0.516	68.9	420	431	635
1.79	0.146	0.438	94.6	310	619	462

DISCUSSION

As Figures 5 and Table 1 show the equation (1) fails to estimate the maximum energy of bremsstrahlung spectrum. By increasing the Bmin field the gradB has been decreased. According to the consideration based on Equation (1) this should increase the end-point energy of bremsstrahlung spectrum. This agrees with the experiments. However, at the same time the size of the plasma, i.e. length l, has decreased substantially as is presented in Table 1. Consequently, the calculated adiabatic heating limit Wa decreases, which disagrees with the experiments. One possible explanation is that the equation does not include relativistic effects.

In the case of high electron energies the mass has increased and consequently the resonance takes place at higher magnetic field values. This means that the distance between B_{min} and B_{res} for relativistic electrons increases. Due to the larger distance between the resonances the heating remains stochastic with higher electron energies – as is supposed by Eq. (1). In this consideration we have focused only on the extraction side of the JYFL 6.4 GHz ECRIS for two reasons: 1) $B_{ext} \leq B_{rad} < B_{inj}$, i.e. the extraction side limits the size of the maximum closed resonance surface and 2) the radial magnetic field profile cannot be estimated using Equation (1) because in the radial direction there are the components of axial and radial magnetic field. For the settings shown in Fig. 2 the distance between the B_{min} and B_{res} has increased from 68.9 mm for cold electrons to 132 mm for the 300 keV electrons. By increasing the energy further the resonance finally takes place at the extraction of the source and consequently the fixed maximum length l = 210 mm has been reached. This also corresponds to largest closed resonance surface. The energy corresponding to resonance at B_{ext} has been denoted by $W_{rel,max}$ in Table 1. If in Eq. (1) it is justified to use the length *l* for relativistic electrons the heating limit increases substantially as can be seen in Fig. 3. As a result it is possible that the adiabatic heating limit is not reached with the JYFL 6.4 GHz ECRIS because the maximum energy is limited by the magnetic field structure. It should be noticed also that if the relativistic length *l* is used much lower electric field of microwaves is needed to reach the same experimental end-point energy. For example, the energy of about 400 keV is reached with the electric field of the order of 100 – 200 kV/m if the length of l = 210 mm is used.

REFERENCES

[1] D. Leitner et al., Rev. Sci. Instrum. 79, 033302, (2008).
[2] S. Gammino et al., Plasma Source Sci. Technol. 18, 045016 (2009).
[3] T. Ropponen, Thesis, JYFL Res. Report No. 1/2010, https://www.jyu.fi/fysiikka/en/studies/theses/theses2010.html.
[4] T. Ropponen, et al., Nucl. Instrum. Meth. A, Vol 600 (3), p. 525, (2009).
[5] N.C. Wyeth, A. J. Lichtenberg and M.A. Lieberman, Plasma physics, Vol. 17, p. 679, (1975).

COMMISSIONING OF THE ECRIS CHARGE STATE BREEDER AT TRIUMF

F. Ames, R. Baartman, P. Bricault, K. Jayamanna, TRIUMF, 4004 Wesbrook Mall, Vancouver, BC, V6T 2A3, Canada
T. Lamy, LPSC UJF-CNRS/IN2P3-INPG, 53 Rue des Martyrs, 38026 Grenoble, France

Abstract

Radioactive isotopes produced at the ISOL facility ISAC at TRIUMF are usually extracted as singly charged ions from the target ion source system. If the mass of these ions exceeds A=30 their acceleration requires breeding to highly charged ions. A modified version of an electron cyclotron ion source (ECRIS) charge state breeder (14.5 GHz PHOENIX from Pantechnik) has been installed and a first on-line test resulting in the successful acceleration of $^{80}Rb^{14+}$ has been performed already in 2008. During the radioactive beam time periods of 2009 and 2010 further measurements with stable and radioactive ions from different target ion source combinations have been performed to further commission the system. Breeding efficiencies of several percent in the maximum of the charge state distribution have been achieved. A major problem for experiments using those beams is the background from residual gas and other ions, which are also produced in the ECR charge state breeder and which result in similar mass to charge ratios than the radioactive isotope.

INTRODUCTION

At the ISAC radioactive ion beam facility at TRIUMF radioactive ions are produced by bombarding solid targets with up to 100 μA of protons from TRIUMF's 500 MeV cyclotron. The target material is operated at high temperature to allow fast diffusion and effusion of the reaction products into an ion source. Mainly singly charged ions are extracted [1]. The desired isotopes are separated with a magnetic mass separator and the ion beam can be transported to low energy experiments at an energy of several 10 keV or injected into a post accelerator for serving high energy experiments. The intensity of the radioactive ion beam covers a broad range from single ions for the most exotic ones up to about 10^9 per second for isotopes close to stability. The acceptance of the post accelerator allows a maximum A/q value of 30. However, this applies only to the first accelerator stage, a 4 rod radio frequency quadrupole (RFQ), which accelerates to 150 A keV. The following drift tube and superconducting cavity sections are able to accelerate ions up to 5 A MeV. They require A/q<7. Up to now this has been achieved by a stripping foil after the RFQ. If additional losses from this stripping process, which becomes less efficient for heavy ions, are to be avoided the charge breeding should directly lead to A/q<7.

Charge state breeding with an ECRIS has been chosen because of its capability to work efficiently in a continuous mode and because of the high charge capacity, which allows the charge state breeding of high intensity ion beams.

SET – UP OF THE SYSTEM

A modified version of a 14.5 GHZ PHOENIX booster from Pantechnik has been installed in a shielded area directly after the mass separation of the radioactive ions. They can be directed to the charge breeder source via a movable electrostatic deflector. The PHOENIX source is operated at a high voltage close to the one of the on – line ion source, so that singly charged ions are decelerated and stopped in the plasma. After extraction of the highly charged ions they are accelerated again to ground potential and separated according to their mass to charge ratio with a combination of a magnetic and electrostatic sector field. This combination assures the separation of scattered and charge exchanged ions out of the beam and thus, guaranties higher beam purity. The mass resolving power ΔM/M of the system is better than 1/100. A small surface ion source for Cs ions in front of the charge breeder source allows for the set-up and tuning of the charge breeder independent from the on-line target ion source system. A more detailed description of the set-up can be found in [2] and [3].

COMMISSIONING RESULTS

The installation has been finished already in 2008 and a first test, cumulating in the first successful acceleration of charge bred radioactive ions ($^{80}Rb^{14+}$) has been performed in November 2008. Results have been already reported in [3]. Final commissioning took place during the beam time periods of 2009 and the beginning of 2010.

With the test ion source a breeding efficiency of 3.5% for Cs^{21+} has been achieved. This is the same as the maximum value, which has been reached before when the source was installed on a test bench [3]. A variety of stable and radioactive ions from different target ion source combinations have been injected and efficiency and charge state distributions have been measured. In order to determine the breeding efficiency for the stable isotopes, current measurements before the charge state breeder and after the A/q selection have been performed. For the radioactive species the beam has been sent first directly to a detection station in the ISAC experimental hall. In this detection station ions can be implanted into a tape, which is surrounded by detectors for α, β and γ radiation. After a measurement the tape can be transported behind a lead shield leaving a fresh spot for a new measurement. After the intensity of the singly

charged ion beam has been determined the ions have been sent into the charge state breeder and the extracted highly charged ions have been sent again to the detector station. The efficiency of the charge state breeding is defined as the ratio of both measurements. Mostly γ measurements have been used, as they allow a clear identification of the isotopes. The implantation times into the tape and the counting times have been chosen to reach a measurement accuracy of about 10%.

Table 1 summarizes results for the charge state breeding of radioactive ions so far. Some variations in the breeding efficiencies for the different isotopes also reflect the different amount of time spent on tuning. A general trend to higher efficiency, when going to higher mass ions can be seen. The efficiency for the metallic elements is lower than for the gaseous elements Kr and Br. This effect has been seen before at the test bench and has been reported by other groups as well [4]. The difference can be explained by the possibility of recycling atoms from the plasma chamber walls for the non condensable elements. This leads to an efficiency of more than 6% for ^{74}Kr.

In the case of Br also singly charged molecular ions have been injected. Within the accuracy of about 10% the efficiency for the charge state breeding from the injection of singly charged molecules or atoms can be considered the same. The injection of some species as molecular ions can be beneficial if the release from the target is preferable in the molecular state. In the case of AlBr the method can be used to purify the beam from the isobaric rubidium isotopes, which are normally released and ionized at a much higher rate. Rubidium doesn't form this molecule. $^{78}Br^{14+}$ charge bred in this way has been injected into the accelerator and accelerated to 5 A MeV. The radioactive isotopes were then detected at the TIGRESS experimental station and identified by their decay scheme. For a more detailed description of this detector facility see for example [5] and references therein.

Table 1: charge breeding efficiencies from different radioactive ions

isotope	$T_{1/2}$ [s]	q	A/q	efficiency [%]	I(in) [pps]	injected ion	background [pA]
^{46}K	115	9	5.11	0.5	$4.0 \cdot 10^4$	K^+	340
^{64}Ga	157	13	4.92	0.75	$4.9 \cdot 10^6$	Ga^+	7
^{64}Ga	157	14	4.57	0.7	$4.9 \cdot 10^6$	Ga^+	44
^{74}Br	1524	14	5.28	3.1	$3.2 \cdot 10^7$	Br^+	10000
^{74}Br	1524	15	4.93	2.1	$3.2 \cdot 10^7$	Br^+	25
^{78}Br	388	14	5.57	4.5	$2.8 \cdot 10^7$	$^{27}Al^{78}Br^+$	20
^{74}Kr	690	15	4.93	6.2	$2.1 \cdot 10^6$	Kr^+	25
^{76}Rb	37	15	5.07	1.68	$3.8 \cdot 10^6$	Rb^+	15
^{80}Rb	30	13	6.15	1.17	$5.7 \cdot 10^7$	Rb^+	35
^{80}Rb	30	14	5.71	1.1	$5.7 \cdot 10^7$	Rb^+	70000
^{122}Cs	21	19	6.42	1.1	$3.1 \cdot 10^5$	Cs^+	6
^{124}Cs	31	20	6.2	1.37	$2.75 \cdot 10^7$	Cs^+	50

The last column of the table shows the background from stable elements extracted at the same A/q value from the charge breeder. Those are mainly isotopes of oxygen, carbon and nitrogen from the residual gas, but also helium and other noble gases from the support gas of the source. Additionally there are contributions from sputtered ions from the stainless steel plasma chamber. Although, their beam intensity is only in the range of pico Amperes, for most cases this is several orders of magnitude higher than the intensity of the radioactive beam. Furthermore, the beam may contain more than one contaminant and the composition and intensity may change with time and source condition.

Figure 1 shows a mass spectrum of ions extracted from the charge state breeder in the range between A/q = 5 to 6. In total 18 peaks with intensities above 5 pA can be found, the most intense being charge states from oxygen, carbon and argon. The spectrum represents the source condition after about 1 week of running and after being optimized for the breeding of radioactive rubidium isotopes. The cesium ions, which are normally not present, occur in this spectrum as the initial set-up with

the test ion source has been done before. Table 2 gives a summary with the most probable constituents in the mass peaks.

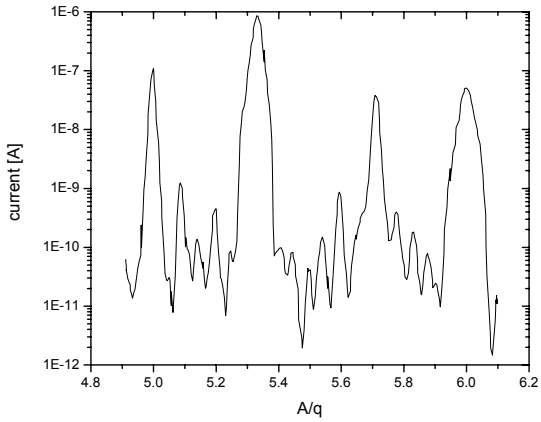

Figure 1: Mass spectrum of ions extracted from the charge state breeder in the range between A/q=5 to 6.

CONCLUSION AND OUTLOOK

Commissioning of the ECRIS charge state breeder at TRIUMF has shown that the system can be used to efficiently produce beams of highly charged radioactive ions suitable for the acceleration with the ISAC accelerators. The desired mass to charge ratio A/q < 7 can be reached for isotopes with masses up to about 150 amu with efficiencies up to about 2% for metallic and 6% for non condensable elements. Further increases in efficiency can be expected with improved understanding, mainly of the injection into the charge state breeder. The injection of molecules into the charge state breeder can be used as a method for beam purification from unwanted isobaric contaminations. Up to now only relatively long lived isotopes have been used. If their half-life approaches the breeding time, which is in the range of several 100 ms [2] a reduction in efficiency can be expected.

Beam purity after the charge state breeder has been found to be the main problem for experiments. The low signal to background ratio makes it difficult to identify reactions from the radioactive isotopes. Although research grade helium with impurity levels in the ppm range has been used as a support gas, further purification from the other noble gases may be necessary. Two cryogenic pumps, one on either side of the charge state breeder are already in place to keep the residual gas pressure at about $5 \cdot 10^{-8}$ T. The amount of background originating from the stainless steel plasma chamber may be reduced by exchanging it to aluminium. A similar approached has been chosen for example at TRIAC [6].

ACKNOWLEDGEMENT

TRIUMF receives federal funding via a contribution agreement through the National Research Council of Canada.

Table 2: Most likely constituents of peaks in the A/q spectrum of figure 1. An accuracy of 0.005 amu/e for the determination of the peak centre has been assumed

A/q	isotopes
5	$^{40}Ar^{8+}$, $^{20}Ne^{4+}$,…
5.11	$^{133}Cs^{26+}$
5.14	$^{36}Ar^{7+}$
5.2	$^{52}Cr^{10+}$, $^{78}Kr^{15+}$, $^{130}Xe^{25+}$
5.24	$^{84}Kr^{16+}$, $^{131}Xe^{25+}$
5.33	$^{16}O^{3+}$
5.41	$^{54}Cr^{10+}$, $^{54}Fe^{10+}$, $^{130}Xe^{24+}$
5.44	$^{136}Xe^{25+}$
5.5	$^{22}Ne^{4+}$, $^{132}Xe^{24+}$
5.54	$^{61}Ni^{11+}$, $^{133}Cs^{24+}$
5.6	$^{28}Si^{5+}$, $^{56}Fe^{10+}$
5.66	$^{17}O^{3+}$, $^{136}Xe^{24+}$
5.71	$^{40}Ar^{7+}$
5.78	$^{52}Cr^{9+}$, $^{133}Cs^{23+}$
5.83	$^{134}Xe^{23+}$
5.88	$^{129}Xe^{22+}$
5.90	$^{53}Cr^{9+}$, $^{124}Xe^{21+}$
6	$^{12}C^{2+}$, $^{18}O^{3+}$, $^{54}Cr^{9+}$, $^{54}Fe^{9+}$, $^{60}Ni^{10+}$,…

REFERENCES

[1] P. Bricault et al., Rev. Scient. Instr. 79 (2008) 02A908
[2] F. Ames et al., Rev. Scient. Instr. 79 (2008) 02A902
[3] F. Ames et al., Rev. Scient. Instr. 81 (2010) 02A903
[4] T. Lamy et al., Rev. Scient. Instr. 77 (2006) 03B101
[5] P. E. Garrett et al Nucl. Instr. Meth. Phys. Res. B 261 (2007) 1084
[6] N. Imai et al., Rev. Scient. Instr. 79 (2008) 02A906

RECENT PERFORMANCE OF THE ANL ECR CHARGE BREEDER*

R. Vondrasek, R. Scott, R. Pardo, A. Kolomiets, ANL, Argonne, IL 60439, U.S.A.

Abstract

The construction of the Californium Rare Ion Breeder Upgrade (CARIBU) [1], a new radioactive beam facility for the Argonne Tandem Linac Accelerator System (ATLAS), is complete and the project is now in the commissioning phase. The facility will use fission fragments, with charge 1+ or 2+, from a 1 Ci ^{252}Cf source; thermalized and collected into a low-energy particle beam by a helium gas catcher. An existing ATLAS ECR ion source was modified to function as a charge breeder in order to raise the ion charge sufficiently for acceleration in the ATLAS linac. A surface ionization source and an RF discharge source provide beams for charge breeding studies. An achieved efficiency of 11.9% for $^{85}Rb^{19+}$, with a breeding time of 200 msec, and 15.6% for $^{84}Kr^{17+}$ has been realized. Both results are with the source operating with two RF frequencies (10.44 + 11.90 GHz). After modification to the injection side iron plug, the charge breeder has been operated at 50 kV, a necessary condition to achieve the design resolution of the isobar separator.

ECR CHARGE BREEDER

The charge breeder is a room temperature ECR ion source with an open structure NdFeB hexapole with a wall field of 0.86 T [2]. The open hexapole structure allows for pumping through the six 17 mm x 41 mm radial slots, resulting in a source pressure of $2x10^{-8}$ mbar without plasma and $8x10^{-8}$ mbar with plasma. The pressure in the extraction region is typically $4x10^{-8}$ mbar. The source is capable of accepting multiple frequencies with the RF launched through the hexapole radial slots. This scheme allows a large amount of iron to be retained on the injection side of the source resulting in a high magnitude and symmetric axial field. The low charge state ions are introduced into the plasma through a stainless steel tube mounted on a linear motion stage which has a 30 mm range of travel. This allows the deceleration point of the low charge state ions to be adjusted on line without disturbing the source conditions.

Injection Region Modifications

For the isobar separator to achieve the required resolution of 1:20,000, beam extraction from the gas catcher must occur at 50 kV. Hence, the high voltage isolation of the source was upgraded to allow 50 kV operation. However, penning discharges in the injection region occurred at 30 kV bias. An iron plug in this region was modified to increase the gap size from 6.5 mm over a 100 mm length to 10.8 mm at a discrete location as shown in Fig. 1. After several weeks of conditioning, the source operates reliably at 50 kV.

* This work was supported by the U.S. Department of Energy, Office of Nuclear Physics, under Contract No. DE-AC02-06CH11357.

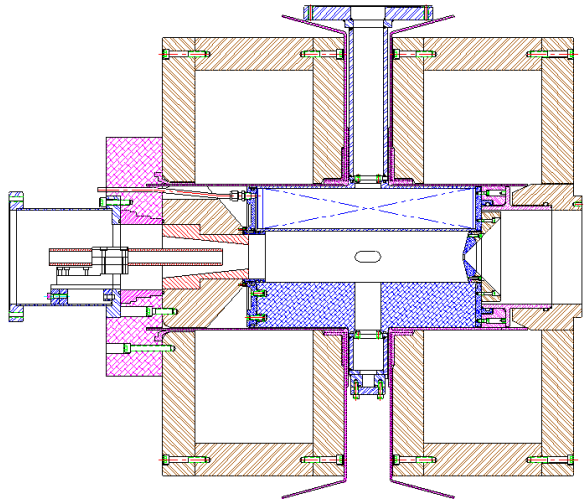

Figure 1: Schematic of the ANL ECR charge breeder. The 1+ beam is injected from the left via the transfer tube. The iron plug which was modified is highlighted with diagonal red. The radial slots where the RF is launched are visible on the source mid-plane.

CHARGE BREEDING RESULTS

The 1+ beam is mass analyzed and injected into the ECR source via a grounded transfer tube. The ions decelerate into the plasma region where a sub-set of them are ionized and captured by the plasma [3].

It was observed that the tune of the 1+ injection line was critical for breeding efficiency. For beams from elemental solids, the optimum injection channel was extremely narrow with a high degree of sensitivity to the entrance einzel lens. With gaseous elements, the einzel lens setting was not as critical, but steering constraints remained very stringent. The position of the transfer tube was also found to be an important variable. A summary of achieved charge breeding efficiencies is given in Table 1. The breeding time was measured by pulsing the incoming 1+ beam and measuring the n+ response time.

Table 1: Summary of charge breeding results.

Ion Species	n+ Charge State	Efficiency (%)	Breeding Time (msec)
Kr-86	17+	15.6	-
Rb-85	19+	11.9	200
Xe-129	25+	13.4	~250
Cs-133	20+	2.9	-

Position of the Transfer Tube

In previous work, it was found that the breeding efficiency increased as the transfer tube was retracted from the plasma [4]. At that time, the linear motion slide was at the limit of its travel. The source was opened and the transfer tube repositioned so that it could be further retracted. The results of the subsequent tests of charge breeding efficiency versus transfer tube position are shown in Fig. 2. The tests took place in three series over the course of several years, but the trend within each data set is clear.

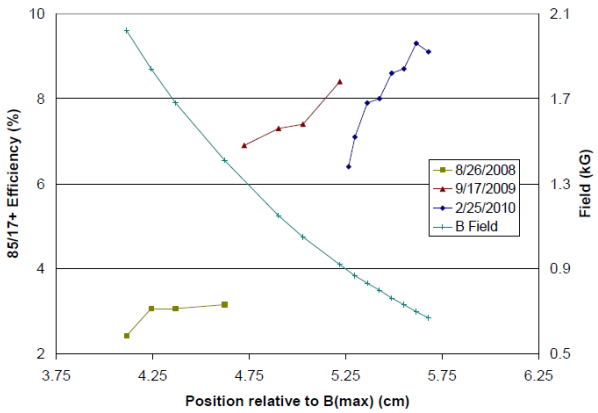

Figure 2: Efficiency of $^{85}Rb^{17+}$ as a function of the transfer tube position. The position is defined as the distance from B_{max} to the end of the transfer tube.

All data sets are taken with a $^{85}Rb^{17+}$ beam provided by a surface ionization source. The source was optimized at each tube position for maximum efficiency in Rb^{17+}. In general, the parameters which were adjusted were the einzel lens, the injection side solenoid, and the ΔV voltage. The tube position is defined as the distance from B_{max} to the end of the transfer tube.

Efficiency Versus ΔV

During charge breeding, the 1+ source and the ECR source are biased with the same power supply. An additional 'tweaker' power supply is in series with the ECR source providing a ΔV voltage, either positive or negative depending on the particulars of the 1+ source, which serves to decelerate the 1+ ions into the ECR plasma. With solid elements (Cs and Rb), it was found that the optimum ΔV was -15 V with a narrow acceptance window of ~5 V. For the gaseous elements (Kr and Xe), the optimum ΔV was +10 V with a very large acceptance window as shown in Fig. 3. There is a steep drop-off in efficiency between +20 and +30 V where the incoming 1+ ions are repelled by the potential and do not enter the plasma chamber. On the other side of the curve, the ions are too energetic and pass through the plasma. However, unlike the solid elements which stick to the cold plasma chamber walls, the gaseous elements are re-emitted and some are charge bred albeit with a lower efficiency and almost certainly a longer hold up time.

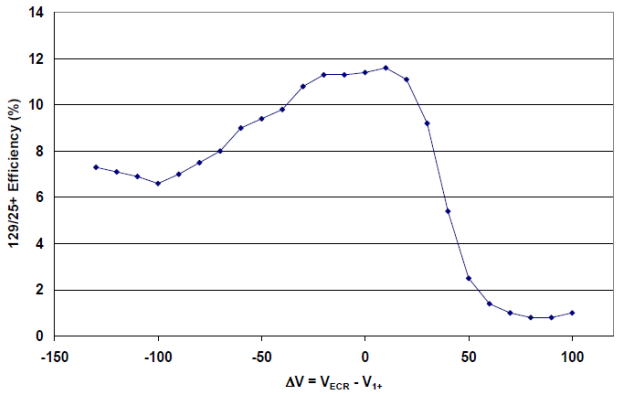

Figure 3: Efficiency of $^{129}Xe^{25+}$ as a function of ΔV.

Multiple Frequency Heating

The effect of multiple frequency heating on the breeding efficiency was previously tested with Cs-133 and Rb-85 with moderate success [4]. These tests were continued with Xe-129 provided by the RF discharge source utilizing a 98% enriched Xe-129 sample. A travelling wave tube amplifier (TWTA) provided RF between 11-13 GHz in addition to a 10.44 GHz klystron. The total RF power was kept constant to serve as a direct comparison of the various RF injection schemes.

With the source running on an oxygen plasma and an extraction voltage of 20 kV, a 65 nA beam of $^{129}Xe^{+}$ was injected into the ECR charge breeder and the breeding efficiency measured as a function of RF power distribution with the results shown in Fig. 4. There is a clear shift in the peak of the charge state distribution when going from single to two-frequency heating. In addition, the global efficiency improved – 42% for 10.44 GHz alone, 46% for 11.90 GHz, and 50% for 10.44+11.90 GHz. In the best configuration, with 350 W of RF injected, the global efficiency was 63% with a maximum efficiency of 13.4% into $^{129}Xe^{25+}$.

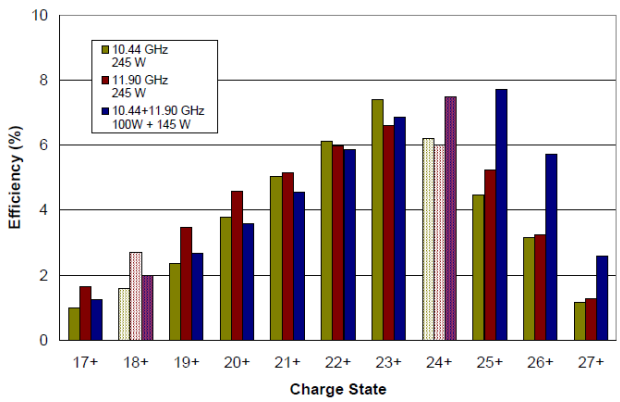

Figure 4: Efficiency of Xe-129 as a function of RF power distribution. The total amount of RF power launched into the source was kept constant. Charge states 18+ and 24+ were obscured by intense background peaks.

Krypton Charge Breeding

A similar set of tests were performed with Kr-86. With the source running on an oxygen plasma at 25 kV extraction, a global efficiency of 77% was observed with a maximum single charge state efficiency of 15.6% into $^{86}Kr^{17+}$. An efficiency spectrum is shown in Fig. 5 with the shaded columns indicating charge states which could not be observed due to interference peaks. Their values are inferred by the general shape of the distribution.

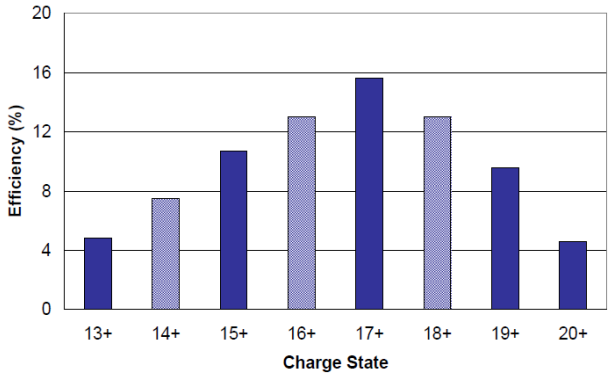

Figure 5: Efficiency spectrum of Kr-86 with the shaded columns indicating charge states which could not be directly observed due to interference peaks.

DISCUSSION

The results in Table 1 demonstrate that the typical relationship of solid elements being half as efficient as gaseous ones is not observed. While not achieving the same level of efficiency as the Kr and Xe, the Rb efficiency is still within a few percent of the gaseous elements. The low breeding efficiency for Cs is attributed to the surface ionization source failing during the testing period. The injection optics could not be optimized, and this led to the reduced efficiency.

A possible explanation for the observed behaviour lies in the design of the 1+ injection region, specifically the iron plug. With shifting the RF injection to the radial ports, a symmetrical magnetic field was maintained in the injection region, whereas with axial RF injection, the waveguide cut-outs introduce a field asymmetry, as shown in Fig. 6 where the center of the magnetic field does not align with the center of the charge breeder and transfer tube. This can introduce steering effects which negatively impact the 1+ injection (particle tracing calculations are being performed to study this hypothesis). It is suggested that the incoming 1+ particles are steered towards the plasma chamber wall before entering the plasma region. In the case of gaseous elements, this is less of an issue due to their not condensing onto the walls of the plasma chamber. However, for solid elements, this would mean that those incoming particles that do impact the wall are lost to the plasma.

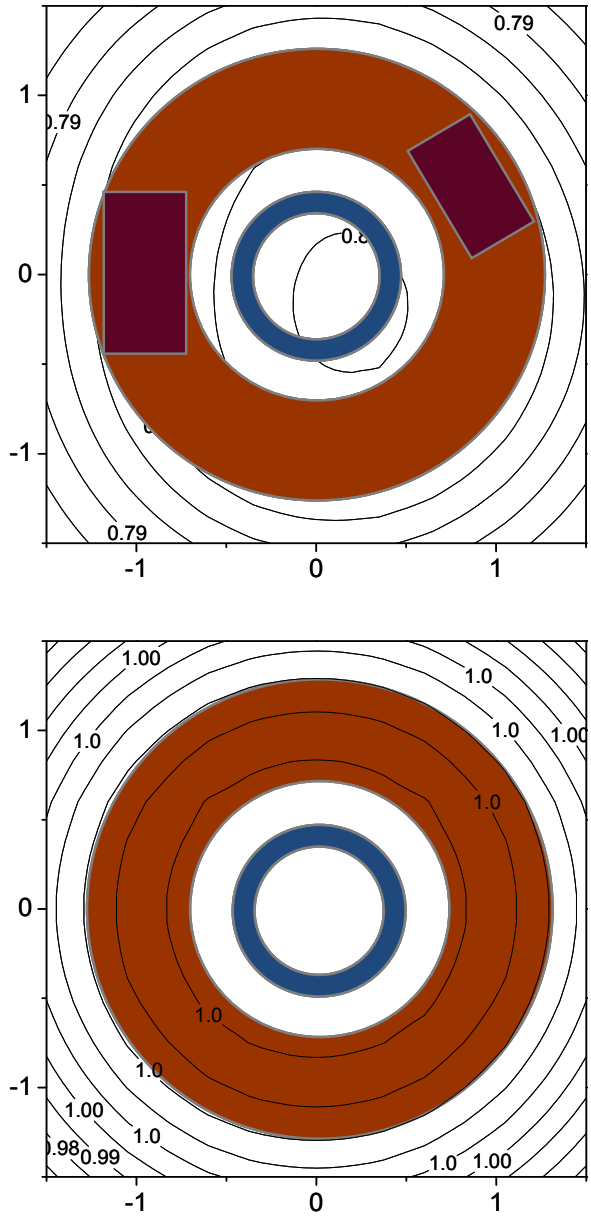

Figure 6: The magnetic field in the injection region with the waveguide cut-outs on top and without on bottom. The overlaid shapes show the position of the transfer tube in blue, the iron plug in brown, and the waveguides in red.

The observed global efficiencies (77% for Kr-86 and 57% for Rb-85) are consistent with a very efficient injection and capture of the 1+ ions. The higher efficiencies for Kr and Xe continue to support the wall recycling model for gaseous elements.

REFERENCES

[1] R. Pardo *et al.*, NIM-B 261, Issues 1-2 (2008) 965.
[2] R. C. Vondrasek, R. Scott, J. Carr, R. C. Pardo, Rev. Sci. Instrum. 79, 02A901 (2008).
[3] R. Geller, Rev. Sci. Instrum. 71, (2000) 612.
[4] R. Vondrasek *et al.,* Rev. Sci. Instrum. 81, 02A907 (2010)

FINE FREQUENCY TUNING OF THE PHOENIX CHARGE BREEDER USED AS A PROBE FOR ECRIS PLASMAS

Lamy Thierry, Angot Julien, Marie-Jeanne Melanie, Medard Jerome, Sortais Pascal, Thuillier Thomas, LPSC - UJF - CNRS/IN2P3 - INPG, Grenoble, France
Galata Alessio, INFN-Legnaro National Laboratories, Legnaro, Italy
Koivisto Hannu, Tarvainen Olli, University of Jyväskylä, Department of Physics, Jyväskylä, Finland

Abstract

Fine frequency tuning of ECR ion sources is a main issue to optimize the production of multiply charged ion beams. The PHOENIX charge breeder operation has been tested in the range 13.75 – 14.5 GHz with an HF power of about 400 W. The effect of this tuning is analyzed by measuring the multi-ionization efficiency obtained for various characterized injected 1+ ion beams (produced by the 2.45 GHz COMIC source). The 1+/n+ method includes the capture and the multi ionization processes of the 1+ beam and may be considered as a plasma probe. The n+ spectra obtained could be considered, in first approach, as an image of the plasma of the charge breeder. However, in certain conditions it has been observed that the injection of a few hundreds of nA of 1+ ions (i.e.: Xe^{+}) in the plasma of the charge breeder, is able to destroy the charge state distribution of the support gas (i.e.: up to 40 % of O^{6+} and O^{7+} disappears). The study of this phenomenon will be presented along with plasma potential measurements for various charge states. This study may help to understand the creation (or destruction) of highly charged ions inside an ECRIS.

INTRODUCTION

When we inject a characterized 1+ ion beam into a plasma, then extract and analyse all the ion species from it, one may expect some information about the characteristics of this plasma : its ability to capture 1+ ions and its ability to multi ionize the 1+ ions injected (i.e. plasma temperature and density). The 1+/n+ method developed for radioactive ion beams could be considered as a kind of non perturbative probe because the number of ions injected is exactly known (1+ beam intensity measurement), and extremely low with respect to the initial number of ions present in the plasma. In this paper, we propose to check the validity of these assumptions, by using fine frequency tuning of the microwaves injected to modify the characteristics of the ECR plasma, and by measuring the plasma potential to quantify the plasma characteristics variations.

THE 1+ COMIC SOURCE

The availability of a reliable ion source to produce cw 1+ ion beams in the range of 100 nA up to 1 µA with good stability is crucial for the 1+/n+ method in order to have a rather confident experimental simulation of low intensity radioactive ion beams and enough signal to have a precise measurement of the n+ efficiency yield. The microwave coupling of the ultra compact 2.45 GHz COMIC ion source developed at LPSC [1] has been particularly optimized, so the necessary HF power for the ignition and the maintaining of the plasma is extremely low (from 100 mW to 5 W depending on the pressure) and can be delivered by a solid state amplifier (see Fig. 1) leading to an extremely stable operation.

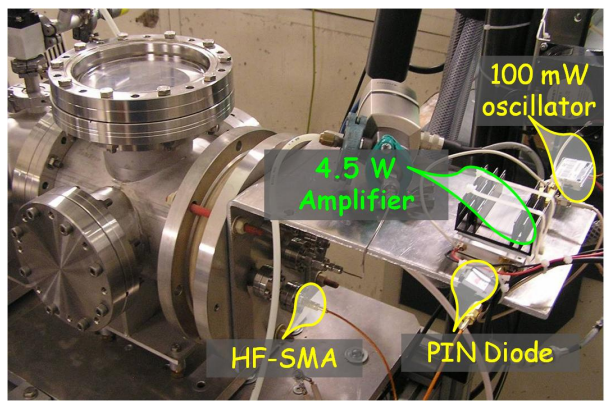

Figure 1: HF circuit of the COMIC Source on the 1+/n+ test stand.

LOW INTENSITY 1+ BEAM INJECTION INTO A PLASMA

Experiment

Oxygen gas is injected to produce the plasma in the PHOENIX charge breeder. The ions extracted from this plasma are analysed in a magnetic spectrometer and the intensities are plotted on Fig. 2 (blue spectrum). In this spectrum, 267 µAe (i.e. 110 µAp) are extracted from the source. Then, a 500 nA $^{132}Xe^{+}$ beam produced by the COMIC source is injected into the charge breeder. The capture is optimized and a second spectrum is performed (red spectrum on Fig. 2). In this second spectrum, the multicharged oxygen ion intensities are lower: the sum of the peaks is 234 µAe, equivalent to 103 µAp. Considering that about 50 % of the $^{132}Xe^{+}$ has been captured by the plasma, we can deduce that the 0.25 µA of $^{132}Xe^{+}$ has destroyed 7 µAp of multicharged oxygen ions, in other words one Xe ion destroys about thirty oxygen ones.

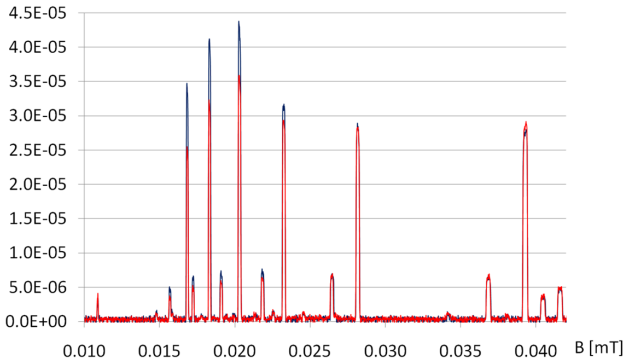

Figure 2: Evolution of the multicharged oxygen ion intensities when injecting a $^{132}Xe^{+}$ beam.

Discussion

One may think that the decrease of the measured intensities of the multicharged ions could be due to an emittance variation of the beams, showing a transmission problem of the beam line. We have measured, with an Allison type emittancemeter, the emittance of O^{6+} without and with 1+ injection. Fig. 3 shows that the emittance in the two cases has almost the same shape and the same value (10 π.mm.mrad at 1σ).

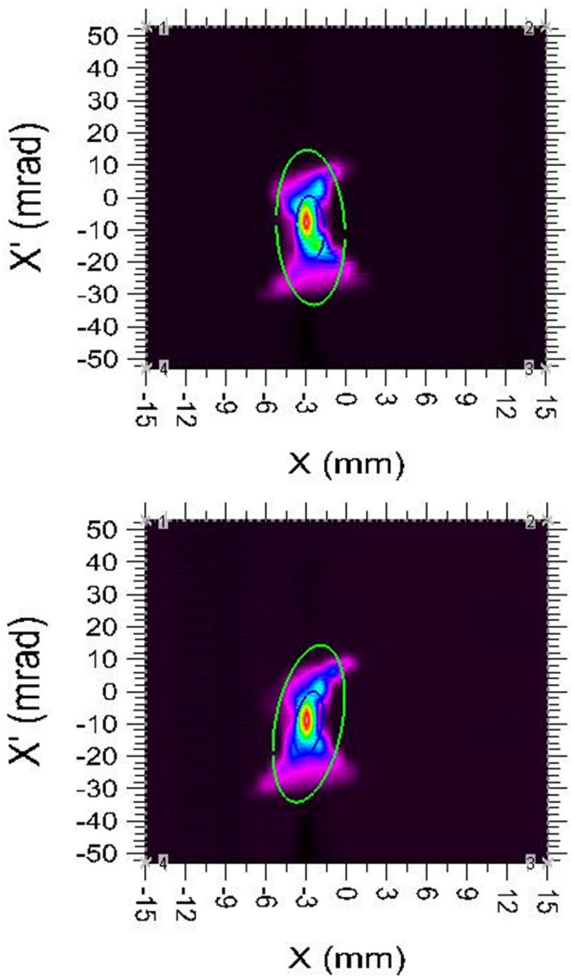

Figure 3: O^{6+} emittance, top – without Xe^{+} injection, bottom – with Xe^{+} injection

The other possibility investigated is a change in the plasma characteristics. For this, the plasma potential has been measured using a retarding potential in front of a Faraday cup [2]. Fig. 4 shows the currents measured in the Faraday cup while varying the retarding potential with (black curve) or without (red curve) injecting Xe^{+} into the charge breeder. The plasma potential is almost the same for the two experiments (about 16 V) and so plasma characteristics may not change sufficiently to explain the destruction of multicharged ions. Finally, let us note that this phenomenon cannot be explained by charge exchange, the low charge states remaining constant when the multicharged ones disappear.

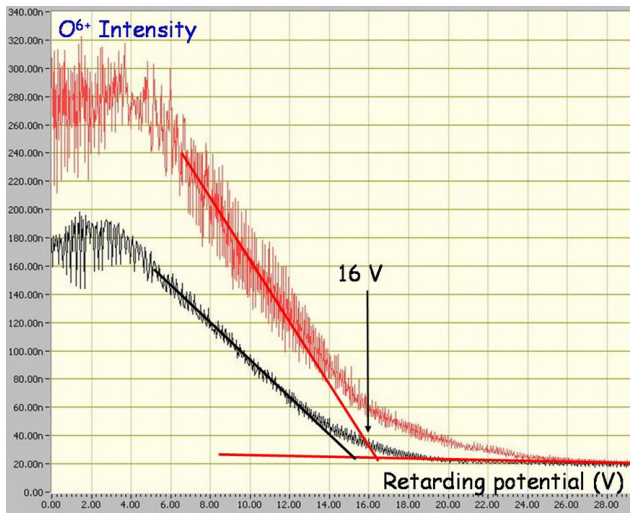

Figure 4: Plasma potential measurements on O6+

FINE FREQUENCY TUNING OF THE ECR CHARGE BREEDER

Context

Fine frequency tuning (in the range of a few MHz around the well known 14 GHz frequency, for example) of ECR ion sources, is known to have a great influence on the extracted ion current intensities and a significant effect on the optical characteristics of the beams [3]. One may take advantage of this effect to increase the efficiency yield of a charge breeder or to optimize it on a specific charge state.

Experimental setup

The microwaves (MW) injected into the PHOENIX charge breeder are delivered by a 14.5 GHz klystron. The plasma chamber has two WR62 MW ports. It has been decided to explore the fine frequency tuning by injecting on the second port of the plasma chamber MW delivered by a Travelling Wave Tube Amplifier (TWTA) with a power adjustable from 0 up to 400 W, for a 13.75 to 14.5 GHz frequency range. The low level signal injected into the TWTA is generated by a tunable oscillator (20 µW). The MW injection of the experiment is shown on Fig. 5

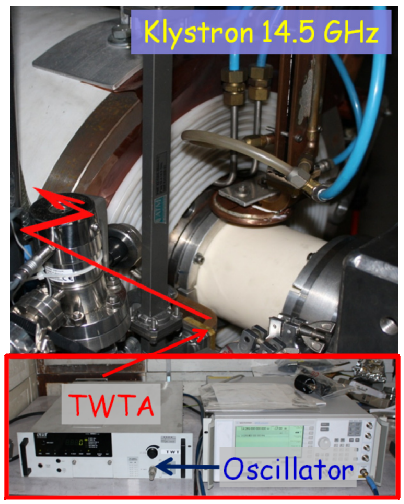

Figure 5: Scheme of the microwaves injections

Experiments and results

The effect of the TWTA frequency tuning on various charge breeding efficiencies and buffer gas ion intensities has been measured in numerous experiments. A few examples of these measurements will be shown below.

It was not possible to initiate and maintain the plasma with the TWTA alone due to its reflected power limitation (10%). Therefore the 14.5 GHz klystron was used first, then its power was decreased (100 W) and the power of the TWTA increased at the highest power (330 W) to allow frequency exploration while maintaining a reflected power of less than 10%. The charge breeding efficiency obtained with the klystron alone was 8.5 % on Ar^{8+}. After the adjustment of the TWTA power, its frequency was decreased from 14.5 down to 14.3 GHz by 10 MHz steps. At each step, Ar^{8+} charge breeding efficiency and O^{5+} intensity were measured (Fig.6). This graph shows:

- An important effect (up to a factor of 2.5) of the fine frequency tuning on the O^{5+} intensity extracted from the charge breeder.
- A moderate effect (up to a factor 1.2) on the charge breeding efficiency for Ar^{8+} (however without improvement).

On Fig. 7, the influence of the fine frequency tuning on the charge breeding of a $^{132}Xe^{+}$ beam is presented.

The initial tuning is performed with the klystron on Xe^{24+} at 14.5 GHz and shown by the blue dot (red and green dots are the efficiencies at 14.5 GHz for charges 20 and 17). Then, the klystron power is decreased and the TWTA power is adjusted to get the same efficiency on the 24+ charge state. The curves are the efficiencies measured when varying the frequency of the TWTA. One can see in these experiments, a slight increase of the charge breeding efficiencies for charges 20 and 24.

Discussion on fine frequency tuning

Reproducibility problems have been noticed during this study. Compared to a standard ECR ion source, the charge breeder MW cavity has an electrical discontinuity

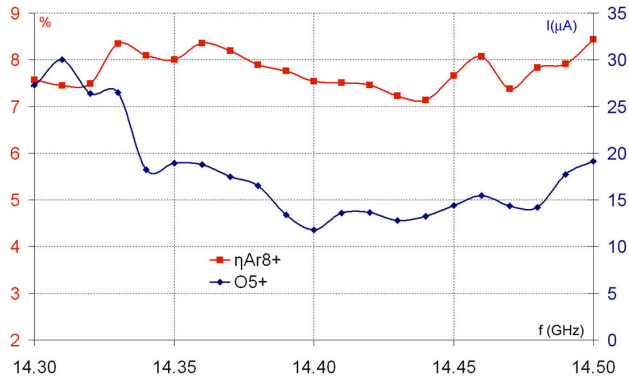

Figure 6: Fine frequency tuning effect on the Ar8+ charge breeding efficiency compared to its influence on O5+ intensity.

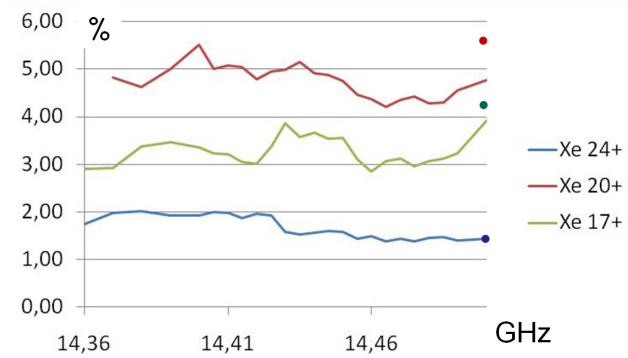

Figure 7: Fine frequency tuning effect on the ^{132}Xe charge breeding efficiency (charge states 17, 20 and 24+).

due to the grounded tube transporting the 1+ beam at high energy towards the plasma. Depending on the tuning of the charge breeder, the coupling of the HF power and so the impedance of the system, may vary substantially, leading to unstable operation. Some studies have been performed in a sweep mode allowing a fast and quasi continuous frequency variation. During such experiments the results were reproducible from sweep to sweep, however due to the variation of the net power coupled to the plasma during a sweep, the influence of the fine frequency tuning could not be properly deduced.

The main conclusion from this study seems to be the difference of behaviour of the buffer gas plasma and the charge bred beams with respect to fine frequency ECR tuning.

GROUNDED TUBE SUPPRESSION

The possibility of removing the grounded tube which permits to transport the high energy 1+ beam towards the plasma, and to fix the position of the deceleration, has been proposed and calculated with SIMION [4]. A cut view of the configuration experimentally tested is shown Fig. 8: on the top, the previous grounded tube configuration (with the last electrode of the double Einzel lens on the left) is represented; on the bottom, the configuration without grounded tube inside the charge breeder is shown.

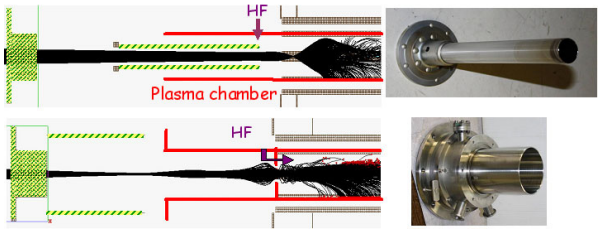

Figure 8: Configuration of the 1+ beam injection in the charge breeder, top – with the grounded tube in the charge breeder, bottom – without grounded tube.

The new electrode has been baked under vacuum and installed one morning. After three hours of pumping, the experiment was performed with a 132Xe+ beam. The n+ signal was found by applying the potential, calculated with SIMION, on the two electrodes of the double Einzel lens. It is interesting to notice that better efficiency than the ones obtained in the last experiments was almost immediately obtained with a power of 85 W (compared to the 400 to the 600 W generally injected to get a reasonable efficiency). The drain current of the high voltage was much lower than in the configuration with the grounded tube (400 µA versus 2 mA), the plasma was much more stable and easier to tune like a standard ECR ion source. The preliminary 132Xe charge breeding spectrum is presented Fig. 9.

This new configuration is promising. Much lower MW power being necessary for operation, the use of a solid state MW generator could be possible. The separation of the injection optics from the ECR charge breeder can simplify the maintenance in the context of radioactive ion production.

Moreover, the HF cavity has no more electrical discontinuity when the grounded tube is removed, thus

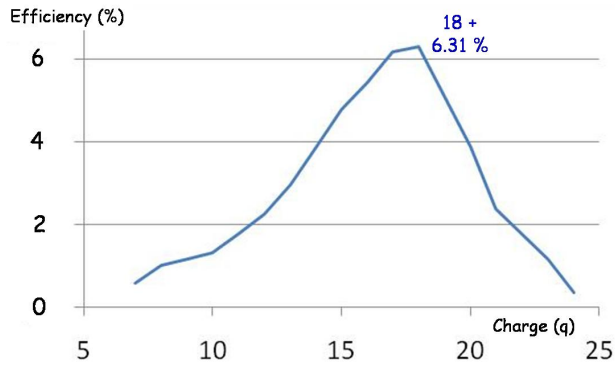

Figure 9: Preliminary charge breeding spectrum obtained without grounded tube

allowing studying properly fine frequency tuning effects. This new configuration has to be tested with alkali and metallic ions in the near future.

REFERENCES

[1] Sortais P.; Lamy T.; Médard J.; Angot J.; Latrasse L.; Thuillier T., Rev. Sci. Instr. 81(2), (2010) 02B314

[2] O. Tarvainen, P. Suominen, and H. Koivisto, Rev. Sci. Instrum. 75, 3138 (2004)

[3] V. Toivanen, H. Koivisto, O. Steczkiewicz, L. Celona, O. Tarvainen, T. Ropponen, S. Gammino, D. Mascali and G. Ciavola, Rev. Sci. Instr. 81(2), (2010) 02A319

[4] T. Lamy, J. Angot, C. Fourel, (http://accelconf.web.cern.ch/AccelConf/HIAT2009/papers/we-06.pdf) Proceedings of the 11th International Conference on Heavy Ion Accelerator Technology, 8-12 June 2009, Venice, Italy.

PRELIMINARY RESULTS OF SPATIALLY RESOLVED ECR ION BEAM PROFILE INVESTIGATIONS*

L. Panitzsch, M. Stalder, R.F. Wimmer-Schweingruber, CAU, Kiel, Germany

Abstract

The profile of an ion beam produced in an Electron Cyclotron Resonance Ion Source (ECRIS) can vary greatly depending on the source settings and the ion-optical tuning. Strongly focussed ion beams form circular structures (hollow beams) as predicted by simulations [1] and observed in experiments [2] and [3]. Each of the rings is predicted to be dominated by ions with same or at least similar m/q-ratios due to ion-optical effects. To check this we performed a series of preliminary investigations to test the reqiured tuning capabilities of our ion source. This includes beam focussing (A) and beam steering (B) using a 3D-movable extraction. Having tuned the source to deliver a beam of strongly focussed ions of different ion species and having steered this beam to match the transmittance area of the sector magnet we also recorded the ion charge state distribution of the strongly focussed beam profile at different, spatially limited positions (C). The preliminary results will be introduced within this paper.

EXPERIMENTAL SETUP

Within this section a short overview of the ECR ion source including the beam line and the profile measuring device, the Faraday Cup Array (FCA), will be given.

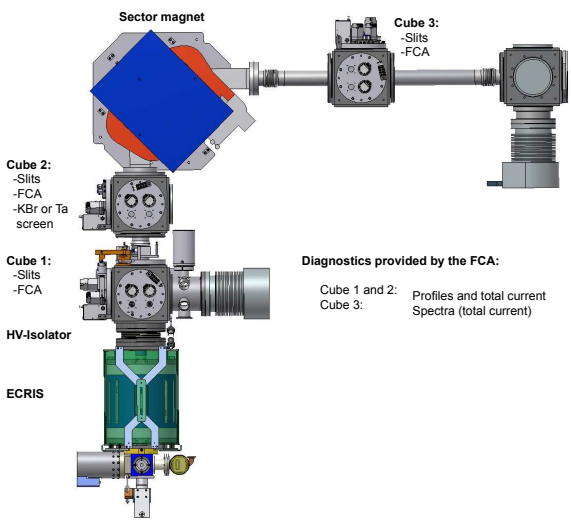

Figure 1: overview of the setup

*Work in parts supported by the German Science Foundation, DFG/HBFG

ECRIS and beam line

The ion source we use to generate the ion beam is an all-permanent magnet ECR ion source. One special feature of this source is the extraction electrode that is movable in three dimensions, along the beam axis and perpendicular to it. After the extraction the ions pass two cubes providing access to the beam (see figure 1). The cubes are equipped with slits to limit the beam and with a profile-measuring device described in the following subsection. A 90° sector magnet is used to separate the ions according to their m/q-ratio. Sweeping the magnetic field we are able to record m/q-spectra using the detector placed in the third cube along beam line.

The tuning of the source was similar during all tests. At a comparatively high pressure in the vacuum chamber of 10^{-5} mbar we axially guide microwaves at a power of 50 W into the plasma.

Faraday Cup Array (FCA)

In order to monitor the ion beam from the source to the experimental chamber we have developed a new kind of beam profile monitor. Its working principle is based on the well-proven Faraday cup (FC). Having arranged a total number of 44 tiny (Ø = 0.3 mm) FCs to an array and driving this arrangement through the beam we record the position and the current for each tiny cup in a repetitive measurement. This allows the reconstruction of the beam profile. We have combined this detector with a standard FC to be able to also determine the total beam current. This detector is characterized by its sensitivity in combination with high durability. The spatial arrangement of the tiny cups allows the detection of profile-structures on mm-scale in a large range of current densities. More detailled information can be found in [4]. A CAD-view of the detector is presented in figure 2.

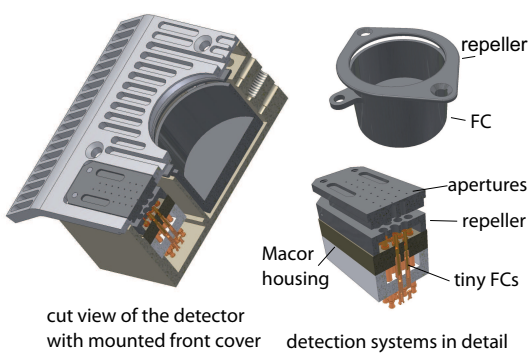

Figure 2: different CAD-views of the FCA

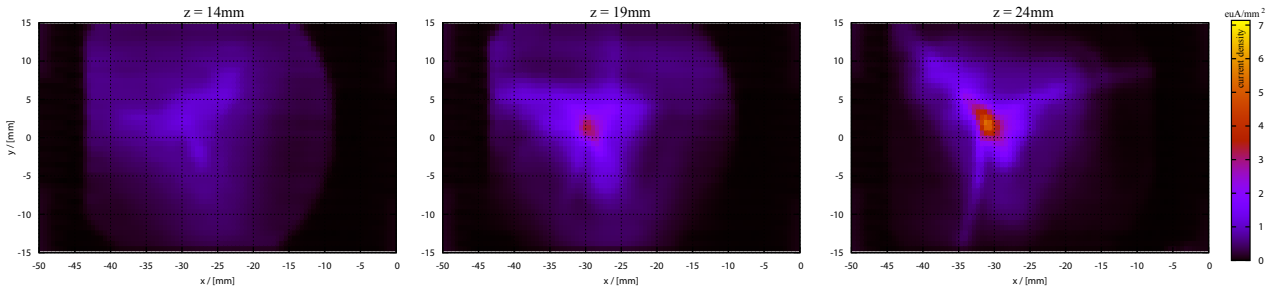

Figure 3: beam profiles recorded at different positions of the extraction electrode along the beam axis show different focussing properties

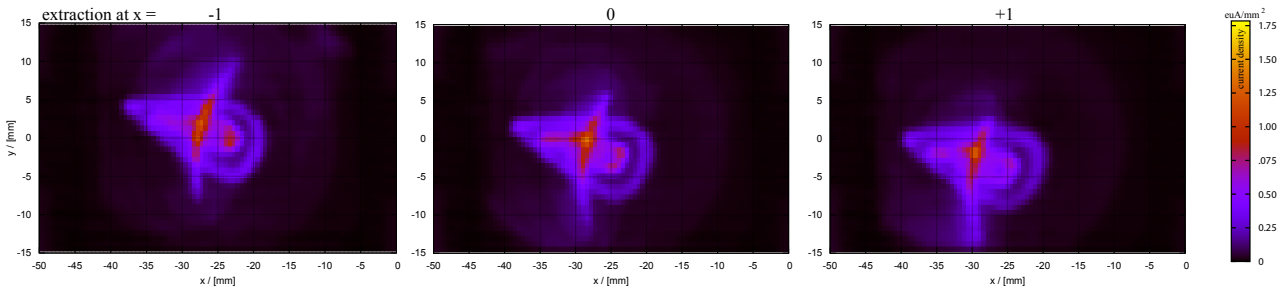

Figure 4: beam profiles for different positions of the extraction in the horizontal direction perpendicular to the beam axis; the stronger focussing in comparison to figure 3 is achieved by additionally lowering the extraction voltage

PROCEDURES AND RESULTS

A *Beam focussing*

For the beam-focussing investigations we move the extraction electrode along the beam line at a constant acceleration voltage and record beam profiles for different distances. A selection of the recorded profiles is shown in figure 3 in the same current density scale. As visibe, the beam is being focussed with increasing distance between the plasma electrode and the extraction electrode. As a result for our beam-focussing investigations we can state that we can focus the beam at a constant acceleration voltage by moving the extraction along beam line. To even increase the focussing effect we additionally can lower the extraction voltage. The higher focussing results in beam profiles similar to those shown in figure 4. We see that the triangular structure changes its shape and more hollow rings appear.

B *Beam steering*

In order to investigate the beam steering capabilities of our source we tuned the source to deliver a strongly focussed beam. Moving the extraction in the plane perpendicular to the beam axis we recorded the movement of the beam in both cubes, again using our profile monitoring device, the FCA. The resulting profiles shown in figure 4 are recorded in cube 1. As we can see the beam moves roughly downwards when the extraction is moved horizontally from left to right. This corresponds a rotation of roughly 90° in the clockwise direction. We can observe the same effect (a rotation of roughly 90° clockwise) when moving the extraction vertically in the same plane. In conclusion we can state that we can effectively steer the beam by changing the position of the extraction in the plane perpendicular to the beam axis. This technique can be used to match a certain, non-central region of the beam into the transmittance area of the sector magnet, i.e. for subsequent m/q-recordings.

C *Spatially resolved charge state distribution*

To check the feasibility of determining the spatially resolved ion charge state distribution of a strongly focussed ion beam we additionally perform this third preliminary

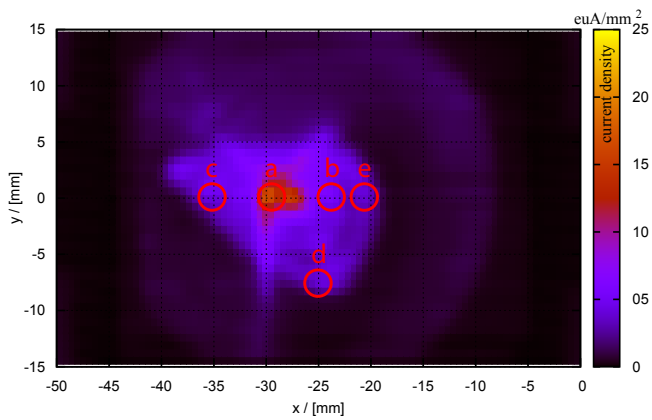

Figure 5: profile with marked positions for m/q-spectra recordings

Table 1: dominant m/q-ratios at the marked spots of figure 5

a	$O^{1+\rightarrow 4+}$ $N^{1+\rightarrow 4+}$
b	N^{2+} O^{2+}
c	N^{2+} O^{2+}
d	O^{2+}
e	O^{2+}

measurement. Therefore, we keep the source tuned to provide a strongly focussed beam of multiple ion species forming the characteristic ring-like structures. We use slits to limit the transmitted beam to the desired spots indicated in figure 5. Only the transmitted beam can pass the sector magnet allowing the determination of m/q spectra or charge-state distributions. For this first feasibility check we only chose a limited number of characteristic points marked ”a-e” in figure 5. To match point ”b” into the transmittable area of the sector magnet we needed to lift the beam slightly by applying our beam steering technique. The results of the different m/q-spectra are summarized in table 1.

From these preliminary results we could assume that the outer ring measured at positions d and e is (under current source settings) dominated by twice ionized oxygen atoms (O^{2+}). Since at position b the dominant ion is N^{2+} with a not negligible amount of O^{2+} one could (assuming a slight misadjustment of the slits) presume that the inner ring mainly consists of twice ionized nitrogen atoms. At position c both hollow rings seem to overlap or at least lay close to each other as visible in figure 5. This is in agreement with the results of the charge state measurement for this point since here the prominent ion species are N^{2+} and O^{2+}. At central position a the higher ionized charge states of nitrogen and oxygen are present.

From these preliminary vaild results we can state that we in principle are able to determine the spatially resolved charge state distribution of a beam profile. However, for reliable data a profile with sharper ring structures should be chosen and the charge state distribution of a higher amount of characteristic points should be determined. This technique can be used to check the theory that the hollow rings often found in strongly focussed ion beams are dominated by ions of the same or at least similar m/q-ratio.

CONCLUSIONS

In conclusion we can state that using our 3D-movable extraction we can effectively steer and focus the ion beam. In combination with our high-resolution beam-profile monitoring device we are able to focus the beam to a strongly focussed beam, steer the regions of interest of the beam into the transmittable area of the analyzing magnet and record a profile of this setting. Using the slits to limit the beam to small areas we are able to determine the spatially resolved ion charge state distribution of the beam profile in the plane perpendicular to the beam axis.

For the final measurements validating the theory mentioned above we tuned our source for multiple ion species whose particular m/q-depending focussing varied from strongly focussed to over-focussed. Then a series of hollow concentric rings appeared that were superimposed by a triangular structure. Using the technique described above we performed more accurate measurements in order to determine the spatially resolved ion charge state distribution of a strongly focussed beam of multiple ion species [5].

REFERENCES

[1] D.S. Todd, D. Leitner, and M. Strohmeier, LOW ENERGY BEAM DIAGNOSTICS AT THE VENUS ECR ION SOURCE, LBNL, Berkeley, CA 94720, USA.

[2] P. Spädtke, K. Tinschert, R. Lang, J. Mäder, and J. Roßbach, J. W. Stetson and L. Celona, Prospects of ion beam extraction and transport simulations, REVIEW OF SCIENTIFIC INSTRUMENTS 79, 02B716, 2008, DOI: 10.1063/1.2823968.

[3] J. Mäder, J. Roßbach, F. Maimone, P. Spädtke, K. Tinschert, R. Lang, L. Sun, Y. Cao, and H. Zhao, Emittance estimation by an ion optical element with variable focusing strength and a viewing target, REVIEW OF SCIENTIFIC INSTRUMENTS 81, 02B720, 2010, DOI: 10.1063/1.3272891.

[4] L. Panitzsch, M. Stalder, and R.F. Wimmer-Schweingruber, Institute for Experimental and Applied Physics (IEAP), University of Kiel, Germany, Direct high-resolution ion beam-profile imaging using a position-sensitive Faraday cup array, REVIEW OF SCIENTIFIC INSTRUMENTS 80, 113302, 2009, DOI:10.1063/1.3246787.

[5] L. Panitzsch, M. Stalder, and R.F. Wimmer-Schweingruber, Institute for Experimental and Applied Physics (IEAP), University of Kiel, Germany, SPATIALLY RESOLVED MEASUREMENTS OF ECR ION SOURCE BEAM PROFILE CHARACTERISTICS, submitted (RSI).

A CORRECTION SCHEME FOR THE HEXAPOLAR ERROR OF AN ION BEAM EXTRACTED FROM AN ECRIS

P. Spädtke*, R. Lang, J. Mäder, F. Maimone, J. Roßbach,
K. Tinschert, GSI Darmstadt

Abstract

The extraction of any ion beam from ECRIS is determined by the good confinement of such ion sources. It has been shown earlier, that the ions are coming from these places, where the confinement is weakest. The assumption that the low energy ions are strongly bound to the magnetic field lines require furthermore, that only these ions starting on a magnetic field line going through the extraction aperture can be extracted. Depending on the setting of the magnetic field, these field lines may come from the loss lines at plasma chamber radius. Because the longitudinal position of these field lines depends on the azimuthal position at the extraction electrode, the ions are extracted from different magnetic flux densities. Whereas the solenoidal component can only be transferred into another phase space projection, the hexapolar component can be compensated by an additional hexapole after the first beam line focusing solenoid. The hexapole has to be rotatable in azimuthal direction and moveable in longitudinal direction. For a good correction the beam needs to have such a radial phase space distribution, that the force given by this hexapole acts on the aberrated beam exactly in such a way that it create a linear distribution after that corrector.

INTRODUCTION

The ion beam extracted from an ECRIS suffers from the magnetic field designed for a good confinement of the plasma. Both magnetic field components, the solenoidal part and the hexapolar part have influence on the properties of the ion beam. Whereas the error caused by the solenoidal component can only be shifted between different projections of the 4d-phase space[1, 2], the negative influence of the hexapole should be possible to be removed. The solenoidal component will stay with the beam, because ions are born within the plasma where the magnetic flux density is high, and therefore $\int \vec{B} ds \neq 0$ which is responsible for twisted trajectories. The experimental evidence for the density structure within the beam has been demonstrated by viewing targets and by emittance measurements with a suitable device[3, 4], showing a typical behavior for all ECRIS beams[5]. This can be explained when ions are extracted only on magnetic field lines going through the extraction hole[6]. A picture behind a pepper plate shows also experimental evidence of a certain structure, see Fig. 1.

The idea of compensation relies on the assumption that it is possible to set the ion beam profile within the known field of a hexapole in such a way that the actual field reverse the aberration of the incoming beam. For the compensation it is essential that the ion beam can be matched in phase space relative to the hexapole position. The orientation of the hexapole correction needs to be variable as well.

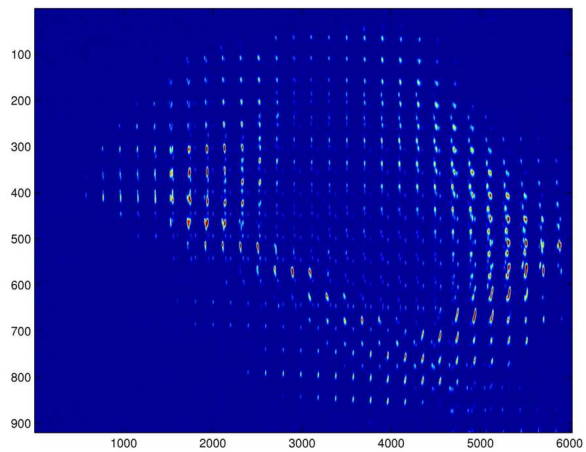

Figure 1: Beam spots behind a pepper plate. The $^{40}Ar^{8+}$ beam is extracted in cw-mode by a single hole of an accel-decel extraction system with 15 kV/-2kV. Both axis are scaled in pixel.

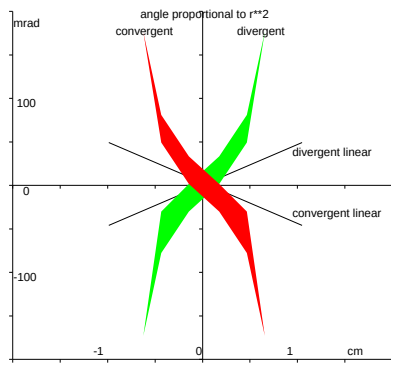

Figure 2: Both possible beam emittance orientations to remove the hexapolar error: divergent emittance in green, and the convergent emittance in red.

If the angle of the radial profile increases with r^2 as shown in Fig. 2, a hexapolar field can be used to change it to a linear distribution again. Such a setting should be possible to create by the help of the focusing force of the solenoid and its distance to the hexapolar field. However, this model assumes linear optic without any coupling. If the radial position of a trajectory changes within the compensation hexapole, the integral focusing force will apply. To minimize possible errors, the hexapole field should be as short as possible. The effective length has to be chosen such that the device can be designed with normal con-

* p.spaedtke@gsi.de

ducting coils. Additional simulation should verify these assumptions.

SIMULATION

To perform a simulation of such a system, the 3d code KOBRA3-INP[7] has been used. The computation has been made in several steps:

1. Simulation of extraction region including the plasma chamber for correct starting conditions of trajectories. The starting location is where the plasma confinement is weakest. The full charge state spectrum has been assumed to produce a correct solution of Poisson's equation within the extraction system. The electron density close to the plasma potential has been solved analytically. Plasma potential, particle density, and electron temperature have to be defined by the user. The space charge of the drifting ion beam is assumed to be compensated by electrons. These electrons are generated by collisions of primary ions with residual gas atoms and will be trapped in the space charge potential, whereas the secondary ions are repelled from this potential. Only one charge state has been saved for further transport simulation in a second area of simulation.

2. For the simulation of the optical section of the beam line, shown in Fig.3 with drift, magnetic solenoid, hexapole correction, it is necessary to use all six phase space coordinates for each trajectory (path of the particle) to take correlation effects into account. The distribution of the magnetic flux density has been calculated with an integral method, saturation effects are neglected. The hexapole is added analytically to the solenoid field. The hexapole component by its own is shown in Fig. 4.

3. For diagnostic reason, different projections of the six dimensional phase space are used. Here we investigate whether the projection of the six dimensional phase space can be used, or a more resolved quantity should be used instead. Projections were made with an additional slit perpendicular to the axis of the measurement to develop the charge density at a local spot in space. This is shown in Fig. 5: the first line shows the integrated emittance, whereas in the following lines a slit is moved in perpendicular direction to obtain spatial resolution. In each line the actual fraction of the beam is shown in real space (y-z) together with both projections y-y', and y-z'. The next three pictures in each line show the same for the perpendicular direction y-z, z-z', and z-y'. Beam direction x.

4. The assumption of a constant phase space volume along the beam line is correct, but it is valid in the six dimensional phase space only. Whether projections of this phase space show similar behavior needs to be proven in each specific case. In case of any coupling between these sub spaces the projection is not necessarily an invariant. Space charge force and magnetic force are examples for coupling forces.

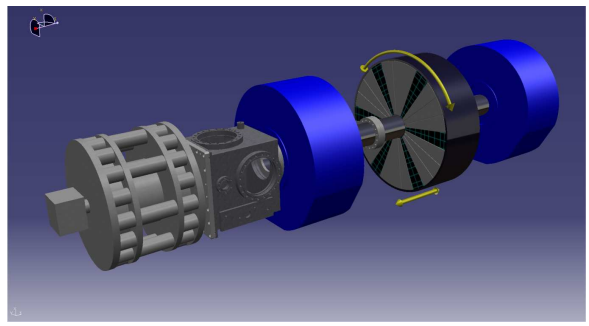

Figure 3: Top: artist view of the compensation device.

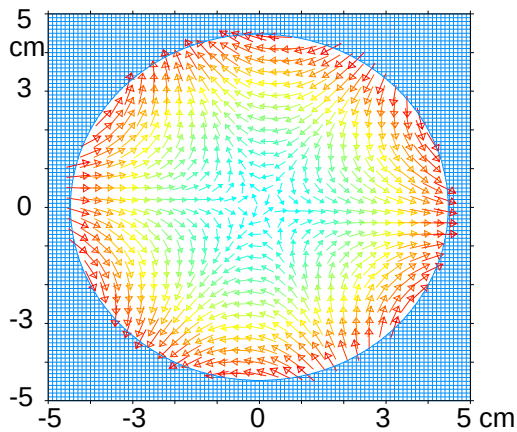

Figure 4: Cross section of the beam tube at the location of the hexapole. Arrows show the strength and the direction of the magnetic flux density.

Different intermediate states of focusing of the extracted ion beam by the solenoid are shown in Fig. 6. Using the particle distribution given by the simulation of the extraction system a slightly different behavior of the ion beam has been found compared to the experimental results. Whereas the hollow beam structure is present if the beam is under focused on the target, the appearance of three arms when over focused are not as visible in this simulation as experimentally observed.

There is a clear structure on the simulated beam, however, it does not depend on r^2 and this error cannot be corrected. Possible reasons to fail the required beam parameter in the simulation could be, that the hexapolar field combined with the solenoidal field will cause another error than a sequential application of both fields separately (coupling), or the initial energy of ions within the plasma differs from expected values and might depend on the origin of ions. Assuming higher starting energy of the ions in simulation seems to increase the effect caused by the hexapole.

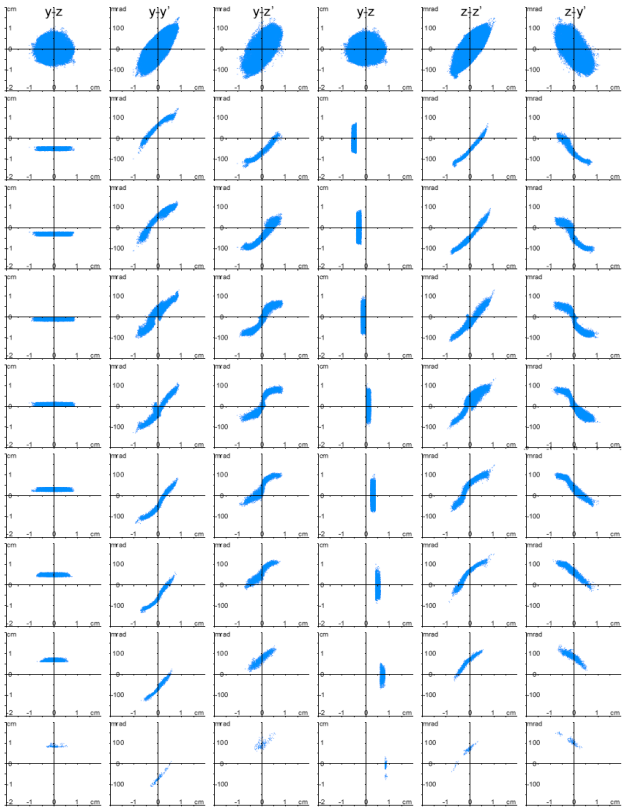

Figure 5: Different diagnostic: first line: real space, phase space, mixed phase space projection, for both transverse directions. Next lines: additional vertical respectively horizontal slit. Behind solenoid at x=0.7 m.

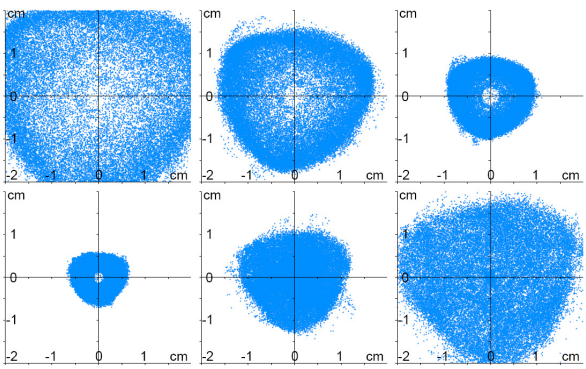

Figure 6: Influence of increasing focal strength of the solenoid on the ion beam profile. The beam is hollow if under focused (first line, focusing force 76%, 83%, and 90%), and becomes triangular afterwards (second line, focusing force 96%, 103%, and 110%).

At that time experiments with frequency ramping were made with the CAPRICE at the EIS test bench[8], showing a strong influence of the frequency on the extracted beam. In these experiments the beam shape on target can be interpreted as fixed surface or volume, containing a local ion density defined by the frequency. The dependence clearly verifies the assumption that collisions within the plasma are not important for the path of the ions. Otherwise these structures clearly defined within the plasma chamber before extraction would not be visible after the beam transport.

CONCLUSION

If the beam is correctly matched to a compensation hexapole, an emittance reduction due to straightening of the emittance figure seems to be possible. A change of the radial position of a trajectory within the hexapole modifies the action of the hexapole. This effect should be avoided, therefore a shorter and stronger hexapole seems to be more useful rather than a weaker but longer one. A normal conducting hexapole seems to be sufficient, but this depends on the required radius.

The simulation of the problem is not an easy task, because already the properties of the extracted beam depend on several parameters, which require always the full scan of computation (variation of each parameter). The optical matching condition to the compensator again will require to scan all optical parameters for the full range.

The strong influence of frequency ramping on the extracted beam indicates that the model in the simulation is still not perfect; the interaction of frequency, geometry, and plasma is neglected in the simulation, which is not acceptable according to the experimental results. The influence of the microwave on the starting conditions of ions needs to be formulated.

REFERENCES

[1] J. Reich, H. Beuscher, FA Jülich, R.K. Bhandari, Bhaba ARC, J.I.M. Botman, H.L. Hagedoorn, Eindhoven University, Partial beam decorrelation of sources providing ions out of axial magnetic fields, EPAC 1988, Rom, Italy.

[2] J.I.M. Botman, H.L. Hagedoorn, Eindhoven University, J. Reich, FA Jülich, The beam emittance of cyclotrons with an axial injection system, EPAC 1988, Rom, Italy.

[3] J.P.M. Beijers, H.R. Kremers, V. Mironov, J. Mulder, S. Saminathan, and S. Brandenburg, Ion source development at KVI, RSI Vol. **79** No 2, 2008.

[4] L. Panitzsch, M. Stalder, R.F. Wimmer-Schweingruer, Direct high-resolution ion beam-profile imaging using a position-sensitive Faraday cup array, Review of Scientific Instruments, Vol. **80**, 113302, 2009.

[5] P. Spädtke, R. Lang, J. Mäder, J. Roßbach, K. Tinschert, GSI Darmstadt, Beam transport effects for ECRIS, Proceedings of LINAC08, Victoria, BC, Canada

[6] P. Spädtke, K. Tinschert, R. Lang, J. Mäder, J. Roßbach, GSI Darmstadt, J.W. Stetson, MSU Michigan, L. Celona, INFN Catania, Prospects of Ion Beam Extraction and Transport Simulations, RSI Vol. **79** No 2, 2008.

[7] KOBRA3-INP, Junkernstr. 99, 65205 Wiesbaden, Germany.

[8] F. Maimone, K. Tinschert, P. Spädtke, J. Mäder, J. Roßbach,, R. Lang, GSI Darmstadt, L. Celona, INFN-LNS Catania, Microwave frequency dependence of the properties of the ion beam extracted from a CAPRICE type ECRIS, these proceedings.

KINETIC PLASMA SIMULATION OF ION BEAM EXTRACTION FROM AN ECR ION SOURCE

S.M. Elliott, Thin Film Consulting, Longmont, CO 80501 U.S.A
J. Simkin, Cobham Technical Services, Vector Fields Software, Oxford, OX5 1JE, UK
E.K. White, Thin Film Consulting, Longmont, CO 80501 U.S.A.

Abstract

Designing optimized ECR ion beam sources can be streamlined by the accurate simulation of beam optical properties in order to predict ion extraction behavior. The complexity of these models, however, can make PIC-based simulations time-consuming. In this paper, we first describe a simple kinetic plasma finite element simulation of extraction of a proton beam from a permanent magnet hexapole electron cyclotron resonance (ECR) ion source. Second, we analyze the influence of secondary electrons generated by ion collisions in the residual gas on the space charge of a proton beam of a dual-solenoid ECR ion source. The finite element method (FEM) offers a fast modeling environment, allowing analysis of ion beam behavior under conditions of varying current density, electrode potential, and gas pressure.

INTRODUCTION

The first simulation reported here represents proton extraction from a hexapole ECR ion source similar, but not identical, to an existing 10 GHz source [1], [2] and with a magnet system for higher frequency operation. The v14 SCALA/TOSCA 3d FEM software [3] is used for reasonably fast prediction of ion beam formation with automatically generated secondary charged particles from gas in the ionization chamber. A second model of a dual-solenoid ECR ion source [4] is used to simulate space charge beam compensation with gas secondary electrons.

PART 1: KINETIC PLASMA SIMULATION

The simulation includes space charge interactions of electrons and ions in the ionization chamber of a hexapole ECR ion source with a solenoid magnet lens (Fig. 1), extracting a proton beam from the plasma volume. The simulation predicts a three spoke ion beam cross-section.

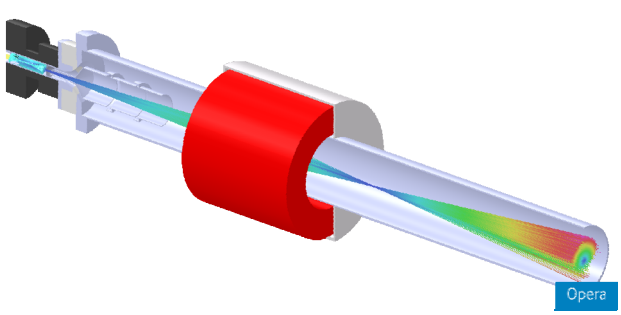

Figure 1: Source geometry with solenoid lens.

The source is composed of a magnet system and ionization chamber. An extractor is held at -10 kV. An einzel lens is also included (Fig. 2).

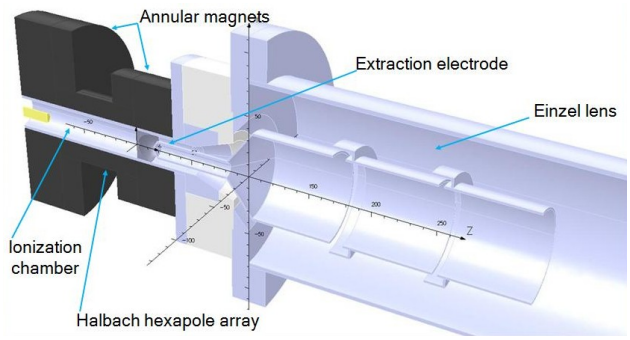

Figure 2: Source and einzel lens.

SIMPLE PLASMA SIMULATION

A small current of ions launched from the ECR surface initializes emission of volume secondary electrons and ions. The plasma fills the magnetic volume in the ionization chamber. Electrons and ions can be given energy and angular distributions, energy and current loss and scattering may be calculated, and surface secondary particles may be added as well.

RESULTS

The minimum B axial magnetic field is simulated with non-linear magnetic materials and has a minimum of about 0.47 T on axis (Fig. 3).

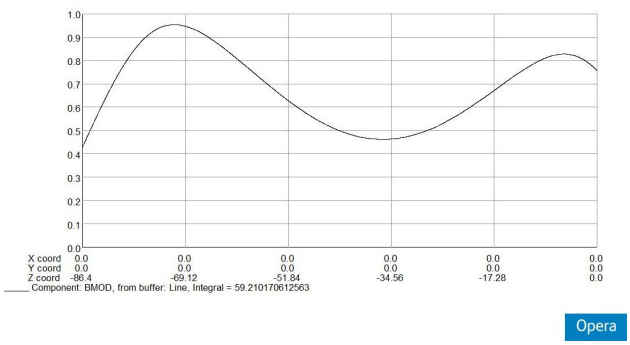

Figure 3: Ionizer on-axis magnetic flux density.

The space charge distribution in the ionization chamber is inhomogeneous due to the magnetic field (Fig. 4).

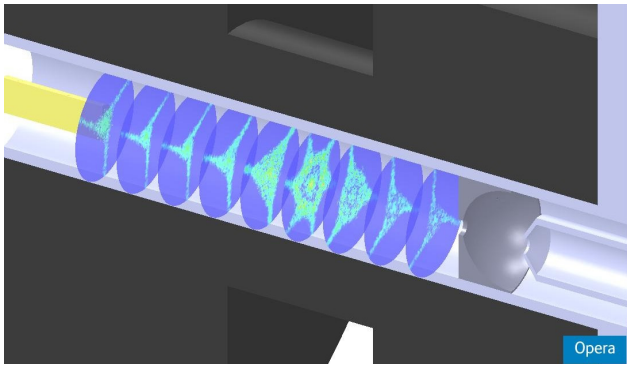

Figure 4: Ionization chamber space charge.

The ionizer plasma is visible by displaying trajectories (Fig. 5).

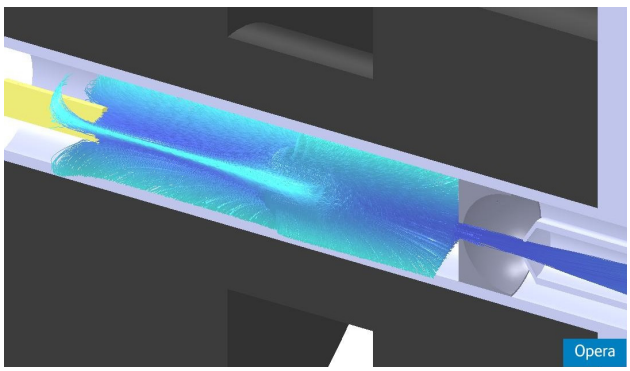

Figure 5: Ionizer plasma.

The extracted ion beam contains three spokes and is embedded in a partial ring halo (Fig. 6). Varying conditions in the ionization chamber can result in variations of the beam profile.

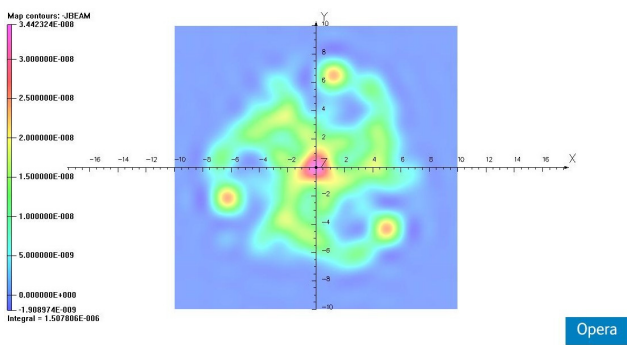

Figure 6: Ion beam profile at Z = 140 mm.

PART 2: BEAM COMPENSATION

The second simulation illustrates the influence of secondary charged particles generated by ion collisions in the drift space residual gas on the space charge in a proton beam. The simulation predicts a decrease in beam divergence with gas secondary electron space charge compensation. The finite element model is composed of two solenoid magnets, a three-electrode accel-decel extraction system and a downstream, partially reflecting termination (Fig. 7).

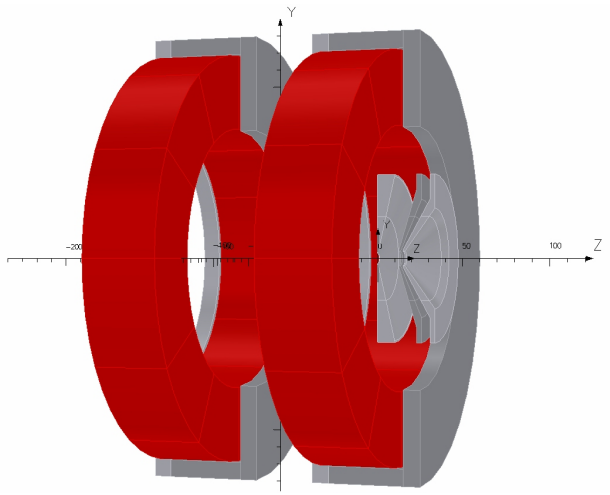

Figure 7: Source geometry with non-linear magnetic materials.

The source is held at 15 kV, the extractor at -4 kV, and the electron suppressor and reflector at -0 V.

BEAM INTERACTIONS

The basic simulation and primary emission method is described elsewhere [4]. Secondary emission from background gas, with user specified energy and angular distributions, is automatically simulated.

Secondary particles are generated from a volume representing the background gas. Volume secondaries are generated at a randomized, user-defined characteristic length along the primary beam trajectories.

RESULTS

The maximum magnetic flux density along the ion source axis is about 0.11 T [Fig. 8].

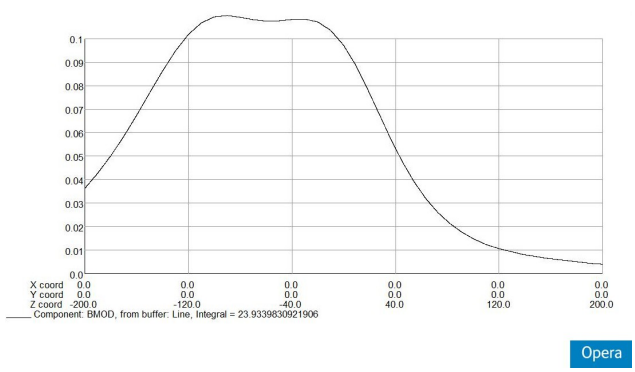

Figure 8: On-axis magnetic flux density.

The gas secondary electrons are highly magnetized and are confined near the ion beam by both the magnetic field and the ion beam space charge [Fig. 9].

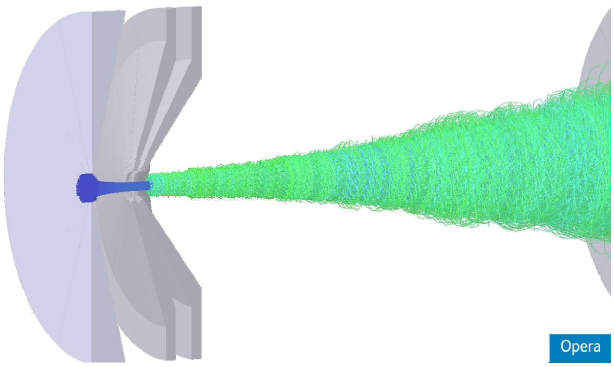

Figure 9: Magnetized secondary electrons.

The ion beam envelope divergence is reduced with space charge compensation (Figs. 10 and 11).

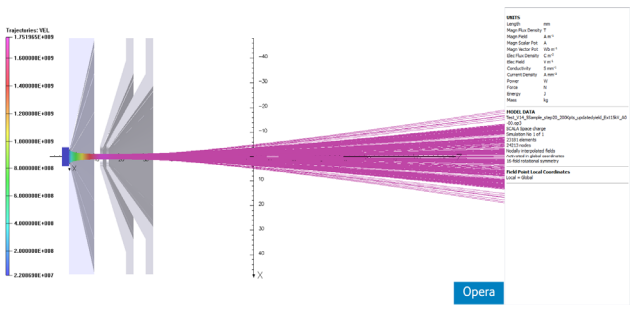

Figure 10: Ion beam without compensation.

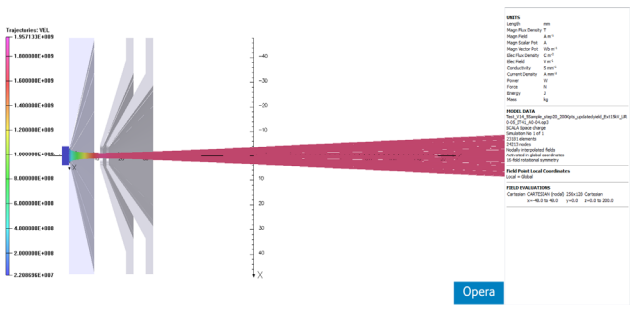

Figure 11: Ion beam with compensation.

The ion beam axial electric potential is reduced with space charge compensation as expected (Figs. 12 and 13).

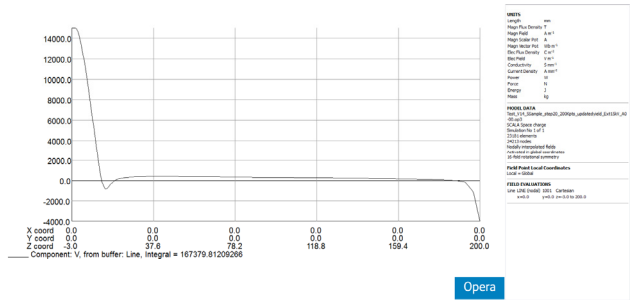

Figure 12: Ion beam axial voltage without compensation.

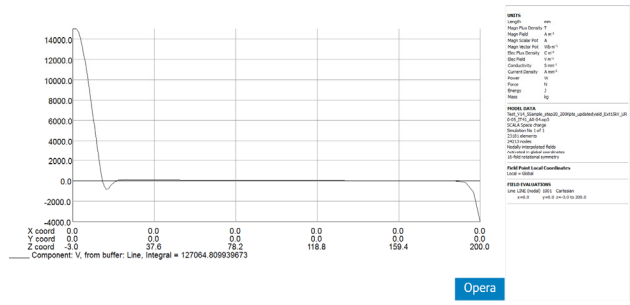

Figure 13: Ion beam voltage with compensation.

CONCLUSIONS

The new version of SCALA/TOSCA, v14, permits simulation of extraction of a structured ion beam from a hexapole ECR ion source as well as simulation of ion beam neutralization by trapped gas secondary electrons. The simulations run in tens of minutes to a few hours on standard computer platforms without the need of particle-in-cell methods. This provides a fast means of simulating beam optics in the design stage for optimal ion extraction.

REFERENCES

[1] M. Schlapp, et al., 12th Intern. Workshop on ECR Ion Sources, RIKEN/Japan (1995) 71.
[2] M. Schlapp, R. Trassl, R.W. McCullough, J.B. Greenwood, E. Salzborn, CAARI 96, Denton/Texas, USA (1996).
[3] OPERA 3d, Cobham Technical Services, Vector Fields Software, Oxford, UK.
[4] S.M. Elliott, J. Simkin, E.K. White, Proceedings of the 18th International Workshop on ECR Ion Sources, Chicago/Illinois (2008).

DIPOLE MAGNET OPTIMIZATION FOR HIGH EFFICIENT LOW ENERGY BEAM TRANSPORT*

S. Saminathan†, J.P.M. Beijers, J. Mulder, V. Mironov, and S. Brandenburg
Kernfysisch Versneller Instituut, University of Groningen, Groningen 9747AA, The Netherlands

Abstract

Losses in the low-energy beam transport line from the KVI-AECRIS to the AGOR cyclotron are estimated to be around 50 %. Numerical simulations of beam extraction and transport have been performed up to the image plane of the analyzing magnet. The simulations show overall good agreement with measurements of beam profiles and emittances. It was found that the beam losses are caused by a too small gap of the analyzing magnet. This magnet also suffers from large second-order aberrations causing a significant increase of the effective beam emittance in both horizontal and vertical directions. We show that by increasing the magnet gap and suitably modifying the pole surfaces the beam losses can be suppressed and the second-order aberrations significantly reduced. This results in a substantially lower effective emittance of the transported beam.

INTRODUCTION

The low-energy beam transport (LEBT) line connecting the electron cyclotron resonance ion source (ECRIS) with the AGOR cyclotron at KVI, Groningen suffers from undesired beam losses of up to 50%. A program has therefore been initiated to improve the transport efficiency of the beam line. We started with a detailed simulation of beam extraction from the ECRIS and transport of the beam through the 110° analyzing magnet. The simulations have been bench marked against measurements of the full 4D emittance of the beams in the image plane of the analyzing magnet with a pepperpot [4] emittance meter and measurements of beam profiles at the source exit. The simulations clearly show that the analyzing magnet is the cause of significant beam losses. In addition, aberrations caused by the magnet's fringe fields lead to a large increase of the effective beam emittance. The next step was to start an improvement program of the ion-optical properties of the analyzing magnet. By increasing the magnet gap and modifying the shape of the pole faces of the analyzing magnet its ion-optical properties can be greatly improved leading to an increase of the beam transport efficiency of the LEBT line.

The paper is organized as follows. First we will present a detailed discussion of the beam extraction and transport simulations and comparison with the emittance measurements. Then the first results of the work on the improvement of the analyzing magnet will be presented and discussed. The paper ends with a summary and outlook.

BEAM TRANSPORT

The ECRIS and the 110° analyzing magnet are shown in Fig. 1. The ECRIS is an ion source of the AECR type of LBNL, Berkeley with the Al plasma chamber built by the Jyväskylä group [1]. More details of our source are given in Refs. [2] and [3]. The analyzing magnet is an unclamped double focusing magnet with straight 37° tilted edges and a vertical gap of 67 mm. The dipole bends the beam over 110° with a bending radius of 400 mm. Two BaF_2 viewing

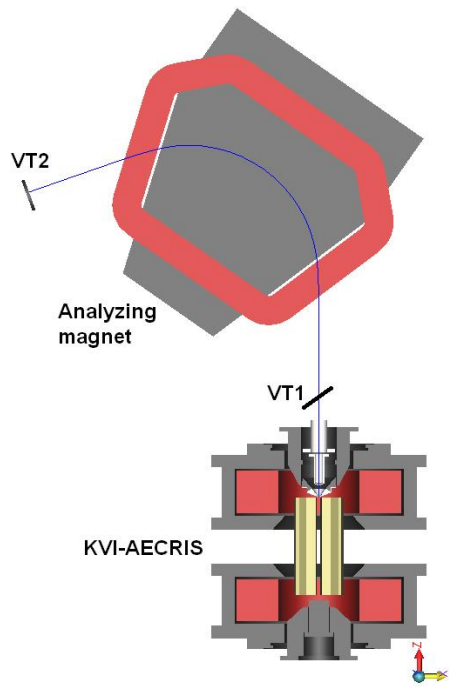

Figure 1: The KVI ECRIS and the 110° analyzing magnet.

targets have been installed, i.e. VT1 located directly behind the extraction system and VT2 located close to the image plane of the analyzing magnet. Later the viewing target VT2 has been replaced by a pepperpot emittance meter [4]. There are no optical elements between ECRIS and analyzing magnet.

Several computer codes have been used in the simulation process including an ECRIS simulation code PIC-MCC [5], and the particle tracking codes LORENTZ-3D [6] and

* This work has been supported by the Rijksuniversiteit Groningen and by the European Union through EURONS, contract 506065. It has been performed as part of the research programme of the "Stichting voor Fundamenteel Onderzoek der Materie" (FOM), with support of the "Nederlandse Organisatie voor Wetenschappelijk Onderzoek" (NWO)."
† saminathan@kvi.nl

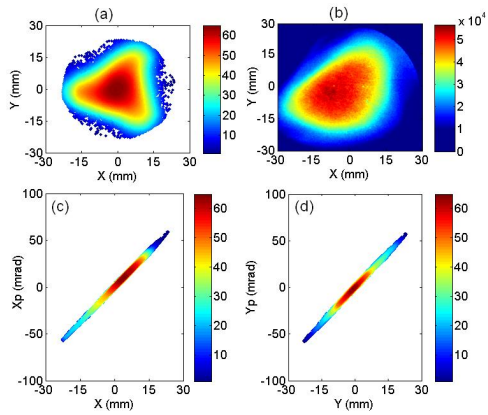

Figure 2: Calculated spatial distribution of a fully space-charge compensated He^+ beam behind the ground electrode at the location of VT1 (a). Measured He^+ beam profile at the same location (b). Calculated horizontal (c) and vertical (d) emittance plot at the same location.

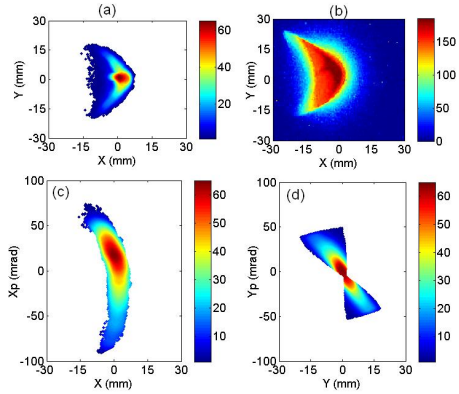

Figure 3: Calculated spatial distributions of a fully space-charge compensated He^+ beam in the image plane of the analyzing magnet at the location of VT2 (a). Measured He^+ beam profile at the same location (b). Calculated horizontal (c) and vertical (d) emittance plot at the same location.

COSY INFINITY [7]. We used LORENTZ-3D also to calculate the electric field in the accel-decel extraction system and the magnetic fields of the ECRIS and the analyzing magnet. All simulations and measurements have been done for a 24 keV He^+ beam. First the initial 5D phase-space distribution of the He^+ ions at the ECRIS extraction aperture is calculated with our PIC-MCC code. This distribution yields the start values of the spatial and angular coordinates of the ions for the subsequent calculation of the ion trajectories through the extraction system and analyzing magnet using the LORENTZ-3D code. Previous work has shown that space-charge forces are not important, so these have not been taken into account in the present simulations [8]. Finally, from the calculated ion trajectories various 2D cross sections of the 4D transverse phase space are extracted, e.g. 2D beam profiles and emittance plots, which can then be compared with measurements. Emittance values are always given as effective RMS emittances incorporating 95% of the beam.

The calculated and measured beam profiles and the calculated horizontal and vertical emittances of the extracted He^+ beam at the location of VT1 directly behind the extraction system and at the location of VT2 close to the image plane of the analyzing magnet are shown in Fig. 2 and 3, respectively. More details about the simulation can be found in Ref. [8]. As can be seen, the calculated and measured beam profiles at both locations compare favorably. The simulations indicate that $\approx 30\%$ of the beam is lost during the transport through the analyzing magnet, mostly because of its too small gap. Furthermore, the parabolic envelope of the beam profile behind the analyzing magnet indicates a large second order image aberration caused by the analyzing magnet. This also leads to a significant increase of the effective beam emittances. The calculated horizontal and vertical emittance at the location of VT1 is 65 π mm mrad, which is increased by as much as five times in the horizontal plane and four times in the vertical plane at the location of VT2 behind the analyzing magnet.

A more stringent test of the beam transport simulations is comparing the calculated emittances with measured ones. We have therefore measured the 4D phase-space distributions with a pepperpot emittance meter installed at the location of VT2 behind the analyzing magnet. Measured horizontal and vertical emittance plots are shown in Fig. 4. The measured value of the horizontal emittance is 390 π mm mrad and of the vertical emittance 320 π mm mrad. Since the agreement between measurements and simulations is satisfactory we conclude that the most important factors determining beam extraction and transport are well understood.

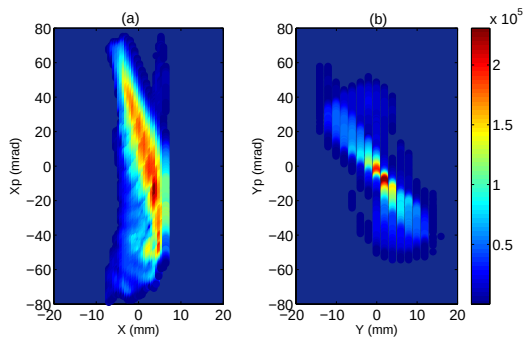

Figure 4: Measured horizontal (a) and vertical (b) beam emittances at the location of VT2 behind the analyzing magnet.

MAGNET OPTIMIZATION

As a next step we used our simulation tools to investigate ways to improve the transport and imaging properties

of the analyzing magnet. To decrease the beam losses the pole gap is increased from 67 to 110 mm. The second order aberrations of the analyzing magnet can be compensated by adding sextupole components to the dipole field of the analyzing magnet. We started with a similar pole face shape as used in the design of the VENUS analyzing magnet of LBNL [9]. The pole faces at the entrance and exit sections are shaped in such a way that a quadratically increasing field is obtained to correct the vertical sextupole component, while the central pole face shape is modified to obtain a quadratically decreasing magnetic field to correct the horizontal sextupole component. The modified pole face shape of the analyzing magnet is shown in Fig. 5. First we used COSY INFINITY to quickly estimate the required sextupole strengths and then the LORENTZ-3D code for the fine tuning.

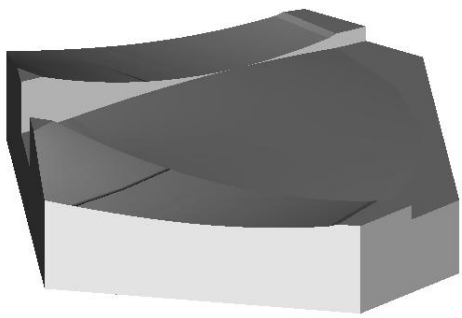

Figure 5: Pole face of the analyzing magnet including the sextupole correction.

The calculated beam profile and emittance plots for the optimized pole shape are shown in Fig. 6. As can be seen in Fig. 6a and 6b a small ($\approx$ 12%) fraction of the beam particles is deflected too much. The simulation shows that these particles are also on the left side of the beam before entering the analyzing magnet. By carefully decreasing the field integral on the inner side of the magnet we might remove this tail without affecting the vertical focusing too much. This is currently being investigated. According to the simulations the full beam is transported to the location of VT2 and the horizontal and vertical emittances are decreased with a factor of two compared to the uncorrected values.

SUMMARY AND OUTLOOK

We have simulated the extraction and transport of a He^+ beam from the KVI ECRIS to the image plane of the analyzing magnet. The good agreement between calculated and measured beam profiles and emittance plots shows that the basic physics is well reproduced in the simulations. We have shown that the analyzing magnet causes beam losses and suffers from large second-order aberrations yielding a four-fold increase in the effective beam emittance. Finally we have shown that the beam losses can be prevented by

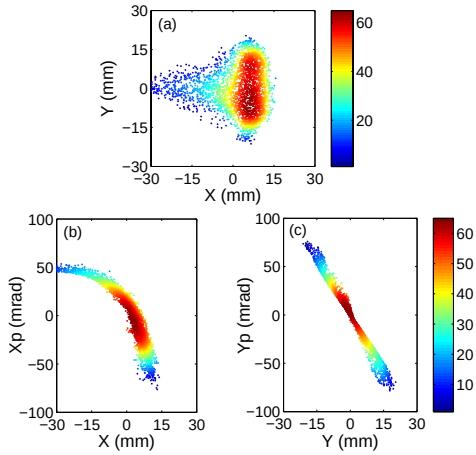

Figure 6: Calculated spatial distribution for a fully space-charge compensated He^+ beam at the location of VT2 behind the modified analyzing magnet (a). Calculated horizontal (b) and vertical (c) emittance plots at the same location.

increasing the magnet gap and that the second-order aberrations can be significantly reduced by modifying the shape of the magnet poles.

Based on our simulations we will modify the pole face of the existing analyzing magnet to include the second order correction optics and extend the simulations to the entire low-energy beam line.

REFERENCES

[1] H. Koivisto *et al.*, Nucl. Instrum. Methods Phys. Res. B **174**, 379 (2001).

[2] H.R. Kremers, J.P.M. Beijers, and S. Brandenburg, Rev. Sci. Instrum. **77**, 03A311(2006).

[3] H.R. Kremers *et al.*, High Energy Phys. Nucl. Phys. **31**, 90 (2007).

[4] H.R. Kremers, J.P.M. Beijers, and S. Brandenburg, Proceedings of DiPAC07, Venice, p. 169-171 (2007).

[5] V. Mironov and J.P.M. Beijers, Phys. Rev. ST Accel. Beams **12**, 073501 (2009).

[6] See the homepage of the LORENTZ-3D code at www.integratedsoft.com/products/lorentz/default.aspx.

[7] K. Makino and M. Berz, Nucl. Instrum. Methods Phys. Res. A **427**, 338 (1999).

[8] S. Saminathan *et al.*, Rev. Sci. Instrum. **81**, 02B706 (2010).

[9] M. Leitner *et al.*, ECRIS02 workshop, Jyväskylä (FI), June 2002.

MODELING ECRIS USING A 1D MULTIFLUID

Michael Stalder#, CAU, Kiel, Germany

Abstract

The Department of Experimental and Applied Physics (IEAP) at the University of Kiel (CAU Kiel) is establishing a solar wind laboratory for the calibration of space instrumentation. The main item of this facility is a 11GHz (Plateau) ECR ion source. It can be operated at two different radial magnetic confinements, using a set of permanent magnets in either hexapole or dodekapole arrangement. While beam focussing by moving the extraction along the beam line to match the ion beam into the analysing magnet is well known, little is known about beam steering by moving the extraction in the plane perpendicular to the beam line. For the hexapole-configuration we will present our results about the feasibility of ion beam focussing and steering using a 3D-movable extraction. The beam profiles of these measurements will be recorded in comparatively high resolution with a Faraday cup array (see paper doi: 10.1063/1.3246787). This method will be shortly introduced within this talk, as well.

Paper not received

#michael.stalder@gmmx.net

CLOSING REMARKS FOR ECRIS'10

T. Nakagawa, RIKEN, Japan

Abstract

The scientific topics of the ECRIS10 Workshop are introduced. New results presented by a selection of authors during the sessions are summarized.

INTRODUCTION

ECRIS'10, the 19th ECRIS workshop, was held in Grenoble, France, from the 23rd through the 26th of August 2010 with 100 participants. It is well known that Grenoble is the Mecca for ECRIS, as it has already played host two previous times (1982 and 1988). The programs this year covered the foremost topics related to the design and operation of ECR ion sources, including status reports, new developments, radioactive ion beam production, plasma physics and plasma diagnostics, beam extraction and transport, and applications. In this workshop, we found several clear trends in the development of ECR ion sources: 1) intense beam production for secondary beams (including radioactive beams); 2) pulsed mode operation for beta-beam projects; 3) new applications; and 4) plasma diagnostics, beam extraction, and transportation. Several highlights in these trends are presented in this short report.

TOPICS

Several facilities using ECR ion sources for radioactive beams are currently in operation. Requirements in this field lead us to employ higher magnetic fields and microwave frequencies to increase the beam current of ions in a medium charge state such as U^{33-35+}. H. W. Zhao demonstrated the effect of the microwave frequency (18 and 24 GHz) on the intensity of beams of highly charged heavy ions with SECRAL. D. Leitner presented the excellent results of VENUS after the re-commissioning. The NSCL team reported the excellent results of their 18 GHz ECR ion source (SuSI) and the requirements of the ECR ion source for the FRIB project. The experimental results of these ion sources clearly show that the beam intensity is not saturated at the highest RF power (~0.7 kW/L). This indicates that there is some scope to increase the beam intensity. The NSCL team made systematic bremsstrahlung and ion beam current measurements to examine the production mechanisms of highly charged heavy ions in the ion source. For the first time, they experimentally demonstrated the effect of the field gradient at the resonance zone on the beam intensity and bremsstrahlung X-rays.

For fourth-generation designs, the technical challenges in attaining the optimum magnetic field strength at 56 GHz were independently proposed by D. Leitner and Z. Q. Xie on the basis of their own concepts. Two Korean teams proposed and designed a new 28 GHz SC-ECRIS for the Korean Rare Isotope Beam Accelerator (KoRIA) project and a compact heavy ion linear accelerator facility.

ECR ion sources are used for the production of other secondary beams. A 2.45 GHz ECR ion source is used to produce thermal neutrons for a neutron imaging facility in Peking University. The CEA and CNRS have undertaken a research and development program on very high beam power accelerators, such as the Accelerator Driven Transmutation of Waste, a new generation of exotic ion facilities, and neutrino and muon production. The CEA is also involved in projects such as the European Spallation Source and IFMIF.

Utilizing metallic particles of rubidium, the charge breeder CARIBU (ANL) project has reached an extraction efficiency of 11.9% from an ECR ion source. Multiple-frequency operations also exhibit the potential to increase the beam intensity for the charge breeding system. The TRIUMF team achieved high-efficiency charge breeding for radioactive ions (1.4% efficiency for $^{124}Cs^{20+}$, 1.7% efficiency for $^{76}Rb^{15+}$, and 6.2% for $^{74}Kr^{15+}$). T. Lamy reported that grounded tube removal is very promising for charge breeding. In the SPIRAL project, a new multi-charged ion source, based on an asymmetric magnetic structure, was both proposed, and designed by L. Maunoury.

An intense short-pulse beam plays a crucial role in the Beta-Beam project. For meeting the requirements, the IAP-RAS and LPSC teams both experimentally and theoretically investigated the mechanisms behind the preglow of a multi-charged heavy ion beam from an ECR ion source. They reported that the effective generation in the short preglow peak is possible under powerful heating at a high frequency. In the study of the time evolution of plasma potential, O. Tarvainen concluded that the plasma potential is higher during the plasma build-up and decay compared with that under steady-state conditions; however, the processes explaining the potential fluctuations are different for preglow and afterglow. For realization of the intense short-pulse beam for the Beta-Beam project, a 60 GHz ECR ion source (megawatt-class) was proposed and tested in Grenoble.

ECR ion sources have several advantages as ion sources for trace element analysis (high ionization efficiency, production of stable plasma under the very low gas pressure ($<10^{-6}$ Torr), long plasma confinement for multi-charged ion production, etc.). Recently, the ANSTO ECR ion source was successfully used for measuring the isotopic ratios of elements such as carbon, nitrogen, and oxygen. An ECR ion source was successfully used as an ion source for AMS at Argonne to detect the noble gas elements (^{39}Ar, ^{81}Kr). R. Pardo proposed a new plan for laser ablation of actinides into an ECR ion source for AMS. P. Sortais fabricated a very small ECR ion source

(COMIC) that produces multiple or broad beams for new industrial applications (ion implanter, surface treatment, etc.). The number of facilities for heavy ion therapy is now increasing rapidly. It is clear that the ECR ion source is one of the important devices for this purpose. The status and development of the ECR ion sources at HIMAC, Gunma University, and HIT were reported. A. Villari presented the status of their commercial ECR ion source, which included the new liquid-He-free SC-ECRIS (PK-ISIS).

The basic studies for ECR plasma, beam extraction, and transportation are perennially important to improving ECR ion source performance. C. Lyneis reported on microwave coupling of the plasma chamber, which is interesting not only for the static properties, but also for dynamical processes. A new simulation code (PIC + Monte Carlo simulation) was developed by D. Mascali in order to understand the plasma dynamics, plasma–microwave interaction, and so on. Visible light emitted from a plasma was systematically measured by S. Biri. The X-rays from a plasma were carefully measured by H. Koivisto and T. Ropponen. In order to investigate the heating mechanism of electrons in the ECR plasma, they studied the maximum energy of bremsstrahlung and the relation between the magnetic field gradient and the average kinetic energy of the X-rays. C. Peaucelle presented the status of the heavy ion low energy beam transport line of SPIRAL 2. The Spiral 2 specifications could be met by an increase in RF power (2 kW) and high voltage extraction (60 kV). The intense U ion beam from VENUS was simulated with the WARP code, and the calculated emittance was in reasonable agreement with the measurements. The beam extracted from the ECR ion source was measured by the KVI4D pepper pot emittance meter and it was observed that the dipole magnet induced a second order aberration of the beam. At end of the workshop, it was announced that O. Tarvainen was awarded the Richard Geller Prize for his contributions to "physics experiments on ECR plasmas that resulted in a deeper understanding of the plasma physics of ECR ion sources."

CONCLUSION

The performance of ECR ion sources is rapidly improving. We do not yet know of any performance ceiling for ECR ion sources. Although the ECR plasma is especially complicated, we are able to gradually deepen our understanding. The applications of ECR ion sources continue to expand. It is obvious that the future of the ECR ion source is still open. There is a tremendous amount of work to be done.

ECRIS’10 was an enormous success due to the efforts of both the participants and the contributors. We thank the chairman, T. Thuillier, the local organizing committee, and the international advisory committee. The next workshop is scheduled for 2012 in Sydney, Australia, which is a new world for the ECR ion source community. See you there!

List of Authors

Bold papercodes indicate primary authors

Institutes List

AEC
Chiba, Japan
- Sakuma, T.
- Sasaki, N.
- Sasano, T.
- Takasugi, W.

ANL
Argonne, USA
- Kolomiets, A.
- Kondev, F.G.
- Kondrashev, S.A.
- Nair, C.
- Palchan, T.
- Pardo, R.C.
- Rehm, E.
- Scott, R.H.
- Vondrasek, R.C.

ANSTO
Menai, Australia
- Button, D.
- Hotchkis, M.A.C.

ATOMKI
Debrecen, Hungary
- Biri, S.
- Rácz, R.

AVS
Eibar, Gipuzkoa, Spain
- Carrera, M.A.
- Galipienzo, J.H.

Bilbao, Faculty of Science and Technology
Bilbao, Spain
- Bermejo, F.J.

CEA/DSM/IRFU
France
- Adroit, G.
- Bourdelle, G.
- Chauvin, N.
- Delferrière, O.
- Duperrier, R.D.
- Gauthier, Y.
- Girardot, P.
- Gobin, R.
- Harrault, F.
- Marolles, C.
- Napoly, O.
- Pottin, B.
- Sauce, Y.
- Senée, F.
- Tuske, O.
- Uriot, D.
- Vacher, T.V.
- Van Hille, C.

CEA/IRFU
Gif-sur-Yvette, France
- Gauthier, Y.
- Gobin, R.
- Mateo, C.M.
- Nyckees, S.

CERN
Geneva, Switzerland
- Stora, T.
- Suominen, P.

CIMAP
Caen, France
- Pierret, C.

CSFNSM
Catania, Italy
- Mascali, D.

DMFCI
Catania, Italy
- Maimone, F.

DU
Debrecen, Hungary
- Pálinkás, J.

Elytt Energy
Madrid, Spain
- Lucas, J.

ESS Bilbao
Bilbao, Spain
- Bustinduy, I.
- Cortazar, D.
- de Cos, D.
- Djekic, S.
- Fernandez-Cañoto, D.
- Hassanzadegan, H.
- Munoz, J.L.

ESS-Bilbao
Zamudio, Spain
- Feuchtwanger, J.
- Rueda, I.

FRIB
East Lansing, Michigan, USA
- Pozdeyev, E.
- Tanke, E.

GANIL
Caen, France
- Bajeat, O.
- Barue, C.
- Canet, C.
- Delahaye, P.
- Dubois, M.
- Dupuis, M.
- Flambard, J.L.
- Frigot, R.
- Jardin, P.
- Leboucher, C.
- Lecesne, N.
- Lecomte, P.
- Lehérissier, P.
- Lemagnen, F.
- Leroy, R.
- Maunoury, L.
- Michel, M.
- Osmond, O.
- Pacquet, J.Y.
- Pichard, A.

GHMFL
Grenoble, France
- Debray, F.
- Matera, J.
- Pfister, R.
- Trophime, C.

Graduate School of Medicine, Dentistry and Pharmaceutical Sciences, Okayama University
Okayama, Japan
- Enomoto, S.

Graduate School of the Chinese Academy of Sciences
Beijing, People's Republic of China
- Lu, W.

GSI
Darmstadt, Germany
- Lang, R.
- Mäder, J.
- Maimone, F.
- Roßbach, J.
- Spädtke, P.
- Tinschert, K.

Gunma University, Heavy-Ion Medical Research Center
Maebashi-Gunma, Japan
- Torikai, K.
- Yamada, S.

HIT
Heidelberg, Germany
- Cee, R.
- Haberer, Th.
- Naas, B.
- Peters, A.
- Winkelmann, T.

IAP/RAS
Nizhny Novgorod, Russia
- Golubev, S.
- Izotov, I.
- Mansfeld, A.
- Razin, S.
- Sidorov, V.
- Skalyga, V.
- Vodopyanov, A.
- Zorin, V.

Idaho National Laboratory
Idaho, USA
- McGrath, C.
- Palmotti, G.
- Salvatores, M.
- Youinou, G.

IEAP
Kiel, Germany
- Panitzsch, L.
- Peleikis, T.
- Stalder, M.
- Wimmer-Schweingruber, R.F.

IEE
Beijing, People's Republic of China
- Ruan, L.
- Song, F.C.
- Xiong, B.
- Yu, S.
- Yuan, J.

IFIN
Magurele- Bucuresti, Romania
- Dobrescu, S.
- Schächter, L.

IGCAR
Channai, India
- Baskaran, R.

IKF
Frankfurt-am-Main, Germany
- Stiebing, K.E.

IMP
Lanzhou, People's Republic of China
- Cao, Y.
- Feng, Y.C.
- Guo, X.H.
- Li, J.Y.
- Li, X.X.
- Lu, W.
- Sun, L.T.
- Xie, D.
- Zhang, W.H.
- Zhang, X.Z.
- Zhao, H.W.
- Zhao, H.
- Zhu, Y.H.

IN2P3 IPNL
Villeurbanne, France
- Peaucelle, C.

INFN-Bologna
Bologna, Italy
- Cuffiani, M.
- Malferrari, L.
- Odorici, F.
- Rizzoli, R.
- Veronese, G.P.

INFN/LNL
Legnaro (PD), Italy
- Galatà, A.

INFN/LNS
Catania, Italy
- Castro, G.
- Celona, L.
- Ciavola, G.
- Gambino, N.
- Gammino, S.
- Mascali, D.
- Miracoli, R.
- Neri, L.
- Romano, F.P.

Institute of High Current Electronics
Tomsk, Russia
- Yushkov, G.

IPN
Orsay, France
- Biarrotte, J.-L.

ISU
Pocatello, Idaho, USA
- Imel, G.

IUAC
New Delhi, India
- Dutt, R.N.
- Kanjilal, D.
- Lakshmy, P.S.
- Mathur, Y.
- Rao, U.K.
- Rodrigues, G.
- Roy, A.

JINR
Dubna, Moscow Region, Russia
- Bekhterev, V.B.
- Bogomolov, S.L.
- Drobin, V.M.
- Efremov, A.
- Gikal, B.
- Gulbekyan, G.G.
- Kostyukhov, Yu.K.
- Lebedev, N.
- Loginov, V.N.
- Seleznev, V.V.
- Yazvitsky, Yu.

JRC/IRMM
Geel, Belgium
- Chavez-de-Jesus, C.
- Gamboni, T.
- Geerts, W.
- Giorginis, G.
- Jaime Tornin, R.
- Lövestam, G.
- Mondelaers, W.

JYFL
Jyväskylä, Finland
- Aho, V.P.
- Ärje, J.
- Jones, P.
- Kauppinen, J.A.
- Koivisto, H. A.
- Peura, P.
- Ropponen, T.
- Sarén, J.H.
- Tarvainen, O.A.
- Toivanen, V.A.

KAERI
Daejon, Republic of Korea
- Chang, D.S.
- Hwang, C.K.
- In, S.R.
- Jeong, S.H.
- Jin, J.T.
- Lee, K.W.
- Oh, B.H.
- Seo, C.S.

KEK
Ibaraki, Japan
- Arai, T.
- Koyama, K.
- Wake, M.

Korea Basic Science Institute
Busan, Republic of Korea
- Lee, B.S.
- Won, M.

KVI
Groningen, The Netherlands
- Beijers, J.P.M.
- Brandenburg, S.
- Drentje, A.G.
- Kremers, H.R.
- Mironov, V.
- Mulder, J.
- Saminathan, S.

LBNL
Berkeley, California, USA
- Benitez, J.Y.
- Ferracin, P.
- Hodgkinson, A.
- Kireeff Covo, M.
- Leitner, D.
- Leitner, M.
- Loew, T.J.
- Lyneis, C.M.
- Noland, J.D.
- Sabbi, G.L.
- Strohmeier, M.M.
- Todd, D.S.
- Winklehner, D.

LLNL
Livermore, California, USA
- Covo, M.K.
- Grote, D.P.

LPSC
Grenoble Cedex, France
- Angot, J.
- Coly, A.
- Jacob, J.
- Lamy, T.
- Latrasse, L.
- Marie-Jeanne, M.
- Médard, J.
- Sortais, P.
- Thuillier, T.
- Grandemange, P.
- Lamy, T.
- Médard, J.
- Sortais, P.
- Thuillier, T.

Mitsubishi Electric Corp., Energy & Public Infrastructure Systems Center
Kobe, Japan
- Kijima, Y.

Mitsubishi Electric Corp., Energy Systems Centre
Kobe, Japan
- Tsuchiyama, M.
- Ueda, S.

National Institute of Radiological Sciences
Chiba, Japan
- Fujita, T.F.

National Research Institute of Police Science
Chiba, Japan
- Kishi, S.
- Seto, Y.

NFRI
Daejon, Republic of Korea
- You, H.J.

Nippon Advanced Technology Co. Ltd.
Ibaraki-prefecture, Japan
- Okazaki, K.

NIRS
Chiba-shi, Japan
- Hojo, S.
- Kitagawa, A.
- Muramatsu, M.
- Sakamoto, Y.

NSCL
East Lansing, Michigan, USA
- Brandon, J.
- Cole, D.G.
- Doleans, M.
- Kester, O.K.
- Machicoane, G.
- Morris, D.
- Pozdeyev, E.
- Ropponen, T.
- Stolz, A.
- Sun, L.T.
- Tobos, L.
- Wu, X.

ORNL
Oak Ridge, Tennessee, USA
- Bannister, M.E.
- Deng, S.
- Draganić, I.N.
- Hale, J.W.

- Harris, P.R.
- Havener, C.C.
- Krause, H.F.
- Meyer, F.W.
- Vane, C.R.

Osaka University, Graduate School of Engineering
Osaka, Japan
- Kato, Y.

PANTECHNIK
BAYEUX, France
- Bieth, C.
- Bougy, W.
- Brionne, B.N.
- Donzel, X.
- Gaubert, G.
- Leroy, R.
- Sineau, A.
- Tasset, O.
- Vallerand, C.
- Villari, A.C.C.

PKU/IHIP
Beijing, People's Republic of China
- Chen, J.E.
- Guo, Z.Y.
- Lu, P.N.
- Lu, Y.R.
- Peng, S.X.
- Ren, H.T.
- Song, Z.Z.
- Yu, J.X.
- Yuan, Z.X.
- Zhang, M.
- Zhao, J.

RIKEN Nishina Center
Wako, Japan
- Fujimaki, M.
- Goto, A.
- Haba, H.
- Higurashi, Y.
- Ikezawa, E.
- Kamigaito, O.
- Kase, M.
- Kidera, M.
- Komiyama, M.
- Nakagawa, T.
- Ohnishi, J.
- Watanabe, Y.

RIKEN
Saitama, Japan
- Takahashi, K.

SHI Accelerator Service Ltd.
Tokyo, Japan
- Aihara, T.
- Tamura, M.
- Uchiyama, A.

SHI
Ehime, Japan
- Miyazaki, H.
- Sawada, K.
- Ueno, T.

Sokendai
Ibaraki, Japan
- Adachi, T.
- Leo, K.W.

Tateyama Machine Co. Ltd.
Toyama-shi, Japan
- Asaji, T.
- Tanaka, K.

Texas A&M University Cyclotron Institute
College Station, Texas, USA
- May, D.P.

Texas A&M University, Cyclotron Institute
College Station, USA
- Tabacaru, G.

The Hebrew University of Jerusalem, The Racah Institute of Physics
Jerusalem, Israel
- Paul, M.

Thin Film Consulting
Longmont, Colorado, USA
- Elliott, S.M.
- White, E.K.

TIT
Yokohama, Japan
- Takayama, K.

Tokyo University of Science, Faculty of Engineering Division I
Tokyo, Japan
- Nagamatsu, T.
- Tanaka, T.

Toyo University
Kawagoe-shi, Saitama, Japan
- Minezaki, H.
- Uchida, T.
- Yoshida, Y.

TRIUMF, Canada's National Laboratory for Particle and Nuclear Physics
Vancouver, Canada
- Ames, F.
- Baartman, R.A.
- Bricault, P.G.
- Jayamanna, K.

UCB
Berkeley, California, USA
- Verboncoeur, J.

University of Notre Dame
Notre Dame, USA
- Collon, P.

University of the Basque Country, Faculty of Science and Technology
Bilbao, Spain
- Etxebarria, V.
- Jugo, J.
- Portilla, J.

Università di Messina
Messina, Italy
- Serafino, T.

Vector Fields Ltd.
Oxford, United Kingdom
- Simkin, J.

Participants List

— A —

Ames, Friedhelm
TRIUMF
Vancouver, BC, Canada

Angot, Julien
LPSC
Grenoble, France

— B —

Barue, Christophe
GANIL
Caen, France

Benitez, Janilee
LBNL
Berkeley, CA, United States

Biri, Sandor
ATOMKI
Debrecen, Hungary

Bogomolov, Sergey
JINR
Dubna, Russian Federation

Bourdeauducq, Sebastien
CEA/Saclay
Gif Sur Yvette, France

— C —

Celona, Luigi
INFN-LNS
Catania, Italy

Cole, Dallas
NSCL
East Lansing, United States

Coly, Arona
LPSC
Grenoble, France

— D —

Debray, Francois
LNCMI
Grenoble, France

Djekic, Slobodan
ESS Bilbao
Leioa (Vizcaya), Spain

Donzel, Xavier
Pantechnik
Bayeux, France

Dubois, Mickael
GANIL
Caen, France

— E —

Efremov, Andrey
FLNR JINR
Dubna, Russian Federation

Elliott, Stephen
Thin Film Consulting
Longmont, CO, United States

— G —

Galatà, Alessio
INFN-LNL
Legnaro, Italy

Gammino, Santo
INFN-LNS
Catania, Italy

Gaubert, Gabriel
Pantechnik
Bayeux, France

Gobin, Raphaël
CEA/Saclay
Gif Sur Yvette, France

Grandemange, Pierre
LPSC
Grenoble, France

— H —

Higurashi, Yoshihide
RIKEN
Wako, Japan

Hotchkis, Michael
ANSTO
Kirrawee DC, Australia

— I —

Izotov, Ivan
IAP RAS
Nizhny Novgorod, Russian Federation

— J —

Jeppesen, Henrik Bak
Siemens A/S
Jyllinge, Denmark

— K —

Kester, Oliver
NSCL
East Lansing, United States

Kidera, Masanori
RIKEN
Saitama, Japan

Kitagawa, Atsushi
NIRS
Chiba, Japan

Koivisto, Hannu
JYU
Jyväskylä, Finland

Kremers, Herman Robert
KVI
Groningen, Netherlands

Küchler, Detlef
CERN
Geneva, Switzerland

— L —

Lamy, Thierry
LPSC
Grenoble, France

Lee, ByoungSeob
KBSI
Busan, Republic of Korea

Leitner, Daniela
LBNL
Berkeley, United States

Leo, Kwee Wah
The Graduate University for Advanced Studies
Tsukuba, Japan

Leroy, Renan
PANTECHNIK
Bayeux, France

Lettry, Jacques
CERN
Geneva, Switzerland

Loiselet, Marc
Université Catholique De Louvain - CRC
Louvain-la-Neuve, Belgium

Lu, Wang
IMP, CAS
Lanzhou, China

Lyneis, Claude
LBNL
Berkeley, CA, United States

— M —

Machicoane, Guillaume
NSCL
East Lansing, United States

Maimone, Fabio
GSI
Darmstadt, Germany

Marie-Jeanne, Mélanie
LPSC
Grenoble, France

Marletta, Salvatore
INFN-LNS
Catania, Italy

Mascali, David
INFN-LNS & CSFNSM
Catania, Italy

Mateo, Cherry May
CEA/Saclay
Gif Sur Yvette, France

Maunoury, Laurent
GANIL
Caen, France

May, Donald
Texas A&M University
College Station, TX, United States

Medard, JérÃ'me
LPSC
Grenoble, France

Meyer, Fred W
ORNL
Oak Ridge, United States

Mironov, Vladimir
KVI
Groningen, Netherlands

Mulder, Jan
KVI
Groningen, Netherlands

Muramatsu, Masayuki
NIRS
Chiba, Japan

— N —

Nakagawa, Takahide
RIKEN
Wako, Japan

Nyckees, Sebastien
CEA/Saclay
Gif Sur Yvette, France

— O —

Oh, Byung-Hoon
KAERI
Daejeon, Republic of Korea

— P —

Panitzch, Lauri
IEAP
Kiel, Germany

Pardo, Richard
ANL
Argonne, IL, United States

Peaucelle, Christophe
IPNL
Villeurbanne, France

Peleikis, Thies
IEAP
Kiel, Germany

Penescu, Liviu Constantin
CERN
Geneve, Switzerland

Peng, Shixiang
IHIP
Haidian, China

Pozdeyev, Eduard
NSCL
East Lansing, United States

— R —

Rodrigues, Gerard
IUAC
New Delhi, India

Ropponen, Tommi
NSCL
East Lansing, United States

— S —

Saminathan, Suresh
KVI
Groningen, Netherlands

Schachter, Leon
NIPNE
Magurele, Romania

Scott, Robert
ANL
Argonne, IL, United States

Skalyga, Vadim
IAP RAS
Nizhny Novgorod, Russian Federation

Sortais, Pascal
LPSC
Grenoble, France

Spädtke, Peter
GSI
Darmstadt, Germany

Stalder, Michael
IEAP
Kiel, Germany

Sun, Liangting
NSCL
East Lansing, United States

Suominen, Pekka
CERN
Geneve, Switzerland

— T —

Tabacaru, Gabriel
Texas A&M University
College Station, United States

Takayama, Ken
KEK
Tsukuba, Japan

Tarvainen, Olli
JYU
Jyväskylä, Finland

Thuillier, Thomas
LPSC
Grenoble, France

Tinschert, Klaus
GSI
Darmstadt, Germany

Toivanen, Ville
JYU
Jyväskylä, Finland

— V —

Villari, Antonio c.c.
PANTECHNIK
Bayeux, France

Vondrasek, Richard
ANL
Lemont, United States

— W —

Winkelmann, Tim
HIT
Heidelberg, Germany

Winklehner, Daniel
LBNL
Berkeley, United States

Won, MiSook
KBSI
Busan, Republic of Korea

— X —

Xie, Daniel
IMP„CAS
Lanzhou, China

— Y —

You, Hyun Jong
NFRI
Daejeon, Republic of Korea

— Z —

Zhao, Hongwei
IMP, CAS
Lanzhou, China

Zorin, Vladimir
IAP RAS
Nizhny Novgorod, Russian Federation